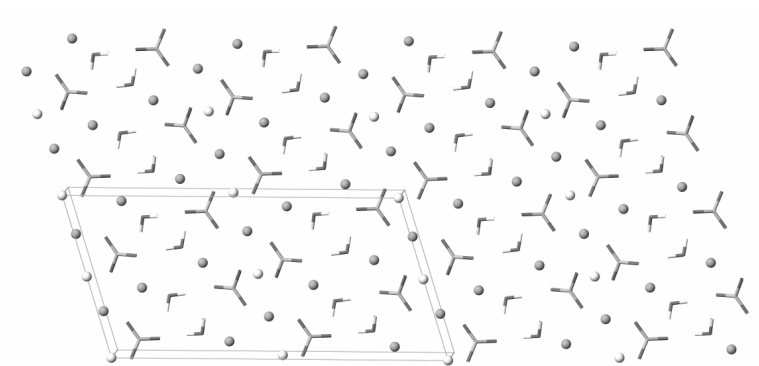


**MIXED SOLVENT REACTIVE RECRYSTALLIZATION**  
**OF**  
**SODIUM CARBONATE**

Robert S. Gärtner





**MIXED SOLVENT REACTIVE RECRYSTALLIZATION**  
**OF**  
**SODIUM CARBONATE**

Proefschrift

ter verkrijging van de graad van doctor  
aan de Technische Universiteit Delft,  
op gezag van de Rector Magnificus, professor dr. ir. J.T. Fokkema,  
voorzitter van het College van Promoties,  
in het openbaar te verdedigen op dinsdag 15 maart 2005 om 15:30 uur

door

Robert Sebastian GÄRTNER  
Dipl.-Ing. Chemietechnik, Universität Dortmund  
geboren te Borgå, Finland

Dit proefschrift is goedgekeurd door de promotor:

Prof. dr. G.J. Witkamp

Samenstelling promotiecommissie:

Rector Magnificus	voorzitter
Prof. dr. G.J. Witkamp	Technische Universiteit Delft, promotor
Prof. H. W. Haynes Jr., PhD	University of Wyoming, Laramie, Wyoming, VS
Prof. dr. ir. G.M. van Rosmalen	Technische Universiteit Delft
Prof. Dr.-Ing. Habil. J. Ulrich	Martin-Luther Universität Halle-Wittenberg, Duitsland
Prof. dr. M. Wessling	Universiteit Twente
Dr. H. Oosterhof	Umicore, België
Dr. M.M. Seckler	IPT, CENATEC, Brasilië
Prof. dr. J.S. Dhillon	Technische Universiteit Delft, reservelid

Dr. M.M. Seckler heeft als begeleider in belangrijke mate aan de totstandkoming van het proefschrift bijgedragen

This research was financially supported by the Ministry of Economical Affairs, the Ministry of Housing, Spatial Planning and Environment, the Ministry of Education and Science of the Netherlands through the EET program of Senter and Novem.

*Cover: Recycle glass bottles and detergent foam – examples of everyday products derived from sodium carbonate (soda). Design by Dima Gärtner.*

ISBN 90-9016165-8

Copyright © 2005 by Robert S. Gärtner  
Printed by Febodruk BV, Enschede



# TABLE OF CONTENTS

<b>CHAPTER 1 :</b> .....	<b>9</b>
INTRODUCTION TO MIXED SOLVENT REACTIVE RECRYSTALLIZATION (MSRR)	
1.1. Introduction.....	9
1.2. Mixed Solvent Recrystallization.....	9
1.3. The Invention of this Work: Mixed Solvent Reactive Recrystallization.....	10
1.4. An Aspect of Crystallization: Facing the Multitude of Solid Phases .....	11
1.5. A Short Thermodynamic Consideration on Solubility and Stability.....	14
1.6. The Effect of “Unintended Additives”: Impurities in Crystallization .....	15
1.7. Outline of This Thesis.....	16
1.8. General Remarks on the Use and Applicability of this Research.....	17
1.9. Literature References .....	18
<b>CHAPTER 2 :</b> .....	<b>19</b>
MIXED SOLVENT RECRYSTALLIZATION FOR THE DENSIFICATION AND PURIFICATION OF SODA ASH	
2.1. Introduction.....	20
2.1.1. The Na <sub>2</sub> CO <sub>3</sub> -H <sub>2</sub> O system.....	20
2.1.2. Process Routes for the Production of Dense Soda.....	20
2.1.3. The Mixed-Solvent-Double-Recrystallization of Sodium Carbonate.....	24
2.2. Influence of Impurities on the Double Recrystallization.....	26
2.3. Experimental .....	27
2.3.1. General Overview .....	27
2.3.2. Influence of Sulfate, Chloride, Fluoride and Borate.....	27
2.3.3. The Accumulation of Chloride in the Mixed Solvent Recycle.....	28
2.3.4. Sulfate Incorporation during Double Recrystallization .....	28
2.4. Results.....	29
2.4.1. Influence of Sulfate, Chloride, Fluoride and Borate.....	29
2.4.2. Accumulation of Chloride in the Mixed Solvent Recycle .....	33
2.4.3. Sulfate Incorporation during Double Recrystallization .....	34

2.5. Conclusions.....	39
2.6. Acknowledgements.....	42
2.7. Literature References.....	42
2.8. Addendum.....	44
2.8.1. Solid Phase Analysis by Heating-Weight-Loss .....	44
2.8.2. A Comment on the Recoverability of the Mixed Solvent.....	45
<b>CHAPTER 3 :.....</b>	<b>47</b>
REACTIVE RECRYSTALLIZATION OF SODIUM BICARBONATE	
3.1. Introduction.....	48
3.2. NaHCO <sub>3</sub> Decomposition in the Solid State .....	49
3.3. NaHCO <sub>3</sub> Decomposition in Aqueous Solution.....	52
3.4. NaHCO <sub>3</sub> Decomposition in the Mixed Solvent.....	59
3.4.1. Experimental.....	59
3.5. Results.....	60
3.5.1. Transition Temperature of Nahcolite Recrystallization.....	60
3.5.2. Solubility of Nahcolite in the Mixed Solvents.....	62
3.5.3. Reaction Kinetics of Decomposition in Mixed Solvent .....	65
3.6. Discussion.....	70
3.7. Conclusions.....	71
3.8. Notation.....	72
3.8.1. Indices.....	73
3.9. Literature References.....	74
3.10. Addendum.....	78
3.10.1. Calculation of the Equilibrium Concentrations in Aqueous Solution .....	78
3.10.2. Solubility of Nahcolite (NaHCO <sub>3</sub> (s)) in the Mixed Solvents .....	81
3.10.3. Heating-Weight-Loss-Analysis for Solid Phase Carbonate-Bicarbonate .....	81
3.10.4. Automated pH Titration for Dissolved Carbonate-Bicarbonate .....	83
3.10.5. Mass Balance in the Decomposition Experiments.....	85

**CHAPTER 4 :..... 89**

RECRYSTALLIZATION OF TRONA (SODIUM SESQUICARBONATE) INTO SODA (SODIUM CARBONATE ANHYDRATE) IN A MIXED SOLVENT, PART I: FUNDAMENTAL CONVERSION STEPS

4.1. Introduction.....	90
4.2. Experimental procedures .....	93
4.2.1. Solubility and Stability Determination in Shake tests .....	93
4.2.2. Batch Recrystallization Experiments.....	94
4.3. Results and Discussion .....	95
4.3.1. Predicted and Observed Transition Lines of Trona .....	95
4.3.2. Kinetics of the Trona Conversion.....	101
4.3.3. Crystallization of Soda (Sodium Carbonate Anhydrate) .....	117
4.4. Conclusions.....	118
4.5. Notation.....	119
4.6. Indices .....	120
4.7. Literature References.....	120
4.8. Addendum.....	124
4.8.1. Experimental Set-Up for Batch Recrystallization Experiments .....	124
4.8.2. Analytical Methods.....	124
4.8.3. Water Activity in Different Mixed Solvent Solutions .....	130
4.8.4. Estimation of the Crystal Surface Area .....	131
4.8.5. Analysis of the Dissolution Mechanism .....	134
4.8.6. Thermodynamic Solubility Products .....	135
4.8.7. Solid State Conversion – Contracting Cube and Contracting Disc Mechanism .....	137

**CHAPTER 5 :..... 139**

RECRYSTALLIZATION OF TRONA (SODIUM SESQUICARBONATE) INTO SODA (SODIUM CARBONATE ANHYDRATE) IN A MIXED SOLVENT. PART II: ALTERNATIVE RECRYSTALLIZATION ROUTES

5.1. Introduction.....	140
------------------------	-----

5.2. Theory .....	141
5.2.1. The System $\text{Na}_2\text{CO}_3\text{-NaHCO}_3\text{-H}_2\text{O}$ .....	141
5.2.2. The Conversion of Trona in Current Industrial Practice .....	143
5.2.3. The Conversion of Trona by Mixed Solvent Reactive Recrystallization .....	143
5.3. Experimental procedures .....	145
5.3.1. Solubility and Stability Determination in Shake tests .....	145
5.3.2. Batch Recrystallization Experiments .....	146
5.3.3. Continuous Recrystallization Experiments.....	147
5.4. Results.....	147
5.4.1. Mixed Solvent Reactive Recrystallization of Trona.....	147
5.4.2. 1-Step Mixed Solvent Reactive Recrystallization (1-Step MSRR) .....	148
5.4.3. 2-Step Mixed Solvent Reactive Recrystallization (2-Step MSRR) .....	156
5.4.4. Wet Calcination and Monohydrate-Recrystallization (3-Step MSRR) .....	166
5.5. Conclusions.....	170
5.6. Literature References .....	171
5.7. Addendum.....	174
5.7.1. Experimental Set-Ups .....	174
5.7.2. Analytical Methods.....	175
<b>CHAPTER 6 :.....</b>	<b>177</b>
OCCURRING SOLID PHASES AND THEIR SOLUBILITIES IN THE SYSTEM $\text{Na}_2\text{CO}_3 - \text{NaHCO}_3 - \text{ETHYLENE GLYCOL} - \text{WATER}$ FROM 50 TO 90°C	
6.1. Introduction.....	179
6.1.1. The System $\text{Na}_2\text{CO}_3 - \text{NaHCO}_3 - \text{H}_2\text{O}$ .....	179
6.2. Experimental Solubility and Stability Determination.....	182
6.3. Results.....	185
6.3.1. Measured Solubilities in the Mixed Solvent.....	185
6.3.2. Phase Stabilities in the Mixed Solvent System.....	187
6.4. Conclusion .....	194
6.5. Literature References .....	195
6.6. Addendum: Solubility Tables & Additional Phase Diagrams .....	197

6.6.1. Phase Diagrams for 60, 80 and 100%-w (salt-free solvent) Ethylene Glycol	208
---	-----

**CHAPTER 7 :..... 211**

NEUTRAL EXTRACTANTS FOR THE SELECTIVE REMOVAL OF ALUMINUM FROM A PICKLING BATH LIQUID

7.1. Introduction.....	212
7.1.1. General.....	212
7.1.2. Extractant selection.....	213
7.1.3. Calixarenes.....	214
7.1.4. Extraction Mechanism .....	216
7.2. Experimental .....	218
7.2.1. Shake Tests .....	218
7.2.2. Analysis.....	219
7.3. Results.....	220
7.4. Conclusions.....	222
7.5. Acknowledgements.....	222
7.6. Notation.....	222
7.7. Literature References .....	223
7.8. Measured Distribution Coefficients.....	225
7.9. Calculation of the Given Standard Deviations.....	226

**CHAPTER 8 :..... 229**

REGENERATION OF MIXED SOLVENT BY ION EXCHANGE RESIN: SELECTIVE REMOVAL OF CHLORIDE AND SULFATE

8.1. Introduction.....	230
8.2. Theory .....	231
8.3. Experimental .....	235
8.4. Results.....	237
8.4.1. Swelling in the Mixed Solvents .....	237
8.4.2. Chloride and Sulfate Sorption.....	238

8.5. Conclusions.....	249
8.6. Acknowledgements.....	250
8.7. Notation.....	251
8.8. Indices.....	251
8.9. Literature References.....	251
8.10. Addendum.....	252
<b>CHAPTER 9 :.....</b>	<b>255</b>
REGENERATION OF MIXED SOLVENT BY ELECTRODIALYSIS: SELECTIVE REMOVAL OF CHLORIDE AND SULFATE	
9.1. Introduction.....	256
9.2. Theory.....	257
9.3. Experimental.....	265
9.3.1. Membrane Swelling.....	265
9.3.2. Ethylene Glycol Retention.....	266
9.3.3. Membrane Electrical Resistance Measurement.....	267
9.3.4. Selectivity of the Ion Exchange Membranes.....	268
9.4. Results.....	269
9.4.1. Membrane Swelling.....	269
9.4.2. Ethylene Glycol Retention.....	272
9.4.3. Membrane Electrical Resistance Measurement.....	280
9.4.4. Selectivity of the Ion Exchange Membranes.....	286
9.5. Conclusions.....	291
9.6. Literature References.....	292
9.7. Notation.....	295
9.7.1. Indices.....	296
9.8. Addendum.....	297
<b>CHAPTER 10.....</b>	<b>301</b>
SUPER DENSE SODA BY MIXED SOLVENT RECRYSTALLIZATION: PROCESS DESIGN AND ECONOMICAL EVALUATION	

10.1. Introduction.....	302
10.1.1. Current Soda Production.....	302
10.1.2. Mixed Solvent Recrystallization.....	306
10.2. Process Design of the Mixed Solvent Recrystallization Processes .....	307
10.2.1. Mixed Solvent Double Recrystallization (MSDR).....	308
10.2.2. 1-step Mixed Solvent Reactive Recrystallization (1-step MSRR) .....	309
10.2.3. 2-step Mixed Solvent Reactive Recrystallization (2-step MSRR) .....	310
10.2.4. 3-Step Mixed Solvent Reactive Recrystallization (3-Step MSRR).....	311
10.2.5. Sodium Bicarbonate Reactive Recrystallization (NaHCO <sub>3</sub> MSRR) .....	313
10.3. Economical Evaluation .....	315
10.3.1. Required Capital Investment.....	315
10.3.2. Required Annual Costs (Operation Costs).....	321
10.3.3. Economical Comparison of the Process Alternatives .....	324
10.4. Bottom Line of the Economical Evaluation.....	333
10.5. Conclusions.....	333
10.6. Literature References .....	334
<b>SUMMARY .....</b>	<b>337</b>
Literature References .....	341
<b>ACKNOWLEDGEMENTS .....</b>	<b>342</b>
<b>CURRICULUM VITAE .....</b>	<b>343</b>
Publications.....	343





## **Chapter 1 :**

### **INTRODUCTION TO MIXED SOLVENT REACTIVE RECRYSTALLIZATION (MSRR)**

#### ***1.1. Introduction***

A large fraction of the separations performed in modern process industry are performed with thermodynamically inefficient processes like distillation and evaporative crystallization. They consume a large amount of energy, which is actually not used for the extraction of the desired product, but for the vaporization of the solvent – which just has to be condensed again in an additional process step. Methods like multi-stage evaporation, vapor recompression and/or vacuum distillation can reduce the energy consumption, but they do not change the large, inherent energy requirement of these processes. The energy is only ‘recycled’ inside the process. Considering the large amount of additional process equipment and engineering required for this recycle, the question suggests itself, whether these resources would not be better spent in the long run in the development and application of separation processes, which require inherently less energy. After all: Energy stored in the heat recycle of a process is dead capital, evaporating with common heat loss instead of inflation.

Such intrinsically more energy efficient separation processes are e.g. membrane processes [1], eutectic freeze crystallization [2, 3], supercritical crystallization (i.e. crystallization from supercritical carbon dioxide as solvent) [4] – and Mixed Solvent Recrystallization [5-7] and Mixed Solvent Reactive Recrystallization.

#### ***1.2. Mixed Solvent Recrystallization***

Mixed Solvent Recrystallization is a novel separation technology aimed to transform one solid phase of a compound into a desired new one by the use of a mixed solvent, composed of the main solvent and a miscible antisolvent. The aim here is to shift the

stabilities of the solid phases of the solute compound in such a way, that a specific, desired solid phase is formed. This can be used to recrystallize an undesired solid phase to the desired solid phase in the mixed solvent solution - without the need of complete dissolution and evaporative or cooling crystallization. The driving force for the recrystallization is provided by the instability of the undesired solid phase itself.

Oosterhof et al. [5-7] successfully applied this technique in the recrystallization of sodium carbonate monohydrate to sodium carbonate anhydrate (soda) and vice versa. The aim of their study was to crystallize the anhydrate solution mediated, which is not possible in aqueous solution, to increase bulk density, mechanical stability and chemical purity in comparison to commercially available soda. While the anhydrate is not a stable phase in aqueous solution, it became a stable phase with increasing amounts of the employed antisolvent, ethylene glycol.

In current practice, the undesired sodium carbonate monohydrate has first to be crystallized by evaporative crystallization and recovered by filtration, to be subsequently converted by an energy intensive calcination step (recrystallization in the dry state at high temperatures) to the desired anhydrate. By Mixed Solvent Recrystallization the energy intensive evaporation and calcination can be completely avoided, as the anhydrate can be crystallized from solution plus recrystallization of monohydrate to anhydrate and vice versa requires only a small temperature shift of the mixed solvent. In this way, e.g. commonly produced Light or Dense Soda Ash can be recrystallized to *super dense soda*, increasing its bulk density and mechanical stability significantly.

### **1.3. The Invention of this Work: Mixed Solvent Reactive Recrystallization**

The process developed by Oosterhof et al. [5-7] is limited to an industrial product: *Light Soda Ash* ( $\text{Na}_2\text{CO}_3(\text{s})$ ), which is already the product of a quite energy-consuming production process.

*The aim of this work was to develop novel, alternative process routes based on the principle of Mixed Solvent Recrystallization to replace the entire, energy-consuming, current production routes.*

Soda is a bulk commodity, which is produced globally on a scale of several million tons per year [8], but which is derived from basically two principal sources:

In natural deposits, sodium carbonate occurs together with sodium bicarbonate ( $\text{NaHCO}_3$ ) [9], and also in the industrial, synthetic route for the production of bulk soda, the well-known Solvay process [10], sodium bicarbonate occurs as an intermediate, which has to be converted into sodium carbonate anhydrate (soda).

It was found in this work, that the chemical reaction, which converts bicarbonate into carbonate, could be performed in the mixed solvent solution simultaneously to the recrystallization. The novel production routes are therefore based on a new hybrid process, which combines Mixed Solvent Recrystallization with the decomposition reaction: *By the Mixed Solvent Reactive Recrystallization process any bicarbonate containing solid source of sodium carbonate – even pure solid sodium bicarbonate ( $\text{NaHCO}_3(s)$ , nahcolite) - can directly be recrystallized to high quality crystalline soda.*

With the aim to fundamentally understand and to control this complex, new, hybrid process, not only the process routes were developed and tested experimentally, but also the fundamental conversion mechanisms were investigated and their kinetics measured. Thermodynamic and kinetic models were developed to allow predictive calculations of the process. Central to the experimental investigation and the modeling was the complex crystallization behavior in the new, mixed solvent system.

#### **1.4. An Aspect of Crystallization: Facing the Multitude of Solid Phases**

The aim of most applications of crystallization is the recovery of a chemical compound as a solid from its melt or its solution. In many cases, the compound can form more than one solid phase, and in some cases, the crystallization can even produce more than one of these possible solid phases.

The different cases of a compound forming multiple solid phases are:

- Polymorphism: The compound crystallizes in different crystal forms with different crystal lattices (polymorphs). While the chemical composition of the different polymorphs is identical, they usually differ in solubility and crystal shape (morphology) and might also have very different physical properties like

e.g. hardness, refraction index, color, transparency and electrical conductivity. A well-known example of polymorphism is carbon with graphite and diamond as polymorphs.

- Pseudopolymorphism: The compound co-crystallizes with the solvent (or even with 2 or more solvents), incorporating one or more moles of solvent(s) per mole of compound in the crystal lattice. Such solids are commonly called solvates, or hydrates for solids with incorporated water. The incorporated solvent is an integral part of the crystal lattice and can only be removed under decomposition of the crystal. Solvates and hydrates only occur for compounds, which strongly interact with the respective solvent. Almost all hygroscopic, inorganic salts form hydrates, e.g.  $\text{Na}_2\text{SO}_4 \cdot 10\text{H}_2\text{O}(\text{s})$  (mirabilite),  $\text{MgCl}_2 \cdot 6\text{H}_2\text{O}(\text{s})$  (bischofite) or  $\text{CuSO}_4 \cdot 5\text{H}_2\text{O}(\text{s})$  (chalcantite). Often, an inorganic salt can form more than one hydrate. The more strongly hydrated forms (i.e. containing the most crystal water per mole of salt) occur at low temperatures, while with increasing temperature the degree of water incorporation decreases as water becomes more volatile. It has to be noted, that each solvate and hydrate is an individual solid phase with a specific crystal lattice that determines the stoichiometric ratio between compound and incorporated solvent. They should not be confused with solid solutions (see below).
- Mixed Solid Phases: Similar to pseudopolymorphs, they consist of two (or more) compounds which form one crystal lattice. Unlike solid solutions, they have a fixed stoichiometry, which is determined by the crystal lattice. Like solvates and hydrates, compounds, which strongly interact with each other, are most likely to form mixed solid phases. It should be noted, that these compounds do not need to have similar atomic / molecular / ionic radii or conformation (as in the case of impurity incorporation). Even compounds of vastly different size and conformation can combine to form stable crystal lattices. Particularly in geological deposits, which usually contain a large variety of different inorganic compounds, many mixed solid phases occur. In this context, terms like “double salt” (e.g. dolomite:  $\text{MgCO}_3 \cdot \text{CaCO}_3(\text{s})$ ) and “triple salt” (e.g. carnallite:

$\text{KCl}\cdot\text{MgCl}_2\cdot 6\text{H}_2\text{O}(\text{s})$ ) are used to describe these solids. Also most metal alloys are mixed solid phases.

- Solid Solutions: These kinds of solids are less common than the other types, as they require that the participating two (or more) compounds integrate so well, that the formed, single crystalline solid phase has no fixed stoichiometric composition. Usually this requires, that the participating compounds have (almost) identical atomic / molecular / ionic radii, charge distribution and conformation to allow the indiscriminate substitution of one compound by another in the crystal lattice. The similarity has to be either very close and/or the lattice has to allow for some variation, as usually even minor differences can prohibit the incorporation of one species into a 'foreign' lattice.
- Amorphous Solids: These solids are commonly described as 'frozen liquids', as they are not composed of a rigidly ordered, symmetric, crystalline lattice with a clearly definable unit cell (as the smallest unit of the repetitive symmetry of the crystal). Rather, the single atoms / molecules / ions form random bridges and branches, which are sufficiently strongly bonded to give the resulting macrostructure the hardness and permanency of shape that commonly define a solid. As the symmetric order and homogeneous bonding of a true crystal lattice are energetically more favorable than this loosely knit amorphous structure, amorphous solids are actually metastable. *Apparently* stable amorphous solids like common (silicate) glass are only kinetically inhibited in their recrystallization to a stable crystalline phase.

Irrespective of its type, each solid phase of a compound has its own, specific solubility in solution. The solid phase with the lowest solubility is the thermodynamically stable phase of the system and all other present solid phases of the compound in contact with the solution will eventually recrystallize into that stable phase.

To obtain a *specific* solid phase, operating conditions, i.e. temperature, pressure, supersaturation, (mixed) solvent, etc., have to be found, in which this phase is stable. In some cases, it is possible to crystallize a solid phase metastably and recover it from solution, before it can recrystallize to the stable phase. But if no feasible operating

conditions can be found to crystallize the desired solid phase by either of these ways, then the desired phase is technically not accessible – at least by crystallization.

### **1.5. A Short Thermodynamic Consideration on Solubility and Stability**

The solubility of a given solid phase is actually a complex function of temperature, pressure and the composition of the solution. The transition of a compound A from the dissolved (or molten) state into a solid state is actually a physical reaction:



The dissolved (or molten) state as well as the solid state can each be attributed with a chemical potential  $\mu_A$ , indicating its thermodynamical stability and its tendency to convert to another state by physical or chemical reaction.

The compound A will crystallize, if the chemical potential of the solid state  $\mu_{A,solid}$  is lower than the chemical potential of the compound in the solution or melt  $\mu_{A,dissolved}$ . While  $\mu_{A,solid}$  is only a function of temperature and pressure (except for the case of a solid solution),  $\mu_{A,dissolved}$  is also dependent on the activity of A in the solution or melt:

$$\mu_{A,dissolved} = \mu_{A,dissolved}^0(p,T) + R \cdot T \cdot \ln(a_A) \quad \text{Eq. 1-2}$$

with  $\mu_{A,dissolved}^0$  being the standard chemical potential of A in solution (or melt). For the case, that the solution or melt is in equilibrium with the solid, i.e. the solution is saturated with A or the melt is in adiabatic equilibrium at the melting point, the chemical potential of solid and solution or melt are equal:

$$\mu_{A,solid}(p,T) = \mu_{A,dissolved}^0(p,T) + R \cdot T \cdot \ln(a_A^x) \quad \text{Eq. 1-3}$$

$$\Leftrightarrow \exp\left(\frac{\mu_{A,solid}(p,T) - \mu_{A,diss}^0(p,T)}{R \cdot T}\right) = a_A^x = \gamma_A^x \cdot c_A^x \quad \text{Eq. 1-4}$$

The activity of the compound at the equilibrium,  $a_A^x$ , determines the solubility of the compound in solution, i.e. the saturation concentration  $c_A^x$ . As can be seen from Eq. 4, the equilibrium activity can be derived from the difference between the chemical potential of the solid and the standard chemical potential of the solution. Both of these chemical potentials are only functions of temperature and pressure, and therefore the

solubility concentration  $c_A^x$  is only a function of temperature, pressure – and the activity coefficient  $\gamma_A^x$ .

For the melt of pure A, the equilibrium activity is equal to one – the melting point is only dependent on the ambient pressure. For an impure melt, i.e. the activity of A is not equal to one, the melting point is shifted to a different, usually lower, temperature at the same ambient pressure.

In a solution, the activity coefficient  $\gamma_A^x$  is not only dependent on the concentration of A, but also on the overall solution composition. This means, that additives - like other solutes or miscible co-solvents - can significantly change the solubility of a solid. This change can even affect the thermodynamical stability of the solid, if the change makes another solid phase of the compound less soluble and thereby the new stable phase of the system.

This effect is well known and employed technically e.g. in antisolvent precipitation of well soluble substances or in the “salting out” of proteins in protein precipitation. In antisolvent precipitation a miscible solvent is added, which not only has a low solubility for the solute compound, but also further reduces the solute’s solubility in the initial solvent. In protein precipitation a well soluble salt (most commonly ammonium sulfate ( $\text{NH}_4\text{SO}_4(\text{s})$ )) is added to the protein solution to reduce the protein’s solubility due to the interaction of the protein with the salt and thereby promote the protein to precipitate from solution.

### **1.6. The Effect of “Unintended Additives”: Impurities in Crystallization**

The explanations of the previous section also imply, that not only the chosen additives affect the solubility and phase stability in solution – also any impurity in the solution might have significant effect as well. And as with any unexpected effect in a technical process, the results are rarely desired or beneficial.

Additionally, impurities, which are incorporated into the crystal lattice, also affect the chemical potential of the solid, usually making the solid less stable, so that higher driving forces, e.g. supersaturation, are required for the crystallization. Such impurities can even prevent the crystallization of this solid phase – making another phase the stable solid of

the system. Therefore, in any crystallization, especially in such crystallizations, where the solid is known to form different solids, it is vital to investigate the influence of common or even just possible impurities.

Any impurity, which can endanger the operation of the crystallization, has to be reduced to levels, where its influence is negligible. As most continuous industrial crystallizers operate with mother liquor recycle loops, inline purification techniques are recommended, to remove such impurities from the recycle, before they build up to critical levels.

### **1.7. Outline of This Thesis**

In **Chapter 2**, a more detailed outline of the Mixed Solvent Recrystallization process of Oosterhof et al. is given. Furthermore, the influence of common impurities on the recrystallization is investigated, which demonstrates the necessity of the removal of critical impurities from the recycled mixed solvent solution.

In **Chapter 3**, the chemical reaction for the conversion of bicarbonate to carbonate is investigated. The reaction mechanism is discussed and identified, the rate of reaction is quantified and kinetic parameters for the reaction are presented.

In **Chapter 4**, the fundamental conversion mechanisms for the Mixed Solvent Reactive Recrystallization of trona (sodium sesquicarbonate,  $\text{Na}_2\text{CO}_3 \cdot \text{NaHCO}_3 \cdot 2\text{H}_2\text{O}(\text{s})$ ), the most ubiquitously occurring carbonate mineral, are identified and investigated. The kinetics of the rate determining steps are given. These kinetics can be used to model the conversion of any sodium bicarbonate containing solid source phase of sodium carbonate.

In **Chapter 5**, the different, new process routes for the application of the Mixed Solvent Reactive Recrystallization process for the conversion of trona are described and evaluated for their technical feasibility.

In **Chapter 6**, the solubilities and stability ranges of all occurring solid phases of the sodium carbonate and sodium bicarbonate for a range of temperatures and ethylene glycol – water mixed solvent compositions are given.

In **Chapter 7**, an investigated application of liquid-liquid reactive extraction is described, the extraction of trace metals by calix-[4]-arenes. While liquid-liquid reactive extraction



was initially deemed to be a possible method to extract critical ionic impurities from the recycled mixed solvent solution, it was not feasible with the tested reactive extractant solutions for the employed antisolvent, ethylene glycol. This technique still presents an attractive inline purification technique for similar applications.

In **Chapter 8**, the investigations on the extraction of critical ionic impurities from mixed solvent solutions by commercially available ion exchange resins are presented and discussed.

In **Chapter 9**, the results of the application of electrodialysis for the extraction of the critical ionic impurities are presented. This study also investigated the effects of the organic co-solvent on the electrodialysis process - a topic that despite its fundamental relevance to electrodialysis is still sparsely investigated and described in literature.

In **Chapter 10**, an economic evaluation of the process routes of the different Mixed Solvent Recrystallization processes and the different Mixed Solvent Reactive Recrystallization processes for the production of soda from trona and solid sodium bicarbonate is given, including comparisons to currently applied industrial processes. The required capital investments as well as the operation costs of these processes are compared and the economic feasibility of the different processes is evaluated.

### ***1.8. General Remarks on the Use and Applicability of this Research***

Although the application of Mixed Solvent (Reactive) Recrystallization is limited in this work to the  $\text{Na}_2\text{CO}_3\text{-NaHCO}_3\text{-H}_2\text{O}$ -Ethylene Glycol system, the theoretical background for the thermodynamic modeling and prediction of the stability of solid phases demonstrates, that this technique can be efficiently applied to other pseudopolymorphic, polymorphic or mixed solid phase systems to influence the formation of specific desired (or undesired) phases.

In addition to this, the research performed in this project provides further understanding of the complex system  $\text{Na}_2\text{CO}_3\text{-NaHCO}_3\text{-CO}_2\text{-H}_2\text{O}$ , its reaction equilibria, its solid phase stability ranges and the associated solubilities.

The influence of impurities and additives on crystallization is a topic of much scientific and industrial interest, especially for such a bulk commodity as sodium carbonate.

The presented research also yields insight into the influence of organic co-solvents on ion exchange resins and on electrodialysis, which is an important topic for many applications of these processes in the process industry.

And last but not least, it presents new, more energy and cost efficient process routes for the production of soda – a bulk commodity produced annually on a global scale of several million tons [8].

### **1.9. Literature References**

- [1] Rautenbach, R., “Membranverfahren – Grundlagen der Modul- und Anlagenauslegung”, Springer-Verlag, Berlin, 1997
- [2] Van der Ham, F., “Eutectic Freeze Crystallization”, PhD thesis Delft University of Technology, Delft University Press, Delft, 1999
- [3] Vaessen, R.J.C., “Development of Scraped Eutectic Crystallizers”, PhD thesis Delft University of Technology, Ponsen & Looijen, Wageningen, 2003
- [4] Wubbolts, F.E., “Supercritical Crystallisation – Volatile Components as (Anti-) Solvents”, PhD thesis Delft University of Technology, Delft University Press, Delft, 2000
- [5] Oosterhof, H., de Graauw, J., Witkamp, G.J., van Rosmalen, G.M., “Continuous Double Recrystallization of Light Soda Ash into Super Dense Soda Ash”, *Crystal Growth & Design*, 2 (2), 2002, p. 151
- [6] Oosterhof, H., Witkamp, G.J., van Rosmalen, G.M., “Antisolvent Crystallization of Anhydrous Sodium Carbonate at Atmospheric Conditions”, *AIChE J.* 47(3), 2001, p. 602-608
- [7] Oosterhof, H., de Graauw, J., Witkamp, G.J., van Rosmalen, G.M., “Process for the production of sodium carbonate anhydrate”, European and US Patent application, 1998
- [8] <http://www.isonex.com:8080/iu.html>
- [9] Garret, D.E., “Natural Soda Ash – Occurrences, Processing, And Use”, Van Nostrand Reinhold (publ.), New York, 1991, pp. 3-27
- [10] Thieme, C., “sodium hydrogen carbonate” in *Ullmann’s Encyclopedia of Chemical Technology*, 6<sup>th</sup> ed., 2000, electronic release, Wiley-VCH

## Chapter 2 :

### MIXED SOLVENT RECRYSTALLIZATION FOR THE DENSIFICATION AND PURIFICATION OF SODA ASH

R.S. Gärtner, G.J. Witkamp

#### ***Abstract***

At atmospheric conditions, soda (sodium carbonate anhydrate) does not form from its aqueous solution, as only hydrates are formed. In a mixed solvent solution, composed of an organic antisolvent (ethylene glycol) and water, the anhydrate is stable and can be crystallized by evaporative crystallization [1] or more energy-efficiently by a double recrystallization process [2-4].

In this work, currently available process routes for the production of dense soda are compared, based on product quality, production costs and energy efficiency. The mixed solvent recrystallization process route is found to offer the best potential for reductions in production costs and for improvements in product quality.

Crystallization is a highly selective separation process and since the soda is grown under controlled conditions in the mixed solvent solution, a significant purification effect is expected. The purifying effect of the recrystallization was studied in this work. The effect of anionic impurities, which commonly occur in current soda production processes, was investigated: Sulfate, borate, chloride and fluoride.

It was found that fluoride, chloride and borate were only incorporated in ppm levels in the solid, while sulfate was incorporated almost quantitatively.

## **2.1. Introduction**

### **2.1.1. The $\text{Na}_2\text{CO}_3\text{-H}_2\text{O}$ system**

Like many other hygroscopic salts, sodium carbonate forms hydrates, i.e. it crystallizes as mixed solid phases that contain crystal water. The tendency to incorporate water in its crystal structure is so strong, that under atmospheric conditions, only hydrated phases can be crystallized from the pure saturated aqueous sodium carbonate solution [5]:

From the freezing point at  $-2.05$  up to  $32^\circ\text{C}$ , sodium carbonate decahydrate (natron,  $\text{Na}_2\text{CO}_3\cdot 10\text{H}_2\text{O}_{(s)}$ ) is the stable phase, followed by sodium carbonate heptahydrate ( $\text{Na}_2\text{CO}_3\cdot 7\text{H}_2\text{O}_{(s)}$ ) from  $32$  to  $35^\circ\text{C}$  [6-9]. From  $35^\circ\text{C}$  to the boiling point of the saturated sodium carbonate solution at  $104.8^\circ\text{C}$ , sodium carbonate crystallizes as monohydrate ( $\text{Na}_2\text{CO}_3\cdot \text{H}_2\text{O}_{(s)}$ ). The stability of the monohydrate actually extends beyond the boiling point of the solution to about  $109^\circ\text{C}$  – so that at temperatures above  $109^\circ\text{C}$  the anhydrate ( $\text{Na}_2\text{CO}_{3(s)}$ ) can be crystallized, e.g. at elevated pressure to increase the boiling point of the solution [6, 7, 10].

### **2.1.2. Process Routes for the Production of Dense Soda**

#### *2.1.2.1. Current Production Processes*

For most industrial applications, like the production of glass or washing powder, the sodium carbonate is required in its anhydrous form as soda.

Soda (sodium carbonate,  $\text{Na}_2\text{CO}_{3(s)}$ ) is produced industrially either from trona ore [11] or from sodium chloride and carbon dioxide by the Solvay process [5]. In both process routes, the sodium carbonate is recovered from its aqueous solution as sodium carbonate monohydrate by atmospheric evaporative crystallization. The monohydrate is then converted to anhydrous sodium carbonate by calcining, i.e. by removing the crystal water through heating of the monohydrate to temperatures of  $120^\circ\text{C}$  or higher [11].

The calcination results in a (pseudo) solid phase recrystallization of the monohydrate into anhydrate [12]. In the calcination or wet calcination of trona (see Chapter 4), this solid phase recrystallization produces pseudomorphous material: the actual anhydrate crystals

remain small (1-10 micron) and form agglomerates, which retain the shape of the original monohydrate crystals. The pseudomorphs are very porous structures and the produced soda from these processes has therefore not only a low bulk density, but is also prone to breakage and dusting, and retains considerable amounts of impurities.

#### *2.1.2.2. Process Alternatives*

Different processes have been proposed to increase the mechanical stability and the bulk density of the soda produced from an aqueous sodium carbonate solution [13-16], from the monohydrate [17-20] or directly from trona [20-22] or sodium bicarbonate [22, 23, 35]. These processes can be roughly distinguished into 3 groups:

- a) The first group [17-21] employs a densification of pseudomorphic soda - produced from monohydrate or trona - under addition of a small amount of water before it enters the calciner - by sintering the soda at temperatures from 300 to 600°C to a higher density and mechanical stability. Another option for increasing the bulk density of (pseudomorphous) soda ash is mechanical compaction in hydraulic presses combined with classification, as described by Bakele [24].
- b) The second group [14, 15, 22, 23, 35] proposes the crystallization of anhydrous sodium carbonate under pressure, to increase the solution's boiling point above the transition point of sodium carbonate monohydrate (in aqueous solution 107 to 109°C). Van Lotringen et al. [22] recommend a temperature of 150°C (at least  $T > 135^\circ\text{C}$ ), which requires a pressure of at least 4 bar in the crystallizer(s) [7, 22].
- c) The third group [13, 14, 16] proposes the crystallization of anhydrous soda from a solution of concentrated sodium hydroxide or sodium chloride. The presence of high concentrations of these compounds allows crystallization of anhydrous soda, because they significantly reduce the water activity in solution and thereby also the stability of the hydrate phases.

#### *2.1.2.3. Drawbacks in the Alternative Process Routes*

The drawbacks of the process routes outlined above are:

- a) For the first group, the final product is still composed of agglomerates, which will be prone to some degree of breakage and dusting. Still they deliver a well handle-able product, which makes these densification procedures the commonly employed ones.
- b) The second group requires pressurized crystallization units, which are not only more expensive in construction and maintenance, but require also more complex operating procedures and safety measures, i.e. an increased amount of instrumentation and more frequent inspection.
- c) The third group offers an apparently simple, cost-efficient solution, as relatively cheap salts are used to modify the crystallization system. These salts (should) remain in the mother liquor - so this mother liquor can be purified (if necessary) and recycled in the process. Sodium hydroxide appears here to be the modifier of choice, as it is the least source of impurity to the system. Additionally, sodium hydroxide absorbs carbon dioxide from the air over time, converting to sodium bicarbonate. This again would either require to replace the mother liquor regularly, before the sodium bicarbonate concentration has risen to levels, where unwanted carbonate-bicarbonate mixed phases (wegscheiderite,  $\text{Na}_2\text{CO}_3 \cdot 3\text{NaHCO}_3(\text{s})$  or trona,  $\text{Na}_2\text{CO}_3 \cdot \text{NaHCO}_3 \cdot 2\text{H}_2\text{O}(\text{s})$ ) start to form [11] – or the crystallizers and mother liquor recycle have to be air-tight to prevent contact with carbon dioxide from the air. Another stringent drawback of this route is that evaporative crystallization faces the problem of co-crystallizing the sodium hydroxide (or sodium chloride) after a certain degree of sodium carbonate recovery. To prevent this, the sodium carbonate recovery in this process has to be reduced, which severely reduces the productivity in comparison to the conventional process. E.g., by evaporative crystallization ca. 12.7 g  $\text{Na}_2\text{CO}_3$  per 100g of evaporated water can be recovered as the anhydrate from a sodium hydroxide containing solution [14], while 30.8 g  $\text{Na}_2\text{CO}_3$  are recovered as (36.1 g) monohydrate per 100g of evaporated water from the regular, aqueous solution [7, 10]. Finally, the auxiliary salt is a source of impurity, as a small amount of it will always remain - e.g. from rests of adhering mother liquor - in the produced soda.

#### *2.1.2.4. A New Process Alternative: Mixed Solvent Recrystallization*

Another method to reduce water activity and increase the stability of the anhydrous phase is the use of an antisolvent [25, 26]. This possibility was first explored for sodium carbonate by Weingaertner et al. [25] and more recently further investigated by Bowman [27] and Oosterhof et al. [1-4]. In these techniques, the organic antisolvent is used to reduce water activity and the stability of the hydrates. While the antisolvent precipitation technique [27] only allows precipitation of anhydrous soda from solution as a fine precipitate of low filterability, the mixed solvent process of Oosterhof et al. allows continuous evaporative crystallization of anhydrous soda of excellent filterability and bulk densities of up to 1550 kg/m<sup>3</sup> [1]. An alternative of the mixed solvent process allows continuous double recrystallization of light soda ash or sodium carbonate monohydrate to high bulk density crystalline soda [2, 4]. Based on the change of the transition temperature with water activity, i.e. antisolvent content, recrystallization can be caused by a minor shift of temperature beyond the transition point of the current solid phase. This will cause the solid to recrystallize to the stable phase. The driving force of this recrystallization, by which the process (i.e.: nucleation and growth rate) can be controlled, is the temperature difference to the transition temperature. Neither evaporation nor excessive cooling is required and due to the control of crystallization conditions, high mean particle sizes and high bulk densities can be achieved.

#### *2.1.2.5. The Drawbacks of Mixed Solvent Recrystallization*

In the antisolvent or mixed solvent crystallization of any compound originally crystallized from its aqueous solution, not only the water activity and thereby the hydrate-phase stability is affected by the addition of the organic antisolvent. Especially the solubility of the compound can change dramatically – and in the case of most (polar) substances well soluble in water, a strong decrease of solubility in the usually less polar, mixed aqueous-organic medium can be expected. Also the growth rate, morphology, metastable zone width, nucleation and agglomeration behavior can be affected significantly by the change in solvent.

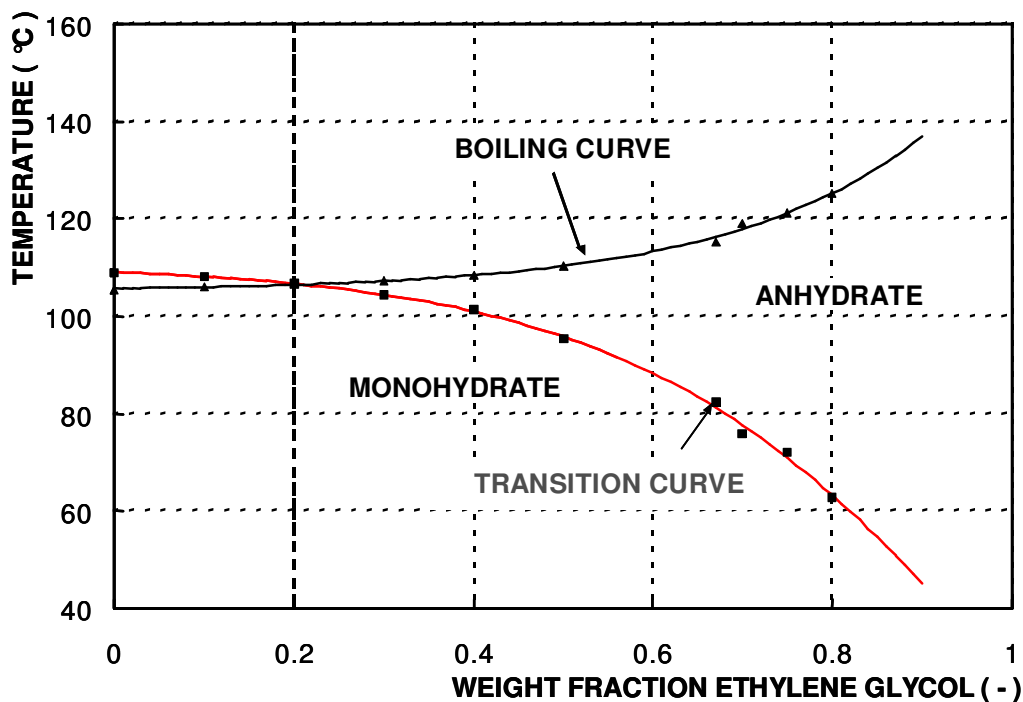


**Figure 2-1:** Boiling and transition curve as a function of antisolvent content with ethylene glycol as antisolvent [28]

The impact of these changes on the crystallization behavior has to be studied in recrystallization experiments and may require a great degree of antisolvent screening to find a suitable antisolvent for a given system. Additionally, the mixed solvent needs to be efficiently separated from the final product. Residual organic solvent might not only impair product quality, but the solvent also needs to be recycled to the recrystallization process with as little loss as possible. Replacement of the organic solvent is an important cost factor for the process, see Chapter 10.

Antisolvent or mixed solvent crystallization offers the greatest potential for energy savings as well as improvement of product quality of all the presented alternative processing routes [1-4].

### 2.1.3. The Mixed-Solvent-Double-Recrystallization of Sodium Carbonate

While the evaporative antisolvent recrystallization was found by Oosterhof et al. [1] to produce a crystalline soda of a higher bulk density (up to 1550 kg/m<sup>3</sup>), the double



continuous recrystallization of soda by temperature shift (see Figure 2 and refer to Oosterhof et al. [2, 3]) is an economically more attractive alternative for the densification of light soda ash produced by either the Solvay process or from trona. Here, it is not necessary to dissolve the treated soda completely as in evaporative crystallization. A soda slurry of up to 20%-w soda can be treated by this process.

The temperature and antisolvent content in the first crystallizer are chosen to cause the introduced light soda ash (anhydrate) to spontaneously recrystallize into monohydrate at conditions below the transition curve in Figure 1. After complete monohydration, which requires a residence time of approximately ½ hour [2], the slurry is recrystallized to anhydrate in the following crystallizers. In these crystallizers, the temperature is set, so that for the same antisolvent content, the system is now *above* the transition line, making anhydrate the stable phase – resulting in spontaneous recrystallization. The second step was found to require a total residence time of app. 1 h [2].

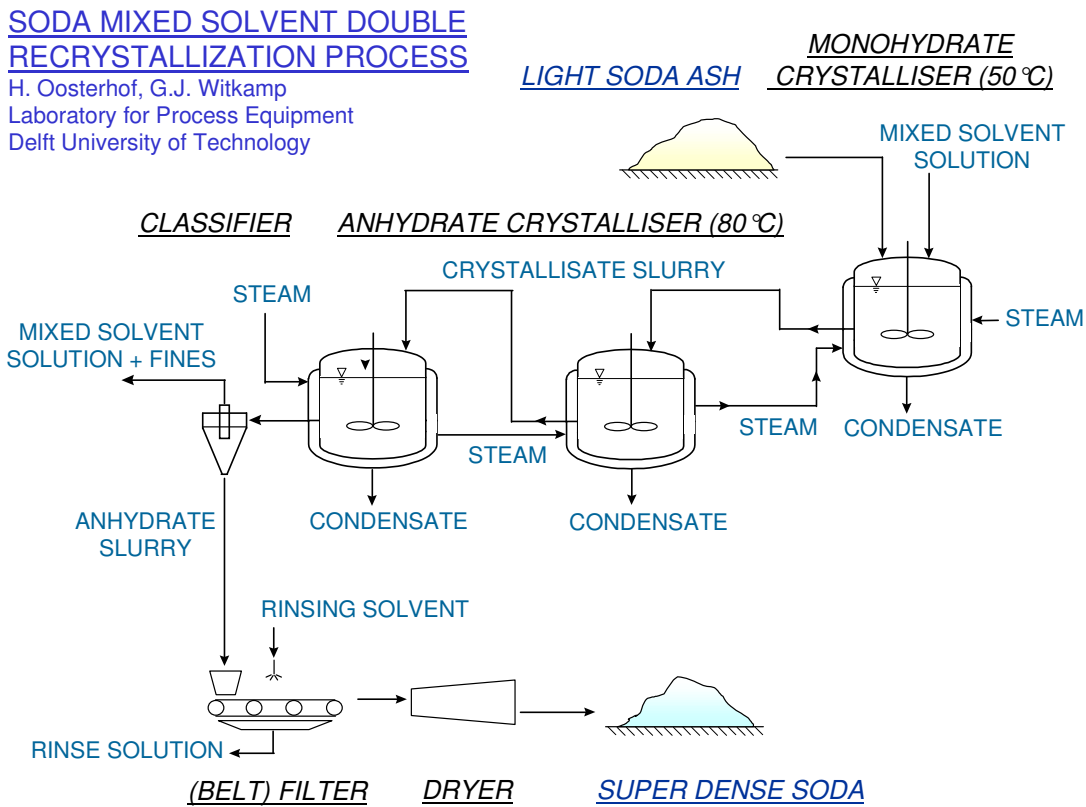


**Figure 2-2:** Process flowsheet of the double recrystallization process of Oosterhof et al. [2-4, 28]

The most favorable antisolvent and its content in the mixed solvent to perform this recrystallization was found to be ca. 70%w (salt-free solvent) ethylene glycol, see Oosterhof et al. [3, 28].

In the optimization of this process for maximum bulk density of the produced crystalline soda [2], it was found that the monohydration should be performed at 50 to 60°C and the recrystallization to anhydrate at 80°C.

The maximum bulk density produced in these experiments [2] was 1350 kg/m<sup>3</sup>, but Oosterhof et al. indicate that with further optimization, bulk densities of 1400 kg/m<sup>3</sup> or more could be attained.

This bulk density is significantly higher than that of commercially available dense soda ash of a bulk density of ca. 1000 to 1200 kg/m<sup>3</sup> [29].

## ***2.2. Influence of Impurities on the Double Recrystallization***

Impurities, which are contained in the feed, may be excluded from or incorporated into the final sodium carbonate anhydrate crystals. As crystallization is a highly selective process, it is very likely that the purity of the soda increases with the double recrystallization. This increased purity is an added value of the super dense soda for some its industrial applications.

However, recycling of antisolvent introduces the risk of accumulating impurities, introduced with the feed or formed during the process.

Therefore, it was investigated in this work, whether anionic impurities, which occur commonly in soda processing, are incorporated into the final soda crystals during the recrystallization and whether they affect the recrystallization process.

The investigated impurities are fluoride, chloride, sulfate and borate. These compounds commonly occur in the production of soda from trona [11]. In the production of soda from sodium chloride by the Solvay process [5], chloride is the main impurity [29].

## **2.3. Experimental**

### **2.3.1. General Overview**

Three series of experiments were performed to investigate the influence of impurities on the double recrystallization. The influence of all of the 4 impurity species (sulfate, chloride, fluoride and borate) during double recrystallization was investigated in batch experiments, while the accumulation of chloride in the mixed solvent was further investigated in continuous stirred tank experiments. For sulfate, further batch recrystallization experiments with increasing amounts of sulfate in the feed soda were performed.

In all experiments, samples were taken every half-hour, the solid fraction was filtered off in 15 $\mu$ m pore size glass filters and rinsed with acetone. The weight loss for the determination of the crystal water content of the solid samples was measured with a Mark II Moisture Analyzer of Denver Instruments and the solid samples were analyzed for their respective content of sulfate, chloride, fluoride and borate by a Dionex DX-120 ion chromatograph from dilutions in ultra pure water. Scanning electron microscope (SEM) images were taken of the samples to study the influence of the present impurities on the sodium carbonate monohydrate and anhydrate morphology.

### **2.3.2. Influence of Sulfate, Chloride, Fluoride and Borate**

In the first series of batch experiments, commercial light soda ash (99.5%, Brunner Mond, The Netherlands) was recrystallized to super dense soda. Sodium sulfate ( $\text{Na}_2\text{SO}_{4(s)}$ ), sodium chloride ( $\text{NaCl}_{(s)}$ ), sodium fluoride ( $\text{NaF}_{(s)}$ ) and sodium tetraborate ( $\text{Na}_2\text{B}_4\text{O}_7 \cdot 10\text{H}_2\text{O}_{(s)}$ ) were added to the feed soda to adjust its impurity content to 4.5%-weight of sulfate ( $\text{SO}_4^{2-}$ ), 2.5%-weight of chloride ( $\text{Cl}^-$ ), 0.25 %-weight of boron (B) and 0.06%-weight of fluoride ( $\text{F}^-$ ). All of the added salts were of analytical purity (99.9%, Merck). The 1.5 liter stirred tank was thermostated by its double jacket. The crystallizer was filled with the mixed solvent (composed of 70%-weight technically pure ethylene glycol and 30%-weight water) and was heated to the initial temperature of 50°C. Then the soda ash with the added impurities was added for a soda content of 20%-weight in the crystallizer. The first conversion step was conducted at 50°C, which recrystallized the

light soda ash (sodium carbonate anhydrate) into sodium carbonate monohydrate. Then the temperature was increased to 80°C to start the second recrystallization step, where the monohydrate was recrystallized into the desired, dense, crystalline soda product (sodium carbonate anhydrate).

### **2.3.3. The Accumulation of Chloride in the Mixed Solvent Recycle**

The accumulation of the chloride anion was investigated a continuous reactor cascade of two, thermostated, stirred-tank crystallizers of 1.5 liters. The first crystallizer was kept at 50°C to perform the conversion to monohydrate with a residence time of 30 minutes; the second crystallizer was thermostated to 80°C to conduct the conversion from monohydrate to anhydrate with a residence time of 1 hour. The first reactor was fed continuously with commercial light soda ash and the recycled mixed solvent. The feed rates were set to install a soda content of 20%-weight in the crystallizers. The second reactor was fed with the overflow of the first reactor. The product stream exited the second reactor by overflow as well. No chloride was added to the feed soda, which already contained an impurity chloride content of 0.2%-weight.

The formed super dense soda was recovered from the overflow stream of the second crystallizer by settling and the decanted, clear mixed solvent was recycled to the first crystallizer.

### **2.3.4. Sulfate Incorporation during Double Recrystallization**

Three experiments were performed to identify the occurring phases during recrystallization in the presence of bulk amounts of sulfate. The recrystallization was performed in a 1.5 liter, discontinuous stirred tank crystallizer with 70%-w (salt-free) ethylene glycol mixed solvent as described previously. The soda ash was monohydrated at 40 to 50°C and recrystallized to anhydrate at 80 to 90°C. Sodium sulfate (Merck, analytical quality) was added to the light soda ash to produce salt mixtures of 10%-mol, 25%-mol and 50%-mol sodium sulfate. The recrystallization was performed with 20%-w salt (solid or dissolved) in the reactor content. At regular intervals samples were taken, which were processed as described above. In addition to analysis with the Mark II

Moisture Analyzer and the ion chromatograph, the solid samples were analyzed by powder x-ray diffraction and their diffraction patterns compared to those of sodium sulfate anhydrate, sodium carbonate anhydrate, sodium carbonate monohydrate and burkeite ( $\text{Na}_2\text{CO}_3 \cdot 2\text{Na}_2\text{SO}_{4(s)}$ ). The diffraction patterns were obtained from  $d^0$ -spacing data published by Garrett [11] or from mineralogical data-bases [30]. To observe the morphology of the formed crystals during the recrystallization, scanning electron microscope (SEM) images of the solid samples were taken. As sulfate and carbonate were found to form strongly agglomerated compound crystals, the samples were additionally analyzed by SEM-EDS (Philips SEM 525M with Noran EDAX), to qualitatively determine the chemical composition of the single crystallites in the observed compound crystals.

## **2.4. Results**

### **2.4.1. Influence of Sulfate, Chloride, Fluoride and Borate**

The development of the content of sulfate, chloride, boron and fluoride in the solid and the solution during the recrystallization for the first series of experiments is shown in Figures 3 and 4.

The content of fluoride, chloride and boron in the solid decreased strongly shortly after the start of the recrystallization. After this initial decrease, the contents remained approximately constant or decreased only very slightly during the progressing recrystallization. This indicated that these impurities rapidly dissolved in the mixed solvent and only a fraction of them was built into or adsorbed onto the intermediate sodium carbonate monohydrate crystals and the final crystalline soda. The content of these impurities in the crystalline soda was reduced to less than 0.5%-weight for the chloride (from initially 2.5%-weight) and less than 0.005%-weight for both boron (initially 0.25%-weight) and fluoride (initially 0.06%-weight).

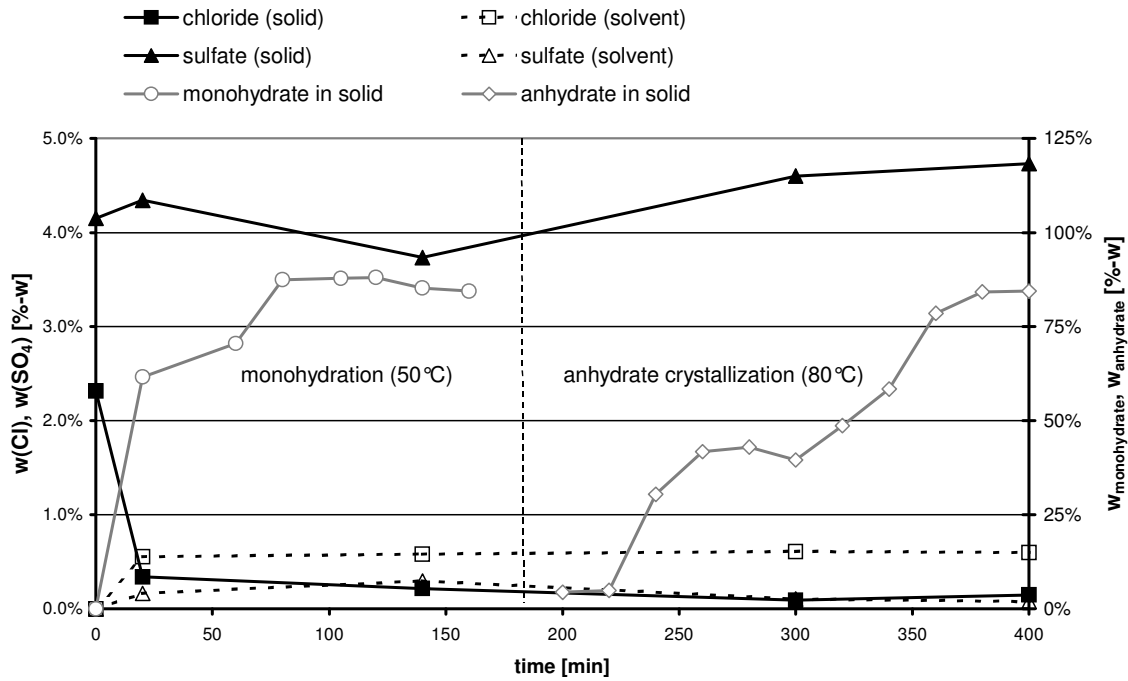


**Figure 2-3:** Chloride and sulfate contents of the solid and the solution during batch double recrystallization in 70%-weight ethylene glycol mixed solvent

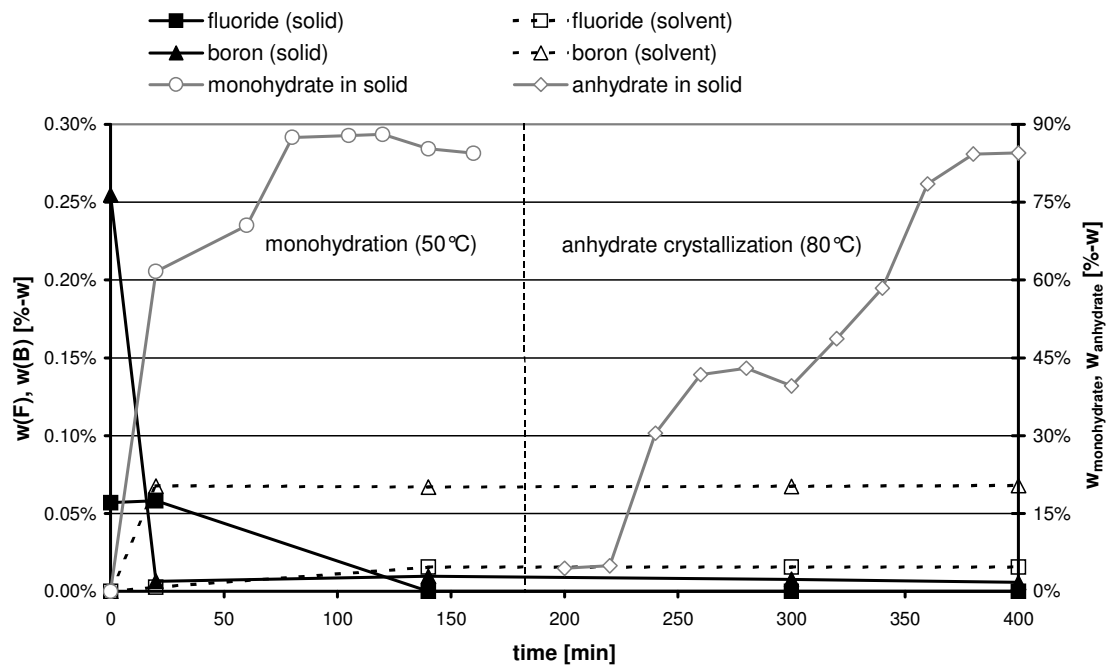


**Figure 2-4:** Fluoride and boron (from borate) contents of the solid and the solution during batch double recrystallization in 70%-weight ethylene glycol mixed solvent

**Table 2-1:** Estimated distribution coefficients between soda (anhydrate) and mixed solvent solution, see Eq.1, for the recrystallization experiments of Figure 3 and 4

	$D_{SO_4}$	$D_{Boron}$	$D_{Cl}$	$D_F$
[g solution/g solid]	40-60	~ 0.1	~ 0.1	< 0.01

As can be seen from Figure 3, the sulfate content of the solids remained almost unchanged. There is a slight decrease of the solid's sulfate content at the end, but considering the uptake of crystal water into the solid, the sulfate to carbonate ratio in the solid remains almost constant. No co-precipitation of any sulfate compound was observed from the SEM images. The crystal morphology of the monohydrate and the anhydrate changed remarkably, see Figure 5. While the anhydrate crystallizes from the mixed solvent without added impurities as well defined hexagonal platelets, the anhydrate formed under the addition of the impurities as flake-like platelets with irregular, serrated edges. This strongly suggested that sulfate was integrated into the crystal lattice of the sodium carbonate solid.

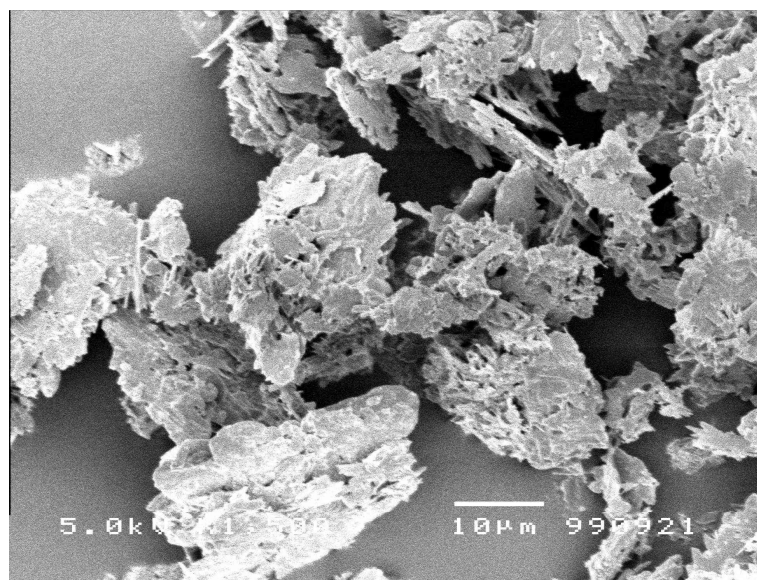


**Figure 2-5:** SEM image of sodium carbonate anhydrate formed by mixed solvent double recrystallization with added impurities (4.5%  $SO_4^{2-}$ , 2.5% Cl, 0.25% B and 0.06% F), bar = 10 micron

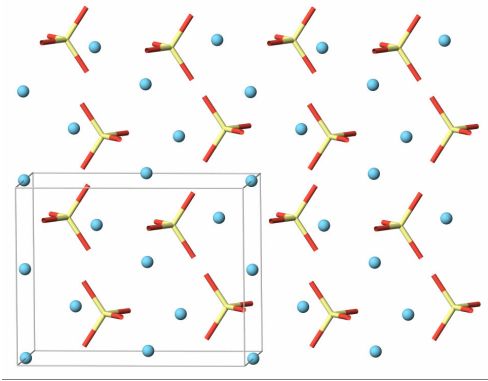


**Figure 2-6:** Unit cell of the sodium sulfate (thenardite) crystal lattice

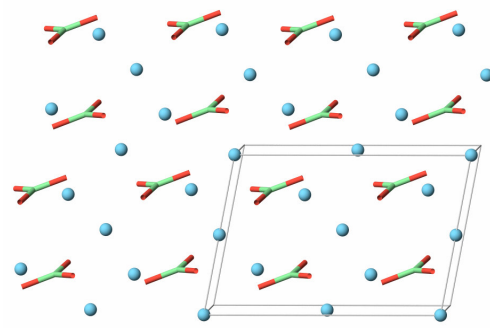


**Figure 2-7:** Unit cell of the sodium carbonate (natrite) crystal lattice

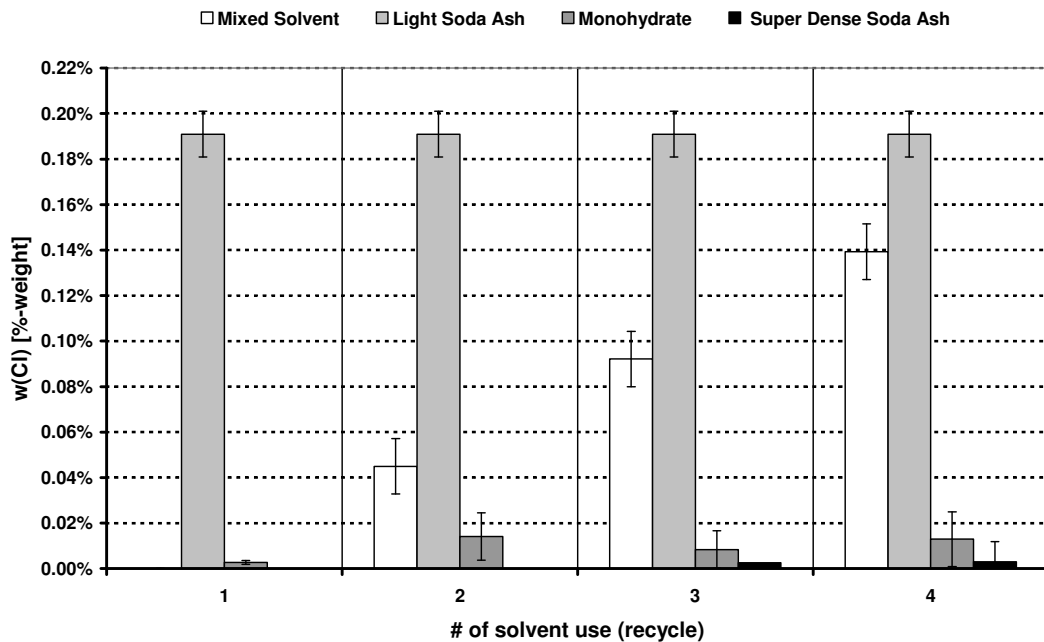


**Figure 2-8:** Chloride contents of the solids and of the (feed) solution in the recrystallization steps in the continuous recrystallization under recycling of the mixed solvent

In the case of incorporation into the crystal lattice, this incorporation will seriously affect the recrystallization of sodium carbonate anhydrate and sodium carbonate monohydrate, as the sulfate ions are larger ( $r_{\text{ion}} = 230\text{pm}$ ) than the carbonate ions ( $r_{\text{ion}} = 178\text{pm}$ ) [31] and, while carbonate ions are planar, the sulfate ions are tetrahedral in conformation. The integration of sulfate ions into e.g. the sodium carbonate anhydrate crystal lattice would cause significant strain in the crystal lattice and would decrease growth rate. Still, the crystal lattices of sodium carbonate anhydrate and sodium sulfate anhydrate are similar



enough, i.e. identical geometrical packing and similar lattice spacing, see Figures 6 and 7, to allow such integration.

#### 2.4.2. Accumulation of Chloride in the Mixed Solvent Recycle

The development of the chloride contents of the intermediate sodium carbonate monohydrate and the produced crystalline super dense soda ash during the continuous 2-batch-cascade experiments with recycling of the mixed solvent is shown in Figure 8.

The chloride content of the used light soda ash was already low with 0.2%-weight. The two-step recrystallization reduced the content in the solid even further to about 0.015%-weight (150ppm) in the sodium carbonate monohydrate and 0.003%-weight (30ppm) in the final anhydrous soda, both produced during the 4<sup>th</sup> recycle of the mixed solvent. It is notable, that in the beginning with fresh mixed solvent the chloride content of the crystalline, super-dense soda was even below the detection limit of the ion chromatograph, i.e. below 0.0005%-weight (5ppm).

The chloride-content of the crystalline soda increased slightly with each cycle of mixed solvent recycle due to the accumulation of the excluded chloride from the feed light soda ash in the mixed solvent. A similar development was noticed for the chloride content of the intermediate sodium carbonate monohydrate.

Distribution coefficients for chloride, see Eq. 1 (i.e. weight fraction chloride in the solid to weight fraction chloride in the mixed solvent) were in the range of 0.1 to 0.3 for the monohydrate crystallization and around 0.03 for the anhydrate recrystallization.

$$D_{Cl^-} = \frac{c_{solid}(Cl^-)}{c_{solution}(Cl^-)} = \frac{w_{solid}(Cl^-)}{w_{solution}(Cl^-)} \quad \text{[g solution / g solid]} \quad \text{Eq. 2-1}$$

The chloride did not have a noticeable effect on the morphology of the formed monohydrate and anhydrate crystals, i.e. they displayed the usual morphology of monohydrate and anhydrate formed during mixed solvent double recrystallization, see Figure 15 and 16.

The chloride – as well as the fluoride and borate - is most probably incorporated into the soda solid by mother liquor inclusion or surface adsorption.

### 2.4.3. Sulfate Incorporation during Double Recrystallization

With no sulfate added to the solid, the recrystallization of anhydrous soda into the monohydrate form occurs rapidly within less than half an hour, while the recrystallization to anhydrate proceeds noticeably slower, see Figure 9.

The recrystallization into monohydrate did occur for all of the three sulfate contents investigated, but the recrystallization to anhydrate did apparently only occur with the 10%-mol  $\text{Na}_2\text{SO}_4$  and also only after the increase of the crystallization temperature to minimally  $80^\circ\text{C}$ . At the higher sulfate contents, the weight loss of the solid samples did not decrease in the second step at 80 to  $90^\circ\text{C}$ , indicating that the sodium carbonate did not recrystallize to anhydrate, but obviously remained monohydrate, see Figure 10 and 11.

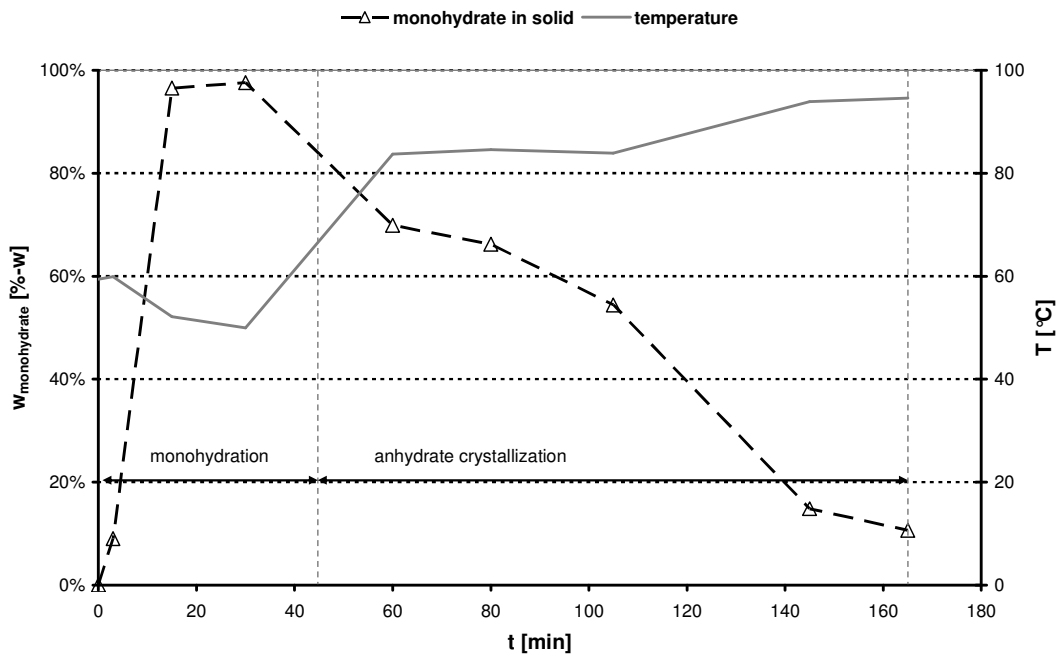
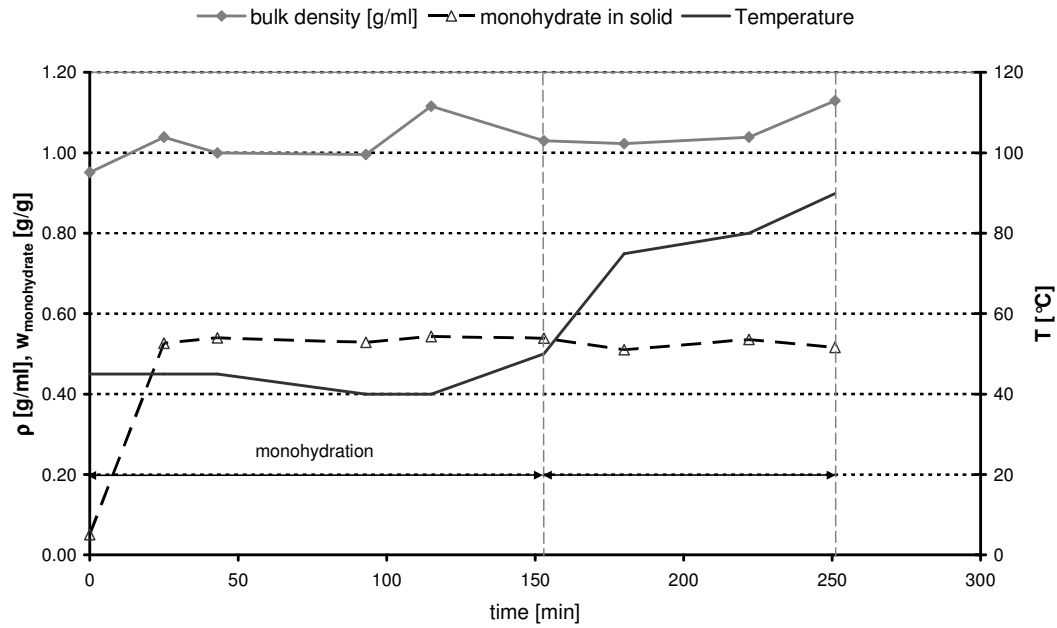
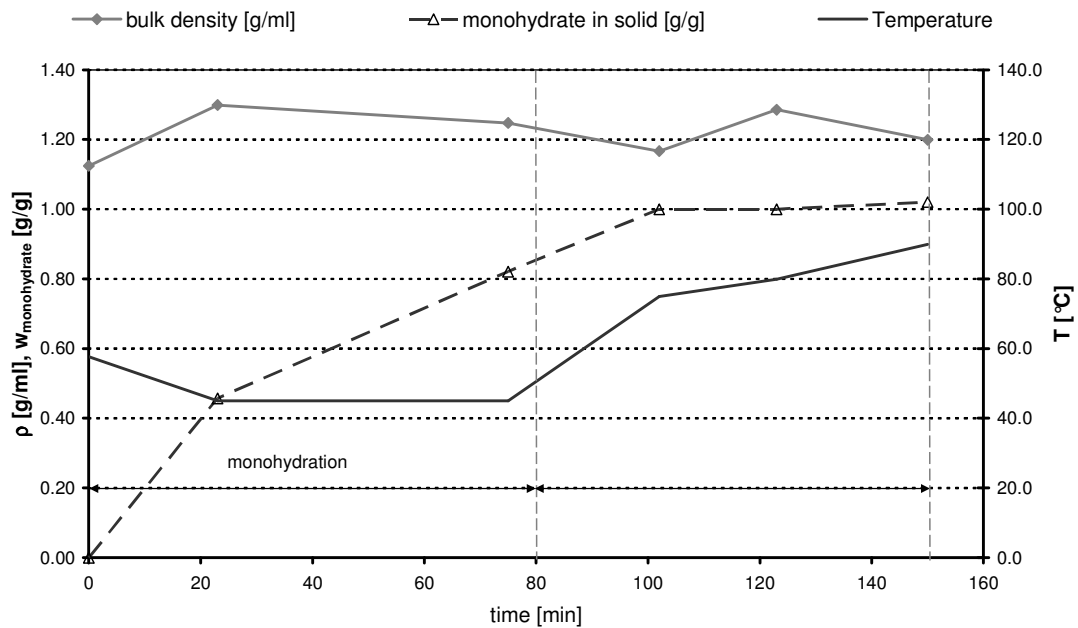


Figure 2-9: Double recrystallization of soda in 70%-w ethylene glycol mixed solvent



**Figure 2-10:** Double recrystallization in 70%w ethylene glycol mixed solvent with 25%-mol  $\text{Na}_2\text{SO}_4$  in the soda, monohydration and anhydrate recrystallization



**Figure 2-11:** Double recrystallization in 70%w ethylene glycol mixed solvent with 50%-mol  $\text{Na}_2\text{SO}_4$  in the soda, monohydration and anhydrate recrystallization

This observation was confirmed by the analysis of the XRD-patterns of the samples:

For all of the three sulfate compositions, an increasing amount of monohydrate could be noticed, while the characteristic peaks of the anhydrate got weaker. For the experiment with 10%-mol sulfate, the anhydrate pattern reappeared during the anhydrate recrystallization cycles. In the other two experiments, the anhydrate pattern did not reappear and monohydrate was identified as the dominating sodium carbonate solid phase.

It was noticeable, that the monohydration proceeded slightly slower than in experiments without sulfate, while the recrystallization into anhydrate in the 10%w sulfate experiment proceeded slower than in the case without sulfate.

During the first hydration cycle no conversion from monohydrate to anhydrate could be found, and only partial conversion was achieved in the second temperature cycle. In the experiments with 25 %-mol and 50 %-mol, see Figure 10 and 11, the monohydration proceeded slower than in the experiment without sulfate, see Figure 9. It appears, that the monohydration rate even decreased with increasing amount of sulfate in the experiment.

The uptake of trace amounts of sulfate during crystallization of sodium carbonate monohydrate was also reported by Garret [11] for the crystallization from aqueous soda solutions, but from their aqueous solution, sodium sulfate and sodium carbonate form a mixed phase, burkeite ( $\text{Na}_2\text{CO}_3 \cdot 2\text{Na}_2\text{SO}_{4(s)}$ ). A recent study of the crystallization of burkeite was performed by Rousseau et al. [32-33], indicating that reduced water activity due to the presence of NaOH and small amounts (1%-weight) of organic impurities did reduce the solubility and the respective metastable zone-width of  $\text{Na}_2\text{SO}_{4(s)}$  and  $\text{Na}_2\text{CO}_{3(s)}$ . Burkeite was still found as the stable phase formed from the solution - unaffected by these additives. They even crystallized a previously unknown mixed solid phase of the composition  $2\text{Na}_2\text{CO}_3 \cdot \text{Na}_2\text{SO}_{4(s)}$ , which they referred to as *dicarbonate* [33].

No burkeite, ( $\text{Na}_2\text{CO}_3 \cdot 2\text{Na}_2\text{SO}_{4(s)}$ ) was identified from the analysis of the XRD-patterns of the samples. Sodium sulfate anhydrate was identified as the only occurring sulfate phase.

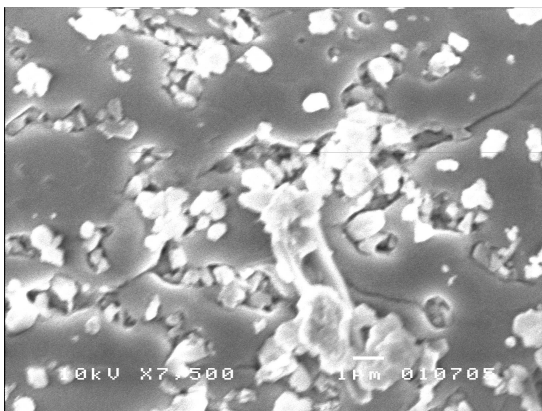


**Figure 2-12:** SEM-EDS image of the surface of a sodium carbonate monohydrate crystal (formed in the 50%-mol sulfate experiment), covered with small sodium sulfate anhydrate crystallites, bar = 1 micron

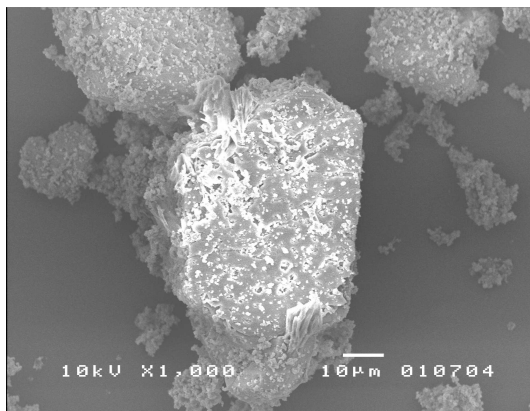


**Figure 2-13:** SEM-EDS image of a sodium carbonate monohydrate crystal (formed in the 50%-mol sulfate experiment), covered with small sodium sulfate anhydrate crystallites, bar = 10 micron

The size of the formed crystals decreased with increasing sulfate content in the solid, compare Figure 13 and 16. Additionally, their surfaces became rougher and slight changes in the morphology were observed.

While sodium carbonate monohydrate crystallized as needle-like lozenges, see Figure 18, and sodium carbonate anhydrate crystallized as hexagonal platelets, see Figure 19, from the mixed solvent without added sulfate, the monohydrate formed in the presence of the sulfate was cubic-like in morphology, see Figure 16.

Although the anhydrate formed in the presence of the sulfate appeared to display also the same cubic-like morphology, see Figure 17, this was actually not the case. The monohydrate underwent a (pseudo) solid-state conversion, which maintained the shape of the monohydrate crystals. I.e. these crystals are pseudomorphous, while the anhydrate formed as 1µm crystallites.

Although the monohydrate particles had a defined morphology, they displayed large pores, and their surfaces as well as the interior of these pores were covered with small crystallites, see Figure 12 and 13. Additional analysis by SEM-EDS showed, that these small crystallites consisted of sodium sulfate, which most probably formed by heterogeneous nucleation on the surface of the (growing) sodium carbonate monohydrate.

Additionally, the studies of the product crystals by SEM-EDS (Philips SEM 525M with Noran EDAX) confirmed, that although the solid carbonate contained significant traces of sulfate incorporated into the carbonate crystal lattice (ca. 1 to 5 %mol), most of the sulfate was still present as a separate solid phase: either in the form of agglomerates of sulfate crystallites (1-10 micron) or as sulfate crystallites of similar size adhering to the surfaces of the larger carbonate crystals. It was even found, that these crystallites were not only adhering to the surface, but that the recrystallizing carbonate monohydrate was growing around these sulfate crystallites, forming small cavities in the carbonate crystal, literally engulfing the sulfate crystallites in the course of the growth.

This behavior certainly provides the following explanation of the decreased sodium carbonate monohydrate and anhydrate recrystallization rates and the inhibition of the recrystallization to the anhydrate in the experiments with 25 and 50%-mol of sulfate: Apart from the obvious obstruction of the carbonate surface by the adhering sulfate crystals, the engulfment of the sulfate crystallites definitely introduces significant strain to the crystal lattice – in addition to the strain by the observed incorporation of sulfate ions into the carbonate lattice. Such strained crystal lattices require higher driving forces to form, i.e. their growth rate is decreased in comparison to the unstrained crystal for the same supersaturation.

Furthermore, if crystal growth was strongly impeded by the blocking of the growth sites by the impurity, i.e. sulfate ions, the supersaturation, which was created by the higher solubility of the dissolving solid phase, could only release itself in an increased degree of nucleation. This is most probably the explanation for the pseudomorph formation during the anhydrate recrystallization in the 10%-mol sulfate experiment: The supersaturation on the surface of the dissolving monohydrate reached a high level, because as the monohydrate was itself strained, it dissolved more rapidly, than unstrained monohydrate at the given temperature. Assuming the anhydrate was impeded in its growth by the sulfate, this resulted in increased anhydrate nucleation to release the built-up supersaturation. The forming anhydrate followed the shrinking monohydrate crystal by continuing nucleation and growth – resulting in a (pseudo) solid phase conversion and in the formation of pseudomorphs.

The lack of anhydrate formation in the experiments with 25%-mol and 50%-mol sulfate could then be explained by the inhibited growth of the anhydrate in the presence of sulfate. This inhibition could have been so strong that even the supersaturation produced by the instable monohydrate could not drive the small amount of growth required for the outgrowth of the anhydrate nuclei. As the supersaturation could not release itself, the monohydrate remained metastable in the system.

The formed carbonate crystals were porous, which resulted in significant retention of mixed solvent solution. This retained mixed solvent then impaired the weight loss analysis with the Mark II Moisture Analyzer. As the mixed solvent would evaporate at the same temperature stage as the crystal water of the monohydrate, the exact degree of conversion could actually only be determined from the weight loss of the samples with an uncertainty of ca. 5 to 7%. Although the morphology of the crystals was strongly distorted by the incorporation and/or engulfment of the sulfate, it appears from the SEM-EDS analysis, that also in the experiments with 25%mol and 50%mol sulfate, at least a small fraction of sodium carbonate anhydrate was formed during the anhydrate recrystallization cycles, which was apparently too low to be detected by the XRD or the heating weight loss analysis (due to error induced by the retained mixed solvent).

Also with SEM-, no burkeite was found. It was confirmed that the only sulfate-containing phase in the solid was sodium sulfate anhydrate. Additionally, with the temperature increase from 50 to 80°C, the number of sulfate crystallites on the carbonate crystal surface and suspended in solution increased. The most probable explanation for this effect was that the sulfate solubility decreased with increasing temperature in the employed mixed solvent.

## **2.5. Conclusions**

Mixed solvent recrystallization of soda ash allows the production of a more dense, crystalline soda (sodium carbonate anhydrate) at atmospheric conditions than by the industrially employed processes. Also the purity of the soda can be improved by mixed solvent recrystallization as impurities, like e.g.: fluoride, chloride and borate, are excluded to a high degree from the produced crystalline soda. This selectivity allowed

reduction of e.g. the chloride content of commercial light soda ash to the parts-per-million (ppm) range.

Sulfate was apparently still incorporated and would have to be removed by additional treatment. A reduction of this sulfate content appears therefore only possible during the recrystallization, when the sulfate is set free into the mixed solvent during the dissolution of the initial feed soda ash or of the intermediately formed monohydrate.

Sulfate is incorporated to a very high degree into the sodium carbonate monohydrate crystal lattice to approx. up to 5%-weight. Distribution coefficients between carbonate crystal and mixed solvent solution of up to 60 were estimated. In the experiments with larger bulk amounts of sulfate, the larger fraction of the sulfate co-crystallized with the carbonate. Small sulfate crystallites adhered to the surface of the crystallizing carbonate and were incorporated into the sodium carbonate monohydrate solid by engulfment, i.e. the carbonate crystal grew around them, incorporating mixed solvent in these pores and cavities as well as the sulfate crystallites.

This peculiar form of growth resulted in slower conversion rates than in recrystallization experiments without the sulfate. The exact degree of this decrease was not quantified since the porous nature of the formed carbonate and the resulting incorporation of the mixed solvent prevented exact determination of the degree of conversion by the heating weight loss method employed.

As no burkeite (and neither the *dicarbonate* phase discovered by Rousseau et al. [33]) was observed during the double recrystallization experiments, it is suspected that the region of burkeite stability is significantly shifted in the mixed solvent in comparison to the aqueous solution (see e.g. Garrett [34] for the aqueous system).



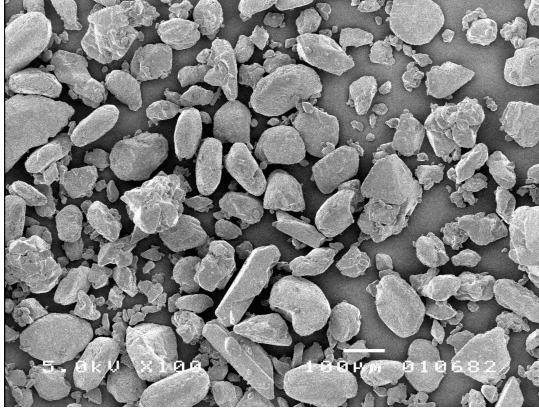


**Figure 2-14:** SEM image of the initial sodium sulfate added to the soda (Merck, Germany, bar = 100 micron)

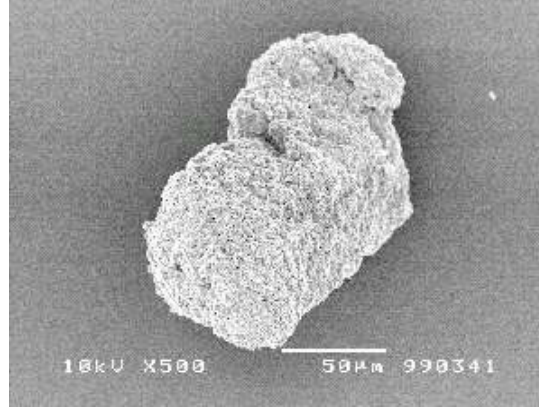


**Figure 2-15:** SEM image of a commercial light soda ash particle (Brunner Mond, The Netherlands, bar = 50 micron)

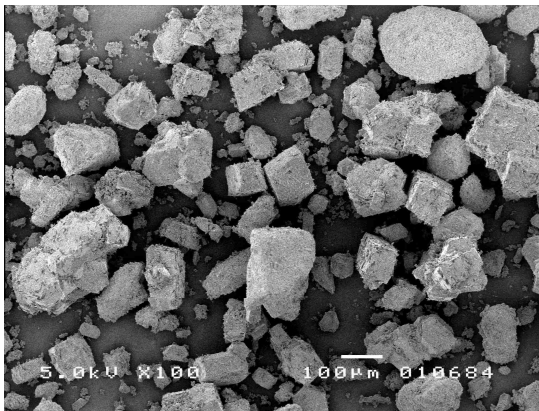


**Figure 2-16:** Monohydrate crystallized in the presence of 10%-mol sodium sulfate (bar = 100 micron)

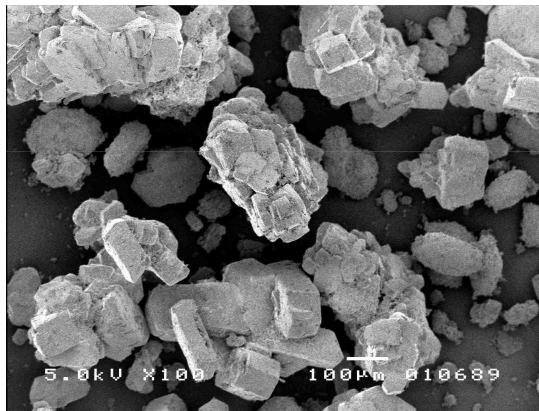


**Figure 2-17:** Anhydrate crystallized in the presence of 10%-mol sodium sulfate. (bar = 100 micron)



**Figure 2-18:** Sodium carbonate monohydrate from double recrystallization without impurity addition (bar = 50 micron)



**Figure 2-19:** Sodium carbonate anhydrate from double recrystallization without impurity addition (bar = 100 micron)

## **2.6. Acknowledgements**

The support and contribution of Mr. Paul Durville with the SEM images, Dr. Sean D. Fleming with the molecular modeling simulations of the sulfate incorporation into the sodium carbonate monohydrate and anhydrate lattices and Dr. Ömer Ünal with the SEM-EDS analysis are gratefully acknowledged.

## **2.7. Literature References**

- [1] Oosterhof, H., Witkamp, G.J., van Rosmalen, G.M., “Evaporative Crystallization of Anhydrous Sodium Carbonate at Atmospheric Conditions”, *AIChE J.*, 47(10), 2001, p. 2220-2225
- [2] Oosterhof, H., de Graauw, J., Witkamp, G.J., van Rosmalen, G.M., “Continuous Double Recrystallization of Light Soda Ash into Super Dense Soda Ash”, *Crystal Growth & Design*, 2 (2), 2002, p. 151-157
- [3] Oosterhof, H., Witkamp, G.J., van Rosmalen, G.M., “Antisolvent Crystallization of Anhydrous Sodium Carbonate at Atmospheric Conditions”, *AIChE J.*, 47(3), 2001, p. 602-608
- [4] Oosterhof, H., de Graauw, J., Witkamp, G.J., van Rosmalen, G.M., “Process for the production of sodium carbonate anhydrate”, European and US Patent application, 1998
- [5] Thieme, C., “sodium hydrogen carbonate” in *Ullmann’s Encyclopedia of Chemical Technology*, 6<sup>th</sup> ed., 2000, electronic release, Wiley-VCH
- [6] Waldeck, W.F., Lynn, G., Hill, A.E., “Aqueous Solubility of Salts at High Temperatures. I. Solubility of Sodium Carbonate from 50 to 348°C”, *J. Am. Chem. Soc.*, 54, 1932, p. 928-936
- [7] Taylor, C.E., “Thermodynamics of Sodium Carbonate in Solution”, *J. Phys. Chem.*, 59, No. 1, p. 653-657
- [8] Hill, A.E., Bacon, L.R., “Ternary Systems. VI. Sodium Carbonate, Sodium Bicarbonate and Water”, *J. Am. Chem. Soc.*, Vol. 59, 1927, p. 2487-2495
- [9] Seidell, A., “Solubilities of Inorganic and Metal Organic Compounds”, Van Nostrand (publ.), New York, 1940
- [10] Kobe, K. A.; Sheehy, T. M., “Thermochemistry of Sodium Carbonate and Its Solution”, *Ind. Eng. Chem.*, 40, 1948, p. 99-102

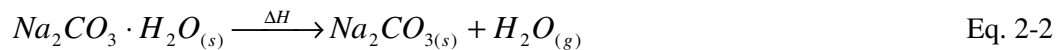
- [11] Garret, D.E., "Natural Soda Ash – Occurrences, Processing, And Use", Van Nostrand Reinhold (publ.), New York, 1991, pp. 267-383
- [12] Ball, M.C., Strachan, A.N., Snelling, C.M., "Dehydration of Sodium Carbonate Monohydrate", J. Chem. Soc. Faraday Trans., 81, 1985, p. 1761-66
- [13] United States Patent 2,267,136, H.R. Robertson, Solvay Process Company, NY, 1940
- [14] United States Patent 3,656,892, D.J. Bourne, F.E. Lamb, Duval Co., 1972
- [15] United States Patent 1,907,987, G. Lynn, Pittsburg Plateglass Co., 1933
- [16] United States Patent, 2,133,455, A.P. Julien, P.A. Keene, The Solvay Process Co., 1938
- [17] United States Patent 3,309,171, A.B. Gancy, Intermountain Research & Development Co., 1967
- [18] United States Patent 2,770,524, M.Y. Seaton, R.D. Pike, FMC Co., 1956
- [19] United States Patent 2,970,037, N.A. Caldwell, W.C. Bauer, FMC Co., 1961
- [20] United States Patent 3,336,105, W.F. Beck, P.M. Di Bello, FMC Co., 1967
- [21] United States Patent 3,028,215, W.R. Frint, FMC Co., 1962
- [22] European Patent Application, EP 85-201753 19851029, T.J.M. van Lotringen, G. van den Berg, AKZO N.V., The Netherlands, 1987
- [23] United States Patent 3,479,134, F.M. Warzel, Phillips Petroleum Co., 1969
- [24] W. Bakele, W., "New developments in the production of heavy soda-ash via compacting method", Powder Technology, 130,, 2003, p. 253-256
- [25] Weingaertner, D.A., Lynn, S., Hanson, D.N., "Extractive crystallization of salts from concentrated aqueous solution", Ind. Eng. Chem. Res., 30, 1991, p. 490-501
- [26] Nordhoff, S., Bechtloff, B., Ulrich, J., "Pseudopolymorphs in industrial use", Crystal Research and Technology, 36(12), 2001, p. 1315-1328
- [27] United States Patent 6,022,385, R.W. Bowman, 2000
- [28] Oosterhof, H., Witkamp, G.J., van Rosmalen, G.M., "Some antisolvents for crystallisation of sodium carbonate", J. Fluid Phase Equilibria, 155(2), 1999, p. 219-227
- [29] Kirk Othmer Encyclopedia of Chemical Technology, 3<sup>rd</sup> edition, Volume 1, p. 866-883, "Sodium Carbonate", J. Wiley & Sons, New York, 1978
- [30] <http://www.webmineral.de>
- [31] Marcus, Y., "Ion Properties", Marcel Dekker (Publ.), New York, NY, 1997
- [32] Bing Shi, Rousseau, R.W., "Crystal Properties and Nucleation Kinetics from Aqueous Solutions of Na<sub>2</sub>CO<sub>3</sub> and Na<sub>2</sub>SO<sub>4</sub>", Ind. Eng. Chem. Res., 40, 2001, p. 1541-1547

- [33] Bing Shi, Frederick, Jr., W.J., Rousseau, R.W., “Nucleation, Growth, and Composition of Crystals Obtained from Solutions of  $\text{Na}_2\text{CO}_3$  and  $\text{Na}_2\text{SO}_4$ ”, *Ind. Eng. Chem. Res.*, 42, 2003, p. 6343-6347
- [34] Garret, D.E., “Natural Soda Ash – Occurrences, Processing, And Use”, Van Nostrand Reinhold (publ.), New York, 1991, pp. 590-592
- [35] United States Patent 3,451,767, W.C., Saeman, J.A. Wood, Olin Mathieson Chemical Co., 1969

## 2.8. Addendum

### 2.8.1. Solid Phase Analysis by Heating-Weight-Loss

As the crystal water of the monohydrate becomes instable upon heating above ca. 120°C, it desorbs to the surrounding air and the monohydrate recrystallizes to the anhydrate:



The accompanying weight loss of the sample due to the desorption of the water can be used to determine the amount of monohydrate in the sample.

The weight loss for pure sodium carbonate monohydrate is:

$$X_{\text{Na}_2\text{CO}_3 \cdot \text{H}_2\text{O}} = \frac{M_{\text{H}_2\text{O}}}{M_{\text{Na}_2\text{CO}_3 \cdot \text{H}_2\text{O}}} = 0.1453 \quad \text{[g/g initial solid]} \quad \text{Eq. 2-3}$$

The weight loss for pure sodium carbonate anhydrate is:

$$X_{\text{Na}_2\text{CO}_3} = 0 \quad \text{[g/g initial solid]} \quad \text{Eq. 2-4}$$

Most samples of the recrystallization experiments contained mixtures of both solid phases. For the double recrystallization experiments w/o addition of sulfate, the solid compositions were calculated directly from the heating-weight-loss. The weight fraction monohydrate  $w_{\text{monohydrate}}$  was calculated as:

$$w_{\text{monohydrate}} = \frac{X}{X_{\text{Na}_2\text{CO}_3 \cdot \text{H}_2\text{O}}} \quad \text{[g/g solid]} \quad \text{Eq. 2-5}$$

The identification of a crystal phase was, of course, not only based on the weight loss of a sample, but also verified either from light microscopy, SEM images and/or powder XRD.

The weight loss analysis was primarily employed to monitor the degree of conversion and to determine the amount of adhering solvent for a great amount of samples.

For the experiments in which 10, 25 or 50%-mol sulfate was added to the solid, the calculated degree of conversion was corrected for the amount of carbonate present in the sample. As sodium sulfate did not form a hydrate in the experiments, it did not contribute to the heating weight loss.

To exactly determine and characterize the amount of adhering liquid (e.g. also adhering acetone as washing liquid from the filtration), the samples were heated in a 2-stage program. The sample was first heated for at least 3 min. at 60°C to evaporate adhering moisture and then for at least 5 min. at 200°C to calcine the sample, i.e. to desorb the crystal water. The Moisture Analyzer was set to keep the samples at constant temperature at each stage, till the sample showed constant weight. Due to the relatively short exposure times, only negligible calcination would occur at 60°C.

The reproducibility of this method was found to depend strongly on sample morphology. For samples of very fine crystallites or an otherwise high degree of intercrystalline porosity, the first stage would not completely remove adhering moisture due to retention by capillary forces. Too high weight losses would be obtained in the second heating stage, especially for samples containing high amounts of pseudomorphs.

### **2.8.2. A Comment on the Recoverability of the Mixed Solvent**

Since the cost of the ethylene glycol is about for times the sales value of the produced soda, see section 10.3.2.7, even the losses of adhering mixed solvent during filtration deserve some attention.

During the filtration test in the glass filter, it was found that the fraction of adhering mixed solvent depended strongly on the particle size and quality of the produced soda crystals. For large, well shaped, unagglomerated soda crystals, as in Figure 4-17, simple vacuum filtration ( $\Delta p = 0.5$  bar) without washing yielded an adhering liquor fraction of 0.5%w for a cake height of about 2.5 cm. For a product that contained pseudomorphic fragments or other agglomerates, as in Figure 2-19, the adhering liquor content (without washing) could increase to 2%w (or more) for the same cake height.



## Chapter 3 :

### REACTIVE RECRYSTALLIZATION OF SODIUM BICARBONATE

R.S. Gärtner, M.M. Seckler, G.J. Witkamp

#### **Abstract**

The thermal decomposition of sodium bicarbonate,  $\text{NaHCO}_3$ , in mixed solvents composed of ethylene glycol and water was found to occur solution mediated, i.e. bicarbonate ions ( $\text{HCO}_3^-$ ) convert in solution to carbonate ions ( $\text{CO}_3^{2-}$ ), carbon dioxide and water. The equilibrium shifts with increasing temperature towards the bicarbonate decomposition. Above  $90^\circ\text{C}$ , the decomposition of the bicarbonate ions in solution results in the conversion (recrystallization) of solid  $\text{NaHCO}_3(\text{s})$  (nahcolite) in contact with the solution. This recrystallization of  $\text{NaHCO}_3(\text{s})$  at temperatures above  $90^\circ\text{C}$  is independent of the water content for the tested mixed solvents. Thus, slurries of solid sodium bicarbonate ( $\text{NaHCO}_3(\text{s})$ ) above  $90^\circ\text{C}$  recrystallize solution mediated via wegscheiderite ( $\text{Na}_2\text{CO}_3 \cdot 3\text{NaHCO}_3(\text{s})$ ) - as an intermediately formed solid phase - to sodium carbonate anhydrate ( $\text{Na}_2\text{CO}_3(\text{s})$ ). The decomposition rates were measured and the kinetics fitted to the most probable mechanism, i.e. first order in concentration of the bicarbonate ion in solution. Additionally, the solubility of nahcolite ( $\text{NaHCO}_3(\text{s})$ ) was determined for a range of mixed solvent compositions and temperatures.

### **3.1. Introduction**

The thermal decomposition of sodium bicarbonate,  $\text{NaHCO}_3$ , to sodium carbonate,  $\text{Na}_2\text{CO}_3$ , is a key step in soda production, as bicarbonate occurs as an intermediate or a by-product in most process routes [1, 2]. Not only do most natural sources of soda contain a greater or lesser amount of bicarbonate, also the Solvay process, the current source of synthetically produced soda, produces bicarbonate, which is transformed to soda by dry thermal decomposition (calcination). This calcination is commonly performed with the dry salt in huge rotary calciners at temperatures of 160 to 200°C [1, 2].

The bicarbonate decomposition in aqueous solution is less well documented in literature [3-7] and its technical application is only documented in a few patents [8]. The decomposition in a mixed solvent has apparently only been studied by our group [9]. Neither the conversion mechanism, nor the conversion rates in the mixed solvent are known. Therefore, both were investigated in this study.

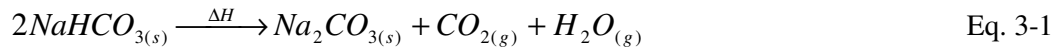
The mixed solvent recrystallization of sodium carbonate monohydrate ( $\text{Na}_2\text{CO}_3 \cdot \text{H}_2\text{O}(\text{s})$ , thermonatrite) to sodium carbonate anhydrate ( $\text{Na}_2\text{CO}_3(\text{s})$ , soda, natrite) was studied by Oosterhof et al. [10-13] and Weingärtner et al. [14] and mixtures of ethylene glycol and water were found to be the most suitable mixed solvents for the crystallization of the anhydrate. These mixed solvents are high boiling and increase the stability of sodium carbonate anhydrate in solution.

From the study of the conversion of sodium bicarbonate in aqueous solution and in the dry state, it is known [1, 15-26], that the thermal decomposition can occur solution mediated, i.e. via the dissolved ions, as well as in the solid state simultaneously to a (pseudo) solid-state recrystallization. Due to the special conditions in the mixed solvent, both of these mechanisms are considered possible and are discussed in the following sections.



### 3.2. $\text{NaHCO}_3$ Decomposition in the Solid State

The decomposition of sodium bicarbonate in the dry solid state is well studied [15-26] and a clear idea of the decomposition mechanism can be established from these publications. The basic reaction equation is:



$$\Delta H_{R, 298.15\text{K}} = 133.39 \text{ kJ/mol [17]}$$

The decomposition and recrystallization mechanism of solid sodium bicarbonate apparently follows till ca. 160°C a 1<sup>st</sup> order reaction (Avrami-Erofeyev  $n=1$ , see [19]) and at higher temperatures a phase boundary controlled (contracting cube, see [19]) mechanism according to [15, 16]. Other authors state, though, that the 1<sup>st</sup> order mechanism applies up to ca. 180°C [20-22]. Keener et al. [24] confirm the contracting cube mechanism for temperatures above 177°C. Tanaka et al. [25] claim to determine kinetic parameters without influence of mass and heat transfer by minimizing sample size and reducing heating rate, but they still find an Avrami-Erofeyev type mechanism followed by a phase boundary controlled mechanism at higher temperatures.

There is a significant variation in the determined activation energy for both stages of the decomposition. E.g., the activation energy of the first order mechanism is given as: 64 kJ/mol (nitrogen atmosphere) and 118 kJ/mol (carbon dioxide atmosphere) [16], 68.0 to 120 kJ/mol (nitrogen atmosphere) [25], 105.8 kJ/mol (nitrogen atmosphere) [15], 98.1 (nitrogen atmosphere) and 119.4 (carbon dioxide atmosphere) [21] and 102 kJ/mol (helium) [20]. The activation energy of the phase boundary controlled stage is given as 27 kJ/mol to 38 kJ/mol [20-25]. The variation in the pre-exponential factor is even more pronounced - while all authors present good kinetic fits to experimental data. Apparently, the reaction is so strongly influenced by mass and heat transfer effects, that particle size, heating rate and purging gas flow significantly affect the decomposition rate and the decomposition mechanism.

The high temperature in industrial bicarbonate calcinations appears to be required, because of the inhibiting effect of the formed carbon dioxide on the decomposition reaction. Ifrim et al. [15] and Ball et al. [16] found that this inhibition in carbon dioxide atmosphere decreased with increasing temperature, so that the rate in carbon dioxide

matched the decomposition rate in carbon-dioxide-free atmosphere at 160°C [15] to 166°C [16]. This change in decomposition rate could be attributed to the change in decomposition mechanism, as also the extrapolated activation energy for the reaction changed from < 160°C to > 160°C. The first order decomposition mechanism for solid-state conversion of sodium bicarbonate is thus dependent on CO<sub>2</sub> partial pressure.

The water partial pressure on the other hand has very little effect on the dry decomposition: Water shows no inhibiting effect on the reaction. It is rather found [15, 16, 18], that the decomposition is accelerated by high ambient relative humidity and/or moisture sorption in the temperature range from 50 to 90°C, indicating that surface bound water has a catalytic effect on the decomposition.

As can be seen from Figure 1, the reaction Gibbs free energy  $\Delta G_R$  is in the temperature range till ca. 90°C significantly lower for the reaction producing liquid water (unbroken line) than the for the one producing water vapor (dotted light gray line) - due to the Gibbs free energy of water evaporation.

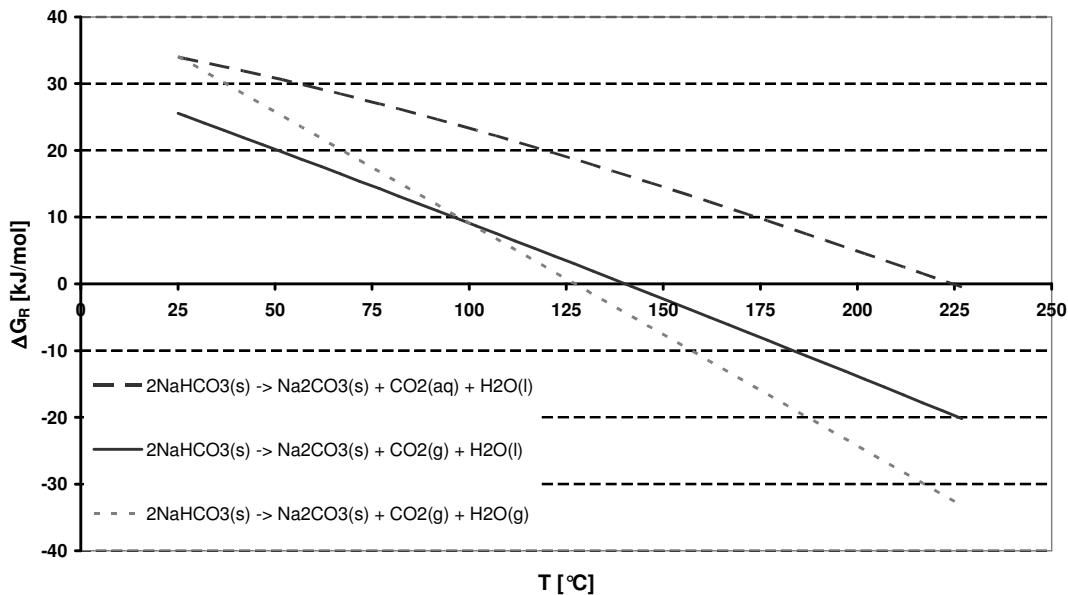


**Figure 3-1:** Reaction Gibbs free energy for the thermal decomposition of solid NaHCO<sub>3</sub>

Therefore, absorbed surface water would lower the total reaction Gibbs free energy in this temperature range, since the water produced by the reaction could be taken up as liquid water by the surface water, instead of having to evaporate.

The values of the given Gibbs free enthalpies of reaction have been calculated by the common thermodynamic relationships from enthalpy and entropy data given in [27].

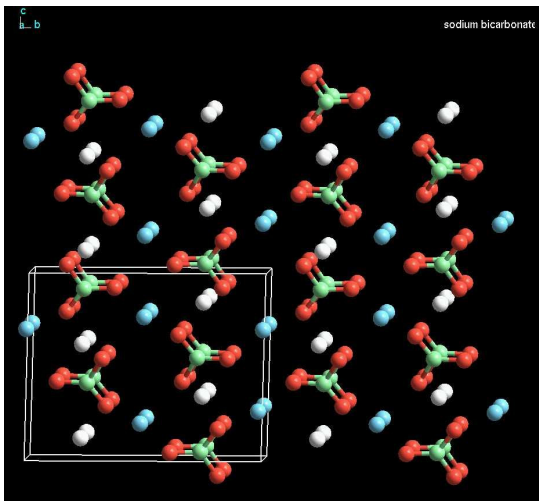
This catalytic effect might also stem from the higher mobility of ions, e.g.  $\text{OH}^-$ , in the surface water (compared to solid or gas phase) and/or the presence of bicarbonate as  $\text{HCO}_3^-$  ion in the adsorbed water (i.e. dissolution of the crystal lattice in the absorbed water layer). Ball et al. [16] propose a combination of a temperature dependent decomposition reaction (Eq. 2) and a diffusion / mass transfer controlled neutralization (Eq. 3) as a possible reaction mechanism.



Figure 1 also offers an explanation, why the change of decomposition mechanism occurs at temperatures around 160°C: In this temperature range the reaction Gibbs free energy becomes significantly negative, indicating a significant shift of the (theoretical) thermodynamic equilibrium towards the products of the reaction. Here, ambient or even slightly increased  $\text{CO}_2$  partial pressure would not suffice anymore to reverse (i.e.: inhibit) the reaction towards bicarbonate formation.

Even at these high temperatures, the presence of liquid surface water in the bicarbonate cannot be ruled out: The formed sodium carbonate crystallites are very fine (~1micron) and form agglomerates, which retain the shape of the bicarbonate crystals (pseudomorphs). The pores in these agglomerates are very fine and might keep the reaction water liquid by capillary condensation. The unconverted bicarbonate at the core of the agglomerate would then have to decompose in contact with liquid water.

As indicated by the topmost line in Figure 1, the solid state reaction has a significantly increased reaction Gibbs free energy for sodium bicarbonate in contact with aqueous solution, because here, the carbon dioxide would have to form as  $\text{CO}_2(\text{aq})$ . This shifts the equilibrium of the conversion reaction strongly towards the solid bicarbonate.



**Figure 3-2:** Crystal lattice of sodium bicarbonate ( $\text{NaHCO}_3(\text{s})$ )

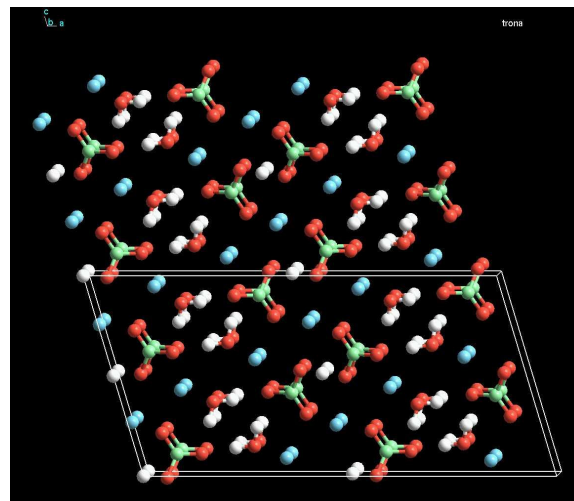


**Figure 3-3:** Crystal lattice of trona ( $\text{Na}_2\text{CO}_3 \cdot \text{NaHCO}_3 \cdot \text{H}_2\text{O}(\text{s})$ )

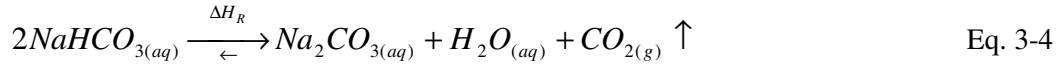
Therefore, sodium bicarbonate in aqueous slurries does not convert in the solid state but rather solution mediated, see next section.

The technically employed decomposition temperatures of bicarbonate are also rather high compared to e.g. the temperature for the calcination of trona (see Chapter 4) of 120 to 160°C.

This is most likely due to the crystal structure of bicarbonate: While in trona layers of sodium ions and hydrogen bonded carbonate-bicarbonate pairs alternate with layers of crystal water, bicarbonate is formed of ordered layers of chains of hydrogen bonded bicarbonate ions, see Figures 2 and 3. Not only the presence of the more volatile crystal water in the trona, but rather also its hydrogen-bonded chain structure appear to make the crystalline bicarbonate (nahcolite) more resistant to thermal decomposition: While in both structures the  $\text{HCO}_3^-$  decomposition was found to start at a significant rate at ca. 50 to 60°C in the dry solid state [1, 9, 17], the  $\text{HCO}_3^-$  decomposition in trona proceeds significantly faster than in bicarbonate.

### ***3.3. $\text{NaHCO}_3$ Decomposition in Aqueous Solution***

The decomposition of dissolved sodium bicarbonate in aqueous solution is commonly described by the following sum equation:



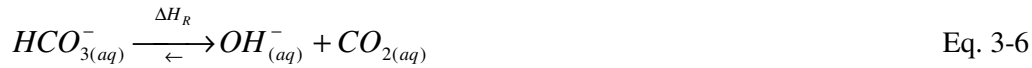
$\Delta H_{R, 298.15K} = 27.50 \text{ kJ/mol}$  [26, 28] or  $25.29 \text{ kJ/mol}$  [26, 29]

Babb et al. [30, 31] have proven with radioactive tracers and potentiometric measurement of the bicarbonate activity, that the thermal decomposition of dissolved sodium bicarbonate in aqueous solution is first order in relation to the activity of the bicarbonate ion. The first order mechanism was confirmed by the work of Stumper [4] and Morgunov [6] for dilute solutions, leading to the following relations for dilute aqueous solutions:

$$\frac{dc_{HCO_3^-(aq)}(t)}{dt} = -k \cdot c_{HCO_3^-(aq)}(t) \Rightarrow c_{HCO_3^-(aq)}(t) = c_{HCO_3^-(aq)}(t_0) \cdot \exp(-k(t - t_0)) \quad \text{Eq. 3-5}$$

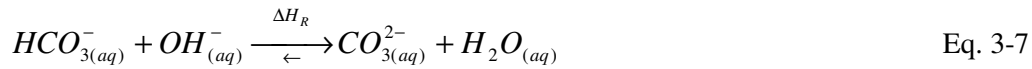
The following reaction scheme was established by Harned et al. [32, 33] and Babb et al. [30, 31] as the dominating route of reaction for  $\text{pH} > 8$ :

1. Thermal decomposition of the bicarbonate ion:



$\Delta H_{R, 298.15K} = 48.74 \text{ kJ/mol}$  [26, 28] or  $46.66 \text{ kJ/mol}$  [26, 29]

2. Neutralization of the excess hydroxide by bicarbonate:



$\Delta H_{R, 298.15K} = -40.99 \text{ kJ/mol}$  [26, 28] or  $-41.12 \text{ kJ/mol}$  [26, 29]

3. Desorption of the excess carbon dioxide:



$\Delta H_{R, 298.15K} = 19.75 \text{ kJ/mol}$  [26, 28]

The rate-determining step is the bicarbonate decomposition reaction of Eq. 6.

The whole reaction chain is reversible, so the proper expression for the decomposition / formation rate is:

$$r_{HCO_3^-} = \frac{dc_{HCO_3^-}}{dt} = -k_d \cdot a_{HCO_3^-} + k_f \cdot a_{CO_2} \cdot a_{OH^-} \quad \text{Eq. 3-9}$$

This leads to a temperature and carbon dioxide partial pressure dependent, dynamic equilibrium between dissolved carbon dioxide, carbonate and bicarbonate in solution. This equilibrium determines e.g. the minimal concentration to which bicarbonate decomposes for a given carbon dioxide partial pressure.

At the equilibrium point, the rate of decomposition equals the formation rate:

$$k_d \cdot a_{\text{HCO}_3^-} = k_f \cdot a_{\text{CO}_2} \cdot a_{\text{OH}^-} \quad \text{Eq. 3-10}$$

The equilibrium constant  $K_R$  is:

$$K_R = \frac{k_d}{k_f} = \frac{a_{\text{CO}_2} \cdot a_{\text{OH}^-}}{a_{\text{HCO}_3^-}} \equiv \exp\left(-\frac{\Delta G_R}{R \cdot T}\right) \quad \text{Eq. 3-11}$$

As can be seen from Eq. 9, 10 and 11, the equilibrium is independent of the water activity, as water is not a participant of the rate determining reaction step.

The Gibbs free energy of the reaction of Eq. 6,  $\Delta G_R$ , and the equilibrium constant  $K_R$  are given in Figure 4.

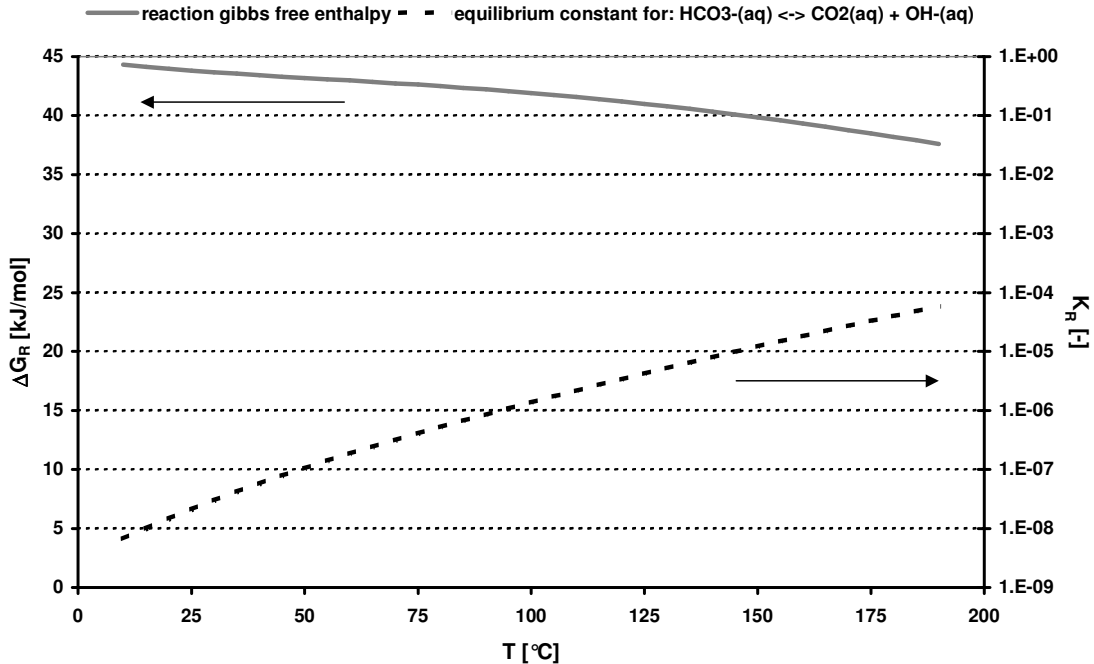


**Figure 3-4:** Reaction Gibbs free energy  $\Delta G_R$  and equilibrium constant  $K_R$  of the reaction of Eq. 9 versus temperature based on [27, 30-34]

These values were calculated using thermodynamical data of Chase et al. [27] and Helgeson et al. [34], and verified against the measured values of Harned et al. [32, 33] and Babb et al. [30, 31].

$K_R$  increases rapidly with temperature, i.e. the equilibrium shifts towards complete dissociation with increasing temperature. From  $K_R$  as a function of temperature, the atmospheric partial pressure of carbon dioxide ( $p_{CO_2} = 10^{-3.5}$  atm) [35], the hydroxide activity  $a_{OH^-}$ , calculated from the pH-buffer-equilibria of the carbonate-bicarbonate system (as functions of temperature) [35], the solubility lines of the different solid phases [36, 37] and the activity coefficients of dissolved carbonate and bicarbonate, calculated with the Pitzer model [38-40], the equilibrium concentrations of carbonate and bicarbonate have been derived and are displayed as the bold, black line in Figure 5, see Addendum.

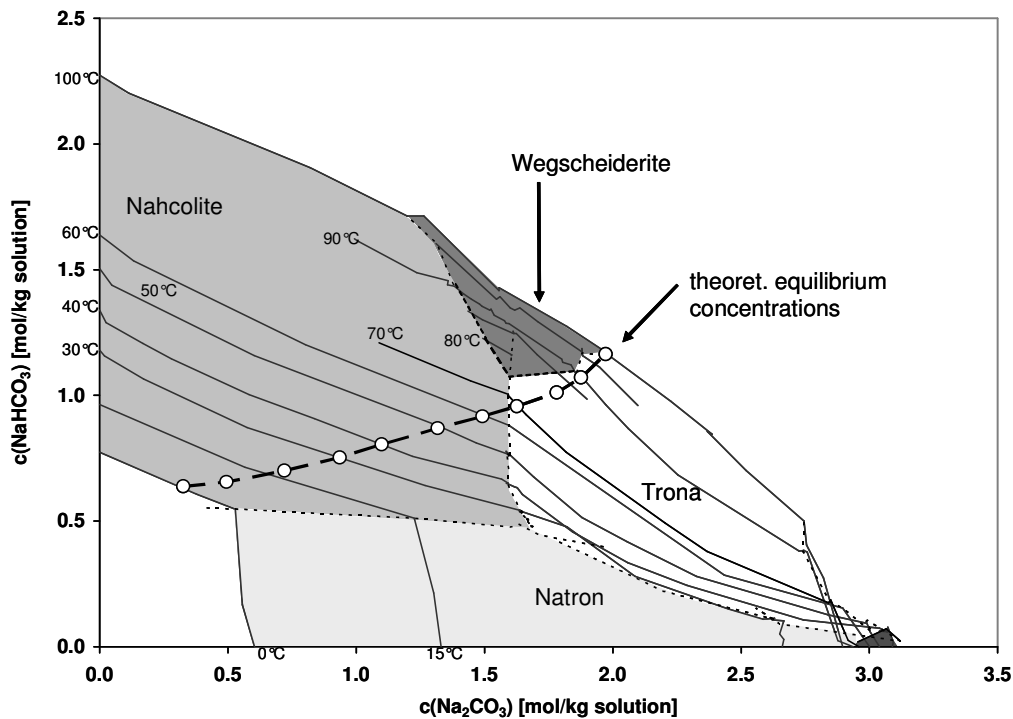


**Figure 3-5:** Theoretical equilibrium concentrations of carbonate and bicarbonate for saturated aqueous solutions in contact with atmospheric carbon dioxide, derived from calculations based on models and data from [27, 34-40] and the  $K_R$  values given in Figure 4

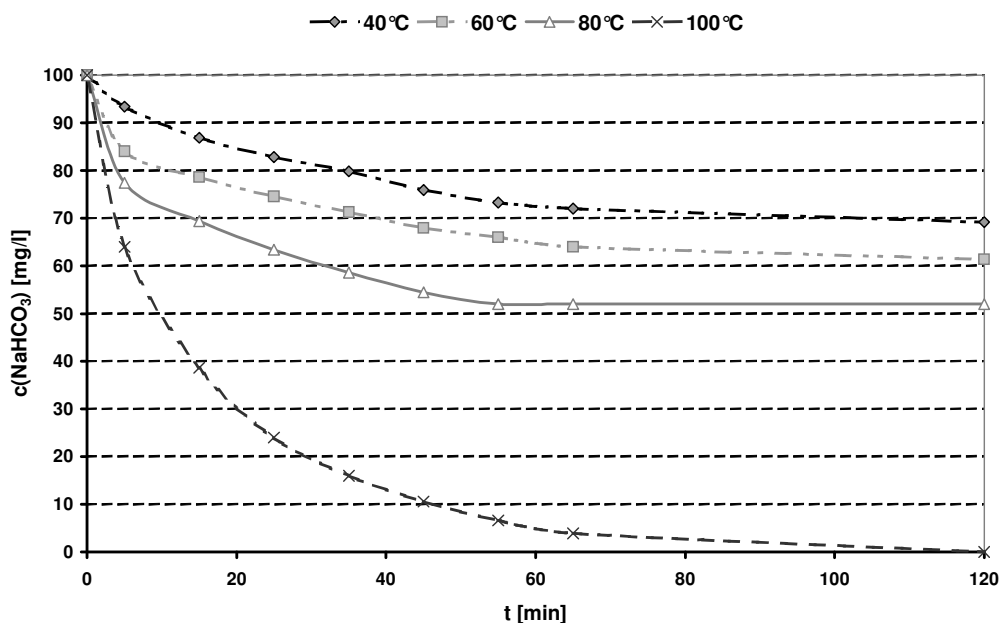


**Figure 3-6:** Thermal decomposition of aqueous  $\text{NaHCO}_3$  [3]

In Figure 5, the isothermic solubility lines for temperatures between  $0^\circ\text{C}$  and  $100^\circ\text{C}$  of the system  $\text{Na}_2\text{CO}_3\text{-NaHCO}_3\text{-H}_2\text{O}$  are given, displaying the solubilities of nahcolite ( $\text{NaHCO}_3(\text{s})$ ), wegscheiderite ( $\text{Na}_2\text{CO}_3\cdot 3\text{NaHCO}_3(\text{s})$ ), natron ( $\text{Na}_2\text{CO}_3\cdot 10\text{H}_2\text{O}(\text{s})$ ) and trona ( $\text{Na}_2\text{CO}_3\cdot \text{NaHCO}_3\cdot 2\text{H}_2\text{O}(\text{s})$ ). For more information on the system and the stability of the occurring phases, see [36, 41].

The predictive calculations indicate, that solid sodium bicarbonate is stable in contact with aqueous solution till about  $70^\circ\text{C}$ , i.e. carbon dioxide absorption / desorption will shift the composition of any saturated carbonate-bicarbonate slurry to form solid bicarbonate. Above  $70^\circ\text{C}$ , trona is predicted as the stable phase at atmospheric conditions.

The uncertainty in the calculated concentrations is about 10%, which implies that the true transition temperature could lie between  $60$  and  $90^\circ\text{C}$ .

Experimental data for *dilute* aqueous solutions from Splittgerber [3] indicate that at  $40$ ,  $60$  and  $80^\circ\text{C}$ , the decomposition remains incomplete, reaching an equilibrium state between carbonate and bicarbonate, see Figure 6. This equilibrium is shifted towards almost complete bicarbonate decomposition with increasing temperature and at  $100^\circ\text{C}$  complete conversion was achieved in two hours. This is coherent with observations of



Stumper [4] and Tsuchiya [5], who observed the formation of dissolved bicarbonate in dilute ( $\sim 0.03\text{mol/l}$ ) carbonate solutions by absorption of carbon dioxide in the temperature range from 20 to 60°C and the decomposition of bicarbonate in dilute bicarbonate solutions from 80 to 100°C. In Gmehlin's Handbook [7], the temperature, at which the decomposition (recrystallization) of solid sodium bicarbonate in contact with aqueous solution starts, is given as 87.7°C.

It can be concluded that the transition temperature for the recrystallization of solid sodium bicarbonate lies between 70 and 100°C, most probably around 90°C.

There is a quite large discrepancy in literature on the values of  $k_d$  and  $k_f$  of Eq. 9 The decomposition [3-6, 30, 31] as well as the formation [30-33, 34, 42-46] of bicarbonate in carbonate solutions has been studied by several research groups, but mostly no activities but only concentrations of carbon dioxide, carbonate and bicarbonate are given. Since the activities of carbonate and bicarbonate can differ up to 2 orders of magnitude from their concentrations, the kinetic parameters determined by these authors differ significantly with ionic strength and concentration.

Only Babb et al. [30, 31] and Harned et al. [32, 33] obtained their data from measurements of carbonate and bicarbonate activities via electrode potential. They obtained equilibrium coefficients  $K_R$  that match the ones derived from the thermodynamic data from Chase et al. [27] and Oelkers et al. [34], but their kinetic coefficients for decomposition ( $k_d$ ) and formation ( $k_f$ ) of bicarbonate are by an order of magnitude higher than those obtained in the other studies. This might be due to the fact, that they defined their reaction rates as the change of bicarbonate *activity* with time (i.e.  $r_{\text{HCO}_3^-} = d(a_{\text{HCO}_3^-})/dt$ ), instead of the change of bicarbonate *concentration* with time (i.e.  $r_{\text{HCO}_3^-} = d(c_{\text{HCO}_3^-})/dt$ ), which is the thermodynamically more suitable expression, see Eq. 9.

Pohorecki et al. [47, 48] give an excellent overview of previous studies and derive an expression for  $k_f$  as function of temperature by extrapolation to infinite dilution. From this  $k_f$ -function and the relationship for  $K_R$ , given in Figure 4 and Table 1, a relationship for  $k_d$  was calculated via Eq. 11. Values of the thus calculated  $k_d$  are given in Table 1 as well.

The following fit for  $K_R$  was obtained from the listed data (see Addendum):

$$\ln(K_R) = 3.312 + \frac{-6269.1K}{T} \quad \text{with: } \Delta G_R = R \cdot T \cdot \ln(K_R) \quad \text{Eq. 3-12}$$

The temperature dependence of  $k_f$  and  $k_d$  can be described by Arrhenius expressions:

$$k_i = k_{i,0} \cdot \exp\left(-\frac{E_i}{R \cdot T}\right) \Leftrightarrow \ln(k_i) = \ln(k_{i,0}) - \frac{E_i}{R \cdot T} \quad \text{Eq. 3-13}$$

The respective rate constants  $k_{i,0}$  and activation energies  $E_i$  are given in Table 1.

**Table 3-1:** Kinetic coefficients for the rate of bicarbonate decomposition / formation in aqueous solution, see Eq. 9 (Pohorecki et al. [47, 48], Babb et al. [30, 31] and Harned et al. [32, 33])

T [°C]	Derived from	derived from [27, 34, 47, 48]	
	[27, 30-34]	$k_d$	$k_f$
	$K_R$	[mol·L <sup>-1</sup> ·s <sup>-1</sup> ]*	[mol·L <sup>-1</sup> ·s <sup>-1</sup> ]*
	[-]		
0	2.748·10 <sup>-9</sup>	4.311·10 <sup>-6</sup>	1,569
10	6.687·10 <sup>-9</sup>	2.132·10 <sup>-5</sup>	3,188
20	1.474·10 <sup>-8</sup>	9.096·10 <sup>-5</sup>	6,173
40	5.750·10 <sup>-7</sup>	0.001172	20,390
60	1.840·10 <sup>-7</sup>	0.01073	58,350
80	5.201·10 <sup>-7</sup>	0.07710	148,250
100	1.359·10 <sup>-6</sup>	0.4631	340,800
$\ln(k_{i,0})$	-	30.750	27.438
$E_i$ [kJ/mol]	-	97.73	45.60

\* as activities are by definition dimensionless,  $k_f$  and  $k_d$  are given as [mol·L<sup>-1</sup>·s<sup>-1</sup>]

### **3.4. $\text{NaHCO}_3$ Decomposition in the Mixed Solvent**

#### **3.4.1. Experimental**

Slurries of 15 to 20%-w sodium bicarbonate in mixed solvents containing 50 to 100%-w ethylene glycol (salt-free base) were prepared and progressively heated in a thermostated, stirred batch reactor of 1-liter volume. Each temperature point, see Figure 7, was maintained for at least 1 hour. Samples of the slurry were taken every 30 minutes, the solvent was filtered off and the solid was rinsed with acetone. The solid was then analyzed for heating-weight-loss in a Mark II Moisture Analyzer thermobalance (Denver Instruments). From the heating-weight-loss the degree of decomposition and recrystallization of the solid sodium bicarbonate was determined (see Addendum for the procedure). The general accuracy of this method was found to be ca. 0.5% weight loss, i.e. 2.5% uncertainty in the calculated weight fraction.

The solid phases in the solid samples were identified visually by polarized light microscopy (Nicon Optishot) and in some cases by powder XRD.

In a second set of experiments, 10g sodium bicarbonate and 40g of mixed-solvent solution were shaken in 50ml Nalgene PTFE-bottles in a thermostated shaking bath. Ethylene glycol contents of 50, 60, 70, 80, 90 or 100%-w (salt-free base) were used. The bottles were shaken at constant temperature for one day. The experiments were started at 50°C and the temperature was increased daily after analysis by 10K till 90°C.

The concentrations of  $\text{CO}_3^{2-}$  and  $\text{HCO}_3^-$  were determined from titration with 0.1 M HCl using a Radiometer VIT 90 Video Titrator. The accuracy of this method was found to be in the range of 0.5 to 2.5% accuracy of the measured concentration. The solid phases were identified visually. All solid samples were tested additionally after conclusion of the experimental series for any indication of recrystallization of the solid by the heating-weight-loss method.

In a third set of experiments, slurries of 15%w sodium bicarbonate were decomposed in the thermostated batch reactor in three different mixed solvent compositions (70, 80 and 90%w ethylene glycol) and at 4 different temperatures (100°C, 110°C, 120°C and 130°C). Samples of the slurry were taken every 20 to 30 minutes. The solid was filtered off in 16-40 micron glass filters and samples of the filtered mixed solvent were titrated in

the Radiometer VIT 90 Videotitrator for their carbonate and bicarbonate content. The solid was rinsed with acetone, dried by suction in the glass filter, analyzed for weight loss. The present crystal morphologies were identified visually by the polarized light microscope. The extent of the bicarbonate decomposition was then calculated from the carbonate and bicarbonate contents in the solid and in solution.

### 3.5. Results

#### 3.5.1. Transition Temperature of Nahcolite Recrystallization

In the first set of experiments, it was found that the conversion of the solid started at app. 90°C, with no apparent dependence on the water content of the mixed solvent, see Figure 7.

The solid bicarbonate (nahcolite,  $\text{NaHCO}_{3(s)}$ ) recrystallized into wegscheiderite (decimite,  $\text{Na}_2\text{CO}_3 \cdot 3\text{NaHCO}_{3(s)}$ ) and at higher temperatures and sufficient reaction times to sodium carbonate anhydrate (natrite,  $\text{Na}_2\text{CO}_{3(s)}$ ).

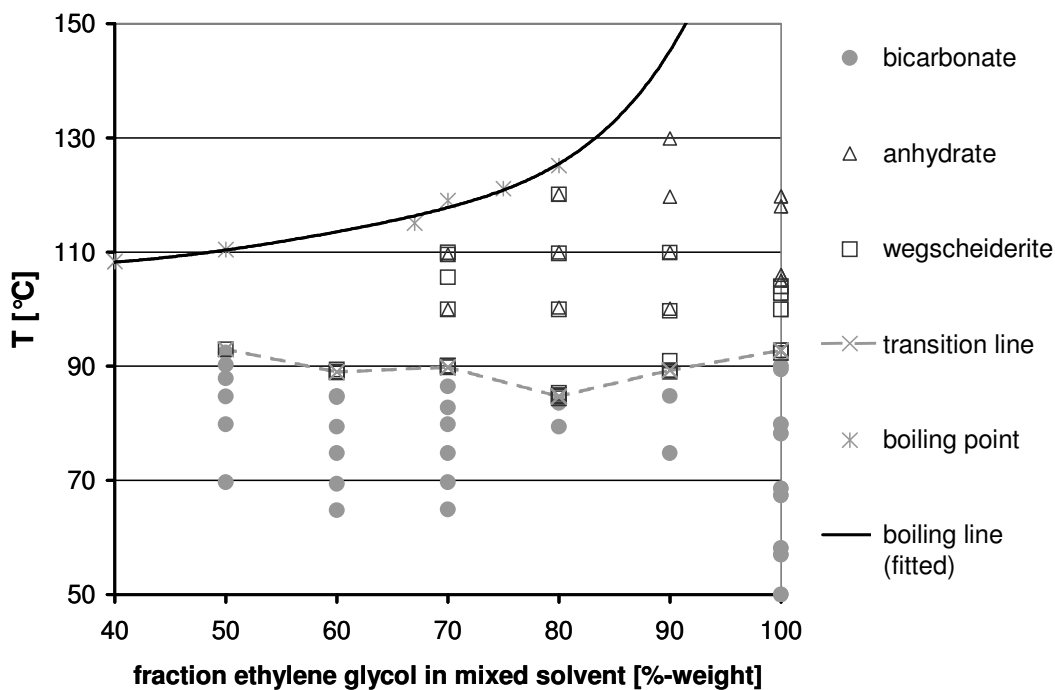


**Figure 3-7:** Transition line of sodium bicarbonate in ethylene glycol – water mixed solvents

It was observed in-situ by optical microscopy that the new phase formed from solution, while the previous phase dissolved. The decomposition occurred therefore most probably in solution. The recrystallization would then be driven by

A) a decrease of bicarbonate and an increase in carbonate concentration in the solution and

B) the progressive decomposition of bicarbonate to carbonate

Although the final solid product obtained was pure anhydrate (natrite), this did not prove yet that the dissolved bicarbonate in the experiment was completely decomposed, since solid anhydrate is stable in a mixed solvent which still contains a significant concentration of dissolved bicarbonate, see Chapter 6 [41].

In the shake tests of the second set of experiments, no significant amounts of dissolved or solid carbonate were found for the whole range of temperatures (50 to 90°C) and antisolvent concentrations (50 to 100%w ethylene glycol). This indicates that no significant decomposition of dissolved bicarbonate to carbonate (i.e. less than 1%-w) had occurred during the experimental period of 24h. The analysis of the solid composition at the end of the experimental series proved, that all solids were still solely composed of sodium bicarbonate (within the error range of this method, i.e. 1.4%-w - or a minimal bicarbonate content of 98.6%-w).

The recrystallization of the solid bicarbonate to wegscheiderite in the first set of experiments (at temperatures above 90°C) was complete after ca. 1 hour, and it was expected, that in the experiments of the second set at temperatures up to 90°C an equilibrium between the dissolved bicarbonate and the dissolved carbonate would establish with a noticeable amount of dissolved carbonate formed by the decomposition - as in the aqueous case, see Figures 5 and 6.

The lack of carbonate formation in the second set of experiments is most probably caused by the increased partial pressure of carbon dioxide in the closed shaking bottles. The equilibrium between bicarbonate and carbonate is greatly affected by carbon dioxide partial pressure, and the partial pressure of carbon dioxide in the atmosphere is very low

( $10^{-3.5}$  atm [35]). Even a minor (i.e. non-detectable) decomposition of bicarbonate of ~ 0.1% could easily increase the partial pressure of carbon dioxide in the ca. 10ml gas space of the bottles by a factor of 500. This increase could shift the equilibrium proportionally (compare e.g. Eq. 11) towards so high bicarbonate-carbonate ratios, that the formed carbonate would remain undetectable, while nahcolite would remain the stable solid phase.

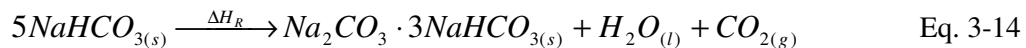
### 3.5.2. Solubility of Nahcolite in the Mixed Solvents

The solubility of sodium bicarbonate increased strongly with increasing temperature, see Figure 8. The solubility also decreased with increasing ethylene glycol content till ca. 80 to 90%w ethylene glycol (salt-free base), where the concentration reached a solubility minimum for all temperatures. In 100%w ethylene glycol (salt-free base), the solubility of sodium bicarbonate was sharply increased. The complete data set is given in the Addendum.

This indicates a strong solvating effect of ethylene glycol for sodium bicarbonate in absence of water. Probably, ethylene glycol and bicarbonate form some kind of complexes. Ethylene glycol with a hydration number of ca. 1.8 [49] forms hydrogen bridges with water molecules. In the absence of water, such hydrogen bridges might be formed with bicarbonate ions, increasing their solubility.

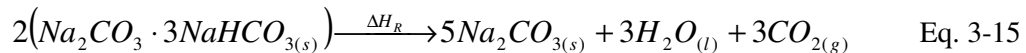
From the batch bicarbonate decomposition experiments, i.e. the first and the third set described in the Experimental section, the following recrystallization scheme for the solid was established.

1. Sodium bicarbonate ( $\text{NaHCO}_{3(s)}$ ) conversion to wegscheiderite ( $\text{Na}_2\text{CO}_3 \cdot 3\text{NaHCO}_{3(s)}$ ):



$$\Delta H_{R, 298.15\text{K}} = 81.39 \text{ kJ/mol [50]}$$

2. Wegscheiderite ( $\text{Na}_2\text{CO}_3 \cdot 3\text{NaHCO}_{3(s)}$ ) conversion to anhydrate ( $\text{Na}_2\text{CO}_{3(s)}$ ):



$$\Delta H_{R, 298.15\text{K}} = 284.15 \text{ kJ/mol [50]}$$

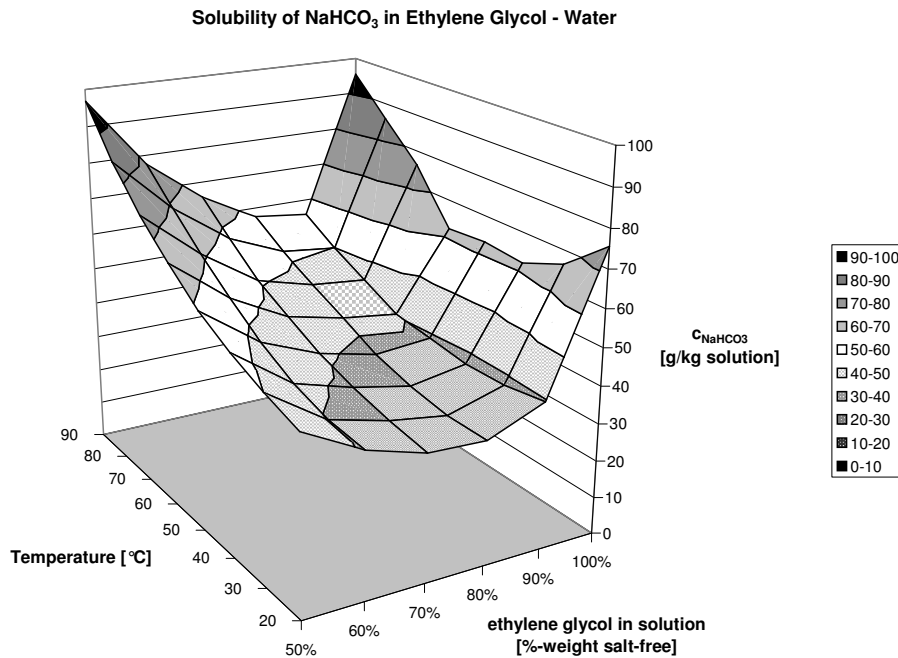


**Figure 3-8:** Solubility of NaHCO<sub>3</sub> in ethylene glycol – water mixed solvents in dependence of temperature

An example of the concentration development in the solution during the conversion is given in Figure 9: The initial bicarbonate concentration in solution  $c(\text{HCO}_3^-)$  equaled the solubility of the solid bicarbonate, which was added initially to the heated mixed solvent. As dissolved bicarbonate decomposed in solution to carbonate, the solid bicarbonate became instable with increasing carbonate concentration and recrystallized slowly to wegscheiderite - simultaneously with the proceeding decomposition. This caused the bicarbonate concentration  $c(\text{HCO}_3^-)$  to drop over time until only wegscheiderite was left as solid, where  $c(\text{HCO}_3^-)$  reached a minimum. As the decomposition progressed, passing the NaHCO<sub>3</sub>-Na<sub>2</sub>CO<sub>3</sub>-stability range of wegscheiderite, anhydrate became the most stable solid phase of the system. As the carbonate solubility of anhydrate was lower than the one of wegscheiderite, the wegscheiderite dissolved slowly, which increased  $c(\text{HCO}_3^-)$ .  $c(\text{HCO}_3^-)$  reached a maximum, when the last wegscheiderite dissolved (leaving no bicarbonate containing solid phase in the system). From then on,  $c(\text{HCO}_3^-)$  decreased slowly by the continuing decomposition, slowly approaching its equilibrium concentration for the bicarbonate decomposition/formation reaction, see Eq. 10 and 11.

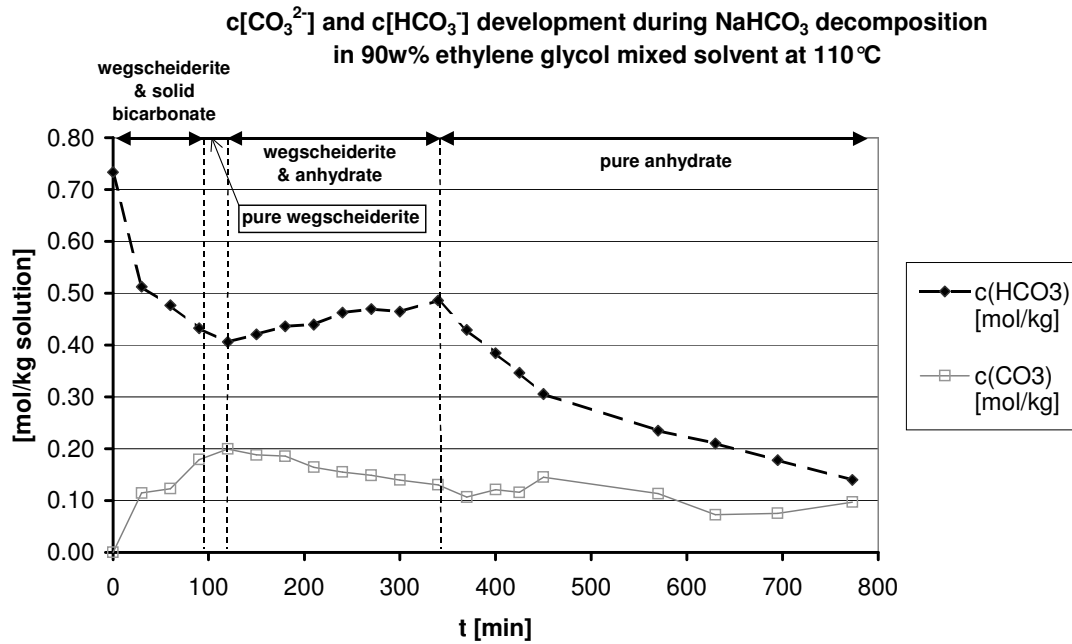


**Figure 3-9:**  $c(\text{CO}_3^{2-})$  and  $c(\text{HCO}_3^-)$  development during  $\text{NaHCO}_3$  decomposition in 90%-w ethylene glycol mixed solvent at 110°C



**Figure 3-10:** In-situ light microscope photograph taken during recrystallization of nahcolite ( $\text{NaHCO}_3(\text{s})$  = dissolving prism-shaped crystals) to wagscheiderite ( $\text{Na}_2\text{CO}_3 \cdot 3\text{NaHCO}_3(\text{s})$  = spherulitically growing, needle shaped crystals); bar = 200 micron



It was observed under the polarised light microscope, that the new phases formed from solution, see Figure 10. This also indicated a solvent mediated mechanism for the decomposition of the bicarbonate ion.

This recrystallization scheme applied to all experiments except the one performed at 90%w ethylene glycol and 130°C, in which the solid bicarbonate (nahcolite) directly recrystallized to sodium carbonate anhydrate (natrite). In this experiment, the decomposition of the bicarbonate apparently proceeded too fast to allow intermediate formation of wegscheiderite.

Especially noteworthy is here, that anhydrate is the stable phase of the decomposition/formation equilibrium above 90°C in the mixed solvent, while the equilibrium's stable phase(s) in aqueous solution at atmospheric carbon dioxide partial pressure is wegscheiderite or trona. Because of this shift in stability *in mixed solvent solution*, see also Gärtner et al. [41], *soda (anhydrate) can be produced directly by reactive recrystallization from solid bicarbonate (nahcolite), wegscheiderite or trona.*

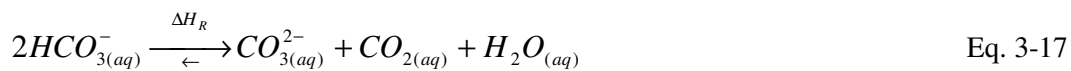
### 3.5.3. Reaction Kinetics of Decomposition in Mixed Solvent

From the third set of experiments, the decomposition rates of bicarbonate and the formation rate of carbonate were calculated.

$$r_{NaHCO_3} = \frac{dn_{NaHCO_3}}{m_{solution} \cdot dt} = -2 \cdot \frac{dn_{Na_2CO_3}}{m_{solution} \cdot dt} = -2 \cdot r_{Na_2CO_3} \quad \text{Eq. 3-16}$$

with  $n_{NaHCO_3}$  and  $n_{Na_2CO_3}$  being the total amount of sodium bicarbonate and sodium carbonate in the reactor (thus in the solid and in the solution). It was found from plots of the reaction rate  $r_{HCO_3^-}$  against  $c(HCO_3^-)$  as well as against  $c(HCO_3^-)^2$ , that the reaction rate would fit both - a first as well as a second order mechanism, see Figure 11.

A monomolecular, i.e. Eq. 6, or a bimolecular mechanism, as given in Eq. 17, could be the rate-determining step of the decomposition in mixed-solvent solution.



$$\Delta H_{R, 298.15K} = 5.54 \text{ kJ/mol [26]}$$

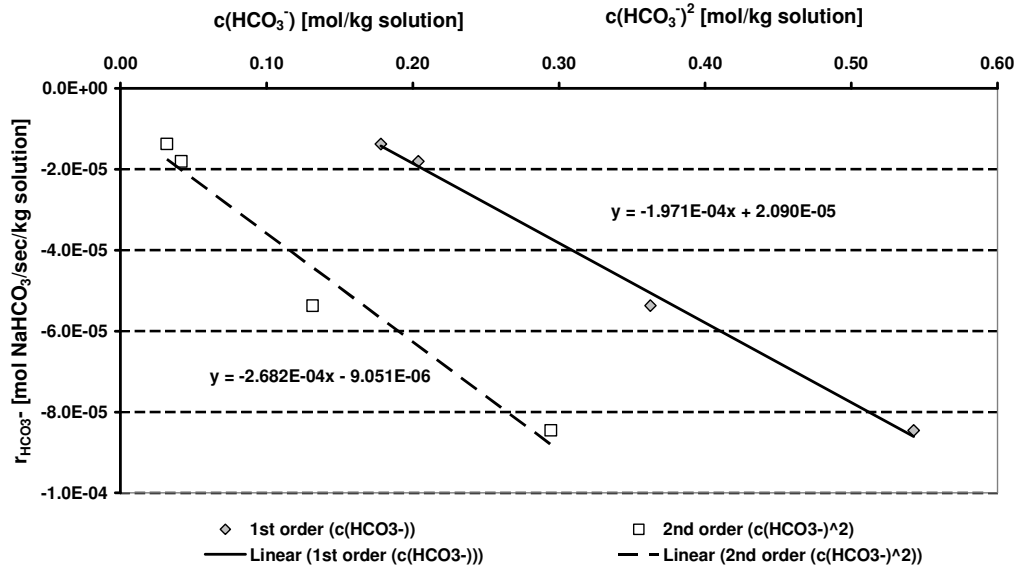


**Figure 3-11:** Reaction rate  $r_{\text{HCO}_3^-}$  vs. concentration  $c(\text{HCO}_3^-)$  plot for decomposition in 90%-w ethylene glycol at 100°C

A bimolecular mechanism, as given in Eq. 17, would imply that the rate of the bicarbonate-forming counter-reaction would depend on the activity of carbonate, carbon dioxide and water, for a total reaction rate of:

$$r_{\text{HCO}_3^-} = -k_1 \cdot a_{\text{HCO}_3^-}^2 + k_2 \cdot a_{\text{CO}_3^{2-}} \cdot a_{\text{CO}_2} \cdot a_{\text{H}_2\text{O}} \quad \text{Eq. 3-18}$$

Neither a significant dependence of the reaction rate on carbonate concentration nor on water activity, i.e. the composition of the mixed solvent, was observed. Therefore, it is most likely, that the monomolecular mechanism of Eq. 6 to 8 is the one, which applies to the decomposition in the mixed solvent – and that Eq. 9 describes the reaction rate in the mixed solvent correctly.

It is also noticeable, that stripping carbon dioxide from the reactor, by bubbling air at a rate of app. 3 litres/hr through the reactor during the whole decomposition period did result in a significant increase of the decomposition rate.

An overview of the third set of experiments is given in Table 2 along with the results for the reaction-rate coefficients of the decomposition reaction and the rates of the counter reaction (bicarbonate formation).

**Table 3-2:** Decomposition experiments and kinetic parameters obtained from the reaction rate – concentration plots for 1<sup>st</sup> order reaction (Eq. 9)

No.	T [°C]	t <sub>exp</sub> [min]	w <sub>EG</sub> [%-w]	k <sub>HCO<sub>3</sub><sup>-</sup></sub> [sec <sup>-1</sup> ]	r <sub>f,HCO<sub>3</sub><sup>-</sup></sub> [mol/kg/sec]	ρ <sub>solid,bulk</sub> [g/ml]	air	sequence of solid phases
0.	80	240	70%	2.07·10 <sup>-4</sup> R <sup>2</sup> = 93.2%	5.91·10 <sup>-5</sup>	na	yes	na
1.	100	899	70%	1.70·10 <sup>-4</sup> R <sup>2</sup> = 88.0%	3.80·10 <sup>-5</sup>	1.18	no	bicarbonate wegscheiderite anhydrate
2.1.	110	450	70%	6.46·10 <sup>-4</sup> R <sup>2</sup> = 88.7%	2.17·10 <sup>-4</sup>	1.03	no	bicarbonate wegscheiderite anhydrate
2.2.	110	185	70%	8.33·10 <sup>-4</sup> R <sup>2</sup> = 99.8%	2.83·10 <sup>-4</sup>	1.04	yes	bicarbonate wegscheiderite anhydrate
3.1.	100	1110	80%	6.83·10 <sup>-5</sup> R <sup>2</sup> = 78.5%	-1.61·10 <sup>-6</sup>	1.44	no	bicarbonate wegscheiderite anhydrate
3.2.	100	290	80%	9.86·10 <sup>-4</sup> R <sup>2</sup> = 93.3%	3.81·10 <sup>-4</sup>	na	yes	bicarbonate wegscheiderite anhydrate
4.1.	110	482	80%	5.94·10 <sup>-4</sup> R <sup>2</sup> = 97.4%	2.00·10 <sup>-4</sup>	0.87	no	bicarbonate wegscheiderite anhydrate
4.2.	110	565	80%	7.06·10 <sup>-4</sup> R <sup>2</sup> = 77.5%	2.07·10 <sup>-4</sup>	na	no	bicarbonate wegscheiderite anhydrate
5.	120	245	80%	1.57·10 <sup>-3</sup> R <sup>2</sup> = 88.2%	5.90·10 <sup>-4</sup>	1.00	no	bicarbonate wegscheiderite anhydrate
6.	100	817	90%	1.97·10 <sup>-4</sup> R <sup>2</sup> = 99.6%	2.09·10 <sup>-5</sup>	1.16	no	bicarbonate wegscheiderite anhydrate
7.1.	110	620	90%	2.45·10 <sup>-4</sup> R <sup>2</sup> = 71.5%	7.22·10 <sup>-5</sup>	0.97	no	bicarbonate wegscheiderite anhydrate
7.2.	110	773	90%	5.35·10 <sup>-4</sup> R <sup>2</sup> = 84.5%	1.86·10 <sup>-4</sup>	Na	yes	bicarbonate wegscheiderite anhydrate
8.1	120	215	90%	3.51·10 <sup>-4</sup> R <sup>2</sup> = 94.2%	8.22·10 <sup>-5</sup>	1.07	no	bicarbonate wegscheiderite anhydrate
8.2	120	265	90%	3.52·10 <sup>-4</sup> R <sup>2</sup> = 50.0%	7.78·10 <sup>-5</sup>	na	no	bicarbonate wegscheiderite anhydrate
9.	130	130	90%	2.78·10 <sup>-4</sup> R <sup>2</sup> = 83.9%	3.71·10 <sup>-5</sup>	0.87	no	bicarbonate anhydrate

The values k<sub>HCO<sub>3</sub><sup>-</sup></sub> and the rates of bicarbonate formation r<sub>f,HCO<sub>3</sub><sup>-</sup></sub>, were derived from the slope and y-intercept in reaction rate vs. concentration plots, similarly to those in Figure

11. The rate coefficient  $k_{\text{HCO}_3^-}$  was obtained as the inclination of the fit-line, while  $r_{f,\text{HCO}_3^-}$  was obtained as the intercept with the y-axis.

$$r_{\text{HCO}_3^-} = -k_{\text{HCO}_3^-} \cdot c_{\text{HCO}_3^-} + r_{f,\text{HCO}_3^-} \quad \text{Eq. 3-19}$$

$$r_{f,\text{HCO}_3^-} = k_f \cdot a_{\text{CO}_2} \cdot a_{\text{OH}^-} \quad \text{Eq. 3-20}$$

Table 2 shows that the highest bulk densities were produced at the lowest temperature (100°C). This was most likely due to the effect, that the (carbonate) supersaturation for the nucleation and growth of the anhydrate was created by the decomposition reaction. For higher temperatures and higher decomposition rates, the higher supersaturation level resulted in significant nucleation and a lower mean particle diameter, which yielded a lower bulk density.

It can be seen from Table 2, that the kinetic coefficient  $k_{\text{HCO}_3^-}$  for 130°C is slightly lower than for 120°C ( $2.8$  vs  $3.5 \times 10^{-4}$ ). This coincides with the observation that the bulk of the bicarbonate in the experiment at 130°C reacted in the first 10 minutes, effectively converting all the *solid* bicarbonate to carbonate.

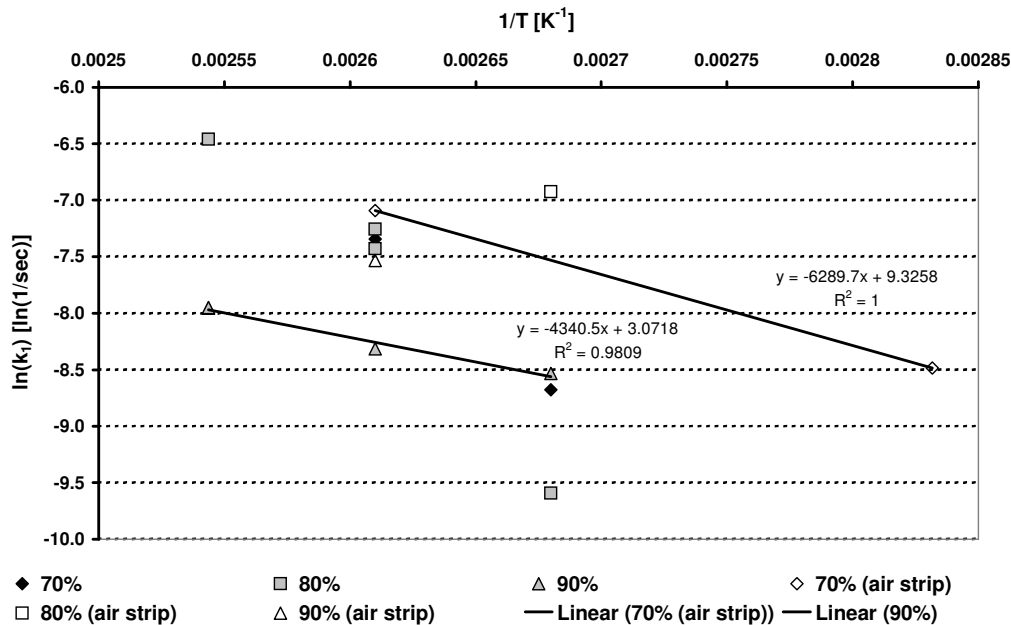


**Figure 3-12:** Arrhenius plot for the rate coefficient  $k_{\text{HCO}_3^-}$  for the decomposition of  $\text{HCO}_3^-$  in the mixed solvent solutions, see Table 2

The dissolved bicarbonate in solution was converted more slowly in the course of the rest of the experimental period. It appears therefore, that at this temperature and mixed solvent composition, the solid-state conversion mechanism of bicarbonate became more favorable than the solution mediated one.

The strong temperature dependence of the reaction is apparent from Table 2 and from Figure 12. Although the observed temperature dependence varies with ethylene glycol content, there is no clear relationship between reaction rate and ethylene glycol content or water activity. The reaction rates in 70 and 80%-w ethylene glycol are almost identical, while the rate in 90%- ethylene glycol appears to be significantly lower - at least for temperatures above 100°C ( $1/T = 0.00268 \text{ K}^{-1}$ ).

Stripping carbon dioxide by air bubbling through the reactor has a strong influence on the reaction rate. The stripping accelerates the reaction in all cases. This indicates, that the slurry in the reactor had increased carbon dioxide levels under non-stripped conditions, which enhanced the counter reaction and slowed down the decomposition. From Table 2, it appears, that the kinetic coefficient  $k_{\text{HCO}_3^-}$  increases under stripped conditions. This kinetic parameter should actually be independent of the reactant concentrations. The observed increase is most probably rather the effect of the decreasing carbon dioxide partial pressure during the non-stripped experiments. I.e. the partial pressure decreases as less carbon dioxide would be formed as the bicarbonate is depleted and the solution composition approaches equilibrium. This would lead in the reaction rate – concentration plots to slightly too low kinetic coefficients  $k_{\text{HCO}_3^-}$  and slightly too low formation reaction rates  $r_{f,\text{HCO}_3^-}$ . While the experimental results show a good reproducibility, compare experiment 4.1 and 4.2 and 8.1 and 8.2, the stripped experiments (0., 2.2, 7.2) should yield more accurate values of  $k_{\text{HCO}_3^-}$  and  $r_{f,\text{HCO}_3^-}$ .

Since the reaction appears to be strongly affected by even slightly increased carbon dioxide levels, it is very likely that more intense stripping can further accelerate the decomposition.

Due to the complex composition of the mixed solvent solution, no activities for carbonate, bicarbonate and hydroxide could be obtained or calculated, so the given  $k_{\text{HCO}_3^-}$  is derived from the concentration instead and does therefore *not directly* correspond to

the reaction rate coefficient  $k_d$ . Therefore, any Arrhenius fit to the given data points could only yield a vague estimation of e.g. the activation energy of the decomposition reaction. The reaction rates in Figure 12 and Table 2 provide nonetheless a good overview of the rates of the bicarbonate decomposition for the tested range of mixed solvent composition (70 to 90%-w ethylene glycol) and temperature (100 to 130°C).

### 3.6. Discussion

On first consideration, it may appear surprising, that the transition temperature for the recrystallization of sodium bicarbonate is constant and independent of the composition of the solvent. It is, after all, a complex function of the solubility and phase stability of the participating sodium carbonate – bicarbonate solid phases, the formation/decomposition equilibrium of bicarbonate and the pH (or rather pOH) of the solution, i.e. the pH-buffer equilibrium of carbonate – bicarbonate.

The solubility of the solid phases is determined by their thermodynamic solubility products ( $K_{sp}$ ), which is only a function of temperature and independent of solution composition:

$$K_{sp,xyz} = a_{Na^+}^{(2x+y)} \cdot a_{CO_3^{2-}}^x \cdot a_{HCO_3^-}^y \cdot a_{H_2O}^z \quad \text{Eq. 3-21}$$

with  $x$ ,  $y$ ,  $z$  representing the stoichiometry of the solid phase, i.e.  $x = 1$ ,  $y = 1$ ,  $z = 2$  for trona ( $Na_2CO_3 \cdot NaHCO_3 \cdot 2H_2O(s)$ ) or  $x = 0$ ,  $y = 1$ ,  $z = 0$  for nahcolite ( $NaHCO_3(s)$ ).

The activity of bicarbonate and carbonate in solution is thus determined by the solid's solubility product, as the dissolution is a much faster reaction than the bicarbonate decomposition. The decomposition equilibrium and the buffer-equilibrium are independent of water activity and are therefore not affected by the mixed solvent composition, but determine in all cases the equilibrium ratio of the activities of carbonate and bicarbonate for a given temperature and carbon dioxide activity. The activity of carbon dioxide in solution should be close to identical to the one in the gas phase, as also the absorption and desorption of carbon dioxide is assumed to occur at a far faster rate than the bicarbonate decomposition, which took several hours. At the equilibrium, the carbon dioxide activity in solution is of course identical to the one in the gas phase.

The transition temperature is therefore only a function of the (atmospheric) carbon dioxide partial pressure and the solubility products of nahcolite and of its ‘successor’ solid phase in the course of the decomposition. And although trona is the ultimately resulting phase for the composition in aqueous solution, while in the mixed solvent solution the ultimately stable solid is sodium carbonate anhydrate (natrite, soda), this successor phase of the recrystallization is in both cases wegscheiderite. With the consequence, that the transition temperature is constant - irrespective of the solvent composition!

For all mixed solvent compositions from 50 to 100%-w ethylene glycol (salt-free base), the same transition temperature of 90°C was observed. This temperature also matches the one identified from literature as the transition point of the aqueous system. This also suggests, that the reaction mechanism in aqueous solution still applies in the mixed solvent system.

From comparison of Table 1 and Table 2, it appears that the reaction proceeds much faster in aqueous solution than in the mixed solvent solution, as  $k_d$  (Table 1) is larger by 3 orders of magnitude than  $k_{\text{HCO}_3^-}$  (Table 2) for 100°C. The actual reaction rate (decomposition rate) differs only by about 2 orders of magnitude between aqueous ( $r_{\text{HCO}_3} \approx 0.03 \text{ mol}\cdot\text{L}^{-1}\cdot\text{s}^{-1}$ ) and mixed solvent ( $r_{\text{HCO}_3} \approx 0.0001 \text{ mol}\cdot\text{L}^{-1}\cdot\text{s}^{-1}$ ) at 100°C. From the presented results, it is not entirely clear, whether this is the effect of the increased carbon dioxide concentration – and the reaction rate in the mixed solvent could be brought to the levels in aqueous solution by sufficient stripping – or an effect of the less polar mixed solvent itself. Based on the degree of increase of the reaction rate in the stripped experiments, it is more likely, that the later is the case.

### **3.7. Conclusions**

1. Unlike the recrystallization of trona (see Gärtner et al. [51]), the nahcolite recrystallization is purely caused by the bicarbonate decomposition and proceeds entirely solution mediated from 90 till app. 130°C.
2. The decomposition initiates the recrystallization of solid bicarbonate (nahcolite) independent of the water activity at around 90°C, which coincides with observations

of other authors made for aqueous solution. The produced, stable solid phase of the recrystallization in the mixed solvent is sodium carbonate anhydrate (soda, natrite), while in aqueous solution it is trona (sodium sesquicarbonate).

3. The solubility of nahcolite ( $\text{NaHCO}_3(\text{s})$ ) reached a minimum around 80 to 90%w ethylene glycol and increased again significantly in pure ethylene glycol. The solubility increased significantly with temperature irrespective of ethylene glycol content.
4. The recrystallization of sodium bicarbonate to sodium carbonate (anhydrate) in the mixed solvent was found to proceed via wegscheiderite as intermediate phase, except at increased temperatures of 130°C and higher, where no intermediate phase was formed.
5. The decomposition rate was measured over the range of 70 to 90%-w (salt-free base) ethylene glycol and of 100 to 130°C. From the obtained kinetic data, the first order mechanism observed for decomposition in aqueous solution was also confirmed for the mixed solvent solution.

### 3.8. Notation

$A_\phi$	: Debye Hückel coefficient	[-]
$a_i$	: activity coefficient of species i	[-]
$B_{ij}$	: Pitzer binary interaction parameter for the species i and j	[-]
$B_{ij}^\phi$	: Pitzer binary interaction parameter for the osmotic coefficient	[-]
$C_{ij}$	: Pitzer binary interaction parameter for the species i and j	[-]
$c_i$	: concentration of species i	[mol/kg solution]
$E_i$	: activation energy of the reaction I	[J/mol]
$f_i$	: fugacity of species i	[-]
$I$	: ionic strength	[mol/kg solvent]
$K_{\text{CO}_3}$	: equilibrium constant for 2 <sup>nd</sup> deprotonation of $\text{H}_2\text{CO}_3$	[-]
$K_{\text{sp}}$	: thermodynamic solubility product	[-]
$K_{\text{R}}$	: equilibrium constant of $\text{HCO}_3^-$ decomposition	[-]
$K_{\text{w}}$	: equilibrium constant of water self dissociation	[-]



$k$	: concentration base kinetic coefficient	[1/sec]
$k_i$	: activity based kinetic coefficient	[mol·L <sup>-1</sup> ·s <sup>-1</sup> ]
$k_{i,0}$	: pre-exponential kinetic rate factor	[mol·L <sup>-1</sup> ·s <sup>-1</sup> ]
$k_d$	: kinetic coefficient of the decomposition reaction	[mol·L <sup>-1</sup> ·s <sup>-1</sup> ]
$k_f$	: kinetic coefficient of the formation reaction	[mol·L <sup>-1</sup> ·s <sup>-1</sup> ]
$k_1$	: 2 <sup>nd</sup> order kinetic coefficient decomposition reaction	[mol/s/kg solution]
$k_2$	: 2 <sup>nd</sup> order kinetic coefficient formation reaction	[mol/s/kg solution]
$k_{\text{HCO}_3^-}$	: kinetic coefficient of decomposition in mixed solvent	[mol/s/kg solution]
$M_i$	: molar mass of compound i	[g/mol]
$m$	: mass	[g]
$m_i$	: molal concentration of species i (in Pitzer model only)	[mol/kg solvent]
$n_i$	: mol number of species i	[mol]
$p_i$	: partial pressure of compound i	[Pa]
$p_0$	: atmospheric pressure (101,325 Pa)	[Pa]
$R$	: gas constant (8.3144 J/mol/K)	[J/mol/K]
$r$	: reaction rate	[mol/s/L] or [mol/s/kg solution]
$T$	: temperature	[K]
$t$	: time	[s]
$V$	: volume	[ml]
$w_i$	: mass fraction of component i	[g/g]
$Z$	: charge density	[mol/kg solvent]
$z_i$	: charge of species i	[-]
$\gamma_i$	: activity coefficient of species i	[-]
$\Delta H_R$	: enthalpy of reaction	[kJ/mol]
$\Delta G_R$	: Gibbs free energy of reaction	[kJ/mol]
$\rho$	: density	[g/ml]

### 3.8.1. Indices

aq : in aqueous solution

- g : in gaseous state  
l : in liquid state  
s : in solid state  
0 : initial conditions

### **3.9. Literature References**

- [1] Ch. Thieme, "sodium hydrogen carbonate" in Ullmann's Encyclopedia of Chemical Technology, 6<sup>th</sup> ed., 2000, electronic release, Wiley-VCH
- [2] Garret, D.E., "Natural Soda Ash – Occurrences, Processing, And Use", Van Nostrand Reinhold (publ.), New York 1991, p. 364-382
- [3] Splittgerber, A., "Zerfall von Natriumbikarbonat in wässriger Lösung", Vom Wasser, Vol. 8, 1934, p. 173-177
- [4] Stumper, R., "Untersuchung über Dynamik und Katalyse der thermischen Bicarbonatzersetzung in wässriger Lösung", Zeitschr. Anorg. Allgem. Chem., No. 210, 1933, p. 264-268
- [5] Tsuchiya, R., "Decomposition of bicarbonates. I. Decomposition velocity of sodium bicarbonate in an aqueous solution containing free carbon dioxide", J. Chem. Soc. Japan, Pure Chem. Sect., Vol. 74, 1953, p. 12-16
- [6] Morgunov, A.N., Perchenko, A.A., "Dissociation kinetics of sodium bicarbonate in aqueous solutions", Maslo-Zhir. Prom-st., Vol. 12, 1975, p. 20-22
- [7] DuMaire, M., Gmelins Handbuch der Anorganischen Chemie, 8<sup>th</sup> ed., Number 21: "Natrium", Verlag Chemie, Leipzig, 1928, p. 730
- [8] European Patent Application, EP 85-201753 19851029, T.J.M. van Lotringen, G. van den Berg, AKZO N.V., The Netherlands, 1987
- [9] Gärtner, R.S., Witkamp, G.J., "Wet Calcining of Trona (Sodium Sesquicarbonate) and Bicarbonate", J. Crystal Growth, Vol. 237-239, (2002), p. 2199-2204
- [10] Oosterhof, H., Witkamp, G.J., van Rosmalen, G.M., "Evaporative Crystallization of Anhydrous Sodium Carbonate at Atmospheric Conditions", AIChE J., 47(10), 2001, p. 2220-2225
- [11] Oosterhof, H., de Graauw, J., Witkamp, G.J., van Rosmalen, G.M., "Continuous Double Recrystallization of Light Soda Ash into Super Dense Soda Ash", Crystal Growth & Design, Vol. 2, No. 2, 2002, p. 151

- [12] Oosterhof, H., Witkamp, G.J., van Rosmalen, G.M., "Antisolvent Crystallization of Anhydrous Sodium Carbonate at Atmospheric Conditions", *AIChE J.*, 47(3), 2001, p. 602-608
- [13] Oosterhof, H., de Graauw, J., Witkamp, G.J., van Rosmalen, G.M., "Process for the production of sodium carbonate anhydrate", European and US Patent application, 1998
- [14] Weingaertner, D.A., Lynn, S., Hanson, D.N., "Extractive crystallization of salts from concentrated aqueous solution", *Ind. Eng. Chem. Res.*, Vol. 30, 1991, p. 490-501
- [15] Ifrim, L., Calistru, C., "Macrokinetics of  $\text{NaHCO}_3$  Thermal Decomposition", *Buletinul Institutului Politehnic din Iași, Secția II: Chimie*, Vol. 19(1-2), 1973, p. 51-57
- [16] Ball, M.C., Snelling, Ch.M., Strachan, A.N., Strachan, R.M., "Thermal Decomposition of Solid Sodium Bicarbonate", *J. Chem. Soc. Faraday Trans. 1*, 82, 1986, p. 3709-3715
- [17] Ball, M.C., Snelling, Ch.M., Strachan, A.N., Strachan, R.M., "Thermal Decomposition of Solid Sodium Sesquicarbonate,  $\text{Na}_2\text{CO}_3 \cdot \text{NaHCO}_3 \cdot 2\text{H}_2\text{O}$ ", *J. Chem. Soc. Faraday Trans.*, 88(4), 1992, p. 631-636
- [18] Kuu, W.Y., Chilamkuri, R., Chen, C., "Effect of relative humidity and temperature on moisture sorption and stability of sodium bicarbonate powder", *Int. J. Pharmaceutics*, 166, 1998, p. 161-175
- [19] Bramford, C.H., Tipper, C.H.F., "Comprehensive Chemical Kinetics, Vol. 22: Reactions in the Solid State", Elsevier, Amsterdam, 1980, pp. 41-113
- [20] Hu, W., Smith, J.M., Doğu, T., Doğu, G., "Kinetics of Sodium Bicarbonate Decomposition", *AIChE J.*, 32 (9), 1986, p. 1483-1490
- [21] Wu, Y. L., Shih, S. M., "Intrinsic kinetics of the thermal decomposition of sodium bicarbonate", *Thermochimica Acta*, 223, 1993, p. 177-186
- [22] Heda, P. K., Dollimore, D., Alexander, K.S., Chen, D., Law, E., Bicknell, P., "A method of assessing solid state reactivity illustrated by thermal decomposition experiments on sodium bicarbonate", *Thermochimica Acta*, 255, 1995, p. 255-272
- [23] Vanderzee, C.E., "Thermodynamic relations and equilibria in  $(\text{Na}_2\text{CO}_3 + \text{NaHCO}_3 + \text{H}_2\text{O})$ : standard Gibbs energies of formation and other properties of sodium hydrogen carbonate, sodium carbonate heptahydrate, sodium carbonate decahydrate, trona:  $(\text{Na}_2\text{CO}_3 \cdot \text{NaHCO}_3 \cdot 2\text{H}_2\text{O})$ , and Wegscheider's salt:  $(\text{Na}_2\text{CO}_3 \cdot 3\text{NaHCO}_3)$ ", *J. Chem. Thermodynamics*, 14, 1982, p. 219-238
- [24] Keener, T.C., Frazier, G.C., Davis, W.T., "Thermal Decomposition of Sodium Bicarbonate", *Chem. Eng. Commun.*, 33, 1985, p. 93-105

- [25] Tanaka, H., Takemoto, H., "Significance of the Kinetics of Thermal Decomposition of  $\text{NaHCO}_3$  Evaluated by Thermal Analysis", *J. Thermal Anal.*, 38 (3), 1992, p. 429-435
- [26] Vanderzee, C.E., Berg, R.L., "Thermodynamics of carbon dioxide and carbonic acid: (a) the standard enthalpies of solution of  $\text{Na}_2\text{CO}_3(\text{s})$ ,  $\text{NaHCO}_3(\text{s})$ , and  $\text{CO}_2(\text{g})$  in water at 298.15 K; (b) the standard enthalpies of formation, and standard entropies of  $\text{CO}_2(\text{aq})$ ,  $\text{HCO}_3^-(\text{aq})$ ,  $\text{NaHCO}_3(\text{s})$ ,  $\text{Na}_2\text{CO}_3(\text{s})$ ,  $\text{Na}_2\text{CO}_3 \cdot \text{H}_2\text{O}(\text{s})$ , and  $\text{Na}_2\text{CO}_3 \cdot 10\text{H}_2\text{O}(\text{s})$ ", *J. Chem. Thermodynamics*, 10, 1978, p. 1113-1136
- [27] Chase et al., NIST Chemistry webbook, National Institute of Standards, 2003, <http://webbook.nist.gov/chemistry/>
- [28] Markus, Y., "Ion Properties", Marcel Dekker, New York, 1997
- [29] Lide, D. R. (Editor), Handbook of Chemistry and Physics, CRC Press, Boca Raton, 1994, table 5.2-5.3
- [30] Himmelblau, D.M., Babb, A.L., "Kinetic Studies of Carbonation Reactions Using Radioactive Tracers", *AIChE J.*, 4(2), 1958, p. 143-152
- [31] Mai, K.L., Babb, A.L., "Vapor-Liquid Equilibria by Radioactive Tracer Techniques", *Ind. Eng. Chem.*, 47(9), 1955, p. 1749-1757
- [32] Harned, H.S., Bonner, F.T., "The First Ionization of Carbonic Acid in Aqueous Solutions of Sodium Chloride", *J. Amer. Chem. Soc.*, 67, 1945, p. 1026-1031
- [33] Harned, H.S., Davis, R., J. "The Ionization Constant of Carbonic Acid in Water and the Solubility of Carbon Dioxide in Water and Aqueous Salt Solutions from 0 to 50°C", *Amer. Chem. Soc.*, 65, 1943, p. 2030-2037
- [34] Oelkers, E. C., Helgeson, H. C., Shock, E. L., Sverjensky, D. A., Johnson, J. W., Pokrovskii, V. A., "Summary of the Apparent Molal Gibbs Free Energies of Formation of Aqueous Species, Minerals, and Gases at Pressures 1 to 5000 Bars and Temperatures 25 to 100°C", *J. Phys. Chem. Ref. Data*, 24, 1995, p. 1401-1560
- [35] Butler, J.N., "Carbon Dioxide Equilibria and their Applications", Lewis Publ., Chelsea, Michigan, 1991, p. 15-43
- [36] Garret, D.E.: "Natural Soda Ash – Occurrences, Processing, And Use", Van Nostrand Reinhold (publ.), New York 1991, p. 565
- [37] Seidell, A., "Solubilities of Inorganic and Metal Organic Compounds", Vol. I, Van Nostrand, New York, 1940, p. 1193-1200
- [38] Pitzer, K. S., "Activity Coefficients in Electrolyte Solutions, 2<sup>nd</sup> ed.", CRC Press: Boca Raton (Florida), 1991

- [39] Haynes, H.W. Jr., DeFilippis, P., “An Equation of State for Trona Brines”, Proceedings XXI International Mineral Processing Congress, Rome, 2000, B10-9 – B10-15
- [40] Haynes, H.W., “A Thermodynamic Solution Model for Trona Brines”, *AIChE J.*, 49 (7), 2003, p. 1883-1894
- [41] Gärtner, R.S., Seckler, M.M., Witkamp, G.J., “Solid Phases and Their Solubilities in the System  $\text{Na}_2\text{CO}_3 - \text{NaHCO}_3 - \text{Ethylene Glycol} - \text{Water}$  from (50 to 90) °C”, *J. Chem. Eng. Data*, 49(1), p. 116-125
- [42] Kloosterman, E.G., de Vries, S.M., Kalsbeek, H., Drinkenburg, B., “Influence of Ionic Strength on the Absorption of  $\text{CO}_2$  in Carbonate/Bicarbonate Buffer Solutions”, *Ind. Eng. Chem. Res.*, 26, 1987, p. 2216-2222
- [43] Danckwerts, P.V., Roberts, D., “Kinetics of  $\text{CO}_2$  absorption in alkaline solutions – I, Transient absorption rates and catalysis by arsenite”, *Chem. Eng. Sci.*, 17, 1962, p. 961-969
- [44] Roughton, F.J.W., Pinsent, B.R.W., Pearson, L., “The Kinetics of Combination of Carbon Dioxide with Hydroxide Ions”, *Trans. Faraday Soc.*, 52, 1956, p. 1512-1520
- [45] Roughton, F.J.W., Pinsent, B.R.W., “The Kinetics of Combination of Carbon Dioxide with Water and Hydroxide Ions”, *Trans. Faraday Soc.*, 47, 1951, p. 263-269
- [46] Roughton, F.J.W., Booth, V.H., “CCLXVI. The Catalytic Effect of Buffers on the Reaction  $\text{CO}_2 + \text{H}_2\text{O} \rightleftharpoons \text{H}_2\text{CO}_3$ ”, *Biochem. J.*, 32, 1938, p. 2049-2069
- [47] Pohorecki, R., Kucharski, E., “Desorption with chemical reaction in the system  $\text{CO}_2$ -aqueous solution of potassium carbonate”, *Chem. Eng. J.*, 46, 1991, p. 1-7
- [48] Pohorecki, R., Moniuk, W., “Kinetics of Reaction between Carbon Dioxide and Hydroxyl Ions in Aqueous Electrolyte Solutions”, *Chem. Eng. Sci.*, 43(7), p. 1677-1684
- [49] Zavitsas, A.A., “Properties of Water Solutions of Electrolytes and Nonelectrolytes”, *J. Phys. Chem. B*, Vol. 105, 2001, p. 7805-7817
- [50] Vanderzee, C.E., 1982, “Thermodynamic relations and equilibria in ( $\text{Na}_2\text{CO}_3 + \text{NaHCO}_3 + \text{H}_2\text{O}$ ): standard Gibbs energies of formation and other properties of sodium hydrogen carbonate, sodium carbonate heptahydrate, sodium carbonate decahydrate, trona: ( $\text{Na}_2\text{CO}_3 \cdot \text{NaHCO}_3 \cdot 2\text{H}_2\text{O}$ ), and Wegscheider’s salt ( $\text{Na}_2\text{CO}_3 \cdot 3\text{NaHCO}_3$ )”, *J. Chem. Thermodynamics*, 14, p. 219-238
- [51] Gärtner, R.S., Witkamp, G.J., “Recrystallization of Trona (Sodium Sesquicarbonate) into Soda (Sodium Carbonate Anhydrate) in a Mixed Solvent, Part I: Fundamental Conversion Steps”, submitted for publication to *AIChE Journal* (Chapter 4)

- [52] Ball, M.C., Strachan, A.N., Strachan, R. M., “Thermal Decomposition of Solid Wegscheiderite,  $\text{Na}_2\text{CO}_3 \cdot 3\text{NaHCO}_3$ ”, J. Chem. Soc. Faraday Trans., 187(12), 1991, p. 1911-1914
- [53] Barral, E.M., Rogers, L.B., “Differential Thermal Analysis of the Decomposition of Sodium Bicarbonate and its Simple Double Salts”, J. Inorg. Nucl. Chem., 1966, 28, 1966, p. 41-51

### 3.10. Addendum

#### 3.10.1. Calculation of the Equilibrium Concentrations in Aqueous Solution

The equilibrium concentrations of carbonate and bicarbonate for free absorption and desorption of atmospheric carbon dioxide and for the solution in contact with the respective stable solid phase (salt) of the system (see Eq. 6 and Eq. 11) are of special interest to this work, as the recrystallization of  $\text{Na}_2\text{CO}_3\text{-NaHCO}_3$  slurries is studied here. The equilibrium concentrations determine, whether a given salt is thermodynamically stable in solution – or whether the salt will recrystallize over time due to solution mediated bicarbonate formation / decomposition and carbon dioxide absorption / desorption. As these equilibrium concentrations were not readily available from literature, they have been calculated from reaction, electrolyte activity and solubility data under the following assumptions:

The dissolved carbon dioxide has to be in equilibrium with the gas phase, i.e. with the atmospheric carbon dioxide partial pressure ( $= 10^{-3.5}\text{atm} = 3.16 \cdot 10^{-4}\text{atm}$  [35]). The activity of carbon dioxide in solution is equal to the activity in the gas phase:

$$a_{\text{CO}_2, \text{aq}} = a_{\text{CO}_2, \text{g}} = \frac{f_{\text{CO}_2, \text{g}}}{f_{\text{CO}_2}^0} \approx \frac{p_{\text{CO}_2, \text{g}}}{p_0} = 10^{-3.5} \quad \text{Eq. 3-22}$$

The activity of the hydroxide ion in solution is determined by the buffer-equilibrium between carbonate and bicarbonate (bicarbonate dissociation):

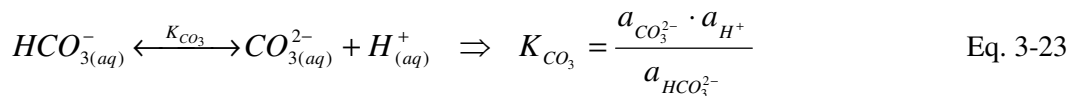
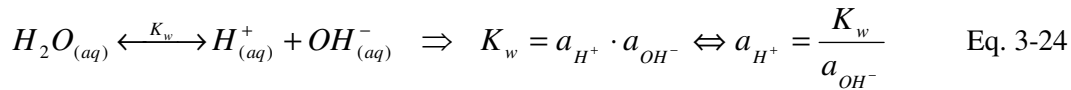


**Table 3-3:** Self dissociation constants  $pK_w$  and  $pK_{CO_3}$  for 10 to 150°C [35]

T [°C]	$pK_w$ [-]	$pK_{CO_3}$ [-]
10	14.54	10.49
15	14.337	10.43
20	14.161	10.377
25	13.999	10.329
30	13.833	10.29
35	13.676	10.25
40	13.533	10.22
50	13.263	10.172
100	12.27	10.16
150	11.64	10.33



The two relations above yield:

$$K_{CO_3} = \frac{a_{CO_3^{2-}} \cdot K_w}{a_{HCO_3^-} \cdot a_{OH^-}} \Leftrightarrow a_{OH^-} = \frac{a_{CO_3^{2-}} \cdot K_w}{a_{HCO_3^-} \cdot K_{CO_3}} \quad \text{Eq. 3-25}$$

This relationship is used to estimate the hydroxide activity from the activities of carbonate and bicarbonate at the decomposition / formation equilibrium (Eq. 6) and the dissociation constants  $K_w$  and  $K_{CO_3}$  at the respective temperature. These dissociation constants were taken from Butler [35], see the Table 3.

The equilibria were calculated for solutions in contact (i.e. in solubility equilibrium) with the stable solid phase of the  $Na_2CO_3$ - $NaHCO_3$ - $H_2O$  system. The solubility concentrations were taken from Garret [36] and Seidell and Linke [37]. The activities of the carbonate and bicarbonate in solution were calculated according to the Pitzer electrolyte activity model [38]:

In the Pitzer electrolyte model, the activity coefficient ( $\gamma_i$ ) of any ion in solution is expressed by a virial expansion function of terms representing the interaction of this ion

with every other ion in solution. An expression for the osmotic coefficient ( $\phi$ ) is also provided in a similar fashion. The expressions, in a summarized form, are:

$$\ln(\gamma_i) = -z_i^2 \cdot A_\phi \cdot f(I) + \sum_j m_j (2B_{ij} + Z \cdot C_{ij}) + |z_i| \cdot \sum_c \sum_a m_c \cdot m_a \cdot C_{ca} \quad \text{Eq. 3-26}$$

$$\phi = 1 + \frac{2}{\sum_i m_i} \cdot \left[ -A_\phi \cdot I \cdot f(I) + \sum_c \sum_a m_c \cdot m_a \cdot (B_{ca}^\phi + Z \cdot C_{ca}) \right] \quad \text{Eq. 3-27}$$

$$f(I) = \left[ \frac{I^{0.5}}{1 + b \cdot I^{0.5}} + \frac{2}{b} \cdot \ln(1 + b \cdot I^{0.5}) \right] \quad \text{Eq. 3-28}$$

$$Z = \sum_i m_i \cdot |z_i| \quad \text{Eq. 3-29}$$

where  $m_i$  represents the molalities of the ions in solution,  $m_j$  the molalities of their possible counter-ions, and  $m_a$  and  $m_c$  the molalities of the anions and cations, respectively.  $b$  is a universal parameter with a value of  $1.2 \text{ (kg/mol)}^{0.5}$ .  $I$  is the ionic strength of the solution,  $A_\phi$  is the Debye-Hückel-parameter,  $z_i$  the charge of the ion species  $i$ , and  $B_{ij}$  and  $C_{ij}$  (i.e.  $C_{ca}$ ) species-dependent binary interaction parameters.  $B_{ca}^\phi$  is the species-dependent binary interaction parameter for the osmotic coefficient. For the activity calculations, the interaction parameter sets of Pitzer et al. [38] as well as those of Haynes et al. [39, 40] were used.

From the respective solubility concentrations, the activities calculated with the Pitzer model, the fixed carbon dioxide activity and Eq. 30, which was obtained from Eq. 11 and Eq. 25, the equilibrium concentrations were calculated iteratively:

$$K_R = \frac{a_{CO_2} \cdot a_{CO_3^{2-}}}{(a_{HCO_3^-})^2} \cdot \frac{K_w}{K_{CO_3}} \Leftrightarrow \frac{K_R \cdot K_{CO_3}}{K_w \cdot a_{CO_2}} = \frac{a_{CO_3^{2-}}}{(a_{HCO_3^-})^2} \quad \text{Eq. 3-30}$$

The  $K_R$  values used for these calculations were obtained from a large array of thermodynamic data to achieve a high accuracy, and the fit of Eq. 12 reproduces these values with a correlation factor of 99.97%. The following relationship reproduces the employed  $K_R$  values exactly (i.e. accurately beyond the limit of these values' own uncertainty):



$$\ln(K_R) = 3.0385636 + \frac{-3.3249984 \cdot 10^4 K}{T} + \frac{8.8933939 \cdot 10^6 K^2}{T^2} + \frac{-9.6945289 \cdot 10^8 K^3}{T^3} \quad \text{Eq. 3-31}$$

### 3.10.2. Solubility of Nahcolite (NaHCO<sub>3</sub>(s)) in the Mixed Solvents

**Table 3-4:** Solubility of nahcolite (NaHCO<sub>3</sub>(s)) in ethylene glycol – water mixed solvents

w <sub>EG</sub> :	50%w	60%w	70%w	80%w	90%w	100%w
T [°C]	c(NaHCO <sub>3</sub> ) [g/kg solution]	c(NaHCO <sub>3</sub> ) [g/kg solution]	c(NaHCO <sub>3</sub> ) [g/kg solution]	c(NaHCO <sub>3</sub> ) [g/kg solution]	c(NaHCO <sub>3</sub> ) [g/kg solution]	c(NaHCO <sub>3</sub> ) [g/kg solution]
15	45.79 +/- 7.35	39.08 +/- 1.06	33.36 +/- 0.20	33.96 +/- 2.41	41.02 +/- 1.10	95.05 +/- 10.97
50	58.82 +/- 0.30	47.53 +/- 0.14	41.20 +/- 0.17	37.69 +/- 0.02	38.98 +/- 0.14	62.86 +/- 0.37
60	66.053 +/- 0.22	53.98 +/- 0.04	45.80 +/- 0.08	42.34 +/- 1.05	40.39 +/- 0.59	62.02 +/- 2.76
70	74.03 +/- 0.09	60.94 +/- 0.61	50.77 +/- 0.25	46.71 +/- 0.57	45.18 +/- 0.14	76.11 +/- 2.94
80	84.04 +/- 0.52	69.06 +/- 0.63	57.99 +/- 0.05	51.55 +/- 0.43	49.89 +/- 0.55	85.75 +/- 0.60
90	96.83 +/- 0.59	77.45 +/- 1.53	65.70 +/- 0.20	57.36 +/- 0.38	55.62 +/- 1.15	95.44 +/- 2.08

### 3.10.3. Heating-Weight-Loss-Analysis for Solid Phase Carbonate-Bicarbonate

As described in the introduction to this chapter, sodium bicarbonate will thermally decompose in the solid state to sodium carbonate. This conversion can be used to quantify the bicarbonate content in a solid sample, provided, that it is known, that either the sample only contains sodium bicarbonate and carbonate or the other compounds of the sample are known and thermally stable. Mixed phases of carbonate and bicarbonate like wegscheiderite and trona can also be identified by this method, since their bicarbonate content decomposes similarly to solid sodium bicarbonate [17, 52, 53] and

the crystal water content of trona desorbs even faster than its bicarbonate content decomposes.

The crystal phase present in a sample can be identified from its specific heating weight loss:

$$x_{loss} = \frac{m_{start} - m_{end}}{m_{start}} \quad [\text{g/g}] \quad \text{Eq. 3-32}$$

for pure solid sodium bicarbonate:

$$x_{NaHCO_3} = \frac{M_{CO_2} + M_{H_2O}}{2M_{NaHCO_3}} = 0.3692 \quad [\text{g/g}] \quad \text{Eq. 3-33}$$

for wegscheiderite:

$$x_{Na_2CO_3 \cdot 3NaHCO_3} = \frac{3M_{CO_2} + 3M_{H_2O}}{2M_{Na_2CO_3 \cdot 3NaHCO_3}} = 0.2599 \quad [\text{g/g}] \quad \text{Eq. 3-34}$$

for sodium carbonate anhydrate

$$x_{Na_2CO_3} = 0 \quad [\text{g/g}] \quad \text{Eq. 3-35}$$

The degree of conversion in only partially recrystallized samples, i.e. when e.g. both solid bicarbonate and solid wegscheiderite were present, was calculated as follows:

1. The weight loss  $x$  of a sample containing a weight fraction of  $w_b$  bicarbonate, while the rest has recrystallized to wegscheiderite, can be calculated by:

$$x = w_b \cdot x_{NaHCO_3} + (1 - w_b) \cdot x_{Na_2CO_3 \cdot 3NaHCO_3} \quad [\text{g/g}] \quad \text{Eq. 3-36}$$

Therefore, the weight fraction bicarbonate can be calculated as:

$$w_b = \frac{x - x_{Na_2CO_3 \cdot 3NaHCO_3}}{x_{Na_2CO_3} - x_{Na_2CO_3 \cdot 3NaHCO_3}} \quad [\text{g/g}] \quad \text{Eq. 3-37}$$

2. Similarly, the weight fraction wegscheiderite  $w_w$  in a sample, that has partially recrystallized to anhydrate, can be calculated from its heating weight loss:

$$w_w = \frac{x - x_{Na_2CO_3}}{x_{Na_2CO_3 \cdot 3NaHCO_3} - x_{Na_2CO_3}} = \frac{x}{x_{Na_2CO_3 \cdot 3NaHCO_3}} \quad [\text{g/g}] \quad \text{Eq. 3-38}$$

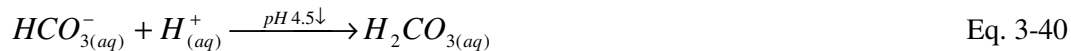
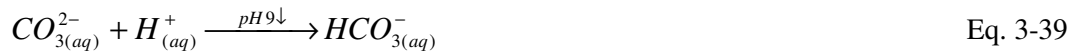
The identification of a crystal phase was of course not based on the weight loss of a sample, but also from light microscope, SEM images and powder XRD. The weight loss analysis was primarily employed in this research to determine the degree of conversion for a great amount of samples, once the reaction path and the occurring crystal phases had been established by the previously mentioned techniques.

To eliminate errors of weight loss from evaporation of adhering liquid (i.e. acetone as washing liquid during filtration), the samples were heated in a 2-stage program. First at least 3 min. at 60°C to evaporate adhering moisture and then at least 5 min. at 200°C to decompose the bicarbonate. The Moisture Analyzer was set to keep the samples at constant temperature at each stage, till the sample showed constant weight. Due to the short exposure times, no solid-state bicarbonate decomposition would occur at 60°C.

The reproducibility of this method was found to depend strongly on sample morphology. For samples of very fine crystallites, the first stage would not completely remove adhering moisture due to retention by capillary forces. Too high weight losses would be obtained in the second stage. In these experiments this effect occurred only with a few wegscheiderite-containing samples and the general accuracy of the weight loss analysis was found to be ca. 0.5% weight loss, i.e. 2-5% error in the calculated weight fraction.

#### 3.10.4. Automated pH Titration for Dissolved Carbonate-Bicarbonate

Sodium carbonate-bicarbonate forms a buffer system, as under addition of a strong acid like HCl, first carbonate ions will be protonated to bicarbonate ions, while under continuing addition of acid beyond the complete protonation of carbonate, bicarbonate will be protonated to carbonic acid. Carbonic acid dissociates into water and carbon dioxide, which usually quickly desorbs from solution, when its saturation concentration (for the ambient CO<sub>2</sub> partial pressure) is exceeded.



For the titration a sample of 0.5 to 1 ml of the filtered test solution was taken, the weight of the sample determined and diluted with app. 10 ml of ultra pure water. This solution was then titrated with 0.1 M HCl (Merck Titriplex) while being stirred by a magnetic stirrer. The pH of the solution was continuously measured by a Radiometer glass pH electrode and recorded by the Radiometer VIT 90 Videotitrator. The derivative curve of pH-volume HCl titration was automatically calculated to gain the inflexion (buffer) points of the pH titration. At the first inflexion point,  $V(\text{CO}_3^{2-})$ , the carbonate content of the sample has been completely protonated to bicarbonate, see Eq. 39, while at the second inflection point,  $V(\text{CO}_3^{2-}+\text{HCO}_3^-)$ , the bicarbonate in the sample has been quantitatively converted to carbonic acid, which of course then dissociates to  $\text{CO}_2$  and water, see Eq. 41. The formation of  $\text{CO}_2$  becomes actually apparent, immediately after the first inflexion point is reached, as gas bubbles spontaneously from the solution. The accuracy of this method and the used equipment was tested every day prior to the actual experimental samples with calibration solutions, prepared from analytical grade solid sodium bicarbonate or solid sodium carbonate and ultra pure water. The reproducibility was found to be in the range of 0.5 to 2.5% of the measured concentration.

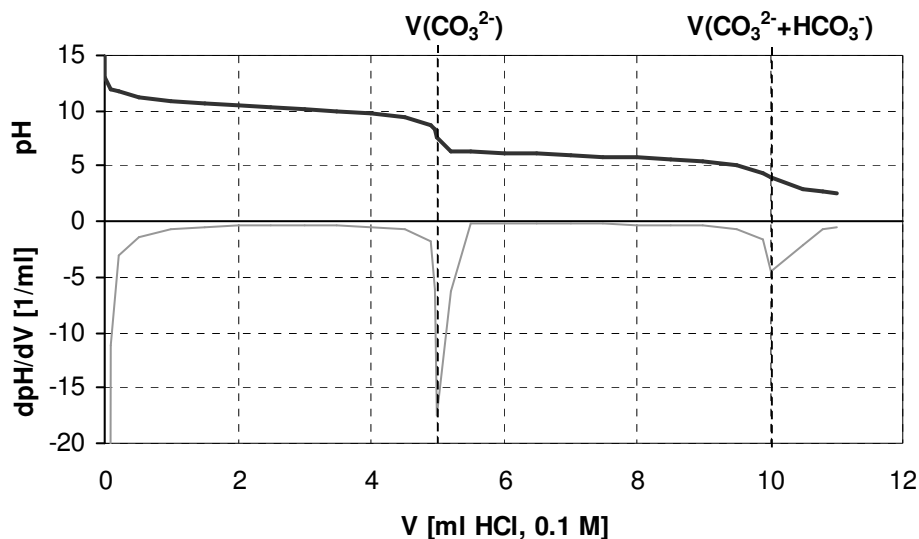


**Figure 3-13:** pH-Titration curve for the determination of  $[\text{CO}_3^{2-}]$  and  $[\text{HCO}_3^-]$

All titrations were performed in triplicate and the amount of sample was chosen for  $V(\text{CO}_3^{2-} + \text{HCO}_3^-) \geq 5 \text{ ml HCl}$  to achieve good resolution with the titration. Significantly higher deviations were found with the solubility of bicarbonate in pure ethylene glycol. These deviations rather seem to stem from differences in the triplicate samples. Most likely minute amounts of water (most likely as steam or droplets from the shaking bath adhering to the cap of the sample bottles) got into the samples. In case of the other, i.e. water containing, samples these tiny amounts would show no significant influence. But in case of the hygroscopic pure ethylene glycol and the strong dependency of bicarbonate solubility on the water content between 90%w and 100%w (salt-free base) ethylene glycol, these small amounts would be sufficient to cause the given deviations in the results.

### **3.10.5. Mass Balance in the Decomposition Experiments**

In the last set of experiments, the decomposition rate of bicarbonate was determined from the decrease of its total content, i.e. the amount contained in the solid as well as in the solution. This decrease could therefore only be calculated. The concentration of bicarbonate in the solid,  $[\text{NaHCO}_3]_{(s)}$ , which would be present as sodium bicarbonate crystals,  $\text{NaHCO}_{3(s)}$ , and/or as component of wegscheiderite crystals,  $\text{Na}_2\text{CO}_3 \cdot 3\text{NaHCO}_{3(s)}$ , was determined from the weight loss during heating (Denver Instruments Mark II). Since the solids were entirely composed of sodium carbonate and sodium bicarbonate, the remaining fraction of the solid would then be the content of sodium carbonate in the solid,  $[\text{Na}_2\text{CO}_3]_{(s)}$ , since no hydrates were formed in these experiments and no other crystallizing compounds were present.

The concentration of carbonate,  $[\text{CO}_3^{2-}]$ , and bicarbonate,  $[\text{HCO}_3^-]$ , in the solution was measured by titration.

The amount of mixed solvent in the system was known from the start of the experiment. It was assumed that this amount was not affected by evaporation since the vapor escaping from the reactor was fed back by reflux cooling, see Figure 14.

The amount of solid in the reactor could not be measured with sufficient accuracy and was therefore calculated from the starting amount of sodium bicarbonate,  $\text{NaHCO}_3(\text{s})$ , added to the reactor and the mass balance of the system:

From  $[\text{HCO}_3^-]$  and  $[\text{CO}_3^{2-}]$  and the amount of mixed solvent, the amount of carbonate and bicarbonate in solution was calculated by solving the following set of equations:

$$m_{\text{Solution}} = m_{\text{Solvent}} + m_{\text{NaHCO}_3,\text{sol}} + m_{\text{Na}_2\text{CO}_3,\text{sol}} \quad \text{Eq. 3-43}$$

$$m_{\text{NaHCO}_3,\text{sol}} = M_{\text{NaHCO}_3} \cdot [\text{HCO}_3^-] \cdot m_{\text{Solution}} \quad \text{Eq. 3-44}$$

$$m_{\text{Na}_2\text{CO}_3,\text{sol}} = M_{\text{Na}_2\text{CO}_3} \cdot [\text{CO}_3^{2-}] \cdot m_{\text{Solution}} \quad \text{Eq. 3-45}$$

Resulting in:

$$m_{\text{Solution}} = \frac{m_{\text{solvent}}}{1\text{kg} - M_{\text{Na}_2\text{CO}_3} \cdot [\text{CO}_3^{2-}] - M_{\text{NaHCO}_3} \cdot [\text{HCO}_3^-]} \quad \text{Eq. 3-46}$$

$$m_{\text{NaHCO}_3,\text{sol}} = \frac{M_{\text{NaHCO}_3} \cdot [\text{HCO}_3^-] \cdot m_{\text{solvent}}}{1\text{kg} - M_{\text{Na}_2\text{CO}_3} \cdot [\text{CO}_3^{2-}] - M_{\text{NaHCO}_3} \cdot [\text{HCO}_3^-]} \quad \text{Eq. 3-47}$$

$$m_{\text{Na}_2\text{CO}_3,\text{sol}} = \frac{M_{\text{Na}_2\text{CO}_3} \cdot [\text{CO}_3^{2-}] \cdot m_{\text{solvent}}}{1\text{kg} - M_{\text{Na}_2\text{CO}_3} \cdot [\text{CO}_3^{2-}] - M_{\text{NaHCO}_3} \cdot [\text{HCO}_3^-]} \quad \text{Eq. 3-48}$$

Since all sodium carbonate present resulted from decomposition of sodium bicarbonate, the dissolved amounts of carbonate and bicarbonate present in the reactor could be calculated back to the corresponding amount of original sodium bicarbonate (added to the reactor in the beginning), from which they resulted:

$$n_{\text{NaHCO}_3,\text{org}} = n_{\text{NaHCO}_3,\text{sol}} + 2 \cdot n_{\text{Na}_2\text{CO}_3,\text{sol}} \quad \text{Eq. 3-49}$$

$$\Rightarrow m_{\text{NaHCO}_3,\text{org},\text{sol}} = M_{\text{NaHCO}_3} \cdot \left( \frac{m_{\text{NaHCO}_3,\text{sol}}}{M_{\text{NaHCO}_3}} + 2 \cdot \frac{m_{\text{Na}_2\text{CO}_3,\text{sol}}}{M_{\text{Na}_2\text{CO}_3}} \right) \quad \text{Eq. 3-50}$$

This fraction of the original sodium bicarbonate (i.e. sodium bicarbonate added to the reactor in the beginning) corresponded to the amounts of carbonate and bicarbonate in solution at this stage of the experiment. The other fraction of the original sodium bicarbonate would then corresponded to the amount of carbonate and bicarbonate in the solids in the reactor:

$$m_{NaHCO_3,org.,solid} = m_{NaHCO_3,org.}^0 - m_{NaHCO_3,org.,sol} \quad \text{Eq. 3-51}$$

With the weight fractions of carbonate and bicarbonate in the solid from the heating-weight-loss analysis, the true amount of solid in the reactor  $m_{solid}$  can be calculated from the following set of equations:

$$m_{NaHCO_3,solid} = w_{NaHCO_3} \cdot m_{solid} \quad \text{Eq. 3-52}$$

$$m_{Na_2CO_3,solid} = w_{Na_2CO_3} \cdot m_{solid} \quad \text{Eq. 3-53}$$

$$m_{NaHCO_3,org.,solid} = M_{NaHCO_3} \cdot \left( \frac{m_{NaHCO_3,solid}}{M_{NaHCO_3}} + 2 \cdot \frac{m_{Na_2CO_3,solid}}{M_{Na_2CO_3}} \right) \quad \text{Eq. 3-54}$$

Resulting in:

$$m_{solid} = \frac{m_{NaHCO_3,org.,solid}}{M_{NaHCO_3} \cdot \left( \frac{w_{NaHCO_3}}{M_{NaHCO_3}} + 2 \cdot \frac{w_{Na_2CO_3}}{M_{Na_2CO_3}} \right)} \quad \text{Eq. 3-55}$$

$$m_{NaHCO_3,solid} = w_{NaHCO_3} \cdot \frac{m_{NaHCO_3,org.,solid}}{M_{NaHCO_3} \cdot \left( \frac{w_{NaHCO_3}}{M_{NaHCO_3}} + 2 \cdot \frac{w_{Na_2CO_3}}{M_{Na_2CO_3}} \right)} \quad \text{Eq. 3-56}$$

$$m_{Na_2CO_3,solid} = w_{Na_2CO_3} \cdot \frac{m_{NaHCO_3,org.,solid}}{M_{NaHCO_3} \cdot \left( \frac{w_{NaHCO_3}}{M_{NaHCO_3}} + 2 \cdot \frac{w_{Na_2CO_3}}{M_{Na_2CO_3}} \right)} \quad \text{Eq. 3-57}$$

From the amounts of sodium carbonate in the solid  $m_{NaHCO_3,solid}$  and in the solution  $m_{NaHCO_3,sol}$ , the total amount of sodium bicarbonate in the reactor  $m_{NaHCO_3,tot}$  for every sampling could be calculated.

$$m_{NaHCO_3,tot} = m_{NaHCO_3,sol} + m_{NaHCO_3,solid} \quad \text{Eq. 3-58}$$

This value is essential for the calculation of the decomposition rate: Although the decomposition was found to occur in the solution, the recrystallization of the solid occurred simultaneously. Sodium carbonate is released and taken up by the solid during the dissolution of the sodium bicarbonate crystals (nahcolite) and the formation of wegscheiderite.

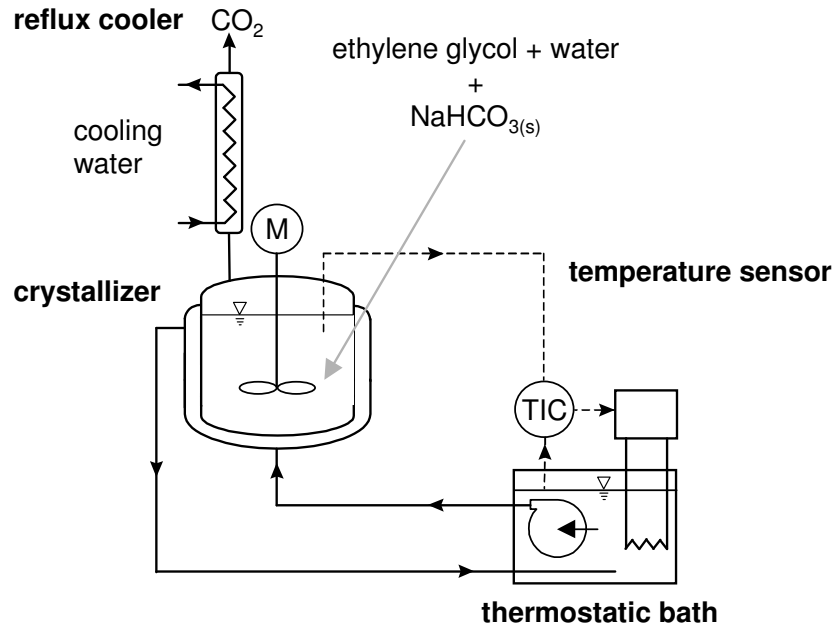


**Figure 3-14:** Batch crystallization set-up for the NaHCO<sub>3</sub> decomposition experiments

For the correct calculation of the decomposition rate this variation of the bicarbonate content of the solid had to be taken into account and the decomposition rate was derived from the change of  $m_{\text{NaHCO}_3, \text{tot}}$  with time:

$$r = \frac{dn_{\text{NaHCO}_3}}{m_{\text{Solution}} \cdot dt} = \frac{dm_{\text{NaHCO}_3}}{M_{\text{NaHCO}_3} \cdot m_{\text{Solution}} \cdot dt} \approx \frac{1}{M_{\text{NaHCO}_3} \cdot m_{\text{Solution}}(t)} \cdot \frac{\Delta m_{\text{NaHCO}_3, \text{tot}}}{\Delta t} \quad \text{Eq. 3-59}$$



## Chapter 4 :

### RECRYSTALLIZATION OF TRONA (SODIUM SESQUICARBONATE) INTO SODA (SODIUM CARBONATE ANHYDRATE) IN A MIXED SOLVENT, PART I: FUNDAMENTAL CONVERSION STEPS

R.S. Gärtner, G.J. Witkamp

#### **Abstract**

A new conversion process for the production of soda ( $\text{Na}_2\text{CO}_{3(s)}$ ) from trona ( $\text{Na}_2\text{CO}_3 \cdot \text{NaHCO}_3 \cdot 2\text{H}_2\text{O}_{(s)}$ ) and other sodium bicarbonate containing sodium carbonate sources is presented. By using a mixed solvent consisting of ethylene glycol and water, the boiling point of the solution was increased and the stability of trona could be decreased to such a degree, that it spontaneously recrystallized to anhydrous soda ( $\text{Na}_2\text{CO}_{3(s)}$ ) and wegscheiderite ( $\text{Na}_2\text{CO}_3 \cdot 3\text{NaHCO}_{3(s)}$ ). Additionally, the sodium bicarbonate content could be completely decomposed thermally in the mixed solvent to sodium carbonate, which crystallized as stable, pure anhydrous soda.

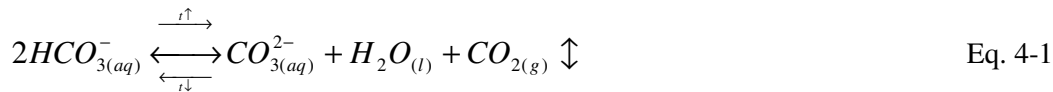
The fundamental mechanisms of this process are discussed in this paper: The stability of trona as a function of mixed solvent composition, water activity and temperature is reported. The dissolution rate, the bicarbonate decomposition rate as well as the (pseudo) solid phase conversion rate of trona were investigated as functions of mixed solvent composition and temperature.

It was found that beyond a certain temperature, depending on the mixed solvent composition, the trona would convert in the (pseudo) solid state.

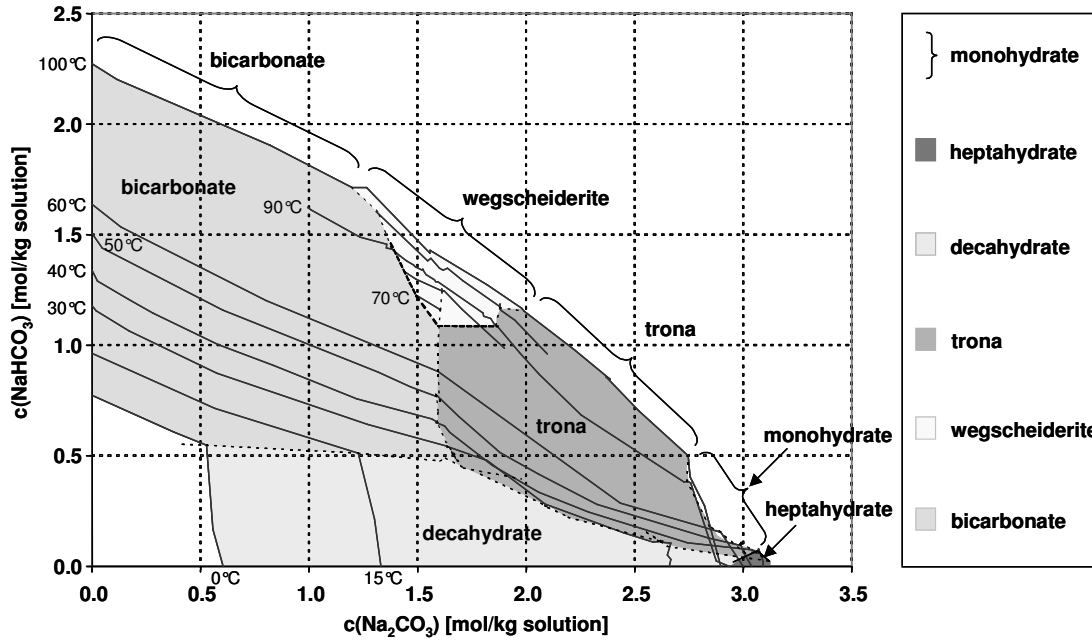
#### 4.1. Introduction

Trona, sodium sesquicarbonate, is a hydrate double salt of sodium carbonate and bicarbonate:  $\text{Na}_2\text{CO}_3 \cdot \text{NaHCO}_3 \cdot 2\text{H}_2\text{O}_{(s)}$ . Trona occurs as a natural ore at locations all over the world, e.g. in the United States (e.g.: the Green River Territory, Wyoming or Searles Lake, California), Mexico (Sosa Texcoco), Turkey (Beypazari) and Kenya (Lake Magadi) [1]. This abundant availability makes trona ore an attractive source material for soda production (soda =sodium carbonate anhydrate,  $\text{Na}_2\text{CO}_{3(s)}$ ).

Almost all natural deposits of sodium carbonates consist either of trona or nahcolite ( $\text{NaHCO}_{3(s)}$ ), since these crystal forms are most likely to form from natural carbonate brines. Trona is the more common mineral. This is due to two factors: the equilibrium between carbonate and bicarbonate in solution and the incongruent solubility of trona, see Figure 1. The equilibration occurs via desorption of  $\text{CO}_2$  to the air or via absorption of atmospheric  $\text{CO}_2$ :



This equilibrium shifts significantly with temperature. With decreasing temperature the formation of bicarbonate is favored. The equilibrium solution composition for atmospheric  $\text{CO}_2$  partial pressure has actually nahcolite as stable solid phase till about  $90^\circ\text{C}$ , see Chapter 3 [2]. But with the (evaporative) crystallization of nahcolite, the brine enriches rapidly in carbonate. The amount of carbon dioxide in the atmosphere is too low to allow conversion of the excess carbonate to bicarbonate (Eq. 1) in competition with the natural evaporation rate. Therefore, the composition of the brine increases in carbonate till trona becomes the stable solid phase. With the crystallization of trona, the same stoichiometric amounts of bicarbonate and carbonate are removed from solution – and the brine composition stabilizes. Therefore, only lower temperatures, solutions (brines) of low alkalinity and low evaporation rates actually result in nahcolite formation in nature.



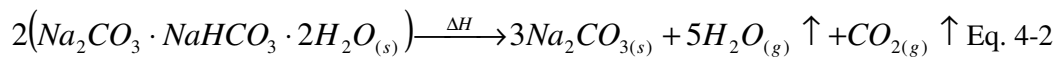
**Figure 4-1:** Phase diagram for the System  $\text{Na}_2\text{CO}_3\text{-NaHCO}_3\text{-H}_2\text{O}$  from 0 to 100°C [3-8]

Figure 1 was constructed from solubility data from different literature sources [3-8]. Comparable diagrams are given by Garret [8].

The conversion of trona to soda (anhydrate) requires the following 3 process steps:

1. The break-up of the trona crystal lattice and the discharge of the crystal water
2. The conversion of bicarbonate to carbonate and the discharge of  $\text{CO}_2$
3. The formation of the soda crystals (nucleation and growth)

The overall conversion reaction is:



$$\Delta H_{R, 298.15\text{K}} = 133.39 \text{ kJ/mol [9]}$$

The equilibrium between carbonate and bicarbonate ions in aqueous solution determines the stable solid phase in saturated solutions and the corresponding solubility concentrations of carbonate and bicarbonate. This equilibrium is strongly affected by the  $\text{CO}_2$  partial pressure, see Eq. 1. At  $T < 90^\circ\text{C}$  and ambient  $\text{CO}_2$  partial pressure, solid bicarbonate (nahcolite) is the thermodynamically stable solid. At  $T > 90^\circ\text{C}$  the equilibrium is sufficiently shifted towards carbonate to make trona the stable phase. The equilibrium can theoretically be shifted further towards carbonate by reducing the

ambient carbon dioxide partial pressure. Intense carbon dioxide stripping could then allow crystallizing sodium carbonate monohydrate and achieving complete conversion into a bicarbonate-free solid phase.

In aqueous solution only the recrystallization of solid bicarbonate to trona can be achieved at ambient CO<sub>2</sub> partial pressure, and an operating temperature  $T > 90^{\circ}\text{C}$  and intense CO<sub>2</sub>-stripping have to be applied. For the complete conversion of bicarbonate to carbonate in solution, CO<sub>2</sub> has to be removed completely from the ambient gas phase and higher temperatures need to be applied. The highest available operating temperature at atmospheric pressure in aqueous solution is the boiling point of the saturated bicarbonate/carbonate solution which lies in the range between 101.4°C, (for a saturated NaHCO<sub>3</sub> solution), and 104.8°C, (for a saturated Na<sub>2</sub>CO<sub>3</sub> solution).

From aqueous carbonate solutions containing little or no bicarbonate, sodium carbonate decahydrate ( $\text{Na}_2\text{CO}_3 \cdot 10\text{H}_2\text{O}_{(s)}$ , *natron*: till ca. 32°C [10, 11]), heptahydrate ( $\text{Na}_2\text{CO}_3 \cdot 7\text{H}_2\text{O}_{(s)}$ , from 32 till ca. 34°C [10, 11]) and monohydrate ( $\text{Na}_2\text{CO}_3 \cdot \text{H}_2\text{O}_{(s)}$ , *thermonatrite*: from 34°C till 109°C [10, 11]) can be crystallized.

At atmospheric pressure the anhydrate ( $\text{Na}_2\text{CO}_3_{(s)}$ , *natrite*) is normally not formed since the boiling point of the solution of 104.8°C [3, 11] is lower than the transition temperature of 109°C [10].

The crystallization of anhydrous soda from a *modified* solution at atmospheric pressure is possible, though: Robertson et al. [12] and Bourne et al. [13] crystallized the anhydrate from solutions containing high concentrations of NaCl or NaOH, while Bowman et al. precipitated anhydrate using methanol as antisolvent [14].

An explanation for this was given by Oosterhof et al. [15-18], who showed that the anhydrous transition temperature decreases according to a simple function with decreasing water activity of the solution. Addition of a component, which reduces the water activity sufficiently, allows crystallization of the anhydrate. Oosterhof et al. predicted the change of transition temperature in mixed solvents of water and ethylene glycol [15, 17, 18] and of water and di-ethylene glycol [18] with high accuracy based on thermodynamic modeling. They also proved, that for mixed solvents with antisolvent contents >30%-w (salt free solvent), sodium carbonate will crystallize as the desired anhydrate from solution [18].

In this work, it will be shown that a sufficient reduction in water activity will force trona ( $\text{Na}_2\text{CO}_3 \cdot \text{NaHCO}_3 \cdot 2\text{H}_2\text{O}(\text{s})$ ) to spontaneously recrystallize to more stable, anhydrous crystal forms such as wegscheiderite and anhydrate. Under conditions where in addition solution mediated decomposition of bicarbonate to carbonate takes place, a complete and fast but controlled conversion of trona into soda (anhydrate) is possible.

This control is obtained by tuning the transition temperature and bicarbonate decomposition rate through the antisolvent content and process temperature. In this way the carbonate supersaturation is controlled which in turn implies that the particle size distribution can be influenced via the nucleation and growth rates.

In this way high bulk densities of the produced soda can be achieved – up to  $1500 \text{ kg/m}^3$  [15, 18]. This reactive recrystallization under controlled supersaturations also increases significantly the purity of the anhydrate product crystals compared to the feed material as well as to common soda ash, see Chapter 2 [19]. Since the recrystallized soda consists of comparatively large crystals instead of agglomerates of fine crystallites (as in the commercially available soda ash), it has an improved filterability and is far less prone to breakage, dusting and caking than the currently produced soda (from calcination of the monohydrate).

Three possible process routes to use the mixed solvent reactive recrystallization method to produce a soda of improved quality are described in Chapter 5 [20].

The aim of this work was to provide a thermodynamic and kinetic description of the mixed solvent reactive recrystallization of trona to soda.

## ***4.2. Experimental procedures***

### **4.2.1. Solubility and Stability Determination in Shake tests**

To determine phase stability and the corresponding carbonate-bicarbonate solubility of a range of temperatures and mixed-solvent compositions a large number of samples needed to be prepared, thermostated and analyzed. This was done in shake-tests: 15g of solid and 40g of mixed-solvent solution were shaken in 50ml Nalgene™ PTFE-bottles in a thermostated shaking bath. In these tests, mixed solvents with ethylene glycol contents of 50, 60, 70, 80, 90 and 100%-w (salt-free) were used. Two different series of experiments

were performed. The first started with a solid, composed of a mixture of sodium carbonate and bicarbonate of technical purity (> 99.5%) in a molar ratio of 1 : 3. In the second series, trona, supplied by Solvay, France, was used as starting solid. The bottles were shaken at constant temperature for one day. The experiments were started at 50°C and the temperature was increased daily by 10K till 90°C. Solution samples were taken and titrated with 0.1 M HCl with a Radiometer VIT 90 Video Titrator. The  $\text{CO}_3^{2-}$  and  $\text{HCO}_3^-$  concentrations in the solution were determined by titration, their concentrations in the solid (after completion of the experiment) were determined from the weight loss on heating (by a Mark II Moisture Analyzer thermobalance (Denver Instruments)). See Addendum for further explanation of the analytical methods.

No significant decomposition of either dissolved or solid bicarbonate was found. The complete solubility data set is given in [21], while the phase stability information is summarized in Figure 2, 3 and 18.

#### **4.2.2. Batch Recrystallization Experiments**

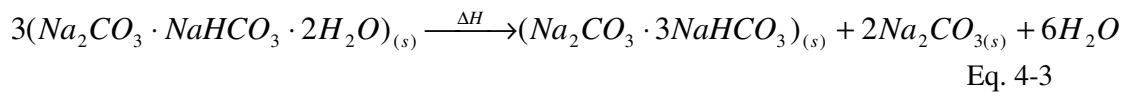
Slurries of 15 to 20%-w trona in mixed solvents, containing 50 to 100%-w ethylene glycol, were recrystallized in a thermostated, stirred batch reactor of 1 or 1.5 liter. Samples of the slurry were taken every 30 minutes, the solvent was filtered off, the solid was rinsed with acetone and air-dried on the filter. The solid was then analyzed for heating-weight-loss, from which the degree of decomposition of the solid sodium bicarbonate was determined (see Addendum). The occurring crystal phases were identified by polarized light microscopy, SEM images and/or powder XRD. For experiments, where trona would recrystallize to wegscheiderite and anhydrate and the  $\text{HCO}_3^-$  in the system would then decompose solution mediated, the carbonate and bicarbonate concentrations were additionally determined titrimetrically for the solution and the solid samples. A sketch of the experimental set-up is given in the Addendum.

### 4.3. Results and Discussion

#### 4.3.1. Predicted and Observed Transition Lines of Trona

Oosterhof et al. [15, 18] predicted the transition temperatures of sodium carbonate monohydrate to anhydrate. The transition temperatures of trona have been estimated in a similar fashion. The estimation is based on the following relationships:

Above the transition temperature (assuming no significant decomposition of bicarbonate to carbonate occurs) trona recrystallizes to wegscheiderite and anhydrate:



$\Delta H_{R,298.15K} = 88.96$  kJ per mol wegscheiderite [9]

At the transition point of Eq. 3, i.e. the thermodynamic conditions at which all 3 solid phases are stable in contact with the solution, the mixed solvent system consists of 4 phases (P), i.e. trona, wegscheiderite, anhydrate and the solution, formed from 4 components (C), i.e.  $\text{Na}_2\text{CO}_3$ ,  $\text{NaHCO}_3$ ,  $\text{H}_2\text{O}$ , and ethylene glycol. The system has therefore 2 degrees of freedom (f) according to the Gibbs phase rule:

$$f = C - P + 2 \Rightarrow f = 4 - 4 + 2 = 2$$

Eq. 4-4

The aqueous system has one component less (missing the ethylene glycol) and has therefore only 1 degree of freedom. This means, that in the aqueous system the transition point of Eq. 3 is fixed for e.g. atmospheric pressure to one specific transition temperature, which is actually *above* the atmospheric boiling point of the aqueous solution. The transition temperature of trona in aqueous solution is actually estimated at ca. 111°C by our model. For the mixed solvent system, the atmospheric transition temperature of Eq. 3 can be varied with the ethylene glycol content. The purpose here is to lower the transition temperature so far, that trona recrystallizes spontaneously to wegscheiderite and anhydrate.

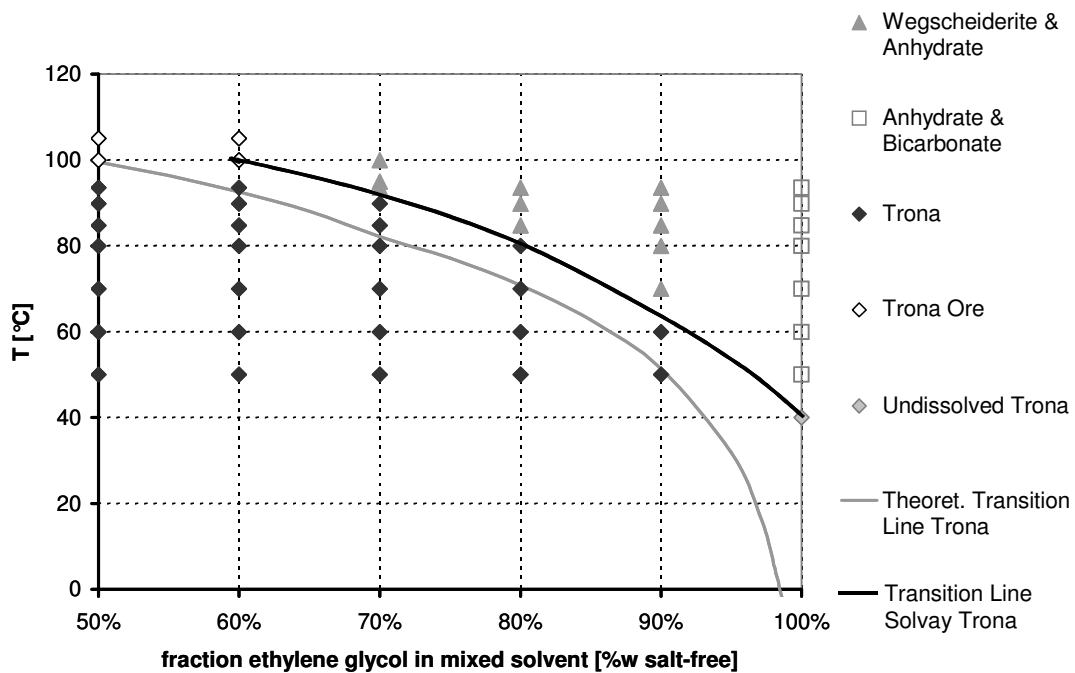


**Figure 4-2:** Stability of trona supplied by Solvay, France, (i.e. formed from aqueous solution) in the mixed solvent in dependence of ethylene glycol content

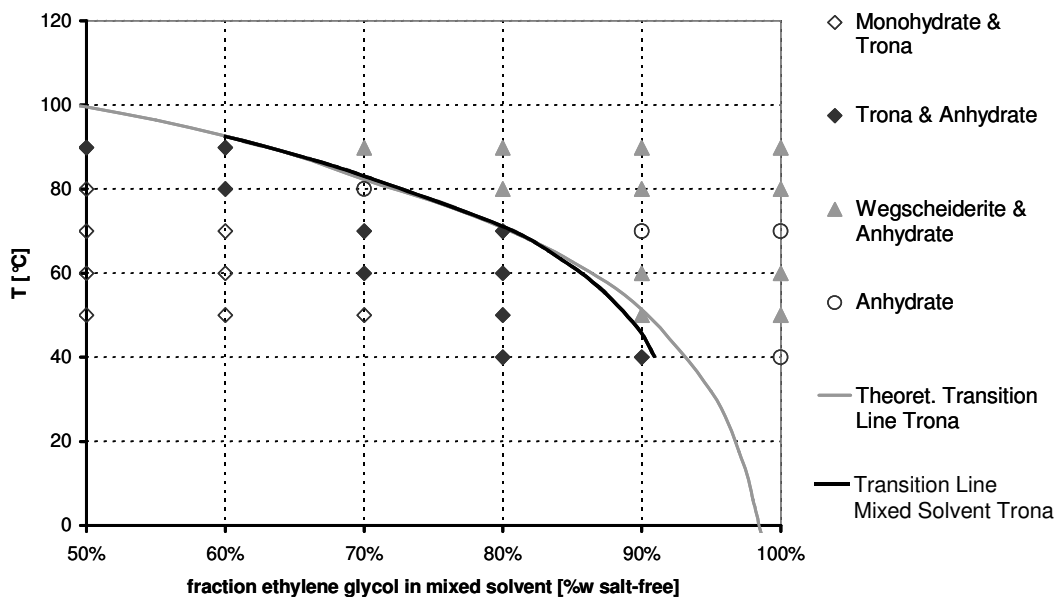


**Figure 4-3:** Stability of trona formed by recrystallization in the mixed solvent solution in dependence of ethylene glycol content



As trona is a hydrate, the change in transition temperature is caused by the decrease of water activity in solution with increasing ethylene glycol content. For the prediction of the transition temperature at a particular ethylene glycol content, a relation between the water activity and the temperature of the transition point has been derived in the following way:

At the solubility line of trona, i.e. at equilibrium between solid and solution, the activities of the ions in solution obey its thermodynamic solubility product:

$$K_{sp,trona} = a_{Na^+}^3 \cdot a_{CO_3^{2-}} \cdot a_{HCO_3^-} \cdot a_{H_2O}^2 \quad \text{Eq. 4-5}$$

At conditions where wegscheiderite and anhydrate are both in solubility equilibrium, the activities of the ions in solution simultaneously obey the thermodynamic solubility products of both these salts:

$$K_{sp,weg} = a_{Na^+}^5 \cdot a_{CO_3^{2-}} \cdot a_{HCO_3^-}^3 \quad \text{Eq. 4-6}$$

$$K_{sp,anh} = a_{Na^+}^2 \cdot a_{CO_3^{2-}} \quad \text{Eq. 4-7}$$

At the transition point of Eq. 3 all three phases are stable, and the solution obeys all three solubility products. With the stoichiometry of the reaction of Eq. 3, this yields the condition for the water activity:

$$K_{sp,trona}^3 = K_{sp,weg} \cdot K_{sp,anh}^2 \cdot a_{H_2O}^6 = a_{Na^+}^9 \cdot a_{CO_3^{2-}}^3 \cdot a_{HCO_3^-}^3 \cdot a_{H_2O}^6 \quad \text{Eq. 4-8}$$

$$\Rightarrow \left( \frac{K_{sp,trona}^3}{a_{H_2O}^6} \right) = (K_{sp,weg} \cdot K_{sp,anh}^2) \quad \text{Eq. 4-9}$$

$$\Leftrightarrow a_{H_2O} = \sqrt[6]{\frac{K_{sp,trona}^3}{K_{sp,weg} \cdot K_{sp,anh}^2}} \quad \text{[at the transition point]} \quad \text{Eq. 4-10}$$

Vapor pressure data of glycol mixtures from Oosterhof [17] were used to convert the water activity into a respective mixed solvent composition. A plot of the water activity for different antisolvent compositions for sodium carbonated saturated solutions as a function of temperature is given in the Addendum. The resulting theoretical transition line from Eq. 10 is given as the grey line in Figure 2 and Figure 3.

Haynes et al. [22, 23] have calculated the thermodynamic solubility products of anhydrate, trona and wegscheiderite as functions of temperature from thermodynamic data of the solid and dissolved species. The set of thermodynamic solubility product functions for the sodium carbonate – bicarbonate system, which is used in our calculations, was published by Haynes in a recent work [23] (T in Kelvin):

$$K_{sp, \text{trona}} = \exp(-87930.16/T + 3786.877 - 701.5103 \cdot \ln(T) + 1.973255 \cdot T - 9.662326 \cdot T^2) \text{ Eq. 4-11}$$

$$K_{sp, \text{weg}} = \exp(-120952.7/T + 4776.029 - 868.0586 \cdot \ln(T) + 2.226852 \cdot T - 10.29110 \cdot T^2) \text{ Eq. 4-12}$$

$$K_{sp, \text{anh}} = \exp(-70816.77/T + 2919.663 - 529.0907 \cdot \ln(T) + 1.290843 \cdot T - 5.648249 \cdot T^2) \text{ Eq. 4-13}$$

The method, by which these functions were obtained, is outlined in the Addendum to this chapter. Thermodynamic solubility products for some of the given salts can also be found in the work of Marion [24], Harvie et al. [25] and Königsberger et al. [26].

Great care has to be taken when determining equilibrium data. For example Wegscheider et al. [27] found, that the system  $\text{Na}_2\text{CO}_3\text{-NaHCO}_3\text{-H}_2\text{O}$  did not equilibrate well under all conditions. They still observed apparently stable trona or natron under conditions, which were clearly outside the proven stability regions for these phases. Hill et al. [7] observed trona at high temperature conditions, where this hydrate is very unlikely to occur. Oosterhof et al. [15, 17] found in their mixed solvent recrystallization experiments of sodium carbonate monohydrate to anhydrate, that the recrystallization would not always initiate spontaneously. Significant superheating was required to start the recrystallization. Two different transition lines were observed experimentally in our work in the mixed solvents: One for trona, Figure 2, which was obtained from Solvay, France, and which was formed by evaporative crystallization from aqueous solution (purity: 99.5%-w): “Solvay trona”. The other line, see Figure 3, was observed for trona, which was recrystallized from soda,  $\text{Na}_2\text{CO}_{3(s)}$ , and solid sodium bicarbonate,  $\text{NaHCO}_{3(s)}$ , in mixed solvent solution: “mixed solvent trona”. The observed higher transition temperatures found for Solvay trona (Figure 2) compared to mixed solvent trona (Figure 3) and the theoretical temperatures could be the result of such a metastability.

**Table 4-1:** Calculated and measured transition temperatures for mixed-solvent-formed trona and aqueous-formed trona acquired from Solvay, France

$w_{EG}$ ethylene glycol fraction in solvent [%-w, salt-free]	$T_{trans}$ calculated [°C]	$T_{trans}$ mix. solv. trona [°C]	$T_{solvay}$ Solvay trona [°C]
60%	92.3	90 - 100	100 ± 0.5
70%	81.0	80 - 90	92 ± 0.2
80%	70.6	70 - 80	80 ± 2
90%	49.6	40 - 50	67 ± 2
100%	na	na	40 ± 2.5

It might be that the Solvay trona did not dissolve and recrystallize at the lower temperature, because the driving force of the system was insufficient to initiate these processes – as in the case of the high temperature trona of Hill et al. [7].

An overview of the observed transition temperatures is given in Table 1. In pure glycol a theoretical transition temperature could not be calculated since the water activity is zero. This lack of water also prevented synthesis of mixed solvent trona.

The thermodynamically predicted transition temperatures agree better with those of the mixed solvent trona than with those of the Solvay trona. The higher temperatures for Solvay trona seem to point at greater metastability effects for this trona.

However, there were some observations indicating that metastability alone is not a sufficient basis for an explanation of the observed difference:

First, the solubility of the Solvay trona at temperatures above the transition line of the mixed solvent trona was not consistently higher than the solubilities of wegscheiderite and anhydrate, see Chapter 6 [21]. This would be expected, if the Solvay trona was metastable under these conditions, as a metastable phase has a higher solubility than the stable one(s).

Second, since trona was reasonably well soluble in the mixed solvent [21], the rate limiting step causing the metastability of the trona, would normally be the nucleation and/or growth of the stable phases anhydrate and wegscheiderite. Contrary to this, it was

observed that in some solubility tests with 70% -w and 80% -w ethylene glycol, Solvay trona, anhydrate and wegscheiderite would be present at the same time in solution without visible signs of continuing recrystallization. This indicated, that formation of anhydrate and wegscheiderite did not impede the recrystallization. It was also found, that the Solvay trona in these cases dissolved inhomogeneously: Only parts of the crystals would dissolve – resulting in holes and rough surfaces of the remaining trona crystals. This observation could be an indication that the system was at the transition line, where all three solid phases were equally stable, which would imply that the solubility of the Solvay trona is just lower than predicted, and lower than that of the mixed solvent formed trona.

Third, the XRD pattern of the Solvay trona and the mixed solvent trona differed slightly. While both patterns contained the same characteristic peaks for trona, the pattern of the mixed solvent trona showed a slight, but noticeable peak broadening. This indicated that the mixed solvent trona had a lower degree of crystallinity. Less crystalline trona would be more soluble and less stable than trona consisting of well-formed crystals (like the Solvay trona).

The aqueous solution grown crystals of the Solvay trona were quite large (ca. 2 to 5mm length, ca. 100 to 200 micron thickness) and more well formed, see Figure 5, than the crystals of the mixed solvent trona, which were significantly smaller (20 to 100 micron length), and displayed a tendency to twinning and epitaxial growth, see Figure 4.



**Figure 4-4:** Mixed solvent trona formed from 70%-w ethylene glycol mixed solvent, bar = 50 micron

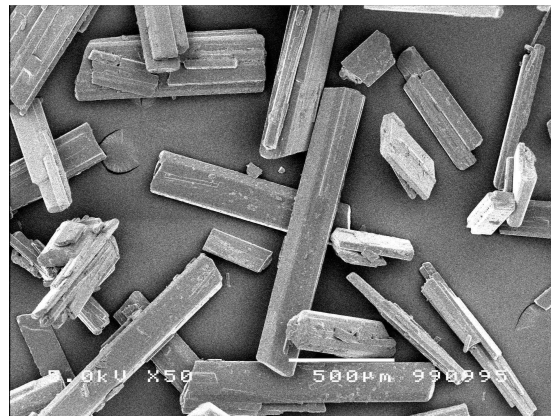


**Figure 4-5:** Solvay trona, bar = 500 micron

These observations suggest, that the transition line of the Solvay trona would be the most representative one – and that the theoretical transition line is not accurate enough.

However, the modeling approach is based on reliable thermodynamic data of the aqueous system (i.e. trona formed from aqueous solution), which should of course also be valid for the (Solvay) trona in the mixed solvent. Therefore, the dissolution of the trona was studied in more detail, as described in the following section.

For the conversion of solid trona in the mixed solvent it is expected, that most trona, which will serve as starting material of the process, is formed from aqueous solutions and will follow the behavior of the Solvay trona (Figure 2) rather than the mixed solvent trona (Figure 3).

#### **4.3.2. Kinetics of the Trona Conversion**

Two factors promote the break-up of the trona:

- a) The instability of the crystal water
- b) The (thermal) decomposition of the bicarbonate

##### *4.3.2.1. Trona dissolution due to the instability of the crystal water*

###### *4.3.2.1.1. General Observations*

Above the transition temperature, the instability of the crystal water will cause trona to spontaneously recrystallize into an anhydrous form, i.e. a mixture of wegscheiderite and anhydrate, see Eq. 3.

It was found, that the rate-determining step of Eq. 3 was the dissolution of the trona crystals: With the occurrence of wegscheiderite and anhydrate in the recrystallization experiments, the concentrations of bicarbonate and carbonate dropped almost instantly to the solubility of the new phases, while trona was still present, see e.g. Figure 3 (*“Solid and solution composition during discontinuous 1-step recrystallization in a stirred tank in 60%-w ethylene glycol mixed solvent”*) of chapter 5 [20]. This supports the hypothesis of the occurrence of a “metastable” Solvay trona, but indicates rather a dissolution

limited metastability than a limitation in the formation of the new solid phases (anhydrate and wegscheiderite), see also Davey et al. [28].

Therefore, dissolution kinetics were used to model this step. While dissolution is commonly found to be diffusion controlled [29], this cannot be assumed in this case. It might be, that the trona dissolution is strongly affected by a surface disintegration step. This is supported by the observation, that trona did not only display rounding of the edges during dissolution but also pits and holes in the crystals. This pitting indicated that the dissolution occurred more strongly on dislocations and stacking faults, where the surface disintegration step was facilitated. A general growth and dissolution expression was applied:

$$\frac{dm_{trona}}{dt} = k_{diss} \cdot \rho_{Trona} \cdot A_{Trona} \cdot \Delta X \quad \text{Eq. 4-14}$$

#### 4.3.2.1.2. Driving Force and Transition Temperature

The driving force  $\Delta X$  for growth and dissolution of trona is the difference in chemical potential  $\Delta\mu_{cryst}$  between the dissolved components of the trona in solution, and the solid trona:

$$\Delta\mu_{cryst}(T) = \mu_{solution}(T) - \mu_{solid}(T) \quad \text{Eq. 4-15}$$

The chemical potential of the solid trona at the process temperature,  $\mu_{solid}(T)$ , is equal to the chemical potential of a trona saturated solution for that temperature:

$$\mu_{solid}(T) = \mu_{solution}^0 + R \cdot T \cdot \ln(K_{sp,trona}(T)) \quad \text{Eq. 4-16}$$

The chemical potential of the dissolved trona,  $\mu_{solution}(T)$ , has to be calculated from the activity product of the species, which the trona is composed of ( $\text{Na}^+$ ,  $\text{CO}_3^{2-}$ ,  $\text{HCO}_3^-$ ,  $\text{H}_2\text{O}$ ), in solution:

$$\mu_{solution}(T) = \mu_{solution}^0 + R \cdot T \cdot \ln\left(\prod_i^{trona} a_i(T)\right) \quad \text{Eq. 4-17}$$

Eq. 16 and 17 yield the following relationship for the driving force for trona dissolution:

$$\Delta\mu_{cryst}(T) = R \cdot T \cdot \ln \left( \frac{\prod_i^{trona} a_i(T)}{K_{sp,trona}(T)} \right) \quad \text{Eq. 4-18}$$

As the concentrations of carbonate and bicarbonate in the solution were close to the solubility of anhydrate and wegscheiderite, the activity product in Eq. 18 can be expressed as a function of the thermodynamic solubility products  $K_{sp,weg}$  and  $K_{sp,anh}$  and the water activity  $a_{H_2O}$ , as already done in the previous section (e.g. in Eq. 8).

The dimensionless, standardized driving force  $\Delta X$  can be expressed as:

$$\Delta X = \frac{\Delta\mu_{cryst}(T)}{R \cdot T} = \ln \left( \frac{\sqrt[3]{K_{sp,anh}^2(T) \cdot K_{sp,weg}(T) \cdot a_{H_2O}^2(T)}}{K_{sp,trona}(T)} \right) \quad \text{Eq. 4-19}$$

The calculated driving forces are presented in Figure 6. Despite the complex relationship between temperature and driving force of Eq. 19, Figure 6 shows, that the driving force  $\Delta\mu_{cryst}/R \cdot T$  is almost linearly proportional to the temperature difference  $\Delta T$  between process and transition temperature.

Such a linear relationship for small temperature differences follows from the Gibbs-Helmholtz [30] relation:

$$\left( \frac{\partial(\Delta\mu/T)}{\partial T} \right)_p = -\frac{\Delta H}{T^2} \Leftrightarrow \left( \frac{\partial \left( \frac{\Delta\mu}{R \cdot T} \right)}{\partial T} \right)_p = -\frac{\Delta H}{R \cdot T^2} \quad \text{Eq. 4-20}$$

Which yields for the dimensionless driving force  $\Delta X$ :

$$\left( \frac{\partial(\Delta X)}{\partial T} \right)_p = -\frac{\Delta H_{diss}}{R \cdot T^2} \quad \text{Eq. 4-21}$$

The enthalpy of dissolution of trona  $\Delta H_{diss}$  is actually a function of temperature. But the assumption can be made, that:  $\Delta H_{diss}(T) \approx \Delta H_{diss}(T_{trans}) \approx \text{const}$ , which is reasonable for temperature differences  $(T - T_{trans})$  of about 10 K or less. Then Eq. 21 yields for the driving force  $\Delta X$  the following approximation:

$$\int_{\Delta X(T_{trans})}^{\Delta X(T)} d(\Delta X) = \int_{T_{trans}}^T -\frac{\Delta H_{diss}(T_{trans})}{R \cdot T^2} dT \quad \text{Eq. 4-22}$$

$$\Delta X(T) - 0 = \frac{\Delta H_{diss}(T_{trans})}{R \cdot T} - \frac{\Delta H_{diss}(T_{trans})}{R \cdot T_{trans}} = \frac{\Delta H_{diss}(T_{trans})}{R \cdot T \cdot T_{trans}} \cdot (T_{trans} - T) \quad \text{Eq. 4-23}$$

$$\Delta X \cong -\frac{\Delta H_{diss}(T_{trans})}{R \cdot T_{trans}^2} \cdot (T - T_{trans}) \Rightarrow \Delta X \propto \Delta T \quad \text{Eq. 4-24}$$

Figure 6 indicates, that Eq. 24 provides a decent approximation of the driving force in comparison to the one calculated from the solubility product data of Haynes [23] by Eq. 19. I.e., the dissolution rate can be related to the temperature difference:

$$\frac{dm_{T_{rona}}}{dt} \propto \Delta T = T - T_{trans} \quad \text{Eq. 4-25}$$

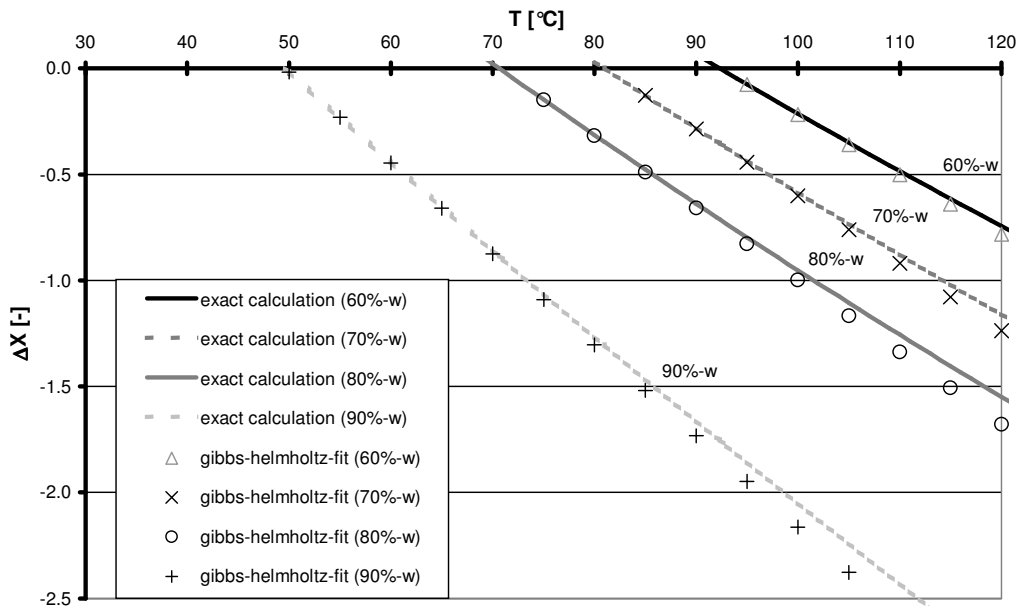


**Figure 4-6:** Comparison of the driving force  $\Delta X$  calculated from the solubility product data of Haynes [23] by Eq. 19 and the Gibbs-Helmholtz-based approximation of Eq. 24



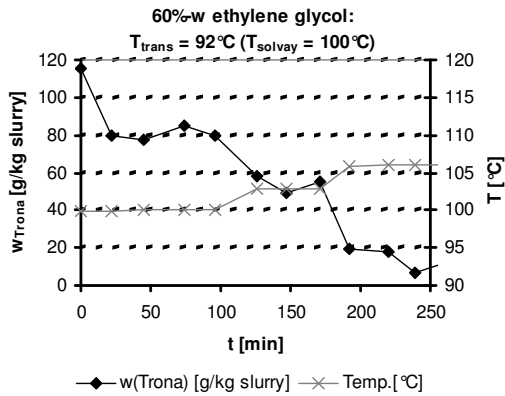


Figure 4-7: Dissolution of Solvay trona in 60%-w ethylene glycol

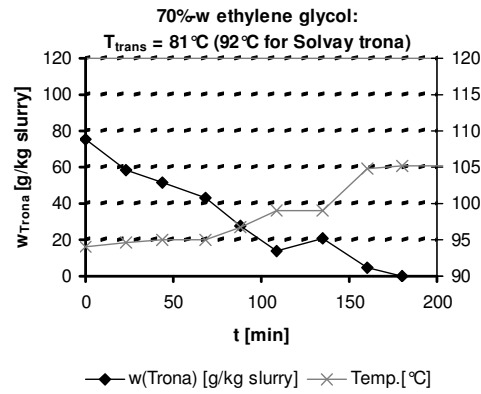


Figure 4-8: Dissolution of Solvay trona in 70%-w ethylene glycol

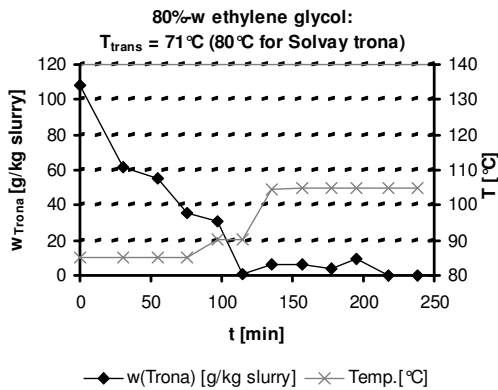


Figure 4-9: Dissolution of Solvay trona in 80%-w ethylene glycol

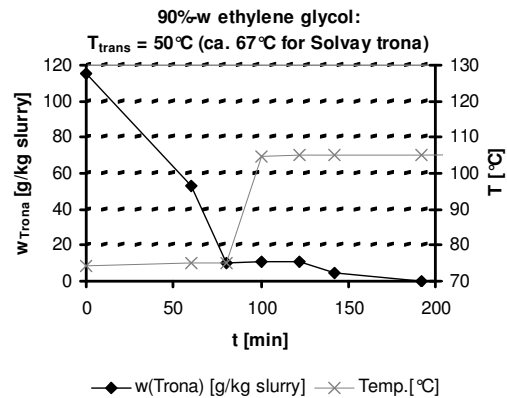


Figure 4-10: Dissolution of Solvay trona in 90%-w ethylene glycol

#### 4.3.2.1.3. The Dissolution Rate of Trona

The actual dissolution rate of trona,  $dm_{Trona}/dt$ , was measured from batch recrystallization experiments, see Figures 7 to 10. In Figures 7 to 10, the weight fraction of trona in the slurry and the reactor temperature are plotted against time.

Figure 7 shows, that the (Solvay) trona dissolution occurred in 60%-w ethylene glycol mixed solvent at ca. 100-103°C. At this temperature the bicarbonate already decomposes to carbonate [2], so the trona dissolution was not only driven by the instability of the crystal water, but also by the decreasing bicarbonate concentration. Since the bicarbonate decomposition rate was still low at this temperature, the dominating effect was the crystal water instability. While dissolution of trona occurred already at 100°C, it did not proceed as steady as at 103°C.

In the dissolution experiments, displayed in Figure 8, 9 and 10, Solvay trona started to recrystallize in all investigated mixed solvent compositions at temperatures that approximately match those found previously, i.e. the observed transition temperatures were increased by a difference of app. 10 to 15 Kelvin compared to the previously found transition temperatures for mixed solvent trona and the temperatures predicted by the model.

The observed dissolution rates of the trona  $dm_{\text{trona}}/dt$  were correlated to the calculated driving force  $\Delta X$ , see Figure 11.

The development of the surface area with decreasing trona mass was estimated from the crystal size distribution of the Solvay trona, as explained in the Addendum. The following relationship between surface area  $A$ , the mass of the crystals  $m$  and the starting crystal mass  $m_0$  was derived:

$$A = m_0 \cdot 0.012959 \cdot \left( \frac{m}{m_0} \right)^{0.84786} \quad \text{Eq. 4-26}$$

The mean material density of trona,  $\rho_{\text{trona}}$ , equals as  $2.13 \text{ g/cm}^3$ , based on our own density measurements of Solvay trona and mineralogical data [31].

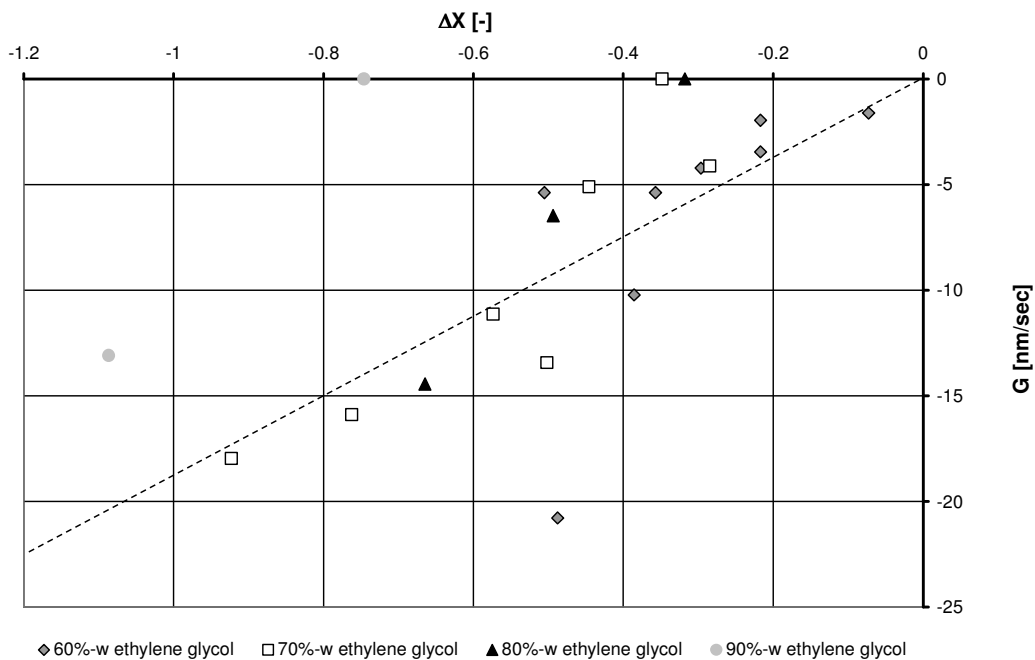


**Figure 4-11:** Dissolution rate of Solvay trona plotted against the driving force  $\Delta X$

The dissolution rates for all mixed solvent compositions plotted against the driving force are roughly scattered around the same line, which implies that  $k_{diss}$  is independent of the ethylene glycol content. This plot also indicates, that the thermodynamic transition temperatures of Solvay trona are not higher than the predictions by the model or the ones observed for mixed solvent trona: Although the onset of the dissolution is delayed for 70, 80 and 90%-w ethylene glycol (salt-free base) to increased driving forces, the dissolution rate in these cases rapidly increases to the same levels as the (almost) un-delayed dissolution in 60%-w (salt-free base) ethylene glycol. Note that the delay in dissolution increases with increasing ethylene glycol content – to the extent, that trona remained metastable in 100%-w (salt-free base) ethylene glycol till 40°C, see Figure 2.

The estimation of a theoretical diffusion border layer based on the measured dissolution rate yielded an unreasonably wide diffusion layer of 1500 to 2000 micron around the crystals. This indicated, that the dissolution is *not* diffusion controlled. The rate limiting mechanism is a surface disintegration step. This matches well with the previously mentioned in-situ light-microscopy observation, that the crystals developed pits, holes and frayed edges during dissolution, i.e. that dissolution occurred preferentially on surface imperfections.

The growth / dissolution rate  $G$  for all mixed solvent compositions can be expressed as:

$$G = \frac{dm_{trona}}{\rho_{trona} \cdot A_{trona} \cdot dt} = k_{diss} \cdot \Delta X \quad \text{Eq. 4-27}$$

From the plot of Figure 11,  $k_{diss}$  was estimated as 18 nm/sec ( $18 \cdot 10^{-9} \text{ m} \cdot \text{s}^{-1}$ ).

As indicated in the previous section, the dissolution rate can also be expressed as a function of the temperature difference  $\Delta T$ . Combining Eq. 27 and 25 a linear relation is obtained, see Figure 12.

$$\frac{dm_{trona}}{dt} = -k'_{diss} \cdot A_{trona} \cdot \rho_{trona} \cdot \Delta T \quad \Leftrightarrow \quad G = -k'_{diss} \cdot \Delta T \quad \text{Eq. 4-28}$$

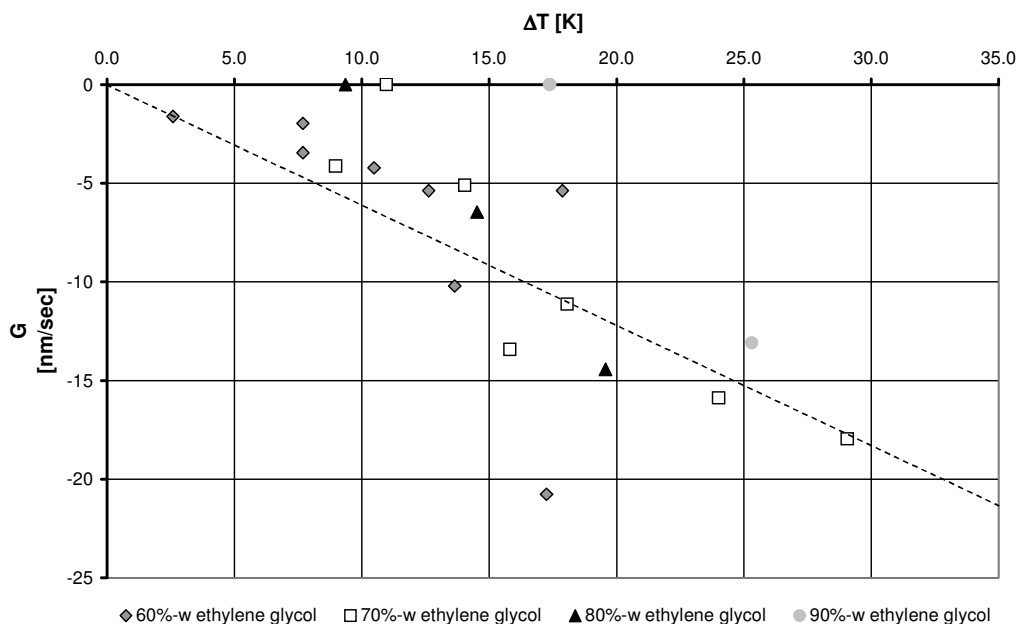


**Figure 4-12:** (Solvay) Trona dissolution rate versus temperature driving force  $\Delta T$  ( $T_{\text{trans}}$  derived from the model)

From Figure 12, a dissolution rate constant  $k'_{\text{diss}}$  of  $-0.6 \text{ nm/sec/K}$  ( $-0.6 \cdot 10^{-9} \text{ m} \cdot \text{s}^{-1} \cdot \text{K}^{-1}$ ) was estimated for (Solvay) trona dissolution in the mixed solvent, independent of the ethylene glycol content.

#### 4.3.2.2. The (Thermal) Decomposition of Bicarbonate.

Equilibrium between the dissolved bicarbonate and dissolved carbonate establishes itself by sorption of carbon dioxide, see Eq. 1. Above  $90^\circ\text{C}$ , sodium carbonate anhydrate (anhydrous soda) is the stable solid phase at the equilibrium composition in mixed solvent solution. Bicarbonate will decompose in solution to carbonate until this equilibrium is reached, and any bicarbonate-containing solid phase will recrystallize to sodium carbonate anhydrate. In the case of trona, the bicarbonate decomposition will accelerate the recrystallization. In the case, that the process temperature does not exceed the transition line of trona, the bicarbonate decomposition alone will result in a slow recrystallization to the anhydrate.

**Table 4-2:** Kinetic coefficients for thermal decomposition of dissolved bicarbonate in some ethylene glycol – water mixed solvents for Eq. 29

T [°C]	$k_{\text{HCO}_3^-}$ [1/sec]		
	70%-w ethylene glycol	80%-w ethylene glycol	90%-w ethylene glycol
100	$(2.08 \pm 0.34) \cdot 10^{-4}$	$(2.44 \pm 0.33) \cdot 10^{-4}$	$(2.72 \pm 0.40) \cdot 10^{-4}$
110	$(5.38 \pm 0.12) \cdot 10^{-4}$	$(4.16 \pm 0.18) \cdot 10^{-4}$	$(2.82 \pm 0.35) \cdot 10^{-4}$
120	-	$(3.77) \cdot 10^{-4}$	$(3.70 \pm 0.24) \cdot 10^{-4}$
130	-	-	$(4.20 \pm 0.12) \cdot 10^{-4}$

The decomposition rates of dissolved bicarbonate in the trona recrystallization were found to match those found in the decomposition-induced recrystallization of solid sodium bicarbonate ( $\text{NaHCO}_{3(s)}$ ) in the mixed solvents, see Chapter 3 [2]. The bicarbonate decomposition could be described by a the first order rate equation:

$$r_{\text{HCO}_3^-} = \frac{dn_{\text{HCO}_3^-}}{m_{\text{solution}} \cdot dt} = -k_{\text{HCO}_3^-} \cdot c_{\text{HCO}_3^-} \quad \text{Eq. 4-29}$$

#### 4.3.2.3. Pseudomorphic Soda

Above 90°C, where both mechanisms, i.e. trona recrystallization due to instable crystal water and bicarbonate decomposition, were in effect, the recrystallization proceeded so fast, that it almost appeared to occur in the solid state. Pseudomorphs were formed, i.e. the resulting soda formed aggregates, which retained the shape of the original trona crystal, see Figure 13. The size of the single soda crystallites in these aggregates decreased with decreasing water content of the mixed solvent, e.g. in 70%-w (salt-free base) mixed solvent this size ranged from 10 to 50 microns, while in experiments in pure ethylene glycol the size range was 1 to 10 microns. This not only indicates, that the soda crystallites were formed via the solution, but also, that they must have been formed in a very thin solution layer on the surface of a rapidly dissolving trona crystal since otherwise they would have been removed by hydrodynamical shear, see Figure 13.

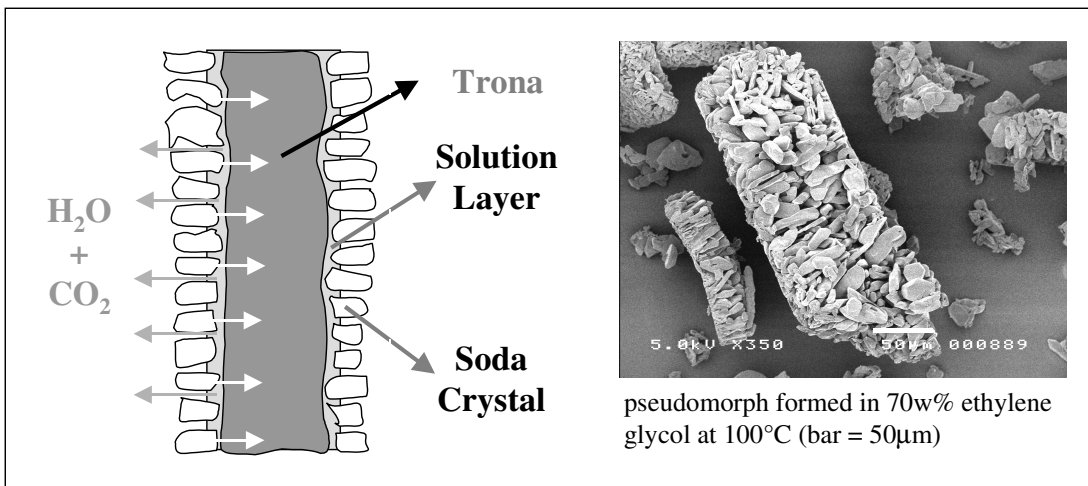


**Figure 4-13:** Mechanism of the formation of the pseudomorph morphology

The fast dissolution of the instable trona plus the decomposition of the bicarbonate in solution created a high carbonate supersaturation in this surface solution layer. This high supersaturation again resulted in continuing nucleation and growth of soda on the surface of the dissolving trona. With continuing dissolution of the trona, the forming soda followed the receding trona surface, resulting in the pseudomorphic morphology as in Figure 13. This also implies, that the solution boundary layer, in which nucleation and growth occurred, migrated with the receding trona surface to the core of the crystal, filling the intercrystalline pores of the pseudomorph with mixed solvent.

Since the solubility of carbonate decreased with increasing ethylene glycol content [16, 21], the highest supersaturation in the surface layer was present in pure ethylene glycol where the pseudomorphs consist of significantly smaller crystallites with a rounded platelet shape and without out any noticeable growth direction alignment.

The morphology of the pseudomorphs, formed in the mixed solvents, resembled the morphology occurring during dry calcinations of trona; see Ball et al. [32]. In dry calcination, though, the size of the constituent soda crystallites is even far smaller with sizes <1micron. This suggested that the conversion mechanism during dry calcinations was similar to the one presented here. Ekmekyapar et al. [33] found 1<sup>st</sup> order reaction kinetics for the dry calcination of trona in non-isothermal decomposition experiments. Ball et al. [32] found, that the conversion rate followed 2<sup>nd</sup> order Avrami-Erofeyev (A-E

$n = 2$ ) kinetics [34] in pure nitrogen and 1<sup>st</sup> order Avrami-Erofeyev (A-E  $n = 1$ ) kinetics [34] in CO<sub>2</sub> atmosphere:

$$\alpha = 1 - \exp[-k \cdot t^n] \quad \text{Eq. 4-30}$$

with  $\alpha$  the degree of conversion, expressed either as volume- or mol-fraction.

The Avrami-Erofeyev model was attributed in this case to a conversion rate determined by rapid nucleation and linear ( $n = 1$ ) or two-dimensional ( $n = 2$ ) (i.e. from e.g. the rim of a disk inwards) growth.

Also the contracting disc ( $n = 2$ ) and contracting cube ( $n = 3$ ) model [34] were considered:

$$\alpha = 1 - (1 - k \cdot t)^n \quad \text{Eq. 4-31}$$

Since the trona dissolved almost linear with time, see Figure 7 to 10 and Figure 12, the contracting cube or disc mechanisms, which implied a time linear conversion, were applied.

A typical data fit to the four models is given in Figure 14. The contracting cube and the 1<sup>st</sup> order Avrami-Erofeyev model produced the best fit to the data points. This would indicate that the conversion proceeded evenly from all side of the crystal to the core.

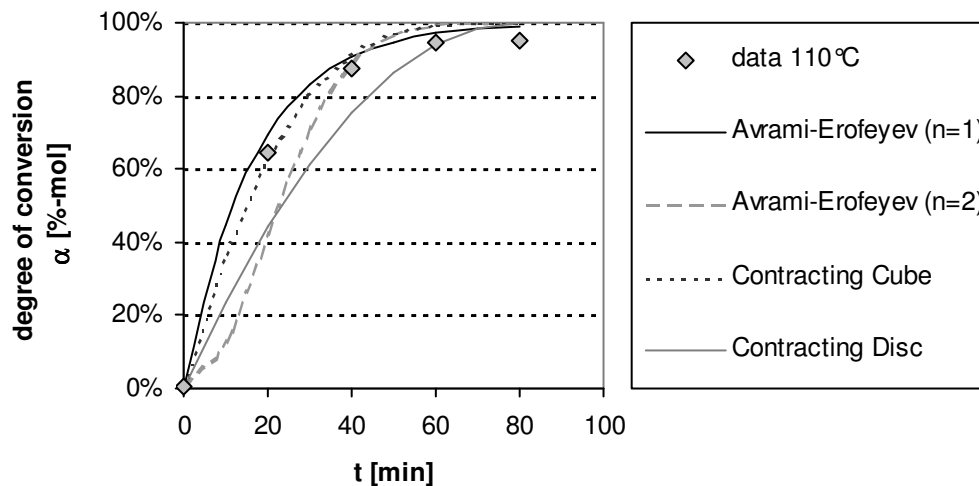


**Figure 4-14:** Fit of solid state conversion models to wet calcinations data of conversion of Solvay trona in pure ethylene glycol at 110°C

Apparently, even the trona's prism shape did not promote a contracting disc or 2<sup>nd</sup> order Avrami-Erofeyev mechanism.

Figure 15 shows that the wet and the dry calcination proceeded with approximately the same rate. The spread of our data points is most probably the effect of remaining mixed solvent in the pores of the pseudomorphs, which resulted in too low values for the measured degree of conversion with the thermogravimetric analysis (see Addendum).

Note that in Figure 15, the kinetic constant for wet-calcination and for dry-calcination in CO<sub>2</sub>-atmosphere were based on the 1<sup>st</sup> order Avrami-Erofeyev (A-E n = 1) equation, while the dry calcination in nitrogen-atmosphere followed 2<sup>nd</sup> order Avrami-Erofeyev (see Eq. 30).

For pure ethylene glycol as solvent, two conversion regimes were identified:

- a) A high temperature region of  $T > \sim 115^{\circ}\text{C}$ , where the conversion was dominated by the formation of pseudomorphs, i.e. by pseudo-solid-state conversion. Dense pseudomorphs of small soda crystallites (1-10 micron) were formed. Because of the pseudo-solid-state conversion, the conversion data fitted the 1<sup>st</sup> order Avrami-Erofeyev as well as the contracting cube model. The reaction rate appeared to match approximately the one found for solid-state conversion in dry nitrogen [32].
- b) A low temperature region of  $T < \sim 115^{\circ}\text{C}$ . Here, the conversion was dominated by dissolution of the trona, due to the instability of the crystal water. Due to the higher solubility of bicarbonate in pure ethylene glycol (see chapter 6 [21]), the remaining solid mainly consisted of anhydrate. Only traces of wegscheiderite were found and only for the temperature region of 54 to 90°C. From 54°C to 90°C the newly formed solid consisted of irregular agglomerates of small (1-10 micron) anhydrate particles with very few wegscheiderite crystallites. Above 70°C the first pseudomorphs appeared, but till ca. 110°C the irregular agglomerates were still found. Since the conversion to the new phase was (bulk) solution mediated in this region, the application of the (pseudo)-solid-state mechanisms was no longer valid. Kinetic constants for 1<sup>st</sup> order Avrami-Erofeyev in this region are given in Figure 15 only for comparison with the actual solid-state conversion rates.

Additional details of the conversion of trona in pure ethylene glycol can be found in [35].



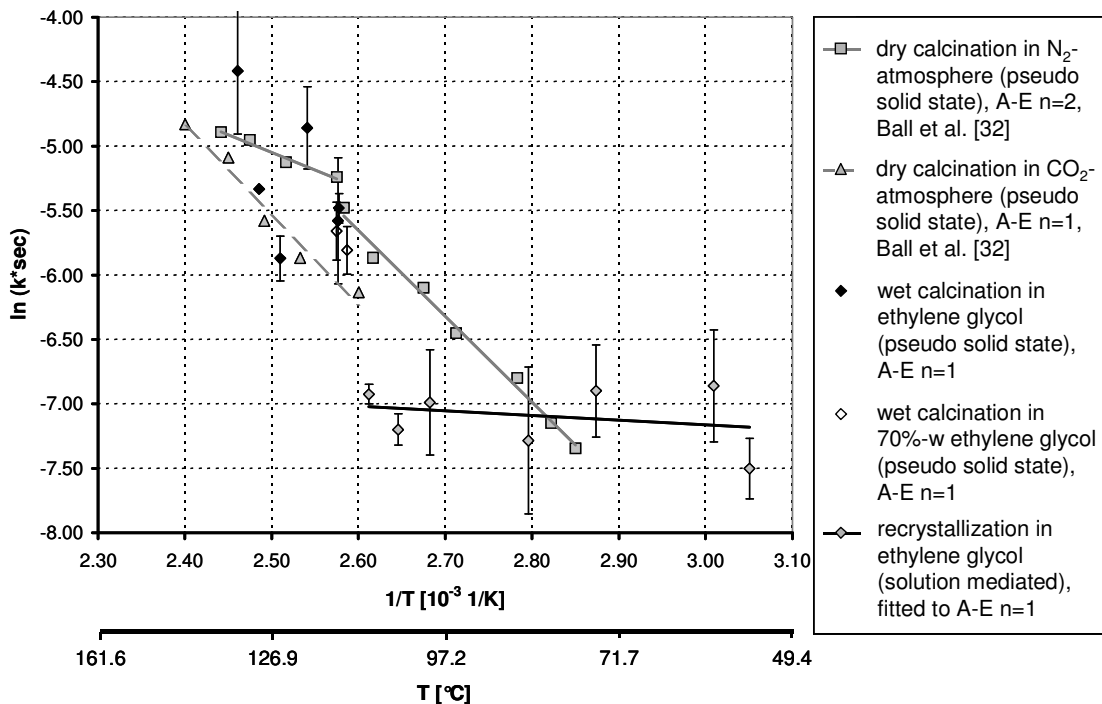


**Figure 4-15:** Arrhenius plot of the kinetic rate constants of the solid-state trona conversion

As can be seen from Figure 15, there was a dramatic increase in conversion rate with the transition from solution-mediated recrystallization to (pseudo-) solid-state recrystallization. This could be attributed to the fact, that in the (pseudo-) solid-state conversion, the conversion of the trona was driven by the instability of the crystal water plus the thermal decomposition of the bicarbonate. For the lower temperature region only the instability of the crystal water acted as the driving force for the recrystallization.

Ball et al. [32] found also for the solid-state conversion in dry nitrogen a change in the mechanism at around 115°C: While the mechanism was identified in both cases as 2<sup>nd</sup> order Avrami-Erofeyev, the activation energy of the reaction changed from 58 kJ/mol below 115°C to 24 kJ/mol above 117°C. They also observed similar inflection points in the thermal decomposition of sodium carbonate monohydrate, wegscheiderite and nahcolite (crystalline sodium bicarbonate) [32, 36, 37]. The activation energy for the decomposition of all 4 solids in the dry solid state is almost identical in the high temperature region with a range of 20 (monohydrate) to 32 kJ/mol (nahcolite), while in the low-temperature region the activation energy for the decomposition of nahcolite (130

kJ/mol) and wegscheiderite (94 kJ/mol) is noticeably higher than for the monohydrate (72 kJ/mol) and trona (58 kJ/mol). The authors note, that in all cases not the nucleation and growth of the new phase but rather the decomposition of the old phase was the rate-limiting step.

For the conversion in the mixed solvent in the low temperature regime, the dissolution (with an estimated activation energy of 3 kJ/mol) is the rate-limiting step instead of the low temperature (pseudo) solid-state conversion ( $E_A = 58$  kJ/mol). The dissolution does not follow the Avrami-Erofeyev (A-E  $n=1$ ) mechanism, but was fitted to it for comparison with the rates in (pseudo) solid-state conversions. (The large standard deviations are in this case the result of the misfit between A-E  $n=1$  and the actual dissolution mechanism.) When the activation energy of the conversion in the low temperature regime in the dry state is expressed as activation energy per mol bicarbonate, it appears that the values for nahcolite (130 kJ/mol), wegscheiderite (125.3 kJ/mol) and trona (116 kJ/mol) are quite similar, indicating that the bicarbonate decomposition is the rate-limiting step. This would suggest, that the dissolution and diffusion of the bicarbonate is rate limiting in the mixed solvent conversion, especially since it was found in Chapter 3 [2], that nahcolite recrystallizes *solvent mediated* to soda (sodium carbonate anhydrate) in ethylene glycol - and not in the (pseudo) solid state.

Apparently, in the high temperature region, the surface disintegration becomes rate limiting instead of the bicarbonate decomposition. As bicarbonate decomposes as fast as it is released from the trona lattice, also the dissolution and diffusion in the mixed solvent are no longer rate limiting – and pseudomorphs are also formed in the mixed solvent.

The pseudomorphs were quite porous structures, since 29.66%-w of the mass of the original trona was released as water and CO<sub>2</sub> during the reactive recrystallization, see Eq. 2. This resulted in a rather low bulk density of the mixed-solvent-formed pseudomorphous soda of 500 to 800 kg/m<sup>3</sup>. Since the pseudomorphs contained measurable amounts of mixed solvent even after washing with acetone and drying at 60°C, the production of soda by direct wet calcination does not appear industrially attractive.

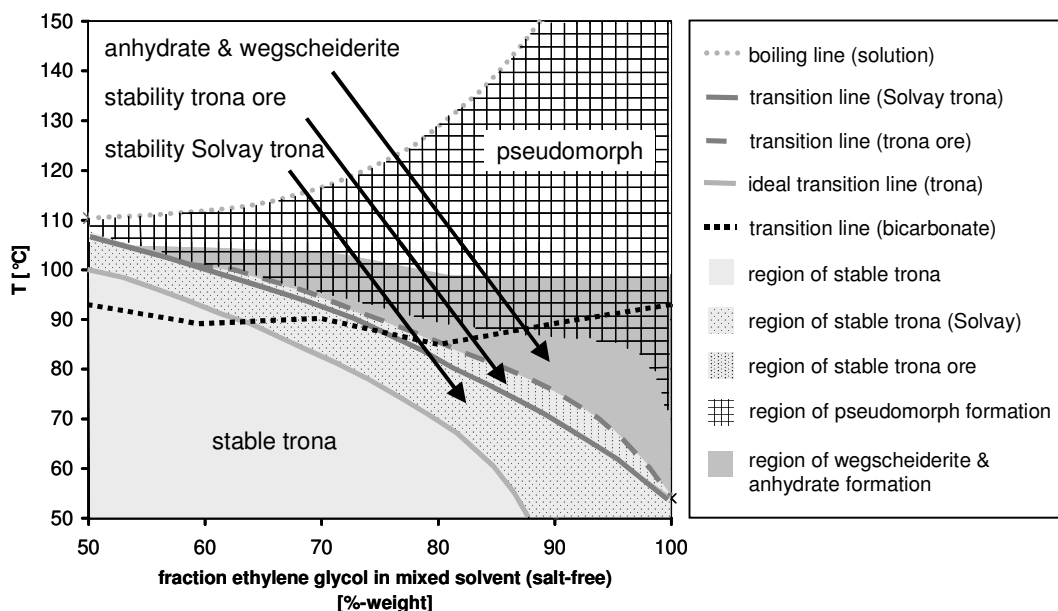


**Figure 4-16:** Phase conversion chart of trona in ethylene glycol-water mixed solvents

#### 4.3.2.4. Overview of the Recrystallization Mechanisms

Each of the described effects, i.e. instability of crystal water, pseudomorphic transition, metastability of trona, etc., could be related to a specific temperature – mixed solvent concentration range. In Figure 16, an overview is given of the regions of the different regimes of the recrystallization of trona in the mixed solvent.

The maximum temperature of stable trona decreased with increasing ethylene glycol content, due to the increasing instability of the crystal water. For the trona obtained from Solvay, which was crystallized from aqueous solution, the stable region was extended by a margin of 10 to 15 Kelvin. This region of extended stability broadens with increasing ethylene glycol content: For pure ethylene glycol (in which trona should not be stable at all due to the complete lack of water!) the Solvay trona did not recrystallize below 54°C in the 1 hour batch recrystallization experiments and was still found till 40°C in the 24h solubility shake tests.

Beyond the transition line of the Solvay trona, the trona recrystallized to an anhydrous form. In regions, where the bicarbonate content of the trona did not rapidly decompose thermally, i.e. around and below 90°C, the trona recrystallized to a mixture of the salts

wegscheiderite ( $\text{Na}_2\text{CO}_3 \cdot 3\text{NaHCO}_3(\text{s})$ ) and sodium carbonate anhydrate ( $\text{Na}_2\text{CO}_3(\text{s})$ ). At temperatures above  $90^\circ\text{C}$  the decomposition of the bicarbonate further accelerated the recrystallization of the trona to such degrees, that *pseudomorphs* were formed. The region of solvent-mediated recrystallization to wegscheiderite and anhydrate and the one of pseudomorph formation overlapped over a range of 10 to 15 Kelvin, in which intermediates of the solid types were formed. Here, usually loose pseudomorphic agglomerates of soda crystals interlaced with wegscheiderite needles occurred. In pure ethylene glycol these agglomerates formed already at  $70^\circ\text{C}$ , while in 60%-w ethylene glycol only few pseudomorphic particles were formed at temperatures slightly above the transition temperature of the Solvay trona, i.e.  $100$  to  $103^\circ\text{C}$ .

Additionally, samples of natural trona ore were obtained from two sources:

**Table 4-3:** Composition and origin of tested trona ore samples

Sample name	crude trona ore	ground trona ore
Origin	Searles Lake, CA, USA	Green River, WY, USA
Supplier	IMC Chemicals, Trona, California, USA	FMC Corp., Philadelphia, Pennsylvania, USA
Trona content $\text{Na}_2\text{CO}_3 \cdot \text{NaHCO}_3 \cdot 2\text{H}_2\text{O}$	~81%-w	~97%-w
Insoluble impurities	~10%-w	~2.5%-w
Soluble impurities	~5.9%-w $\text{Na}_2\text{SO}_4$ (thenardite) ~4.0%-w $\text{NaCl}$ (halite) ~1.2%-w $\text{Na}_2\text{B}_{10}\text{O}_{17} \cdot 4\text{H}_2\text{O}$ (biringuccite) ~0.13%-w $\text{NaF}$	~0.5%-w $\text{NaCl}$ (halite) ~0.025%-w $\text{Na}_2\text{SO}_4$

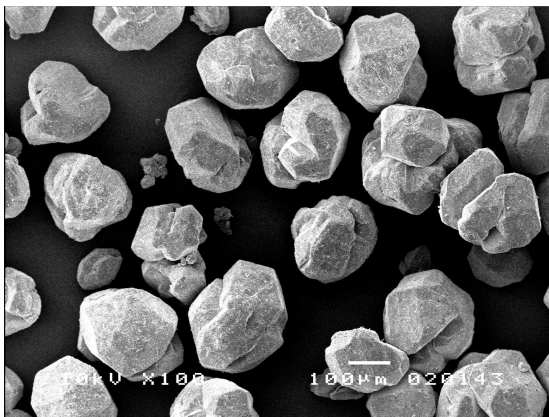


**Figure 4-17:** SEM image of sodium carbonate anhydrate crystallized in 80%-w mixed solvent, bar = 100 micron



**Figure 4-18:** SEM image of wegscheiderite crystallized in 70%-w mixed solvent, bar = 50 micron

The transition line for the Searles Lake trona, obtained from IMC Chemicals, California, was found to lie slightly above the transition line of the Solvay trona, see Figure 16.

The transition points for the Green River trona were only determined for 70 and 80%-w ethylene glycol mixed solvent. Although this trona ore contained far less impurities, the two measured transition points coincided with those of the Searles Lake trona ore.

The recrystallization behavior of the tested trona ores matched quite closely that of the Solvay trona. The slight increase in (apparent) transition temperature might be the effect of a higher stability, as the crystals of the trona ore had had geological time spans to form and (Ostwald-) ripen.

### 4.3.3. Crystallization of Soda (Sodium Carbonate Anhydrate)

The anhydrate was the first new phase to form during the dissolution of the trona, indicating that it nucleated faster than the wegscheiderite from the mixed solvent solution. For the recrystallization of the trona ore, anhydrate was even the only phase to form, probably because some of the impurities in the ore suppressed the formation of the wegscheiderite.

The linear growth rate  $G$  of anhydrate in 70 and 80%-w ethylene glycol (salt-free base) mixed solvent at 100°C was found to be about 4.5 nm/sec. The metastable zone of soda in the mixed solvents, especially in those of 90 and 100%-w ethylene glycol (salt-free

base), appeared to be narrower than in aqueous solution. Strong nucleation occurred in 90 and 100 %-w in experiments with rather small carbonate supersaturations, resulting in a small mean particle size. For 60 to 80%-w ethylene glycol, mean diameters of 150 to 200 micron could be obtained in the discontinuous and continuous experiments.

For comparison, sodium carbonate monohydrate can be grown from aqueous solution at rates of up to 20 micron per minute (833nm/sec) as far higher supersaturation levels can be achieved due to a higher metastable zone width and higher solubility in aqueous solution [38].

The formation and dissolution of wegscheiderite occurred too fast to allow obtaining reliable growth or dissolution parameters. An impression of the rate of formation and dissolution can be gained from the experimental solid-phase composition – time plots given in Chapter 5 [20].

#### **4.4. Conclusions**

By solvent mediated crystallization, trona ( $\text{Na}_2\text{CO}_3 \cdot \text{NaHCO}_3 \cdot 2\text{H}_2\text{O}_{(s)}$ ) can be directly recrystallized to soda of superior quality.

There are two main driving forces for trona recrystallization: The instability of the crystal water and the thermal decomposition of bicarbonate to carbonate. Both of these effects increase with temperature. Above about 100°C, the recrystallization is accelerated so much by the combined effect, that it proceeds in the pseudo-solid state and pseudomorphs (porous agglomerates of fine soda particles, which retain the shape of the original trona crystal) are formed.

Only at temperatures between 70 and 100°C the trona will recrystallize solvent mediated to soda (sodium carbonate anhydrate) of high mean crystal size. In mixed solvents of 50 to 60 %-w ethylene glycol (salt-free base), the recrystallization is only driven by the bicarbonate decomposition and proceeds rather slowly. In mixed solvents of 70 to 90 %-w ethylene glycol (salt-free base), the instability of the crystal water becomes the main driving force and the recrystallization proceeds much more rapidly. As the bicarbonate decomposition at this temperature range is slower than the trona recrystallization, wegscheiderite ( $\text{Na}_2\text{CO}_3 \cdot 3\text{NaHCO}_3(s)$ ) is formed as an intermediate.

The presented models allow predictive calculation of trona recrystallization rate in the mixed solvent for the solvent mediated recrystallization as well as the pseudomorph formation.

#### 4.5. Notation

A	: surface area	[m <sup>2</sup> ]
a	: cube edge length	[m]
a <sub>i</sub>	: activity of species I	[-]
c	: concentration	[mol/kg solution]
c <sub>Pi</sub>	: heat capacity of species I	[J/mol/K]
d <sub>major</sub>	: major characteristic crystal length	[m]
E <sub>A</sub>	: activation energy	[kJ/mol]
G	: linear crystal growth rate	[m/sec]
G <sub>f,i</sub>	: Gibbs free energy of formation of species i	[J/mol]
H <sub>i,f</sub>	: enthalpy of formation of species i	[J/mol]
K <sub>sp</sub>	: thermodynamic solubility product	[-]
k	: rate constant solid state conversion	[1/sec <sup>n</sup> ]
k <sub>A</sub>	: crystal surface area shape factor	[-]
k <sub>C</sub>	: rate constant solid state conversion	[1/sec]
k <sub>diss</sub>	: dissolution rate constant (ΔX)	[m/sec]
k' <sub>diss</sub>	: dissolution rate constant (ΔT)	[m/sec/K]
k <sub>HCO<sub>3</sub><sup>-</sup></sub>	: bicarbonate decomposition rate constant	[1/sec]
k <sub>V</sub>	: crystal volume shape factor	[-]
l	: longitudinal crystal length	[m]
m	: mass	[g]
n	: molar amount	[mol]
R	: ideal gas constant = 8.3144 J/mol/K	[J/mol/K]
r	: crystal radius	[m]
S <sub>i</sub>	: entropy of species i	[J/mol/K]
T	: temperature	[K] or [°C]

t	: time	[sec]
$\Delta T$	: temperature difference	[K]
w	: weight fraction	[%-w]
$x_0$	: mean diameter gaussian distribution	[m]
$\Delta X$	: dimensionless driving force for dissolution	[-]
$\alpha$	: molar or volumetric degree of conversion	[%-mol] or [%-vol]
$\gamma$	: activity coefficient	[-]
$\sigma_x$	: standard deviation of gaussian distribution	[m]
$\mu$	: chemical potential	[J/mol] or [J/g]

#### 4.6. Indices

AS	: antisolvent (i.e. ethylene glycol)	stable:	at stable condition
$\text{CO}_3^{2-}$	: carbonate ion	sol	: solvent
diss	: dissolution	solid	: solid phase
m	: molar property	solution:	solution
$\text{HCO}_3^-$	: bicarbonate ion	solway:	property of Solway trona
$\text{H}_2\text{O}$	: water	trans	: at transition condition
$\text{Na}^+$	: sodium ion	trona	: property of trona

#### 4.7. Literature References

- [1] Garret, D.E., "Natural Soda Ash – Occurrences, Processing and Use", Van Nostrand – Reinhold (Publ.), New York, 1992, p. 30-416
- [2] Gärtner, R.S., Seckler, M.M., Witkamp, G.J., "Reactive Recrystallization of Sodium Bicarbonate", submitted for publication in Ind. Eng. Chem. Res. (Chapter 3)
- [3] Waldeck, W.F., Lynn, G., Hill, A.E., "Aqueous Solubility of Salts at High Temperatures. I. Solubility of Sodium Carbonate from 50 to 348°C", J. Am. Chem. Soc., 54, 1932, p. 928-936
- [4] Seidell, A., "Solubilities of Inorganic and Metal Organic Compounds", Vol. I, Van Nostrand, New York, 1940, p. 1193-1200



- [5] Wegscheider, R., Mehl, J., "Über Systeme  $\text{Na}_2\text{CO}_3\text{-NaHCO}_3\text{-H}_2\text{O}$  und das Existenzgebiet der Trona", *Monatsh. d. Chem., Sitzungsberichte Akademie der Wissenschaften in Wien*, 49, 1928, p. 283-315
- [6] Hill, A.E., Bacon, L.R., "Ternary Systems. VI. Sodium Carbonate, Sodium Bicarbonate and Water", *J. Am. Chem. Soc.*, 59, 1927, p. 2487-2495
- [7] Waldeck, W.F., Lynn, G., Hill, A.E., "Aqueous Solubility of Salts at High Temperatures. II., The Ternary System  $\text{Na}_2\text{CO}_3\text{-NaHCO}_3\text{-H}_2\text{O}$  from 100 to 200°C", *J. Am. Chem. Soc.*, 56, 1934, p. 43-48
- [8] Garret, D.E., "Natural Soda Ash – Occurrences, Processing and Use", Van Nostrand – Reinhold (Publ.), New York, 1992, p. 565
- [9] Vanderzee, C.E., "Thermodynamic relations and equilibria in  $(\text{Na}_2\text{CO}_3 + \text{NaHCO}_3 + \text{H}_2\text{O})$ : standard Gibbs energies of formation and other properties of sodium hydrogen carbonate, sodium carbonate heptahydrate, sodium carbonate decahydrate, trona:  $(\text{Na}_2\text{CO}_3\cdot\text{NaHCO}_3\cdot 2\text{H}_2\text{O})$ , and Wegscheider's salt:  $(\text{Na}_2\text{CO}_3\cdot 3\text{NaHCO}_3)$ ", *J. Chem. Thermodynamics*, 14, 1982, p. 219-238
- [10] Taylor, C.E., "Thermodynamics of Sodium Carbonate in Solution", *J. Phys. Chem.*, 59 (1), 1966, p. 653-657
- [11] Kobe, K.A., Sheehy, T.M., "Thermochemistry of Sodium Carbonate and Its Solution", *Ind. Eng. Chem.*, 40 (1), 1948, p. 99-102
- [12] Robertson, H.R., "Production of Dense Soda Ash", United States Patent 2,267,136, Solvay Process Company, NY, 1940
- [13] Bourne, D.J., Lamb, F.E., "Method of Producing Soda Ash", United States Patent 3,656,892, Duval Co., 1972
- [14] Bowman, R.W., "Process for the manufacture of sodium carbonate crystals from minerals or solutions", United States Patent 6,022,385, 2000
- [15] Oosterhof, H., de Graauw, J., Witkamp, G.J., van Rosmalen, G.M., 2002, "Continuous Double Recrystallization of Light Soda Ash into Super Dense Soda Ash", *Crystal Growth & Design*, 2 (2), 2002, p. 151-157
- [16] Oosterhof, H., Witkamp, G.J., van Rosmalen, "Some antisolvents for crystallisation of sodium carbonate", *Fluid Phase Equilibria*, 155, 1999, p. 219-227
- [17] Oosterhof, H., Witkamp, G.J., van Rosmalen, G.M., 2001, "Antisolvent Crystallization of Anhydrous Sodium Carbonate at Atmospheric Conditions", *AIChE J.*, 47 (3), 2001, p. 602-608

- [18] Oosterhof, H., Witkamp, G.J., van Rosmalen, G.M., 2001, "Evaporative Crystallization of Anhydrous Sodium Carbonate at Atmospheric Conditions", *AIChE J.*, 47 (10), 2001, p. 2220-2225
- [19] Gärtner, R.S., Witkamp, G.J., "Mixed Solvent Recrystallization for the Densification and Purification of Soda Ash", in preparation for publication (Chapter 2)
- [20] Gärtner, R.S., Witkamp, G.J., "Recrystallization of Trona (Sodium Sesquicarbonate) into Soda (Sodium Carbonate Anhydrate) in a Mixed Solvent. Part II: Alternative Recrystallization Routes", in preparation for publication (Chapter 5)
- [21] Gärtner, R.S., Seckler, M.M., Witkamp, G.J., "Solid Phases and Their Solubilities in the System  $\text{Na}_2\text{CO}_3 - \text{NaHCO}_3 - \text{Ethylene Glycol} - \text{Water}$  from (50 to 90) °C", *J. Chem. Eng. Data*, 49(1), 2004, p. 116-125
- [22] Haynes, H.W. Jr., DeFilippis, P.: *Proceedings XXI International Mineral Processing Congress, Rome, 2000*, B10-9 – B10-15
- [23] Haynes, H.W. Jr., "A Thermodynamic Solution Model for Trona Brines", *AIChE J.*, 49 (7), 2003, p. 1883-1894
- [24] Marion, G.M., "Carbonate Mineral Solubility at Low Temperatures in the Na-K-Mg-Ca-H-Cl-SO<sub>4</sub>-OH-HCO<sub>3</sub>-CO<sub>3</sub>-CO<sub>2</sub>-H<sub>2</sub>O System", *Geochimica et Cosmochimica Acta*, 65 (12), 2001, p. 1883-1896
- [25] Harvie, C.E., Møller, N., Weare, J.H., "The Prediction of Mineral Solubilities in Natural Waters: The Na-K-Mg-Ca-H-Cl-SO<sub>4</sub>-OH-HCO<sub>3</sub>-CO<sub>3</sub>-CO<sub>2</sub>-H<sub>2</sub>O System to High Ionic Strengths at 25°C", *Geochimica et Cosmochimica Acta*, 48, 1984, p. 723-751
- [26] Königsberger, E., Königsberger, L.C., Gamsjäger, H., "Low-temperature thermodynamic model for the system  $\text{Na}_2\text{CO}_3\text{-MgCO}_3\text{-CaCO}_3\text{-H}_2\text{O}$ ", *Geochimica et Cosmochimica Acta*, 63 (19/20), 1999, p. 3105-3119
- [27] Wegscheider, R., Mehl, J., "Über Systeme  $\text{Na}_2\text{CO}_3\text{-NaHCO}_3\text{-H}_2\text{O}$  und das Existenzgebiet der Trona", *Monatsh. d. Chem., Sitzungsberichte Akademie der Wissenschaften in Wien*, 49, 1928, p. 283-315
- [28] Davey, R.J., Cardew, P.T., "The kinetics of solvent-mediated phase transformations", *Proc. R. Soc. Lond.*, A398, 1985, p. 415-428
- [29] Mullin, J.W., "Crystallisation", 4<sup>th</sup> ed., Butterworth-Heinemann (publ.), Oxford, 2001, pp.225
- [30] Ott, B.V., Boerio-Goates, J., "Chemical Thermodynamics – Principles and Applications", Academic Press, London, 2000, p. 281
- [31] crystallographical data taken from: <http://webmineral.com/data/Trona.shtml>

- [32] Ball, M.C., Snelling, Ch.M., Strachan, A.N., Strachan, R.M., “Thermal Decomposition of Solid Sodium Sesquicarbonate,  $\text{Na}_2\text{CO}_3 \cdot \text{NaHCO}_3 \cdot 2\text{H}_2\text{O}$ ”, *J. Chem. Soc. Faraday Trans.*, 88 (4), 1992, p. 631-636
- [33] Ekmekyapar, A., Erşahan, H, Yapici, S., “Nonisothermal Decomposition Kinetics of Trona”, *Ind. Eng. Chem. Res.*, 35, 1996, p. 258-262
- [34] Bramford, C.H., Tipper, C.H.F., “Comprehensive Chemical Kinetics, Vol. 22: Reactions in the Solid State”, Elsevier, Amsterdam, 1980, pp. 41-113
- [35] Gärtner, R.S., Witkamp, G.J., “Wet Calcining of Trona (Sodium Sesquicarbonate) and Bicarbonate in a Mixed Solvent“, *J. Crystal Growth*, 237-239 (3), 2002, p. 2199-2205
- [36] Ball, M.C., Strachan, A.N., Strachan, R. M., “Thermal Decomposition of Solid Wegscheiderite,  $\text{Na}_2\text{CO}_3 \cdot 3\text{NaHCO}_3$ ”, *J. Chem. Soc. Faraday Trans.*, 187 (12), 1991, p. 1911-1914
- [37] Ball, M.C., Snelling, C.M., Strachan, A.N., Strachan, R. M., “Thermal Decomposition of Solid Sodium Bicarbonate”, *J. Chem. Soc. Faraday Trans. I*, 82, 1986, p. 3709-3715
- [38] Hazen, W.C., Denham, D.L. Jr., Prusko, R., Baughman, D.R., Tacoma, R.B, “Sodium Carbonate Recrystallization”, United States Patent 6,284,005 B1, Hazen Inc., Colorado, 2001
- [39] Wesselingh, J.A., Krishna, R., “Mass Transfer”, Ellis Horwood Ltd. (publ.), Chichester – England, 1990, Chapter 11: “Electrolytes”, p. 84-94
- [40] Nasün-Sagili, G., Okutan, H., “Mechanism of dissolution of Turkish trona”, *Hydrometallurgy*, 43, 1996, p. 317-329
- [41] Pitzer, K.S.: “Activity Coefficients in Electrolyte Solutions”, 2<sup>nd</sup> ed., 30-153, CRC Press, Boca Raton (Florida), 1991
- [42] Pitzer, K.S., Peiper, J.C., “Thermodynamics of Aqueous Carbonate Solutions including Mixtures of Sodium Carbonate, Bicarbonate and Chloride”, *J. Chem. Thermodynamics*, 14, 1982, p. 613-638
- [43] Oelkers, E.C., Helgeson, H.C., Shock, E.L., Sverjensky, D.A., Johnson, J.W., Pokrovskii, V.A., “Summary of the Apparent Molal Gibbs Free Energies of Formation of Aqueous Species, Minerals, and Gases at Pressures 1 to 5000 Bars and Temperatures 25 to 100°C”, *J. Phys. Chem. Ref. Data*, 24 (4), 1995, p. 1401-1560

## 4.8. Addendum

### 4.8.1. Experimental Set-Up for Batch Recrystallization Experiments

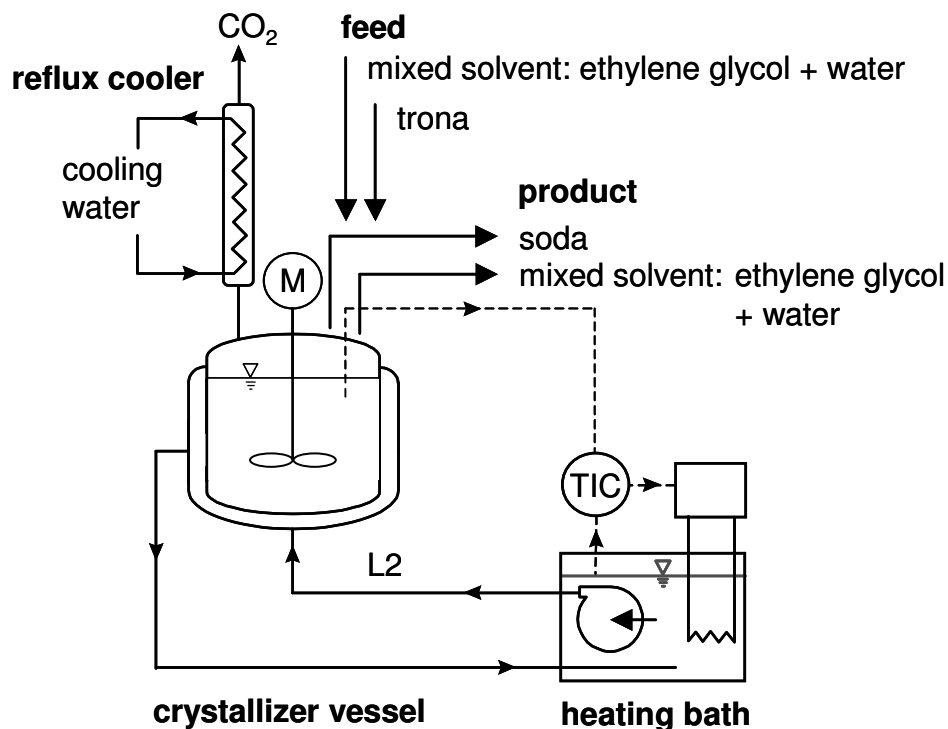


**Figure 4-19:** Thermostated batch set-up for discontinuous recrystallization experiments

### 4.8.2. Analytical Methods

#### 4.8.2.1. Solid Phase Analysis by Heating-Weight-Loss

Sodium bicarbonate thermally decomposes in the solid state to sodium carbonate. This conversion was used to quantify the bicarbonate content in a solid sample, as it was known that either the sample only contained sodium bicarbonate and sodium carbonate or the other compounds in the sample were known and thermally stable. Also mixed phases of carbonate and bicarbonate like wegscheiderite and trona were identified by this method, since their bicarbonate content decomposed similarly to solid sodium bicarbonate [32, 35-37] and the crystal water content of trona desorbed even faster than its bicarbonate content decomposed. The crystal phases present in a sample were identified by polarized light and/or SEM (scanning electron microscopy) and the phase

composition calculated from its specific heating mass loss  $X_i$ , which was measured in a Denver Instruments Mark II Moisture Analyzer thermo balance:

$$X_{loss} = \frac{m_{start} - m_{end}}{m_{start}} \quad [\text{g/g}] \quad \text{Eq. 4-32}$$

for pure solid sodium bicarbonate:

$$X_{NaHCO_3} = \frac{M_{CO_2} + M_{H_2O}}{2M_{NaHCO_3}} = 0.3692 \quad [\text{g/g}] \quad \text{Eq. 4-33}$$

for pure trona:

$$X_{Na_2CO_3 \cdot NaHCO_3 \cdot 2H_2O} = \frac{M_{CO_2} + 5M_{H_2O}}{2M_{Na_2CO_3 \cdot NaHCO_3 \cdot 2H_2O}} = 0.2966 \quad [\text{g/g}] \quad \text{Eq. 4-34}$$

for pure wegscheiderite:

$$X_{Na_2CO_3 \cdot 3NaHCO_3} = \frac{3M_{CO_2} + 3M_{H_2O}}{2M_{Na_2CO_3 \cdot 3NaHCO_3}} = 0.2599 \quad [\text{g/g}] \quad \text{Eq. 4-35}$$

for pure sodium carbonate monohydrate:

$$X_{Na_2CO_3 \cdot H_2O} = \frac{M_{H_2O}}{M_{Na_2CO_3 \cdot H_2O}} = 0.1453 \quad [\text{g/g}] \quad \text{Eq. 4-36}$$

for pure sodium carbonate anhydrate:

$$X_{Na_2CO_3} = 0 \quad [\text{g/g}] \quad \text{Eq. 4-37}$$

Most samples of recrystallization experiments contained mixtures of some of these solid phases. In the 1- and 2-step recrystallization experiments the solid samples could contain trona, wegscheiderite and anhydrate. In the wet calcination and monohydrate recrystallization experiments, the solid samples consisted of mixtures of trona and anhydrate or mixtures of monohydrate and anhydrate, provided that the wet calcination had completely converted the bicarbonate fraction of the trona to bicarbonate.

The quantitative composition of mixed trona / wegscheiderite / anhydrate samples could not be determined from their heating-weight-loss alone, since no clear distinction could be made between the weight-loss of the wegscheiderite fraction and the one of the trona

fraction. Additional information of the carbonate, bicarbonate and water content was necessary, which was acquired by titration. The heating-weight-loss was used here to countercheck the compositions calculated from the titration results (see below) and gave additional information about the amount of adhering solvent.

For the simpler phase compositions in the wet calcination and monohydrate recrystallization experiments, the compositions were calculated directly from the heating-weight-loss:

The weight loss  $X$  of a sample containing a weight fraction of  $w_{\text{Trona}}$  trona, while the rest had recrystallized to anhydrate, was:

$$X = w_{\text{Trona}} \cdot X_{\text{Na}_2\text{CO}_3 \cdot \text{NaHCO}_3 \cdot 2\text{H}_2\text{O}} + (1 - w_{\text{Trona}}) \cdot X_{\text{Na}_2\text{CO}_3} \quad \text{Eq. 4-38}$$

Therefore, the weight fraction trona was calculated as:

$$w_w = \frac{X - X_{\text{Na}_2\text{CO}_3}}{X_{\text{Na}_2\text{CO}_3 \cdot \text{NaHCO}_3 \cdot 2\text{H}_2\text{O}} - X_{\text{Na}_2\text{CO}_3}} = \frac{X}{X_{\text{Na}_2\text{CO}_3 \cdot \text{NaHCO}_3 \cdot 2\text{H}_2\text{O}}} \quad \text{Eq. 4-39}$$

Similarly, the weight fraction monohydrate  $w_{\text{monohydrate}}$  was calculated from:

$$w_{\text{monohydrate}} = \frac{X}{X_{\text{Na}_2\text{CO}_3 \cdot \text{H}_2\text{O}}} \quad \text{Eq. 4-40}$$

The identification of a crystal phase was, of course, not only based on the weight loss of a sample, but also verified either from light microscopy, SEM images and/or powder XRD. The weight loss analysis was primarily employed in this research to monitor the degree of conversion and to determine the amount of adhering solvent for a great amount of samples, once the reaction path had been established and the occurring crystal phases had been identified.

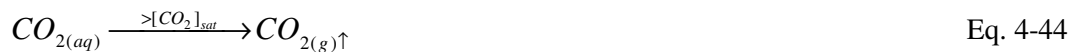
To exactly determine and characterize the amount of adhering liquid (e.g. also the acetone as washing liquid during filtration), the samples were heated in a 2-stage program. The sample was first heated for at least 3 min. at 60°C to evaporate adhering moisture and then for at least 5 min. at 200°C to calcine the sample, i.e. to desorb the crystal water and decompose the bicarbonate fraction. The Moisture Analyzer was set to keep the samples at constant temperature at each stage, till the sample showed constant

weight. Due to the relatively short exposure times, only negligible calcination would occur at 60°C.

The reproducibility of this method was found to depend strongly on sample morphology. For samples of very fine crystallites, the first stage would not completely remove adhering moisture due to retention by capillary forces. Too high weight losses would be obtained in the second heating stage, especially for samples containing high amounts of pseudomorphs. In general, the accuracy of the weight loss analysis was found to be ca. 0.5% weight loss, i.e. an error of 2 to 5% in the calculated weight fractions.

#### 4.8.2.2. Dissolved Carbonate-Bicarbonate Concentration by Automated pH Titration

Sodium carbonate-bicarbonate forms a buffer system. Under addition of a strong acid like HCl, carbonate ions will first be protonated to bicarbonate ions, and under continuing addition of acid beyond the complete protonation of carbonate, bicarbonate will be protonated to carbonic acid. Carbonic acid dissociates into water and carbon dioxide, which will usually quickly desorb from solution.



For the determination of the solution concentrations, a sample of 0.5 to 1 ml of the filtered mixed solvent solution was taken, weighed and then diluted with app. 10 ml of ultra-pure water. This solution was then titrated with 0.1 M HCl (Merck Titriplex) while being mixed by a magnetic stirrer.

For the 1-step and 2-step reactive recrystallization experiments, the composition of the solid was also analyzed by titration in addition to the heating-weight-loss analysis described above. For the titrimetric analysis of the solid, app. 0.5g sample of the solid was taken, weighed, and dissolved in app. 10 ml ultra-pure water. This solution was then titrated with 1 M HCl (Merck Titriplex).

During titration, the pH of the solution was continuously measured in both cases by a Radiometer glass pH electrode and recorded by a Radiometer VIT 90 Videotitrator. The Videotitrator automatically calculated the derivative curve of the pH – V<sub>HCl</sub> titration to gain the inflexion (buffer) points of the titration curve.

At the first inflexion point, V(CO<sub>3</sub><sup>2-</sup>), the carbonate content of the sample was completely protonated to bicarbonate, see Eq. 41, while at the second inflection point, V(CO<sub>3</sub><sup>2-</sup> + HCO<sub>3</sub><sup>-</sup>), the bicarbonate in the sample was quantitatively converted to carbonic acid. The formed carbonic acid of course then dissociated to CO<sub>2</sub> and water, according to Eq. 43. The formation of CO<sub>2</sub> became actually apparent, immediately after the first inflexion point was reached, as gas bubbles spontaneously formed in solution.

The titrations of the mixed solvent samples yielded their carbonate and bicarbonate concentrations immediately.

The titrations of the solid samples of the 1- and 2-step reactive recrystallization experiments yielded the bicarbonate and carbonate concentrations in the solid as [mol/ kg solid]. The amount of crystal water,  $m_{H_2O,cryst.}$ , was calculated from the mass balance of the sample and under consideration of the amount of adhering solvent  $m_{adh.liq.}$ , obtained from the heating-weight-loss analysis:

$$m_{NaHCO_3} + m_{Na_2CO_3} + m_{H_2O,cryst.} + m_{adh.liq.} = m_{sample} \quad \text{Eq. 4-45}$$

$$m_{sample} \cdot (c_{HCO_3^-} \cdot M_{NaHCO_3} + c_{CO_3^{2-}} \cdot M_{Na_2CO_3} + c_{H_2O} \cdot M_{H_2O} + x_{adh.liq.}) = m_{sample} \quad \text{Eq. 4-46}$$

$$c_{H_2O} = (1 - c_{HCO_3^-} \cdot M_{NaHCO_3} - c_{CO_3^{2-}} \cdot M_{Na_2CO_3} - x_{adh.liq.}) / M_{H_2O} \quad \text{Eq. 4-47}$$

The total number of moles carbonate, bicarbonate and water in the solid,  $n_{solid}$ , was then calculated as:

$$n_{solid} = n_{NaHCO_3} + n_{Na_2CO_3} + n_{H_2O} = (c_{HCO_3^-} + c_{CO_3^{2-}} + c_{H_2O}) \cdot m_{sample} \quad \text{Eq. 4-48}$$

From these values the following solid-state mol fractions were calculated:

1. Fraction bicarbonate in the dry solid,  $x_{NaHCO_3}$ :

$$x_{NaHCO_3} = \frac{c_{HCO_3^-}}{c_{HCO_3^-} + c_{CO_3^{2-}} + c_{H_2O}} \quad \text{Eq. 4-49}$$



2. Since of the occurring phases only trona contained crystal water, 1 mol of trona contained 2 moles of crystal water and 4 total moles of sodium carbonate, sodium bicarbonate and crystal water, the mol fraction of trona in the solid,  $x_{Trona}$ , was calculated from:

$$x_{Trona} = \frac{4 \cdot n_{Trona}}{n_{solid}} = \frac{4 \cdot (n_{H_2O}/2)}{n_{solid}} = \frac{2 \cdot (m_{sample} \cdot c_{H_2O})}{n_{solid}} \quad \text{Eq. 4-50}$$

3. As trona and wegscheiderite were the only bicarbonate containing solids, 1 mol of trona contained 1 mol of sodium bicarbonate and 1 mol of wegscheiderite contained 3 moles of sodium bicarbonate, the mol fraction wegscheiderite,  $x_{wesch.}$ , was calculated as:

$$x_{wesch.} = \frac{n_{NaHCO_3} - n_{Trona}}{3 \cdot (n_{solid}/4)} = \frac{4}{3} \cdot \frac{m_{sample} \cdot (c_{HCO_3^-} + c_{H_2O}/2)}{n_{solid}} \quad \text{Eq. 4-51}$$

4. With the mol fractions of all other solid phases known, the mol fraction anhydrate,  $x_{anh.}$ , was derived from the sodium carbonate balance: 1 mol anhydrate, 1 mol trona and 1 mol wegscheiderite each contained 1 mol sodium carbonate:

$$x_{anh.} = \frac{n_{Na_2CO_3} - n_{Trona} - n_{wesch.}}{n_{solid}} \quad \text{Eq. 4-52}$$

$$x_{anh.} = \frac{n_{Na_2CO_3} - n_{H_2O}/2 - (n_{NaHCO_3} - n_{H_2O}/2)/3}{n_{solid}} \quad \text{Eq. 4-53}$$

$$x_{anh.} = \frac{m_{sample} \cdot (c_{CO_3^{2-}} - c_{H_2O}/6 - c_{HCO_3^-}/3)}{n_{solid}} \quad \text{Eq. 4-54}$$

Since mol fractions more properly reflected the degree of conversion than mass fractions, in most figures mol fractions are given. They can be converted to mass fractions by:

$$w_i = \frac{x_i \cdot M_i}{\sum_j x_j \cdot M_j} \quad \text{Eq. 4-55}$$

$$\text{e.g.: } w_{Trona} = \frac{x_{Trona} \cdot M_{Trona}}{x_{Trona} \cdot M_{Trona} + x_{wesch.} \cdot M_{wesch.} + x_{anh.} \cdot M_{anh.}} \quad \text{Eq. 4-56}$$

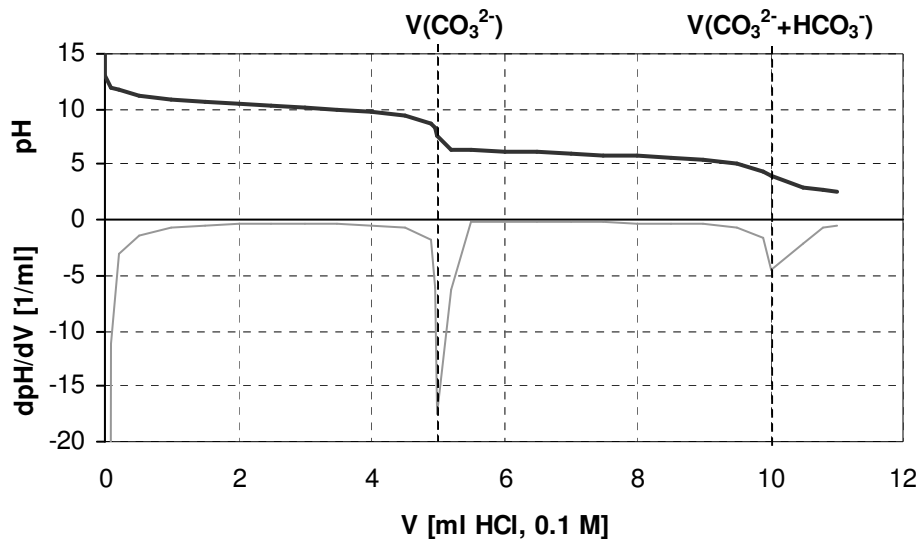


**Figure 4-20:** pH-Titration curve for the determination of  $[\text{CO}_3^{2-}]$  and  $[\text{HCO}_3^-]$

The accuracy of the used titration equipment was tested every day prior to the actual experimental samples with calibration solutions, prepared from analytical grade solid sodium bicarbonate and/or solid sodium carbonate and ultra pure water.

The reproducibility was found to be in the range of 0.5 to 2.5% of the measured concentration. All titrations were performed in triplicate and the amount of sample was chosen for  $V(\text{CO}_3^{2-} + \text{HCO}_3^-) \geq 5 \text{ ml HCl}$  to achieve good resolution with the titration. As the mol fractions in the solid could not be obtained directly, they were derived from the concentrations by the calculation procedures described above.

#### 4.8.3. Water Activity in Different Mixed Solvent Solutions

Oosterhof et al. [17] determined the water activity in sodium carbonate saturated mixed solvent solutions of different ethylene glycol content by measurement of the partial pressure of the water vapor above the solution. From their data, the following plot was derived.

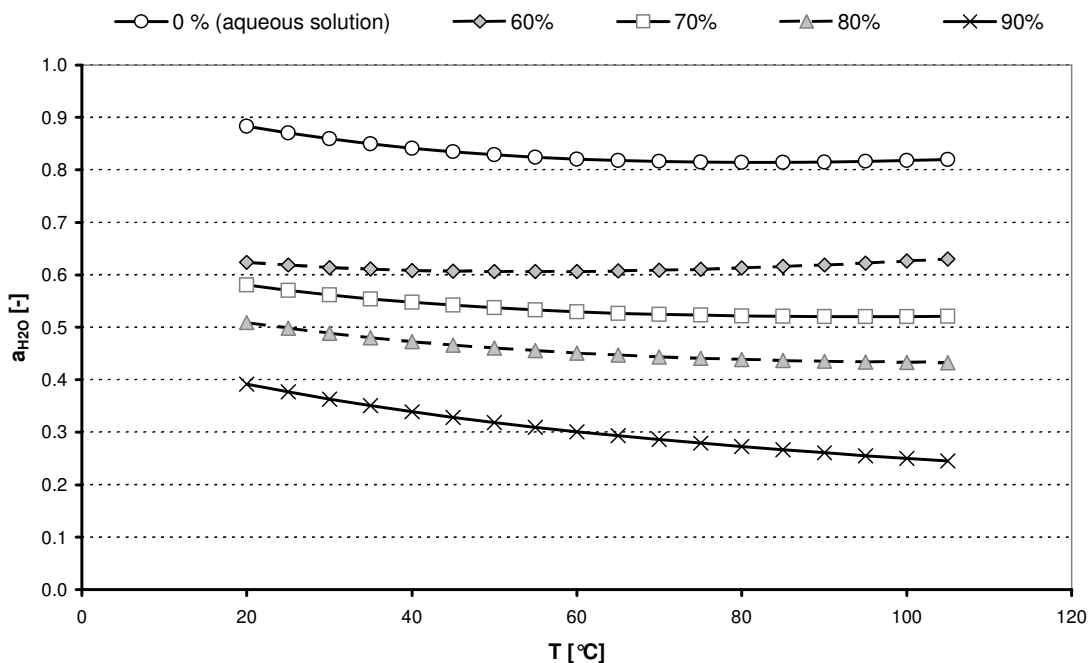


**Figure 4-21:** Water activity as a function of temperature for different sodium carbonate saturated mixed solvent solutions. Ethylene glycol content is given as %-weight (solvent-free base).

#### 4.8.4. Estimation of the Crystal Surface Area

As the dissolution of trona is a surface dependent process, the surface area of the trona crystals during dissolution had to be estimated. The occurrence of two additional phases (wagscheiderite and anhydrate) during the dissolution made the measurement of the crystal size distribution of the trona crystals too difficult to perform. Only the CSD of the starting material was measured by SEM and light-microscope particle image analysis. Therefore, the decline of surface area with decreasing trona mass was estimated mathematically assuming size independent linear dissolution. Three estimation functions of this approach are displayed in Figure 22:

- a) The dissolution of a monodispers distribution of trona crystals with the same starting surface area as the Solvay trona ( $A_0/m_0 = 0.0126\text{m}^2/\text{g}$ ). This corresponded to trona crystals with a major characteristic crystal diameter of 888 micron.

The surface area to mass ratio of the trona crystals was calculated as:

$$\frac{A}{m} = \frac{k_A \cdot d_{major}^2}{\rho_{trona} \cdot k_V \cdot d_{major}^3} = \frac{k_A}{\rho_{trona} \cdot k_V} \cdot \frac{1}{d_{major}} = \frac{k_A}{\rho_{trona} \cdot k_V} \cdot \sqrt[3]{\frac{\rho_{trona} \cdot k_V}{m}} \quad \text{Eq. 4-57}$$

$$\frac{A}{m_0} = \frac{A}{m} \cdot \frac{m}{m_0} = \frac{k_A}{(\rho_{trona} \cdot k_V)^{2/3}} \cdot \frac{1}{\sqrt[3]{m}} \cdot \frac{m}{m_0} \quad \text{Eq. 4-58}$$

$$\Leftrightarrow \frac{A}{m_0} = \frac{k_A}{(\rho_{trona} \cdot k_V)^{2/3} \cdot \sqrt[3]{m_0}} \cdot \left(\frac{m}{m_0}\right)^{2/3} = \frac{k_A}{\rho_{trona} \cdot k_V \cdot d_{major,0}} \cdot \left(\frac{m}{m_0}\right)^{2/3} \quad \text{Eq. 4-59}$$

$d_{major}$  was the major (longitudinal) characteristic length of the trona crystal, the surface area shape factor  $k_A$  ( $\approx 0.84$ ), the volume shape factor  $k_V$  ( $\approx 0.037$ ) and the density  $\rho_{trona}$  ( $\approx 2.13 \text{ g/cm}^3$ ) of the trona crystal [31].

With Eq. 57, Eq. 59 yielded of course:

$$\frac{A}{m_0} = \frac{A_0}{m_0} \cdot \left(\frac{m}{m_0}\right)^{2/3} \quad \text{Eq. 4-60}$$

- b) The linear dissolution of trona crystals with the measured crystal size distribution.

The initial crystal size distribution of the used trona was obtained by measuring a representative amount of crystals from light microscope and SEM images. The surface area and the mass of each crystal in the distribution were calculated using  $k_A$ ,  $k_V$  and  $\rho_{trona}$ . They were then added up to obtain total area and total mass, from which the overall initial surface area to mass ratio  $A_0/m_0$  was calculated. To simulate dissolution, a fixed length of 50 micron was subtracted from the major diameters in the distribution, negative diameters removed from the distribution and the surface area and mass calculated as described above. This procedure was repeated till only 1% of the original mass remained ( $m/m_0 = 0.01$ ).

- c) A gaussian size distribution was fitted to the measured CSD:

$$n(d) = \frac{1}{\sigma_x \cdot \sqrt{2\pi}} \cdot e^{-\left(\frac{(x-d)^2}{2\sigma_x^2}\right)} \cdot 100\% \quad [\%] \quad \text{Eq. 4-61}$$

The fit to the gaussian distribution yielded a mean diameter  $x$  of 641 micron and a standard deviation  $\sigma$  of 280 micron. The dissolution was simulated for this distribution in the same way as for the measured CSD (see b)). The predicted surface

area – mass ratio matched well with those obtained from the measured CSD. The measured CSD was thus well represented by the gaussian fit. Since the gaussian function is mathematically easier to handle than a measured CSD data set, this method is recommended to simplify predictive calculations:

$$A_{tot}(\Delta d) = \int_0^{\infty} \frac{1}{\sqrt{2\pi} \cdot \sigma_x} \cdot e^{-\frac{(\bar{x}_0 - d_{major} - \Delta d)^2}{2 \cdot \sigma_x^2}} \cdot 2 \cdot k_A \cdot d_{major} \cdot \partial d_{major} \quad \text{Eq. 4-62}$$

$$m_{tot}(\Delta d) = \int_0^{\infty} \frac{1}{\sqrt{2\pi} \cdot \sigma_x} \cdot e^{-\frac{(\bar{x}_0 - d_{major} - \Delta d)^2}{2 \cdot \sigma_x^2}} \cdot 3 \cdot k_V \cdot d_{major}^2 \cdot \rho_{trona} \cdot \partial d_{major} \quad \text{Eq. 4-63}$$

$$\frac{A}{m_0} = \frac{A_{tot}(\Delta d)}{m_{tot}(\Delta d = 0)} \quad \text{Eq. 4-64}$$

$$\frac{m}{m_0} = \frac{m_{tot}(\Delta d)}{m_{tot}(\Delta d = 0)} \quad \text{Eq. 4-65}$$

with  $\Delta d$  the decrease in the major characteristic length  $d_{major}$  by dissolution,  $x_0$  the average of  $d_{major}$  and  $\sigma$  its standard deviation in the gaussian distribution.

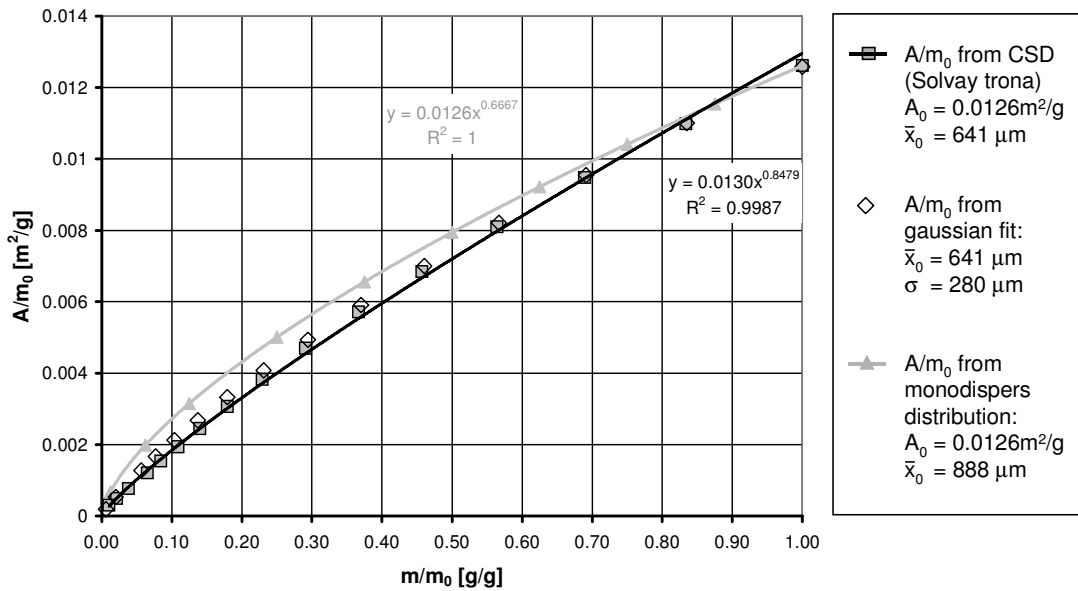


**Figure 4-22:** Surface area to starting mass ratio  $A/m_0$  during dissolution: Calculated from the measured CSD of the Solvay trona, a gaussian fit to the CSD and a monodispers distribution ( $x = 888$  micron) with the same starting surface area

Using the fitted curve to the dissolution function of the measured CSD, the surface area  $A$  of the remaining trona crystals in the batch experiments during dissolution in the solvent mediated recrystallization were calculated from the mass of the remaining crystals  $m$ :

$$A = m_0 \cdot 0.012959 \cdot \left( \frac{m}{m_0} \right)^{0.84786} \quad \text{Eq. 4-66}$$

#### 4.8.5. Analysis of the Dissolution Mechanism

Based on the measured correlation between the dissolution rate  $dm_{\text{trona}}/dt$  and the driving force  $\Delta X$ , given in Figure 9, the dissolution mechanism can be discussed further. Under the **assumption**, that trona dissolution was diffusion controlled, the dissolution coefficient  $k_{\text{diss}}$  could be derived from the diffusion coefficient of trona  $D_{\text{trona}}$  and the mean width of the concentration (i.e. diffusion) border layer around the trona crystals  $\delta_c$ :

$$\frac{dm_{\text{trona}}}{dt} = M_{\text{trona}} \cdot \rho_{\text{solution}} \cdot c_{\text{trona}} \cdot \frac{D_{\text{trona}}}{\delta_c} \cdot A_{\text{trona}} \cdot \Delta X_{\text{solway}} \quad \text{Eq. 4-67}$$

With the use Eq. 67, two simplifications are made implicitly:

First, trona actually breaks down into 4 species in solution –  $\text{Na}^+$ ,  $\text{CO}_3^{2-}$ ,  $\text{HCO}_3^-$  and  $\text{H}_2\text{O}$ . Each of these diffuses separately according to its individual diffusion coefficient and driving force [39]. For the rough estimation of diffusion-controlled dissolution, an overall the diffusion coefficient  $D_{\text{trona}}$  and the corresponding overall driving force  $\Delta X$  are used here.

Second, the mean concentration  $c_{\text{trona}}$  of trona in the border layer  $\delta_c$  was estimated from the concentrations of the 4 species in solution.

For a simple estimation of the order of magnitude of  $\delta_c$ , the uncertainties introduced by these simplifications are acceptable:

$$\delta_c = M_{\text{trona}} \cdot \rho_{\text{solution}} \cdot c_{\text{trona}} \cdot \frac{D_{\text{trona}}}{dm_{\text{trona}}/dt} \cdot A_{\text{trona}} \cdot \Delta X_{\text{solway}} \quad \text{Eq. 4-68}$$

An overall diffusion coefficient for trona in aqueous solution was given by Nasün-Sagili et al. [40] as a function of molar carbonate concentration:

$$D_{trona} = (8.6 + 1.19 \cdot c_{CO_3^{2-}} / \text{mol} \cdot \text{l}^{-1}) \cdot 10^{-10} \quad [\text{m}^2/\text{s}] \quad \text{Eq. 4-69}$$

It can be assumed that the diffusion rate of trona in the mixed solvent should be in the same order of magnitude. With a solution density of 1.10 to 1.15 kg/liter and a mean trona concentration of 0.25 to 0.45 mol/kg solution, Eq. 68 yields a mean border layer width of  $\delta_c = 1500 - 2000$  micron.

This value of  $\delta_c$  is unreasonable for a mixed vessel, especially since it is even in the range of the starting size of the trona crystals (500 to 5000 micron). The mean eddy scale in the dissolution experiments was calculated to be in the range of 40 microns, and the actual border layer width would therefore be significantly smaller than 40 microns.

This indicates that the trona dissolution was *not diffusion controlled*, but dominated by a surface disintegration step. The found dissolution coefficient  $k_{\text{diss}}$  represents the disintegration rate constant of this step.

#### 4.8.6. Thermodynamic Solubility Products

The solubility products given by Haynes [22, 23] were calculated from thermodynamic data of the occurring solid and dissolved species. While they could also be derived from solubility data, i.e. an array of solubility concentrations, and calculated activity coefficients with e.g. the Pitzer model [41, 42], this method was not as reliable: No electrolyte activity model appeared to be fitted with sufficient accuracy for this system for the required temperature and concentration range.

$$K_{sp,i}(T) = a_{Na^+}^{(2x+y)}(T) \cdot a_{CO_3^{2-}}^x(T) \cdot a_{HCO_3^-}^y(T) \cdot a_{H_2O}^z(T) \quad \text{Eq. 4-70}$$

$$K_{sp,i}(T) = \gamma_{Na^+}^{(2x+y)}(T) \cdot \gamma_{CO_3^{2-}}^x(T) \cdot \gamma_{HCO_3^-}^y(T) \cdot c_{Na^+}^{(2x+y)}(T) \cdot c_{CO_3^{2-}}^x(T) \cdot c_{HCO_3^-}^y(T) \cdot a_{H_2O}^z(T) \quad \text{Eq. 4-71}$$

With x, y and z the respective stoichiometric coefficients of carbonate, bicarbonate and crystal water in a given solid i (  $i = (\text{Na}_2\text{CO}_3)_x \cdot (\text{NaHCO}_3)_y \cdot (\text{H}_2\text{O})_z$  - e.g. trona: x = 1, y = 1, z = 2).

Haynes [22, 23] derived the thermodynamic solubility products from the apparent molar Gibbs free enthalpies of dissolution of the solids:

$$R \cdot T \cdot \ln(K_{sp,i}(T)) = \Delta G_{\text{Dissolution},m,i}(T) = \Delta G_{f,m,\text{solution},i}(T) - \Delta G_{f,m,\text{solid},i}(T) \quad \text{Eq. 4-72}$$

These Gibbs free enthalpies were derived from exact enthalpy, heat capacity, and entropy data for the occurring gases, liquids and solids and apparent molar Gibbs free energy data for dissolved species found in literature [43]. The molar Gibbs free energy of a substance *i* at the temperature *T* can be calculated as:

$$\Delta G_{f,m,i}(T) = \Delta H_{f,m,i}(T_0) + \int_{T_0}^T \Delta c_{Pm,i}(T) dT - T \cdot \left( \Delta S_{f,m,i}(T_0) + \int_{T_0}^T \frac{\Delta c_{Pm,i}(T)}{T} dT \right) \quad \text{Eq. 4-73}$$

$$\Delta H_{f,m,i}(T_0) = H_{m,i}(T_0) - \sum \nu \cdot H_m(T_0) \quad \text{Eq. 4-74}$$

$$\Delta S_{f,m,i}(T_0) = S_{m,i}(T_0) - \sum \nu \cdot S_m(T_0) \quad \text{Eq. 4-75}$$

$$\Delta c_{Pm,i}(T) = c_{Pm,i}(T) - \sum \nu \cdot c_{Pm}(T) \quad \text{Eq. 4-76}$$

$H_{m,i}$ ,  $S_{m,i}$ ,  $c_{Pm,i}$  were the molar enthalpy, entropy and heat capacity of the respective salt *i* and  $H_m$ ,  $S_m$ ,  $c_{Pm}$  the molar enthalpies, entropies and heat capacities of the elements, of which the salt *i* was composed of – with  $\nu$  their respective stoichiometric coefficients.  $\Delta c_{Pm,i}$  was required as a function of temperature, as it was used to calculate the temperature dependence of the molar Gibbs free energy  $\Delta G_{f,m,i}$ .

These solubility products were derived from thermodynamic properties of the pure solids and the dissolved ions. They were assumed valid for the mixed solvent system, provided that the Gibbs free energy of the dissolved state of the ions does not differ significantly between the aqueous solution and the mixed solvent.

Since in both cases, the ions were present in a standard ionized state, solubilized only by different numbers of solvent molecules (due to differences in polarity and polarizability of the solvents, i.e. reflected in e.g. their dielectric constant), this assumption appeared valid. The non-ideal behavior of the solubilization in the mixed solvent was after all reflected in the ions' activity coefficients - as is also non-ideal behavior of the solubilization in aqueous solution. This non-ideal behavior does not affect the standard state, for which the Gibbs free energy of dissolution is calculated. The activity coefficient can be expressed as a function of the *excess* Gibbs free energy of dissolution,  $\Delta G_{\text{diss},m}^E(T)$ , see Pitzer [41].



#### 4.8.7. Solid State Conversion – Contracting Cube and Contracting Disc Mechanism

The contracting cube model assumes equal conversion on all surfaces of cube or sphere shaped particles (i.e. all surfaces are approx. equidistant from the particle center). This implies, that the conversion also proceeds with equal rates from all surfaces into the core of the particle, leaving the unconverted material a proportionally shrinking cube, Eq. 77, or sphere, Eq. 78:

$$\alpha = \frac{a^3 - (a - 2 \cdot k_C \cdot t)^3}{a^3} = 1 - \left(1 - \frac{2 \cdot k_C}{a} \cdot t\right)^3 \quad \text{Eq. 4-77}$$

$$\alpha = \frac{4/3 \cdot \pi \cdot r^3 - 4/3 \cdot \pi \cdot (r - k_C \cdot t)^3}{4/3 \cdot \pi \cdot r^3} = \frac{r^3 - (r - k_C \cdot t)^3}{r^3} \quad \text{Eq. 4-78}$$

with  $a$  the edge length of the cube,  $r$  the radius of the sphere and  $k_C$  the linear conversion rate.

The contracting disc model could be deduced similarly for the assumption, that the conversion of a cylinder or prism shaped particle was dominated by the conversion on its longitudinal surface(s):

$$\alpha = \frac{\pi \cdot r^2 \cdot l - \pi \cdot (r - k_C \cdot t)^2 \cdot (l - 2 \cdot k_C \cdot t)}{\pi \cdot r^2 \cdot l} \quad \text{Eq. 4-79}$$

$$\Leftrightarrow \alpha = 1 - \left(1 - \frac{k_C}{r} \cdot t\right)^2 \cdot \left(1 - \frac{2k_C}{l} \cdot t\right) \quad \text{Eq. 4-80}$$

for:  $l \gg r$ , i.e.  $\frac{2k_C}{l} \ll \frac{k_C}{r}$  :

$$\Rightarrow \alpha = 1 - \left(1 - \frac{k_C}{r} \cdot t\right)^2 \quad \text{Eq. 4-81}$$



## Chapter 5

### RECRYSTALLIZATION OF TRONA (SODIUM SESQUICARBONATE) INTO SODA (SODIUM CARBONATE ANHYDRATE) IN A MIXED SOLVENT. PART II: ALTERNATIVE RECRYSTALLIZATION ROUTES

R.S. Gärtner, G.J. Witkamp

#### **Abstract**

The production of soda ash from trona ( $\text{Na}_2\text{CO}_3 \cdot \text{NaHCO}_3 \cdot 2\text{H}_2\text{O}_{(s)}$ ) in current industrial practice is very energy consuming: The recovered trona (ore) is first calcined at 120 to 160°C to sodium carbonate ( $\text{Na}_2\text{CO}_{3(s)}$ ) to remove crystal water and break down the bicarbonate content. The sodium carbonate is then dissolved to remove insoluble impurities and to crystallize sodium carbonate monohydrate ( $\text{Na}_2\text{CO}_3 \cdot \text{H}_2\text{O}_{(s)}$ ) by multi-effect evaporative crystallization. The monohydrate is then calcined and densified into the commercially available soda ash.

The energy consuming calcination and evaporative crystallization are avoided by the *mixed solvent reactive recrystallization* process presented here. This process is driven by the thermodynamic instability of the trona in the mixed solvent and the controlled thermal bicarbonate decomposition, and is performed without need for evaporation of solvent in the temperature range of 90 to 110°C. Additionally, the soda is crystallized from solution, allowing manipulation of its crystal size and crystal size distribution. Through this controlled crystallization the produced soda has not only higher purity and mechanical strength than the commercially available one, but also superior bulk densities of 1200 kg/m<sup>3</sup> and more can be obtained.

By circumventing the calcination and evaporative crystallization steps of the industrial process, savings in heating energy of 70 to 90% can be achieved.

Three alternative process routes for mixed solvent reactive recrystallization are presented: 1-step and 2-step reactive recrystallization and wet calcination.

## **5.1. Introduction**

Trona, sodium sesquicarbonate,  $\text{Na}_2\text{CO}_3 \cdot \text{NaHCO}_3 \cdot 2\text{H}_2\text{O}$ , is an important source material for the production of soda (sodium carbonate anhydrate). Trona occurs as a natural ore in the United States (e.g.: Green River Territory, Wyoming and Searles Lake, California) and is mined there for soda production since the first half of the last century [1]. Both regular and solution mining have been performed in trona recovery. While solution mining is considered to have less environmental impact, in the United States the larger part of trona is still recovered by regular mining due to insoluble compounds, impurities and the low solubility of bicarbonate, which appear to impair solution-mining operations. Over 600 published articles and patents can be found dealing with process improvements, process alternatives, measurement of process parameters and physical properties of the system, testifying to the industrial relevance of trona as a source material and the importance of soda as a bulk commodity. Garret [1], Haynes [2] and Aitala [3] give excellent reviews of the current state-of-the-art processes and feasible process alternatives.

In Europe, the plans for the exploitation of the large Beypazari trona deposit west of Ankara, Turkey, [4] have increased the interest in trona-related research in the last years [5-10]. Beypazari trona (> 99 %w [4]) may be easily processed by solution mining, as it appears to contain little soluble and insoluble impurities, according to Garret [4]. This high purity applies apparently only to individual strata in the overall deposit, as Nasün-Saygili et al. [5] estimated the overall grade of the deposit as ca. 84 %w trona. The studies on the dissolution rate of Beypazari trona [5, 6] have shown, that the dissolution behavior of the Beypazari trona is similar to the one found in American trona ores, like the ones investigated in Chapter 4 [11].

A significant economic bottleneck for the production of soda from trona compared to the Solvay process [12], which is commonly employed in Europe, is the remoteness of the mining sites. The produced soda needs to be transported over considerable distances for use in glass manufacturing, detergent production, etc. at production sites close to larger population centers or to larger harbors (for e.g. international export). Increasing the bulk density of the produced soda can significantly lower the transport costs and thereby make

a trona-based soda production economically more attractive, as a larger region becomes accessible for sales and marketing.

In this chapter, a number of energy efficient alternative processes, based on the mixed solvent reactive recrystallization of trona, for the production of super dense soda from solid trona with a yield of almost 100% are presented.

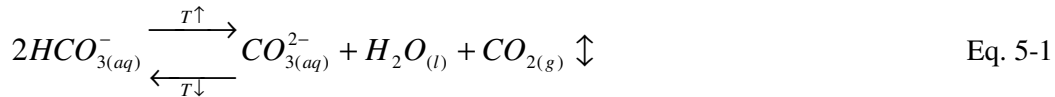
Soda (sodium carbonate anhydrate, natrite,  $\text{Na}_2\text{CO}_{3(s)}$ ) is crystallized in the last step and bulk densities of  $1400 \text{ kg/m}^3$  can be achieved. Since this soda consists of comparatively large (mean diameter ca. 150 micron) crystals, it is also more resistant to breakage and dusting than the commercially available soda. Also the impurity content of the super dense soda is lower compared to the commercially available soda, due to its lower intercrystalline porosity, see Chapter 2 [13].

The aim of this work is develop and illustrate different alternative process routes based on *mixed solvent reactive recrystallization*, see Chapter 4 [11].

## 5.2. Theory

### 5.2.1. The System $\text{Na}_2\text{CO}_3\text{-NaHCO}_3\text{-H}_2\text{O}$

Trona, sodium sesquicarbonate, is a hydrate double salt of sodium carbonate and bicarbonate:  $\text{Na}_2\text{CO}_3\cdot\text{NaHCO}_3\cdot 2\text{H}_2\text{O}_{(s)}$ . Almost all natural deposits of sodium carbonates consist of either trona or nahcolite ( $\text{NaHCO}_{3(s)}$ ). This is due to the fact, that in all aqueous carbonate-bicarbonate solutions the carbonate / bicarbonate content will shift towards equilibrium compositions that favor the formation of these solids.



This equilibrium shifts significantly with temperature. With decreasing temperature the equilibrium shifts towards the bicarbonate ion.

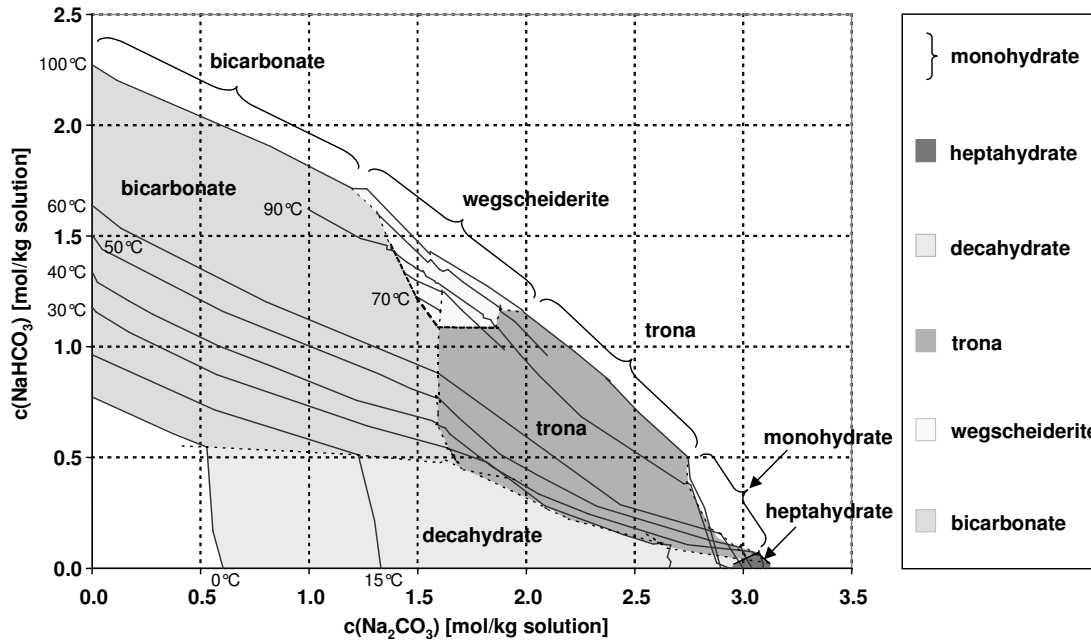


**Figure 5-1:** Phase and solubility diagram of the system  $\text{Na}_2\text{CO}_3\text{-NaHCO}_3\text{-H}_2\text{O}$ , derived from phase and solubility data from [14-17]

Wegscheiderite,  $\text{Na}_2\text{CO}_3 \cdot 3\text{NaHCO}_3(s)$ , the only other known double salt of sodium carbonate and bicarbonate, is only formed at temperatures above  $70^\circ\text{C}$  from aqueous solution, see Figure 1, and is therefore only rarely found in nature.

From aqueous carbonate solutions containing little or no bicarbonate, sodium carbonate decahydrate ( $\text{Na}_2\text{CO}_3 \cdot 10\text{H}_2\text{O}$ , *natron*: till ca.  $32^\circ\text{C}$  [7, 8]), heptahydrate ( $\text{Na}_2\text{CO}_3 \cdot 7\text{H}_2\text{O}$ , from  $32$  till ca.  $34^\circ\text{C}$  [14, 15]) and monohydrate ( $\text{Na}_2\text{CO}_3 \cdot \text{H}_2\text{O}$ , *thermonatrite*: from  $34^\circ\text{C}$  till  $109^\circ\text{C}$  [14, 15]) can be crystallized. At atmospheric pressure the anhydrate ( $\text{Na}_2\text{CO}_3$ , *natrite*) cannot be crystallized (unless the growth of the monohydrate can be inhibited), since the saturated solution's boiling point at  $104.8^\circ\text{C}$  [15, 16] is lower than the anhydrous transition temperature of  $109^\circ\text{C}$  [14].

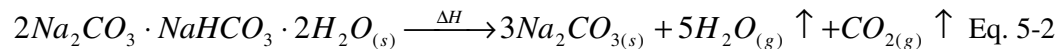
In current industrial practice, sodium carbonate is therefore crystallized as monohydrate by evaporative crystallization. The monohydrate is then dehydrated by *calcination* (heating of the solid to remove volatile compounds of the crystal like the crystal water) at  $100$  to  $160^\circ\text{C}$  [1], resulting in a (pseudo) solid phase conversion to anhydrous soda.

The crystallization of anhydrous soda from solution at atmospheric pressure is possible, though, by lowering the anhydrous transition temperature [18-20]. Any significant

reduction in the water activity in solution reduces the stability of the hydrates and lowers the transition temperature, i.e. the temperature, at which e.g. the monohydrate will recrystallize to the anhydrate. Introducing well-soluble electrolytes into the solution - like NaCl or NaOH in high concentrations [21, 22] - reduces the water activity. It can also be reduced by adding a hygroscopic antisolvent like methanol [23], ethylene glycol [20] or glycerol [18, 19]. The possibility of crystallizing the anhydrate (instead of the monohydrate) directly from solution with the help of ethylene glycol as antisolvent was investigated by Oosterhof et al. [18-20, 24], and is also used in the presented processes.

### 5.2.2. The Conversion of Trona in Current Industrial Practice

The conversion of trona to soda (sodium carbonate anhydrate,  $\text{Na}_2\text{CO}_{3(s)}$ ), is most often performed in current industrial practice in the dry state by calcination (i.e. thermal decomposition) of the solid salt at temperatures between 120 and 160°C [1]:



$$\Delta H_{R, 298.15\text{K}} = 133.39 \text{ kJ/mol [6]}$$

Calcination is the technically most uncomplicated conversion method. However, it is neither the most energy efficient one, nor does it yield a product of high quality. The resulting soda consists of *pseudomorphs*, i.e. aggregates of the formed soda crystallites, which retain the shape and approximate size of the original trona crystals. The soda crystallites in the aggregates remain small due to the poor growth conditions in the solid-state conversion (<1µm). Due to the removal of the  $\text{CO}_2$ , the crystal water and the reaction water, the aggregates are very porous and have low bulk density and poor mechanical stability - resulting in breakage and dusting during production, packing, transport, and further processing. Additional processing is required to improve the handling and transport qualities of this soda.

### 5.2.3. The Conversion of Trona by Mixed Solvent Reactive Recrystallization

The conversion of trona to soda can be broken down into three fundamental steps:

- 1) The break-up of the trona crystal lattice & the discharge of the crystal water

- 2) The decomposition of bicarbonate to carbonate and the discharge of CO<sub>2</sub>
- 3) The formation of the soda crystals (nucleation and growth)

As presented in Chapter 3 [25], temperatures >90°C and/or intense CO<sub>2</sub>-stripping need to be applied, to achieve complete conversion at ambient CO<sub>2</sub> partial pressure. The bicarbonate conversion rate increases exponentially with temperature following an Arrhenius relation. In aqueous solution at atmospheric pressure the conversion rate is limited by the boiling point of the saturated bicarbonate/carbonate solution, which is in the range of 101.4°C (saturated NaHCO<sub>3</sub> solution) to 104.8°C (saturated Na<sub>2</sub>CO<sub>3</sub> solution). Furthermore, only monohydrate can be crystallized at these conditions.

Attempts to perform this conversion in slurries of trona and its aqueous solution had only limited success, since the conversion remained incomplete – most probably due to the carbonate-bicarbonate equilibrium (Eq. 1). Not all bicarbonate in solution was decomposed, most likely due to insufficient CO<sub>2</sub> desorption, and trona remained the predominant solid phase in the system.

Since trona is a hydrate, its phase stability, especially in solution, depends on the ambient water activity. A significant reduction in water activity will force the trona to recrystallize to an anhydrous form. As shown in Chapter 3 [25], the bicarbonate content of the trona will convert solution mediated to carbonate at temperatures above 90°C for ambient CO<sub>2</sub> partial pressure and natural CO<sub>2</sub> desorption rates. Additionally, for mixed solvents with antisolvent contents >30%-w (salt free), sodium carbonate can be crystallized as anhydrate instead of the monohydrate from solution [20]. Combining these two processes for the conversion of trona, crystalline soda can be directly produced from trona.

Furthermore, not only the stability of trona can be modified - also its rate of dissolution and the growth of the anhydrate can be controlled via process temperature, mixed solvent content and the bicarbonate decomposition rate. Thereby, the crystal size distribution of the formed anhydrate can be influenced and high bulk densities can be achieved – up to 1500 kg/m<sup>3</sup> [15, 18].

These processes can be described by the following relationships:



- a) The trona dissolution rate is a linear function of the temperature difference  $\Delta T$  between the process temperature and the anhydrous transition temperature:

$$\frac{dm_{trona}}{dt} = k'_D \cdot A_{trona} \cdot \Delta T = k'_D \cdot A_{trona} \cdot (T - T_{trans}) \quad \text{Eq. 5-3}$$

- b) The anhydrous transition temperature is a rather complex function of the water activity.
- c) The bicarbonate composition rate is a function of the concentration of the dissolved bicarbonate. For the tested temperature and mixed solvent composition range, a first order relationship can be used to estimate the decomposition rate:

$$r_{HCO_3^-} = \frac{dn_{HCO_3^-}}{m_{solution} \cdot dt} \equiv k_{HCO_3^-}(T) \cdot c_{HCO_3^-} \quad \text{Eq. 5-4}$$

The mixed solvent composition appeared to have no influence on the bicarbonate decomposition rate.

Values for the kinetic parameters  $k'_D$  and  $k_{HCO_3^-}$  are given in Chapter 4 [11] and Chapter 3 [25].

Since the crystallization of the soda yields comparatively large single crystals, it has an improved filterability and is far less prone to breakage, dusting and caking than the soda produced by calcining.

### **5.3. Experimental procedures**

#### **5.3.1. Solubility and Stability Determination in Shake tests**

The phase stability and the corresponding carbonate-bicarbonate solubility of a range of temperatures and mixed-solvent compositions were determined in shake-tests: 15g of solid and 40g of mixed-solvent solution were shaken in 50ml Nalgene™ PTFE-bottles in a thermostated shaking bath. In these tests, mixed solvents with ethylene glycol contents of 50, 60, 70, 80, 90 and 100%-w (salt-free) were used. Two different series of experiments were performed. The first started with a solid composed of a mixture of sodium carbonate and bicarbonate of technical purity (> 99.5%) in a molar ratio of 1 : 3. In the second series, trona, supplied by Solvay, France, was used as starting solid, see

Figure 1. The bottles were shaken at constant temperature for one day. The experiments were started at 50°C and the temperature was increased daily after analysis by 10°K till 90°C. It had been found in previous work, that solid bicarbonate recrystallized above 90°C in the mixed solvent. Since the sodium bicarbonate solubility was the parameter of interest for this investigation, the presented series of experiments were only conducted till 90°C. Solution samples were taken and titrated with 0.1 M HCl with a Radiometer VIT 90 Video Titrator. The concentration of  $\text{CO}_3^{2-}$  and  $\text{HCO}_3^-$  were determined from the titration curves, see Addendum. The heating-weight-loss of the solid was determined after completion of the experimental series. No significant decomposition of either dissolved or solid bicarbonate was found. The complete solubility data set is given in Chapter 6 [26], while some of the phase stability information is summarized in Figure 1, 2, 6 and 9.

### 5.3.2. Batch Recrystallization Experiments

Slurries of 15 to 20%-w trona in mixed solvents containing 50 to 100%-w ethylene glycol were prepared and recrystallized according to the required temperature profiles of the different conversion routes in a thermostated, stirred tank reactor of 1.5 liter volume. A sketch of the experimental set-up is given in the Addendum.

Samples of the slurry were taken app. every 30 minutes, the solvent was filtered off and the solid was rinsed with acetone. The solid was then analyzed for heating-weight-loss in a Mark II Moisture Analyzer thermobalance (Denver Instruments). From the heating-weight-loss the degree of decomposition of the solid sodium bicarbonate was determined (see Addendum). The occurring crystal phases were identified by (polarized) light microscopy, SEM images and/or powder XRD. For process routes, where trona would recrystallize to wegscheiderite and anhydrate and the bicarbonate fraction would decompose (bulk) solution mediated, the carbonate and bicarbonate concentrations were additionally determined titrimetrically in the solution and in the solid samples taken.

### **5.3.3. Continuous Recrystallization Experiments**

The continuous experiments for the different recrystallization routes were performed in a continuously operated tank-reactor cascade of 3 thermostated stirred tanks. The first reactor had a volume of 1.7 litres and was mixed by a propeller-turbine stirrer combination supported by baffles. The following two reactors had a volume of 5 litres (each) and were mixed by a propeller-draft tube arrangement. Each reactor was thermostated to a constant operation temperature individually by a heating bath. Mixed solvent solution was fed to the first reactor in the cascade by a dosage pump, the solid trona fed to the first reactor by a powder feeder. Feed rates were adjusted to receive a desired slurry density and residence time profile in the cascade. Between the reactors, the slurry flowed on to the following reactor by overflow from a side outlet. The slurry from the last reactor was split into a solid and a solution fraction by sedimentation in settling vessel. The solution was recycled to the solution storage vessel and from there back to the reactor cascade. A process flow diagram of the set-up is given in the Addendum.

5 ml slurry samples were taken by pipette at intervals of app. 1 hour from the center of the reactors. The solution of the sample was filtered off and recovered for analysis; the solid was washed with acetone and dried by suction in the filtration set-up for 15 minutes. The solution and the solid samples were titrated for their bicarbonate and carbonate content. The solid samples' heating-weight-loss was determined additionally for the amount of adhering solvent (acetone and/or mixed solvent), and for counter checking the titration results.

## **5.4. Results**

### **5.4.1. Mixed Solvent Reactive Recrystallization of Trona**

The mixed solvent technique is not only less process intensive and less energy consumptive than the current production routes [1], but also higher bulk densities can be achieved with it: The crystalline soda was found to reach bulk densities of up to 1550 kg/m<sup>3</sup> [18]. The material density of sodium carbonate anhydrate is 2540 kg/m<sup>3</sup>.

This high density of crystalline soda can of course only be achieved by careful monitoring of the crystal growth rate and particle size distribution during the solvent

mediated recrystallization. The dissolution rate of the trona and the bicarbonate decomposition rate have to be reduced to levels, which allow the slow continuous growth of the soda crystals. Especially increases in supersaturation, which would result in excessive nucleation and an undesired broadening of the particle size distribution, have to be avoided.

Three different *mixed solvent reactive recrystallization* (MSRR) process routes have been developed to achieve these objectives:

1-Step MSRR, 2-Step MSRR and Wet Calcination & Double Recrystallization

#### **5.4.2. 1-Step Mixed Solvent Reactive Recrystallization (1-Step MSRR)**

To convert trona directly to crystalline soda (anhydrate) by solvent mediated crystallization, the trona crystals have to be dissolved slowly to prevent pseudomorph formation, while operating at temperatures, where the bicarbonate content of the trona will decompose to carbonate. This is only possible in a narrow window of operating conditions for the trona + mixed-solvent system. As is sketched in Figure 2, the operating range for the 1-step conversion lies between the region of pseudomorph formation and the line of bicarbonate decomposition (which runs approximately at constant 90°C). The metastable transition line of (Solvay) trona should not be exceeded, to ensure, that pseudomorph formation is effectively suppressed. Since the bicarbonate decomposition rate increases with temperature, the temperature of the metastable transition line was chosen as operating temperature, since the maximal feasible decomposition rate was desirable to reduce processing time.

Previous work has shown [11], that at around 100°C, the growth of carbonate is still faster than the bicarbonate decomposition, so the bicarbonate decomposition at the transition line conditions did not lead to excessive supersaturation and unwanted nucleation.

An ethylene glycol content of 60%-w in the mixed solvent was used, since the transition temperature of ca. 100°C resulted in an acceptable decomposition rate while still being ca. 10K below the boiling point of the mixed solvent.

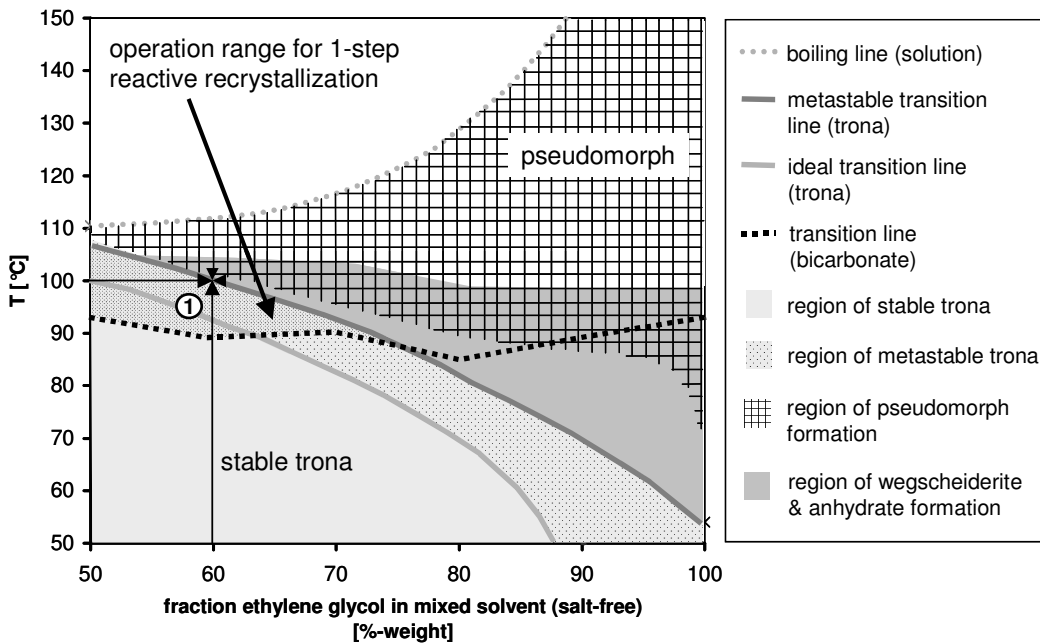


**Figure 5-2:** Operation range for 1-step trona reactive recrystallization in mixed solvent

This margin to the boiling point was found necessary to avoid an excessive degree of evaporation of water from the mixed solvent. Recrystallization experiments were performed in a discontinuous stirred tank reactor and continuous stirred tank-reactor cascade.

#### 5.4.2.1. Batch Recrystallization

The conversion of trona was first tested in discontinuous, thermostated stirred-tank experiments with 60%-w ethylene glycol mixed solvent. An amount of trona was added to the reactor of 20%-w of the total reactor content. The aim was to convert the trona to crystalline soda at almost constant temperature, i.e. with a minimal temperature shift. Starting from the transition temperature of 100°C the temperature was increased stepwise and the recrystallization monitored.

In Figure 3, the changes in solid and solution composition with time are displayed at the different temperature steps. For the first 100 minutes the temperature was kept at 100°C.

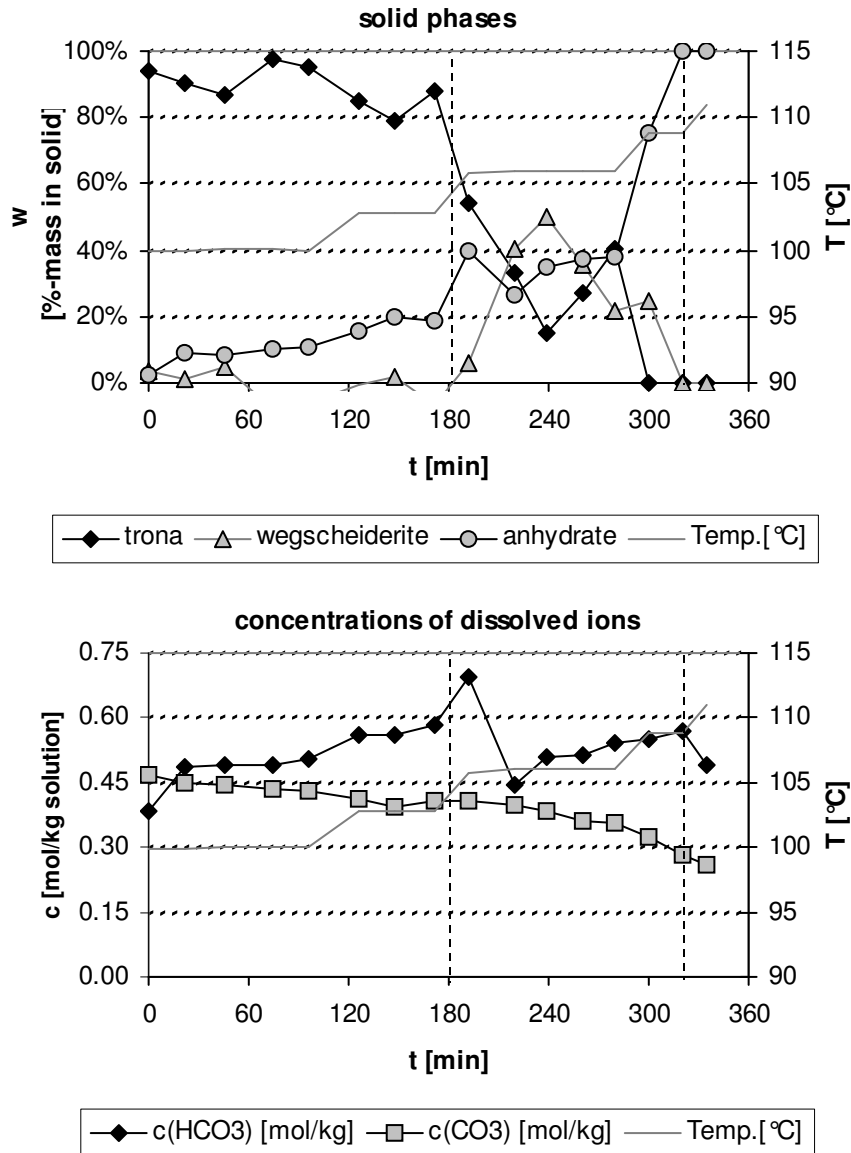


**Figure 5-3:** Solid and solution composition during discontinuous 1-step recrystallization in a discontinuous, stirred tank in 60%-w ethylene glycol mixed solvent

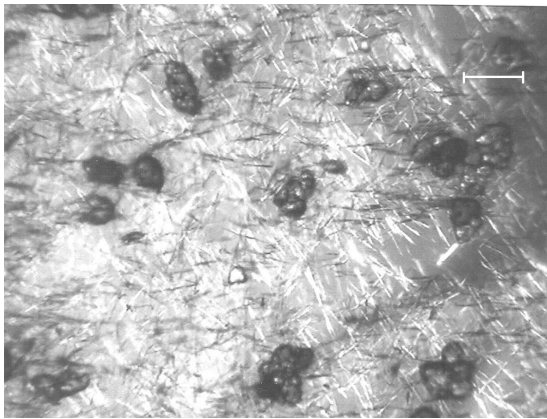
Slow decomposition of bicarbonate in solution occurred, resulting in the dissolution of trona and crystallization of a small amount of sodium carbonate anhydrate.

At a slightly increased temperature of 103°C, more trona dissolved immediately as the solubility of bicarbonate in solution increased with temperature, resulting in crystallization of another small amount of anhydrate. As the bicarbonate concentration increased in solution, the carbonate concentration had to decrease due to the solubility product of the trona.



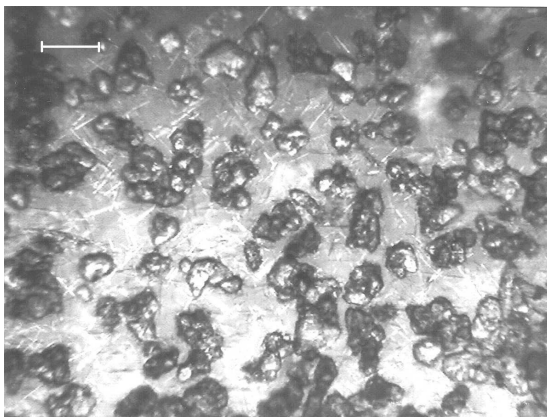
80 minutes: 100°C, bar = 200micron

- trona (large prisms)
- + anhydrate (small dark plates)
- + wegscheiderite (fine needles)



275 minutes: 106°C, bar = 200micron

- anhydrate (dark clusters)
- + wegscheiderite (light needles)



315 minutes: 106°C, bar = 200micron

- anhydrate (dark clusters)
- + wegscheiderite (light needles)

**Figure 5-4:** Solid phases during the batch recrystallization of trona in 60 %-w ethylene glycol by the 1-step process, observed by polarized light microscopy

At the next temperature step of 106°C the trona recrystallized rapidly in solution due to the instability of the crystal water. Wegscheiderite nucleated and grew (see Figure 3 at ca. 180 minutes) as the trona fraction decreased rapidly. A small amount of anhydrate dissolved again, as the forming wegscheiderite took up carbonate from solution. With further progressing time, the bicarbonate content of the reactor decomposed solution

mediated, resulting in the slow dissolution of wegscheiderite and the increase of the anhydrate fraction till finally at ca. 320 minutes the solid phase consisted entirely of anhydrate.

The progression of the phase transformation is illustrated in Figure 4:

In the first image taken at 80 minutes during the experiment of Figure 3, the original prism-shaped trona crystals and small cluster of the newly formed anhydrate platelets can be seen. Already a few fine wegscheiderite needles are visible, indicating that the system is at its transition temperature at 100°C.

In the second image, taken at 275 minutes, only wegscheiderite and anhydrate were present. No pseudomorphs are visible in this picture, but the solid did contain a small fraction of them.

The third image at 315 minutes was taken shortly before the complete disappearance of the wegscheiderite. The anhydrate fraction of the solid has clearly increased compared to the previous image and the anhydrate crystals have grown in size. The anhydrate tends to form agglomerates of a small number (4 to 8) of single crystals.

This experiment proved that trona could be converted to crystalline soda with little variation of temperature or even at constant temperature. This and other 1-step discontinuous recrystallization experiments yielded a crystalline soda of a bulk density of up to 1140 kg/m<sup>3</sup>.

#### *5.4.2.2. Continuous Recrystallization Experiments*

The 1-step crystallization was also tested in continuous recrystallization experiments using a continuous stirred tank cascade of 3 separately thermostated stirred tank reactors. The first reactor vessel had a volume of 1.7 liters; the other two vessels were identical 5-liter draft tube reactors. The input flows of trona and 60%-w (salt-free base) ethylene glycol mixed solvent were set to achieve a slurry density of around 15%-w solid throughout the set-up and residence times of 40 minutes in reactor 1, and 120 minutes in reactor 2 and 3 each.

This residence time profile was chosen, to allow equilibration of the trona at the transition temperature in reactor 1 before conducting the trona dissolution and



bicarbonate decomposition at 105°C in reactor 2. Reactor 3 was operated at 110°C, to decompose any remaining bicarbonate fraction. The details of the operating conditions are summarized in Table 1:

**Table 5-1:** Operating conditions for the continuous 1-step crystallization of trona in 60%-w ethylene glycol mixed solvent in a cascade of 3 stirred tank reactors

	<i>Reactor 1</i>	<i>Reactor 2</i>	<i>Reactor 3</i>
<b>Stirrer Type:</b>	double stirrer: propeller + turbine impeller	propeller	Propeller
<b>Flow Modifier:</b>	baffles	draft tube w. baffles	draft tube w. baffles
<b>Volume:</b>	1.7 [liter]	5 [liter]	5 [liter]
<b>Residence Time:</b>	40 [min]	120 [min]	120 [min]
<b>Stirring Rate:</b>	300-500 [rpm]	350 [rpm]	350 [rpm]
	0.3 [W]	0.3 [W]	0.3 [W]
<b>Temperature:</b>	~100 [°C]	105 [°C]	110 [°C]
<b>Solid Content:</b>	~16 [%-w]	~13.5 [%-w]	~13.5 [%-w]
<b>CO<sub>2</sub> stripping w. air</b>	no	yes	no
<b>Solid phases:</b>	- trona - (wegscheiderite) - (anhydrate)	- trona - wegscheiderite - anhydrate	- anhydrate - (wegscheiderite)
<b>Concentrations:</b>			
	[HCO <sub>3</sub> <sup>-</sup> ] ~0.40 [mol/kg]	~0.50 [mol/kg]	~0.50 [mol/kg]
	[CO <sub>3</sub> <sup>2-</sup> ] ~0.45 [mol/kg]	~0.35 [mol/kg]	~0.20 [mol/kg]

The concentration profiles in a continuous experiment are given in Figure 5:

The equilibration of the trona at a temperature of 102°, i.e. slightly above the transition point, first resulted in trona recrystallization to anhydrate and wegscheiderite. But as the solution in reactor 1 became saturated with carbonate and bicarbonate ions and more trona was fed to the reactor, the recrystallization (dissolution) rate was too low to balance the trona feed stream and trona became the dominant phase in reactor 1. A small amount

of anhydrate formed, which lowered the solubility of carbonate in the reactor from the expected trona equilibrium carbonate concentration given in Table 1.

The recrystallization of trona in reactor 2 did proceed as expected with the formation of only a small amount of pseudomorphs. All trona was converted to wegscheiderite and anhydrate. The decomposition rate of bicarbonate in this stage was as fast as expected at this temperature, so that the bicarbonate fraction contained in the solid was ca. 40%-mol:

$$\frac{\Delta n_{HCO_3^-}}{\Delta t \cdot m_{solution}} \approx \frac{dn_{HCO_3^-}}{dt \cdot m_{solution}} = k_{60\%-w}(105^\circ C) \cdot c_{HCO_3^-} \quad \text{Eq. 5-5}$$

If no bicarbonate had decomposed, the fraction would have been 46.0 %-mol (accounting for the higher solubility of bicarbonate (ca. 0.35 mol/kg solution) compared to carbonate (ca. 0.20 mol/kg solution) at these conditions). The steady state established only slowly in reactor 2 (dotted vertical line at 420 minutes), most probably due to the fact that the system was close to the transition point of trona. In the beginning some wegscheiderite and anhydrate formed until sufficient trona was present.

In Reactor 3, though, the bicarbonate decomposition did not proceed as fast as expected and ca. 20%-mol of the solid phase consisted of bicarbonate. The decomposition rate was about 33% lower than in the discontinuous experiments. This decreased decomposition rate was most likely due to a lower CO<sub>2</sub> desorption rate from reactor 3, since this reactor was not fed with air to enhance CO<sub>2</sub> desorption.

It can be assumed that more intense stripping of CO<sub>2</sub> will increase the decomposition of bicarbonate to the desired levels to achieve complete conversion.

Due to the amount of wegscheiderite remaining in the solid, the bulk density of the solid, was rather low with ca. 800 kg/m<sup>3</sup>.

In the presented experiments, the intermediate formation of wegscheiderite was not completely avoided. Due to the rather low bicarbonate decomposition rate at temperatures below 100°C (i.e. the transition temperature in 60%-w mixed solvent) the transformation would take more than 24 hours. Such a time-intensive process would not be industrially feasible. Therefore temperatures above 100°C were chosen, which were slightly above the transition line, resulting in formation of small amounts of wegscheiderite and anhydrate (see 2-step MSRR below).

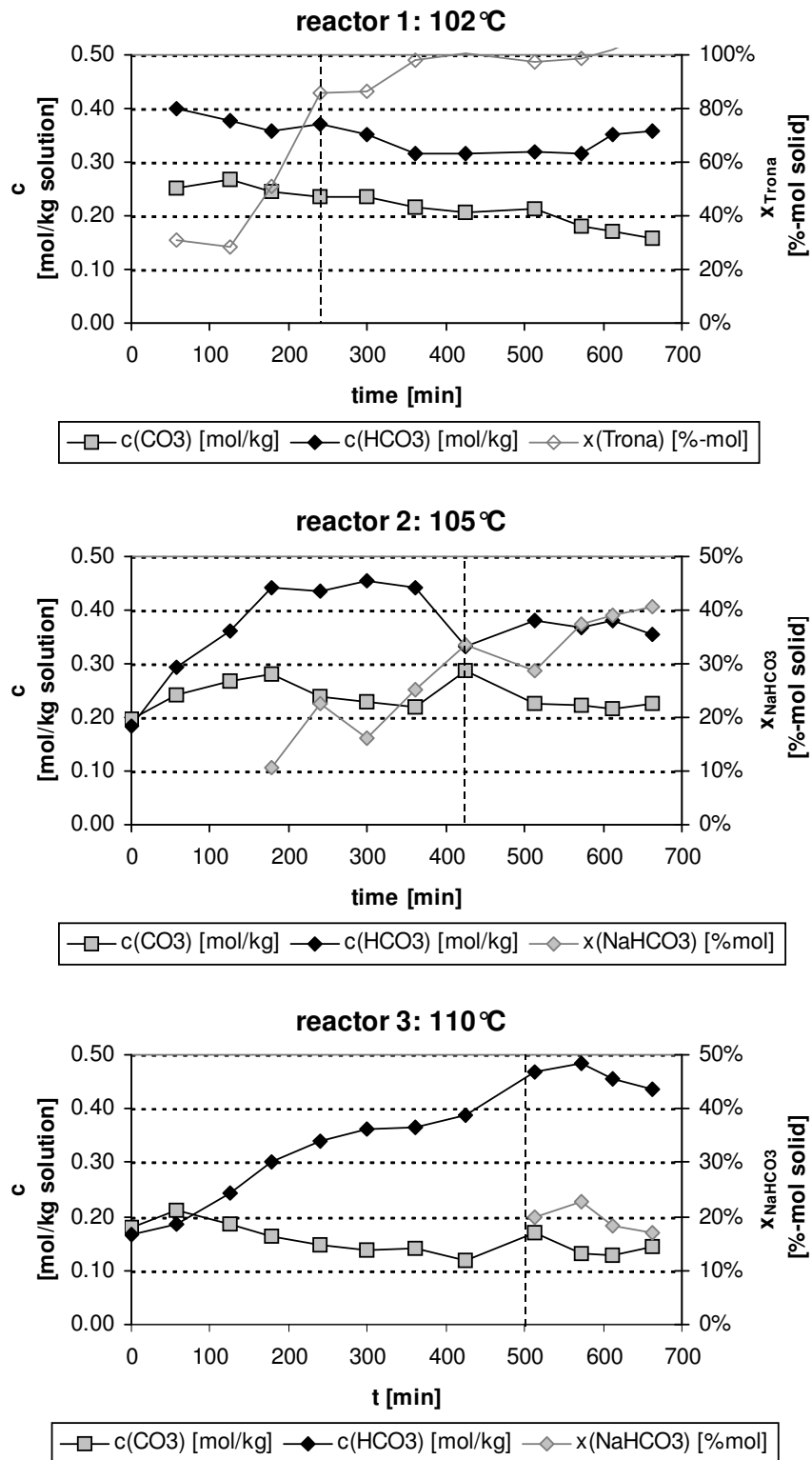


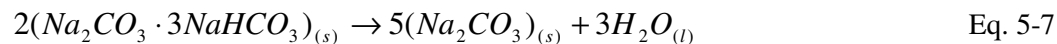
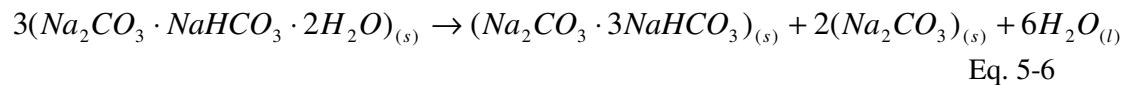
**Figure 5-5:** Composition profiles during continuous 1-step recrystallization of trona to soda (anhydrate) in 60%-w ethylene glycol mixed solvent in a stirred-tank cascade

For lower ethylene glycol contents in the mixed solvent than 60%-w (salt-free base), though, direct recrystallization of trona to anhydrate without any intermediate formation of wegscheiderite could be attempted: By remaining below the trona transition line and above the bicarbonate transition line, the bicarbonate of the trona would decompose, while the crystal water of the trona would still be stable. This would result in a recrystallization only driven by the slow bicarbonate decomposition.

Such a direct conversion would have to be operated close to the boiling point of the solution, where the water evaporation rate is significant. Such an operation would require intense reflux cooling to counter the evaporation, which also decreases the energy efficiency of the process.

#### 5.4.3. 2-Step Mixed Solvent Reactive Recrystallization (2-Step MSRR)

The basic idea of the 2-step conversion of trona was, to recrystallize the trona first completely to wegscheiderite and anhydrate according to Eq. 6 and then to decompose the bicarbonate content in a second step at a higher temperature level according to Eq. 7.



The advantage of this method was, that the amount of pseudomorphs formed could be minimized, since these were only formed from trona, see Chapter 4 [11]. All other bicarbonate-containing phases of the system, i.e. wegscheiderite ( $\text{Na}_2\text{CO}_3 \cdot \text{NaHCO}_3$ ) and nahcolite ( $\text{NaHCO}_3$ ), recrystallized (bulk) solution mediated even at high temperatures.

For the first step, as illustrated in Figure 6, a temperature slightly above the transition line was chosen, but where possible below 90°C, to avoid the accelerating effect of the bicarbonate decomposition on the trona conversion. Still, to minimize the process time of the first step, the chosen temperature was chosen close to the lower edge of the region of pseudomorph formation to take advantage of the higher dissolution rates at these temperatures.

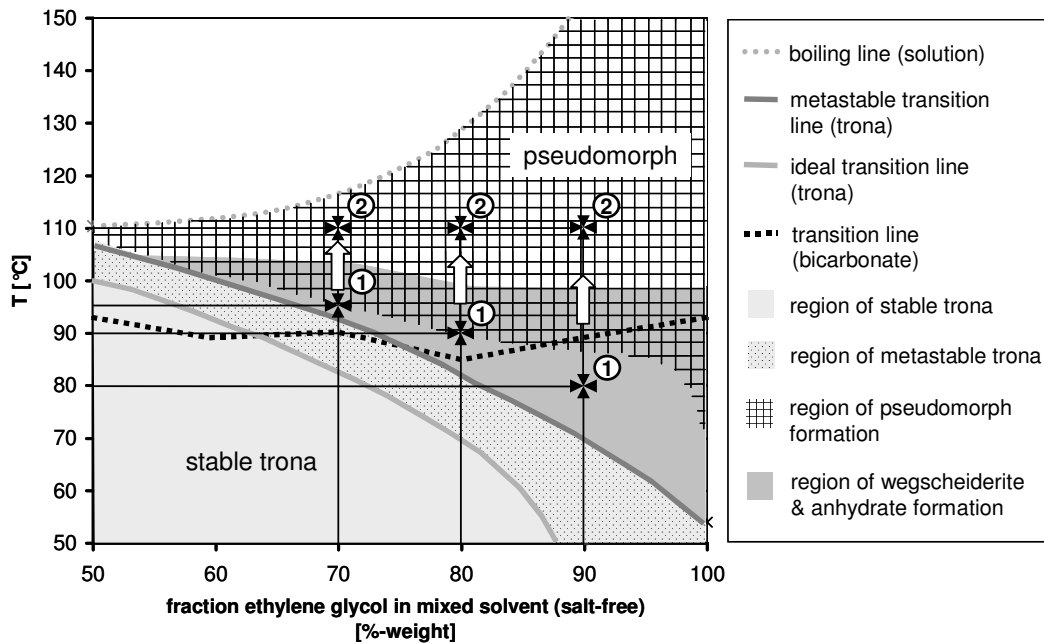


**Figure 5-6:** Operation ranges of the 2-step conversion of trona in the mixed solvent

The second step was set at a temperature, where the bicarbonate decomposition proceeded at a high rate. Still, the decomposition should not proceed faster than the anhydrate growth, to avoid high supersaturation leading to excessive nucleation. An increased fraction of fine particles was found to lower the product bulk density [18, 20, 24]. It was found, that at a temperature of 105 to 110°C anhydrate growth and bicarbonate decomposition were adequately balanced [11], provided a sufficiently high anhydrate seed surface area for growth was present. This seed area was provided here either by the anhydrate crystals formed in the first step, see Eq. 6, or from the constant anhydrate fraction present in the continuous (MSMPR) crystallizers.

#### 5.4.3.1. Discontinuous Batch Experiments

Figure 7 illustrates the processes occurring during the 2-step conversion in 70%-w mixed solvent. Although the solubilities, dissolution and recrystallization rates differed due to the different mixed solvent contents and applied temperature profiles, the basic

mechanisms and processes were identical to the conversions in 80 and 90%-w ethylene glycol.

In the first step, here for 70%-w mixed solvent at ca. 90°C, the trona was recrystallized to wegscheiderite and anhydrate. The anhydrate formed first, see Figure 7, resulting in a built-up of bicarbonate in solution. Due to the solubility product of the trona, which linked the carbonate and bicarbonate concentration, the carbonate concentration dropped slightly with increasing bicarbonate concentration.

When this built-up of bicarbonate had produced sufficient supersaturation to nucleate wegscheiderite (see first vertical dotted line in Figure 7), the bicarbonate concentration dropped slightly to the solubility concentration of wegscheiderite. As can be seen, a small fraction of anhydrate redissolved, because of the take-up of sodium carbonate by the wegscheiderite.

At this moment, the temperature was increased to enable decomposition of the bicarbonate fraction. The increase in bicarbonate concentration (second vertical dotted line) was a result of the increased bicarbonate solubility at the increased temperature (see chapter 6 / [26]). The carbonate concentration also shifted, decreasing in accordance with the solubility products of wegscheiderite and anhydrate. After the wegscheiderite had disappeared, the bicarbonate concentration in solution started to deplete, too. Interestingly, also the carbonate concentration dropped with decreasing bicarbonate concentration. This suggested that the activity coefficient of carbonate increased slightly with decreasing bicarbonate concentration, since the carbonate concentration in solution had now only to obey the anhydrate solubility product (plus a slight supersaturation).

The discontinuous 2-step recrystallization experiments in 70%-w and 80%-w ethylene glycol mixed solvent produced crystalline soda with a reproducible mean bulk density of 1160 kg/m<sup>3</sup>, but some experiments in 70%-w mixed solvent yielded soda of significantly higher bulk densities of up to 1330 kg/m<sup>3</sup>.

The discontinuous 2-step recrystallization experiments in 90%-w ethylene glycol mixed solvent, on the other hand, yielded crystalline soda of lower bulk densities of 450 to 800 kg/m<sup>3</sup>, with the temperature profile given in Figure 7, i.e. 90°C and 110°C. A higher bulk density of 1310 kg/m<sup>3</sup> was achieved with lower temperatures, i.e. 66°C and 100°C, but the complete conversion required 360 minutes in place of ca. 180 minutes.

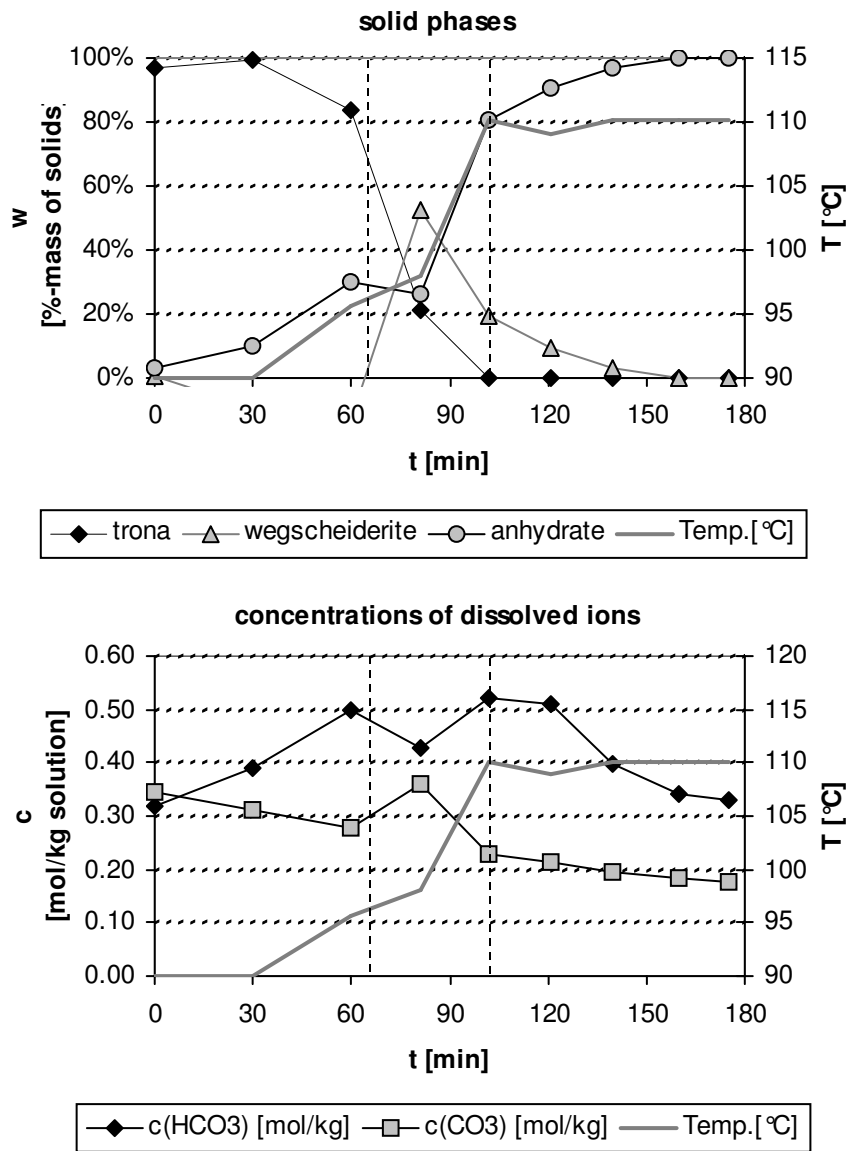


**Figure 5-7:** Composition profiles during discontinuous 2-step trona conversion in 70%-w ethylene glycol mixed solvent in a stirred tank

The reason for this behavior in 90%-w mixed solvent was apparently, that the dissolution rate of trona is directly proportional to the temperature difference  $\Delta T$  to the transition temperature. The relatively high  $\Delta T$  for the recrystallization with the temperature profile 90 and 110°C resulted in fast trona dissolution and in excessive nucleation of anhydrate. As these anhydrate crystals served as seeds for the second step, this resulted ultimately in

small mean crystal sizes and low average bulk densities, as was observed in SEM and light microscope images of the final product.

Additionally, anhydrate appeared to nucleate more readily with increasing ethylene glycol content. This means, that either the metastable zone width or the growth rate of anhydrate decreased with increasing ethylene glycol concentration. This was consistent with the observations made during the reactive recrystallization of nahcolite ( $\text{NaHCO}_3(\text{s})$ ), as described in chapter 3 [25].

From these results, it appears, that a slow trona dissolution rate is beneficial for a high bulk density, as the highest bulk densities were achieved for temperatures barely above the transition point in the first step.

#### *5.4.3.2. Continuous Stirred Tank Cascade Experiments*

The continuous 2-step conversion process was investigated in the same cascade of 3 stirred-tank reactors as the 1-step conversion. Reactor 1 with a volume of 1.7 liters was used to perform the recrystallization of the trona to anhydrate and wegscheiderite; the two 5 liter reactors were operated at the second temperature stage to perform the bicarbonate decomposition. Again, the feed streams were calculated to result in a residence time profile of 40 minutes in reactor 1 and 120 minutes in each of reactors 2 and 3. The temperature of reactor 1 was set to achieve complete trona dissolution within the residence time, while the reactors 2 and 3 were operated at  $110^\circ\text{C}$ , as at this temperature anhydrate growth and bicarbonate decomposition were well balanced for 70%-w and 80%-w ethylene glycol mixed solvent.

An overview of the process conditions for the experiments in the 3 different mixed solvents is given in Tables 2, 3 and 4. An overview of the composition profiles in the reactors is given in Figure 8 for the conversion in 90%-w ethylene glycol mixed solvent, corresponding to the operation conditions given in Table 4.



**Table 5-2:** Process parameters for the continuous 2-step conversion in 70%-w ethylene glycol mixed solvent in a 3 reactor cascade

	<i>Reactor 1</i>	<i>Reactor 2</i>	<i>Reactor 3</i>
<b>Stirrer Type:</b>	double stirrer: propeller + turbine impeller	propeller	Propeller
<b>Flow Modifier:</b>	baffles	draft tube w. baffles	draft tube w. baffles
<b>Volume:</b>	1.7 [liter]	5 [liter]	5 [liter]
<b>Residence Time:</b>	40 [min]	120 [min]	120 [min]
<b>Stirring Rate:</b>	300-500 [rpm]	350 [rpm]	350 [rpm]
	0.3 [W]	0.3 [W]	0.3 [W]
<b>Temperature:</b>	95 [°C]	105 [°C]	110 [°C]
<b>Solid Content:</b>	~15 [%-w]	~12 [%-w]	~11 [%-w]
<b>CO<sub>2</sub> stripping w. air</b>	no	yes	no
<b>Solid Phases</b>	- (trona) - wegscheiderite - anhydrate	- wegscheiderite - anhydrate	- anhydrate - (wegscheiderite)
<b>Solution Content:</b>			
	[HCO <sub>3</sub> <sup>-</sup> ] ~0.27 [mol/kg]	~0.40 [mol/kg]	~0.30 [mol/kg]
	[CO <sub>3</sub> <sup>2-</sup> ] ~0.34 [mol/kg]	~0.30 [mol/kg]	~0.25 [mol/kg]

**Table 5-3:** Process parameters for the continuous 2-step conversion in 80%-w ethylene glycol mixed solvent in a 3 reactor cascade

	<i>Reactor 1</i>	<i>Reactor 2</i>	<i>Reactor 3</i>
<b>Stirrer Type:</b>	double stirrer: propeller + turbine impeller	propeller	Propeller
<b>Flow Modifier:</b>	baffles	draft tube w. baffles	draft tube w. baffles
<b>Volume:</b>	1.7 [liter]	5 [liter]	5 [liter]
<b>Residence Time:</b>	40 [min]	120 [min]	120 [min]
<b>Stirring Rate:</b>	330 [rpm]	350 [rpm]	800 [rpm]
	0.3 [W]	0.3 [W]	2.2 [W]
<b>Temperature:</b>	85 [°C]	105 [°C]	110 [°C]
<b>Solid Content:</b>	~15 [%-w]	~12 [%-w]	~11 [%-w]
<b>CO<sub>2</sub> stripping w. air</b>	no	yes	no
<b>Solid Phases</b>	- (trona) - wegscheiderite - anhydrate	- wegscheiderite - anhydrate	- anhydrate - (wegscheiderite)
<b>Solution Content:</b>			
	[HCO <sub>3</sub> <sup>-</sup> ] ~0.40 [mol/kg]	~0.45 [mol/kg]	~0.25 [mol/kg]
	[CO <sub>3</sub> <sup>2-</sup> ] ~0.20 [mol/kg]	~0.15 [mol/kg]	~0.20 [mol/kg]

**Table 5-4:** Process conditions for the continuous 2-step conversion in 90%-w ethylene glycol mixed solvent in a 3 reactor cascade

	<i>Reactor 1</i>	<i>Reactor 2</i>	<i>Reactor 3</i>
<b>Stirrer Type:</b>	double stirrer: propeller + turbine impeller	propeller	Propeller
<b>Flow Modifier:</b>	baffles	draft tube w. baffles	Draft tube w. baffles
<b>Volume:</b>	1.7 [liter]	5 [liter]	5 [liter]
<b>Residence Time:</b>	40 [min]	120 [min]	120 [min]
<b>Stirring Rate:</b>	500-770 [rpm]	350 [rpm]	300 [rpm]
	1 [W]	0.3 [W]	0.2 [W]
<b>Temperature:</b>	85 [°C]	105 [°C]	110 [°C]
<b>Solid Content:</b>	~12 [%-w]	~12 [%-w]	~9 [%-w]
<b>CO<sub>2</sub> stripping w. air</b>	no	yes	no
<b>Solid Phases</b>	- (trona) - wegscheiderite - anhydrate	- wegscheiderite - anhydrate	- anhydrate - (wegscheiderite)
<b>Solution Content:</b>			
	[HCO <sub>3</sub> <sup>-</sup> ] ~0.45 [mol/kg]	~0.40 [mol/kg]	~0.25 [mol/kg]
	[CO <sub>3</sub> <sup>2-</sup> ] ~0.20 [mol/kg]	~0.15 [mol/kg]	~0.10 [mol/kg]

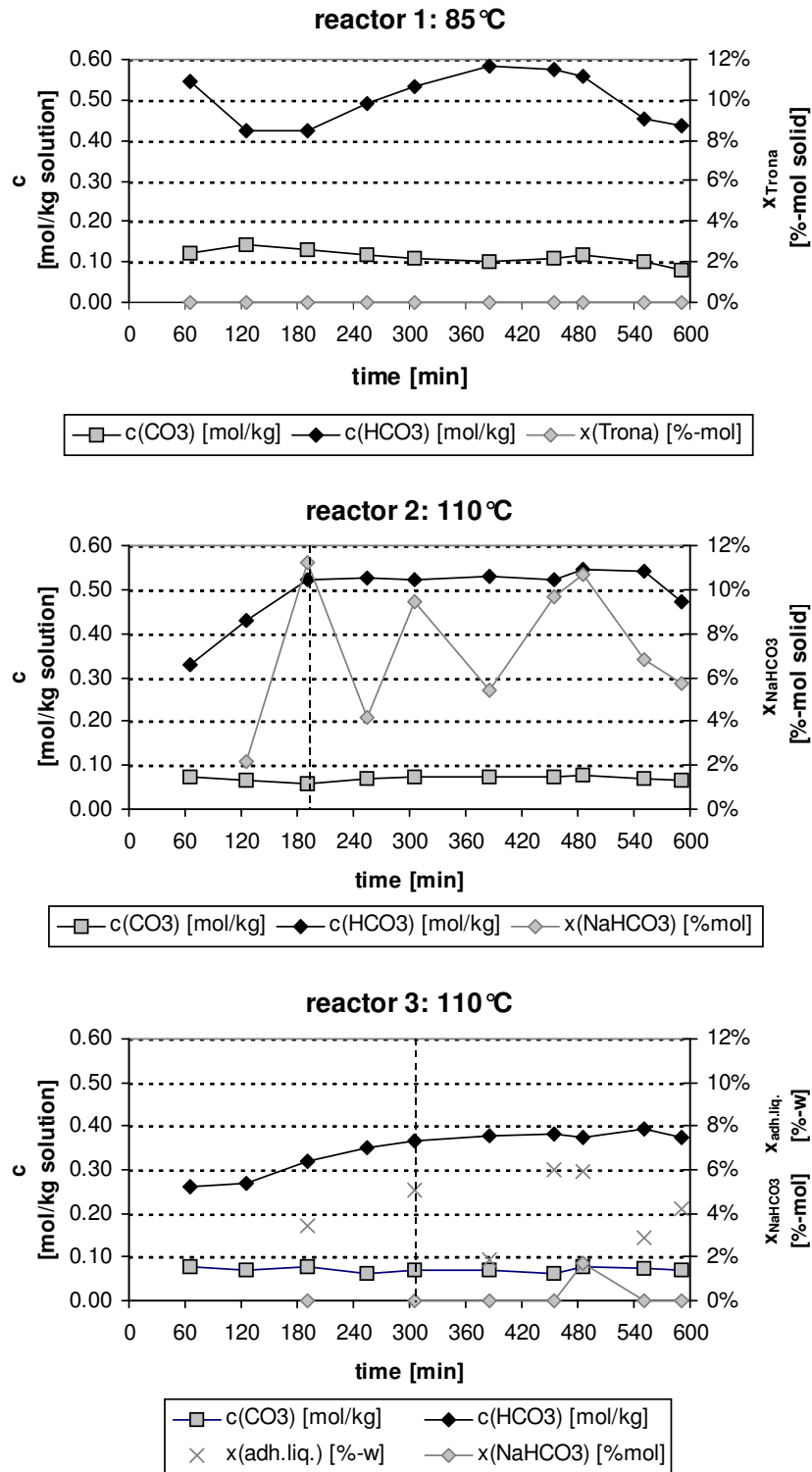


**Figure 5-8:** Continuous 2-temperature step reactive recrystallization of trona in 90%-w ethylene glycol mixed solvent in a cascade of 3 stirred tanks

As an equilibration step – like in the 1-step conversion - was not necessary here, the recrystallization of trona to anhydrate and wegscheiderite was performed immediately in reactor 1. Due to the high driving force for the trona dissolution ( $\Delta T = 15\text{K}$ ) in the presented case of 90%-w mixed solvent, the trona dissolved so fast, that no trona was found by analysis in the solid of reactor 1, see Figure 8.

The bicarbonate concentration in reactor 1 was not steady, i.e. the supersaturation was not constant. This indicated, that the nucleation and growth of wegscheiderite did not reach a steady state. The carbonate concentration was far more constant, showing only small variations, indicating that the growth and nucleation of the anhydrate proceeded more stably.

In the experiments with 70%-w and 80%-w mixed solvents, the solid of reactor 1 still contained 15 to 20%-mol trona. The driving force was far lower here ( $\Delta T = 3$  to  $5\text{K}$ ), so the trona dissolved more slowly. To compensate for this, the temperature of reactor 2 was kept for these mixed solvents at  $105^\circ\text{C}$  instead of  $110^\circ\text{C}$  to give remaining small trona crystals a chance to complete their dissolution in reactor 2. To completely avoid the formation of pseudomorphs from remaining trona in reactor 2, a longer residence time in reactor 1 is recommended to further improve product bulk density.

In all mixed solvents, the recrystallization of the trona produced a slurry consisting mainly of wegscheiderite and anhydrate. At the lower temperature of reactor 1, i.e. without significant bicarbonate decomposition and the higher viscosity of the solution, the very thin, needle-shaped wegscheiderite crystals resulted in a thick, pasty slurry, which was difficult to maintain mixed homogeneously. Proper mixing and thereby the maintenance of the proper residence time in reactor1 was only achieved with the combination of a propeller and a turbine-impeller stirrer with the baffles in the reactor. The mixing problem was especially evident in 90%-w mixed solvent.

The bicarbonate decomposition for 90%-w mixed solvent in reactor 2 and 3 proceeded as expected, reducing the bicarbonate content of the solid in reactor 2 to 2-10%-w and in reactor 3 to the desired 0%-w.

The bicarbonate concentration is steadier in reactor 2 and 3 than in reactor 1. The dissolution of wegscheiderite and the nucleation and growth of anhydrate were apparently far more stable than the nucleation and growth of wegscheiderite in reactor 1. Although complete conversion to anhydrate (soda) was achieved, the product quality was impaired by a rather high degree of adhering solvent in the range of 2-6%-w, see Figure 8. The anhydrate crystals were rather small and formed agglomerates, which retained noticeable amounts of mixed solvent even after washing with acetone. Also the bulk density of the produced soda was rather low.

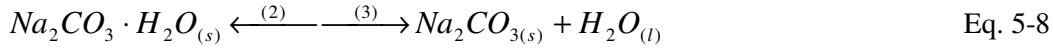
These problems did not occur in the experiments in 70%-w and 80%-w ethylene glycol mixed solvent. The process conditions are given in Table 2 and 3. The product of these experiments was composed of far larger (mean diameter ~150 micron) and less agglomerated crystals. In 80%-w ethylene glycol a product of a mean bulk density of 1160 kg/m<sup>3</sup> containing ~0.5%-w of adhering solvent was produced, while the continuous 2-step recrystallization in 70%-w ethylene glycol yielded a mean bulk density of 1220 kg/m<sup>3</sup> containing only 0.3%-w of adhering solvent. As both products still contained noticeable fractions of pseudomorphs, it is expected, that process optimization, like e.g. a longer residence time and improved mixing in reactor 1, could further increase bulk density and reduce the content of adhering solvent.

The mixed solvent acquired a noticeable yellow discoloration during the first continuous run performed with it. This discoloration was most likely due to an alkaline mediated reaction of the ethylene glycol. Although this discoloration did neither affect transition temperatures nor conversion rates, it might affect the process or the product quality on the long term, especially if it indicated a progressing degradation of the ethylene glycol.

#### **5.4.4. Wet Calcination and Monohydrate-Recrystallization (3-Step MSRR)**

The third method presented here to convert trona to anhydrous soda combines wet calcination with the 2-step-monohydrate-recrystallization process developed by Oosterhof et al. [18, 20]. In the first recrystallization stage the light soda ash was recrystallized to sodium carbonate monohydrate ( $\text{Na}_2\text{CO}_3 \cdot \text{H}_2\text{O}_{(s)}$ ), which was then

recrystallized in the second stage under controlled conditions back to anhydrate, see Eq. 8.



It was found [18, 20], that the transition in 70 to 80%-%-w ethylene glycol provided the best conditions for the formation of a high bulk density soda.

Commercially available light soda ash basically consists of pseudomorphic soda, produced by dry calcinations of monohydrate crystallized from aqueous solution. The commercially available “dense soda ash” is usually produced by increasing the bulk density of light soda ash by sintering [27 - 30] and/or compacting steps [31], which densify the pseudomorphs without significantly increasing the crystallite size of the soda. As pseudomorphic soda can also be formed by wet calcination of trona in the mixed solvent, the double recrystallization process of Oosterhof et al. can be used to adjust the bulk density and content of adhering solvent of soda, which produced in the region of pseudomorph formation, see Figure 9.

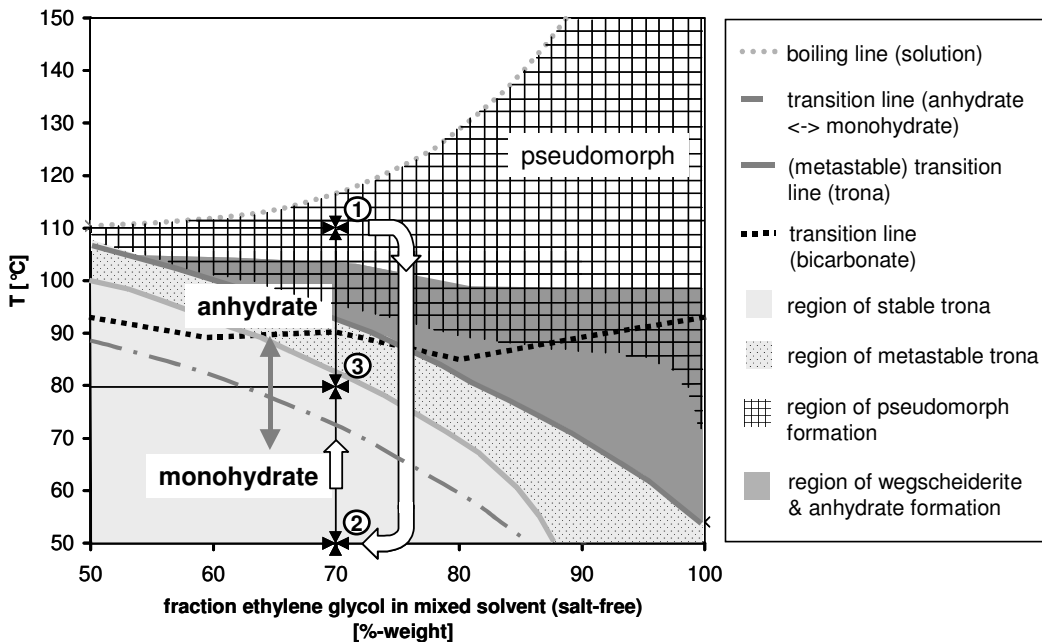
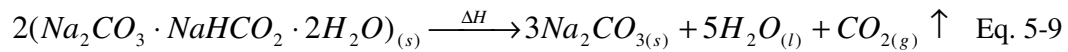


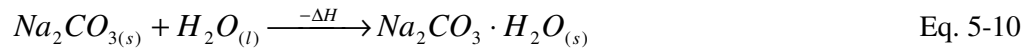
**Figure 5-9:** Process steps during wet calcination and monohydrate recrystallization

The function of the wet calcination in this process scheme is to rapidly decompose the bicarbonate content of the trona. The advantage of the wet calcination, compared to the reactive recrystallization presented above, is that significantly higher process temperatures and thus higher bicarbonate decomposition rates, see Figure 9, can be employed. A point of attention here is, that not only the bicarbonate content in the solid has to be converted, but also a large fraction of the dissolved bicarbonate. Otherwise, since their solubility decreases with temperature, see Chapter 6, bicarbonate-containing phases, i.e. trona, (re)form at the lower temperatures of the monohydrate recrystallization. The steps of the complete process as illustrated in Figure 9:

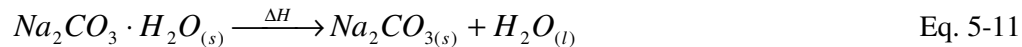
1. Wet calcination of at temperatures of 110 to 120°C:



2. Recrystallization to monohydrate at temperatures below the monohydrate transition line, see Figure 18:



3. Slow recrystallization to anhydrate at temperatures slightly above the monohydrate transition line, see Figure 9:



The results of the batch recrystallization experiment in 70%-w ethylene glycol are given in Figure 10:

In the first stage the solid trona converted to solid anhydrate. Additional time was provided, to allow the dissolved bicarbonate content to decrease below the trona solubility concentration at the temperature of the second stage.

Then the slurry was cooled to a temperature significantly below the monohydrate transition temperature, i.e. ca. 50°C, to allow a relatively fast monohydrate formation (“monohydration”).



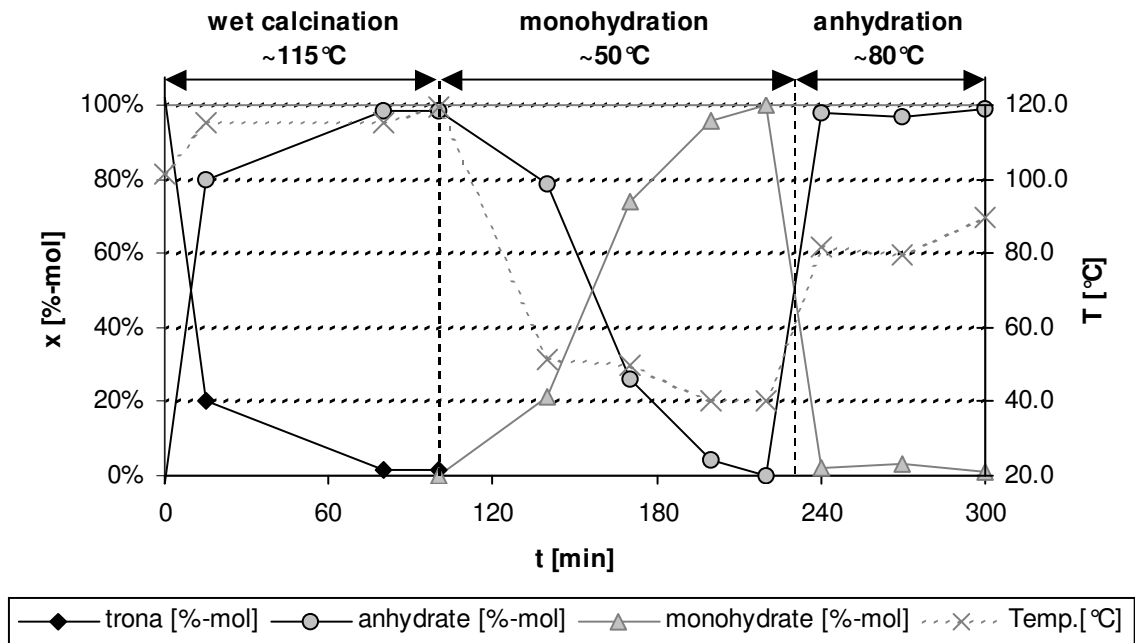


**Figure 5-10:** Solid composition and temperature profile during discontinuous wet calcinations and monohydrate recrystallization in a stirred tank

After the soda of the wet calcination had completely transformed to monohydrate, i.e. the pseudomorphs had completely dissolved, the temperature was increased to a level slightly above the monohydrate transition temperature (ca. 72°C in 70%-w ethylene glycol) to form the anhydrate.

In the example given in Figure 10, this transition was occurring already too fast, although the transition temperature was exceeded by only 8 K by the process temperature of 80°C. The anhydrate formation (“anhydration”) was finished already after 15 minutes. This was most likely due to an excess of undissolved anhydrate crystallites from the wet calcination, which had survived the monohydration step. This anhydrate acted as seeds for the growth of further anhydrate from the dissolving monohydrate. Due to an excess of seed material, the anhydrate did not grow to a high mean size and the bulk density in this experiment remained low with ~890 kg/m<sup>3</sup>.

The great advantage of this process is the fast bicarbonate conversion in the wet calcination, which is due to its pseudo-solid-state mechanism significantly faster than the solvent mediated bicarbonate decomposition, see Chapter 4. This can reduce the total process time significantly: The wet calcination can be completed in less than an hour and

the double recrystallization process was found [15] to require about one and a half hour after adjustment to a stable steady state. The 3-step (wet calcination and monohydrate recrystallization) process takes therefore in total ca. 2½ hours to convert trona to dense crystalline soda, while the 1- and 2-step reactive recrystallization processes require app. 5 hours.

Oosterhof et al. [13, 15] achieved bulk densities of around 1300 kg/m<sup>3</sup> (up to 1400 kg/m<sup>3</sup>) in the monohydrate recrystallization process, which is slightly more than the bulk densities produced yet in the 1- and 2-step reactive recrystallization processes.

Significant temperature changes have to be performed between the different steps in the wet calcination: 110°C → 50°C → 80°C, while in 2-step recrystallization less temperature changes are required: 85°C → 105°C → 110°C. For the 1 step recrystallization no or only a small change (100°C → 105°C) has to be induced. These temperature changes correspond with heating/cooling duties on the crystallizers, i.e. investment of energy for heating/cooling.

A more critical drawback is the fact that the calcination of the trona can also be performed in the dry state. The produced pseudomorphic soda can be recrystallized by the monohydrate recrystallization process to increase the bulk density and mechanical stability of the product. This might have the additional advantage, that the soda crystallites in the dry calcined trona are smaller, i.e. dissolve faster and will probably leave less seed material for the anhydration step.

## **5.5. Conclusions**

Crystalline soda of bulk densities of up to 1330 kg/m<sup>3</sup> was produced directly from trona by reactive recrystallization in the mixed solvent. This is significantly higher than the bulk densities of commercially available dense soda ash (pseudomorphic soda) of around 1000 to 1200 kg/m<sup>3</sup>. Additionally, the crystalline soda has a very good filterability and is more resistant to breakage and dusting, since it consists of comparatively large single soda crystals, while the commercial soda consists of agglomerates of very fine soda particles.

For the desired high bulk densities, a high mean crystal size of the sodium carbonate anhydrate (soda) is necessary. This requires balanced growth conditions, i.e. the trona dissolution and the bicarbonate decomposition have to be adapted to the anhydrate growth rate to prevent high supersaturation levels and excessive nucleation.

At conditions with a high rate in the decomposition, the trona converts in a pseudo-solid-state mechanism to pseudomorphs, i.e. agglomerates of small soda crystallites, which maintain the shape of the original trona crystal. Despite its high conversion rates, the conversion to pseudomorphs is in most cases undesirable, since the formed pseudomorphs are very porous structures, retain noticeable amounts of solvent even after washing and have a low bulk density.

In this work 3 different mixed solvent reactive recrystallization routes were presented, that produce high bulk density crystalline soda from trona: 1-step reactive recrystallization, 2-step reactive recrystallization and wet calcination (+ double recrystallization).

In the 1-step process, trona is directly recrystallized solution mediated to soda. In the 2-step process, the trona is first recrystallized to a mixture of sodium carbonate anhydrate and wegscheiderite, which is then recrystallized in the second step via the decomposition of its bicarbonate fraction to the anhydrate. In the wet calcination process, the trona is first converted to pseudomorphic soda, which is then converted by a double recrystallization via sodium carbonate monohydrate to crystalline soda.

All three processes were shown to convert trona to a high-grade soda, but the highest bulk density was achieved by the 2-step process in 70 to 80%-w ethylene glycol mixed solvent, while the wet calcining process yielded the shortest process residence times.

## **5.6. Literature References**

- [1] Garret, D.E., "Natural Soda Ash – Occurrences, Processing and Use", Van Nostrand – Reinhold (Publ.), New York, 1992, p. 267-416
- [2] Haynes, H.W., "Solution Mining of Trona", In Situ, Vol. 21(4), 1997, p. 357-394
- [3] Aitala, R., Aitala, M., "Process Selection Criteria for Refining Trona to Commercial Products", The First International Soda Ash Conference (ISAC), June 1997, available on: <http://www.isonex.com/isacpaper.html>

- [4] Garret, D.E., "Natural Soda Ash – Occurrences, Processing and Use", Van Nostrand – Reinhold (Publ.), New York, 1992, p. 161-162
- [5] Nasün-Saygili, G., Okutan, H., "Application of the solution mining process to the Turkish trona deposit", *Hydrometallurgy*, 42, 1996, p. 103-113
- [6] Nasün-Saygili, G., Okutan, H., "Mechanism of the dissolution of Turkish trona", *Hydrometallurgy*, 43, 1996, p. 317-329
- [7] Ekmekyapar, A., Erşahan, H., Yapici, S., "Nonisothermal Decomposition Kinetics of Trona", *Ind. Eng. Chem. Res.*, 35, 1996, p. 258-262
- [8] Demirbas, A., "Production of sodium carbonate from soda ash via flash calcination in a drop tube furnace", *Chem. Eng. Proc.*, 41, 2002, p. 215-221
- [9] Dogan, M., Güldür, Ç, Dogu, G., Dogu, T., "Soda ash Production from trona in a spray dryer", *J. Chem. Technol. Biotechnol.*, 68, 1997, p. 157-162
- [10] Çolak, S., Ekmekyapar, A., Erşahan, H., Künükül, A., Modoglu, Ö., "Flash calcination of trona ore in a free fall reactor and production of soda from trona", *Energy Educ. Sci. Technol.*, 4, 2000, p. 48-59
- [11] Gärtner, R.S., Seckler, M.M., Witkamp, G.J., "Recrystallization of Trona (Sodium Sesquicarbonate) into Soda (Sodium Carbonate Anhydrate) in a Mixed Solvent, Part I: Fundamental Conversion Steps" submitted for publication to *AIChE Journal* (Chapter 4)
- [12] Thieme, C., "sodium hydrogen carbonate" in "Ullmann's Encyclopedia of Chemical Technology", 6<sup>th</sup> ed., 2000, electronic release, Wiley-VCH
- [13] Gärtner, R.S., Seckler, M.M., Witkamp, G.J., "Recrystallisation for the Densification and Purification of Soda Ash", in preparation for publication (Chapter 2)
- [14] Vanderzee, C.E., "Thermodynamic relations and equilibria in ( $\text{Na}_2\text{CO}_3 + \text{NaHCO}_3 + \text{H}_2\text{O}$ ): standard Gibbs energies of formation and other properties of sodium hydrogen carbonate, sodium carbonate heptahydrate, sodium carbonate decahydrate, trona: ( $\text{Na}_2\text{CO}_3 \cdot \text{NaHCO}_3 \cdot 2\text{H}_2\text{O}$ ), and Wegscheider's salt: ( $\text{Na}_2\text{CO}_3 \cdot 3\text{NaHCO}_3$ )", *J. Chem. Thermodynamics*, 14, 1982, p. 219-238
- [15] Taylor, C.E., "Thermodynamics of Sodium Carbonate in Solution", *J. Phys. Chem.*, 59 (1), 1955, p. 653-657
- [16] Kobe, K.A., Sheehy, T.M., "Thermochemistry of Sodium Carbonate and Its Solution", *Ind. Eng. Chem.*, 40 (1), 1948, p. 99-102
- [17] Waldeck, W.F., Lynn, G., Hill, A.E., "Aqueous Solubility of Salts at High Temperatures. I. Solubility of Sodium Carbonate from 50 to 348°C", *J. Am. Chem. Soc.*, 54, 1932, p. 928-936

- [18] Oosterhof, H., de Graauw, J., Witkamp, G.J., van Rosmalen, G.M., "Continuous Double Recrystallization of Light Soda Ash into Super Dense Soda Ash", *Crystal Growth & Design*, 2 (2), 2002, p. 151-157
- [19] Oosterhof, H., Witkamp, G.J., van Rosmalen, "Some antisolvents for crystallisation of sodium carbonate, *Fluid Phase Equilibria*, 155, 1999, p. 219-227
- [20] Oosterhof, H., Witkamp, G.J., van Rosmalen, G.M., "Evaporative Crystallization of Anhydrous Sodium Carbonate at Atmospheric Conditions", *AIChE J.* 47(10), 2001, p. 2220-2225
- [21] Robertson, H.R., "Production of Dense Soda Ash", United States Patent 2,267,136, Solvay Process Company, NY, 1940
- [22] Bourne, D.J., Lamb, F.E., "Method of Producing Soda Ash", United States Patent 3,656,892, Duval Co., 1972
- [23] Bowman, R.W., "Process for the manufacture of sodium carbonate crystals from minerals or solutions", United States Patent 6,022,385, 2000
- [24] Oosterhof, H., Witkamp, G.J., van Rosmalen, G.M., "Antisolvent Crystallization of Anhydrous Sodium Carbonate at Atmospheric Conditions", *AIChE J.* 47(3), 2001, p. 602-608
- [25] Gärtner, R.S., Seckler, M.M., Witkamp, G.J., "Reactive Recrystallization of Sodium Bicarbonate", submitted for publication to *Ind. Eng. Chem. Res.* (Chapter 3)
- [26] Gärtner, R.S., Seckler, M.M., Witkamp, G.J., "Solid Phases and Their Solubility in the System  $\text{Na}_2\text{CO}_3 + \text{NaHCO}_3 + \text{Ethylene Glycol} + \text{Water}$  from 50 to 90 °C", *J. Chem. Eng. Data*, 49(1), 2004, p. 116-125
- [27] Caldwell, N.A., Bauer, W.C., "Trona Process", United States Patent 2,970,037, FMC Co., New York, 1961
- [28] Frint, W.R., "Preparation of Sodium Carbonate", United States Patent 3,028,215, FMC Co., 1962
- [29] Gancy, A.B., "Densification of Soda Ash by Vapor Hydration", United States Patent 3,309,171, Intermountain Research & Development Co., 1967
- [30] Beck, W.F., Di Bello, P.M., "Preparation of Soda Ash", United States Patent 3,336,105, FMC Co., 1967
- [31] Bakele, W., "New Developments in the production of heavy soda-ash via compacting method", *Powder Techn.*, 130, 2003, p. 253-256

- [32] Ball, M.C., Strachan, A.N., Strachan, R.M., “Thermal Decomposition of Solid Wegscheiderite,  $\text{Na}_2\text{CO}_3 \cdot \text{NaHCO}_3$ ”, J. Chem. Soc. Faraday Trans., 87(12), 1991, p. 1911-1914
- [33] Ball, M.C., Snelling, Ch.M., Strachan, A.N., Strachan, R.M., “Thermal Decomposition of Solid Sodium Sesquicarbonate,  $\text{Na}_2\text{CO}_3 \cdot \text{NaHCO}_3 \cdot 2\text{H}_2\text{O}$ ”, J. Chem. Soc. Faraday Trans., 88 (4), 1992, p. 631-636
- [34] Barral, E.M., Rogers, L.B., “Differential Thermal Analysis of the Decomposition of Sodium Bicarbonate and its Simple Double Salts”, J. Inorg. Nucl. Chem., 28, 1966, p. 41-51

## 5.7. Addendum

### 5.7.1. Experimental Set-Ups

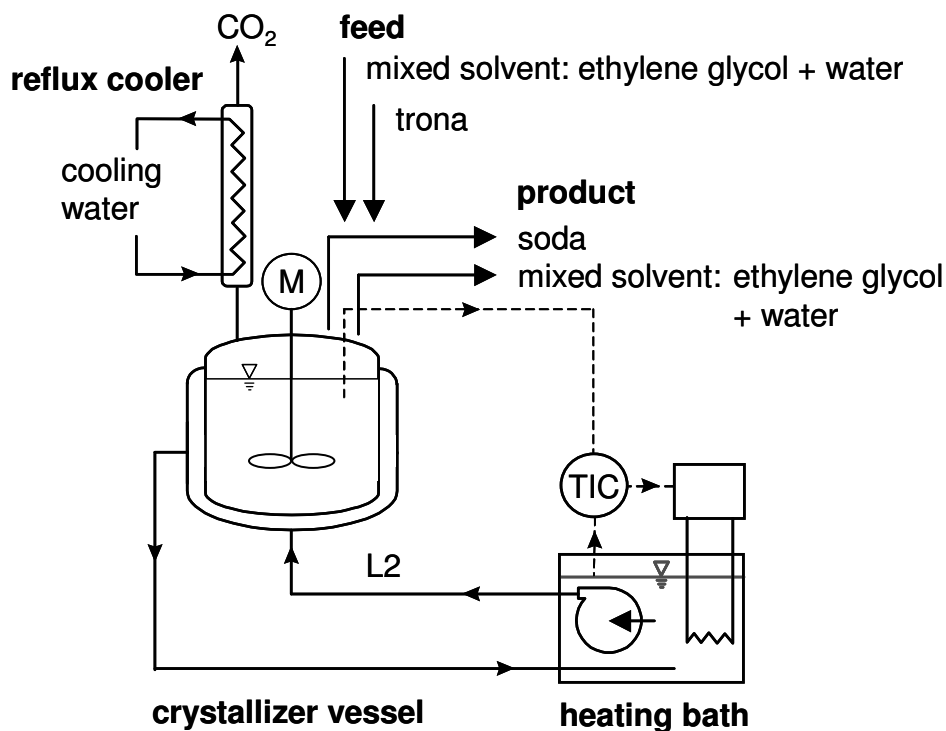


**Figure 5-11:** Thermostated batch set-up for discontinuous recrystallization experiments

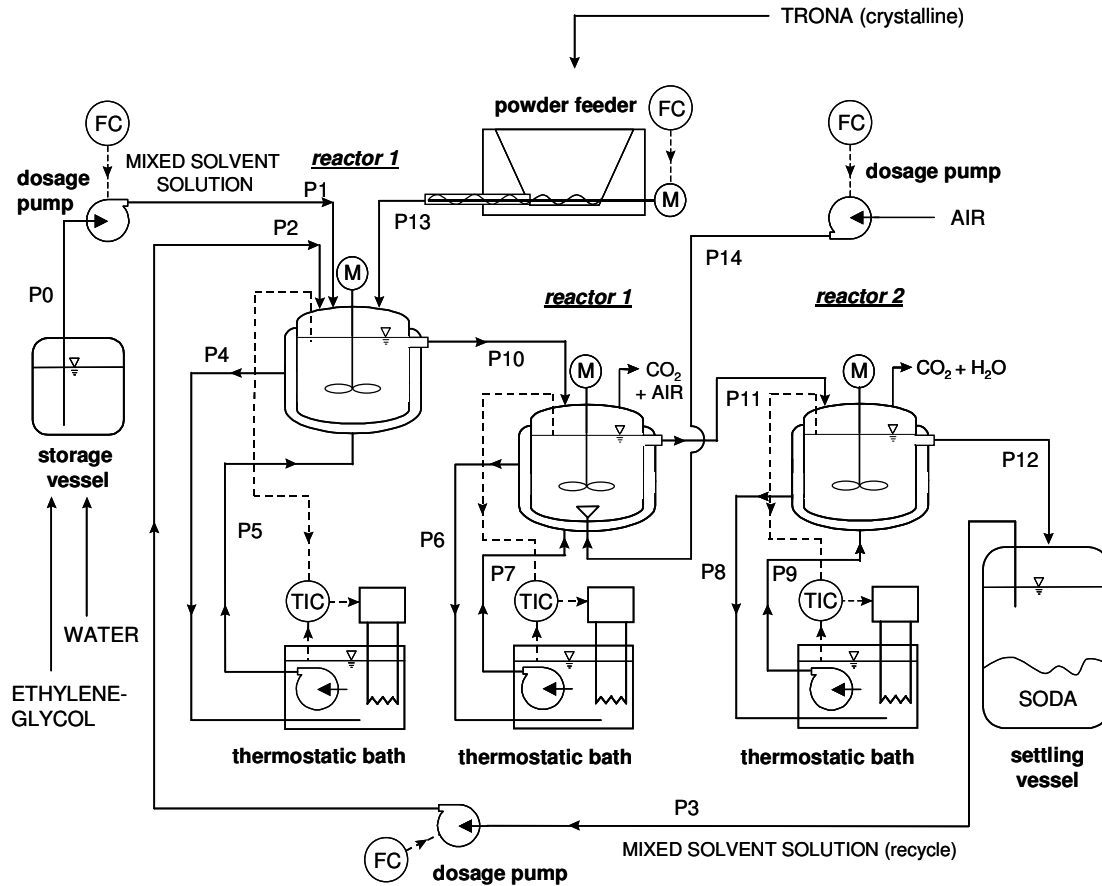


**Figure 5-12:** Tank cascade set-up for continuous trona recrystallization experiments

## 5.7.2. Analytical Methods

### 5.7.2.1. Solid Phase Analysis by Heating-Mass-Loss

See **Chapter 4**, Addendum: 4.8.2 Analytical Methods

### 5.7.2.2. Dissolved Carbonate-Bicarbonate Concentration by Automated pH Titration

See **Chapter 4**, Addendum: 4.8.2. Analytical Methods





## Chapter 6 :

### OCCURRING SOLID PHASES AND THEIR SOLUBILITIES IN THE SYSTEM Na<sub>2</sub>CO<sub>3</sub> - NaHCO<sub>3</sub> - ETHYLENE GLYCOL - WATER FROM 50 TO 90°C

R.S. Gärtner, M.M. Seckler, G.J. Witkamp

#### **Abstract**

Solubilities in the system sodium carbonate - bicarbonate were measured over a range of temperatures from 30 to 90°C in mixed solvents containing 50 to 100%-w (salt free solvent) ethylene glycol. Mixtures of solid sodium carbonate anhydrate (Na<sub>2</sub>CO<sub>3(s)</sub>) and solid sodium bicarbonate (NaHCO<sub>3(s)</sub>) in different ratios and also trona (Na<sub>2</sub>CO<sub>3</sub>·NaHCO<sub>3</sub>·2H<sub>2</sub>O<sub>(s)</sub>) were allowed to recrystallize and equilibrate with the mixed solvents at the given temperatures.

The solubility concentration of CO<sub>3</sub><sup>2-</sup> was generally found to decrease with increasing ethylene glycol content irrespective of the occurring solid phase, while HCO<sub>3</sub><sup>-</sup> solubility concentration displayed a minimum at 80 to 90%-w (salt free solvent) ethylene glycol and then increased sharply.

For pure carbonate phases, CO<sub>3</sub><sup>2-</sup> solubility displayed little temperature dependence. In equilibrium with mixed carbonate-bicarbonate phases, the CO<sub>3</sub><sup>2-</sup> solubility concentration usually decreased with temperature, most likely because it was linked with the HCO<sub>3</sub><sup>-</sup> concentration via the solid's solubility product. The solubility concentration of HCO<sub>3</sub><sup>-</sup> increased significantly with temperature for all sodium bicarbonate containing solid phases.

For the temperature range from 30 to 90°C and an ethylene glycol concentration range between 50 and 100%-w (of salt free solvent), the CO<sub>3</sub><sup>2-</sup> solubility concentration varied between 0.058 and 1.023 mol/kg solution, and the HCO<sub>3</sub><sup>-</sup> solubility concentration ranged between 0.000 (i.e. the lower detection limit of the analytical method) and 1.153 mol/kg solution.

The occurring solid phases were the same as those formed in the aqueous system. They were identified in the recrystallization experiments as: Sodium carbonate anhydrate

( $\text{Na}_2\text{CO}_3(\text{s})$ ), sodium carbonate monohydrate ( $\text{Na}_2\text{CO}_3\cdot\text{H}_2\text{O}(\text{s})$ ), trona ( $\text{Na}_2\text{CO}_3\cdot\text{NaHCO}_3\cdot 2\text{H}_2\text{O}(\text{s})$ ), wegscheiderite ( $\text{Na}_2\text{CO}_3\cdot 3\text{NaHCO}_3(\text{s})$ ) and sodium bicarbonate ( $\text{NaHCO}_3(\text{s})$ ). No solvate phases with ethylene glycol were observed.

## **6.1. Introduction**

Dealing with any kind of electrolyte system in academic research or industrial application requires detailed knowledge of the species occurring in the system, both in the solution as well as the occurring solids. Aqueous systems are reasonably well documented and understood. A variety of electrolyte models, like Chen / Electro-NRTL [1-3], Pitzer [4-6] or Helgeson [7, 8], can be used to describe speciation, phase stability and solubility. Organic or even mixed solvent systems are much less well understood, partly because detailed solubility and solid phase stability data is lacking in most cases. But given extensive mixed solvent solubility and phase stability data, the cited aqueous electrolyte models can already be extended to include mixed solvent systems.

For example, Koo et al. [9, 10] were able to parameterize and model the solubility of the compound L-Ornithine-L-Aspartate (LOLA) in water-methanol mixed solvents with the Chen-model, i.e. based on NRTL and simple Debye-Hückel interactions, based on their detailed solubility and phase data.

Work by Pitzer [4] shows that the ionic interactions in the aqueous system of  $\text{Na}_2\text{CO}_3 - \text{HCO}_3$  are far more complex than predicted by the Debye-Hückel theory, and only limited mixed solvent solubility and solid phase stability data of this important salt system is available in current literature [11, 12].

The aim of this work is to provide solubility and phase stability data of the  $\text{Na}_2\text{CO}_3 - \text{NaHCO}_3 - \text{H}_2\text{O}$  - ethylene glycol system.

### **6.1.1. The System $\text{Na}_2\text{CO}_3 - \text{NaHCO}_3 - \text{H}_2\text{O}$**

The actual solubility concentration of a solute not only depends on the ability of the solvent to solvate the solute, but also on the solid phase of the solute. Most substances can form more than one solid phase, either as polymorphs, pseudopolymorphs (e.g. hydrates), mixed solid phases, solid solutions or amorphous solids. The stable solid phase, i.e. the one with the minimal solubility, determines the solubility concentration.

Four solid phases are known for the aqueous system of  $\text{Na}_2\text{CO}_3$ :

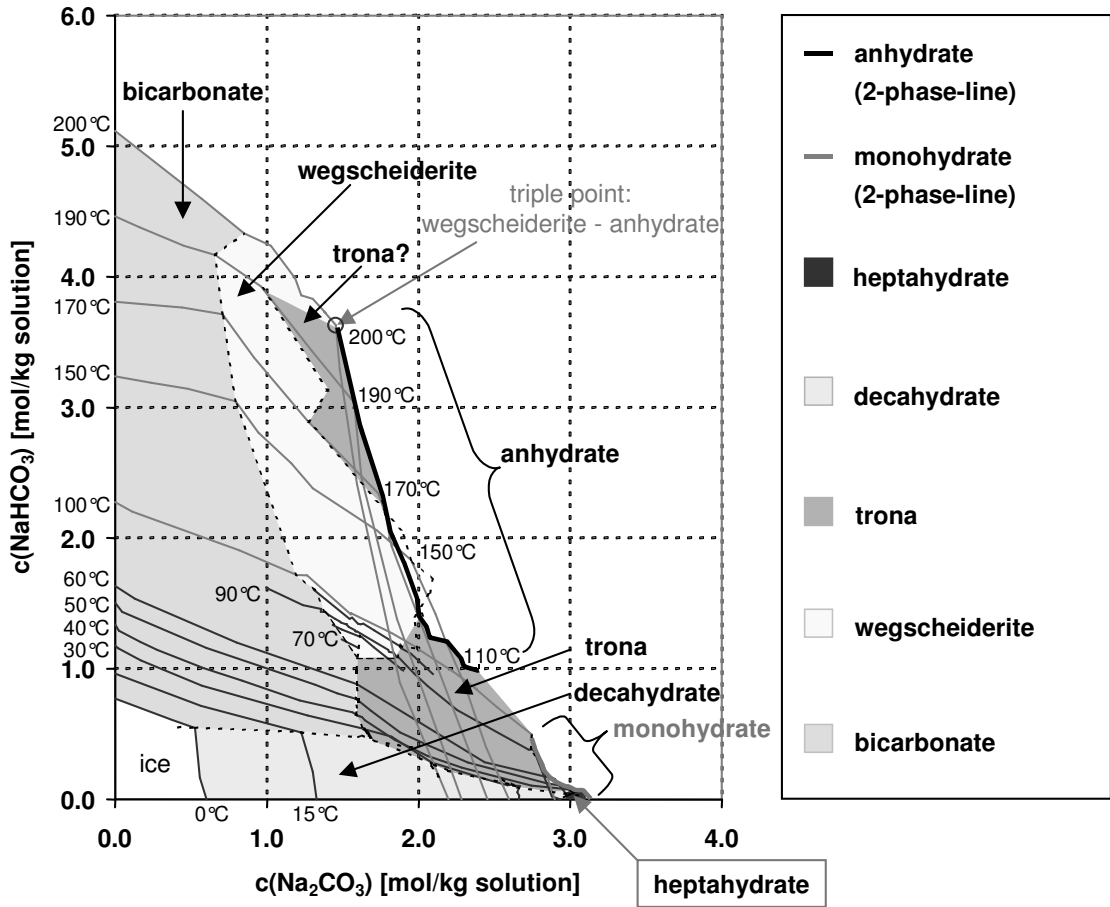


**Figure 6-1:** Phase stability and solubility chart for the system  $\text{Na}_2\text{CO}_3\text{-NaHCO}_3$  in aqueous solution from 0 to 200°C, derived from literature solubility data [13-20]

The anhydrate ( $\text{Na}_2\text{CO}_{3(s)}$ , natrite) and three hydrate phases: monohydrate ( $\text{Na}_2\text{CO}_3\cdot\text{H}_2\text{O}_{(s)}$ , thermonatrite), heptahydrate ( $\text{Na}_2\text{CO}_3\cdot 7\text{H}_2\text{O}_{(s)}$ ) and decahydrate ( $\text{Na}_2\text{CO}_3\cdot 10\text{H}_2\text{O}_{(s)}$ , natron). Each of these hydrate phases is stable in a specific temperature and  $[\text{CO}_3^{2-}] - [\text{HCO}_3^-]$  concentration range, see [13-16]. The anhydrate does not form from its pure aqueous solution at atmospheric pressure, since it is only stable above 109°C, which is above the boiling point of the pure saturated sodium carbonate solution of 104.9°C [13-15].

In the aqueous system of  $\text{Na}_2\text{CO}_3 - \text{NaHCO}_3$ , three additional phases are found:

The pure sodium bicarbonate ( $\text{NaHCO}_{3(s)}$ , nahcolite), and 2 mixed phases: sodium sesquicarbonate ( $\text{Na}_2\text{CO}_3\cdot\text{NaHCO}_3\cdot 2\text{H}_2\text{O}$ , trona) and sodium carbonate tri-bicarbonate ( $\text{Na}_2\text{CO}_3\cdot 3\text{NaHCO}_{3(s)}$ , wegscheiderite or decimite). Again, each of these phases is stable in a specific temperature and  $[\text{CO}_3^{2-}] - [\text{HCO}_3^-]$  concentration range. The stability ranges

of these solid phases were first documented by Wegscheider et al. [17] and extended by Hill et al. [18, 19]. Extensive phase stability / solubility charts of the system are given by Garret [20].

The phase stability chart of Figure 1 was constructed from solubility data from the listed sources [13-20]. Figure 2 displays the solubility over the more limited temperature range from 0 to 100°C for better readability of the naturally occurring compositions of the system. The thin lines represent solubilities of the system  $\text{Na}_2\text{CO}_3$  -  $\text{NaHCO}_3$  at a given temperature, i.e. the *solubility isotherms*. The colored areas outline the ranges of composition and temperature, in which a specific solid phase is stable in contact with the solution, i.e. the *stability range* of a solid phase. The thin, dotted lines indicate conditions of temperature and composition, where the solution is in equilibrium with 2 solid phases, i.e. the *2-phase-lines*. The phase stability ranges of monohydrate and anhydrate could not be outlined as clear as those of the other phases, since they overlap with the ranges of other phases at lower temperatures. Generally, the almost vertically dropping part of each solubility isotherm in Figure 1 is the solubility line of either monohydrate or anhydrate. They can be distinguished by the fact, that monohydrate is only stable till 109°C. Therefore, all isotherms of higher temperature represent the solubility of the anhydrate. For ease of reference, a thick, black line connects the 2-phase points of anhydrate, and a thick, gray line connects those of monohydrate.

It has to be pointed out, that the existence of the high temperature trona region in Figure 1 is rather unlikely, since the stability of hydrates decreases noticeably with increasing temperature, as the crystal water becomes more volatile. The trona found by Hill et al. [19] at this temperature range is more likely to be undissolved (i.e. metastable) trona, since the researchers used crystalline trona as starting material in their recrystallization experiments.

Limited data on the solubilities and phase stabilities of sodium carbonate in mixed solvents of ethanol - water, n-propanol – water, isopropanol - water, isobutanol – water, allyl alcohol – water, glycerol water, pyridine – water, 2-picoline – water and of aliphatic amines in water can be found in the book of Seidell [12].

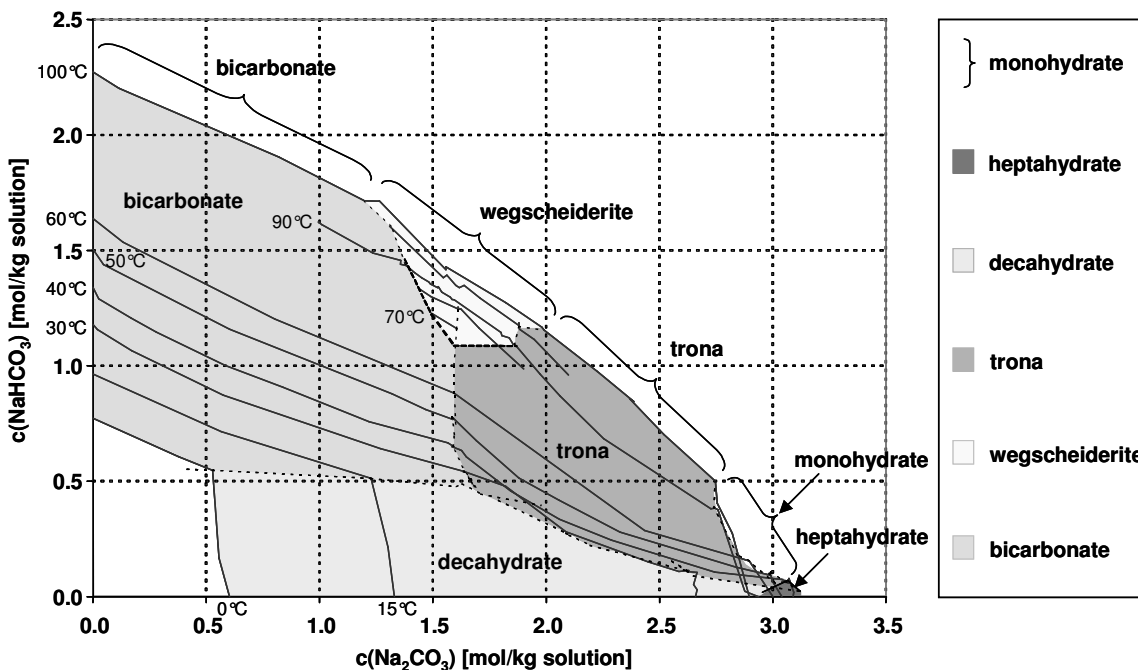


**Figure 6-2:** Phase stability and solubility chart for the system  $\text{Na}_2\text{CO}_3\text{-NaHCO}_3$  in aqueous solution from 0 to 100°C, derived from literature solubility data [13-20]

The solubilities and stabilities of sodium carbonate anhydrate and monohydrate in 0 to 100%-w (salt-free) mixed solvents of ethylene glycol, di-ethylene glycol, glycerol and 1,2-propanediol in a temperature range from 40 to 90°C were measured by Oosterhof et al. [11]. These solubilities and phase stabilities in ethylene glycol are reproduced in Figure 4 and Table 2.

The mixed solvent ethylene glycol – water has special technical relevance for the salt system  $\text{Na} - \text{CO}_3 - \text{HCO}_3$ , because ethylene glycol has been shown by Oosterhof et al. [11, 21] to be a particularly suitable antisolvent for the crystallization of soda (sodium carbonate anhydrate). Its impact on the crystal growth of soda is small compared to other organic solvents and the hygroscopic nature of ethylene glycol [22] makes it an effective antisolvent, because of its tendency to bind the water in solution.

## 6.2. Experimental Solubility and Stability Determination

The phase stabilities and corresponding solubilities at a range of temperatures and mixed-solvent compositions were determined with the following experimental procedure: App. 15g of solid and 40g of mixed-solvent were shaken in 50ml Nalgene™ PTFE-bottles in a

thermostatic shaking bath. Mixed solvents with ethylene glycol contents of 50, 60, 70, 80, 90 and 100%-w (salt-free), prepared from technical grade ethylene glycol and ultra-pure water, were used. The solids added to the mixed solvent mixture were:

sodium bicarbonate of technical grade (purity > 99.5%-w)

a mixture of sodium carbonate and bicarbonate of technical grade (> 99.5%-w) in a molar ratio of 1 : 3

a mixture of sodium carbonate and bicarbonate of technical grade (> 99.5%-w) in a molar ratio of 3 : 1

trona, obtained from Solvay, France, (purity > 99.8%-w)

The bottles were shaken at constant temperature of 50°C for one day. The temperature was increased daily after sampling by 10°C till 90°C. In some of the experiments, the system was then cooled down for one day to room temperature (app. 15°C) or 30°C. All samples were prepared in duplicate to test for reproducibility.

It had been found in previous work [23], that solid bicarbonate recrystallized at temperatures > 90°C in the mixed solvent due to thermal decomposition of the dissolved bicarbonate. Since this thermal decomposition was thought to significantly impair the equilibration of the system, temperatures above 90°C were not investigated.

Solution samples were taken after each shaking period of 24h and titrated with 0.1 M HCl (Merck Titriplex) in a Radiometer VIT 90 Video Titrator. The concentrations of  $\text{CO}_3^{2-}$  and  $\text{HCO}_3^-$  were determined from the titration curves, as exemplified in Figure 3. The error of the method was found to be in the range of 0.5 to 2.5% of the measured concentration. All titrations were performed in triplicate and the amount of sample was chosen for  $V(\text{CO}_3^{2-} + \text{HCO}_3^-) \geq 5\text{ml HCl}$  to achieve good resolution of the titration curve. In the Tables 1, 3, 4, 5, also the standard deviations of the titrations of the duplicate samples are given, to indicate the reliability of each data point.

These deviations do not only reflect the accuracy of the titration method, but also the experimental reproducibility of the respective data point. E.g., for pure ethylene glycol, the reproducibility of the  $[\text{HCO}_3^-]$  concentrations is below average: The measured values deviate by 10% or more.

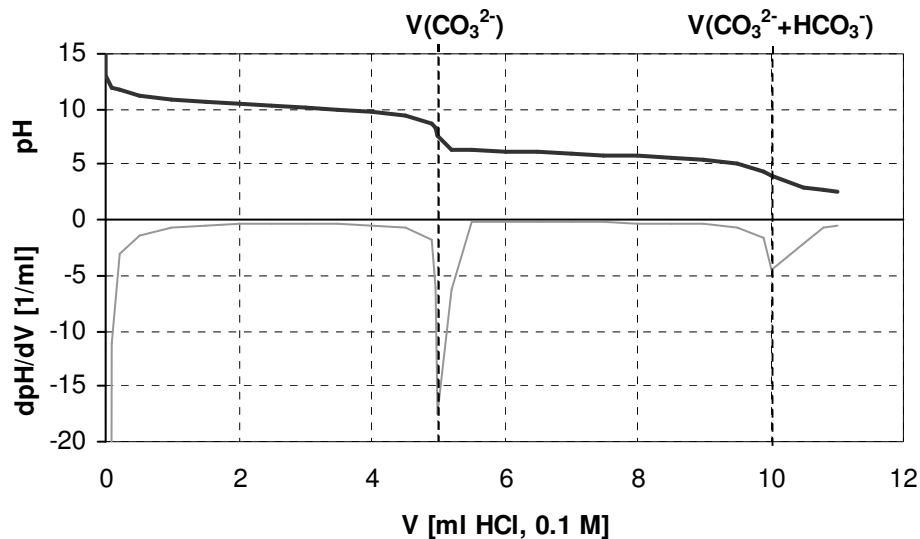


**Figure 6-3:** pH-Titration curve for the determination of  $[\text{CO}_3^{2-}]$  and  $[\text{HCO}_3^-]$

As the  $\text{HCO}_3^-$  concentration increases rapidly from its minimum at 80 to 90%-w ethylene glycol, see Figure 5, small amounts of condensing water vapor from the shaking bath in the sample bottles might have caused these deviations.

The solid phases were identified from (polarized) light microscopy and SEM images. In cases of doubt, samples were additionally analyzed by powder XRD. Additionally, the weight-loss-upon-heating (at  $200^\circ\text{C}$ ) of the solid was determined after completion of the experimental series. No significant decomposition of either dissolved or solid bicarbonate was found below  $90^\circ\text{C}$  from mass balancing the dissolved and solid bicarbonate contents measured at the end of the experimental procedure.

The solution densities given in the tables were obtained by pipeting a known volume of solution and weighing it. No significant temperature dependence of the density was found: The error of this analytical method is estimated to be up to 5% of the measured value, which is in most cases larger than the noted temperature spread.

In addition to the measured solubilities, solubility points are interpolated between  $50^\circ\text{C}$  and room temperature. To distinguish these estimated points from the measured data, these points are rendered in gray and no error range is given for them, see Tables 1, 2 and 3. They were obtained from polynomial fits of at least 4<sup>th</sup> order with a correlation coefficient ( $R^2$ ) of at least 99.9% to the measured data points in the range from 15 to  $90^\circ\text{C}$ . They are only intended to give an impression of the development of the presented



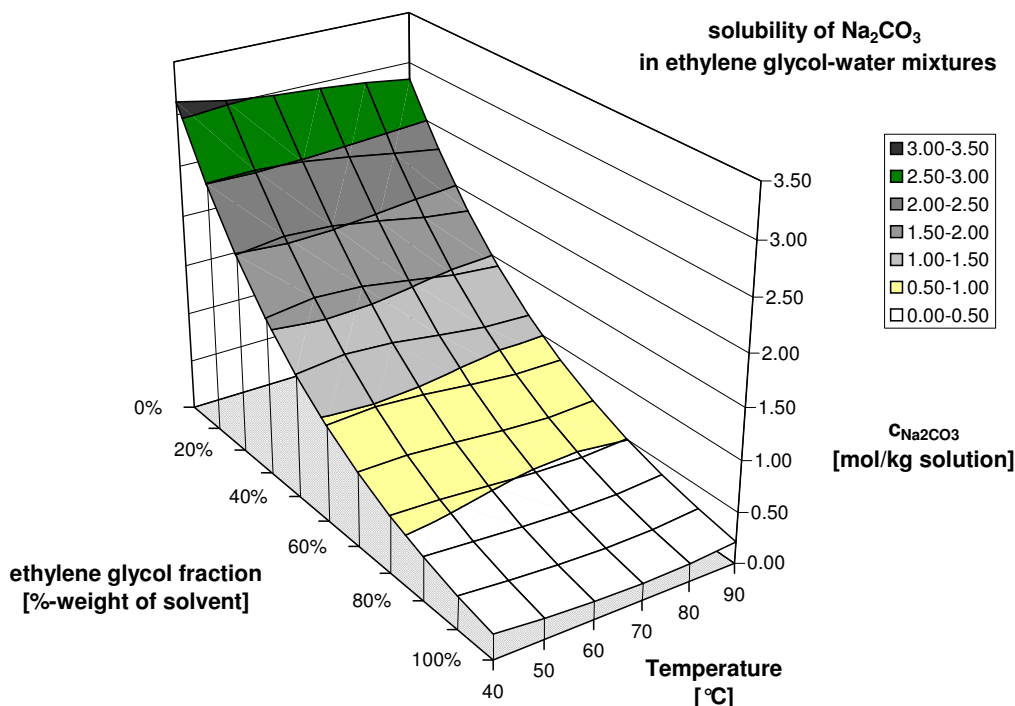
data sets. Although the developments of the solubility lines were steady in these regions, these points might not represent the actual solubilities.

Table 2 lists data points calculated from solubility functions published by Oosterhof et al [11] for sodium carbonate in ethylene glycol - water. These functions were derived as 2<sup>nd</sup> order polynomial fits to their solubility data with correlation coefficients ( $R^2$ ) of at least 99.2%. The data points for 50 and 60°C were extrapolated by 4<sup>th</sup> order polynomial fits to the derived data points. An overview of the solubility results by Oosterhof et al. is given in Figure 4.

### 6.3. Results

#### 6.3.1. Measured Solubilities in the Mixed Solvent

The measured solubilities and the corresponding solid phases are listed in Tables 1, 3, 4 and 5.



**Figure 6-4:** Solubility of  $\text{Na}_2\text{CO}_{3(s)}$  and  $\text{Na}_2\text{CO}_3 \cdot \text{H}_2\text{O}_{(s)}$  in ethylene-glycol – water, derived from solubility data by Oosterhof et al. [11], see Table 2

The solubilities of the pure Na - CO<sub>3</sub> system and of the pure Na – HCO<sub>3</sub> system in the mixed solvent are listed in Tables 2 and 1, and displayed graphically in Figures 4 and 5.

The concentration of dissolved Na<sub>2</sub>CO<sub>3</sub>, i.e. in equilibrium with either anhydrate or monohydrate as solid, see Figure 4 or Table 2, decreased strongly with increasing ethylene glycol concentration, but showed little dependence on temperature.

The solubility of sodium bicarbonate (NaHCO<sub>3(s)</sub>, nahcolite) showed a comparatively slower decline with increasing ethylene glycol content, reached a minimum around 80 to 90%-w ethylene glycol and then sharply increased again towards pure ethylene glycol, see Figure 5. Unlike the solubility concentration of Na<sub>2</sub>CO<sub>3</sub> in Figure 4, the solubility of sodium bicarbonate showed strong temperature dependency and increased with increasing temperature for most bicarbonate containing solid phases, see Figure 10, 11 and 12 in the Addendum. In mixed solvents of 50 to 90%-w ethylene glycol content, the solubility concentration more than doubled from 20 to 90°C. For 90 and 100%-w ethylene glycol, there was a solubility minimum around 40 to 50°C.

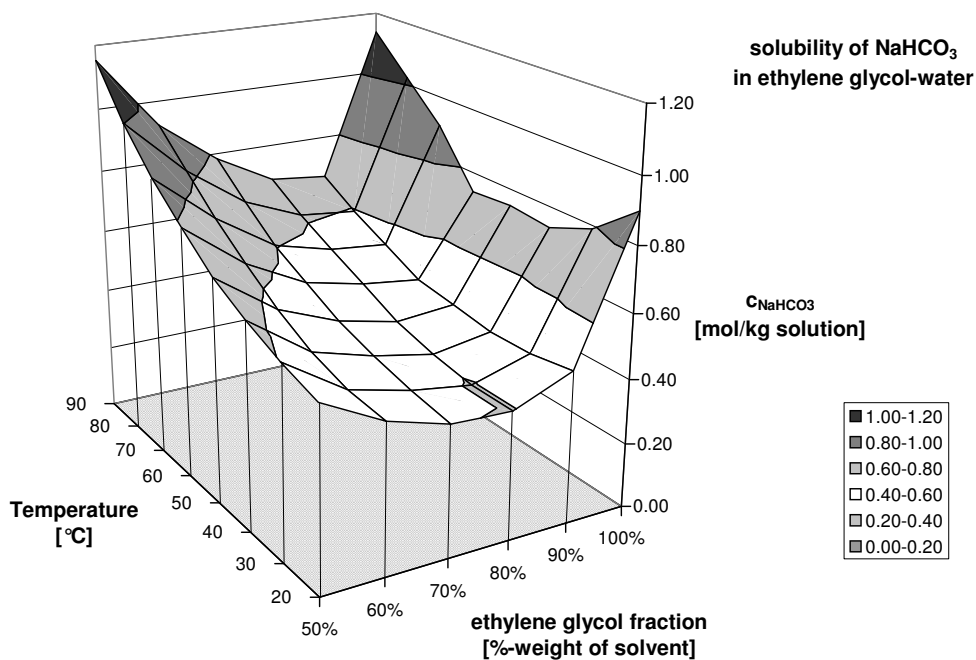


**Figure 6-5:** Solubility of sodium bicarbonate (NaHCO<sub>3(s)</sub>, nahcolite) in ethylene glycol – water

The high solubility of sodium bicarbonate in pure ethylene glycol can probably be explained by the presence of soluble complexes of ethylene glycol with the  $\text{HCO}_3^-$  ion or with neutral, dissolved but undissociated  $\text{NaHCO}_3$ . Small amounts of water apparently break up these complexes and act as an antisolvent in this case. Most likely, the water, with its higher capability for hydrogen bonding, replaces the  $\text{HCO}_3^-$  at the complex-forming bonding sites of the ethylene glycol. The uncomplexed  $\text{HCO}_3^-$  ion and  $\text{NaHCO}_{3(\text{sol})}$  are less soluble in the comparatively unpolar ethylene glycol, because both are rather polar species. The less polar glycol is rather attracted to other glycol molecules or water molecules.

A steady increase of  $\text{HCO}_3^-$  solubility concentration at water contents from 70 to 0%-w (salt-free solvent) ethylene glycol was observed. This could be explained by the formation of hydration hulls, which distribute the ion's charge over the molecules participating in them, reducing long-range ion interactions.

### **6.3.2. Phase Stabilities in the Mixed Solvent System**

As can be seen from the Tables 1 to 5, the different starting solid compositions resulted in the formation of different solid phases after equilibration. The following solid phases were identified by microscopy, heating weight loss analysis and powder XRD: Trona (T), wegscheiderite (W), sodium bicarbonate (B), sodium carbonate anhydrate (A) and sodium carbonate monohydrate (M). The solid phase analysis gave no indication for any further solid phases and the measured solubilities can be adequately explained by the occurrence of the given phases. No solid solvate phases with ethylene glycol were formed in the investigated temperature and concentration range.

Solubility and phase stability diagrams for 50, 70 and 90%-w (salt-free) ethylene glycol mixed solvent are given in Figures 6, 7 and 8. Generally, the solid phases occurred in the same sequence as in the aqueous system: From  $\text{HCO}_3^-$ -rich solutions, sodium bicarbonate (nahcolite) was formed. With increasing  $\text{CO}_3^{2-}$  concentration, first wegscheiderite, then trona and finally sodium carbonate monohydrate or anhydrate became the stable phase of the system. The thin gray lines indicate the solubility isotherms, while the unbroken fat lines mark 2-phase-lines over the investigated temperature range.

Most measured data points correspond to such 2-phase-lines, as a sufficient amount of solid Na-CO<sub>3</sub> as well as solid Na-HCO<sub>3</sub> was present in most experiments to form more than one solid phase. The depicted solubility isotherms are lines between the measured data points. Therefore, they are only approximations of the actual solubilities. It is likely that the actual solubility isotherms have a more hyperbolic shape, due to their dependency on the thermodynamic solubility products of the occurring solid phases:

$$K_{sp,xyz} = a_{Na_2CO_3}^x \cdot a_{NaHCO_3}^y \cdot a_{H_2O}^z = \gamma_{Na_2CO_3}^x \cdot c_{Na_2CO_3}^x \cdot \gamma_{NaHCO_3}^y \cdot c_{NaHCO_3}^y \cdot a_{H_2O}^z \quad \text{Eq. 6-1}$$

$$\Leftrightarrow c_{NaHCO_3} = \sqrt[y]{\frac{K_{sp,xyz}}{\gamma_{NaHCO_3}^y \cdot \gamma_{Na_2CO_3}^x \cdot c_{Na_2CO_3}^x \cdot a_{H_2O}^z}} \quad \text{Eq. 6-2}$$

$$\Rightarrow c_{NaHCO_3} \propto \left( \frac{1}{c_{Na_2CO_3}} \right)^{x/y} \quad \text{Eq. 6-3}$$

In Eq. 1 to 3, x,y and z represent the stoichiometric coefficients of Na<sub>2</sub>CO<sub>3</sub>, NaHCO<sub>3</sub> and H<sub>2</sub>O in the given solid phase, e.g. x = 1, y = 1, z = 2 for trona: Na<sub>2</sub>CO<sub>3</sub>·NaHCO<sub>3</sub>·2H<sub>2</sub>O<sub>(s)</sub>.

In Figure 6, the solubilities of the occurring phases in 50%-w (salt-free) ethylene glycol from 50 to 90°C are given. The solubilities of nahcolite, wegscheiderite and trona increased steadily with temperature, while the solubility of monohydrate decreased with temperature. This resulted in a crossing of solubility isotherms in the trona – monohydrate region. While some anhydrate was formed at 90°C as second solid in equilibrium with trona, from solutions containing no HCO<sub>3</sub> (i.e. along the x-axis of Figure 6) only the monohydrate is formed, see also Table 2.

In Figure 7, the solubilities of the occurring phases in 70%-w (salt-free) ethylene glycol from 50 to 90°C are displayed. Again, the solubilities of bicarbonate (nahcolite), wegscheiderite and trona increased steadily with temperature, while the solubility of monohydrate decreased with temperature and the solubility of anhydrate increased slightly with temperature. This resulted in a crossing of solubility isotherms in the trona – monohydrate/anhydrate region. In solutions containing no HCO<sub>3</sub> (i.e. along the x-axis of Figure 7), monohydrate is stable till ca. 70°C, while anhydrate was found at 80 and 90°C, see also Table 2. The 2-phase lines for bicarbonate – wegscheiderite and wegscheiderite -

anhydrate are given till 95°C. For this reason, these lines are exceeding the 90°C solubility isotherm.

In Figure 8, the solubilities and stabilities of the occurring phases in 90%-w (salt-free) ethylene glycol from 50 to 90°C are plotted. The solubilities of bicarbonate (nahcolite), wegscheiderite and trona was noticeably less temperature dependent than at the lower ethylene glycol contents, see Figures 6 and 7. From solutions containing no HCO<sub>3</sub> (i.e. along the x-axis of Figure 8) only anhydrate formed from 50 to 90°C. The solubility isotherms cross in the region of wegscheiderite, because the solubility of anhydrate decreased from 50 to 70°C and then increased again from 70 to 90°C, see Table 2.

Two solubility plots are given in Figure 8, since a significant difference in phase stability between trona formed during the experiments in mixed solvent solution and the trona obtained from Solvay, France (i.e. formed from aqueous solution), was found. The Solvay trona was stable up to 70°C, while the mixed-solvent-formed trona was only stable till 40°C.

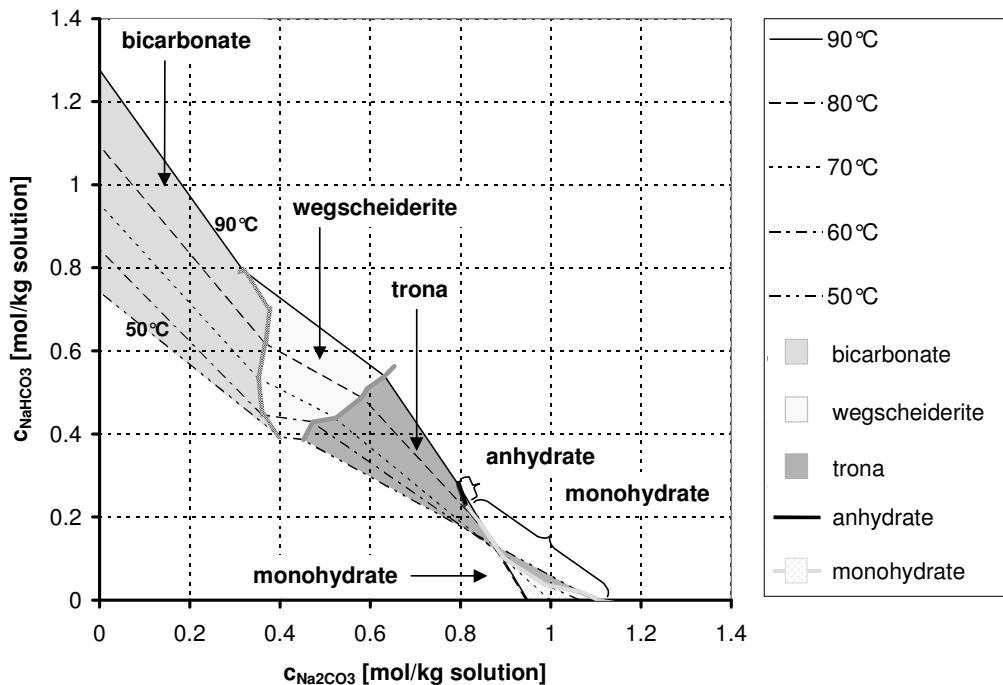


**Figure 6-6:** Phase stability and solubility chart for Na<sub>2</sub>CO<sub>3</sub>-NaHCO<sub>3</sub> in 50%-w (salt-free) ethylene glycol mixed solvent

For the development of the solubilities and phase stabilities with increasing ethylene glycol content, the following effects were observed:

While wegscheiderite only occurred at temperatures above 70°C in the aqueous system, see Figure 1 and 2, it was already found at 50°C in 50%-w (salt-free solvent) ethylene glycol. It appears that for higher ethylene glycol concentrations, wegscheiderite might occur at even lower temperatures.

Also of significance was the fact that, while anhydrate was not a stable phase in aqueous solution, it was a stable phase in 50%-w (salt-free solvent) ethylene glycol at 80°C or higher, see Figure 6.

At higher ethylene glycol concentrations, anhydrate formed at even lower temperatures, effectively replacing monohydrate, trona and even wegscheiderite. In 70%-w (salt-free solvent) ethylene glycol, anhydrate occurred already at 60 to 70°C, and in 90%-w (salt-free solvent) ethylene glycol at a temperature as low as 50°C.

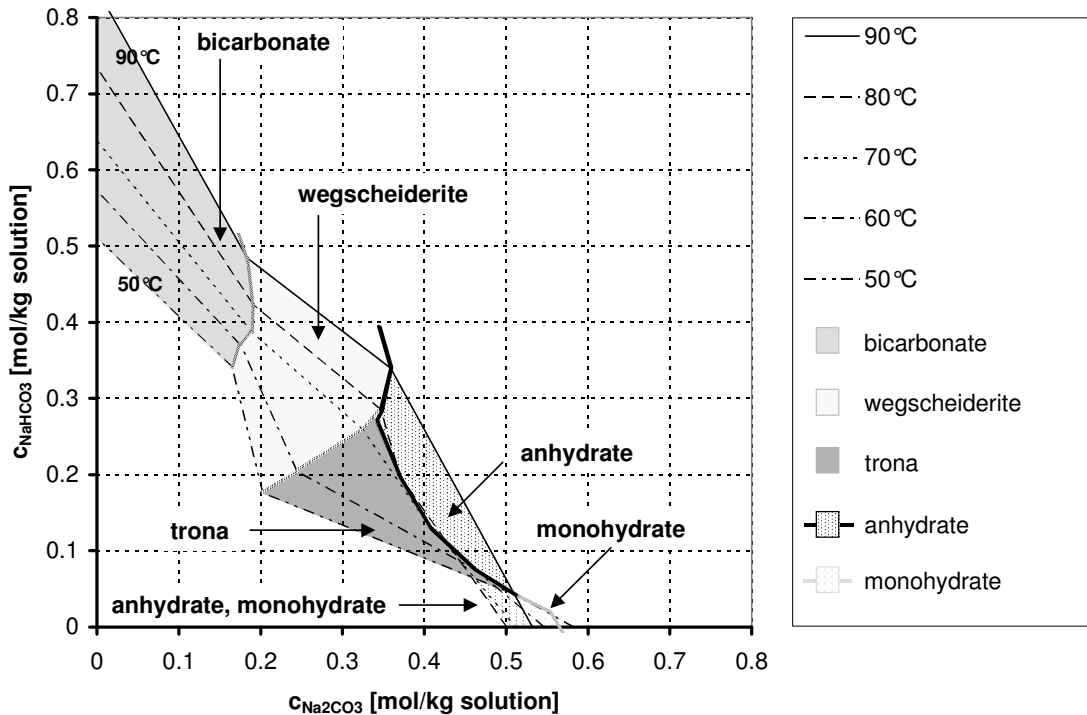


**Figure 6-7:** Phase stability and solubility chart for  $\text{Na}_2\text{CO}_3$ - $\text{NaHCO}_3$  in 70%-w (salt-free) ethylene glycol mixed solvent

These results were not surprising, since monohydrate and trona are hydrates, which stabilities decrease with increasing antisolvent content.

As can be seen from Figure 6, 7 and 8, the mixed solvent's ability to solubilize  $\text{CO}_3^{2-}$  decreased more strongly with increasing ethylene glycol content than its ability to solubilize  $\text{HCO}_3^-$ : e.g. the maximal solubility concentration of  $\text{NaHCO}_3$  (i.e. along the y-axis) became higher than the maximal  $\text{Na}_2\text{CO}_3$  solubility concentration (i.e. along the x-axis). Due to the decreasing solubility of  $\text{CO}_3^{2-}$ , the anhydrate was stable at increasing  $[\text{HCO}_3^-]$  to  $[\text{CO}_3^{2-}]$  ratios with increasing ethylene glycol content. This effect went so far, that in 90%-w (salt-free solvent) ethylene glycol, wegscheiderite was replaced by anhydrate at increased temperature and even no wegscheiderite was found in pure ethylene glycol from 50 to 90°C.

The phase behavior at high contents of ethylene glycol displayed some similarity with the one of the aqueous system at increased temperatures.

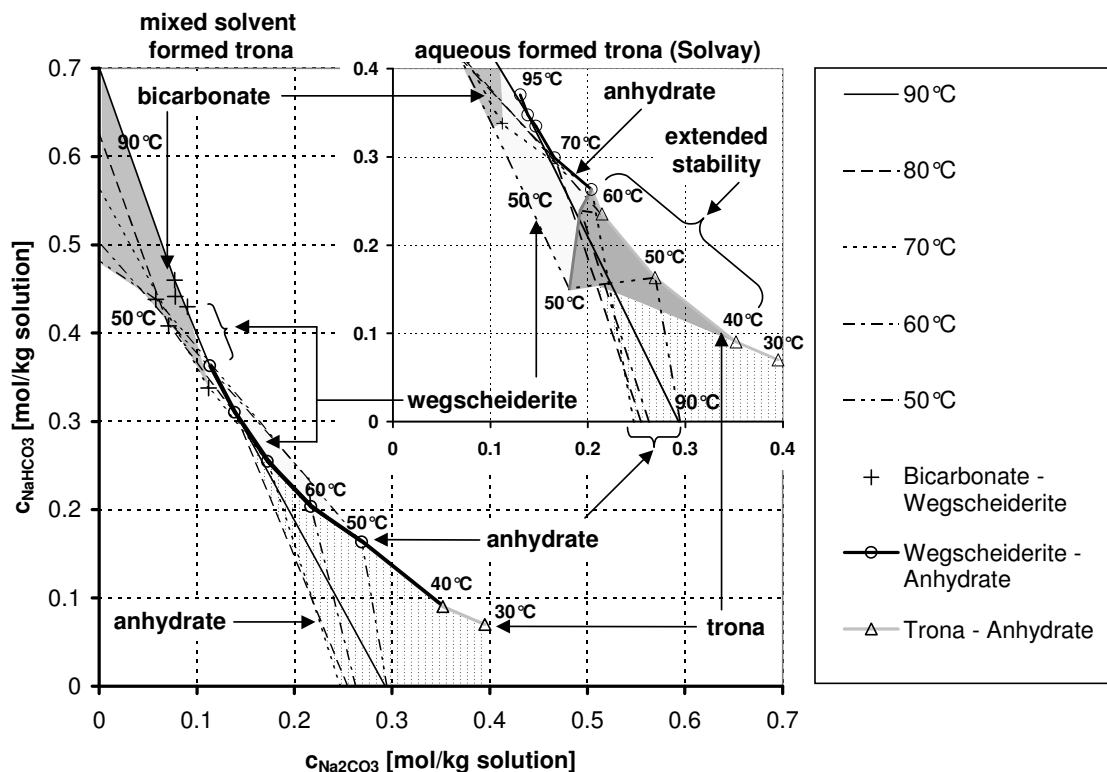


**Figure 6-8:** Phase stability and solubility chart for  $\text{Na}_2\text{CO}_3$ - $\text{NaHCO}_3$  in 90%-w (salt-free) ethylene glycol mixed solvent

E.g. the reduced hydrate stability, or the increasing ratio of the  $[\text{NaHCO}_3]$  solubility concentration in the  $\text{Na-HCO}_3$  system (see y-axis in Figures 1, 2, 6-8) to the  $[\text{Na}_2\text{CO}_3]$  solubility concentration in the  $\text{Na-CO}_3$  system (see x-axis in same Figures):

$$\frac{[\text{NaHCO}_3]_{\text{Na-HCO}_3}}{[\text{Na}_2\text{CO}_3]_{\text{Na-CO}_3}} \left[ \frac{\text{mol}(\text{NaHCO}_3)/\text{kg solution}}{\text{mol}(\text{Na}_2\text{CO}_3)/\text{kg solution}} \right]$$

For 25°C and aqueous solution, this ratio is 0.52, while in aqueous solution at 200°C and in 90%-w (salt-free solvent) ethylene glycol at 90°C the ratio is 2.3.

Unfortunately, the measured phase stability behavior was not completely conclusive:

The stability and solubility of trona (sodium sesquicarbonate) recrystallized from the mixed solvent was lower than the stability and solubility of trona obtained from Solvay, France, i.e. trona crystallized from aqueous solution, see Figure 8. For this effect, it did not matter, whether the trona was recrystallized in the mixed solvent from sodium carbonate anhydrate (soda) and sodium bicarbonate (nahcolite) or from a mixture of wegscheiderite and anhydrate, which had been formed previously by recrystallization of Solvay trona. Therefore, it was unlikely, that this difference in stability is a result of impurities in one of the trona types.

The stability of both types of trona in dependence of temperature and ethylene glycol content is outlined in Figure 9, which is taken from Chapter 4. The difference in solubility and stability increased with increasing ethylene glycol content. Till 50%-w (salt-free) ethylene glycol, both types of trona recrystallized at the same *transition temperature*, but the Solvay trona recrystallizes at 60%-w at a slightly higher temperature than the mixed-solvent-formed one. With increasing ethylene glycol content this difference increased to the extend, that Solvay trona appeared stable in pure ethylene glycol, from which no trona could possibly form by recrystallization, due to the complete lack of sufficient water.

This difference in stability and solubility could not be detected in Figure 6 and 7, although a significant difference in trona transition temperature can be observed in 70%-w (salt-free solvent) ethylene glycol mixed solvent from Figure 9.



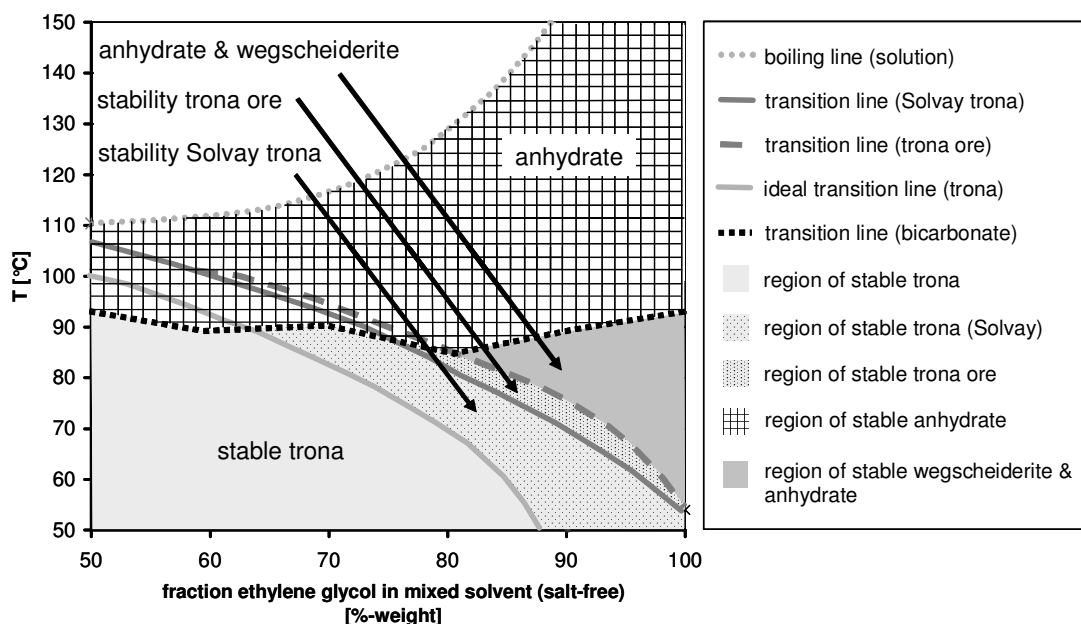


**Figure 6-9:** Stability of trona of different origin in ethylene glycol – water mixed solvents

As  $\text{HCO}_3^-$  undergoes significant thermal decomposition to  $\text{CO}_3^{2-}$  and  $\text{CO}_2$  at  $T > 90^\circ\text{C}$ , only anhydrate was found beyond ca.  $110^\circ\text{C}$  as the thermodynamically stable phase under atmospheric conditions, see Chapter 3 and 4.

Powder XRD showed a slight broadening of the diffraction peak of the mixed solvent trona compared to the Solvay trona. This indicated a possible slight difference of crystallinity in the crystal lattice of the two types of trona. This difference in crystal structure might well explain the difference in stability, but why this difference was only found in mixed solvents of more than 60%-w ethylene glycol, could not be explained on the basis of the presented data.

In Chapter 4, it was found, that thermodynamic data derived from measurements of the aqueous systems predicts the phase transition line of the mixed-solvent-formed trona - and not the aqueous-crystallized Solvay trona.

Trona ore, supplied by IMC Chemicals, California, USA, displayed similar behavior as the trona obtained from Solvay, see Figure 9. The increased stability was therefore not only a property of the Solvay trona, but rather appeared to generally apply to trona formed from aqueous solution.

#### 6.4. Conclusion

The solubilities in the system Na – CO<sub>3</sub> – HCO<sub>3</sub> were measured in mixed solvents of ethylene glycol – water over a range of temperatures and mixed solvent compositions. Sodium carbonate anhydrate (natrite, Na<sub>2</sub>CO<sub>3(s)</sub>), sodium carbonate monohydrate (thermonatrite, Na<sub>2</sub>CO<sub>3</sub>·H<sub>2</sub>O<sub>(s)</sub>), sodium bicarbonate (nahcolite, NaHCO<sub>3(s)</sub>), sodium sesquicarbonate (trona, Na<sub>2</sub>CO<sub>3</sub>·NaHCO<sub>3</sub>·2H<sub>2</sub>O) and sodium carbonate tri-bicarbonate (wegscheiderite or decimite, Na<sub>2</sub>CO<sub>3</sub>·3NaHCO<sub>3(s)</sub>) were identified as the occurring solid phases. No solvate phases with ethylene glycol were formed.

For all observed solid phases, the solubility concentration of CO<sub>3</sub><sup>2-</sup> decreased with increasing ethylene glycol content, while for HCO<sub>3</sub><sup>-</sup> it reached a minimum at 80 to 90%-w (salt-free solvent) ethylene glycol and then sharply increased again. While the CO<sub>3</sub><sup>2-</sup> solubility concentration showed little temperature dependence, the HCO<sub>3</sub><sup>-</sup> solubility concentration was very temperature dependent for all NaHCO<sub>3</sub> containing solid phases. The solubility concentration of HCO<sub>3</sub><sup>-</sup> approximately doubled in the temperature range from 50 to 90°C.

The solubility of nahcolite, wegscheiderite and trona increased steadily with temperature, the solubility of sodium carbonate monohydrate dropped with temperature, and the solubility of sodium carbonate anhydrate showed a slight increase with temperature for all mixed solvent compositions in the investigated temperature range.

Increasing ethylene glycol content decreased the stability of hydrates, like monohydrate and trona, and increased those of anhydrous phases like anhydrate and wegscheiderite. These anhydrous phases occurred therefore in the mixed solvents at significantly lower *transition temperatures* than in aqueous solution.

The stability of trona recrystallized from mixed solvents with ethylene glycol contents higher than 60%-w (salt-free solvent) ethylene glycol was lower than that of trona formed from aqueous solution. This discrepancy in stability could not be explained within the framework of this work, but there was some indication, that the crystal lattice of the mixed-solvent-formed trona differed slightly from the one obtained from aqueous crystallization.

These results offer some interesting possibilities for technical applications of the mixed solvent system of Na – CO<sub>3</sub> – HCO<sub>3</sub>:

The stability range of the industrially relevant sodium carbonate anhydrate (soda) is significantly extended compared to the aqueous system. This allows e.g. the crystallization of sodium carbonate anhydrate from a broader range of sodium carbonate – bicarbonate compositions.

Also the stability range of wegscheiderite ( $\text{Na}_2\text{CO}_3 \cdot 3\text{NaHCO}_3(\text{s})$ ) is increased compared to the aqueous system, which can facilitate the preparation of this salt for e.g. analytical purposes.

### **6.5. Literature References**

- [1] Chen, C.C., Evans, L.B., “Local Composition Model for Excess Gibbs Energy of Aqueous Electrolyte Systems”, *AIChE J.*, 28, 1982, p. 588-596
- [2] Chen, C.C., Evans, L.B., Mock, B., “Thermodynamic Representation of Phase Equilibria of Mixed Solvent Electrolyte Systems”, *AIChE J.*, 32, 1986, p. 1655-1664
- [3] Chen, C.C., Mathias, P.M., Orbey, H., “Use of Hydration and Dissociation Chemistries with the Electrolyte-NRTL Model”, *AIChE J.*, 45, 1999, p. 1576-1586
- [4] Pitzer, K.S., "Activity Coefficients in Electrolyte Solutions", 2<sup>nd</sup> ed., CRC Press, Boca Raton (Florida), 1991
- [5] Pitzer, K.S., Kim, J.J., “Thermodynamics of Electrolytes. IV. Activity Coefficients for Mixed Electrolytes”, *J. Am. Chem. Soc.*, 96, 1974, p. 5701
- [6] Marion, G.M., “Carbonate Mineral Solubility at Low Temperatures in the Na-K-Mg-Ca-H-Cl-SO<sub>4</sub>-OH-HCO<sub>3</sub>-CO<sub>3</sub>-CO<sub>2</sub>-H<sub>2</sub>O System”, *Geochimica et Cosmochimica Acta*, 65 (12), 2001, p. 1883-1896
- [7] Johnson, J.W., Oelkers, E.H., and Helgeson, H.C., “SUPCRT92: A software package for calculating the standard molal thermodynamic properties of minerals, gases, aqueous species, and reactions from 1 to 5000 bars and 0 to 1000°C”, *Computers & Geosciences*, 18 (7), 1992, p. 899-947
- [8] Oelkers, E.C., Helgeson, H.C., Shock, E.L., Sverjensky, D.A., Johnson, J.W., Pokrovskii, V.A., “Summary of the Apparent Molal Gibbs Free Energies of Formation of Aqueous Species, Minerals, and Gases at Pressures 1 to 5000 Bars and Temperatures 25 to 100°C”, *J. Phys. Chem. Ref. Data*, 24 (4), 1995, p. 1401-1560
- [9] Kim, Y., Haam, S., Koo, K.K., Shul, Y.G., Son, J.H., Jung, J.K., “Representation of Solid-Liquid-Equilibrium of L-Ornithine-L-Aspartate + Water + Methanol System Using the

- Chen Model for Mixed Solvent Electrolyte Solution”, *J. Chem. Eng. Data*, 46, 2001, p. 1387-1391
- [10] Kim, Y., Haam, S., Koo, K.K., Shul, Y.G., Kim, W.S., Jung, J.K., Eun, H.C., “Pseudopolymorphic Crystallization of L-Ornithine-L-Aspartate by Drowning Out”, *Ind. Eng. Chem. Res.*, 42 (2), 2002, p. 883-889
- [11] Oosterhof, H., Witkamp, G.J., van Rosmalen, “Some antisolvents for crystallisation of sodium carbonate”, *Fluid Phase Equilibria*, 155, 1999, p. 219-227
- [12] Seidell, A., “Solubilities of Inorganic and Metal Organic Compounds”, Vol. II, Van Nostrand, New York, 1958, p. 940-946
- [13] Taylor, C.E., “Thermodynamics of Sodium Carbonate in Solution”, *J. Phys. Chem.*, 59 (1), 1955, p. 653-657
- [14] Kobe, K.A., Sheehy, T.M., “Thermochemistry of Sodium Carbonate and Its Solution”, *Ind. Eng. Chem.*, 40 (1), 1948, p. 99-102
- [15] Waldeck, W.F., Lynn, G., Hill, A.E., “Aqueous Solubility of Salts at High Temperatures. I. Solubility of Sodium Carbonate from 50 to 348°C”, *J. Am. Chem. Soc.*, 54, 1932, p. 928-936
- [16] Seidell, A., “Solubilities of Inorganic and Metal Organic Compounds”, Vol. I, Van Nostrand, New York, 1940, p. 1193-1200
- [17] Wegscheider, R., Mehl, J., “Über Systeme  $\text{Na}_2\text{CO}_3\text{-NaHCO}_3\text{-H}_2\text{O}$  und das Existenzgebiet der Trona”, *Monatsh. d. Chem., Sitzungsberichte Akademie der Wissenschaften in Wien*, 49, 1928, p. 283-315
- [18] Hill, A.E., Bacon, L.R., “Ternary Systems. VI. Sodium Carbonate, Sodium Bicarbonate and Water”, *J. Am. Chem. Soc.*, 59, 1927, p. 2487-2495
- [19] Waldeck, W.F., Lynn, G., Hill, A.E., “Aqueous Solubility of Salts at High Temperatures. II. The Ternary System  $\text{Na}_2\text{CO}_3\text{-NaHCO}_3\text{-H}_2\text{O}$  from 100 to 200°C”, *J. Am. Chem. Soc.*, 56, 1934, p.43-48
- [20] Garret, D.E., “Natural Soda Ash – Occurrences, Processing and Use”, Van Nostrand – Reinhold (Publ.), New York, 1992, p. 565
- [21] Oosterhof, H., de Graauw, J., Witkamp, G.J., van Rosmalen, G.M., 2002, “Continuous Double Recrystallization of Light Soda Ash into Super Dense Soda Ash”, *Crystal Growth & Design*, 2 (2), 2002, p. 151-157
- [22] Zavitsas, A.A., “Properties of Water Solutions of Electrolytes and Nonelectrolytes”, *J. Phys. Chem. B*, 105, 2001, p. 7805-7817

[23] Gärtner, R.S., Witkamp, G.J., “Wet Calcining of Trona (Sodium Sesquicarbonate) and Bicarbonate in a Mixed Solvent“, J. Crystal Growth, 237-239 (3), 2002, p. 2199-2205

## 6.6. Addendum: Solubility Tables & Additional Phase Diagrams

**Table 6-1:** Solubility of sodium bicarbonate ( $\text{NaHCO}_3(\text{s})$ ) in ethylene glycol – water

		c( $\text{NaHCO}_3$ ) [mol/ kg solution]					
$x_{\text{EG}}$ [%w] (salt-free)	50%	60%	70%	80%	90%	100%	
T [°C]	c [mol/kg]	c [mol/kg]	c [mol/kg]	c [mol/kg]	c [mol/kg]	c [mol/kg]	
15	0.5450 ± 0.0875	0.4651 ± 0.0126	0.3971 ± 0.0024	0.4042 ± 0.0288	0.4883 ± 0.0130	1.1315 ± 0.1305	
20	0.5590	0.4597	0.4040	0.3956	0.4701	0.8998	
30	0.5944	0.4706	0.4238	0.3956	0.4484	0.7896	
40	0.6414	0.5072	0.4526	0.4153	0.4452	0.7358	
50	0.7002 ± 0.0036	0.5657 ± 0.0016	0.4904 ± 0.0020	0.4487 ± 0.0003	0.4640 ± 0.0016	0.7483 ± 0.0044	
60	0.7863 ± 0.0026	0.6425 ± 0.0004	0.5452 ± 0.0009	0.5040 ± 0.0125	0.4808 ± 0.0070	0.7383 ± 0.0328	
70	0.8812 ± 0.0010	0.7254 ± 0.0072	0.6043 ± 0.0030	0.5560 ± 0.0068	0.5378 ± 0.0016	0.9061 ± 0.0350	
80	1.0004 ± 0.0062	0.8221 ± 0.0075	0.6903 ± 0.0006	0.6137 ± 0.0051	0.5939 ± 0.0065	1.0207 ± 0.0072	
90	1.1527 ± 0.0070	0.9219 ± 0.0182	0.7820 ± 0.0023	0.6829 ± 0.0045	0.6621 ± 0.0137	1.1361 ± 0.0247	
$\rho_{\text{solution}}$ [g/ml]	1.074 ± 0.044	1.075 ± 0.026	1.098 ± 0.025	1.096 ± 0.023	1.106 ± 0.005	1.131 ± 0.017	

**Table 6-2:** Solubility of Na<sub>2</sub>CO<sub>3</sub> anhydrate (A) and monohydrate (M) in ethylene glycol – water, calculated from solubility functions given by Oosterhof et al. [9]

c(Na <sub>2</sub> CO <sub>3</sub> ) [mol/kg solution]						
x <sub>EG</sub> [%-w] (salt-free)	0%	10%	20%	30%	40%	
T [°C]	c [mol/kg]	c [mol/kg]	c [mol/kg]	c [mol/kg]	c [mol/kg]	
40	3.12 <sup>M</sup>	2.50 <sup>M</sup>	1.99 <sup>M</sup>	1.57 <sup>M</sup>	1.23 <sup>M</sup>	
50	3.03 <sup>M</sup>	2.52 <sup>M</sup>	2.05 <sup>M</sup>	1.64 <sup>M</sup>	1.28 <sup>M</sup>	
60	2.98 <sup>M</sup>	2.48 <sup>M</sup>	2.02 <sup>M</sup>	1.61 <sup>M</sup>	1.26 <sup>M</sup>	
70	2.94 <sup>M</sup>	2.42 <sup>M</sup>	1.95 <sup>M</sup>	1.54 <sup>M</sup>	1.19 <sup>M</sup>	
80	2.90 <sup>M</sup>	2.34 <sup>M</sup>	1.87 <sup>M</sup>	1.46 <sup>M</sup>	1.13 <sup>M</sup>	
90	2.83 <sup>M</sup>	2.27 <sup>M</sup>	1.81 <sup>M</sup>	1.42 <sup>M</sup>	1.11 <sup>M</sup>	

x <sub>EG</sub> [%-w] (salt-free)	50%	60%	70%	80%	90%	100%
T [°C]	c [mol/kg]	c [mol/kg]	c [mol/kg]	c [mol/kg]	c [mol/kg]	c [mol/kg]
40	0.96 <sup>M</sup>	0.74 <sup>M</sup>	0.57 <sup>M</sup>	0.43 <sup>M</sup>	0.32	0.24 <sup>A</sup>
50	0.98 <sup>M</sup>	0.74 <sup>M</sup>	0.55 <sup>M</sup>	0.40 <sup>M</sup>	0.29	0.20 <sup>A</sup>
60	0.95 <sup>M</sup>	0.71 <sup>M</sup>	0.52 <sup>M</sup>	0.37 <sup>M</sup>	0.26 <sup>A</sup>	0.17 <sup>A</sup>
70	0.90 <sup>M</sup>	0.67 <sup>M</sup>	0.49 <sup>M</sup>	0.35 <sup>A</sup>	0.24 <sup>A</sup>	0.16 <sup>A</sup>
80	0.86 <sup>M</sup>	0.64 <sup>M</sup>	0.48 <sup>A</sup>	0.35 <sup>A</sup>	0.25 <sup>A</sup>	0.18 <sup>A</sup>
90	0.86 <sup>M</sup>	0.66 <sup>A</sup>	0.50 <sup>A</sup>	0.38 <sup>A</sup>	0.28 <sup>A</sup>	0.21 <sup>A</sup>

**Table 6-3:** Solubility of Na<sub>2</sub>CO<sub>3</sub> anhydrate (A), Na<sub>2</sub>CO<sub>3</sub> monohydrate (M), trona (T) and wegscheiderite (W), forming from a starting solid composition ratio of Na<sub>2</sub>CO<sub>3(s)</sub>-NaHCO<sub>3(s)</sub> of 3 : 1 (mol), in ethylene glycol – water

		c(CO <sub>3</sub> <sup>2-</sup> ) [mol/kg solution]					
x <sub>EG</sub> [%-w] (salt-free)	50%	60%	70%	80%	90%	100%	
T [°C]	c [mol/kg]	c [mol/kg]	c [mol/kg]	c [mol/kg]	c [mol/kg]	c [mol/kg]	c [mol/kg]
30	1.0230 ±0.0017	0.7296 ±0.0322	0.5395 ±0.0237	0.4950 ±0.0411	0.3792 ±0.0072	0.2308 ±0.0225	
40	0.9971	0.7117	0.5231	0.4335 ±0.0021	A,T 0.3393 ±0.0018	A,T 0.3120 ±0.0100	A
50	0.9535 ±0.0087	M,T 0.6710 ±0.0005	M,T 0.4905 ±0.0088	M,T 0.3821 ±0.0060	A,T 0.2615 ±0.0012	AW 0.2387 ±0.0379	AW
60	0.8951 ±0.0038	M,T 0.6195 ±0.0031	M,T 0.4451 ±0.0081	A,T 0.3235 ±0.0099	A,T 0.2119 ±0.0006	AW 0.1464 ±0.0179	AW
70	0.8187 ±0.0300	M,T 0.5653 ±0.0094	M,T 0.3901 ±0.0015	A,T 0.2568 ±0.0025	A,T 0.1692 ±0.0027	AW 0.1074 ±0.0196	A
80	0.7735 ±0.0100	M,T 0.5159 ±0.0018	A,T 0.3578 ±0.0135	A 0.2224 ±0.0037	AW 0.1366 ±0.0053	AW 0.0726 ±0.0049	AW
89.8	0.7336 ±0.0125	A,T 0.5314 ±0.0713	A,T 0.3099 ±0.0119	AW 0.2084 ±0.0074	AW 0.1120 ±0.0005	AW 0.0672 ±0.0077	AW

		c(HCO <sub>3</sub> <sup>-</sup> ) [mol/kg solution]					
x <sub>EG</sub> [%-w] (salt-free)	50%	60%	70%	80%	90%	100%	
T [°C]	c [mol/kg]	c [mol/kg]	c [mol/kg]	c [mol/kg]	c [mol/kg]	c [mol/kg]	c [mol/kg]
30	0.0000 ±0.0070	0.0000 ±0.0143	0.0000 ±0.0106	0.0000 ±0.0211	0.0696 ±0.0027	0.3884 ±0.0729	
40	0.0000	0.0146	0.0199	0.0134 ±0.0050	A,T 0.0895 ±0.0091	A,T 0.0886 ±0.0411	A
50	0.0215 ±0.0155	M,T 0.0327 ±0.0029	M,T 0.0391 ±0.0010	M,T 0.0491 ±0.0069	A,T 0.1611 ±0.0045	AW 0.1732 ±0.0407	AW
60	0.0374 ±0.0082	M,T 0.0578 ±0.0076	M,T 0.0714 ±0.0088	A,T 0.1187 ±0.0084	A,T 0.2001 ±0.0033	AW 0.3626 ±0.0201	AW
70	0.1005 ±0.0038	M,T 0.1161 ±0.0094	M,T 0.1308 ±0.0057	A,T 0.2026 ±0.0030	A,T 0.2493 ±0.0031	AW 0.4233 ±0.0181	A

80	0.1817 <sup>M,T</sup>	0.1790 <sup>A,T</sup>	0.1908 <sup>A</sup>	0.2745 <sup>AW</sup>	0.3024 <sup>AW</sup>	0.4820 <sup>AW</sup>
	±0.0121	±0.0079	±0.0234	±0.0248	±0.0227	±0.0050
89.8	0.2712 <sup>A,T</sup>	0.3072 <sup>A,T</sup>	0.3385 <sup>AW</sup>	0.3330 <sup>AW</sup>	0.3522 <sup>AW</sup>	0.5379 <sup>AW</sup>
	±0.0003	±0.0628	±0.0175	±0.0074	±0.0128	±0.0097
$\rho_{\text{solution}}[\text{g/ml}]$	1.108	1.133	1.134	1.113	1.116	1.134
	±0.044	±0.041	±0.022	±0.017	±0.027	±0.028
$x_{\text{EG}} [\%-\text{w}]$ (salt-free)	50%	60%	70%	80%	90%	100%



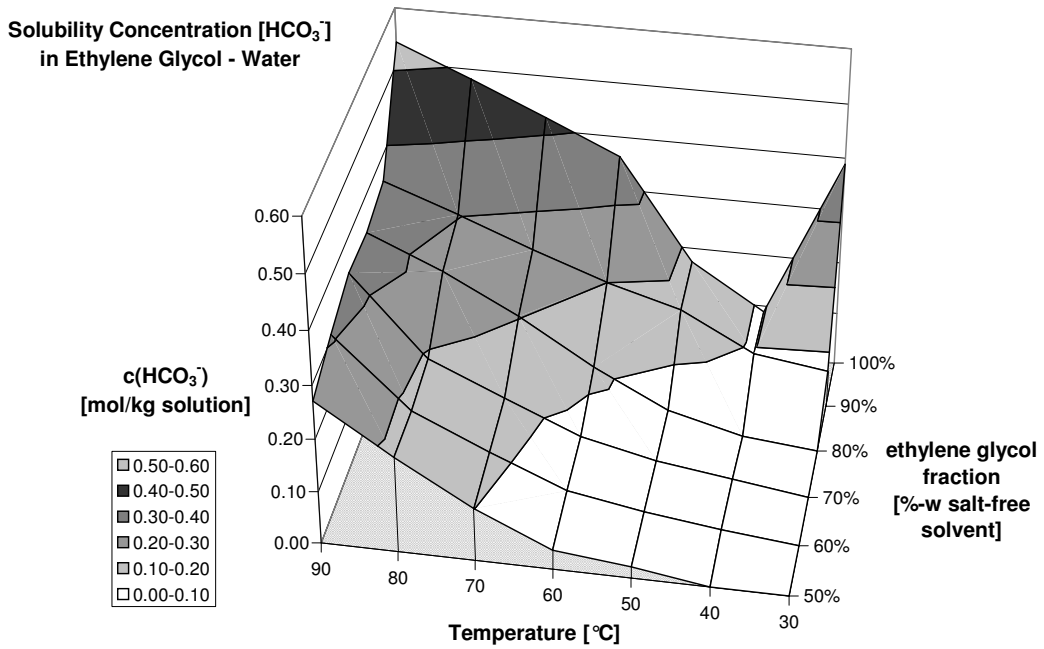
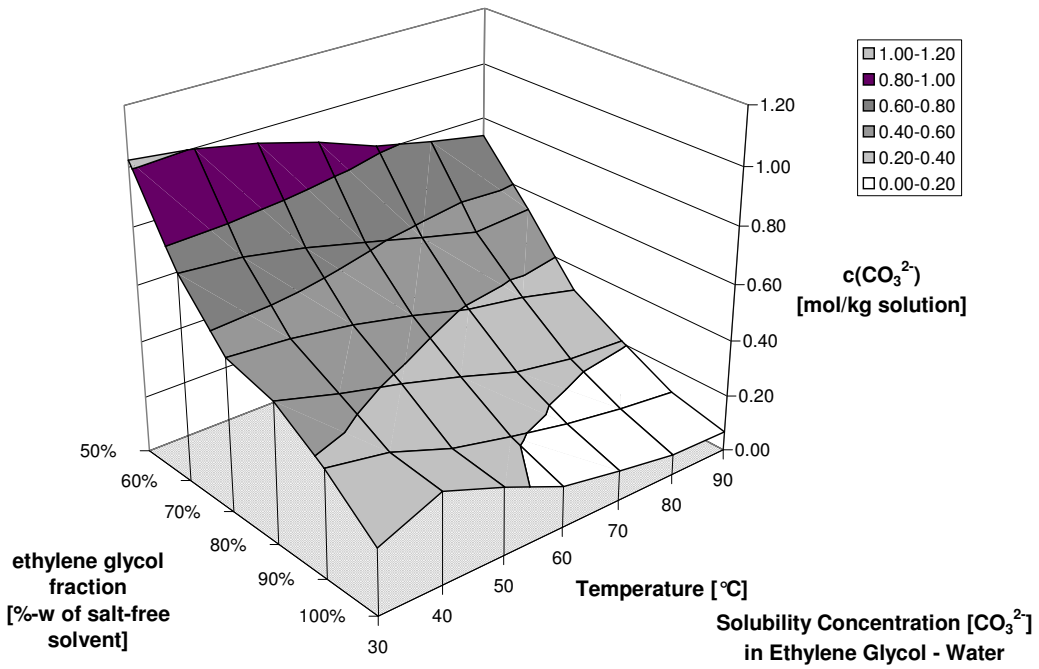


**Figure 6-10:** Solubility Concentrations  $[\text{CO}_3^{2-}]$  and  $[\text{HCO}_3^-]$  in ethylene glycol – water mixed solvents as given in Table 3

**Table 6-4:** Solubility of Na<sub>2</sub>CO<sub>3</sub> anhydrate (A), wegscheiderite (W), trona (T) and nahcolite (NaHCO<sub>3(s)</sub>, B), forming from a starting solid composition ratio of Na<sub>2</sub>CO<sub>3(s)</sub>-NaHCO<sub>3(s)</sub> of 1 : 3 (mol), in ethylene glycol - water

		c(CO <sub>3</sub> <sup>2-</sup> ) [mol/kg solution]					
x <sub>EG</sub> [%-w] (salt-free)		50%	60%	70%	80%	90%	100%
T [°C]		c [mol/kg]	c [mol/kg]	c [mol/kg]	c [mol/kg]	c [mol/kg]	c [mol/kg]
30		0.3833 <sup>W,B</sup>	0.2272 <sup>W,T</sup>	0.1623	0.0676 <sup>W,B</sup>	0.0575 <sup>W</sup>	0.1369 <sup>A,B</sup>
		±0.0198	±0.0031	±0.0230	±0.0015	±0.0062	±0.0003
50		0.3482 <sup>W,B</sup>	0.2431 <sup>W,B</sup>	0.1714 <sup>W,B</sup>	0.1476 <sup>W,B</sup>	0.2097 <sup>W,T</sup>	0.1682 <sup>A,B</sup>
		±0.0043	±0.0024	±0.0061	±0.0022	±0.0017	±0.0044
60		0.3392 <sup>W,B</sup>	0.2348 <sup>W,B</sup>	0.1857 <sup>W,B</sup>	0.1361 <sup>W,B</sup>	0.1107 <sup>W</sup>	0.0998 <sup>A,B</sup>
		±0.0035	±0.0005	±0.0078	±0.0011	±0.0004	±0.0151
70		0.3540 <sup>W,B</sup>	0.2363 <sup>W,B</sup>	0.1873 <sup>W,T</sup>	0.1414 <sup>W</sup>	0.0706 <sup>W</sup>	0.0886 <sup>A,B</sup>
		±0.0036	±0.0017	±0.0014	±0.0072	±0.0060	±0.0108
80		0.3636 <sup>W,B</sup>	0.2361 <sup>W</sup>	0.1959 <sup>W</sup>	0.1015 <sup>W</sup>	0.0894 <sup>W</sup>	0.0731 <sup>A,B</sup>
		±0.0013	±0.0123	±0.0143	±0.0132	±0.0024	±0.0002
84.8		0.3077 <sup>W,B</sup>	0.2260 <sup>W,B</sup>	0.1800 <sup>W</sup>	0.0761 <sup>W</sup>	0.0766 <sup>W</sup>	0.0696 <sup>A,B</sup>
		±0.0106	±0.0016	±0.0033	±0.0021	±0.0268	±0.0025
89.8		0.3017 <sup>W,B</sup>	0.2002 <sup>W,B</sup>	0.1695 <sup>W,B</sup>	0.0703 <sup>W,B</sup>	0.0773 <sup>W</sup>	0.0673 <sup>A,B</sup>
		±0.0092	±0.0173	±0.0336	±0.0013	±0.0037	±0.0046

		c(HCO <sub>3</sub> <sup>-</sup> ) [mol/kg solution]					
x <sub>EG</sub> [%-w] (salt-free)		50%	60%	70%	80%	90%	100%
T [°C]		c [mol/kg]	c [mol/kg]	c [mol/kg]	c [mol/kg]	c [mol/kg]	c [mol/kg]
30		0.3802 <sup>W,B</sup>	0.3688 <sup>W,T</sup>	0.3317	0.4040 <sup>W,B</sup>	0.4226 <sup>W</sup>	0.8621 <sup>A,B</sup>
		±0.0453	±0.0095	±0.0482	±0.0040	±0.0063	±0.0718
50		0.4299 <sup>W,B</sup>	0.3850 <sup>W,B</sup>	0.3607 <sup>W,B</sup>	0.3320 <sup>W,B</sup>	0.1830 <sup>W,T</sup>	0.5595 <sup>A,B</sup>
		±0.0126	±0.0027	±0.0136	±0.0002	±0.0005	±0.0460
60		0.5125 <sup>W,B</sup>	0.4591 <sup>W,B</sup>	0.3756 <sup>W,B</sup>	0.3384 <sup>W,B</sup>	0.3287 <sup>W</sup>	0.7638 <sup>A,B</sup>
		±0.0130	±0.0042	±0.0207	±0.0029	±0.0259	±0.0273
70		0.5883 <sup>W,B</sup>	0.5329 <sup>W,B</sup>	0.4096 <sup>W,T</sup>	0.3530 <sup>W</sup>	0.3948 <sup>W</sup>	0.8477 <sup>A,B</sup>
		±0.0059	±0.0033	±0.0367	±0.0091	±0.0050	±0.0373
80		0.6627 <sup>W,B</sup>	0.5577 <sup>W</sup>	0.4102 <sup>W</sup>	0.4301 <sup>W</sup>	0.4148 <sup>W</sup>	0.8555 <sup>A,B</sup>
		±0.0239	±0.0164	±0.0172	±0.0005	±0.0176	±0.0134

84.8	0.7447 <sup>W,B</sup>	0.6175 <sup>W,B</sup>	0.4655 <sup>W</sup>	0.4310 <sup>W</sup>	0.4429 <sup>W</sup>	0.9946 <sup>A,B</sup>
	±0.0105	±0.0058	±0.0022	±0.0014	±0.0370	±0.0494
89.8	0.7403 <sup>W,B</sup>	0.5151 <sup>W,B</sup>	0.4935 <sup>W,B</sup>	0.3626 <sup>W,B</sup>	0.4257 <sup>W</sup>	0.9443 <sup>A,B</sup>
	±0.0157	±0.0248	±0.0490	±0.0263	±0.0022	±0.0190
$\rho_{\text{solution}}[\text{g/ml}]$	1.087	1.074	1.105	1.122	1.127	1.137
	±0.024	±0.034	±0.019	±0.028	±0.032	±0.014
$x_{\text{EG}} [\%-\text{w}]$ (salt-free)	50%	60%	70%	80%	90%	100%

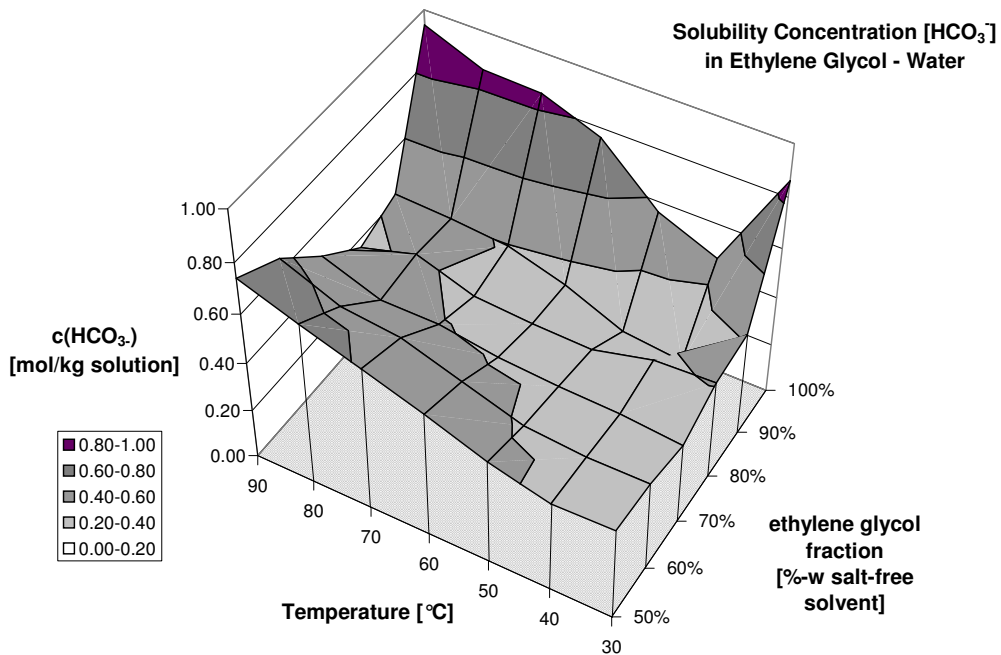
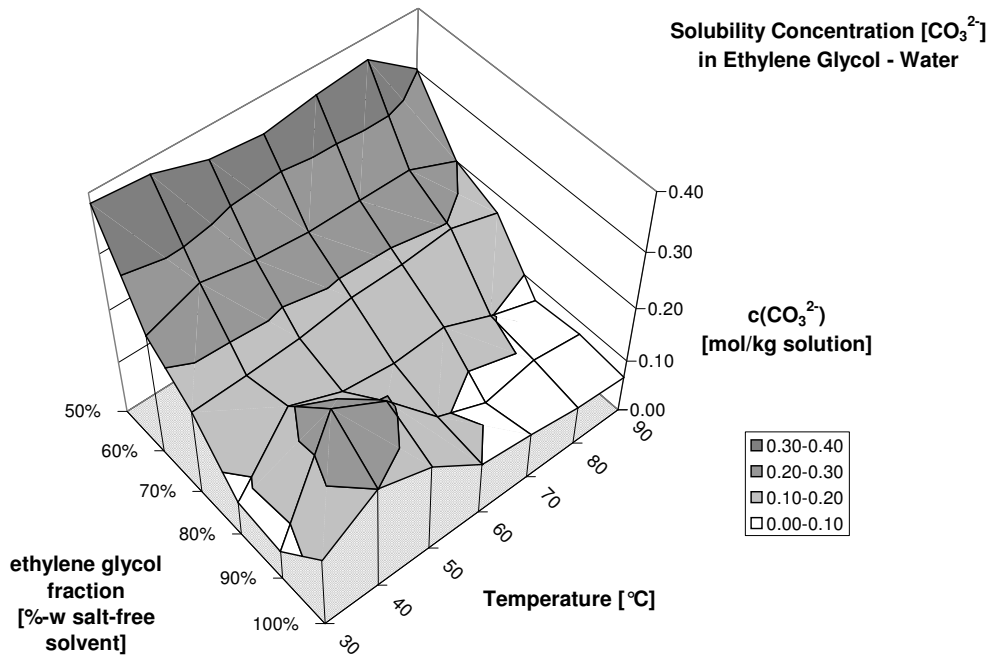


**Figure 6-11:** Solubility Concentrations [ $\text{CO}_3^{2-}$ ] and [ $\text{HCO}_3^-$ ] in ethylene glycol – water mixed solvents as given in Table 4

**Table 6-5:** Solubility of Na<sub>2</sub>CO<sub>3</sub> anhydrate (A), wegscheiderite (W), trona T and nahcolite (NaHCO<sub>3(s)</sub>, B), forming from trona (Solvay, France) as starting solid, in ethylene glycol – water

		c(CO <sub>3</sub> <sup>2-</sup> ) [mol/kg solution]										
x <sub>EG</sub> [%-w] (salt-free)		50%	60%	70%	80%	90%	100%					
T [°C]	C [mol/kg]	c [mol/kg]	c [mol/kg]	c [mol/kg]	c [mol/kg]	c [mol/kg]	c [mol/kg]					
50	0.4315	T	0.3347	T	0.1985	T	0.1884	T	0.1778	T	0.1916	A, B
	±0.0105		±0.0014		±0.0145		±0.0011		±0.0182		±0.0217	
60	0.4500	T	0.3582	T	0.2385	T	0.2125	T	0.1882	T	0.1415	A, B
	±0.0020		±0.0065		±0.0105		±0.0006		±0.0200		±0.0049	
70	0.4961	T	0.3934	T	0.3125	T	0.2687	T	0.1994	A,W	0.0927	A, B
	±0.0081		±0.0078		±0.0007		±0.0006		±0.0024		±0.0066	
80	0.5470	T	0.4209	T	0.3342	T	0.2455	T	0.1629	A,W	0.0656	A, B
	±0.0169		±0.0032		±0.0027		±0.0013		±0.0090		±0.0124	
84.8	0.5581	T	0.4506	T	0.2950	T	0.2203	A,W	0.1445	A,W	0.0714	A, B
	±0.0086		±0.0127		±0.0019		±0.0066		±0.0034		±0.0160	
89.8	0.5927	T	0.4683	T	0.3457	T	0.2208	A,W	0.1364	A,W	0.0537	A, B
	±0.0052		±0.0012		±0.0070		±0.0110		±0.0054		±0.0339	
93.5	0.6109	T	0.4697	T	0.3320	A,W	0.2134	A,W	0.1290	A,W	0.0754	A, B
	±0.0045		±0.0028		±0.0156		±0.0132		±0.0080		±0.0084	

		c(NaHCO <sub>3</sub> ) [mol/kg solution]										
x <sub>EG</sub> [%-w] (salt-free)		50%	60%	70%	80%	90%	100%					
T [°C]	c [mol/kg]	c [mol/kg]	c [mol/kg]	c [mol/kg]	c [mol/kg]	c [mol/kg]	c [mol/kg]					
50	0.3740	T	0.2868	T	0.1741	T	0.1632	T	0.1489	T	0.4470	A, B
	±0.0114		±0.0002		±0.0183		±0.0095		±0.0158		±0.0550	
60	0.4141	T	0.3175	T	0.2017	T	0.1919	T	0.2348	T	0.5382	A, B
	±0.0101		±0.0117		±0.0038		±0.0043		±0.0110		±0.0219	
70	0.4224	T	0.3247	T	0.2544	T	0.2145	T	0.2576	A,W	0.5972	A, B
	±0.0035		±0.0131		±0.0001		±0.0011		±0.0119		±0.0320	
80	0.4683	T	0.3652	T	0.2784	T	0.2812	T	0.2918	A,W	0.7009	A, B
	±0.0054		±0.0047		±0.0068		±0.0020		±0.0099		±0.1029	
84.8	0.4885	T	0.3582	T	0.2648	T	0.2935	A,W	0.3258	A,W	0.6069	A, B
	±0.0089		±0.0042		±0.0098		±0.0006		±0.0027		±0.1868	

89.8	0.5156 <sup>T</sup>	0.3797 <sup>T</sup>	0.3304 <sup>T</sup>	0.3336 <sup>A,W</sup>	0.3377 <sup>A,W</sup>	0.7792 <sup>A,B</sup>
	±0.0072	±0.0007	±0.0065	±0.0033	±0.0006	±0.2342
93.5	0.5380 <sup>T</sup>	0.3964 <sup>T</sup>	0.3820 <sup>A,W</sup>	0.3502 <sup>A,W</sup>	0.3593 <sup>A,W</sup>	0.8612 <sup>A,B</sup>
	±0.0284	±0.0106	±0.0128	±0.0081	±0.0010	±0.0198
$\rho_{\text{solution}}[\text{g/ml}]$	1.036	1.058	1.083	1.081	1.094	1.128
	±0.049	±0.057	±0.040	±0.023	±0.018	±0.027
$x_{\text{EG}} [\%-\text{w}]$ (salt-free)	50%	60%	70%	80%	90%	100%

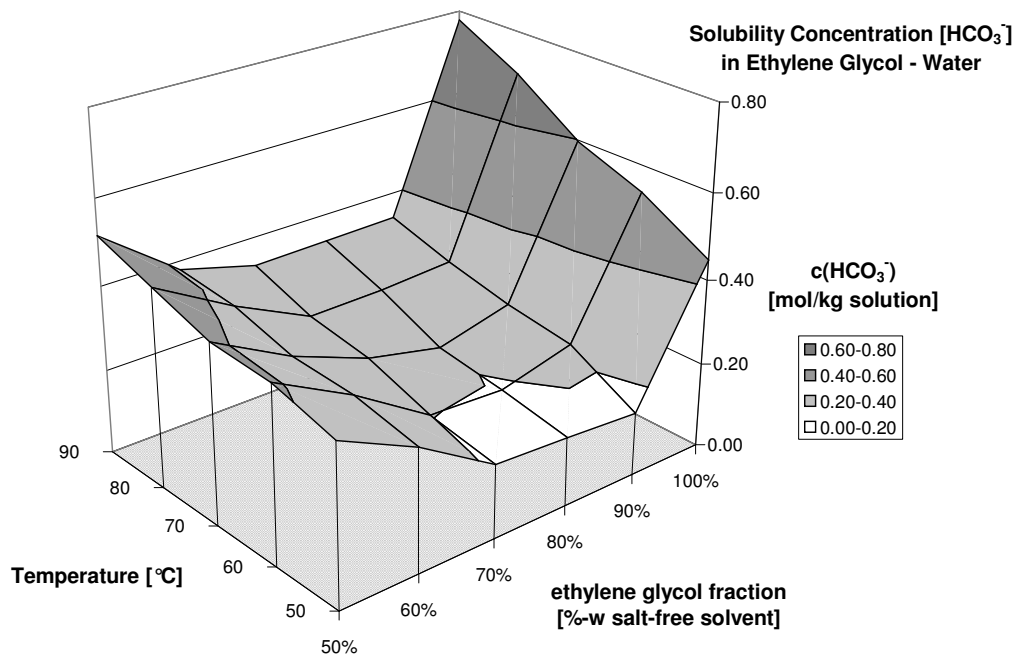
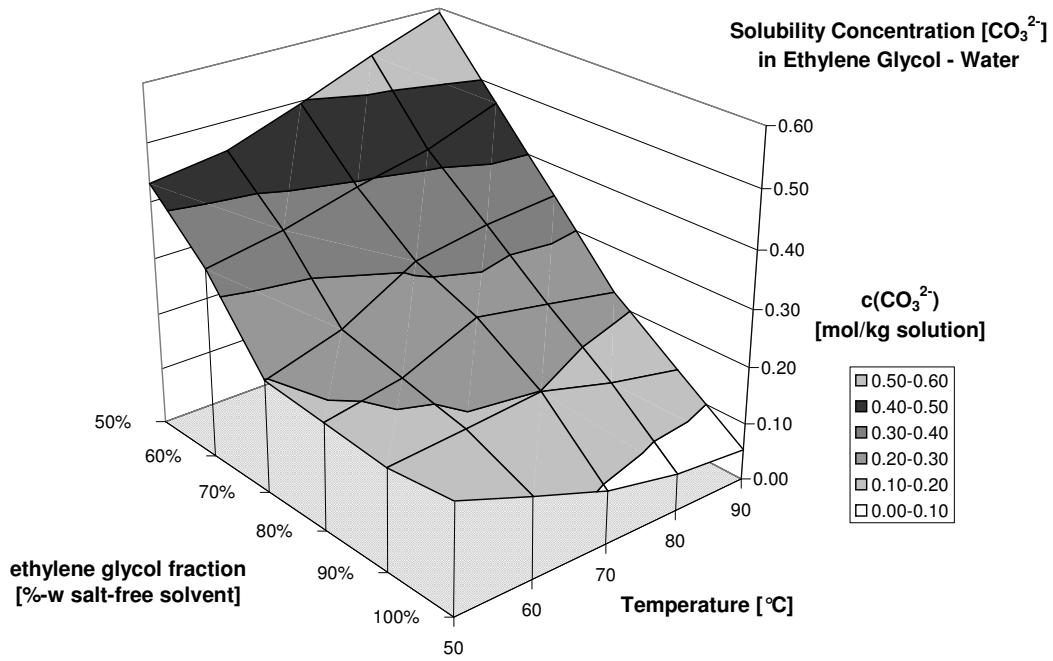


**Figure 6-12:** Solubility Concentrations [ $\text{CO}_3^{2-}$ ] and [ $\text{HCO}_3^-$ ] in ethylene glycol – water mixed solvents as given in Table 5

### 6.6.1. Phase Diagrams for 60, 80 and 100%-w (salt-free solvent) Ethylene Glycol

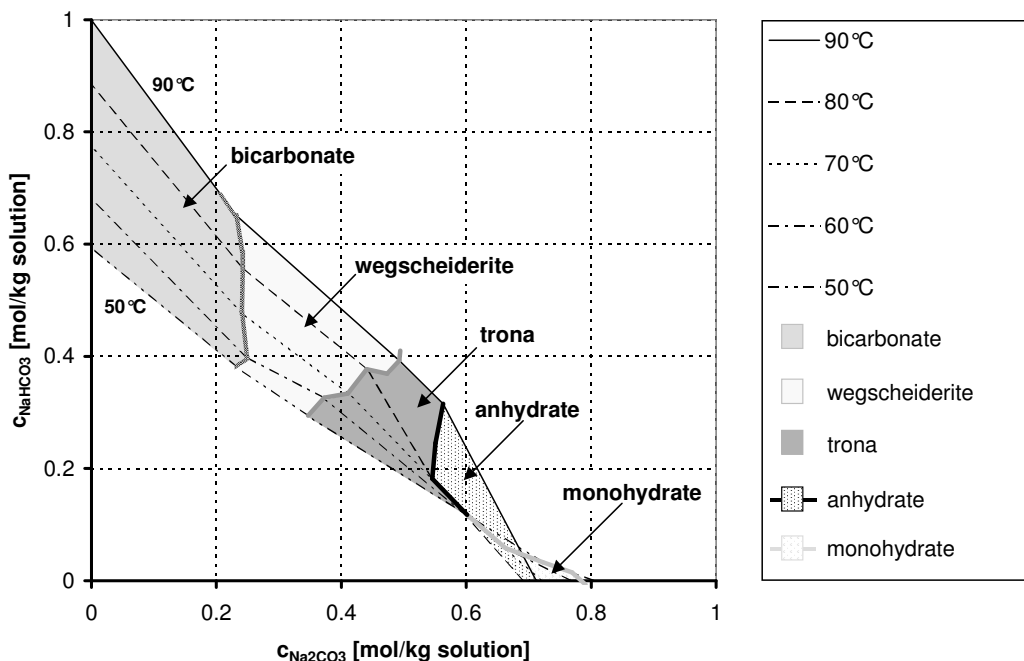


**Figure 6-13:** Phase stability and solubility chart for  $\text{Na}_2\text{CO}_3$ - $\text{NaHCO}_3$  in 60%-w (salt-free) ethylene glycol mixed solvent

The phase stabilities in 100%-w ethylene glycol differed significantly from the phase stabilities in the water containing mixed solvents. The only stable phases observed were sodium bicarbonate (nahcolite), sodium carbonate anhydrate and wegscheiderite.

Which phases would form depended apparently on the composition of the starting solid of the experiment. Wegscheiderite only formed in the experiments with a starting solid  $\text{CO}_3 : \text{HCO}_3$  ratio of 3 : 1, see Table 3. In all other cases only bicarbonate and anhydrate would occur. As can be seen in Figure 15, also the 2-phase line of bicarbonate & anhydrate would differ significantly between experiments. Most probably due to the special mechanism of  $\text{HCO}_3^-$  solvation in ethylene glycol, the solubility concentrations of  $\text{CO}_3^{2-}$  and  $\text{HCO}_3^-$  were not very stable and were apparently easily shifted by outside influences.



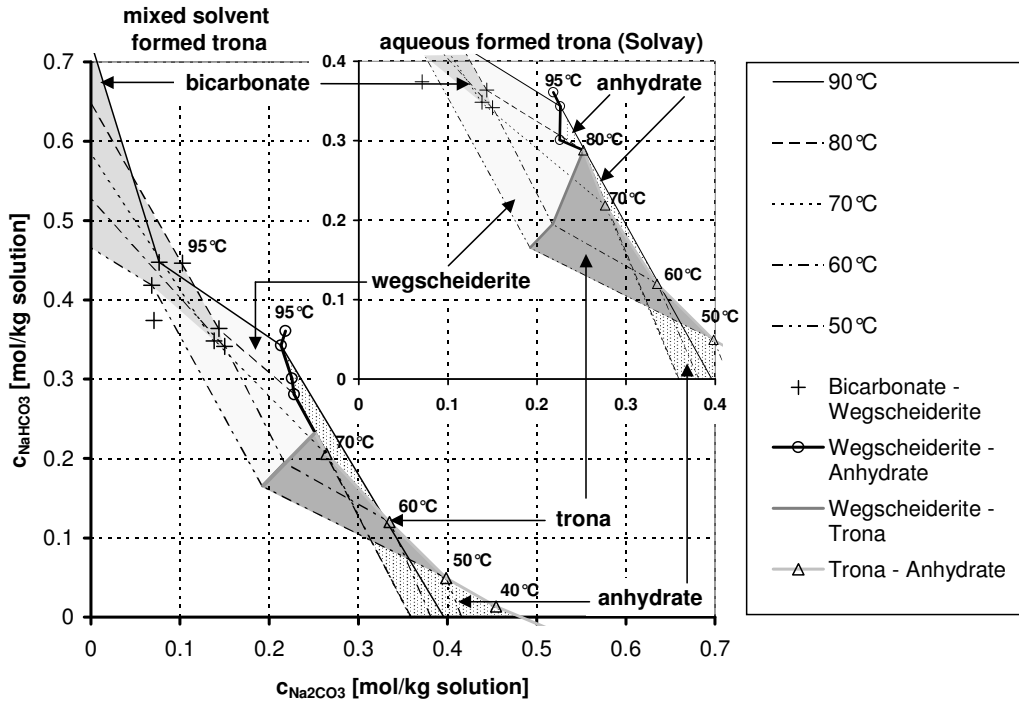


**Figure 6-14:** Phase stability and solubility chart for  $\text{Na}_2\text{CO}_3\text{-NaHCO}_3$  in 80%-w (salt-free) ethylene glycol mixed solvent

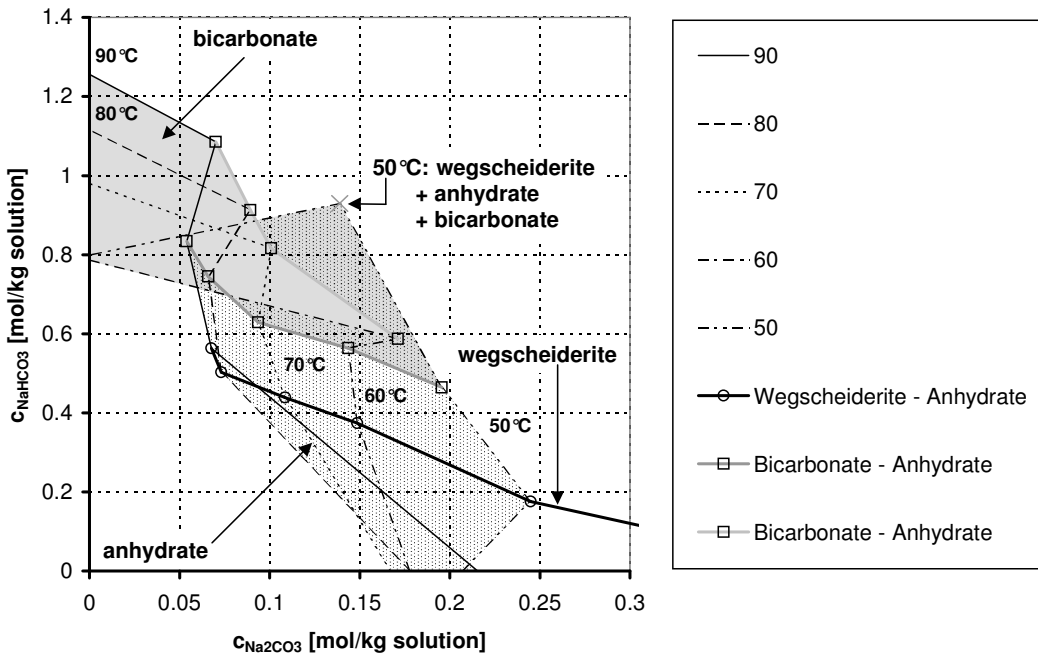


**Figure 6-15:** Phase stability and solubility chart for  $\text{Na}_2\text{CO}_3\text{-NaHCO}_3$  in 100%-w (salt-free) ethylene glycol mixed solvent

The 3-phase point of wegscheiderite, anhydrate and bicarbonate at 50°C is rather surprising, not only due to the occurrence of all 3 phases outside the observed stability range of wegscheiderite, but also due to the high solubility concentrations of  $\text{CO}_3^{2-}$  and  $\text{HCO}_3^-$ . It is possible, that this point reflects a metastable state, with the system still in the process of recrystallization from bicarbonate to wegscheiderite.

The crystals of wegscheiderite and anhydrate formed in pure ethylene glycol were small ( $\leq 10$  micron), while bicarbonate could form crystals of significantly larger size (up to 50 micron). Due to the low solubility of anhydrate and wegscheiderite, these phases would grow only slowly and the recrystallization was dominated by nucleation.

## Chapter 7 :

### NEUTRAL EXTRACTANTS FOR THE SELECTIVE REMOVAL OF ALUMINUM FROM A PICKLING BATH LIQUID

Robert S. Gärtner, Anke M. Berends, Geert-Jan Witkamp

#### ***Abstract***

For the regeneration of an industrial pickling bath by a solvent extraction process different extractants were investigated for their capability to extract aluminum. The two main components of the pickling bath are phosphoric and hydrofluoric acid. This chapter describes the results of shake experiments with different p-tert-butyl-calix[4]arenes. Their capabilities to extract aluminum were compared with the results of Alamine 308. No significant extraction was found for all the calixarenes tested.

## **7.1. Introduction**

### **7.1.1. General**

In the chromium conversion coating of aluminum parts, the removal of their aluminumoxide layer is an important step. It is conducted in an acidic pickling bath, which dissolves the aluminumoxide. Over a period of time the pickling bath solution becomes saturated with dissolved aluminum, thereby loosing its efficiency, and has to be disposed of. As the bath liquid still mainly consists of a mixture of inorganic acids, it is highly corrosive and toxic which makes its disposal rather expensive. The lifetime of the pickling bath could be increased by continuously removing the aluminum in the pickling bath solution by an in-line purification step. An additional advantage is that this allows the aluminum concentration to be kept at a level where the quality of the treated aluminum the highest. Here this is attempted by selectively extracting the aluminum with an extraction process. Our final aim is to design a hollow fiber supported liquid membrane (HFSLM) module process for the continuous in-line removal of aluminum. In supported liquid membrane (SLM) extraction the extractant solution is absorbed into a thin, porous, hydrophobic support material separating the feed and the strip phase. The so-immobilized extractant solution then functions itself as a membrane barrier between the strip and the feed phase, being only permeable for those metal ions, which are complexed by the extractant; see also Figure 1.

The major potential advantage of SLM is the combination of high selectivity and high driving force. The important benefit of hollow fiber SLM or of hollow fiber liquid-liquid extraction is the capability to treat solid-containing streams, since the feed stream and the organic phase are physically separated. With other liquid-liquid extraction methods problems can arise as the organic phase adheres to the particles leading to crud formation, hampering good phase separation and thus inhibiting treatment of these slurries by liquid-liquid extraction. Finally, more expensive extractants like calixarenes can be used more economically with this setup, as only relatively small amounts of extractant solution are required to impregnate the membrane support.

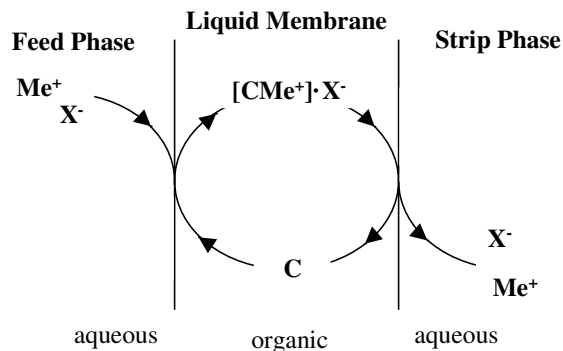


**Figure 7-1:** Metal extraction by a calixarene in liquid membrane extraction with  $\text{Me}^+$  as a metal cation,  $\text{X}^-$  as an anion, C as the calixarene and  $[\text{CMe}^+]\cdot\text{X}^-$  as the metal ion-calixarene complex.

The aim of this work is to investigate whether p-tert-butyl-calix[4]arenes are suitable for the selective extraction of aluminum from the pickling bath solution.

### 7.1.2. Extractant selection

Different basic and acidic extractants have been tested in previous works [1-3] without satisfying results for the technical application. They either did not extract aluminum at all, the transport rate was far too low or precipitation occurred on the membrane. These problems are partially due to the composition of the pickling bath solution, which main active components are hydrofluoric and phosphoric acid in concentrations of 0.01 – 3.0 M. These acids tend to form a variety of fluoro-phosphato-aluminum complexes as described by e.g. Akitt et al. [4]. The presence of these positively or negatively charged complexes makes aluminum extraction by a basic or acidic extractant more complicated and less selective, because phosphate and fluoride ions are co-extracted.

Acidic extractants showed no significant extraction of aluminum from the pickling bath solution [3, 5]. This was surprising, as acidic organophosphorus extractants are recommended by Meyer et al. [6] and Bailey et al. [7] for aluminum extraction from acidic solutions similar to the pickling bath solution. However, Bailey et al. [7] already noted the negative influence of fluoride ions on the aluminum extraction as unextractable aluminum-fluoride complexes are formed.

Only tri-alkyl amines, basic extractants, such as Alamine 308 (tri-iso-octylamine) and Alamine 336 (a mixture of tri-alkyl amines with n-C8 : n-C10  $\approx$  2 : 1), showed extraction capability for aluminum from the pickling bath solution [1, 2]. They were tested in flat

sheet supported liquid membranes with basic strip phases, which caused precipitation of  $\text{Al}(\text{OH})_3$ ,  $\text{Na}_3\text{AlF}_6$  and an unknown compound mainly on the strip side of the membrane [1]. This precipitation slowed down the mass transfer and finally all mass transfer stopped. As  $\text{Al}(\text{OH})_3$  is known to form between pH 5 and 12, an acidic strip phase could be used to avoid pH-induced precipitation. With the tested tri-alkyl amines the transport rate with an acidic strip phase was far too low for technical applications [3].

Because acidic extractants did not extract aluminum, a neutral extractant with a specific affinity for either the aluminum ion or one of the predominant fluoro-phosphato-aluminum complexes is needed. In this work neutral extractants, calixarenes have been tested. They have a high capability for selective complexation of cations, anions and neutral molecules, and the results are described in this chapter. For comparison, results with the extractant Alamine 308 are given as well.

### 7.1.3. Calixarenes

Calixarenes are macrocyclic oligomers, usually produced by poly-condensation of phenol and formaldehyde with sodium hydroxide or potassium carbonate [8, 9]. They possess a high capability for cationic, anionic and molecular inclusion. Their general molecular structure can be given according to Atwood [10] and Andreetti and Ugozzoli [11] as:

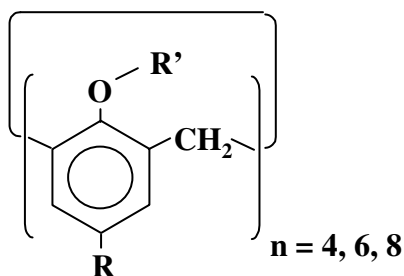


**Figure 7-2:** General structure of a calix[n]arene

In our study six p-tert-butyl-calix[4]arenes (i.e.:  $\text{R} = -\text{C}(\text{CH}_3)_3$ , see Figure 2) were investigated for their capability for aluminum extraction from the pickling bath solution. They are either substituted at the phenol oxygen with acetic-carboxyl-groups (i.e.:  $\text{R}' = -\text{CH}_2-\text{COO}-\text{R}''$ , for calixarenes **A**, **B**, **C** and **D**) or with crownether-like polyglycol bridges (i.e.:  $\text{R}'-\text{R}' = (\text{CH}_2-\text{O}-\text{CH}_2)_n$ , for calixarenes **E** and **F**) to enhance their cation-

complexation capability (see Figures 2 and 3). This produces highly selective chelating arrangements. Due to the attachment to the rigid aromatic calix-ring, the chelating groups are sterically preorganized. This alleviates the complexation of a fitting cation, because according to Atwood [10] the cation complexation involves only a relatively small steric change of the molecule. Here, the chelating groups are the phenol oxygens of the aromatic base structure, and the carboxyl oxygens (calixarene **A**, **B**, **C**, **D**) and/or the ether oxygens (calixarene **D**, **E**, **F**) of the side chains, respectively, see Figure 3.

This sterical preorganization also increases the selectivity of the complexation and thus of the extraction, as the calix-ring determines the size of the chelating cavity. In the case of calixarene **E** and **F** the chelating cavity is further determined by the length of crownether-like polyglycol bridges, which produces a different selectivity from that induced by the calix-ring alone.

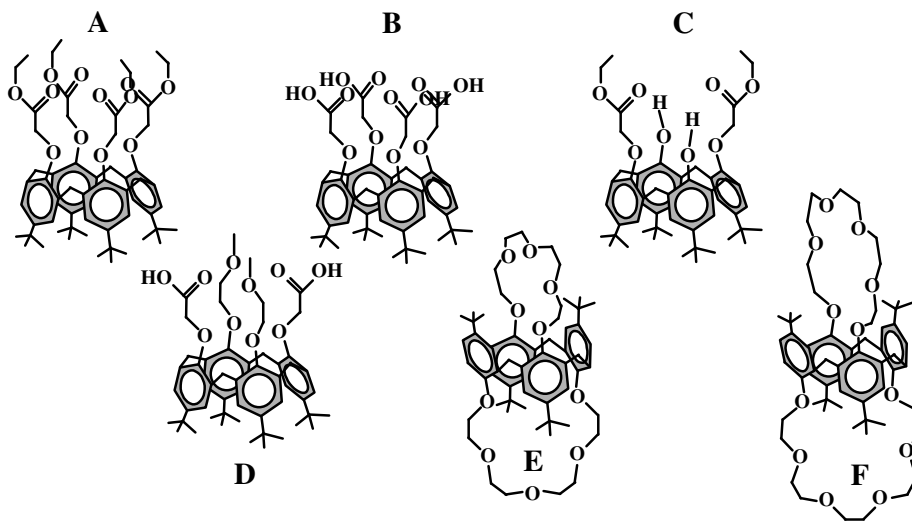


**Figure 7-3:** Molecular structure of the tested calixarenes.

In literature, the following affinities for the tested calixarenes were found:

The tetra-ester-structure of calixarene **A** (see Figure 3) has an affinity for sodium ions according to Schwing and McKervey [12]. Atwood [10] and Gutsche [8] also note an especially high selectivity of calixarene **A** for sodium over other alkali metals under basic extraction conditions. Goto et al. [13] and Ohto et al. [14] report an affinity for sodium for a calixarene very similar to calixarene **B** under acidic conditions. The calixarene tested by these authors has p-tert-octyl-groups instead of the p-tert-butyl-groups of

calixarene **B**, but the groups attached to the phenolic oxygens, which form the chelating cavity, are identical. For calixarene **C**, Gutsche [8] reports a lack of sodium extraction and a small affinity for earth alkali metal ions under basic extraction conditions. Selectivities for calixarenes similar to calixarene **D** listed by Schwing and McKervey [12] indicate a sodium affinity under basic extraction conditions.

The crownether-like bridges determine the selectivity of the doubly bridged calixarenes **E** and **F**: According to Asfari et al. [15], calixarene **E** has a high selectivity for potassium over sodium. The longer glycolether bridges of calixarene **F** induce a high selectivity for cesium over all other alkali metals, which can be used for selective cesium recovery according to Asfari et al. [15] and Gutsche [9].

Although the calixarenes show the greatest affinity towards alkali metal ions, their applications are not limited to that group of ions, as research done by Inoue et al. [15-17] on the extraction of other group metal ions indicates. It was thought possible that they would also be capable of complexing aluminum or its complexes.

#### **7.1.4. Extraction Mechanism**

As already explained above, a calixarene binds a cation selectively by chelating complexation with the phenol oxygens and the attached polar groups (see e.g. Figure 4). Thus one calix[4]arene molecule usually complexes only one cation, but co-extraction of a second cation is known to happen according to Inoue et al. [13, 14, 16-18]. Extraction of two cations of the same species was found by Ohto et al. [16, 18] for p-tert-octyl-calix[4]arene tetracarboxylate for  $\text{Na}^+$  and for  $\text{Pb}^{2+}$ . The second cation is loosely bound by the carboxylate groups at increased pH. But at the low pH of the pickling bath acid only one cation of a species should be complexed per calixarene molecule.

As p-tert-butyl-calixarenes are almost insoluble in aqueous solutions, the complexation of the metal ion by the calixarene can only take place in the organic extractant solution. These metal ions get solubilized into the organic solution as neutral complexes with anions; see Eq. 1. From these neutral complexes in the organic solution the metal ion is complexed by the calixarene; see Eq. 2. The anion is coordinated to the calixarene-cation-complex by the cation's charge and is thus co-extracted with the cation.



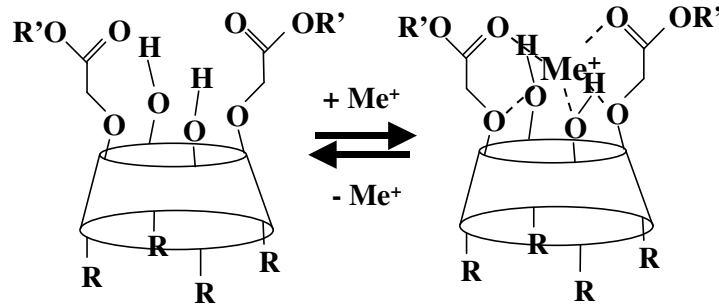


**Figure 7-4:** Metal cation complexation by a calix[4]arene-di-carboxylate.

In the stripping process the steps of this mechanism are reversed to release the cation and the anion to the stripping solution. The following equations summarize this mechanism:



Here  $\text{Me}^+$  represents the metal cation,  $\text{X}^-$  a corresponding anion and C the calixarene. The overbar denotes that the relevant components are solved in the organic extractant solution.

This mechanism, as it is given by Reinhoudt et al. [19, 20], is only accurate for an acidic feed phase like the pickling bath solution. Under basic conditions calixarenes tend to deprotonate, acquiring a negative charge. This decreases the anion co-transport, as the calixarene itself compensates the charge of the cation. According to Gutsche [8], this facilitates extraction, as the cation is additionally attracted to the calixarene by its charge. The affinity of an extractant for an ion is mathematically represented by the distribution coefficient  $m_f$ . The distribution coefficient is calculated as the ratio of the molar concentration of a species in the organic extractant solution  $c_{\text{org}}$  and of the molar concentration of the species in the pickling bath solution  $c_{\text{aq}}$ , both taken after shaking and phase separation:

$$m_f = \frac{c_{\text{org}}}{c_{\text{aq}}} \quad \text{Eq. 7-3}$$

## 7.2. Experimental

### 7.2.1. Shake Tests

The extraction capabilities of the calixarenes were tested in shake tests with the industrial pickling bath solution, which was kindly supplied by a chemical surface treatment company. The calixarenes (obtained from dr. J. Vicens, EHICS, France), were dissolved in two different kerosenes: Shellsol D70 (an aliphatic solvent consisting of 45% naphthenics and 55% paraffinics; Shell) and Solvesso 150 (a high boiling aromatic solvent with a content of 99% of aromatic compounds, mostly alkyl(C3-C5)benzenes; Exxon). The concentrations of these solutions varied with the respective calixarene's solubility. Calixarene A proved to be relatively well soluble in Solvesso 150 and an extractant solution with a concentration of 0.10 M could be prepared. The concentrations of all the calixarenes are listed in Table 1. Shake tests were also conducted with Alamine 308 in Shellsol D70.

The concentration of aluminum in the pickling bath solution is about 0.15 to 0.25 M. The phase ratio in the shake tests was varied according to the different solubilities of the calixarenes to enable significant aluminum extraction from the pickling bath solution; see Table 1.

**Table 7-1:** The prepared calixarene solutions

Compound	Solvent	c [mol/l]	Feed : Membrane [ml/ml]	$\rho_{\text{solution}}$ [g/ml]
calixarene A	Shellsol D70	0.018	1 : 1	0.78
	Solvesso 150	0.100	1 : 1	0.90
calixarene B	Shellsol D70	0.006	1 : 10	0.79
	Solvesso 150	0.012	1 : 10	0.88
calixarene C	Shellsol D70	0.006	1 : 10	0.79
	Solvesso 150	0.013	1 : 10	0.88
calixarene D	Solvesso 150	0.011	1 : 10	0.88
calixarene E	Solvesso 150	0.046	1 : 2	0.89
calixarene F	Solvesso 150	0.010	1 : 10	0.88
Alamine 308	Shellsol D70	0.13	1 : 1	0.79
		1.13	1 : 1	0.80
		2.26	1 : 1	0.82

For each calixarene at least three shake tests were conducted, one membrane phase was made for all three shake tests. Blank shake tests containing only pickling bath solution and the appropriate amount of kerosene were shaken and analyzed parallel with the extractant samples to determine the solubility of the metal ions and the most predominant anions in the solvent. The samples were shaken for 48h at 25°C to reach extraction equilibrium.

### 7.2.2. Analysis

After phase separation, both phases were analyzed for the most predominant metal ions (Na, Al, Cr, Fe, Zn) and total phosphorus (from  $\text{PO}_4^{3-}$ ,  $\text{HPO}_4^{2-}$ ,  $\text{H}_2\text{PO}_4^-$ ,  $\text{H}_3\text{PO}_4$ ) by a Finnigan HR ICP-MS. A sample of 0.2 g of the organic phase of each shake test and of each blank was digested in a Milestone 1200 mls MEGA microwave with a mixture of 5 ml 70% nitric acid and 1 ml 70% perchloric acid to enable its analysis by ICP-MS. The acids used for the digestion of the organic phase were metal-free acids for trace metal analysis (J.T. Baker intra-analyzed<sup>®</sup> reagent). Dilutions prepared for the analysis by ICP-MS were made with 3% nitric acid, prepared from ultra pure water and metal-free 70% nitric acid for trace metal analysis.

The fluoride and phosphate concentrations of the aqueous phases of the shake tests with calixarenes **D**, **E** and **F** were additionally measured with a Dionex DX-120 ion chromatograph. The samples for the ion chromatograph were diluted by a factor of 1000 with ultra pure water. As the ion chromatograph did not measure the fraction of fluoride and phosphate complexed by the aluminum or other cations, the total phosphorus measurements by ICP-MS are used for the data on phosphate given in Figures 5 and 6 and in the Addendum. The phosphate concentrations measured by the ICP-MS were always approximately 10% higher than the concentrations measured with the ion chromatograph. The fluoride data given in the Addendum are derived from the measurements by the ion chromatograph and thus only relate to the concentration of free fluoride in the diluted aqueous samples.

### 7.3. Results

Precipitation occurred in all the shake tests with Shellsol D70, apparently this solvent has insufficient solvating power. No detectable extraction of any of the analyzed elements could be measured, therefore these results are not represented here. Due to these precipitation problems, Solvesso 150 was chosen as solvent for further experiments. This kerosene proved to have more solvating power for the calixarenes tested here. Precipitation occurred with Solvesso 150 only in the extractant solution of calixarene **B** after shaking. The extractant solution of calixarene **B** before shaking did not show precipitation, the solution only became slightly gel-like.

The analysis of Al in the original pickling bath liquid was difficult due to a precipitate. This precipitate was analyzed as well and contained Al:F:P = 1:4:1.5, indicating that the precipitate contains at least two different salts. The concentration of Al between different ICP-MS runs ranged between 0.17-0.21 M, however during 1 run the fluctuation was within 5%. As both aqueous and organic phases of a shake test were always analyzed during one run, it is believed by the authors that the  $m_f$ -values reported in Appendix A are valid. The ICP-MS analysis of phosphates gave no problems.

As can be seen in Figures 5 and 6, none of the calixarenes showed any significant affinity for extracting aluminum from the pickling bath solution. This result can be supported by the results of Ohto et al. [16]. They did find aluminum extraction from a nitric acid solution with a calixarene similar to calixarene **B**, but at pH 3 or higher, whereas the pickling bath solution has a pH of about 1.5. They found that the aluminum was complexed by the carboxylic acid groups of the side chains, which start to deprotonate at pH 3, and not by the chelating cavity as given in Figure 4.

The chelating cavities of **A**, **B** and **D** are quite similar, but apparently not suitable for Al-extraction. Probably the cavities do not have the right sterical configuration for the extraction of aluminum or of an aluminum-complex. Calixarenes **C**, **E** and **F** also do not show any Al-extracting capability, so apparently their chelating cavities also do not have the right sterical configuration. The low anion co-extraction is apparent from the low distribution coefficients of fluoride and phosphate, see also Addendum, which means that the mechanism of Figure 1 does not occur.

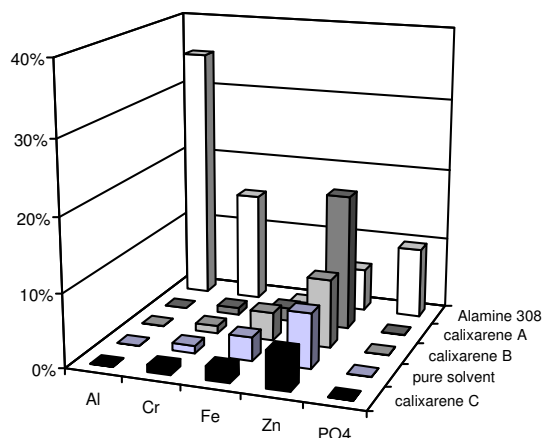


**Figure 7-5:** The extracted amounts of Al, Cr, Fe, Zn and PO<sub>4</sub> for calixarenes **A**, **B** and **C**; for pure solvent (Solvesso 150) and for Alamine 308 in Shellsol D70.

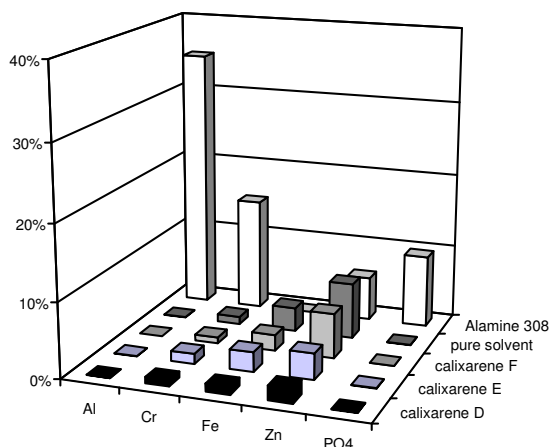


**Figure 7-6:** The extracted amounts of Al, Cr, Fe, Zn and PO<sub>4</sub> for calixarenes **D**, **E** and **F**; for pure solvent (Solvesso 150) and for Alamine 308 in Shellsol D70.

Calixarene **A** is the only extractant which extracts zinc, but  $m_f(\text{Zn})$  is very small, approximately 0.2 (see Addendum). Ohto et al. [16] found for their p-tert-octyl-calix[4]arene tetracarboxylic acid, with a similar cavity as calixarene **A**, no selective zinc complexation, but rather a slight co-extraction of zinc by the carboxylic groups at pH 5 and higher. Probably this co-extraction of zinc occurred here as well.

We could not detect a significant affinity for sodium with calixarene **A**, **B** and **C**, as it is generally attributed to calix[4]arene carboxylates by different authors [8, 9, 11, 13, 14, 21] under acidic as well as basic extraction conditions. The exact analytical quantification of sodium at ppb-level was difficult, as trace level contamination with this common metal was hard to avoid. As sodium extraction was not relevant for our application and due to

the problems with its quantification, sodium was not analytically quantified in the experiments with calixarenes **D**, **E** and **F** and in the experiments with Alamine 308.

#### **7.4. Conclusions**

The tested p-tert-butyl-calix[4]arenes showed no capability to extract aluminum from the pickling bath solution. Apparently, the chelating cavities of the tested calixarenes are not suitable for the complexation of the  $\text{Al}^{3+}$ -ion or an  $\text{Al}^{3+}$ -complex. Furthermore, the acidity of the pickling bath acid is too high to enable co-extraction by the acidic side-groups of the alkyl chains. Only minor extraction of Al, Cr, Fe, Zn, total phosphate and fluoride from the pickling bath solution was found for all of the calixarenes.

#### **7.5. Acknowledgements**

This research was supported financially by the Ministry of Economic Affairs, the Ministry of Housing, Spatial Planning and Environment and the Ministry of Education and Science of the Netherlands. We wish to thank Mr. Wangzhao Zhu and Mr. Duco Bosma for conducting the analysis by HR ICP-MS and ion chromatograph.

#### **7.6. Notation**

##### **Roman**

C	calixarene molecule	
c	molar concentration	[mol/l]
$\text{Me}^+$	metal cation	
m	distribution coefficient	[-]
$\text{X}^-$	anion	

##### **Greek**

$\rho$	density	[ $\text{kg/m}^3$ ]
$\sigma$	absolute standard deviation	[-]
$\sigma\%$	percentile standard deviation	[%]

## Subscripts

aq	aqueous phase
blank	blank test without extractant (only solvent)
f	feed side
feed	pickling bath solution
org	organic phase
solution	extractant solution

## 7.7. Literature References

- [1] A.M. Berends, G.J. Witkamp, G.M. van Rosmalen, *Sep. Sci. Tech.* 34(6&7), 1521-1543 (1999); Chapter 4 of this thesis.
- [2] A.M. Berends, G.J. Witkamp, "Removal of Aluminum from Pickling Bath Liquids by Tertiary and Quarternary Amine Extractants"; *Solv. Extr. Ion Exch.* (2001)
- [3] A.M. Berends, G.J. Witkamp, unpublished data
- [4] J.W. Akitt, N.N. Greenwood, G.D. Lester, *J. Chem. Soc. (A)*, 2450-2457 (1971)
- [5] R.S. Gärtner, G.J. Witkamp, *Preparations for Supported Liquid Membrane (SLM) Extraction of Aluminum from a Pickling Bath Solution II: Organophosphorus Extractants*, in preparation for publication
- [6] G. Meyer, S.O. Fekete, G.R. Wicker, *Selective Extraction of Iron and Aluminum from Acidic Solutions*, US Patent 4,233,273, Nov. 11 1980
- [7] N.T. Bailey, P. Mahi, *Trans. Instn Min. Metall. (Sect. C: Mineral Process. Extr. Metall.)* 95, C70-C78 (1986)
- [8] C.D. Gutsche, *Calixarenes*, Monographs in Supramolecular Chemistry, the Royal Society of Chemistry, Cambridge (1989)
- [9] C.D. Gutsche, *Calixarenes Revisited*, Monographs in Supramolecular Chemistry, The Royal Society of Chemistry Information Services, Cambridge (1998)
- [10] J.L. Atwood in *Cation Binding by Macrocycles – Complexation by Cationic Species by Crown Ethers*, Yoshihisa Inoue, G.W. Gokel, Ed., Marcel Dekker Inc., New York, 1990, Chapter 15

- [11] G.D. Andreetti, F. Ugozzoli in *Calixarenes – A Versatile Class of Macrocyclic Compounds*, J. Vicens, V. Böhmer, Ed., Kluwer Academic Publishers, Dordrecht, 1991, 127-148
- [12] M.-J. Schwing, M.A. McKervey in *Calixarenes – A Versatile Class of Macrocyclic Compounds*, J. Vicens, V. Böhmer, Ed., Kluwer Academic Publishers, Dordrecht, 1991, 149-172
- [13] T. Oshima, T. Kakoi, F. Kubota, K. Ohto, M. Goto, *Sep. Sci. Tech.* *33(13)*, 1905-1917 (1998)
- [14] K. Ohto, K. Shiratsuchi, K. Inoue, M. Goto, F. Nakashio, S. Shinkai, T. Nagasaki, *Solv. Extr. Ion Exch.* *14(3)*, 459-478 (1996)
- [15] Z. Asfari, C. Bressot, J. Vicens, C. Hill, J.-F. Dozol, H. Rouquette, S. Wymard, V. Lamare, B. Tournois, *Anal. Chem* *67*, 3133-3139 (1995)
- [16] K. Ohto, Y. Fujimoto, K. Inoue, *Anal. Chim. Acta* *387*, 61-69 (1999)
- [17] R. Ludwig, K. Inoue, T. Yamato, *Solv. Extr. Ion Exch* *11(2)*, 311-330 (1993)
- [18] K. Ohto, H. Ishibashi, K. Inoue, *Chem. Letters*, 631-632 (1998)
- [19] E.G. Reichwein-Buitenhuis, H.C. Visser, F. de Jong, D.N. Reinhoudt, *J. Am. Chem. Soc.* *117*, 3913-3921 (1995)
- [20] L.A.J. Christoffels, W. Struijk, F. de Jong, D.N. Reinhoudt, *J. Chem. Soc., Perkin Trans.* *2*, 1617-1622 (1996)
- [21] R. Ungaro, A. Pochini in *Frontiers in Supramolecular Organic Chemistry and Photochemistry*, H.J. Schneider, H. Dürr, Ed., VCH Verlagsgesellschaft, Weinheim, 1991



## 7.8. Measured Distribution Coefficients

**Table 7-2:** Distribution Coefficients of the Investigated Extractants

Sample $m_f$	Na	Al	Cr	Fe	Zn	PO <sub>4</sub>	F
Calixarene A	0.33	0.00030	0.010	0.019	0.23	0.00030	na
$\sigma\%$	104%	14%	6%	13%	14%	9%	
Calixarene B	0.14	0.00060	0.011	0.040	0.10	0.00029	na
$\sigma\%$	12%	9%	17%	22%	54%	11%	
Calixarene C	0.06	0.00036	0.010	0.019	0.05	0.00020	na
$\sigma\%$	15%	23%	5%	7%	27%	19%	
Calixarene D	na	0.00016	0.008	0.011	0.020	0.00044	0.0049
$\sigma\%$		20%	12%	30%	15%	23%	≈5%
Calixarene E	na	0.00025	0.014	0.027	0.036	0.00054	0.0017
$\sigma\%$		24%	16%	14%	23%	29%	≈5%
Calixarene F	na	0.00016	0.008	0.022	0.064	0.00030	0.0012
$\sigma\%$		13%	13%	16%	19%	8%	≈5%
0.13 M Alamine 308	na	0.27	0.0039	-0.0033	0.035	0.069	0.40
$\sigma\%$		3.7%	242%	165%	43%	28%	4.4%
1.13 M Alamine 308	na	3.8	6.2	-0.030	0.39	2.7	5.9
$\sigma\%$		0.14%	29%	30%	11%	4.0%	23%
2.26 M Alamine 308	na	6.6	4.6	-0.0026	0.30	4.1	8.1
$\sigma\%$		0.2%	8.8%	36%	11%	14%	0.83%
Shellsol D70	na	-0.017	-0.040	-0.0013	0.0093	-0.0092	0.03
$\sigma\%$		75%	36%	285%	251%	155%	297%
Solvesso 150	0.15	0.00043	0.010	0.048	0.07	0.00025	na
$\sigma\%$	33%	31%	4%	14%	11%	83%	
Pickling bath acid	0.0029	0.18	0.0014	0.0015	0.00040	0.27	0.84
$\sigma\%$	46%	13%	25%	30%	58%	9.6%	3.3%

### 7.9. Calculation of the Given Standard Deviations

The standard deviation of a distribution coefficient was derived from the standard deviations of the concentrations in the extractant solution and in the pickling bath solution after shaking. This calculation procedure was used, because the distribution coefficient was calculated from the average values of these concentrations from the triplicate shake tests in the experiment. As these concentrations were measured separately, they are not mathematically correlated and the standard deviation of the distribution coefficient can be calculated by the formula:

$$\sigma_{m_f}^2 = \sigma_{c,org}^2 \cdot \left( \frac{\partial m_f}{\partial c_{org}} \right)_{c,aq}^2 + \sigma_{c,aq}^2 \cdot \left( \frac{\partial m_f}{\partial c_{aq}} \right)_{c,org}^2 \quad \text{Eq. 7-4}$$

With Eq. 3, this yields after some transformations:

$$\sigma_{m_f}^2 = \frac{\sigma_{c,aq}^2 \cdot c_{org}^2 + \sigma_{c,org}^2 \cdot c_{aq}^2}{c_{aq}^4} \quad \text{Eq. 7-5}$$

with  $\sigma$  as the absolute standard deviation of the respective parameter ( $m_f$ ,  $c_{org}$  or  $c_{aq}$ ).

After introducing percentile standard deviations  $\sigma\%$ :

$$\sigma_{\%,m_f} = \frac{\sigma_{m_f}}{m_f} \cdot 100\% \quad \text{Eq. 7-6}$$

$$\sigma_{\%,c,org} = \frac{\sigma_{c,org}}{c_{org}} \cdot 100\% \quad \text{Eq. 7-7}$$

$$\sigma_{\%,c,aq} = \frac{\sigma_{c,aq}}{c_{aq}} \cdot 100\% \quad \text{Eq. 7-8}$$

equation Eq. 5 can be transformed into:

$$\sigma_{\%,m_f} = \sqrt{\sigma_{\%,c,aq}^2 + \sigma_{\%,c,org}^2} \quad \text{Eq. 7-9}$$

Eq. 9 calculates a conservative estimation of the percentile standard deviation of the distribution coefficient  $m_f$  (as given in Appendix A) from the percentile standard deviations of the concentrations  $c_{org}$  and  $c_{aq}$ . This was done to take correlated errors into account, which would be neglected by simple averaging of the distribution coefficients of the triplicate shake tests of each calixarene. The mass balance of the shake tests was monitored to detect and estimate not only the amount of metal contamination from sample preparation, but also the amount of metal loss from the digestion process for the preparation of the organic phase for analysis by ICP-MS. The mass balance was accurate for all the analyzed elements within 20%.



## Chapter 8 :

### REGENERATION OF MIXED SOLVENT BY ION EXCHANGE RESIN: SELECTIVE REMOVAL OF CHLORIDE AND SULFATE

R.S. Gärtner, G.J. Witkamp

#### ***Abstract***

The selective extraction of sulfate and chloride ions from mixed solvent solutions was investigated. The mixed solvents consisted of water and 50 to 100%-w (salt-free solvent) ethylene glycol. The extraction was measured for mixed solvent solutions containing only sulfate and chloride, and mixed solvent solutions saturated with trona (sodium sesquicarbonate,  $\text{Na}_2\text{CO}_3 \cdot \text{NaHCO}_3 \cdot 2\text{H}_2\text{O}(\text{s})$ ). 3 anion exchange resins, Dowex 1X8-50, Dowex 21K-Cl and Dowex MSA-1, were investigated for their chemical and physical resistance to the mixed solvent carbonate/bicarbonate solutions, for their swelling behavior in the different mixed solvents and for their extraction efficiency for chloride and sulfate.

The loading of the ion exchangers was fitted to a Langmuir-type sorption model. While the extraction from trona-free mixed solvents was well reproduced, the loading of the ion exchangers with chloride and sulfate from trona-saturated mixed solvent solutions did not fit the sorption model. It appears rather, that under these conditions, chloride and sulfate are “salted out” of the bulk solution and driven into the ion exchangers.

## **8.1. Introduction**

Recrystallization as well reactive recrystallization of soda (sodium carbonate) in a mixed solvent have been shown in related work [1 - 7] as energy-efficient, alternative process routes for the production of soda of higher physical quality and chemical purity than currently available soda. The mixed solvent used in these processes consists of water and ethylene glycol.

A vital factor for the economical feasibility of these processes is the recycle of the mixed solvent in the process. Inline purification steps are necessary to remove impurities from the mixed solvent recycle. Ion exchange resins may offer a possibility to selectively remove ionic impurities from the mixed solvent solution while not changing the solvent composition.

The globally most common sodium carbonate source is trona, sodium sesquicarbonate ( $\text{Na}_2\text{CO}_3 \cdot \text{NaHCO}_3 \cdot 2\text{H}_2\text{O}(\text{s})$ ), which occurs as a natural mineral in large, mostly subterranean deposits [8]. It can be converted via the Mixed Solvent Reactive Recrystallization process [5 - 7] to high quality soda.

Trona, recovered by solution mining [9], is a suitable starting material for the Mixed Solvent Reactive Recrystallization, as organic and insoluble particulate impurities have already been removed. This trona would still contain at least traces of soluble inorganic impurities: Traces of chloride and sulfate were found in samples of trona ore from Wyoming and California, see Chapter 2 and 4 [5, 10].

Light soda ash used as starting material in the Mixed Solvent Recrystallization process by Oosterhof et al. [1, 2, 4] is commonly produced by the Solvay process from sodium chloride, and contains measurable traces of sodium chloride.

These trace concentrations of sodium chloride and sodium sulfate remain in the mixed solvent after the recrystallization [10] and should be removed during the recycle.

For these reasons, the inline removal of chloride and sulfate by different techniques has been investigated. Also membrane processes like electrodialysis, reverse osmosis, nano- and hyperfiltration offer feasible methods to remove dissolved ionic impurities from solutions. Especially electrodialysis appeared suitable for the outlined separation and has been tested in a related study [11].

In this work, three strongly basic anion exchange resins, Dowex 1X8-50, Dowex 21K-Cl and Dowex MSA-1, were investigated for their resistance to the mixed solvent solutions, their swelling behavior and their change in selectivity for sulfate and chloride with increasing ethylene glycol content and solution saturation with carbonate/bicarbonate.

## **8.2. Theory**

Ion exchangers usually consist of an inorganic or organic matrix structure, which links and immobilizes the active groups, which are usually ionic themselves. Cation exchangers usually contain anionic groups (e.g. sulfonate, carboxylate), while anion exchangers usually contain cationic groups (e.g. amine).

Most organic-polymer ion exchangers only achieve their ion exchange capability after swelling in solution, i.e. by taking up solution into their “pores” and hydrating (solvating) their ionic functional groups. All transport of ions in the ion exchanger resin takes place as diffusion through this pore solution. A high degree of swelling generally facilitates ion exchange processes, as more pore volume becomes available for diffusive transport. A lack of swelling, on the other hand, can decrease the (available) capacity of an ion exchange resin, as some of the active groups are not accessible by diffusion.

The degree of swelling, i.e. the amount of solution absorbed by the ion exchanger resin, in aqueous solution does not only depend on the active ionic groups, but also on their counter ions in the pore solution and the general ionic strength of the surrounding bulk solution. While highly hydrated counter ions result in an increased degree of swelling, a bulk solution of high ionic strength decreases the degree of swelling.

Phenomenologically, the degree of swelling is determined by the equilibrium of two forces [14]:

- a) The osmotic pressure between bulk and pore solution, i.e. the hydration (solvation) of the fixed active groups by the absorbed pore solution and the ionic interaction between the active groups and their counter ions.
- b) The contractive force of the polymer matrix, which is stretched with the swelling. This force is a result of the tendency of polymer chains to rather take a folded or coiled shape (conformation) than a straight one.

This model does not only explain the increase in swelling with more strongly charged and more heavily hydrated counter ions, but also the order of selectivity for strong ion exchangers, i.e. the preference for smaller, less charged and less hydrated counter ions.

Based on this theoretical consideration, organic co-solvents can have multiple effects on an ion exchange resin.

First, they usually decrease the solubility (and increase the activity) of ionic species in solution, due to these solvents' lower dielectric constant (e.g. the dielectric constant of ethylene glycol (41.4) is  $\sim 1/2$  that of water (80.1) at 20°C [13]), i.e. the decrease in dielectric shielding. The ionic charge is less buffered / distributed by the solvent, and the interactions between the ions become stronger in the bulk solution. This results usually in an increased ion sorption in the resin.

Second, since sorption / swelling is determined by the osmotic pressure (i.e. the chemical potential difference between resin and bulk solution) of each solvent component, the composition of the mixed solvent in the resin is usually not identical to the composition in the bulk solution. One of the solvents, either water or the organic solvent, is absorbed preferentially into the pores of the resin [14]. For dilute solutions of ethylene glycol in water, water is taken up preferentially, resulting in a distribution coefficient for ethylene glycol of ca. 0.6 between resin and bulk solution for low ethylene glycol concentration (50g/l) [14]. At high ethylene glycol concentrations and in pure ethylene glycol, increased swelling was observed [16, 17]. This increase in swelling was explained by the fact, that the dielectric constant of ethylene glycol was high enough to allow dissociation of the ionic species, while it resulted at the same time in a significantly stronger repulsion between ions of the same sign - notably the fixed active groups.

Third, the organic co-solvent can also absorb to the polymer matrix through London or dipole-dipole interactions [14]. As these interactions are weaker than the electrostatic ones, this is usually a minor effect. For high concentrations of the organic co-solvent and a high affinity between it and the polymer matrix – like e.g. for aliphatic hydrocarbon chains – this effect can become a major cause of (apolar) swelling. For ethylene glycol and the polystyrene matrix of the tested resins this affinity is not given and this effect is



assumed irrelevant for the given ion exchangers despite the high ethylene glycol concentrations used in this work.

The equilibrium distribution of a solute  $i$  between resin and solution can be described by an expression similar to a Langmuir-adsorption isotherm:

$$\frac{q_i}{q_0} = \frac{k_i \cdot c_i}{1 + k_i \cdot c_i} \quad \text{Eq. 8-1}$$

with  $q_i$  the loading of the resin with  $i$ ,  $c_i$  the solute's concentration in the bulk solution and  $k_i$  the Langmuir coefficient.

The Langmuir description is applicable to the ion exchange resin despite the fact that the solute, the counter ion, is not necessarily adsorbed (bound) to one specific active site, because all ionic species are - in the ideal case - assumed to be dissociated and the counter ions are therefore present in the pore solution as free species. But because of the electro-neutrality condition, every fixed charge of an active group has to be countered by an opposite charge from a counter ion in the pore solution. Therefore, the number of active-site-charges can be directly related to the number of opposite charges in the pore solution, which is similar to the adsorption described by the Langmuir expression, i.e. one solute molecule per sorption site.

Certain counter ions could draw additional co-ions (of the same charge as the fixed charges) into the pore solution. Under such conditions, the Langmuir expression would no longer properly describe the distribution behavior. A polymolecular-layer-adsorption expression like e.g. BET (Brunauer – Emmet - Teller) could be used to describe such a solute distribution between resin and solution.

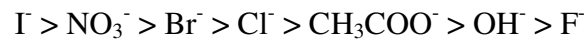
Another complication of the description of the distribution of *one* solute species is the presence of *multiple competing* species, which definitely applies to our case. Not only chloride and sulfate are competing with each other for sorption into the pore solution, but they also have to compete with the other present anions, namely carbonate, bicarbonate and the hydroxide ion.

In the ideal case, this could be described by an extended Langmuir expression:

$$\frac{q_i}{q_0} = \frac{k_i \cdot c_i}{1 + \sum_j k_j \cdot c_j} \quad \text{Eq. 8-2}$$

The presence of the ethylene glycol, which decreases the electrostatic shielding between ionic species and promotes ionic association, adds another complication. Weak acid anions like carbonate and bicarbonate might be forced by this apolar environment to form bonds with the fixed charges, if the concentration of the ethylene glycol in the pore solution was sufficiently high. Such strong sorption could significantly slow the equilibration of the system.

The tested, strongly basic anion exchange resins consist of cross-linked styrene polymer-chains containing trimethyl-benzyl-amine as active groups. These groups give these ion exchangers the following order of (aqueous) selectivity for sorbed counter ions [12]:



An overview of the properties of the 3 tested resins in aqueous solution is given in Table 1. The Dowex 1X8-50 and 21K-Cl resins are gel-type ion exchange resins, which implies that their porosity is dependant on their degree of swelling. Only in a sufficiently swollen state is their ion exchange capacity fully (and readily) accessible to the bulk solution. For this reason, these resins are described as *microporous*. The Dowex MSA-1 resin on the other hand is *macroporous*, i.e. its polymer matrix has wide pores, providing access to the full exchange capacity without dependency on swelling.

These resins were chosen for their high mechanical and chemical stability and their strongly basic character. They have not only to be resistant to the ethylene glycol in the mixed solvent as well as the increased swelling this might cause, but they also have to operate at a pH of 10 to 11, i.e. a trona (carbonate / bicarbonate) saturated solution. For the resin to be functional, its active groups have to be dissociated, which is only given in a strongly basic resin for this pH range.

**Table 8-1:** Properties of the tested ion exchange resins according to supplier [12]

Resin	<b>Dowex 1X8-50</b>	<b>Dowex 21K Cl</b>	<b>Dowex MSA-1</b>
active group	trimethyl amine	trimethyl amine	trimethyl amine
matrix	styrene-DVB, (microporous) gel	styrene-DVB, (microporous) gel	styrene-DVB, macroporous
shipped ionic form	chloride (Cl <sup>-</sup> )	chloride (Cl <sup>-</sup> )	Chloride (Cl <sup>-</sup> )
mean particle size	550 micron	580 micron	640 micron
effective pH range	0-14	0-14	0-14
exchange capacity			
dry resin [meq/g]	3.5	4.5	4.0
wet resin [meq/ml]	1.33	1.25	1.0
general properties	excellent physical and chemical stability	excellent mechanical stability, good kinetics and high regeneration efficiency	excellent mechanical and chemical stability, good kinetics and high regeneration efficiency

### **8.3. Experimental**

Previous to the experiments, the ion exchanger resins were transformed from their chloride form (Cl<sup>-</sup>) into the hydroxide form (OH<sup>-</sup>) by contacting 100g of dry resin successively three times with app. 250g of fresh 5M NaOH. This removed ca. 75% of the chloride from the resins and was sufficient for the experiments, see Addendum.

To investigate the ion exchange behavior of the three resins, the distribution of chloride and sulfate between resin and bulk solution was investigated for different compositions of the mixed solvent as well as with and without addition of trona.

In a first set of experiments, samples of the Dowex MSA-1 resin were contacted for 4h with solutions containing app. 7500ppm chloride ions and 4500ppm sulfate ions at 25°C in resin to solution ratios of 1:2, 1:5 and 1:10. Solutions containing app. 47, 62 and 80%-w (salt-free solvent) ethylene glycol were tested.

In a second set of experiments, the Dowex 21K-Cl and MSA-1 resins were contacted for 4h with solutions containing app. 8500ppm of chloride ions, 4000ppm of sulfate ions. The resins were contacted in ratios of 1:2, 1:5 and 1:10 to the solution (by weight of wet resin to solution) at 50°C. Solutions containing app. 70, 90 and 100%-w (salt-free solvent) ethylene glycol were tested. Solutions saturated with trona and solutions without trona were tested for evaluate the impact of the high carbonate / bicarbonate on the extraction.

To test the extraction of low concentrations of chloride and sulfate, 100ml of mixed solvent solutions saturated with trona containing app. 60ppm of chloride ions and 40ppm of sulfate ions were contacted with the resins in their hydroxide form for 24h at 25°C. The amount of resin in each in this last set of experiments corresponded to app. 2g of dry resin in the original chloride form. Mixed solvents containing 0, 50, 70 and 90%-w (salt-free solvent) ethylene glycol were tested.

The concentrations of chloride and sulfate in solution were measured by ion chromatography before and after contacting with the resin. The loading of the resin with sulfate and chloride was then calculated by mass balance, i.e. the amounts of sulfate and chloride removed from the solution by the resin. As the resin was not completely stripped of chloride in the regeneration with NaOH, the remaining amount of chloride had to be added to the amount from the solution mass balance to obtain the total amount of chloride in the resin.

The swelling of the ion exchangers in trona-saturated solutions of solvents with ethylene glycol contents of 0, 50, 70 and 90%-w (salt-free solvent) was determined at 25°C. 2 to 3g samples of the NaOH regenerated (swollen) resin were contacted with 100ml of solution for 24h. Then the resin was filtered off, rinsed with distilled water, weighed and dried on the filter paper at 50°C for another 24h, after which it was weighed again. The degree of swelling was calculated as the ratio between the swollen weight in the test solutions and the dried weight at the end of the experiments.

$$v_s = \frac{m_{IE,solution}}{m_{IE,dried}} \quad [\% \text{-w dry resin}] \quad \text{Eq. 8-3}$$

The trona was obtained 99.8%-w pure from Solvay, France. The mixed solvents were prepared from technical grade ethylene glycol and ultra-pure water. The saturation concentrations of trona in ethylene glycol – water mixed solvents can be found in Chapter 6 [7]. Sulfate and chloride were introduced to the samples as analytically pure sodium salts (Merck). The three ion exchange resins were obtained from Sigma Aldrich.

All experiments were executed in triplo as shake tests in 50ml Nalgene™ bottles in a thermostatic shaking bath.

## 8.4. Results

### 8.4.1. Swelling in the Mixed Solvents

The results of the swelling experiments are summarized in Figure 1. The degree of swelling first decreased from about 40 to 50%-w in aqueous solution to 18 (Dowex 1X8-50) to 35%-w (Dowex MSA-1 and 21K Cl) in 50%-w (salt-free solvent) ethylene glycol.

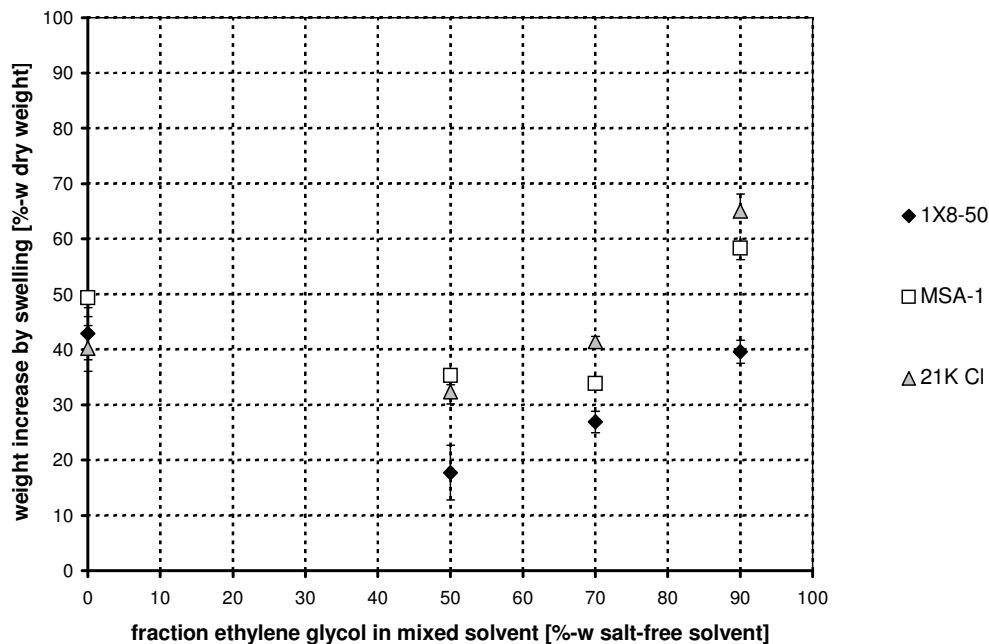


**Figure 8-1:** Swelling of the ion exchange resins in solvents of increasing ethylene glycol content at 25°C

Beyond 50%-w (salt-free solvent) ethylene glycol content the swelling increased almost linearly with increasing glycol content to reach 40%-w for Dowex 1X8-50 and app. 60%-w for Dowex MSA-1 and 21K-Cl in 90%-w ethylene glycol.

The Dowex 1X8-50 resin displayed a similar degree of swelling as the other two resins in the aqueous solution, but a ca. 15 to 20%-w lower degree of swelling in the mixed solvent solutions. Since Dowex 1X8-50 is a gel-type resin, its ion exchange capability (and even capacity, see above) requires a certain degree of swelling. Obviously, its affinity to the ethylene glycol is low, resulting in a decreased solvent sorption at middle ethylene glycol contents, where it preferentially absorbs water.

This is in good agreement with the observations of Helfferich [14], Bodamer et al. [16] and Bonner et al. [17], who found preferential water sorption for low ethylene glycol contents, i.e. low swelling as the water distributes between the resin and the ethylene glycol containing bulk solution, and high swelling, most probably due to increased electrostatic repulsion of the fixed charges in the resin, for high glycol contents.

#### 8.4.2. Chloride and Sulfate Sorption

The chloride and sulfate ions distributed between the resins' pore solution and the bulk solution in accordance with a Langmuir sorption isotherm, see Eq. 1. Based on the Langmuir model, the distribution coefficient of a solute species  $i$ ,  $D_i$ , which is the ratio between resin loading  $q_i$  and bulk solution concentration  $c_i$ , can be expressed as a function of the resin loading  $q_i$ , see Eq. 6:

$$\text{Langmuir: } \frac{q_i}{q_0} = \frac{k_i \cdot c_i}{1 + k_i \cdot c_i} \Leftrightarrow q_i + q_i \cdot k_i \cdot c_i = q_0 \cdot k_i \cdot c_i \quad \text{Eq. 8-4}$$

$$\frac{q_i}{c_i} + q_i \cdot k_i = q_0 \cdot k_i \quad \text{Eq. 8-5}$$

$$D_i = \frac{q_i}{c_i} \Rightarrow D_i = -q_i \cdot k_i + q_0 \cdot k_i \quad \text{Eq. 8-6}$$

Therefore, the distribution coefficient  $D_i$  is plotted versus  $q_i$  to obtain the Langmuir coefficient  $k_i$  and the total exchange capacity  $q_0$ .

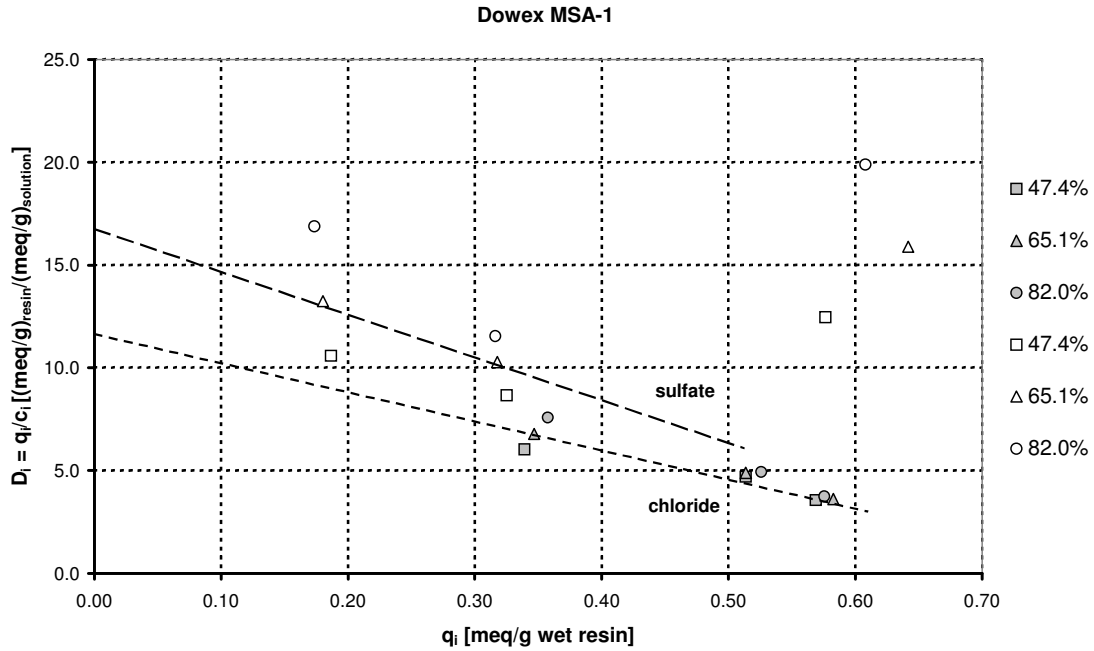


**Figure 8-2:** Distribution coefficient  $D$  versus resin loading  $q$  for sulfate (white symbols) and chloride (gray symbols) loading of the MSA-1 resin at 25°C for 47.4, 65.1 and 82%-w (salt-free solvent) ethylene glycol in the mixed solvent (w/o trona)

For the the Dowex MSA-1 resin at 25°C in 47.4, 65.1 and 82.0%-w (salt-free solvent) ethylene glycol solution, the  $D$  versus  $q$  plots are given in Figure 2, while the derived Langmuir fits together with the experimental data points are given in Figure 3. It can be noted from Figure 2, that the distribution coefficients for both sulfate and chloride displayed a slight increase with increasing ethylene glycol content. This effect was more pronounced for sulfate than for chloride, where it was almost negligible. The reason for this was most likely, that the more polar sulfate ion was more strongly affected by the increasingly apolar bulk solution and was therefore more strongly drawn to the more polar pore solution.

The total exchange capacity of the wet Dowex MSA-1 resin, calculated from the exchange capacity of the dry resin, see Table 1, and the degree of swelling, was ca. 1.17meq/g wet resin. From the plots of Figure 2, an average Langmuir coefficient  $k_i$  of 13g solution/meq for chloride and 21 g solution/meq for sulfate were obtained.

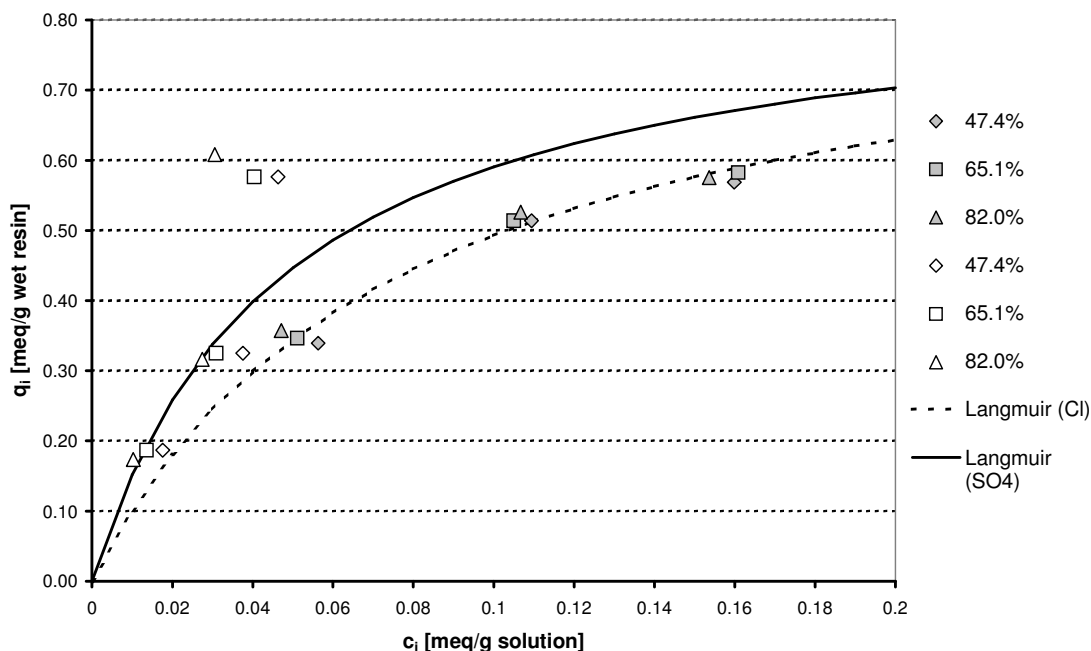


**Figure 8-3:** Resin load  $q$  versus bulk concentration  $c$  for chloride (gray symbols) and sulfate (white symbols) sorption of Dowex MSA-1 resin at 25°C from solutions containing 47.4, 65.1 and 82.0%-w (salt-free solvent) ethylene glycol (w/o trona)

The Langmuir fit in Figure 3 reproduces the distribution of chloride quite well, but the sulfate distribution shows a significant deviation for high sulfate loading. This effect was observed for all three ethylene glycol concentrations. For the deviant conditions, the sulfate loading  $q(\text{SO}_4)$  was 0.60 meq/g wet resin, while the chloride loading  $q(\text{Cl})$  was 0.57 meq/g wet resin, i.e. a combined total load of 1.17 meq/g wet resin, which corresponded exactly to the calculated total exchange capacity.

It is more likely, though, that sulfate was taken up in excess, i.e. together with a co-ion (sodium). The reason for this deviation from the Langmuir-behavior was probably the formation of  $[\text{NaSO}_4]^-$  (or even  $[\text{Na}_2\text{SO}_4]$ ) complexes (due to the apolar mixed solvent), which would be taken up in the pore solution, but would occupy less fixed-charges of the resin than the sulfate ions. As - due to the fixed charges - the pore solution is more polar than the mixed solvent bulk solution, it can also buffer such polar complexes better, resulting in an increased uptake of sulfate by the resin. The total capacity of the ion exchange resin was most probably not reached (or rather: a fraction was still occupied by  $\text{OH}^-$ ).



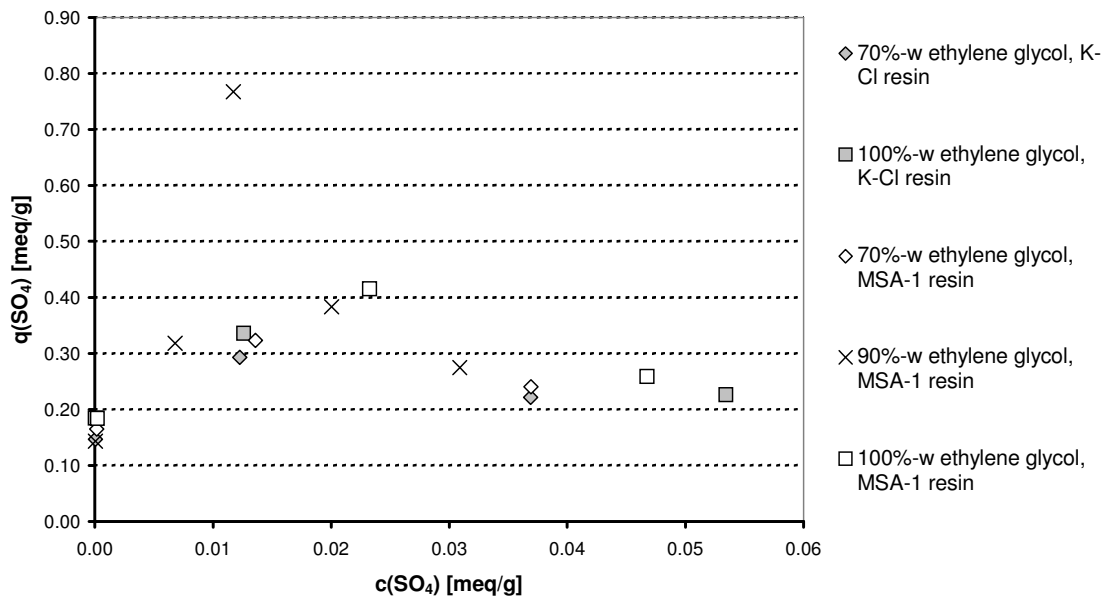
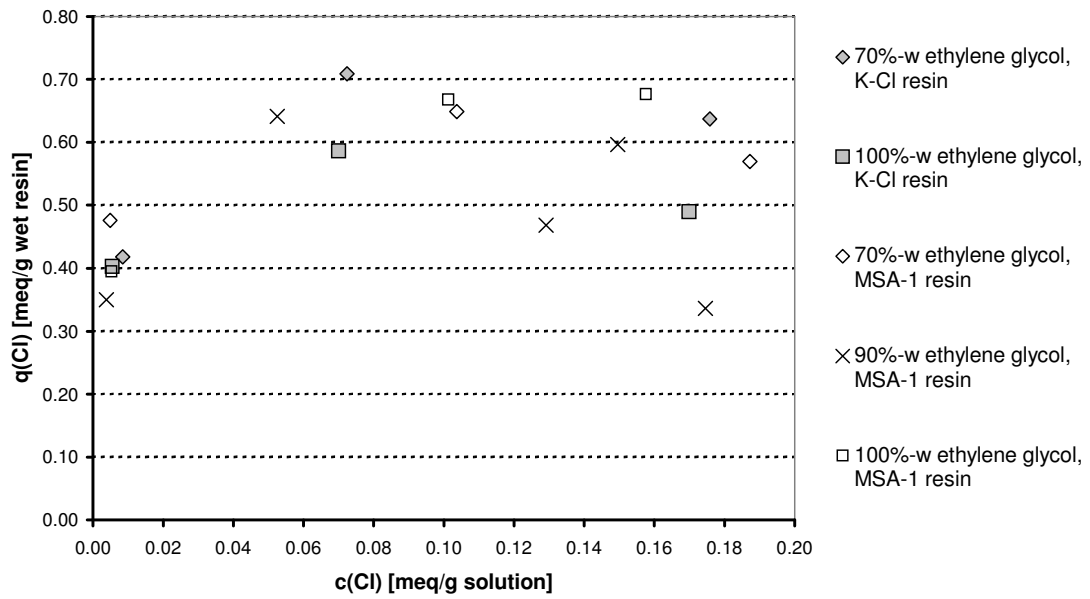


**Figure 8-4:** Resin loading  $q$  versus bulk solution concentration  $c$  for chloride (above) and sulfate (below) for Dowex 21K-Cl and MSA-1 resin in 70, 90 and 100%-w (salt-free solvent) ethylene glycol solutions (without trona) at 50°C

As can be seen from the experiments at 50°C with 70, 90 and 100%-w (salt-free solvent) ethylene glycol mixed solvents in Figure 4, the distribution coefficients for sulfate and chloride strongly increased with temperature. In almost all experiments in solutions without trona, both Dowex 21K-Cl and MSA-1 were loaded to their total exchange capacity with sulfate and chloride at low bulk concentration.

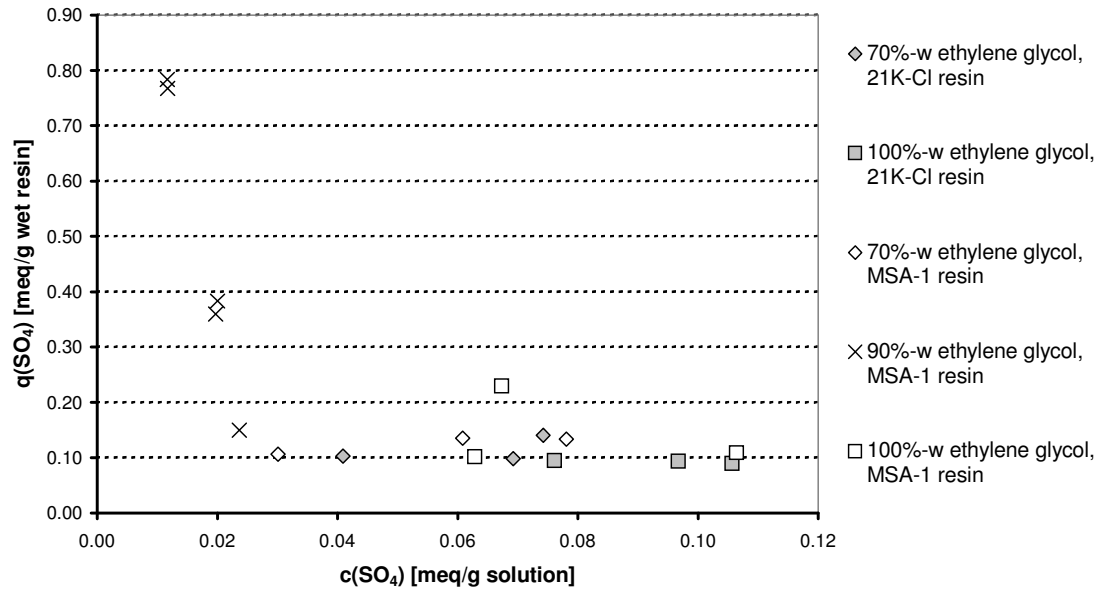
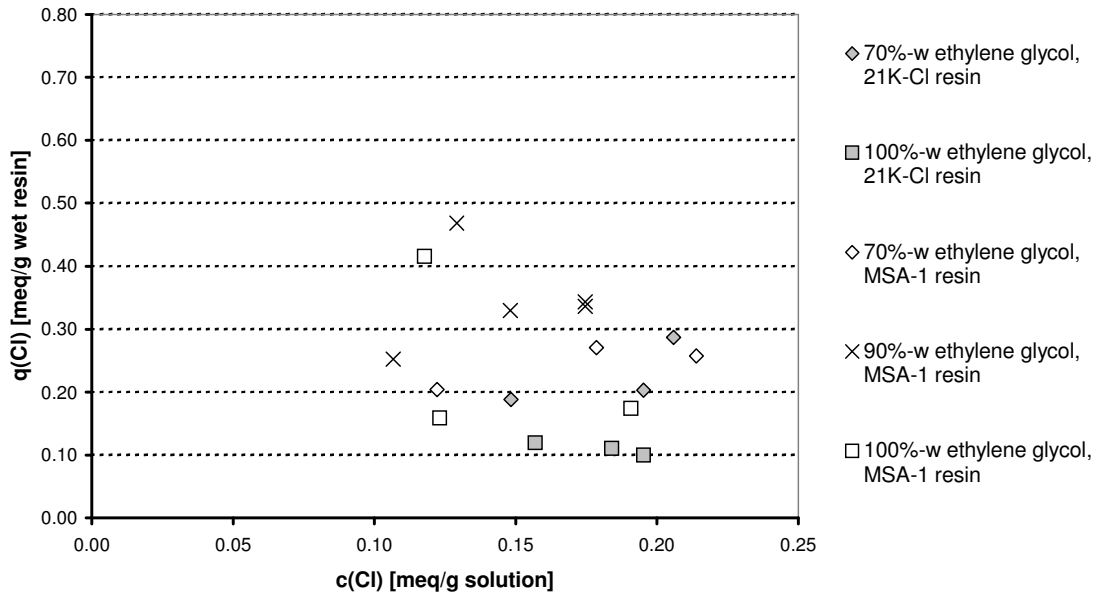
Therefore, it was not possible to obtain reliable Langmuir coefficients from these experiments

Figure 4 shows, that sulfate was reduced to lower levels (max. 0.06meq SO<sub>4</sub>/g solution) in solution than chloride (up to 0.2meq Cl/g solution) and that the maximum loading of chloride was app. 0.6 to 0.7meq/g wet resin, while the maximum sulfate loading varied between 0.2 and 0.4meq/g wet resin. Since these maximum loadings roughly correspond to the initial concentration of 8500ppm chloride and 4000ppm sulfate, the maximum loadings might actually be reversed for reversed initial concentrations. It can still be concluded, that both ion exchange resins show a slightly higher affinity to sulfate than chloride.

In the experiments at 50°C with Dowex 21K-Cl and MSA-1 with solutions saturated with trona, the resins were occupied to a significant fraction by carbonate and bicarbonate, resulting in a decrease in the loading with sulfate and chloride. While the sulfate loading dropped to app. constant 0.1meq/g wet resin (irrespective of bulk concentration), the chloride loading varied between 0.1 and 0.3meq/g wet resin, see Figure 5.

Exceptions were the conditions in the 90%-w (salt-free solvent) ethylene glycol solution, where both chloride and sulfate obtained a maximum in their loadings. This minimum in carbonate and bicarbonate loading of the resin coincides with the solubility minimum of bicarbonate in the mixed solvent solutions, see Chapter 6 [7].

The distribution coefficient of sulfate and chloride did depend significantly on the ethylene glycol content of the solution, as can be seen in Figure 6. Even though no distribution was measured for the Dowex 21K-Cl resin in 90%-w (salt-free solvent) ethylene glycol solution, the values in 70 and 100%-w ethylene glycol are identical enough to assume also a maximum in chloride and sulfate extraction at 90%-w ethylene glycol for Dowex 21K-Cl.



**Figure 8-5:** Resin loading  $q$  versus bulk concentration  $c$  for chloride (above) and sulfate (below) for Dowex 21K-Cl and MSA-1 resin at 50°C in 70, 90 and 100%-w (salt-free solvent) ethylene glycol solutions saturated with trona

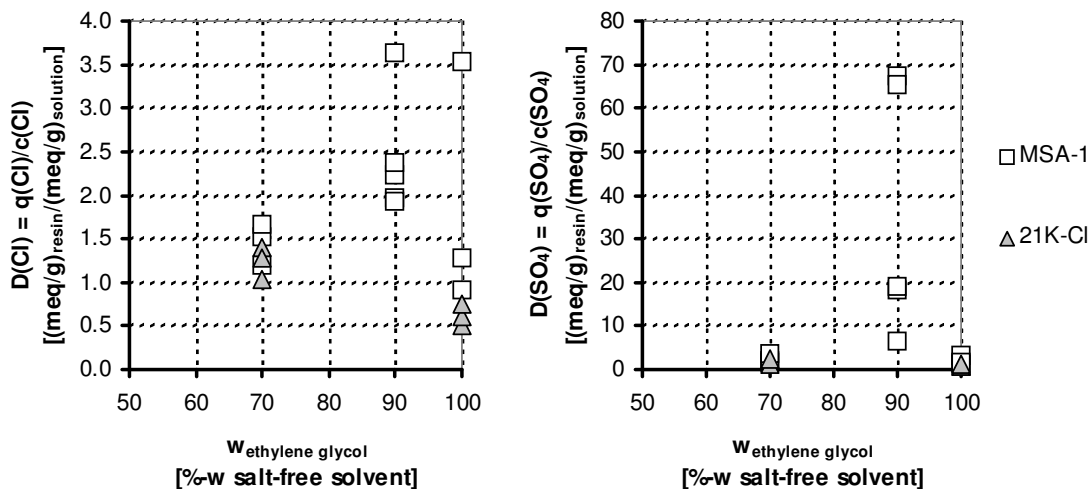


**Figure 8-6:** Dependence of the distribution coefficients for chloride and sulfate of Dowex 21K-Cl and MSA-1 resin on the ethylene glycol content for trona-saturated solutions for 50°C

It should be noted for the peak at 90%-w ethylene glycol, that while the distribution coefficient of chloride remained rather low with maximally 3.6, the distribution coefficient for sulfate reached exceptionally high levels with a value of 65 to 70. This indicates, that the sulfate ions are almost driven out of the bulk solution into the resin.

Another noteworthy effect is the almost linear increase of the chloride and sulfate distribution coefficient with the respective chloride and sulfate loading, see Figure 7, which is actually inverse of what was expected according to the Langmuir expression.

A similar behavior could be observed in the tests with 60ppm chloride and 40ppm sulfate at 25°C. The distribution coefficients of sulfate and chloride increased with increasing glycol content, see Figure 8.

The development of the sulfate distribution coefficient in Figure 8 matched the one in Figure 6 quite well. While in 25°C and far lower sulfate initial concentration, the increase of the distribution coefficient with increasing glycol content was more gradual, in both cases the maximum distribution coefficient at 90%-w (salt-free solvent) glycol was in the range of 60 to 70. This illustrates, that the influence of sulfate concentration on the distribution coefficient is negligible compared to the influence of the glycol content *in saturated-trona solution*.

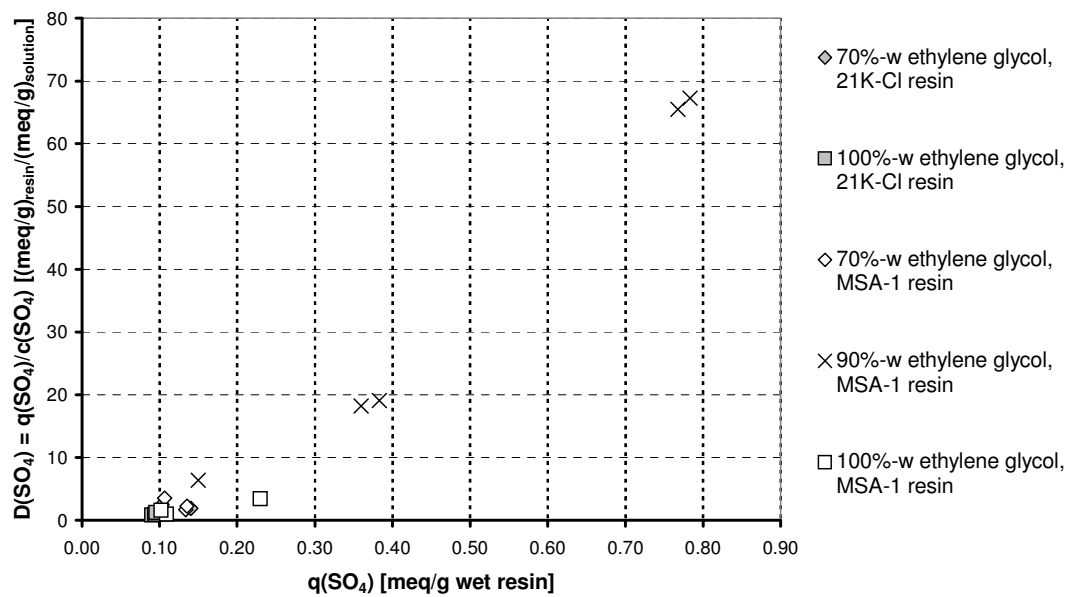
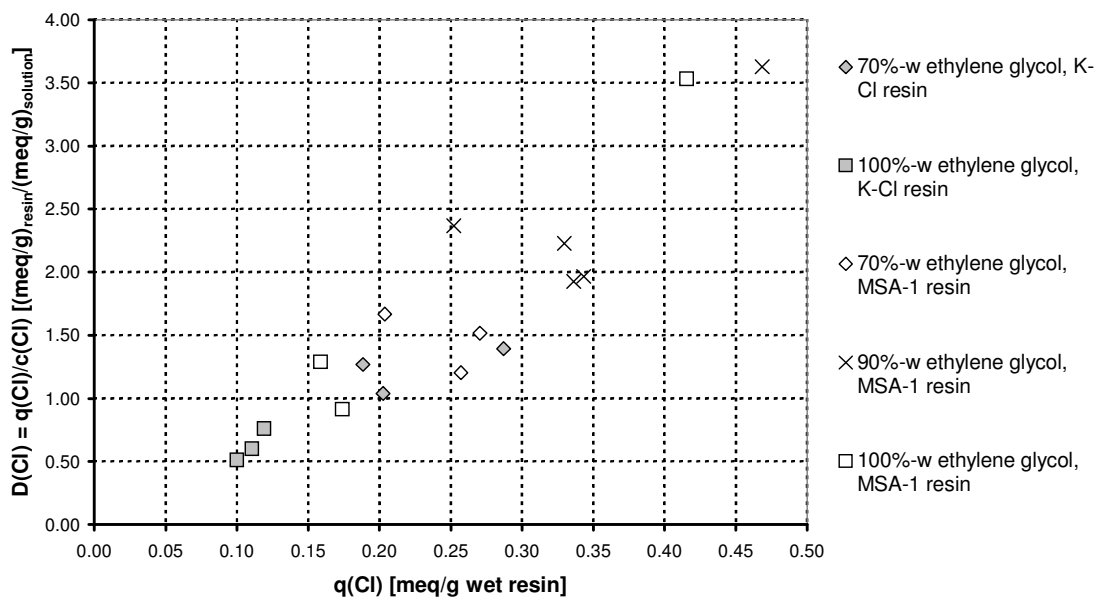


**Figure 8-7:** Distribution coefficient  $D_i$  versus resin loading  $q_i$  of chloride (above) and sulfate (below) for Dowex 21K-Cl and MSA-1 resin at 50°C in 70, 90 and 100%-w (salt-free solvent) ethylene glycol solutions saturated with trona

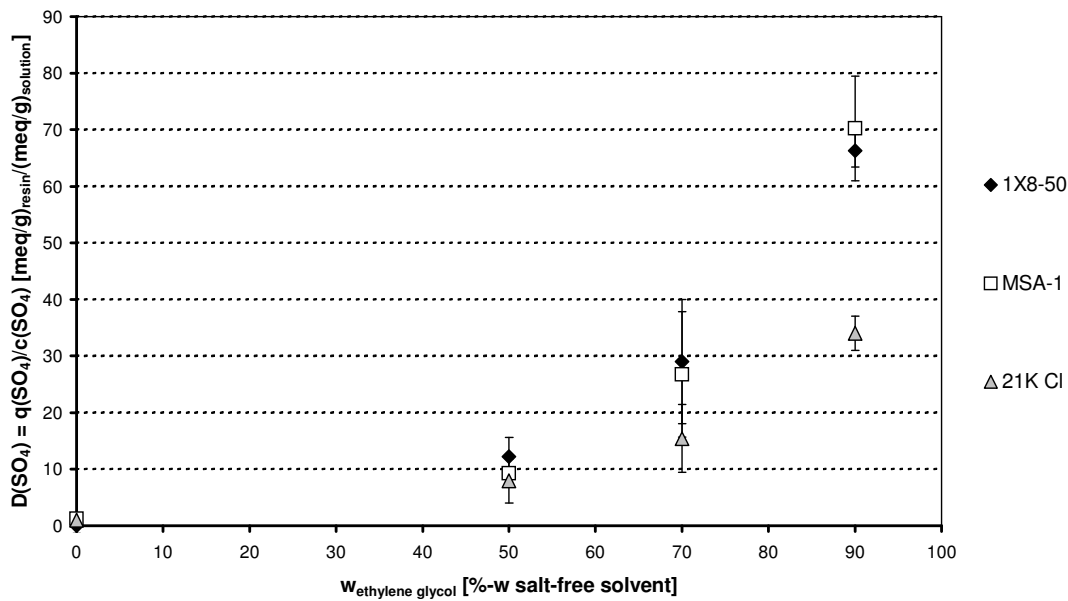
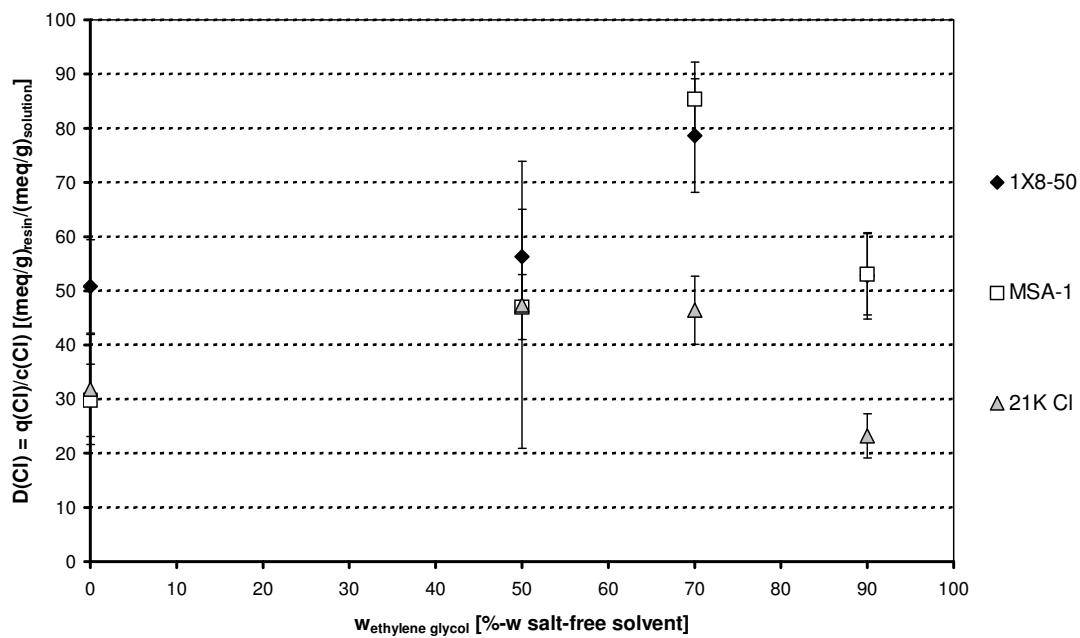


**Figure 8-8:** Dependence of the distribution coefficients for chloride and sulfate of Dowex 1X8-50, 21K-Cl and MSA-1 resin on the ethylene glycol content for trona-saturated solutions for 25°C

The development of the chloride distribution coefficient at 25°C and low chloride concentration in Figure 8 differed significantly from the one observed in Figure 6 at 50°C. Not only were the distribution coefficients at the lower temperature and concentration by more than factor of magnitude higher, i.e. 30 to 90 at 25°C compared to 1.0 to 3.6 at 50°C. Also the maximum distribution coefficient at 25°C was found at 70%-w (salt-free solvent) glycol, while at 50°C the maximum coincided with the one of sulfate at 90%-w (salt-free solvent) glycol.

It can be noted from Figure 6 and 8, that the distribution coefficients for Dowex MSA-1 and 1X8-50 were noticeably higher than the ones for Dowex 21K-Cl for both sulfate and chloride, indicating that the two first resins had a higher affinity for sulfate and chloride in the trona-saturated solution. Since this affinity was not noted for Dowex MSA-1 and 21K-Cl in trona-free solution, see Figure 4, this suggests, that Dowex 21K-Cl might have a higher affinity to carbonate / bicarbonate ions.

The linear relationship between the distribution coefficient  $D_i$  and the resin loading  $q_i$  of Figure 7 was also found in the 25°C experiments with trona-saturated solutions, see Figure 9. The surprisingly good fit between  $D_i$  and  $q_i$  can be explained by the mass balance, as the amount of solute  $\Delta n_i$  taken from the solution was simply added to the loading of the resin, resulting in the following relationship:

$$D_i = \frac{q_i}{c_i} = \frac{q_{i,1} + \Delta q_i}{c_{i,1} - \Delta c_i} = \frac{1}{c_{i,1} - \Delta q_i \cdot \frac{m_{resin}}{m_{solution}}} \cdot q_i = \frac{1}{c_{i,1} - (q_i - q_{i,1}) \cdot \frac{m_{resin}}{m_{solution}}} \cdot q_i \quad \text{Eq. 8-7}$$

Eq. 7 can be simplified into:

$$D_i = \frac{const.}{const. - q_i} \cdot q_i \quad \text{Eq. 8-8}$$

A slight hyperbolic tendency, as implied by Eq. 8, can be seen in the sulfate plot of Figure 9 and is noticeable in the chloride plot of Figure 7. This indicates, that the bulk solution concentration did not (directly) influence the distribution coefficient for the trona-saturated solutions.

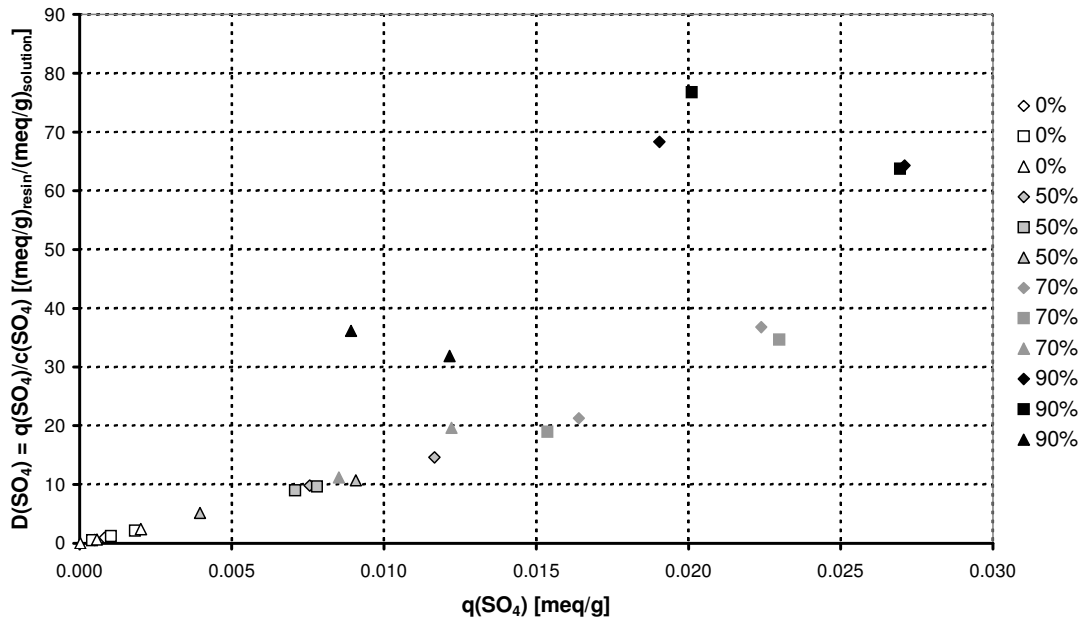
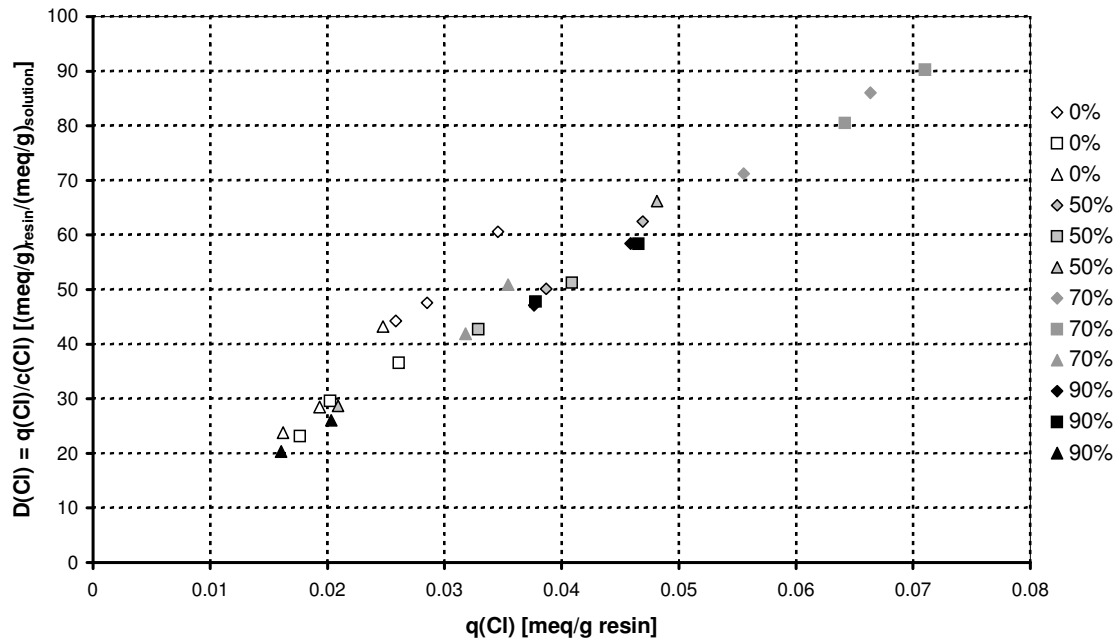


**Figure 8-9:** Apparent distribution coefficient  $D_i$  versus resin loading  $q_i$  of chloride (above) and sulfate (below) for Dowex 1X8-50 (diamond symbols), MSA-1 (square symbols) and 21K-Cl (triangle symbols) resin at 25°C in 0, 50, 70 and 90%-w (salt-free solvent) ethylene glycol solutions saturated with trona



Therefore, the distribution in trona-saturated solutions can apparently not be described by a Langmuir fit or another sorption-isotherm expression as in the experiments without trona.

The only parameter directly affecting the distribution coefficients in the trona-saturated mixed solvents was the ethylene glycol content: The driving force for the sulfate and chloride loading of the resin was apparently dominated by the effect of the glycol content on the activities of the different ionic species in solution. For example, chloride and sulfate were “salted out” of the bulk solution and “salted into” the more polar resin by the combined effect of the glycol and the high carbonate/bicarbonate concentration in the experiments with 90%-w ethylene glycol.

An explanation for the “salting out” effect is, that polar, but uncharged (or less charged) Na-Cl and Na-SO<sub>4</sub> complexes formed in the apolar mixed solvent solution and distributed preferentially to the more polar ion exchanger pore solution, which provide better charge buffering. The “salting out” is in fact a partitioning effect between two liquid phases, the pore solution and the bulk solution - and not limited to specific sorption sites, i.e. the fixed charges. Therefore the Langmuir sorption model does not apply.

As can be seen from Figures 6 and 8, the distribution coefficients were approximately constant for a given ethylene glycol content and the presented measured values can be used to extrapolate it for different ethylene glycol contents. For a different temperature, it appears most feasible to measure the distribution coefficient of interest, as - especially for chloride - the distributions coefficients vary significantly with temperature.

### **8.5. Conclusions**

The mixed solvent alone did not strongly affect the chloride and sulfate loading of the ion exchangers. While the sulfate and chloride loadings slightly increased with increasing glycol content, the loading in trona-free solutions can reliably described by Langmuir isotherms, i.e. as functions of the bulk solution concentration.

In the trona-saturated mixed solvent solutions, on the other hand, the loading was no longer controlled by the bulk solution concentration, but rather by a “salting out” effect of the trona-saturated mixed solvent. The distribution coefficients between resin (pore

solution) and bulk solution were here very strongly affected by the ethylene glycol content. Maximal extraction was achieved in solutions containing app. 90%-w (salt-free solvent) ethylene glycol.

Despite the strong effect of the high carbonate / bicarbonate concentration, satisfactory degrees of chloride and sulfate extraction could be achieved from the trona-saturated solutions. Especially the Dowex MSA-1 and 1X8-50 resins showed good affinities for chloride and sulfate.

The swelling of the resins in trona-saturated solutions was also significantly influenced by the glycol content and was found to drop from purely aqueous solutions till app. 50%-w (salt-free solvent) ethylene glycol, and to increase from there by app. the same amount till 90%-w (salt-free solvent) ethylene glycol.

The extraction of chloride and sulfate from mixed solvent solutions saturated with trona was found possible, but further tests are required to evaluate the influence of temperature and initial chloride and sulfate concentration on the degree of extraction.

For the application of ion exchange for the regeneration of mixed solvent in the Mixed Solvent Recrystallization and Mixed Solvent Reactive Recrystallization processes, not only economical methods for the resin regeneration have to be found, but also loading and regeneration tests with the mixed solvent solutions in actual ion exchange columns are required. From the obtained results, the biggest economical obstacle appears to be the co-extraction of carbonate / bicarbonate, which reduces the available exchange capacity for chloride and sulfate of the resin by up to 70%. Additionally, the co-extraction also results in a loss of product (i.e. carbonate / bicarbonate).

## **8.6. Acknowledgements**

The contribution of Mr. Cahir O'Neill and Mr. Michel van den Brink to the experimental work is gratefully acknowledged.

## 8.7. Notation

$c_i$	: concentration of $i$ in solution	[meq/g solution]
$c_{i,1}$	: initial concentration of $i$ in the solution	[meq/g solution]
$D_i$	: distribution coefficient between pore and bulk solution	[-]
$k_i$	: Langmuir coefficient	[g solution/meq]
$q_0$	: total exchange capacity of the resin	[meq/g wet resin]
$q_i$	: loading of the resin with solute $i$	[meq/g wet resin]
$q_{i,1}$	: initial loading of the resin with $i$ (after regeneration)	[meq/g wet resin]

## 8.8. Indices

$i$	: solute $i$
$j$	: solute $j$
resin	: in the resin
solution:	in the solution

## 8.9. Literature References

- [1] Oosterhof, H., Witkamp, G.J., van Rosmalen, "Some antisolvents for crystallisation of sodium carbonate", *Fluid Phase Equilibria*, 155, 1999, p. 219-227
- [2] Oosterhof, H., Witkamp, G.J., van Rosmalen, G.M., 2001, "Antisolvent Crystallization of Anhydrous Sodium Carbonate at Atmospheric Conditions", *AIChE J.*, 47 (3), 2001, p. 602-608
- [3] Oosterhof, H., Witkamp, G.J., van Rosmalen, G.M., 2001, "Evaporative Crystallization of Anhydrous Sodium Carbonate at Atmospheric Conditions", *AIChE J.*, 47 (10), 2001, p. 2220-2225
- [4] Oosterhof, H., de Graauw, J., Witkamp, G.J., van Rosmalen, G.M., 2002, "Continuous Double Recrystallization of Light Soda Ash into Super Dense Soda Ash", *Crystal Growth & Design*, 2 (2), 2002, p. 151-157
- [5] Gärtner, R.S., Seckler, M.M., Witkamp, G.J., "Recrystallization of Trona (Sodium Sesquicarbonate) into Soda (Sodium Carbonate Anhydrate) in a Mixed Solvent. Part I: Fundamental Conversion Steps", submitted for publication in *AIChE Journal* (Chapter 4)

- [6] Gärtner, R.S., Seckler, M.M., Witkamp, G.J., “Recrystallization of Trona (Sodium Sesquicarbonate) into Soda (Sodium Carbonate Anhydrate) in a Mixed Solvent. Part II: Alternative Recrystallization Routes”, in preparation for publication (Chapter 5)
- [7] Gärtner, R.S., Seckler, M.M., Witkamp, G.J., “Solid Phases and their Solubilities in the System  $\text{Na}_2\text{CO}_3 + \text{NaHCO}_3 + \text{Ethylene Glycol} + \text{Water}$  from (50 to 90) °C”, J. Chem. Eng. Data, 49(1), 2004, p. 116-125
- [8] Garret, D.E., “Natural Soda Ash – Occurrences, Processing and Use”, Van Nostrand – Reinhold (Publ.), New York, 1992, p. 30-416
- [9] Haynes, H.W., “Solution Mining of Trona”, In Situ, 21(4), 1997, p. 357-394
- [10] Gärtner, R.S., Seckler, M.M., Witkamp, “Mixed Solvent Recrystallisation for the Densification and Purification of Soda Ash”, in preparation for publication (Chapter 2)
- [11] Gärtner, R.S., Wilhelm, F.G., Wessling, M., Witkamp, G.J., “Regeneration of Mixed Solvent by Electrodialysis: Selective Removal of Chloride and Sulfate”, accepted for publication in Journal of Membrane Science
- [12] Sigma-Aldrich product information
- [13] Lide, D.R., “CRC Handbook of Chemistry and Physics”, 79<sup>th</sup> edition, CRC Press, Boca Raton, 1999, p. 6-139 – 6-161
- [14] Helfferich, F.G., “Ion Exchange”, Dover Publications Inc., New York, 1995; Chapter 5: “Equilibria”
- [15] Helfferich, F.G., “Ion Exchange”, Dover Publications Inc., New York, 1995; Chapter 10: “Behavior in Non-aqueous and Mixed Solvents”
- [16] Bodamer, G.W., Kunin, R., “Behaviour of Ion Exchange Resins in Solvents Other Than Water”, Ind. Eng. Chem., 45, 1953, p. 2577-2580
- [17] Bonner, O.D., Moorefield, J.C., “Ion Exchange in Mixed Solvents”, J. Phys. Chem., 58, 1954, p. 555-557

### **8.10. Addendum**

For the stripping of the ion exchange resins in preparation for the experiments, it was tested, whether the distribution between resin and solution could be described by a Langmuir-expression according to Eq. 1.

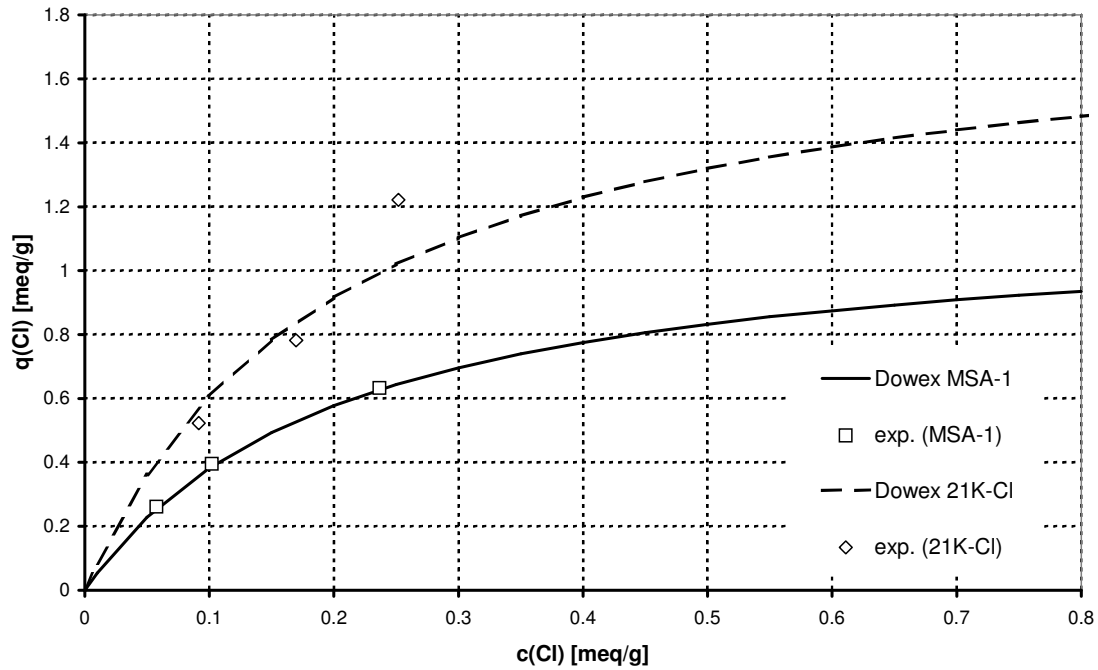


**Figure 8-10:** Langmuir fits for the chloride loading of Dowex 21K-Cl and Dowex MSA-1 and the experimentally observed points during stripping of the resins with 5M NaOH at 50°C

The total capacity of the wet resin was calculated from the dry capacity and the degree of swelling in the 5M NaOH used for chloride stripping. The total capacity  $q_0$  of Dowex 21K-Cl was app. 1.86meq/g wet resin and app. 1.17meq/g wet resin for Dowex MSA-1. The Langmuir-coefficient was fitted from the experimental data and was found to be ca. 4.8 g solution/meq chloride for both resins. The resulting fits are given in Figure 10.

$$\frac{q(Cl)}{q_0} = \frac{4.8 \cdot c(Cl)}{1 + 4.8 \cdot c(Cl)} \quad \text{Eq. 8-9}$$



## Chapter 9 :

### REGENERATION OF MIXED SOLVENT BY ELECTRODIALYSIS: SELECTIVE REMOVAL OF CHLORIDE AND SULFATE

R.S. Gärtner, F.G. Wilhelm, G.J. Witkamp, M. Wessling

#### ***Abstract***

The applicability of electrodialysis for the selective removal of sulfate and chloride ions from a mixed solvent solution of sodium carbonate was investigated. The mixed solvent consisted of 70%-w ethylene glycol and 30%-w water. 6 different ion exchange membranes, the homogeneous membranes Neosepta CM-2, AM-3, AMX and ACM as well as the heterogeneous FuMA Tech CM-A and AM-A, were tested for their chemical and physical resistance to the mixed solvent carbonate solution, their ethylene glycol retention, their electrical resistance in the mixed solvent and their selectivity for sulfate and chloride over carbonate transport.

## 9.1. Introduction

Recrystallization as well reactive recrystallization of soda (sodium carbonate) in a mixed solvent have been shown in related work [1 - 7] as energy-saving, alternative process routes for the production of soda of higher physical quality and chemical purity than currently available soda. The mixed solvent used in these processes consists of water and ethylene glycol as organic antisolvent. The most suitable mixture for the recrystallization contains 70%w ethylene glycol [1, 2, 4, 6, 7] and this composition was also used in this work.

A vital factor for the economical feasibility of these processes is the recycle of the mixed solvent in the process. Inline purification steps are necessary to remove impurities from the mixed solvent recycle. These purification steps should not change the ethylene glycol content of the mixed solvent. As electrodialysis selectively extracts ions from solutions, it offers a possible method to remove ionic impurities from the mixed solvent solution.

The globally most common sodium carbonate source is trona, sodium sesquicarbonate ( $\text{Na}_2\text{CO}_3 \cdot \text{NaHCO}_3 \cdot 2\text{H}_2\text{O}(\text{s})$ ), which occurs as a natural mineral in large, mostly subterranean deposits [8]. It can be converted via the Mixed Solvent Reactive Recrystallization process [5 - 7] to high quality soda. Trona (sodium sesquicarbonate) used for the Mixed Solvent Reactive Recrystallization process should be free of organic impurities, because such impurities can have a strong impact on the recrystallization. Such organic impurities might also be difficult to remove from the partially organic mixed solvent and should therefore be removed from the trona *before* attempting the Mixed Solvent Reactive Recrystallization. It is also preferable to remove any insoluble impurities before the Mixed Solvent Reactive Recrystallization.

Trona, recovered by solution mining [9], would therefore be a suitable starting material for the Mixed Solvent Reactive Recrystallization, as organic and insoluble particulate impurities have already been removed. This trona would still contain at least traces of soluble inorganic impurities: Traces of chloride and sulfate were found in samples of trona ore from Wyoming and California, see Gaertner et al. [5, 10].



The light soda ash used as starting material in the Mixed Solvent Recrystallization process by Oosterhof et al. [1, 2, 4] is commonly produced by the Solvay process, i.e. from sodium chloride, and contains therefore measurable traces of sodium chloride.

These trace concentrations of sodium chloride and sodium sulfate remain in the mixed solvent after the recrystallization [10] and should be removed during the recycle.

For these reasons, the inline removal of chloride and sulfate by different techniques has been investigated. The results of extraction tests for chloride and sulfate removal by anion exchanger resins are described by Gärtner et al. [11].

But also membrane processes like electrodialysis, reverse osmosis, nano- and hyperfiltration offer feasible methods to remove dissolved ionic impurities from solutions. Since it is vital for the recrystallization process to maintain the ethylene glycol content unchanged, especially electrodialysis seemed suitable for the outlined separation.

The selective removal of inorganic ions from partially organic solutions of ethylene glycol by electrodialysis is not only relevant to our case, but was also of interest to other researchers and industrial applications [12 - 15]. These references indicate that the separation is basically possible, but yield only little generally applicable, fundamental information on the influence of the partially organic solvent on the electrodialysis process. The aim of this research was thus not only to conduct a feasibility study of the desalination of the mixed solvent solution for our case, but also to investigate the influence of the partially organic mixed solvent on the ion exchange membranes. Specifically, the change in swelling, in electrical resistance, and in chloride and sulfate selectivity as well as the ethylene glycol retention was investigated.

## **9.2. Theory**

The selective removal of specific ions from a partially organic aqueous solution differs significantly from the usual applications of electrodialysis, i.e. the desalination, concentration or fractionation of aqueous salt solutions.

Electrodialysis membranes are basically nanoporous organic polymer membranes containing charged functional groups like sulfonates, carboxylates, amines, etc.. These groups serve to overcome the hydrophobic nature of the organic polymer network and

allow the membrane to take up aqueous electrolyte solutions into its pores. This swelling, i.e. absorption of electrolyte solution, enables the membrane to conduct electrical current. In the ideal case, the pore solution will only contain the dissolved counter-ions to the fixed charged functional groups, i.e. mobile cations for cation exchange membranes (CEM) with anionic functional groups and mobile anions for anion exchange membranes (AEM) with cationic functional groups. Such ideal membranes would be 100% permselective for cations or anions, since only the counter-ions as the only mobile charged species would be the carriers of the current.

In reality, the pores are so wide, that the fixed charges are not homogeneously distributed in the pore volume. Regions close to the pore “walls” will fit the ideal case above and contain increased levels of counter-ions over co-ions (i.e. ions with the same polarity as the fixed charges), while the composition of pore solution further away from the pore “walls” and the fixed charges will resemble the solution outside the membrane. Pimenskaya et al [16] have given a more detailed description of the membrane and pore solution composition for solutions of  $\text{Na}^+$ ,  $\text{CO}_3^{2-}$  and  $\text{HCO}_3^-$  for some of the Neosepta membranes used in this study.

This inhomogeneous composition of the pore solution results in less than 100% permselectivity as also a certain amount of co-ions is available in the membrane for charge transport. Physical properties such as swelling and pore size have an influence on permselectivity as large pore diameters and increased degrees of swelling will increase the amount of co-ions in the membrane.

Since their hydration hulls, which increase the diameter of the transported charge, surround the migrating ions, the pore size and the degree of swelling also affect the membrane’s selectivity for specific counter-ions. The mass transfer resistance to diffusion/migration for each specific hydrated ion depends on the size of the hydration hull and the mean pore channel width - to the degree that larger hydrated ions are not able to permeate the membrane.

The main impact of the mixed solvent in comparison to the aqueous solution is:

1. The solubility of sodium carbonate is far lower in the mixed solvent than in water.

The organic antisolvent is less polar than water and effectively unable of self-

- dissociation into ionic species. There are thus less mobile charges (free ions) per unit volume present in the mixed solvent solution. The conductivity of the mixed solvent and thereby also the limiting current density [17, 18] are therefore significantly lower than that of the aqueous solution.
2. All electro dialysis membranes are used in a swollen state, containing significant amounts of salt solution in their pore channels. This solution serves as the ion-conducting medium through the membrane. In the mixed solvent this will result in an increased electrical resistance of the membrane, as the partially organic solution in the pores is less polar and has a lower solubility for ionic species.
  3. The membrane will not only absorb the partially organic solution in its pores, but also in its organic polymer lattice. This increased solvent uptake results in a change in pore volume, which has multiple consequences for the characteristics of the membrane: The mechanical stability of the membrane might decrease, and its selectivity for different ions might change with increasing or decreasing pore diameter. Furthermore, excessive swelling can irreversibly damage a membrane – therefore the resistance to the mixed solvent should be checked.
  4. The influence of a mixed solvent on the current efficiency of an electro dialysis (membrane) stack has not yet been tested. Due to the effects listed above, the current efficiency, i.e. the fraction of the electrical current actually used in the electro dialysis membrane stack for ion separation, with the mixed solvent solution might significantly differ from the one in aqueous solution.

Only limited information on mixed solvent electro dialysis is available in current literature [12 - 15] and because of the complexity of interactions in electrolyte systems, extrapolations from first principles are not feasible. All these above listed factors were therefore investigated in this work for the given mixed solvent system to evaluate the feasibility of electro dialysis for the selective removal of trace ionic impurities of sodium chloride and sodium sulfate from the mixed solvent solution. The investigated mixed solvent solution contained 70%-w (salt free solvent) ethylene glycol, 30%-w (salt free solvent) water, 60 g/l  $\text{Na}_2\text{CO}_3$ , 5 g/l  $\text{NaCl}$  and 2.5 g/l  $\text{Na}_2\text{SO}_4$ .

A few of the above outlined phenomena and technical terms need to be correlated by mathematical relationships and definitions:

The current density  $i$  of an electro dialysis cell, i.e. the electrical current  $I$  per area of one membrane sheet  $A_m$  in the stack (cation or anion exchange membrane), is equivalent to the sum of the ion fluxes  $j_{i,M}$  through this membrane, as the ions are the carriers of electrical charge inside the membrane stack [2].

$$i = F \cdot \sum_i |z_i| \cdot j_i \quad \text{Eq. 9-1}$$

Every mobile ion species present in the stack can contribute to the current density, as the electrical field applied to the stack will affect all charged species. Basically, the ion fluxes in the stack can be assumed to result only from the electrical field:

$$j_i = -\frac{D_i \cdot F \cdot c_i}{R \cdot T} \cdot \frac{\partial \phi}{\partial x} = -u_i \cdot c_i \cdot F \cdot \frac{\partial \phi}{\partial x} \quad \text{Eq. 9-2}$$

This yields for the current density:

$$i = F \cdot \sum_i |z_i| \cdot j_i = -\frac{\partial \phi}{\partial x} \cdot F^2 \cdot \sum_i |z_i| \cdot u_i \cdot c_i \quad \text{Eq. 9-3}$$

The transport number of a particular ion  $i$  commonly expresses the fraction of the current transported by these ions:

$$t_i = \frac{|z_i| \cdot j_i}{\sum_i |z_i| \cdot j_i} \quad \text{Eq. 9-4}$$

In the bulk solution, the transport number of the cations,  $t_+$ , has to be identical to the one of the anions,  $t_-$ , i.e. both are equal to  $\frac{1}{2}$ . In an ideal electro dialysis membrane, all current is transported by the counter-ions, which transport number is then equal to 1, while the transport number of the excluded co-ions is equal to 0. In a real membrane, where both counter-ions and co-ions pass through the membrane, the transport number of counter-ions through an electro dialysis membrane ranges therefore theoretically between  $\frac{1}{2}$  and 1, while the transport number of co-ions through a the same membrane would range between 0 and  $\frac{1}{2}$ :

$$t_+^{CEM} = 1 - t_-^{CEM} \quad \text{and} \quad t_-^{AEM} = 1 - t_+^{AEM} \quad \text{Eq. 9-5}$$

Typical transport numbers for commercially available electro dialysis membranes range from 0.85 to 0.99 [19].

The permselectivity of an electro dialysis membrane is commonly defined as its ability to hold-back co-ions and is defined as:

For cation exchange membranes (CEM):

$$\phi^{CEM} = \frac{t_+^{CEM} - t_+}{t_-} \quad \text{Eq. 9-6}$$

and for anion exchange membranes (AEM):

$$\phi^{AEM} = \frac{t_-^{AEM} - t_-}{t_+} \quad \text{Eq. 9-7}$$

The current efficiency of an electro dialysis stack is defined as the ratio between the current used for the intended concentration / separation effect and the total current. The current density used for the *concentration / separation* for an ion i is:

$$i_i = |z_i| \cdot F \cdot \frac{\dot{V}_d}{A_M} \cdot (c_{i,in} - c_{i,out})_d = |z_i| \cdot F \cdot \frac{\dot{V}_c}{A_M} \cdot (c_{i,out} - c_{i,in})_c \quad \text{Eq. 9-8}$$

As long as the applied electrical field only results in ion migration and no water splitting occurs in the stack (see *limiting current density* below), the current efficiency of the process can be calculated from the transport numbers of the membranes. The current efficiency for one anionic species i- can be calculated as:

$$\xi_{i-} = \frac{i_{i-}}{i} = t_{i-}^{AEM} - t_{i-}^{CEM} \quad \text{Eq. 9-9}$$

For a cationic species i+, the current efficiency can be derived from the membrane transport numbers as:

$$\xi_{i+} = \frac{i_{i+}}{i} = t_{i+}^{CEM} - t_{i+}^{AEM} \quad \text{Eq. 9-10}$$

The overall current efficiency of the electro dialysis stack can be derived as:

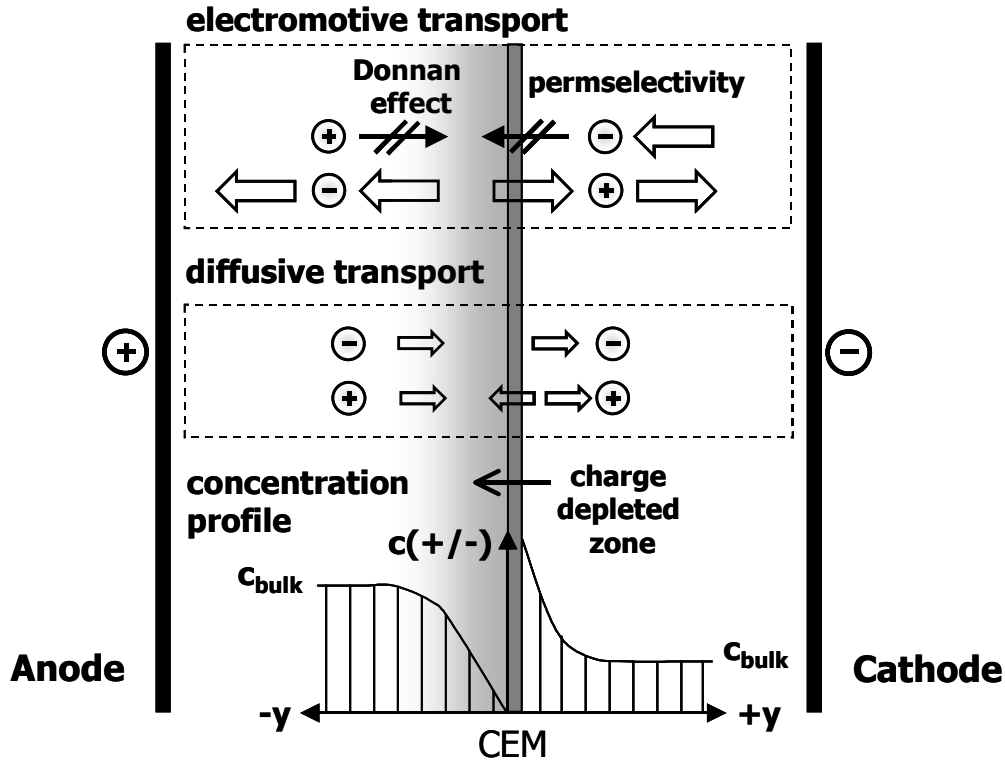


**Figure 9-1:** Diffusion limited current density as result of concentration polarization

$$\xi = \frac{i_{sep}}{i} \equiv \xi_+ = \frac{i_+}{i} = t_+^{CEM} - t_+^{AEM} \equiv \xi_- = \frac{i_-}{i} = t_-^{AEM} - t_-^{CEM} \quad \text{Eq. 9-11}$$

The maximum current density, which can be applied to an electro dialysis stack, is limited by the ion fluxes [17, 18]. Since the membranes are permselective, the counter-ions carry the current through the membrane.

The co-ions, of which only a small fraction can pass, are held back at the concentrate side and migrate off from the diluate side of the membrane, resulting in a strong concentration polarization effect. This effect is especially critical for the diluate side, as the counter-ions are withdrawn through the membrane and the co-ions are depleted by migration. This results in a charge-depleted zone in the membrane concentration border layer. Without the presence of co-ions in this zone, the Donnan effect, i.e. the electroneutrality condition, prevents counter-ions from the bulk solution to enter this zone. The only

mechanism, which promotes co-ion transport into this zone, is regular diffusion, driven by the concentration profile between bulk solution and membrane surface, see Figure 1.

In the steady state the ion flux through the membrane, which can be assumed to be purely electromotive, is equal to the diffusive flux plus the electromotive flux in the border layer:

$$j^M = \frac{t^M \cdot i}{|z| \cdot F} = -D \cdot \left( \frac{dc}{dy} \right) + \frac{t \cdot i}{|z| \cdot F} \Rightarrow i = -\frac{D \cdot |z| \cdot F}{t^M - t} \cdot \frac{dc}{dy} \quad \text{Eq. 9-12}$$

This again yields for the ion fluxes:

$$j_+ = -\frac{D \cdot t_+^M}{t_+^M - t_+} \cdot \frac{dc}{dy} \quad \text{Eq. 9-13}$$

$$j_- = -\frac{D \cdot t_-^M}{t_-^M - t_-} \cdot \frac{dc}{dy} = \frac{D \cdot t_+^M}{t_+^M - t_+} \cdot \frac{dc}{dy} \quad \text{Eq. 9-14}$$

$$j^M = j_+ - j_- = -\frac{D \cdot t_+^M}{t_+^M - t_-} \cdot \frac{dc}{dy}$$

The *limiting current density*  $i_{\text{lim}}$  is reached, when the diffusive transport has reached its physical maximum, i.e. the maximum concentration gradient  $dc/dy$  in the border layer. This is the case when the concentration on the membrane reaches 0, i.e.:

$$i_{\text{lim}} = \frac{D \cdot F}{t^M - t} \cdot \frac{c_{\text{diluate}}}{\delta} \quad \text{Eq. 9-15}$$

In aqueous solutions, the current density can usually be increased beyond the limiting current density. The resulting increase in current stems from water splitting and does not contribute to the intended concentration/separation. Additionally, water splitting can lead to significant pH shifts, as  $\text{OH}^-$  or  $\text{H}^+$  ions accumulate on the membrane surface. Such a pH shift can damage the membrane by e.g. causing a hydrolysis reaction on the functional groups. The maximum applied current density in an electro dialysis application should therefore be equal or lower than  $i_{\text{lim}}$ .

The swelling of a membrane is defined by the following simple relationship:

$$v_M = \frac{V_{wet} - V_{dry}}{V_{dry}} \cdot 100\% \quad [\%-\text{vol}] \quad \text{Eq. 9-16}$$

The swelling can be related to the membrane porosity by:

$$v_M = \frac{\epsilon_{wet} - \epsilon_{dry}}{\epsilon_{dry}} \cdot 100\% \quad [\%-\text{vol}] \quad \text{Eq. 9-17}$$

The dry state of an electro dialysis membrane provides a poor comparison for the degree of swelling in the mixed solvent, as the operational state of an electro dialysis membrane is the one swollen with an electrolyte solution. Therefore a different definition of swelling is used to better reflect the influence of the mixed solvent on the membranes in relation to the operational state of the membrane: The relative swelling in the mixed solvent  $v_{MS}$ .

$$v_{MS} = \frac{V_{MS} - V_{ref}}{V_{ref}} = \frac{\epsilon_{MS} - \epsilon_{ref}}{\epsilon_{ref}} \quad [\%-\text{vol}] \quad \text{Eq. 9-18}$$

The index “ref” refers to the reference state of the membrane, in which the membrane is provided by its producer. For the tested set of membranes, the provided state is in equilibrium with a 0.5 M NaCl solution, which swells the membrane to an immediately usable state for aqueous desalination / concentration applications.

**Table 9-1:** Overview of the tested membranes, their characteristics, their electrical resistance and their applicable pH range as given by their producer [20, 21]]

Name	Producer	Type	Characteristics	pH	$r_M$ [ $\Omega \cdot \text{cm}^2$ ]
Neosepta CM-2	Tokuyama Co.	homogen. CEM	low diffusion	-	2.0-4.5
Neosepta AM-3	Tokuyama Co.	homogen. AEM	low diffusion	-	2.8-5.0
Neosepta AMX	Tokuyama Co.	homogen. AEM	high mechan. strength	-	2.0-3.5
Neosepta ACM	Tokuyama Co.	homogen. AEM	proton blocking	-	3.5-5.5
FT-CM-A	FuMA Tech	heterogen. CEM	mechan. very stable	6-13	5-9
FT-AM-A	FuMA Tech	heterogen. AEM	mechan. Stable	6-13	4-8



### **9.3. Experimental**

6 ion exchange membranes, 2 cation and 4 anion exchange membranes, were chosen for their resistance to organic solvents, operability at pH ranges from 8 to 13 and mechanical burst strength. A listing of the tested membranes is given in Table 1.

For the investigation of the feasibility of electrodialysis for the selective removal of sulfate and chloride ions from the sodium carbonate saturated ethylene glycol – water mixed solvent, 4 types of experiments were performed:

1. Measurement of membrane swelling in different solution compositions
2. Ethylene glycol retention in comparison to water permeability
3. Electrical resistance of the membranes in aqueous soda solution and in mixed solvent
4. Selectivity of transport of chloride, sulfate and carbonate in an electrodialysis stack with a) aqueous soda solution and b) mixed solvent soda solution as diluate stream

#### **9.3.1. Membrane Swelling**

App. 10 cm long and 2 cm broad sample strips of the membranes, which had been previously equilibrated in 0.5M NaCl solution, were submerged in 4 different solutions:

1. demineralized water
2. mixed solvent (70%-weight ethylene glycol, 30%-water)
3. 0.1 M aqueous soda solution
4. 0.1 M soda in mixed solvent

For the anion exchange membranes the solution was refreshed after 24 h, because chloride would be released from the membranes equilibrated in 0.5 M NaCl. By exchanging the solutions after 24h, this change in the environment of the membrane was compensated.

The changes in length, width, thickness and weight were monitored in regular intervals of ca. 40 h. After 120 h, the membrane strips were regenerated in 0.5 M NaCl for another 120 h to check for irreversible swelling of the membranes.

### 9.3.2. Ethylene Glycol Retention

To quantify ethylene glycol retention in comparison to the water permeability of the tested membranes, diffusion dialysis experiments were conducted in a membrane cell. A sketch of the set-up is given in Figure 2. A 0.1 M  $\text{Na}_2\text{CO}_3$  mixed solvent (70 %w ethylene glycol + 30%w water) feed solution and an aqueous 0.1 M  $\text{Na}_2\text{CO}_3$  strip solution were separated by the tested electro dialysis membrane. The circular membrane area of the set-up was  $23.59 \text{ cm}^2$ . The solution compartments of the membrane cell had volumes of ca. 10 ml each, and the starting volume of each solution was 500 ml. The solutions were circulated through the membrane cell by dosage pumps at high rate, to make the influence of the concentration boundary layer on the membrane surface insignificant. The refraction index of the feed and the strip solution was measured every hour and the ethylene glycol concentration of the solution calculated from it, using the calibration line given in the addendum, see Figure 16.

The amounts of feed and strip solution were monitored by weighing every 8 hours.

The experimental duration was varied between 70 and 170 hours depending on the observed ethylene glycol permeation.

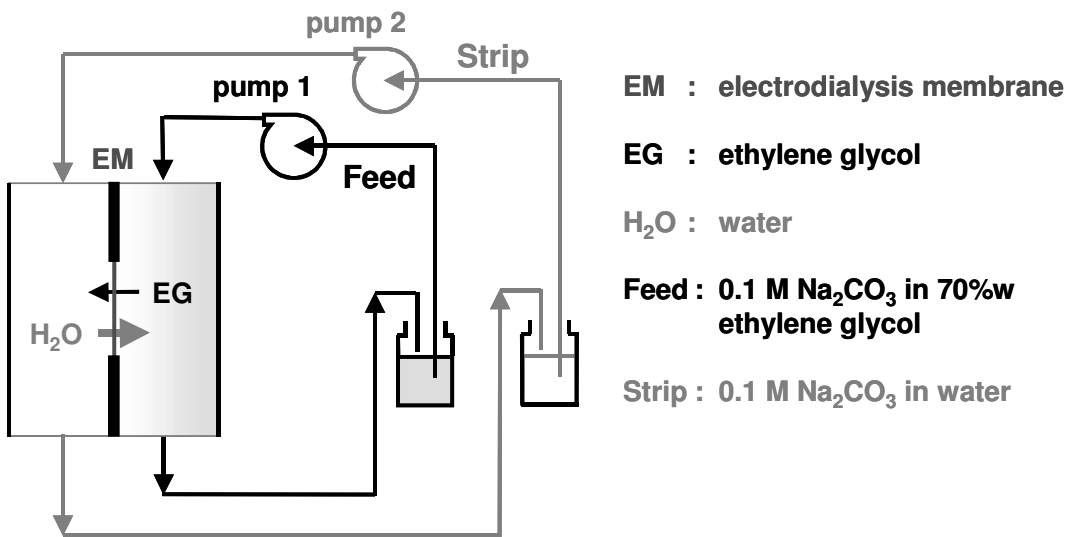


**Figure 9-2:** Diffusion dialysis set-up for testing ethylene glycol retention

### 9.3.3. Membrane Electrical Resistance Measurement

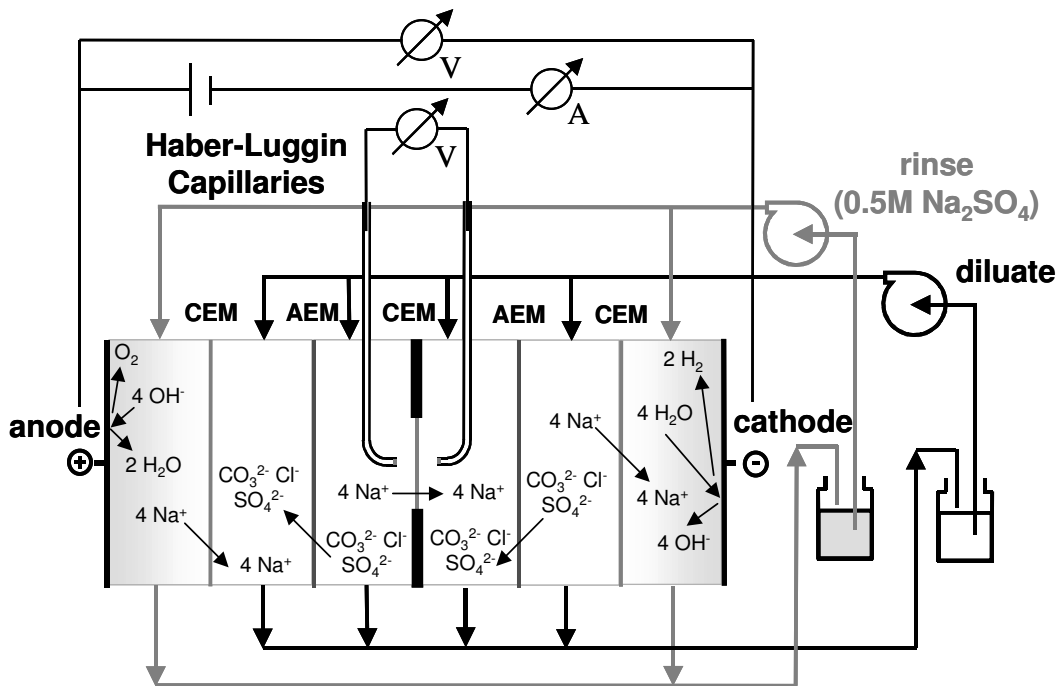
The resistance of the tested membranes was measured in 2 different solutions:

An aqueous 6 %w  $\text{Na}_2\text{CO}_3$  solution containing 0.5 %w  $\text{NaCl}$  and 0.25 %w  $\text{Na}_2\text{SO}_4$ , and a mixed solvent solution containing 6 %w  $\text{Na}_2\text{CO}_3$ , 0.5 %w  $\text{NaCl}$  and 0.25 %w  $\text{Na}_2\text{SO}_4$ .

The mixed solvent consisted of 70 %w ethylene glycol (based on salt free solvent)

$\text{NaCl}$  and  $\text{Na}_2\text{SO}_4$  were added in levels that were expected to accumulate in the soda recrystallization processes. The concentration of  $\text{Na}_2\text{CO}_3$  is the saturation concentration of soda in the mixed solvent. Aqueous 0.5 M  $\text{Na}_2\text{SO}_4$  solution was circulated through the electrode compartments as rinse solution.

Between experiments, the membranes were equilibrated and stored in aqueous 6 %w  $\text{Na}_2\text{CO}_3$  solution. In the mixed solvent experiments, they would equilibrate in the stack.



- diluate: a) 6 %w  $\text{Na}_2\text{CO}_3$ , 0.5 %w  $\text{NaCl}$ , 0.25 %w  $\text{Na}_2\text{SO}_4$  in water**  
**b) 6 %w  $\text{Na}_2\text{CO}_3$ , 0.5 %w  $\text{NaCl}$ , 0.25 %w  $\text{Na}_2\text{SO}_4$  in mixed solvent**

**Figure 9-3:** Electrodialysis set-up for measuring the electrical resistance of the tested membranes; displayed is the membrane arrangement for the measurement of a cation exchange membrane (CEM)

They were left in the stack for 2 hours before measurements to allow them to swell to their equilibrium condition. A schematic of the experimental set-up is given in Figure 3. The tested membrane sample had a surface area of  $3.14 \text{ cm}^2$  and was placed between two Haber–Luggin-capillaries. The distance between the capillaries was 6.6 mm, to allow for some bulging of the swollen membrane. The voltage between the electrodes of the stack was set externally, and the current through the stack and the voltage drop between the Haber-Luggin-capillaries was measured. The other membranes of the stack had a surface area of  $23.59 \text{ cm}^2$ , to allow an even ion flux throughout the stack.

The conductivity of the test solutions was monitored throughout the experiments. The conductivity of the aqueous solution was  $59.5 \text{ mS/cm}$  ( $0.168 \text{ }\Omega\cdot\text{m}$ ) and of the mixed solvent solution was  $7.25 \text{ mS/cm}$  ( $1.33 \text{ }\Omega\cdot\text{m}$ ).

#### **9.3.4. Selectivity of the Ion Exchange Membranes**

The selectivity of the ion transport through the ion exchange membranes was tested in small electro dialysis stacks of 3 CEM and 2 AEM, see Figure 4. The strip solution (concentrate) consisted initially of  $0.1 \text{ M}$  aqueous  $\text{Na}_2\text{CO}_3$  solution, the rinse solution of the electrode chambers of  $0.5 \text{ M}$  aqueous  $\text{Na}_2\text{SO}_4$  solution. The test solution, containing  $60 \text{ g/l}$   $\text{Na}_2\text{CO}_3$ ,  $5 \text{ g/l}$   $\text{NaCl}$  and  $2.5 \text{ g/l}$   $\text{Na}_2\text{SO}_4$  in either water or 70%w ethylene glycol mixed solvent, was fed into the diluate chambers of the stack. Each membrane in the stack had a surface area of  $23.59 \text{ cm}^2$ , while the chamber width between membranes and between membranes and electrodes was app. 20 mm. The stack voltage (on the electrodes) was adjusted to achieve a constant current density of ca.  $30 \text{ mA/cm}^2$  ( $300 \text{ A/m}^2$ ) in all experiments, which was known from the electrical resistance measurements to be at least 10% below the lowest limiting current density of the tested membranes (i.e.  $i_{\text{lim}}$  for Neosepta CM-2 in the mixed solvent carbonate solution, see Figure 11).

The conductivity of the diluate, concentrate and rinse solution was measured in 30-min. intervals to monitor the progress of the desalination. Additionally, samples of the diluate, concentrate and rinse solution were taken in 30 min. intervals for later determination of their  $\text{CO}_3^{2-}$ ,  $\text{SO}_4^{2-}$  and  $\text{Cl}^-$  concentrations by HPLC.

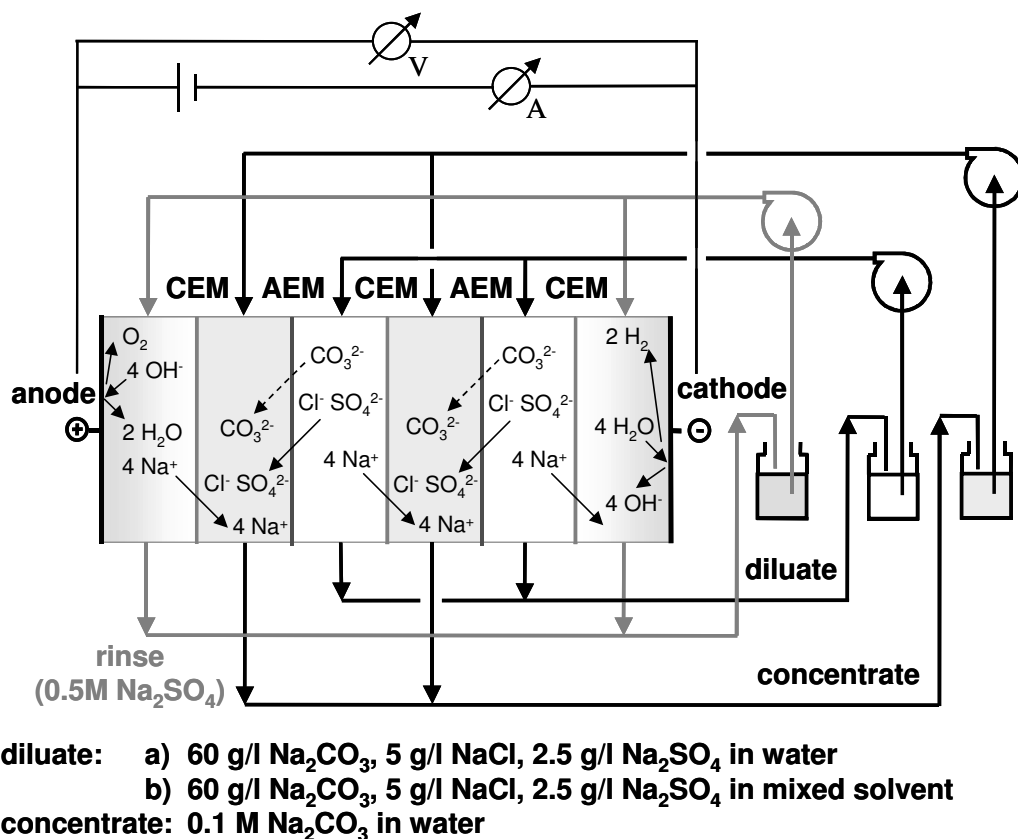


**Figure 9-4:** Experimental set-up for measuring the selectivity of the ion transport by electrodesialysis

The experiments were stopped, when the conductivity of the concentrate reached app. 30 mS/cm.

## 9.4. Results

### 9.4.1. Membrane Swelling

The relative degrees of swelling in aqueous 0.1 M  $\text{Na}_2\text{CO}_3$ , in 70 %-w ethylene glycol mixed solvent and in 0.1 M  $\text{Na}_2\text{CO}_3$  in 70 %-w ethylene glycol and after regeneration for the swelling experiments in 0.1 M  $\text{Na}_2\text{CO}_3$  in 70 %-w ethylene glycol are given in Figure 5 and 6. Volume based swelling is given in Figure 5, and weight based swelling is given in Figure 6. The volume based swelling, according to Eq. 18, yields the more physically correct quantity. It is derived from the 3 separate measurements of length, breadth and

thickness, which were each subject to some degree of analytical uncertainty. Therefore, the weight-based swelling is given to confirm the observed tendencies.

Little or no additional swelling occurred with the membrane samples immersed in demineralized water. It was found that all membranes except Neosepta ACM swelled to at least a moderate degree (i.e. +2 %-vol) in the other 3 tested solutions. Although some swelling was found for Neosepta ACM in the 0.1 M Na<sub>2</sub>CO<sub>3</sub> mixed solvent solution, for all other solutions the membrane sample shrunk by ca. 5 %-vol compared to the reference state.

The highest degree of swelling occurred for all membranes in the 0.1 M Na<sub>2</sub>CO<sub>3</sub> mixed solvent solution. No irreversible swelling was observed, although the degree of swelling for FT-AM-A (with up to +24 %-vol) was rather high. The increase in length and breadth of this membrane of app. 5 % of the starting length due to swelling in the soda mixed-solvent solution is problematic for the installation of the membrane in a stack, as it can result in bulging, wrinkling and distortion of the membrane. This might not only cause gaps between the membrane and the diluate/concentrate chamber spacers and flow maldistribution, but also might result in physical damage to the membrane. Also Neosepta CM-2 and AM-3 show a noticeable amount of swelling in the soda mixed solvent solution and might be subject to the same problems.

Neosepta AMX and FT-CM-A displayed the least degree of additional swelling with 8 %-vol and 2.5 %-vol, respectively.

Also Pourcelly et al. [12] noted an increase of less than 10% in area due to swelling for the tested (homogeneous) Nafion 117 membrane in ethylene glycol. The other organic co-solvents tested in their work, tetrahydrofurane (THF) and N-methylformamide (NMF), caused significantly higher degrees of swelling (e.g. +60% area for 70%-vol THF mixed solvent, +24% area for 70%-vol NMF mixed solvent).

Another observation made during the swelling experiments was the discoloration of some of the membrane samples during exposure to the test solution. This discoloration was homogeneous on the whole membrane area exposed to the test solution.

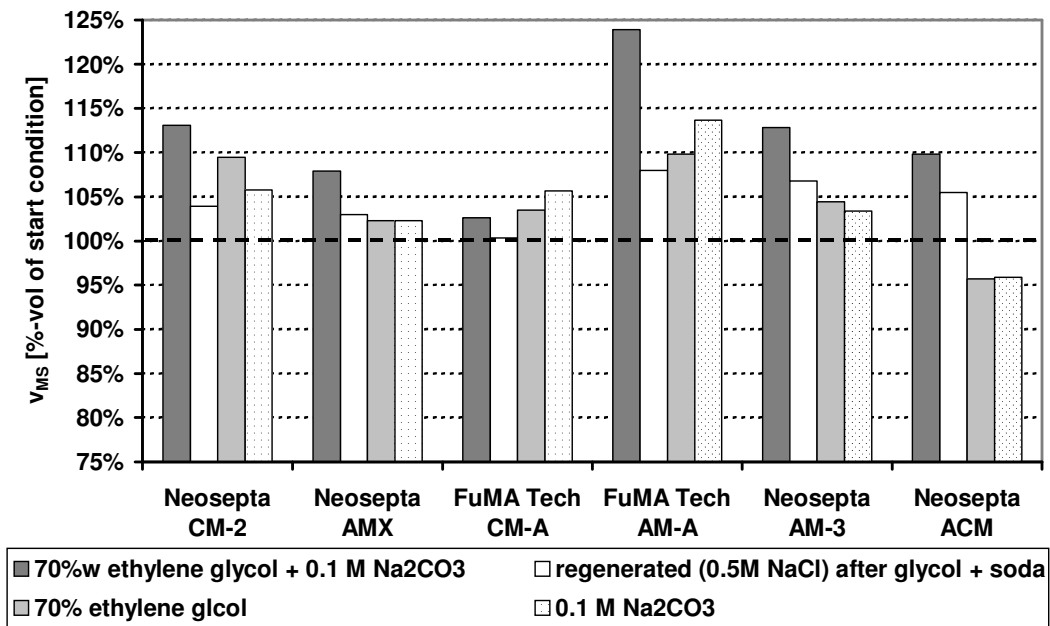


**Figure 9-5:** Volume based relative swelling of the tested membranes in aqueous 0.1 M Na<sub>2</sub>CO<sub>3</sub>, in 70 %-w ethylene glycol mixed solvent and in 70 %-w ethylene glycol + 0.1 M Na<sub>2</sub>CO<sub>3</sub>

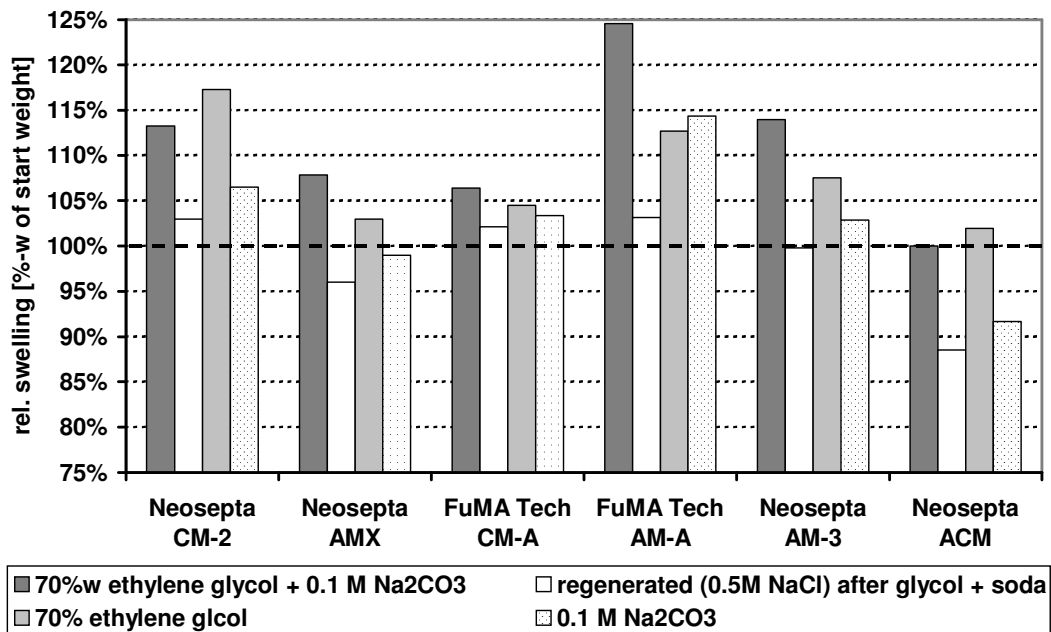


**Figure 9-6:** Weight based relative swelling of the tested membranes in aqueous 0.1 M Na<sub>2</sub>CO<sub>3</sub>, in 70 %-w ethylene glycol mixed solvent and in 70 %-w ethylene glycol + 0.1 M Na<sub>2</sub>CO<sub>3</sub>

**Table 9-2:** Membrane discoloration during exposure to the test solutions

Membrane	demineralized water	70 %-w glycol	0.1 M Na <sub>2</sub> CO <sub>3</sub>	70 %-w glycol 0.1 M Na <sub>2</sub> CO <sub>3</sub>
Neosepta CM-2	no	no	no	no
Neosepta AM-3	no	yellow	brown	brown
Neosepta AMX	no	brown	light brown	dark brown
Neosepta ACM	no	no	no	no
FT-CM-A	bleached	no	light brown	brown
FT-AM-A	no	no	brown	no

The effect was particularly strong for Neosepta AMX in the soda mixed solvent solution, which turned the membrane irreversibly to a dark brown color. A similar discoloration was observed with Neosepta AM-3 in the soda mixed solvent solution and in the aqueous 0.1 M Na<sub>2</sub>CO<sub>3</sub> solution. The discoloration of FT-CM-A was less severe for the soda mixed solvent solution, but more intense in the aqueous 0.1 M Na<sub>2</sub>CO<sub>3</sub> solution. All these discolorations did not disappear with the regeneration. As can be seen from the overview given in Table 2, the discoloration appears to be in general to be caused by the Na<sub>2</sub>CO<sub>3</sub> rather than by the ethylene glycol.

This discoloration indicates an irreversible (chemical) change of the membranes and especially Neosepta AM-3 and AMX as well as FT-CM-A appear susceptible to it. No indication of the nature of this change and its effect on the membrane performance can be given.

#### 9.4.2. Ethylene Glycol Retention

Since the membranes were not equilibrated with the used strip and feed solution, they were changing their state of swelling in the first hours of the dialysis experiments. Since the degree of swelling greatly affects the porosity and thereby permeability of the membrane, all mass transfer calculations are based on data obtained after 24 hours of experimental run time, to ensure that the membrane had achieved an equilibrium state.

Since permeation was slow, experimental times of at least 70 hours were required to properly quantify the mass flows in the diffusion cell experiments.



### Neosepta CM-2

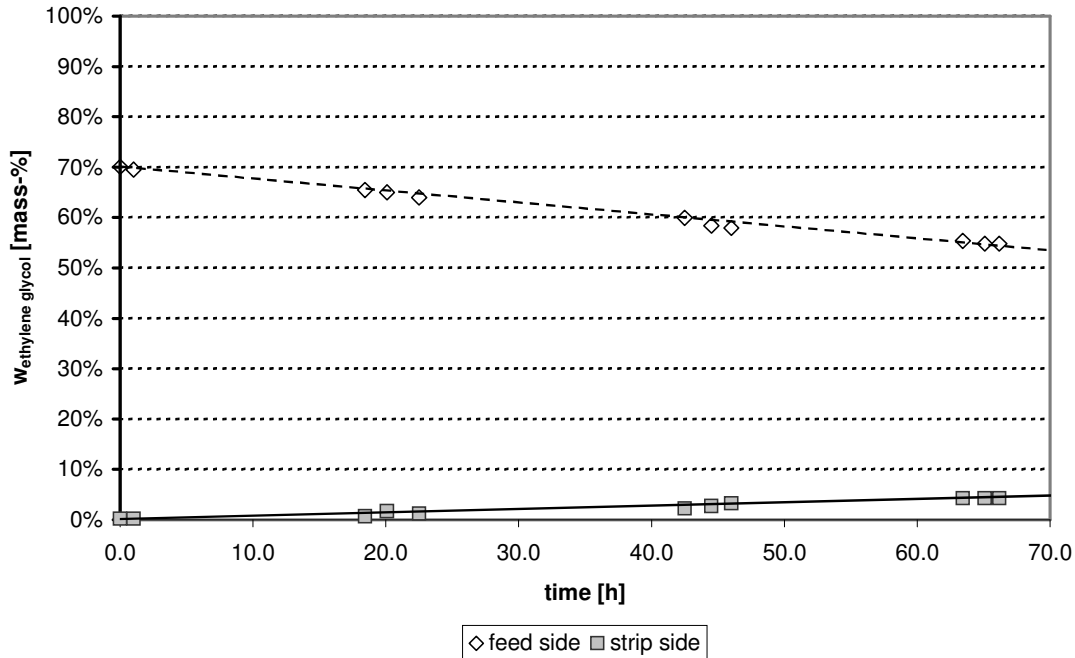


**Figure 9-7:** Concentration – time profiles (%-w ethylene glycol) for the feed (0.1 M Na<sub>2</sub>CO<sub>3</sub> in 70 %-w ethylene glycol) and the strip (aqueous 0.1 M Na<sub>2</sub>CO<sub>3</sub>) of the diffusion dialysis experiment with Neosepta CM-2

An impression of the concentration development in the feed and in the strip can be gained from Figure 7, which displays the concentration–time profiles for the Neosepta CM-2 membrane.

The amount of ethylene glycol and water in the feed and in the strip was calculated for each time step. From the changes in these amounts with time, the flow of ethylene glycol and of water through the membrane was calculated.

$$\text{e.g.: } \frac{dm_{EG}(t_2)}{dt} = \left( \frac{m_{EG}(t_2) - m_{EG}(t_1)}{t_2 - t_1} \right)_{\text{feed}} \equiv - \left( \frac{m_{EG}(t_2) - m_{EG}(t_1)}{t_2 - t_1} \right)_{\text{strip}} \quad \text{Eq. 9-19}$$

From the so obtained fluxes, the membrane area and the mean concentration difference as driving force, an overall mass transport coefficient  $k_D$  for the membrane was calculated:

$$\text{e.g.: } k_{D,EG} \cdot M_{EG} \cdot A_M \cdot (c_{EG,feed}(t) - c_{EG,strip}(t)) = \frac{dm_{EG}(t)}{dt} \quad \text{Eq. 9-20}$$

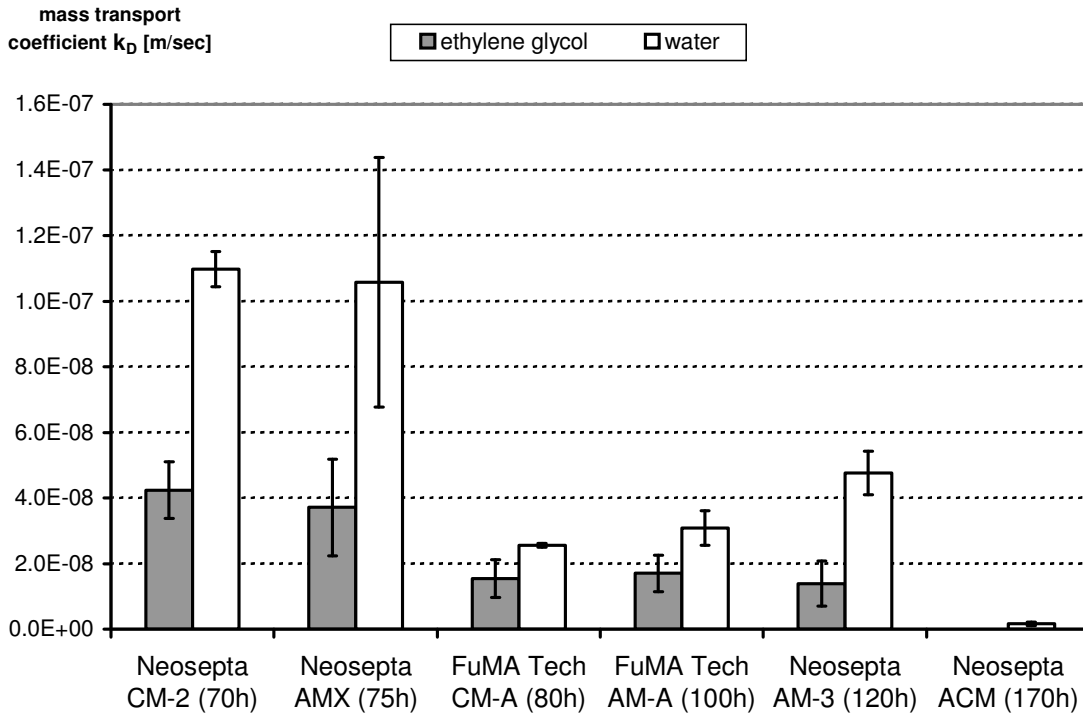


**Figure 9-8:** Mass transport coefficients for water and ethylene glycol for the tested membranes. Experimental duration is given in parentheses on the x-axis

The mass transport coefficient provides a driving force and time independent measure of the water and ethylene glycol permeability of the membranes.

As was expected, the ethylene glycol diffused from the feed into the strip and the water diffused from the strip to the feed. It was generally found that the flow of water was greater, than the flow of ethylene glycol.

The calculated  $k_D$  values are given in Figure 8 and in Table 3.

As can be seen from Figure 8, Neosepta CM-2 and AMX showed the highest water permeability, but at the same time also the highest ethylene glycol permeability. The water permeability of the FuMA Tech membranes was significantly lower as well as their ethylene glycol permeability. The Neosepta AM-3 membrane showed ethylene glycol retention similar to the FuMA Tech membranes, while having a slightly better water permeability. The extremely low water and ethylene glycol permeability of the Neosepta ACM membrane combined with the fact that it did not show any increase in swelling like the other membranes, indicates that this membrane does not adapt well to the sodium

carbonate solution nor the mixed solvent. It is very likely that the poor mass transfer characteristic of this membrane in the given solutions is due to a lack of swelling and solution exchange with the surrounding bulk solution.

The given  $k_D$  values are sufficient to evaluate ethylene glycol loss and mixed solvent dilution, for the given application. In the actual electro dialysis stack, there might occur a slight loss of mixed solvent with the solvation hulls of the transported ions in addition to ethylene glycol diffusion.

The  $k_D$  values do not yield generally applicable mass transfer characteristics of the tested membranes, though, since they only imply Fick diffusion, i.e. the effect of the other present species on the diffusion is not considered. Since water and ethylene glycol are diffusing counter-currently through the membrane pores with mass flows of roughly the same order of magnitude, it is logical, that they will impede each other. This type of diffusion is best described by the Maxwell-Stefan approach [22, 23]. This approach is very fundamental, balancing the gradient of the (chemical potential) driving force against the occurring friction forces (with other species). The diffusion coefficient is defined as an inverse friction coefficient between the diffusing species (i) and the components of the surrounding medium (j). The friction is proportional to the relative velocity of the diffusing species:

$$-\frac{\partial(\mu_i/R \cdot T)}{\partial y} = \sum_j x_j \cdot \frac{v_j - v_i}{D_{ij}} \quad \text{Eq. 9-21}$$

The gradient of the chemical potential resulting from a concentration gradient can be expressed as:

$$\frac{\partial(\mu_i/R \cdot T)}{\partial y} = \frac{\partial(\ln(\gamma_i \cdot x_i))}{\partial y} \approx \frac{\ln\left(\frac{\gamma_i(\delta) \cdot c_i(\delta)}{\gamma_i(0) \cdot c_i(0)}\right)}{\delta} \approx \frac{\ln(c_i(\delta)/c_i(0))}{\delta} \quad \text{Eq. 9-22}$$

For our case, the diffusion path length  $\delta$  can be set equal to the membrane thickness, since the feed and strip compartments are well mixed and the widths of the concentration border layers on the membrane surfaces are therefore far smaller than the membrane thickness.

The Na<sub>2</sub>CO<sub>3</sub>, present in both solutions, might cause an additional diffusive flux, but since its driving force should be rather low, as both solutions contain 0.1 M Na<sub>2</sub>CO<sub>3</sub>, this flux is considered negligible, compared to uncertainties of the component and mass balance, for the following considerations.

This yields for our ethylene glycol – water diffusion the following 2 relationships:

$$-\frac{\ln\left(\frac{C_{EG,strip}}{C_{EG,feed}}\right)}{\delta_M} = x_{H_2O} \cdot \frac{v_{H_2O} - v_{EG}}{D_{H_2O,EG}} + x_M \cdot \frac{0 - v_{EG}}{D_{EG,M}} \quad \text{Eq. 9-23}$$

$$-\frac{\ln\left(\frac{C_{H_2O,feed}}{C_{H_2O,strip}}\right)}{\delta_M} = x_{EG} \cdot \frac{v_{EG} - v_{H_2O}}{D_{EG,H_2O}} + x_M \cdot \frac{0 - v_{H_2O}}{D_{H_2O,M}} \quad \text{Eq. 9-24}$$

The species velocities are calculated from the mass flows by:

$$v_i = \frac{dm_i/dt}{\rho_i \cdot A_M} \quad \text{Eq. 9-25}$$

The positive direction of the velocity (vector) is defined as the direction of the considered diffusive flow. Therefore,  $v_{H_2O}$  and  $v_{EG}$  are actually added in value in the equations above, since their diffusive flows are countercurrent.

As the driving forces as well as the mass flows remain almost constant throughout the performed diffusion dialysis experiments, the exact values of the diffusion coefficients  $D_{EG,H_2O}$ ,  $D_{EG,M}$  and  $D_{H_2O,M}$  could not be extrapolated from the obtained data sets. Assuming, that either the friction of the countercurrent flow of ethylene glycol and water or the membrane friction between the diffusing species and the “pore walls” of the membrane is dominating the mass transfer resistance, the dominating diffusion coefficient can be estimated as either:

$$D_{H_2O,EG} = x_{H_2O} \cdot \delta_M \cdot \frac{|v_{H_2O}| + |v_{EG}|}{-\ln\left(\frac{C_{EG,strip}}{C_{EG,feed}}\right)} \equiv x_{EG} \cdot \delta_M \cdot \frac{|v_{EG}| + |v_{H_2O}|}{-\ln\left(\frac{C_{H_2O,feed}}{C_{H_2O,strip}}\right)} \quad \text{Eq. 9-26}$$

or

$$D_{EG,M} = x_M \cdot \delta_M \cdot \frac{|v_{EG}|}{-\ln\left(\frac{c_{EG,strip}}{c_{EG,feed}}\right)} \quad \text{Eq. 9-27}$$

$$D_{H_2O,M} = x_M \cdot \delta_M \cdot \frac{|v_{H_2O}|}{-\ln\left(\frac{c_{H_2O,feed}}{c_{H_2O,strip}}\right)} \quad \text{Eq. 9-28}$$

An overview of the calculated diffusion coefficients  $D_{EG,H_2O}$  is given in Figure 9 for each of the tested membranes. The calculated diffusion coefficients  $D_{EG,M}$  and  $D_{H_2O,M}$  are displayed in Figure 10. As can be seen from Figure 9, the calculated diffusion coefficients for the ethylene glycol driving force ( $D_{EG,H_2O}$ ) and the driving force of the water ( $D_{H_2O,EG}$ ) do not match each other as exactly as should be expected, if the fluid friction was the dominating mass transfer resistance. Still the agreement between them is noticeable: They do not differ by more than a factor of 2. The calculated values of the diffusion coefficients vary significantly between the different membranes, although this diffusion coefficient should be actually independent of the membrane. The reason for this variation might lie in the differences in free area for diffusion in the different membranes: The diffusing species can only pass through the area of membrane pores, while the area of the “pore walls”, i.e. the polymer matrix, of the membrane is impermeable. To convert the binary diffusion coefficient calculated by Eq. 26 into the generally valid diffusion coefficient, it would have to be corrected for the tortuosity of the membrane pores. For comparison, the water – ethylene glycol diffusion coefficient is estimated with the well-known Wilke-Chang equation [24]:

$$D_{is} = 7.4 \cdot 10^{-8} \cdot \frac{\sqrt{\psi_s \cdot M_s \cdot T}}{\eta \cdot V_{m,i}^{0.6}} \quad [\text{m}^2/\text{s}] \quad \text{Eq. 9-29}$$

$D_{is}$  represents the diffusion coefficient of the dissolved species  $i$  through the solvent  $s$ . In the Wilke-Chang equation, the viscosity  $\eta$  should be entered in [mPa·s] and the molar volume at the atmospheric boiling point as [cm<sup>3</sup>/mol]. The association factor  $\psi_s$  is a correction factor for the self-association of the solvent. For water it has a value of 2.3, for methanol a value of 1.8, for ethanol 1.5 and for non-associating solvents 1.0. For ethylene

glycol an association factor of 1.8 is used. The Wilke-Chang equation yields the following diffusion coefficients for dilute solutions:

Ethylene glycol diffusing in water:

$$D_{EG,H_2O} = 1.33 \cdot 10^{-9} \text{ m}^2/\text{s}$$

Water diffusing in ethylene glycol:

$$D_{H_2O,EG} = 1.94 \cdot 10^{-9} \text{ m}^2/\text{s}$$

As can be seen from Figure 9, the values of  $D_{EG,H_2O}$  calculated by Eq. 26 are by 2 to 3 orders of magnitude lower than the diffusion coefficients predicted by Wilke-Chang, Eq. 29. Even taking some degree of tortuosity, i.e. increased diffusion path length in the membrane (e.g. Rautenbach [25] suggests a tortuosity factor of  $25/12 \approx 2.08$ , while Marshall [26] proposes the following relationship between tortuosity  $\tau$  and porosity  $\epsilon$ :  $\tau = \epsilon^{-1.5}$ . With a porosity of the tested Neosepta membranes of ca. 40% [16], this yields a tortuosity of ca. 4.) into account, these effects do not explain this strong decrease in diffusivity.

Also Wesselingh [22] states, that diffusion coefficients in porous media are lowered by around 1 to 2 orders of magnitude. Based on Maxwell-Stefan diffusion calculations and aqueous ion exchange membrane diffusion data by Narebska et al. [27 - 29] and Scattergod et al. [30], Wesselingh [23] found a tortuosity-reduced water diffusion coefficient of app.  $5 \cdot 10^{-10} \text{ m}^2/\text{s}$  for electrodialysis membranes.

It is therefore more likely, that the friction with the membrane “walls”, according to Eq. 27 and Eq. 28, is the dominating diffusion resistance. In Figure 10, the diffusion coefficients for water are higher by 2 factors of magnitude than those for ethylene glycol. This appears plausible, considering the polar nature of the membrane pores compared to the rather low polarity of the glycol. The glycol would rather be attracted by the apolar polymer lattice [15]. Such an interaction with the immobile polymer would increase the friction for diffusion of ethylene glycol through the membrane.

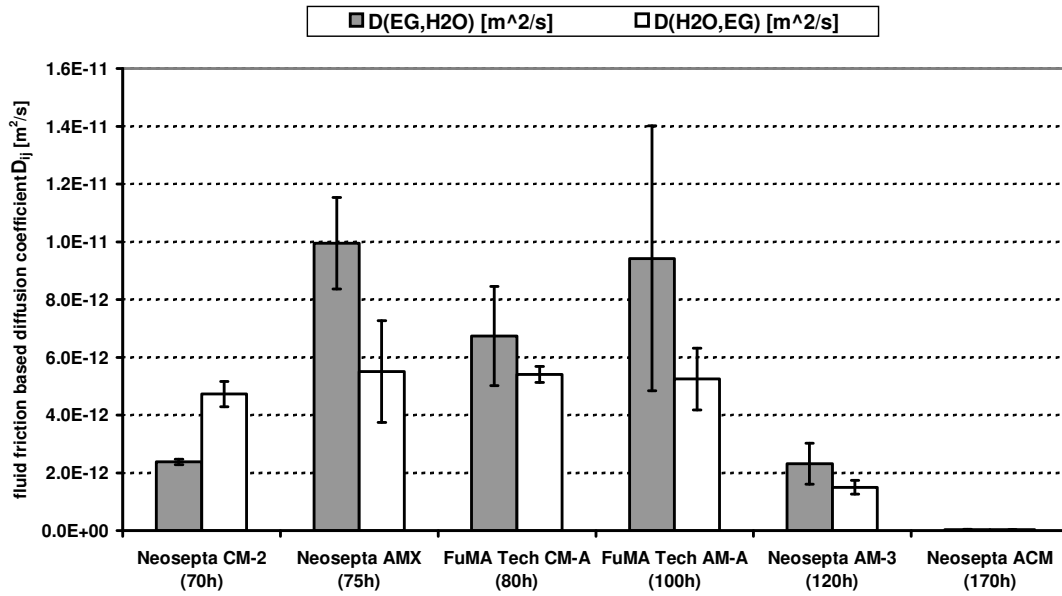


**Figure 9-9:** Fluid friction based diffusion coefficient  $D_{EG,H_2O}$  calculated for the performed diffusion dialysis experiments. The gray columns represent the values of the coefficient calculated based on the ethylene glycol driving force, the white columns those based on the driving force of the water

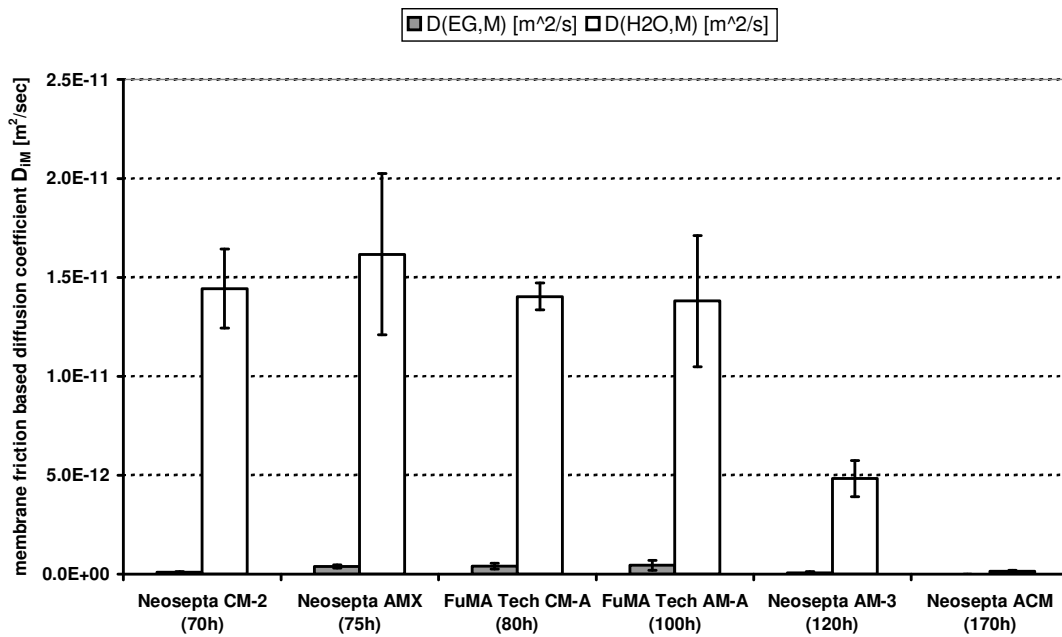


**Figure 9-10:** Membrane friction based diffusion coefficients  $D_{EG,M}$  and  $D_{H_2O,M}$  for the tested ion exchange membranes

**Table 9-3:** Membrane mass transfer parameters obtained from the diffusion cell experiments.

Membrane	$k_{D,EG}$ [m/sec]	$k_{D,H_2O}$ [m/sec]	$D_{EG,M}$ [m/sec]	$D_{H_2O,M}$ [m/sec]	$\delta_M$ [ $10^{-3}m$ ]
Neosepta CM-2	$4.24 \cdot 10^{-8}$	$1.10 \cdot 10^{-7}$	$1.01 \cdot 10^{-13}$	$1.44 \cdot 10^{-11}$	0.125
Neosepta AM-3	$1.39 \cdot 10^{-8}$	$4.76 \cdot 10^{-8}$	$7.83 \cdot 10^{-14}$	$4.84 \cdot 10^{-12}$	0.105
Neosepta AMX	$3.71 \cdot 10^{-8}$	$1.06 \cdot 10^{-7}$	$3.90 \cdot 10^{-13}$	$1.62 \cdot 10^{-11}$	0.160
Neosepta ACM	$-2.30 \cdot 10^{-9}$	$1.61 \cdot 10^{-9}$	$-9.75 \cdot 10^{-15}$	$1.47 \cdot 10^{-13}$	0.110
FT-CM-A	$1.54 \cdot 10^{-8}$	$2.55 \cdot 10^{-8}$	$4.21 \cdot 10^{-13}$	$1.40 \cdot 10^{-11}$	0.620
FT-AM-A	$1.70 \cdot 10^{-8}$	$3.08 \cdot 10^{-8}$	$4.58 \cdot 10^{-13}$	$1.38 \cdot 10^{-11}$	0.500

The diffusion coefficient  $D_{H_2O,M}$  for Neosepta CM-2 and AMX and FuMA Tech CM-A and AM-A is  $1.4 \cdot 10^{-11} \text{ m}^2/\text{s}$ , which is only app. 1 order of magnitude smaller than the  $5 \cdot 10^{-10} \text{ m}^2/\text{s}$  found by Wesselingh [23]. This decrease can be explained by the ethylene glycol swelling of the polymer lattice and the hydrophilic interaction between the bound ethylene glycol and the diffusing water. These effects would increase tortuosity and “wall” friction for water.

The calculated values for the membrane friction based diffusion coefficients  $D_{EG,M}$  and  $D_{H_2O,M}$ , as well as the mass transfer coefficients  $k_D$  calculated with the simplified model of Eq. 20 are given in Table 3.

It has to be noted that the given diffusion and transport coefficients for the Neosepta ACM membrane are negative, which is physically highly unlikely [23]. This effect is most likely either caused by the analytical uncertainty considering the very low flows in these experiments, or the friction caused by the countercurrent diffusion of ethylene glycol and water was not negligible in these experiments. The ethylene glycol was “washed back” by the stronger water diffusion stream.

### 9.4.3. Membrane Electrical Resistance Measurement

The electrical resistance  $r_{\text{gap}}$  of the gap between the Haber-Luggin-capillaries was calculated from the voltage drop  $U_{\text{gap}}$  between the Haber-Luggin-capillaries, see Figure 2, and the current density  $i$  through the membrane stack:



$$r_{gap} = \frac{U_{gap}}{i} \quad [\Omega \cdot m^2] \quad \text{Eq. 9-30}$$

This resistance was measured for both aqueous and mixed solvent solution with and without a test-membrane between the Haber-Luggin-capillaries. The electrical resistance of the membrane  $r_M$  was calculated from the difference of the resistance measured with and without the membrane:

$$r_M = r_{gap+M} - r_{gap,sol} + \rho_{sol} \cdot \delta_M \quad \text{Eq. 9-31}$$

with  $\rho_{sol}$  [ $\Omega \cdot m$ ] the specific resistance of the solution per meter. Since the solution proved far more conductive than the membrane, the correction term  $\rho_{sol} \cdot \delta_M$  could be neglected and the membrane resistance calculated as:

$$r_M = r_{gap+M} - r_{gap,sol} \quad \text{Eq. 9-32}$$

It was found, that the membrane resistance varied between  $(0.2 \text{ to } 1.5) \cdot 10^{-3} \Omega \cdot m^2$  in aqueous solution. In the mixed solvent solution, the resistances were higher by a factor of magnitude and ranged between  $(3 \text{ to } 11) \cdot 10^{-3} \Omega \cdot m^2$ , see Figure 11. An exception was the Neosepta ACM membrane, which displayed resistances of  $0.575 \Omega \cdot m^2$  in aqueous and  $1.90 \Omega \cdot m^2$  in mixed solvent solution, which is another indication, that this membrane was insufficiently swollen and not in an operational state for electro dialysis.

The lowest resistance in the mixed solvent was found for the Neosepta CM-2, followed by the Neosepta AMX, which already displayed more than twice the resistance of the CM-2. Both FuMA Tech membranes had slightly higher resistances, than the Neosepta AMX. The Neosepta AM-3 membrane was not tested, as it already displayed poorer water permeability in the diffusion test than the Neosepta CM-2 and AMX membranes as well as the FuMA Tech CM-A and AM-A membranes. This already indicated that the AM-3 membrane also would have a higher electrical resistance than the Neosepta CM-2 and AMX membranes.

The resistance of the even less water permeable Neosepta ACM membrane was actually only measured to gain an impression of the degree of electrical resistance this poorly swollen membrane would offer and whether the mixed solvent would affect its resistance.

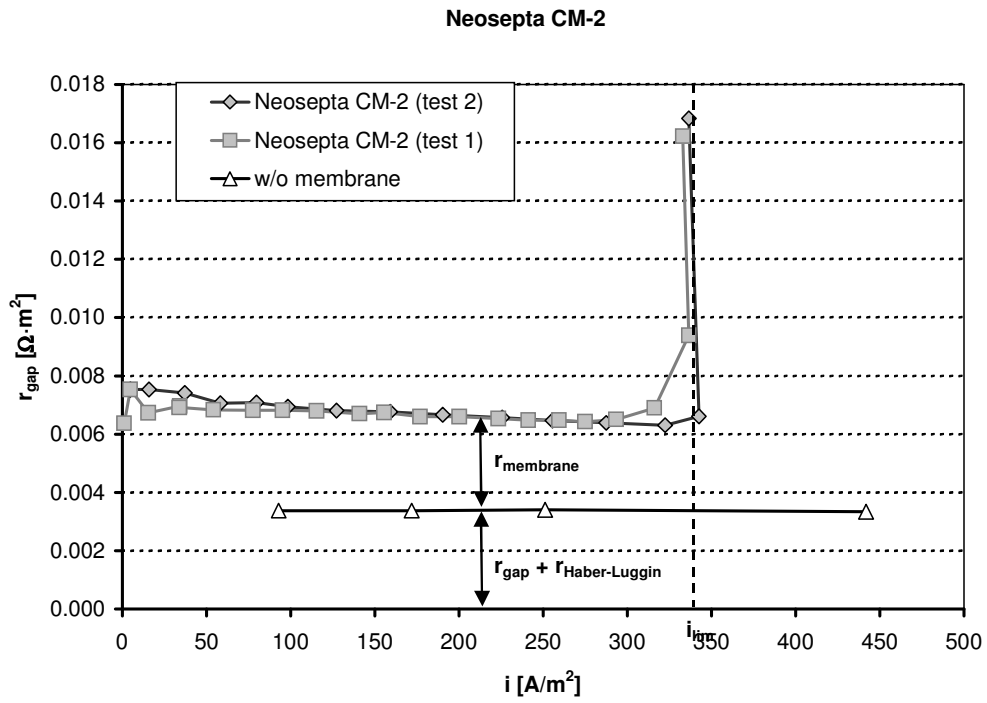
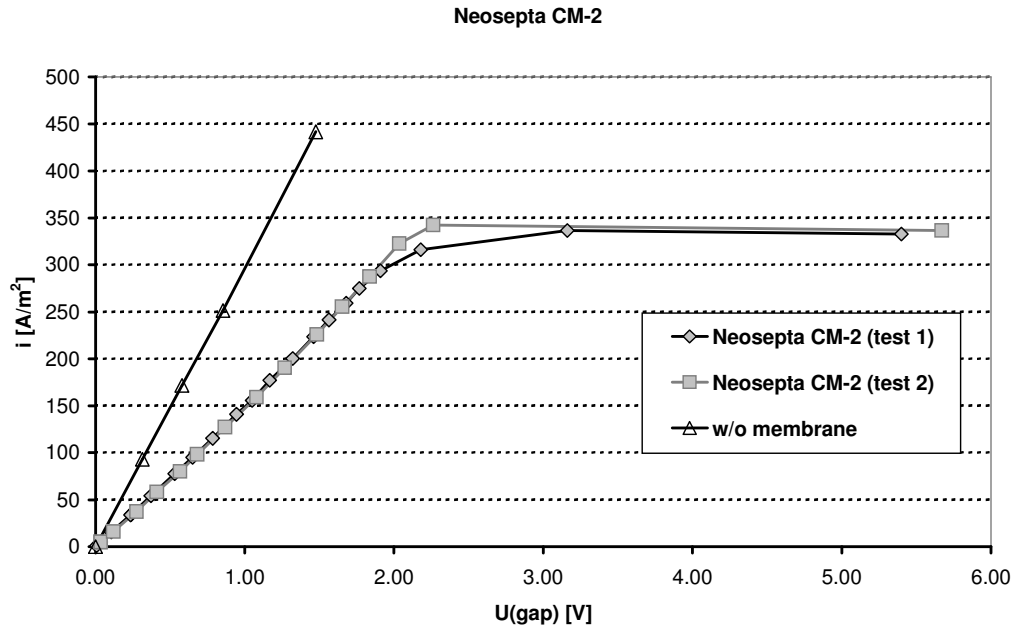


**Figure 9-11:** Current-voltage curve and resistance-current density curve for the measurement of the Neosepta CM-2 membrane

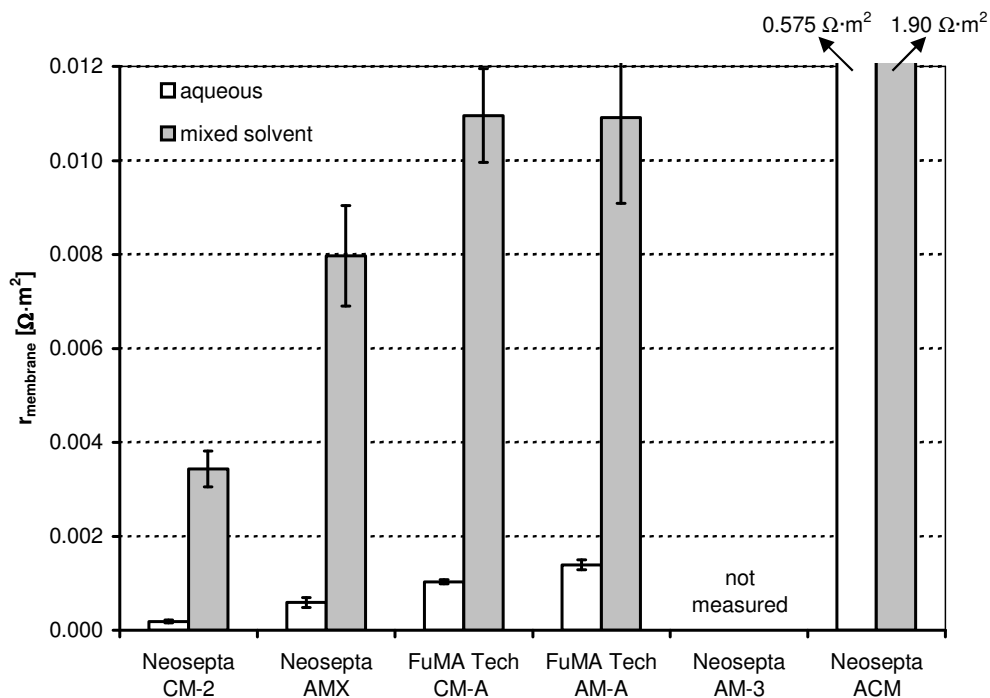


**Figure 9-12:** Membrane specific electrical resistance in aqueous and mixed solvent carbonate solution, containing chloride and sulfate

Although the membrane did show no significant change in its degree of swelling in the mixed solvent, see Figures 5 and 6, it certainly takes up mixed solvent as its increase in electrical resistance, see Figure 12, clearly indicates.

It should be noted from Figure 11 that the current density did not increase beyond the limiting current density with further increase of the voltage. I.e. no effect like water splitting occurred in the mixed solvent, despite the fact that the mixed solvent contained 30%w (salt-free solvent) water. This is attributed to the hygroscopic, but rather apolar nature of the ethylene glycol: The water is bound/complexed by the ethylene glycol, which prohibits it from participating in e.g. the protonation/deprotonation membrane surface reactions, that are thought to cause water splitting [31 - 34].

The low resistance of the Neosepta CM-2 is most likely the result of the presence of the monovalent sodium ion, which should have a higher mobility in the CEM than the divalent carbonate ions in the AEM.

**Table 9-4:** Overview of the electrical resistance of the tested membranes in the mixed solvent and in the aqueous carbonate solution as well as resistance ranges provided by the producers

Membrane	$r_M [\Omega \cdot m^2]$ (mixed solvent)	$r_M [\Omega \cdot m^2]$ (aqueous)	$r_M [\Omega \cdot m^2]$ ([20, 21])
Neosepta CM-2	$34.35 \cdot 10^{-4}$	$1.84 \cdot 10^{-4}$	$(2.0-4.5) \cdot 10^{-4}$
Neosepta AM-3	na	na	$(2.8-5.0) \cdot 10^{-4}$
Neosepta AMX	$79.69 \cdot 10^{-4}$	$5.93 \cdot 10^{-4}$	$(2.0-3.5) \cdot 10^{-4}$
Neosepta ACM	1.9022	0.5747	$(3.5-5.5) \cdot 10^{-4}$
FT-CM-A	$109.6 \cdot 10^{-4}$	$10.32 \cdot 10^{-4}$	$(5-9) \cdot 10^{-4}$
FT-AM-A	$109.1 \cdot 10^{-4}$	$13.93 \cdot 10^{-4}$	$(4-8) \cdot 10^{-4}$

The higher resistance of the heterogeneous FuMA Tech membranes stemmed most probably from the fact, that they had 4 to 5 times the thickness of the homogeneous Neosepta membranes, see Table 3. The effect of their thickness was most likely reduced by their greater degree of swelling, see Table 4, as their resistance was only slightly higher than that of the Neosepta AMX membrane.

From the obtained results, it appeared that a combination of Neosepta CM-2 and Neosepta AMX would provide the lowest overall electrical resistance.

It can be noted from Table 4, that while the resistances of the cation exchange membranes fairly matched the resistance range provided by the producers [20, 21] for aqueous solution, the resistances of the anion exchange membranes were noticeably higher than the producers' specifications. This was most likely due to the carbonate ions, which were the predominant anions in the solution. As carbonate is a weak acid anion and it might have complexed with the functional charges in the membrane.

The increases in membrane resistance from aqueous to mixed solvent solution were also higher than expected, if the aqueous solution ( $\rho_{aq} = 0.166 \Omega \cdot m$ ) was just replaced by mixed solvent solution ( $\rho_{MS} = 1.33 \Omega \cdot m$ ). Roughly, the conductivity of a membrane  $\lambda_M$  can be estimated from the conductivities of its functional components, the polymer lattice

and the pore solution and their relative free projected areas (i.e. orthogonal to the current) in the membrane:

$$\kappa_M = \frac{A_{poly}}{A_M} \cdot \kappa_{poly} + \frac{A_{pore}}{A_M} \cdot \kappa_{solution}, \text{ i.e.: } \frac{1}{\rho_M} = \frac{A_{poly}}{A_M} \cdot \frac{1}{\rho_{poly}} + \frac{A_{pore}}{A_M} \cdot \frac{1}{\rho_{solution}} \quad \text{Eq. 9-33}$$

Since the polymer lattice's conductivity is negligible, due to its lack of mobile charges, this yields:

$$\kappa_M = \frac{A_{pore}}{A_M} \cdot \kappa_{solution} = \frac{A_{pore}}{A_M} \cdot \frac{1}{\rho_{solution}} \quad \text{Eq. 9-34}$$

It should therefore be expected, that the resistance of a membrane in the mixed solvent was app. 8 times higher, i.e. the ratio of  $\rho_{MS} : \rho_{aq} = 8.01$ , than its resistance in aqueous solution. From the experiments it appeared, that the resistance in mixed solvent solution of Neosepta CM-2 was 18.7 times, of Neosepta AMX 13.4 times, of FuMA Tech CM-A 10.6 times and of FuMA Tech AM-A 7.8 times higher than in aqueous solution.

This indicates that especially for the Neosepta membranes not just the pore solution is replaced in the mixed solvent, but also other changes to the membranes occur, which reduce the conductivity. On the basis of this research 2 explanations can be offered for this slight additional increase in membrane resistance:

1. Ion exchange membranes are not homogeneous structures, but consist of the apolar (non-conductive) regions of the polymer-lattice and the polar (conductive) pore channels with the charged functional groups (electrolyte gel). Swelling of the apolar polymer-lattice by bonding of ethylene glycol could greatly increase the apolar volume fraction, block pore area and reduce the dielectric shielding of the charged functional groups and of the free ions in solution (the dielectric constant of ethylene glycol (41.4) is  $\sim 1/2$  the one of water (80.1) at 20°C [35]), thereby reducing conductivity.
2. In the mixed solvent, the hydration hulls of the ions are no longer comprised of only water, but will also contain ethylene glycol. (Actually, considering the significant decrease in conductivity, a large fraction of e.g. soda should even be undissociated.) Since the diffusion of ethylene glycol in the membrane was

strongly impeded – most probably due to strong interactions with the polymer lattice – the movement of solvated ions might be affected, too.

#### 9.4.4. Selectivity of the Ion Exchange Membranes

The ion flux of a species  $i$  and thereby the current, which was transported by that flux in the membrane stack, was calculated from the average of 1) the decrease of that species in the diluate and 2) the increase of that species in the concentrate with time according to Eq. 8. With Eq. 9 and the total current density, the current efficiency of sulfate, chloride and carbonate was calculated for each membrane pairing with the aqueous and the mixed solvent diluate. The obtained current efficiencies are displayed in Figure 13. The carbonate flux carried in all cases more than 60% of the current, which was not high, considering that carbonate constituted about 85 %-mol of the present anions.

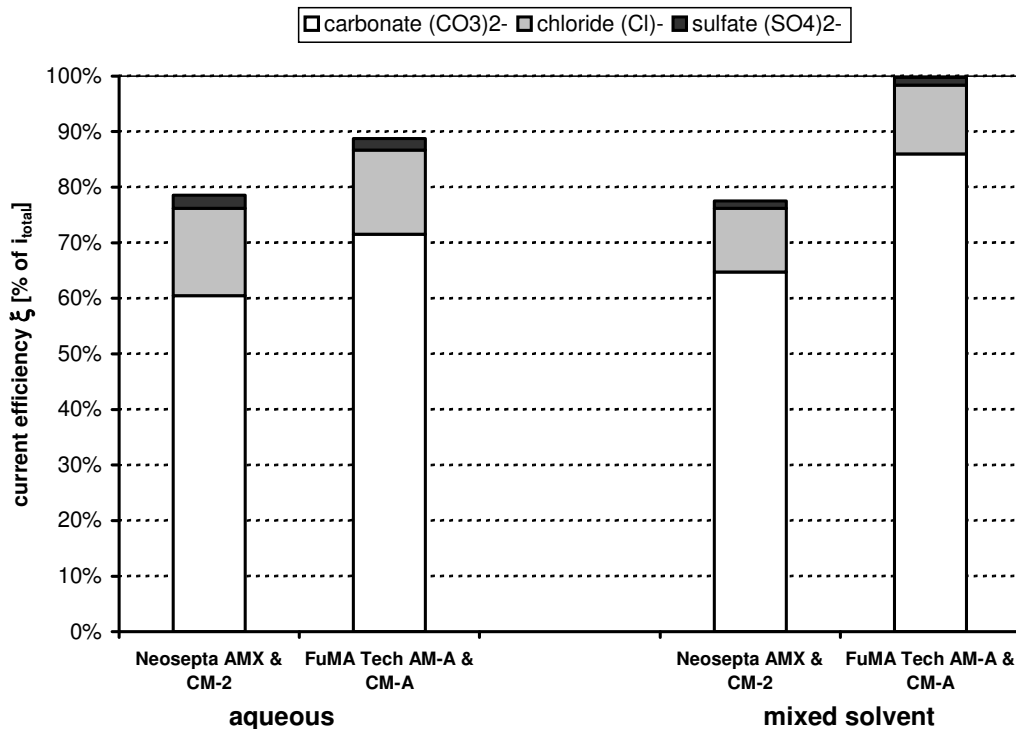


**Figure 9-13:** Current efficiencies of the tested membrane pairings Neosepta AMX & CM-2 and FuMA Tech AM-A & CM-A in aqueous and in mixed solvent carbonate solution

The current efficiency of chloride was ca. 15% and the one of sulfate ca. 2% for both membrane pairings for aqueous solution. The current efficiency for carbonate of the FuMA Tech membranes was ca. 10% higher than for the Neosepta membranes, giving the Neosepta membranes a higher selectivity but also a lower overall current efficiency. With the mixed solvent diluate, the Neosepta membranes showed about the same total current efficiency as in the aqueous case of about 78%, but the chloride current efficiency had decreased to 11% and the sulfate one to 1.4%. The total current efficiency for the FuMA Tech membranes increased with the mixed solvent diluate to almost 100% (99.7%), but the chloride current efficiency decreased to 12% and the sulfate one to 1.4%.

For comparison of the selectivity of the transport between the two membranes pairings and between aqueous and mixed solvent conditions, a dimensionless selectivity  $S$  of the ion transport in the electrodialysis needs to be defined, which is e.g. not influenced by the (starting) concentration of the species in the diluate.

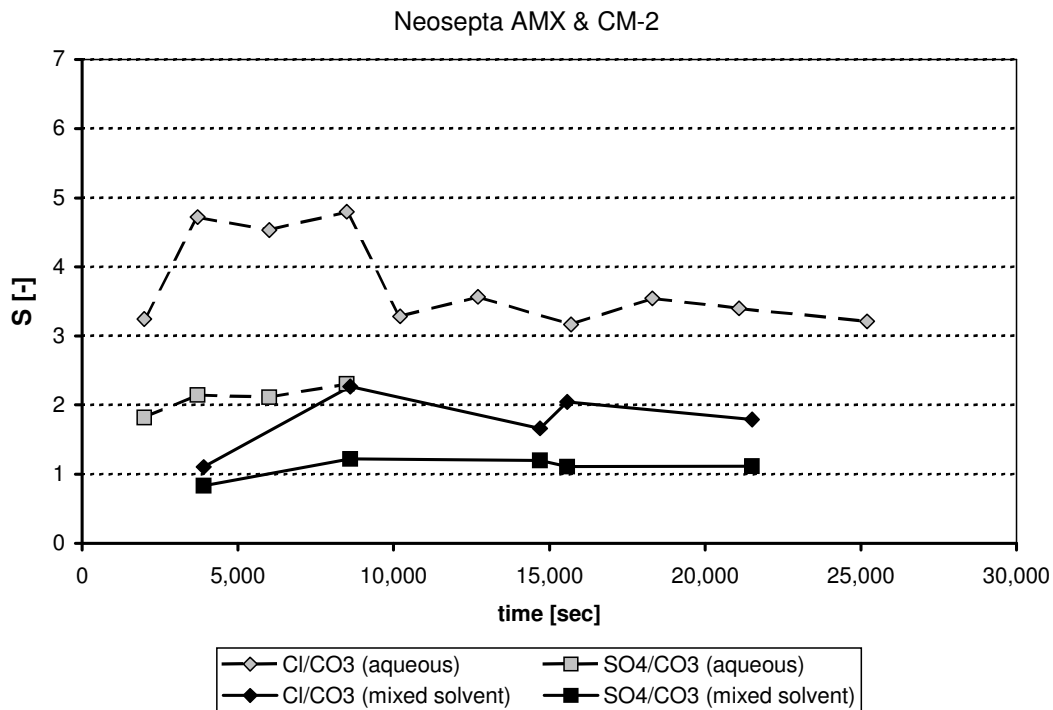


**Figure 9-14:** Selectivity of the transport of sulfate ( $\text{SO}_4^{2-}$ ) and chloride ( $\text{Cl}^-$ ) ions over carbonate ( $\text{CO}_3^{2-}$ ) ions for the Neosepta AMX & CM-2 membrane combination with aqueous and mixed solvent diluate solution

Such a definition of the selectivity is the ratio of the overall mobilities  $u_i$  and  $u_j$  of the compared species  $i$  and  $j$ :

$$S_{ij} = \frac{u_i}{u_j} \quad \text{Eq. 9-35}$$

Since the mobilities are not readily accessible, they have to be derived from the ion fluxes according to Eq. 2, yielding the following relationship for the selectivity:

$$S_{ij} = \frac{j_i/c_i}{j_j/c_j} = \frac{-u_i \cdot F \cdot \frac{\partial \phi}{\partial y}}{-u_j \cdot F \cdot \frac{\partial \phi}{\partial y}} = \frac{u_i}{u_j} \quad \text{Eq. 9-36}$$

From the known ion fluxes and the measured concentrations, the selectivities were derived.

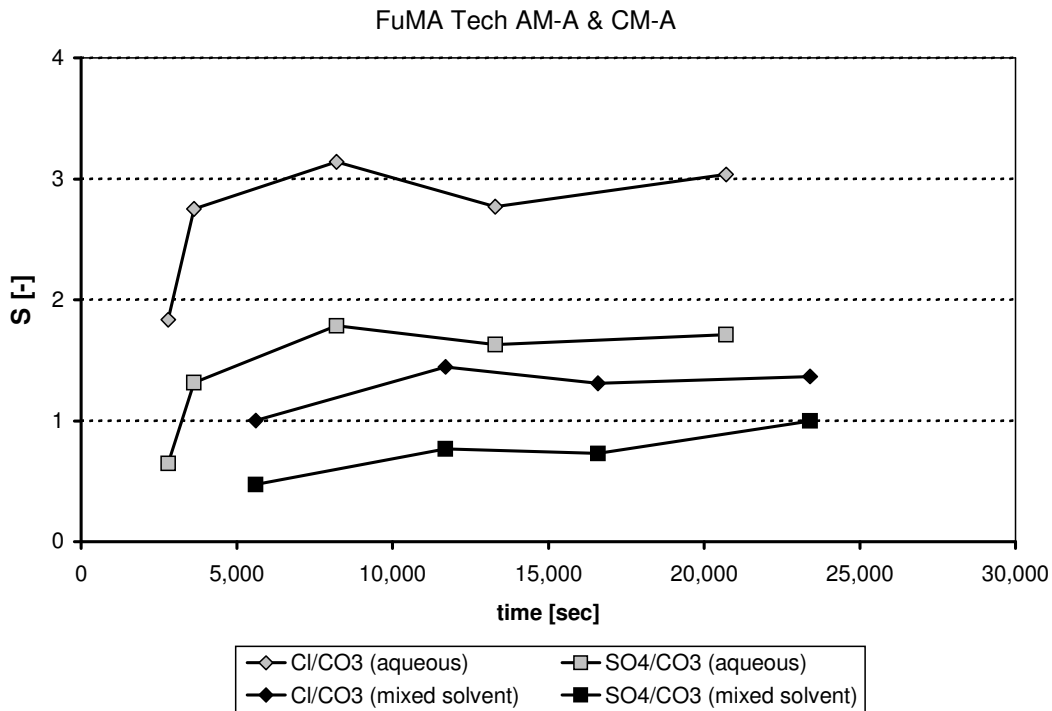


**Figure 9-15:** Selectivity of the transport of sulfate (SO<sub>4</sub><sup>2-</sup>) and chloride (Cl<sup>-</sup>) ions over carbonate (CO<sub>3</sub><sup>2-</sup>) ions for the FuMA Tech AM-A & CM-A membrane combination with aqueous and mixed solvent diluate solution



The development of the selectivities with time in the experiments with the Neosepta membranes is given in Figure 14 and for the FuMA Tech membranes in Figure 15. For both membrane pairings the chloride-carbonate selectivity was app. 3 while the sulfate-carbonate selectivity was app. 2. The selectivities with the Neosepta membranes were higher than with the FuMA Tech membranes, as less carbonate passed the Neosepta membranes.

In the experiment with the Neosepta membranes and aqueous diluate, sulfate ions from the electrode rinse compartments leaked into the diluate and concentrate compartments at around 10,000 seconds and no sulfate selectivity determination was feasible after that. Since the leakage was only minor, the experiment was continued, but it appeared, that the selectivity of chloride over carbonate dropped from app. 4.6 to 3.4. The minor increase in sulfate concentration does not offer an explanation for the drop of the selectivity for chloride transport.

For the mixed solvent diluates, the selectivities dropped significantly:

With the Neosepta membranes, the chloride selectivity dropped to app. 2 and the sulfate to almost 1, i.e. no sulfate selectivity at all. For the FuMA Tech membranes, the chloride selectivity dropped to app. 1.4 and no sulfate selectivity was found.

The reason for this development of the selectivity was most likely the degree of ion dissociation: Chloride and sulfate are strong acid anions and were completely dissociated in aqueous solution, while carbonate as a weak acid anion was only partially dissociated. Carbonate would therefore formed unpolar or single charged species, which contributed less or not at all to the charge transport, see Addendum. Therefore proportionally less carbonate was transported through the AEMs, resulting in the observed chloride and sulfate selectivity.

In the less polar mixed solvent solution, all species, sulfate, carbonate and chloride, were only partially dissociated and the transport of the species also became more even.

The generally noticeable chloride selectivity in these experiments can also be attributed to the higher permeability of the AEMs for this small single charged ion in comparison to the larger double charged sulfate and carbonate ions.

Sata et al. [15] found similar changes in ion selectivity for their AEM in ethylene glycol mixed solvents. They attributed the change in selectivity to the fact, that the membrane became more hydrophilic with the adsorption of ethylene glycols on the apolar polymer lattice. They assumed that this increase in hydrophilicity of the membrane would allow more strongly hydrated ions like sulfate and fluoride to enter and pass the membrane, while less hydrated ions like bromide and nitrate would encounter more resistance.

This explanation is not entirely convincing, since an increased uptake of ethylene glycol does not make a membrane more hydrophilic, simply because an increased ethylene glycol uptake implies that less water is absorbed into the membrane. As Helfferich [36] points out, the amount of swelling of an organic ion exchange polymer resin – like the material of an electrodialysis membrane – is limited by the elastic forces of the polymer lattice, that are directed to contract the resin back into an un-swollen state. These elastic forces are countered by the osmotic pressure between the bulk and the membrane solution, which causes the absorption of solution into the resin and thus swelling. The osmotic pressure of water between bulk and membrane solution decreases with decreasing water content in the bulk solution, as the osmotic pressure of water is a function of the ratio in water activity between bulk solution and membrane pore solution. Even taken the increased membrane swelling in the mixed solvent solution, observed in this work, into account, a membrane impregnated with ethylene glycol can contain significantly less water – and becomes less polar and thereby more hydrophobic!

In our opinion, it appears therefore more likely, that the higher selectivity for more strongly hydrated ions should rather be explained on the basis of the higher degree of dielectric shielding, that a larger hydration hull provides to the ion. The larger hydration hull reduces the polarity of the ion, so that the ion encounters less transport resistance from the more apolar environment in the ethylene glycol impregnated membrane. These resistances consist of charge repulsion between the co-ions in the membrane and the increased strength of bonding (complexation) of the co-ions to the functional groups in the more apolar environment. An ion, shielded by a large and strongly bonded hydration hull, would experience these effects less than an unshielded ion.

## **9.5. Conclusions**

It was found that all of the tested 6 ion exchange membranes showed good chemical and physical resistance to the mixed solvent, which was composed of 70%-w (salt-free solvent) ethylene glycol and 30%-w (salt-free solvent) water, concentrated aqueous carbonate solution and mixed solvent carbonate solution.

The diffusive resistance of the membranes to ethylene glycol was found app. 2 orders of magnitude higher than the diffusive resistance of water. This resulted in decent ethylene glycol retention for a few hours, but noticeable ethylene glycol leakage was found in long-term experiments. The intended selective desalination of the mixed solvent should therefore be performed batch-wise instead of continuous, to reduce ethylene glycol losses.

The electrical resistance of the ion exchange membranes in the mixed solvent was higher by a factor of 8 to 10 for the FuMA Tech membranes and a factor of 14 to 18 for the suitable Neosepta membranes compared to aqueous solution. Still, the heterogeneous Neosepta membranes showed a lower resistance than the thicker, homogeneous FuMA Tech membranes. The thicker FuMA Tech membranes, on the other hand, showed lower ethylene glycol permeability.

In electro dialysis experiments, it was observed that both chosen membrane pairs – FuMA Tech AM-A & CM-A and Neosepta AMX & CM-2 – displayed selective transport of sulfate and especially chloride ions over carbonate ions from aqueous diluate solutions. For the mixed solvent diluate, these selectivities greatly decreased or even disappeared. It is assumed that the aqueous selectivity stems from the effect, that carbonate is only partially dissociated in the concentrated, aqueous carbonate solution, so that not all carbonate “ions” participate in electromigration. Since the mixed solvent is apolar, also chloride and sulfate are only partially dissociated here, and only the small, dissociated fractions of chloride, sulfate and carbonate contribute to the ionic flux.

The heterogeneous Neosepta membranes display the best performance, since they show not only lower electrical resistance and less elongation by swelling, but also achieve higher selectivities for the targeted sulfate and chloride ions. The thicker, heterogeneous FuMA Tech membranes show higher ethylene glycol retention, which might be also an

important factor as ethylene glycol loss is an important economic factor for the given application.

Generally, it appears that the desalination from aqueous solution is more favorable than the direct desalination from the mixed solvent. Not only the electrical resistance (corresponding to the energy cost of the process) is lower by a factor of magnitude, but also the targeted selectivity of transport is significantly higher.

Therefore, it might be economically more feasible to extract the ionic impurities – together with a significant amount of carbonate – from the mixed solvent solution with packed bed ion exchangers, strip the ion exchangers with an aqueous (carbonate) solution and subsequently regenerate this strip solution by electrodialysis, taking advantage of the higher selectivity in the aqueous system.

## **9.6. Literature References**

- [1] Oosterhof, H., Witkamp, G.J., van Rosmalen, “Some antisolvents for crystallisation of sodium carbonate”, *Fluid Phase Equilibria*, 155, 1999, p. 219-227
- [2] Oosterhof, H., Witkamp, G.J., van Rosmalen, G.M., “Antisolvent Crystallization of Anhydrous Sodium Carbonate at Atmospheric Conditions”, *AIChE J.*, 47(3), 2001, p. 602-608
- [3] Oosterhof, H., Witkamp, G.J., van Rosmalen, G.M., “Evaporative Crystallization of Anhydrous Sodium Carbonate at Atmospheric Conditions”, *AIChE J.*, 47(10), 2001, p. 2220-2225
- [4] Oosterhof, H., de Graauw, J., Witkamp, G.J., van Rosmalen, G.M., “Continuous Double Recrystallization of Light Soda Ash into Super Dense Soda Ash”, *Crystal Growth & Design*, 2 (2), 2002, p. 151-157
- [5] Gärtner, R.S., Seckler, M.M., Witkamp, G.J., “Recrystallization of Trona (Sodium Sesquicarbonate) into Soda (Sodium Carbonate Anhydrate) in a Mixed Solvent. Part I: Fundamental Conversion Steps”, submitted for publication in *AIChE Journal* (Chapter 4)
- [6] Gärtner, R.S., Seckler, M.M., Witkamp, G.J., “Recrystallization of Trona (Sodium Sesquicarbonate) into Soda (Sodium Carbonate Anhydrate) in a Mixed Solvent. Part II: Alternative Recrystallization Routes”, in preparation for publication (Chapter 5)

- [7] Gärtner, R.S., Seckler, M.M., Witkamp, G.J., "Solid Phases and their Solubilities in the System  $\text{Na}_2\text{CO}_3 + \text{NaHCO}_3 + \text{Ethylene Glycol} + \text{Water}$  from (50 to 90) °C", *J. Chem. Eng. Data*, 49(1), 2004, p. 116-125
- [8] Garret, D.E., "Natural Soda Ash – Occurrences, Processing and Use", Van Nostrand – Reinhold (Publ.), New York, NY, 1992, p. 30-416
- [9] Haynes, H.W., "Solution Mining of Trona", *In Situ*, 21(4) (1997), p. 357-394
- [10] Gärtner, R.S., Seckler, M.M., Witkamp, "Mixed Solvent Recrystallisation for the Densification and Purification of Soda Ash", in preparation for publication (Chapter 2)
- [11] Gärtner, R.S., Seckler, M.M., Witkamp, "Regeneration of Mixed Solvent by Ion Exchange Resin: Selective Removal of Chloride and Sulfate", submitted for publication in *Separation Science and Technology*
- [12] Ethève, J., Huguet, P., Innocent, C., Bribes, J.L., Pourcelly, G., "Electrochemical and Raman Spectroscopy Study of a Nafion Perfluorosulfonic Membrane in Organic Solvent – Water Mixtures", *J. Phys. Chem. B*, 105 (2001), p. 4151 – 4154
- [13] Hörpel, G., Kuppinger, F.F., Schmidt, F.G., van der Velden, P.M., "Verfahren zur Abtrennung multifunktionaler Alkohole von wasserlöslichen Salzen aus wässrigen Systemen", European Patent Application EP 0 982 283 A2
- [14] Ivashchenko, V.F., Grebenyuk, V.D., Tubol'tseva, L.P. Mal'tseva, O.L., "Solvent Transfer in Electrodialysis of Water-Diethylene Glycol Solutions", *Khimiya i Tekhnologiya Vody*, 9(2) (1987), p. 179-180
- [15] Sata, T. Mine, K., Matsuaki, K., "Change in Transport Properties of Anion-Exchange Membranes in the Presence of Ethylene Glycols in Electrodialysis", *J. Colloid Interface Sci.*, 202 (1997), p. 348-358
- [16] Pimenskaya, N., Laktionov, E., Nikonenko, V., El Attar, A., Auclair, B., Pourcelly, G., "Dependence of composition of anion-exchange membranes and their electrical conductivity on concentration of sodium salts of carbonic and phosphoric acid", *J. Membr. Sci.*, 181, 2001, p. 185-197
- [17] Cowan, D.A., Brown, J.H., "Effect of turbulence on limiting current in electrodialysis cells", *Ind. Eng. Chem.*, 51, 1959, p. 1445-1448
- [18] Spiegler, K.S., "Polarization at ion exchange membrane – solution interfaces", *Desalination*, 9, 1971, p. 367-385
- [19] Scott, K., "Ion-Exchange and Charge Driven Processes", in Scott, K., Hughes, R., "Industrial Membrane Separation Technology", Blackie Academic & Professional (publ.), Glasgow, 1996, pp. 199

- [20] product information, “Neosepta Ion Exchange Membranes”, Tokuyama Corporation (2000), Shibuya, Shibuya-Ku, Tokyo, Japan
- [21] product information, “Umkehrosmose, Nanofiltration, Mikro- und Ultrafiltration, bipolare Membrantechnik”, FuMA Tech GmbH (2000), Vaihingen/Enz, Germany
- [22] Wesselingh, J.A., Krishna, R., “Mass Transfer”, Ellis Horwood Ltd. (Publ.), London, 1990
- [23] Wesselingh, J.A., Vonk, P. Kraaijeveld, “Exploring the Maxwell-Stefan description of ion-exchange”, Chem. Eng. J., 57, 1995, p. 75-89
- [24] Cussler, E.L., “Diffusion – Mass Transfer in Fluid Systems”, Cambridge University Press, Cambridge, 1986
- [25] Rautenbach, R., “Membranverfahren – Grundlagen der Modul- und Anlagenauslegung”, Springer-Verlag, Berlin, 1997
- [26] Marshall, T.J., “Permeability and the Size Distribution of Pores”, Nature, 180, 1957, p. 664-665
- [27] Narebska, A., Kujawski, W., “Transport of electrolytes across charged membranes. Part IV. Frictional interactions of the neutral and alkaline permeants and the permeability/reflection phenomena”, J. Membr. Sci., 56, 1991, p. 99-112
- [28] Narebska, A., Kujawski, W., Koter, S., “Irreversible Thermodynamics of Transport across Charged Membranes”, J. Membr. Sci., 30, 1987, p. 125-140
- [29] Narebska, A., Kujawski, W., Koter, S., “Ions and Water Transport across Charged Nafion Membranes. Irreversible Thermodynamics Approach”, Desalination, 51, 1984, p. 3-17
- [30] Scattergood, E.M., Lightfoot, E.N., “Diffusional Interaction in an Ion-Exchange Membrane”, Trans. Faraday Soc., 64, 1968, p. 1135-1146
- [31] Krol, J., “Monopolar and Bipolar Ion Exchange Membranes – Mass Transport Limitations”, (Chapter 1: Introduction), PhD Thesis, University of Twente, The Netherlands (printed by Print Partners Ipskamp, Enschede, The Netherlands)
- [32] Simons, R., “Electric Field Effects on Proton Transfer between Ionizable Groups and Water in Ion Exchange Membranes”, Electrochim. Acta, 29, 1984, p. 151-158
- [33] Simons, R., “Strong Electric Field Effects on Proton Transfer between Membrane Bound Amines and Water”, Nature, 280, 1979, p. 824-826
- [34] Simons, R., “Water Splitting in Ion Exchange Membranes”, Electrochim. Acta, 30, 1985, p. 275-282
- [35] Lide, D.R., “CRC Handbook of Chemistry and Physics”, 79<sup>th</sup> edition, CRC Press, Boca Raton, 1999, p. 6-139 – 6-161

- [36] Helfferich, F.G., "Ion Exchange", Dover Publications Inc., New York, 1995; Chapter 5: "Equilibria"
- [37] Atkins, P.W., "Physical Chemistry", 3<sup>rd</sup> edition, Oxford University Press, Oxford, 1988, p. 665-673
- [38] Smedley, S.I., "The Interpretation of Ionic Conductivity in Liquids", Plenum Press, New York, NY, 1980, p. 11-47

### 9.7. Notation

$A_M$	: area of one membrane sheet	$[m^2]$
$A$	: area	$[m^2]$
$a$	: coefficient Debye-Hückel-Onsager equation	$[(S \cdot cm^2/mol)/(mol/l)^{1/2}]$
$b$	: coefficient Debye-Hückel-Onsager equation	$[(mol/l)^{-1/2}]$
$c_i$	: concentration of species $i$	$[mol/m^3]$
$D_i$	: diffusion coefficient of species $i$	$[m^2/s]$
$F$	: Faraday constant	$[96485 C/mol]$
$I$	: electrical current	$[A]$
$i$	: electrical current density	$[A/m^2]$
$j_i$	: mole flux of species $i$	$[mol/sec/m^2]$
$n$	: refraction index	$[-]$
$R$	: electrical resistance	$[\Omega]$
$r$	: specific membrane resistance	$[\Omega \cdot m^2]$
$u_i$	: electromobility of species $i$	$[m/sec/V]$
$t_i$	: transport number of species $i$	$[-]$
$V$	: volume	$[m^3]$
$\dot{V}$	: volume flow	$[m^3/sec]$
$v_M$	: membrane swelling	$[\% - vol]$
$v_{MS}$	: relative membrane swelling in the mixed solvent	$[\% - vol]$
$w_{EG}$	: weight fraction ethylene glycol	$[\% - w]$
$X$	: fit parameter Debye-Hückel-Onsager equation	$[kS \cdot cm^5/mol^2]$
$x_i$	: mol fraction of species $i$	$[mol/mol]$
$y$	: length coordinate perpendicular to membrane surface	$[m]$

$z_i$	: charge of ion species i	[-]
$\delta$	: border layer thickness	[m]
$\varepsilon$	: porosity	[m <sup>3</sup> /m <sup>3</sup> ]
$\phi$	: electrical potential	[V]
$\kappa$	: specific electrical conductivity	[mS/cm]
$\Lambda_m$	: molar electrical conductivity	[S·cm <sup>2</sup> /mol]
$\Lambda_m^0$	: limiting molar electrical conductivity for infinite dilution	[S·cm <sup>2</sup> /mol]
$\rho$	: specific material electrical resistance	[Ω·m]
$\tau$	: tortuosity	[m/m]

### 9.7.1. Indices

c	: concentrate
d	: diluate
i	: species i
M	: membrane
m	: molar value
MS	: mixed solvent
poly	: polymer lattice of the membrane
ref	: reference state
s	: solvent
sol	: solution
+	: cation
-	: anion



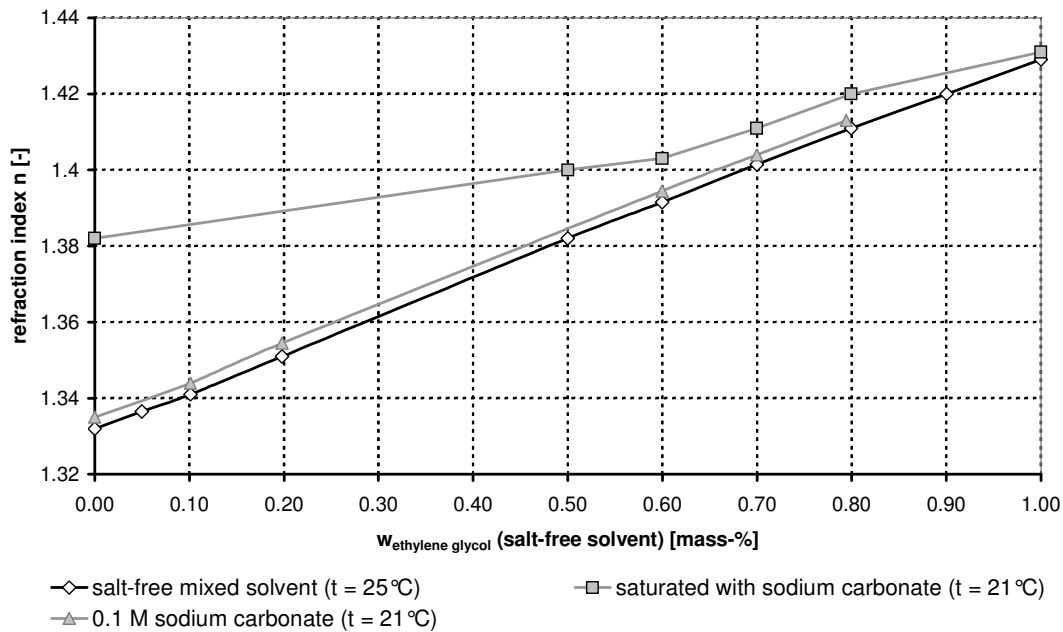


**Figure 9-16:** Calibration line of refractive index versus ethylene glycol mass fraction in mixed solvent

### 9.8. Addendum

It was found that the refraction index was a good parameter for the determination of the ethylene glycol contents of mixed solvents of ethylene glycol and water and dilute carbonate solutions of such mixed solvents. The relationship between refraction index and salt-free ethylene glycol fraction was also linear for mixed solvent carbonate solutions of low constant carbonate concentration, see Figure 16 The used calibration line in the diffusion dialysis experiments for 0.1 M  $\text{Na}_2\text{CO}_3$  solution at 21°C was:

$$n = 1.3348 + 0.09882 \cdot w_{EG} \quad \text{Eq. 9-37}$$

In the electro dialysis experiments for the determination of the sulfate and chloride selectivity, the conductivity of the diluate and concentrate solutions was used to monitor the progress of the desalination. As conductivity of a (mixed) salt solution is a strongly non-linear function of the salt concentration(s) and its sensitivity decreases with increasing salt concentration(s) [37, 38], it was not used to determine the actual concentration(s). These concentrations were obtained from analysis by HPLC.

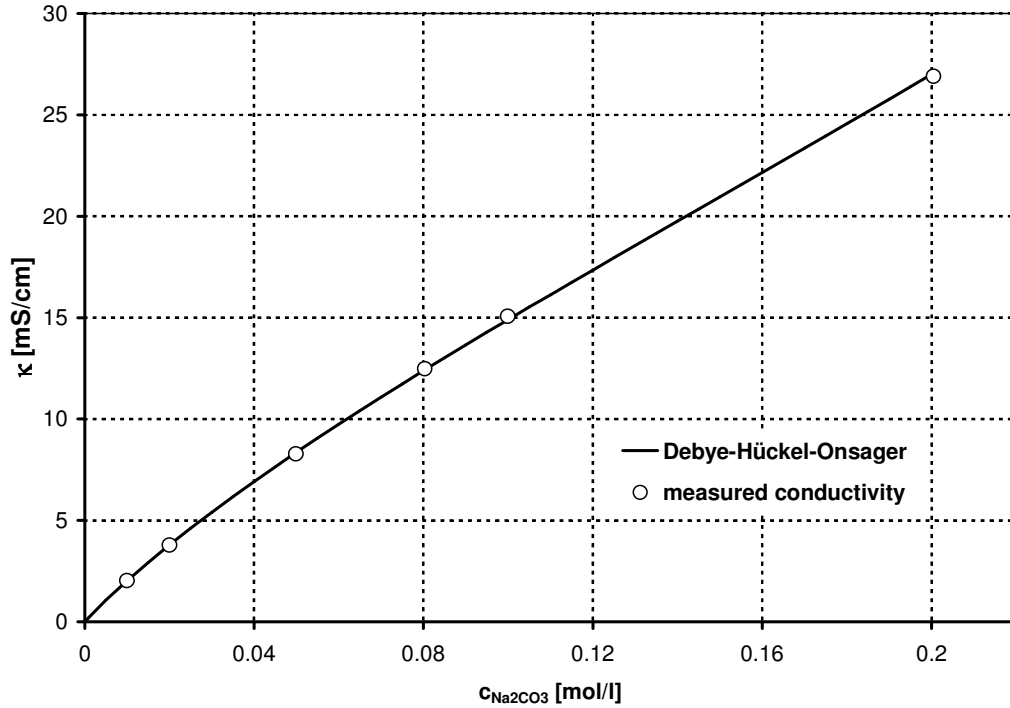


**Figure 9-17:** Conductivity versus sodium carbonate concentration at 25°C – measured values in comparison to Debye-Hückel-Onsager fit [12, 13]

For dilute or weak solutions, usually up to max. 0.1 M, the relationship of *Debye-Hückel-Onsager* [37] can be used to fit and even predict solution conductivity  $\kappa$  and the molar conductivity  $\Lambda_m$ :

$$\kappa = \Lambda_m \cdot c \quad [\text{mS/cm}] \quad \text{Eq. 9-38}$$

$$\Lambda_m = \Lambda_m^0 - (a + b \cdot \Lambda_m^0) \cdot \sqrt{c} + X \cdot c \quad [\text{S}\cdot\text{cm}^2/\text{mol}] \quad \text{Eq. 9-39}$$

For aqueous sodium carbonate solutions, the *Debye-Hückel-Onsager* relationship yielded a good reproduction of the conductivity up to app. 0.2 M. While  $\Lambda_m^0$  and  $(a + b \cdot \Lambda_m^0)$  could be calculated [37, 38], the parameter X in Eq. 36 had to be fitted to measured conductivity values, which yielded the following fit line for 25°C, which is also used in Figure 17:

$$\Lambda_m = 238.8 - 409 \cdot \sqrt{c} + 395.5 \cdot c \quad [\text{S}\cdot\text{cm}^2/\text{mol}] \quad \text{Eq. 9-40}$$

with concentration  $c$  in mol/l.

For higher carbonate concentrations and the mixed solvent solution, the *Debye-Hückel-Onsager* relationship no longer yields good approximations of the actual conductivity. The conductivity is significantly lower than the prediction. The reason for this is most likely the increased degree of association in these solutions. The uncharged  $[\text{Na}_2\text{CO}_3]$  will not contribute to charge transport and the less charged  $[\text{NaCO}_3]^-$  will contribute less than the carbonate ion  $\text{CO}_3^{2-}$ . For the tested aqueous solution of 60g/l  $\text{Na}_2\text{CO}_3$ , 5 g/l  $\text{NaCl}$  and 2.5 g/l  $\text{Na}_2\text{SO}_4$ , a theoretical conductivity  $\kappa_{\text{theo}}$  of 98.7 mS/cm was calculated for complete dissociation of all salts, while the actual measured conductivity  $\kappa$  was 59.5 mS/cm.



## Chapter 10

### **SUPER DENSE SODA BY MIXED SOLVENT RECRYSTALLIZATION: PROCESS DESIGN AND ECONOMICAL EVALUATION**

R.S. Gärtner, G.J. Witkamp, J. de Graauw

#### ***Abstract***

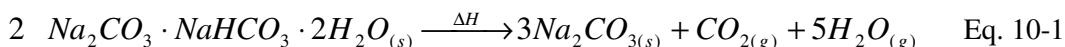
Several new process routes for the production of soda (sodium carbonate anhydrate,  $\text{Na}_2\text{CO}_3(\text{s})$ ) from trona ( $\text{Na}_2\text{CO}_3 \cdot \text{NaHCO}_3 \cdot 2\text{H}_2\text{O}(\text{s})$ ) and sodium bicarbonate ( $\text{NaHCO}_3(\text{s})$ ) based on Mixed Solvent Recrystallization are presented. In Mixed Solvent Recrystallization the stability of the possible occurring crystal phases (trona, bicarbonate, sodium carbonate hydrates) is manipulated by adjusting the mixed solvent composition to allow spontaneous suspension recrystallization of the desired anhydrous soda from e.g. solution mined natural trona or sodium bicarbonate produced by the Solvay process. Thereby, the evaporative crystallization and calcination steps necessary in current processing can be omitted, resulting in significant savings in energy requirements and production costs. Additionally, since the anhydrous soda can be crystallized directly from solution in a well- controllable fashion, higher mechanical stabilities and bulk densities can be achieved with Mixed Solvent Recrystallization than in current production processes.

## 10.1. Introduction

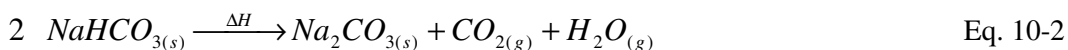
### 10.1.1. Current Soda Production

The two most common source materials for the production of soda (sodium carbonate anhydrate,  $\text{Na}_2\text{CO}_3(\text{s})$ ) are natural trona, occurring e.g. in the United States (the Green River Territory, Wyoming or Searles Lake, California), Mexico (Sosa Texcoco), Turkey (Beypazari) and Kenya (Lake Magadi) [1, 17], and sodium bicarbonate ( $\text{NaHCO}_3(\text{s})$ ), produced from sodium chloride ( $\text{NaCl}(\text{s})$ ) and carbon dioxide ( $\text{CO}_2(\text{g})$ ) by the Solvay Process [2, 3]. While the production of soda from natural trona is usually cheaper than the Solvay process, the remoteness of the mining sites and the resulting transport costs for the produced soda make production from both sources competitive on the global market.

In current industrial practice the production of soda from trona or sodium bicarbonate involves the dry thermal decomposition (calcination) of the source salt, trona or sodium bicarbonate, to anhydrous soda, see Eq. 1 and 2.



$\Delta H_{298.15\text{K}} = 124.68 \text{ kJ per mol Na}_2\text{CO}_3$  [4, 5]



$\Delta H_{298.15\text{K}} = 133.39 \text{ kJ per mol Na}_2\text{CO}_3$  [4, 5]

The soda produced by the thermal decomposition has a low bulk density and poor mechanical stability. The formed soda consists of pseudomorphs, i.e. agglomerates in the shape of the original source crystal of very small ( $\sim 1$  micron) soda crystallites. These agglomerates have a high porosity, roughly corresponding to the amounts of carbon dioxide and water released during the calcination. The weight loss during calcination is 29.66 %-weight for trona and 36.92 %-weight for sodium bicarbonate. This soda is therefore very prone to particle breakage and dusting, which gives it poor transport, packing, storage and handling properties.

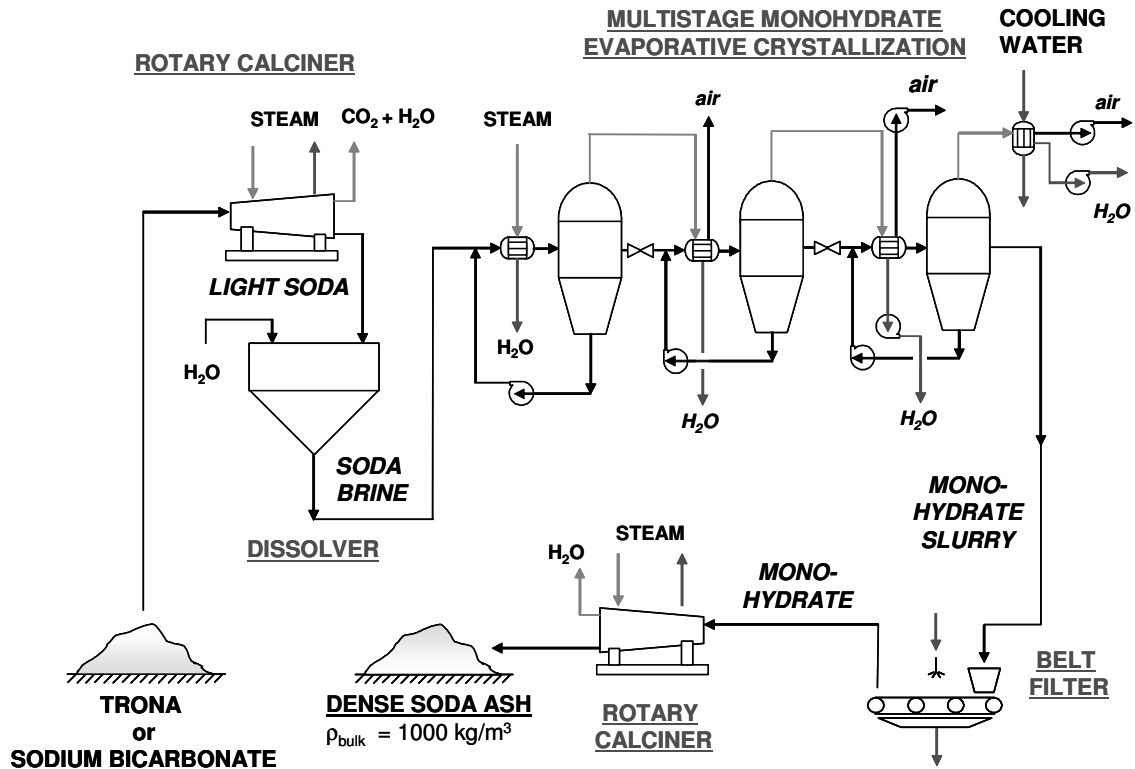


**Figure 10-1:** Flowsheet of the *monohydration* process for the production of soda ash from trona or sodium bicarbonate

It is therefore usually dissolved in water and recrystallized by evaporative crystallization as sodium carbonate monohydrate  $\text{Na}_2\text{CO}_3 \cdot \text{H}_2\text{O}(\text{s})$ , which can be calcined to soda of higher bulk density and mechanical stability [1, 3]. Two grades of soda are commonly produced by this route: Light soda ash with a bulk density of about  $500\text{kg/m}^3$  and dense soda ash with a bulk density of  $1000$  to  $1200\text{kg/m}^3$  [1, 3]. The production of dense soda ash actually requires a second calcinations step, in which water is added to the soda to facilitate a sintering-like Ostwald-ripening process, which densifies the pseudomorphs formed in the first calcination [10-13].

The process flow sheet for this process, commonly referred to as the *monohydration process* in literature [1, 3], is given in Figure 1.

As natural trona ore contains noticeable amounts of inorganic and organic, soluble as well as insoluble impurities, it is not directly fed into the monohydration process, but subjected to prior purification steps.

When the trona is recovered as the solid ore, the purification steps commonly involve calcination to crude soda ash, subsequent dissolution in water to remove insoluble impurities by settling and filtration and treatment of the resulting soda brine by activated carbon to remove organic impurities before the multistage evaporative crystallization [1]. To whiten the soda ash, sodium nitrite is added before the final calcination, to oxidize remaining organic discoloring impurities.

Solution mining of trona is an attractive alternative, as the heavy-equipment- and labor-intensive underground mining operation can be avoided. Instead, several solution-mining wells have to be drilled and subsequently, brine caverns have to be expanded – a process that can take several years. The greatest obstacles in solution mining are the slow mass transfer (driven only by the concentration and density differences between saturated brine and the added fresh water), the blinding of the solubility fronts by insoluble impurities like oil shale, and the incongruent solubility of trona, which results in enrichment of the less soluble and more slowly dissolving bicarbonate in the caverns [6 - 9]. The accumulation of sodium bicarbonate in the caverns can be countered by recycling the incongruently dissolved carbonate fraction diluted with fresh water back to the cavern [8].

From the solution-mined brine, the trona is recovered by evaporative crystallization, calcined to light soda ash, which is then densified by the monohydration process, see Figure 2.

Note, that in both Figures (1 and 2), the multistage evaporative crystallization steps for trona and monohydrate are set-up as a three-stage vacuum evaporation, i.e. the first crystallizer is operated at atmospheric pressure with a boiling point of the saturated brine of ca. 105°C, the second crystallizer is operated at 0.47 bar and a boiling point of 85°C, while the last crystallizer is operated at 0.20 bar and a boiling point of 65°C. The reduced pressures are maintained by barometric condensers and vacuum pumps, which evacuate the air from the condensate.



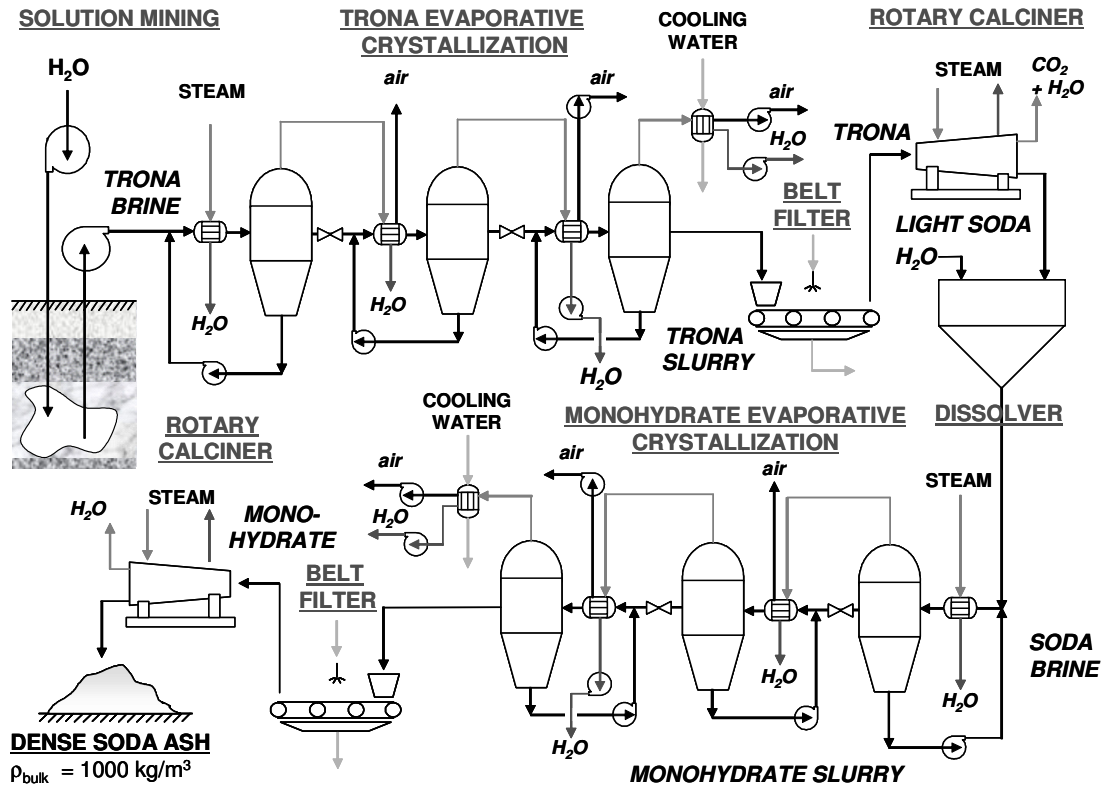


**Figure 10-2:** (Simplified) process flow sheet of soda production from solution mined trona

Multistage vacuum evaporation has two significant advantages to the other alternative, i.e. vapor recompression: First, only the non-condensable gas fraction in the steam from the previous crystallizer has to be evacuated by the vacuum pump (, which is estimated to correspond to max. 3 %-vol of the steam flow, taking dissolved gases in the brine, air leakages and carbon dioxide from bicarbonate decomposition into account), while for vapor recompression the whole steam flow would have to be compressed to a pressure of at least 2 bar (for a condensation temperature of at least 120°C). Second, while the solubility of monohydrate is almost independent of temperature, the solubility of trona decreases significantly with temperature, so less water needs to be evaporated in the trona crystallization for vacuum evaporation in comparison to vapor recompression.

Solution mining has the additional advantage, that the recovered trona brine contains almost no insoluble impurities (which remain in the cavern) and can be far easier transported, handled and processed than the crushed ore from classical underground mining. Especially, the solution-mined brine can be directly treated by settling, filtration,

activated carbon and evaporative crystallization to produce trona of a purity that is suitable for further processing by the monohydration process – or another densification process route - like Mixed Solvent Recrystallization.

### 10.1.2. Mixed Solvent Recrystallization

Mixed Solvent Recrystallization is a process alternative for the production of dense soda. While soda (sodium carbonate anhydrate) in purely aqueous solution is not a stable phase at atmospheric conditions, and cannot be crystallized technically, it can be crystallized from a mixed solvent solution. Oosterhof et al. [14-16] have shown that ethylene glycol – water is a particularly suitable mixed solvent. Mixed Solvent Recrystallization has not only the advantage, that soda can be crystallized to high mean particle sizes with bulk densities of up to  $1500 \text{ kg/m}^3$ , i.e. *super dense soda*, from the mixed solvent solution. It also does not require evaporative crystallization as simple shift in temperature will cause the soda to recrystallize spontaneously to the monohydrate and vice versa, see Chapter 2. Finally, as shown by Gärtner et al. [18 – 21], trona and sodium bicarbonate can be directly converted in suspension with the mixed solvent to high bulk density crystalline soda (*super dense soda*) by reactive recrystallization: The thermal decomposition of sodium bicarbonate to sodium carbonate can be performed solution mediated in the high boiling ethylene glycol – water mixed solvent.

Several processes were designed to employ Mixed Solvent Recrystallization for the production of *super dense soda*:

- The *Mixed Solvent Double Recrystallization (MSDR)* Process by Oosterhof et al. [15, 16], which recrystallizes light soda ash from calcination of trona or sodium bicarbonate to super dense soda (Figure 3)
- The *1-step Mixed Solvent Reactive Recrystallization (1-step MSRR)* Process by Gärtner et al. [20], which converts trona into super dense soda (Figure 4)
- The *2-step Mixed Solvent Reactive Recrystallization (2-step MSRR)* Process by Gärtner et al. [20], which converts trona into super dense soda (Figure 5)
- The *3-step Mixed Solvent Reactive Recrystallization (3-step MSRR)* Process by Gärtner et al. [20], which converts trona into super dense soda (Figure 6)

- The *Sodium Bicarbonate Mixed Solvent Reactive Recrystallization (NaHCO<sub>3</sub> MSRR)* Process by Gärtner et al. [21] for reactive recrystallization of sodium bicarbonate to super dense soda (Figure 7)

In this work the process designs of these processes are presented and an economical evaluation is given for comparison of the feasibility of these process alternatives. For comparison with the industrial practice, the economical evaluation of the monohydration process (**MH**), as outlined in Figure 1, and of the evaporative crystallization of trona (**TEC**) as addition to the monohydration process for the solution mining of trona, see Figure 2, are presented as well.

## **10.2. Process Design of the Mixed Solvent Recrystallization Processes**

All Mixed Solvent Recrystallization processes have in common, that they only require a minimal amount of evaporation to remove the released crystal water of the recrystallization of monohydrate and trona to maintain the water content of the mixed solvent constant. Therefore, the crystallization vessels do not require the large vapor heads of the common evaporative crystallizers. In the MSRR processes on the other hand carbon dioxide stripping is required, with the volume fraction of strip gas (air) amounting to 5 to 8 %-vol of the crystallizer content, corresponding to a superficial gas velocity of 0.2 to 0.3 m/sec. This requires a bubbling/degassing volume in the top section of the crystallizer of ca. 15 to 25% of the crystallizer volume to minimize mixed solvent entrainment in the strip gas.

Still, the mixed solvent re-crystallizers are smaller in dimensions and therefore less expensive for the same slurry content than evaporative crystallizers.

Additionally, the mixed solvent re-crystallizers require far smaller heat exchangers than the evaporative crystallizers, as only the slurry needs to be brought to / kept at the recrystallization temperature and the recrystallization enthalpy has to be supplied. This amount of heat is only a fraction ( $\sim 1/10^{\text{th}}$ ) of the evaporation enthalpy required in the evaporative crystallization processes.

Each of the Mixed Solvent Recrystallization processes has a specific, optimized residence time profile, temperature profile and carbon dioxide discharge / stripping rate, according to the crystal dissolution and growth rates as well as the bicarbonate decomposition reaction rate applied in the process.

### 10.2.1. Mixed Solvent Double Recrystallization (MSDR)

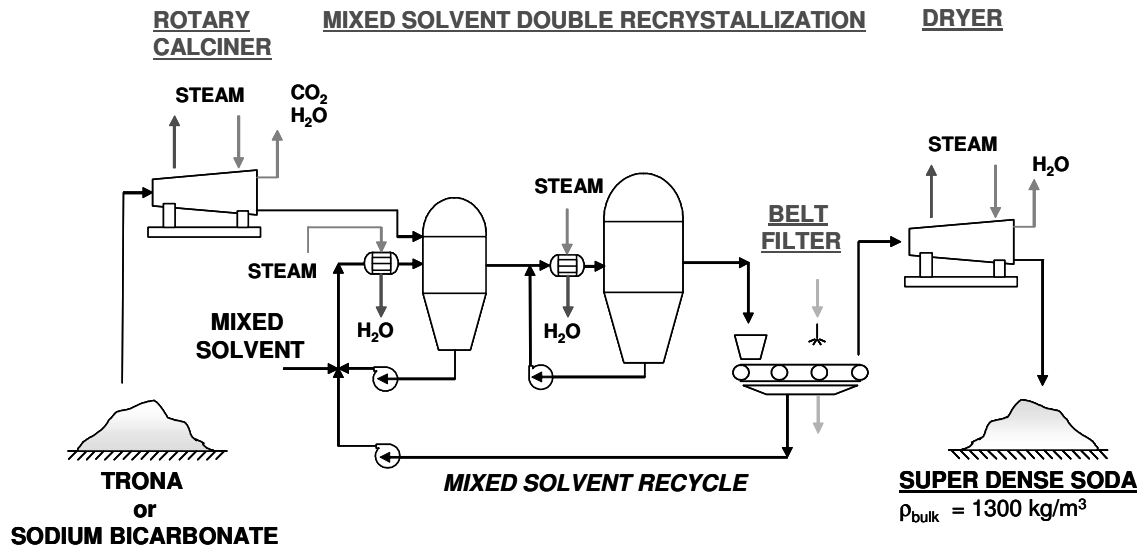


**Figure 10-3:** Process flow sheet for the Mixed Solvent Double Recrystallization Process for the production of super dense soda from trona or sodium bicarbonate

The mixed solvent double recrystallization process was designed by Oosterhof et al. [15, 16] to recrystallize light soda ash via sodium carbonate monohydrate into super dense soda. To produce soda from trona or sodium bicarbonate, the source salt is first calcined in a rotary calciner to light soda ash according to Eq. 1 or Eq. 2. Trona is typically [1] calcined at 120 to 160°C, while sodium bicarbonate is more thermally stable and requires calcination temperatures of 160 to 200°C [22]. The formed light soda ash is then fed into the mixed solvent recrystallization, wherein it is recrystallized in a mixed solvent containing 70%-weight (salt-free basis) ethylene glycol at a slurry density of max. 20%-weight. In the first crystallizer, the light soda ash is recrystallized at 50°C to sodium carbonate monohydrate with a residence time of 30 to 40 minutes. In the second crystallizer, the monohydrate is recrystallized at 70 to 80°C with a residence time of ca. 1

to 1.5 h to the super dense soda, which is then filtered off, washed on a belt filter and dried in a drum dryer from adhering traces of washing liquid (which is preferably a warm, saturated, aqueous sodium carbonate solution).

The mixed solvent is recovered from the belt filter and recirculated to the first crystallizer. Losses of solvent are compensated by addition of fresh mixed solvent.

### 10.2.2. 1-step Mixed Solvent Reactive Recrystallization (1-step MSRR)

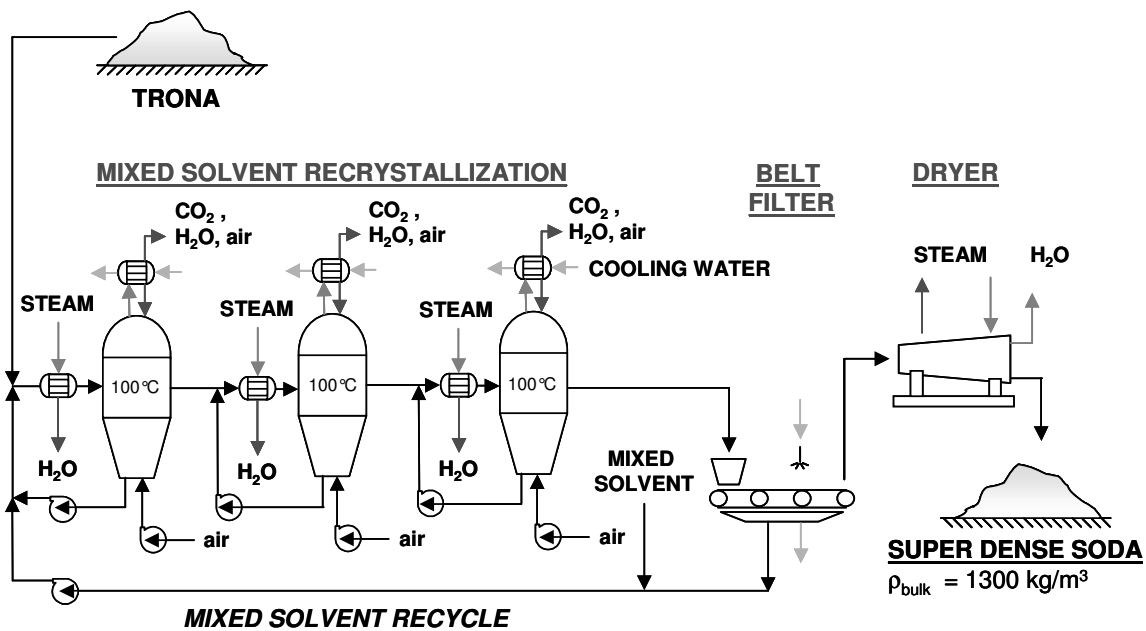


**Figure 10-4:** Process flow sheet of the 1-step Mixed Solvent Reactive Recrystallization Process for the production of super dense soda from trona

In the 1-step Mixed Solvent Reactive Recrystallization Process [20], trona is directly recrystallized into super dense soda. The recrystallization is performed in a mixed solvent containing 60 %-weight (salt-free basis) at 100°C with a slurry density of max. 20 %-weight trona. As the bicarbonate fraction of the trona is decomposed solution mediated during the reactive recrystallization, carbon dioxide is released and has to be stripped from the solution, as it has an impeding effect on the recrystallization. The strip gas (air) is fed to the crystallizers by compressors and is also used to suspend the crystals and mix the solution.

The significant feature of this process is that the recrystallization is only driven by the decomposition of bicarbonate to carbonate in solution. Thereby, the trona directly recrystallizes to sodium carbonate anhydrate. The decomposition rate of bicarbonate has been adjusted to the growth rate of the anhydrate to achieve slow, continuous growth of the anhydrate with minimal primary nucleation. In a mixed solvent with 60%-weight (salt free solvent) at a constant temperature of 100°C a residence time profile is recommended of 1 hour in the first and 1.5 to 2 hours in the second and third crystallizer [20] in order to prevent the formation of pseudomorphs from trona [19]. The super dense soda is again filtered, washed and dried as in the MSDR process. Mixed solvent losses are compensated by addition of fresh mixed solvent to the recycle.

### 10.2.3. 2-step Mixed Solvent Reactive Recrystallization (2-step MSRR)

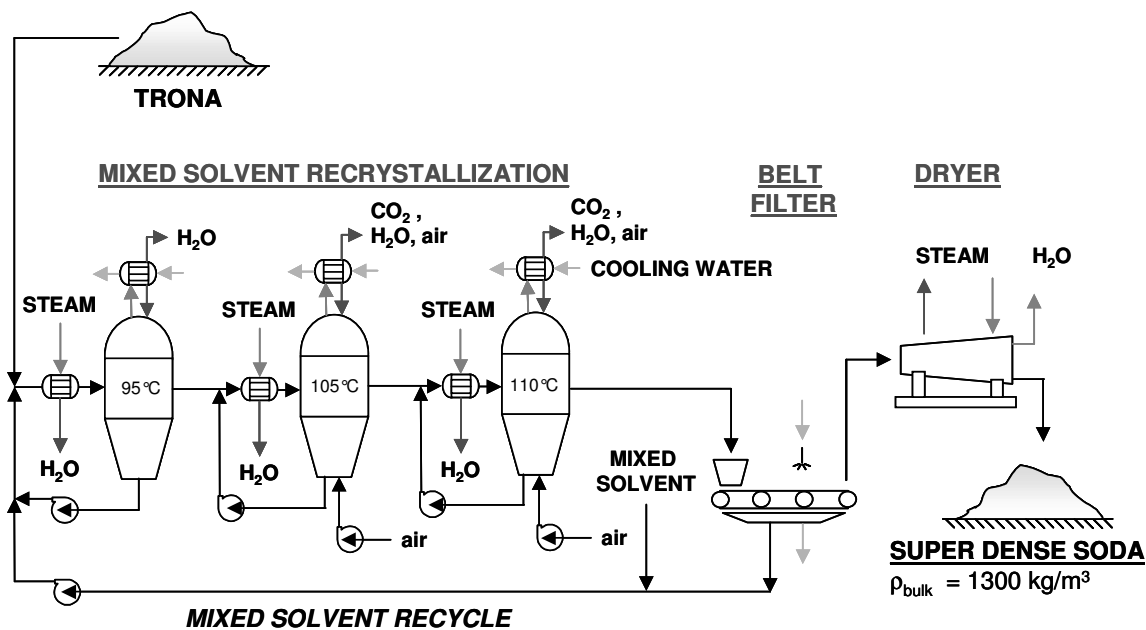
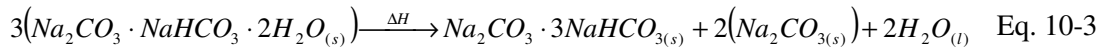


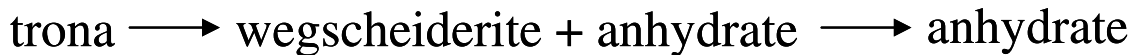
**Figure 10-5:** Process flow sheet of the 2-step Mixed Solvent Reactive Recrystallization Process for the production of super dense soda from trona

While the employed equipment is very similar to that in the 1-Step MSRR process, the trona in the 2-step MSRR process is first recrystallized to wegscheiderite ( $\text{Na}_2\text{CO}_3 \cdot 3\text{NaHCO}_3(\text{s})$ ) and sodium carbonate anhydrate in the first crystallizer, see Eq. 3.



$\Delta H_{298.15\text{K}} = 88.96 \text{ kJ per mol Na}_2\text{CO}_3 \cdot 3\text{NaHCO}_3(\text{s})$  [4, 5]

This has the significant advantage that the bicarbonate decomposition can be performed at higher temperatures - and thus at higher reaction rates - in the second and third crystallizer, as there are already sufficient seed crystals present from the recrystallization in the first reactor. More importantly, the trona is completely dissolved in the first crystallizer, and the operation temperature is no longer limited by the formation of pseudomorphic soda, see Gärtner et al. [19] and [20]. As the bicarbonate decomposition only occurs in the second and third crystallizer, only these vessels are stripped by compressed air. The total recrystallization route is thus:



A limiting factor in this process is the intermediate formation of the needle shaped wegscheiderite crystals, which form a very viscous slurry. This limits the maximum solid fraction to 15%-weight trona. As described in [20], a mixed solvent of 70%-weight (salt free solvent) ethylene glycol is recommended. This requires a temperature of 95°C with a residence time of 1h in the first crystallizer, and a temperature of 105°C in the second and 110°C in the third crystallizer with a residence of ca. 2h in both of them.

#### 10.2.4. 3-Step Mixed Solvent Reactive Recrystallization (3-Step MSRR)

The 3-Step MSRR process is more similar to the MSDR process, as the trona is calcined in the mixed solvent at min. 115°C to pseudomorphic soda, see Gärtner et al. [19, 20]. The advantage compared to the MSDR process is the enhanced heat transfer in the mixed solvent solution compared to the one in the rotary calciner. The wet calcination can effectively be performed at 120°C with a residence time of 20 to 30 minutes.

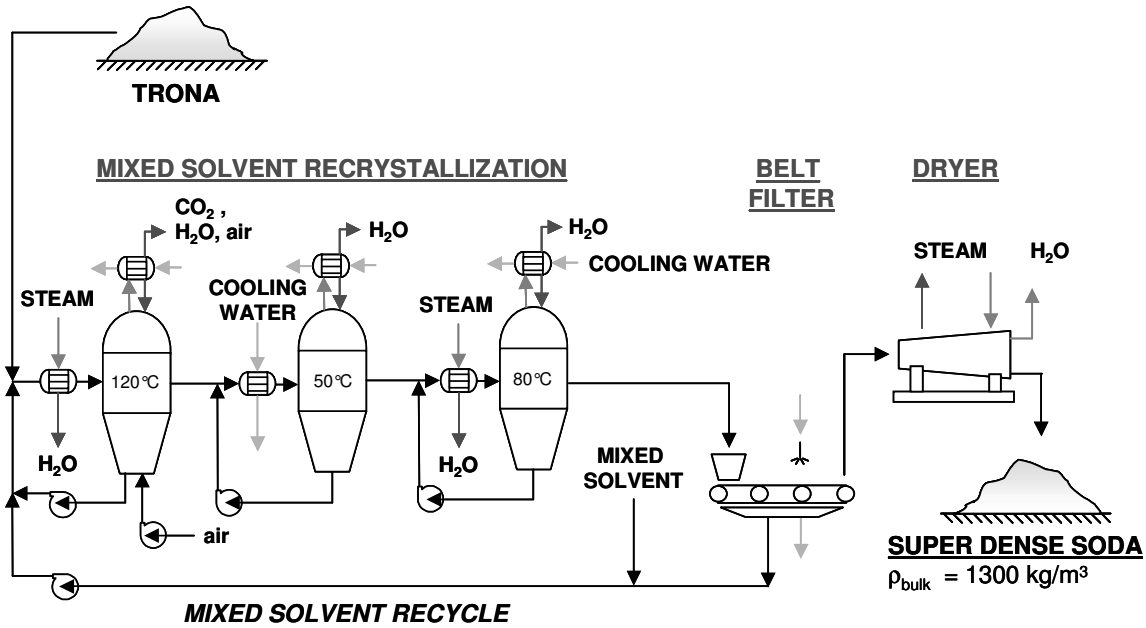
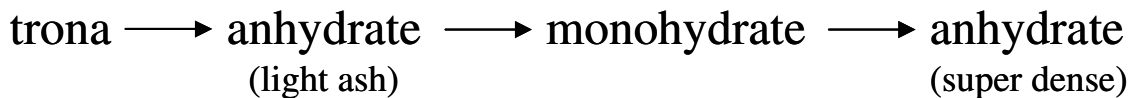


**Figure 10-6:** Process flow sheet of the 3-step Mixed Solvent Reactive Recrystallization Process for the production of super dense soda from trona

Since the carbon dioxide is very rapidly set free during the reaction, the required stripping with compressed air is less intense, i.e. it requires only an air hold-up of 1 to 2%-vol of the solution, corresponding to a superficial velocity of 0.04 to 0.08 m/sec.

The recrystallization in the second and third reactor is identical to the MSDR process: In 70%-weight (salt-free basis) ethylene glycol mixed solvent, the pseudomorphic (light) soda is recrystallized at 50°C with a residence time of 30 to 40 minutes to monohydrate, which is then recrystallized at 70 to 80°C with a residence time of 1 to 1.5h to super dense soda.

The overall recrystallization route can be summarized as:



The drawback of this process is, of course, that the slurry has to be cooled from 120°C to 50°C, and then heated from 50°C to about 80°C. The recycle solution has then again to



be heated from 80°C to 120°C. This is more energy intensive, than the previously presented processes

A possible solution is the heat integration of these process streams, but since most of these streams consist of recrystallizing slurries, the heat integration could face the risk of heat exchanger scaling and blockage. It has therefore not been integrated in the following economic evaluation. However, the pre-heating of the mixed solvent recycle stream from 80°C to 105°C by cooling the product stream of the first crystallizer from 120°C to 95°C would save 5300 kW of heating as well as the same amount of cooling duty in the projected case of a 500,000t/a soda plant. This corresponds to savings of about 1,293k€/a in heating and 334k€/a in cooling costs with no significant change in the required heat exchanger surface area.

#### **10.2.5. Sodium Bicarbonate Reactive Recrystallization (NaHCO<sub>3</sub> MSRR)**

The NaHCO<sub>3</sub> MSRR is similar to the 1-Step MSRR process as the recrystallization of the source salt, sodium bicarbonate, is driven by the decomposition of the dissolved bicarbonate to carbonate. Unlike the 1-stepp MSRR process, wegscheiderite (Na<sub>2</sub>CO<sub>3</sub>·3NaHCO<sub>3</sub>(s)) occurs as an intermediate in this process. The sodium bicarbonate recrystallizes first with proceeding decomposition to wegscheiderite, which subsequently recrystallizes to sodium carbonate anhydrate:



Since twice the amount of bicarbonate has to be decomposed solution mediated, a significantly longer residence time is required, than in the previously described MSRR processes. In the process outlined in Figure 7, the recrystallization is performed in a cascade of 5 crystallizers of about the same size for a residence time of about 2h in each crystallizer. In the first crystallizer at 100°C the recrystallization of sodium bicarbonate to wegscheiderite is initiated and it contains a mixed slurry of wegscheiderite and sodium bicarbonate.

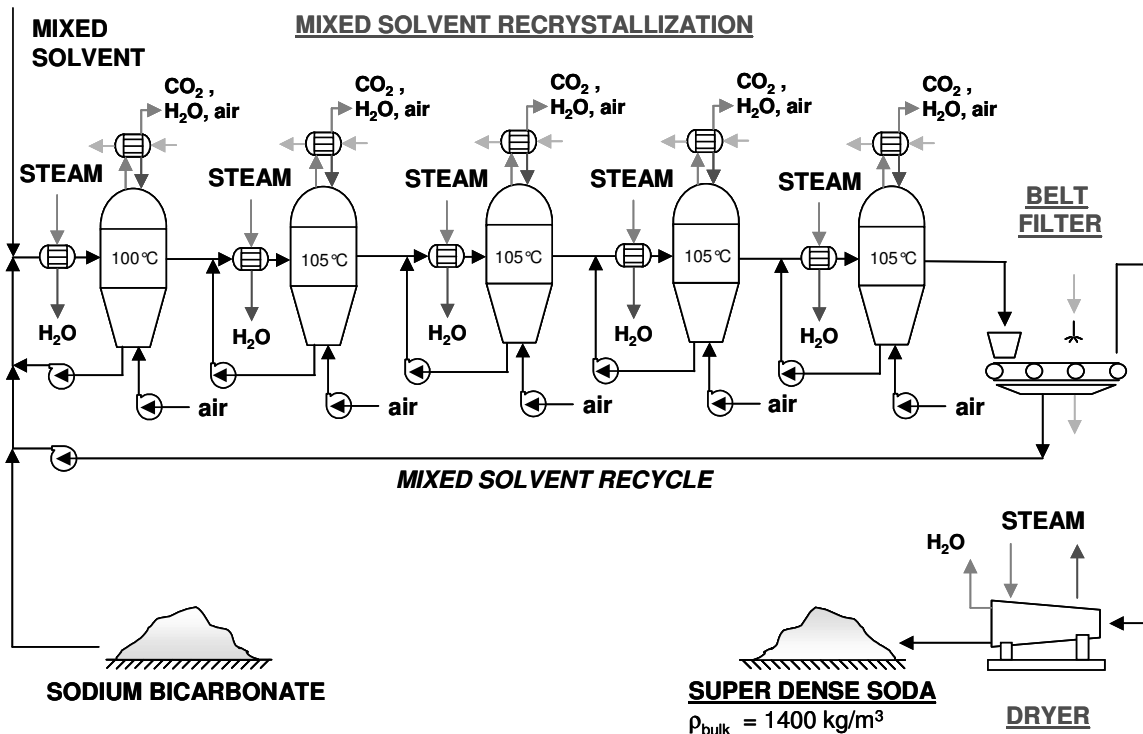


**Figure 10-7:** Process flow sheet of the 3-step Mixed Solvent Reactive Recrystallization Process for the production of super dense soda from trona

This recrystallization is completed in the second crystallizer (at 105°C), which contains only wegscheiderite as solid phase. In the following 3 crystallizers at 105°C, the wegscheiderite content is continuously recrystallized into anhydrate, so that the final crystallizer only contains sodium carbonate anhydrate, which is then subsequently filtered off, washed and dried into super dense soda.

Each of the crystallizers was stripped by a stream of compressed air of the formed carbon dioxide. The airflow (plus the formed carbon dioxide) was calculated to produce a gas fraction of 5%-vol in the crystallizer with a residence time of ca. 10 seconds. This also introduced sufficient turbulence to mix the solution and to suspend the crystals, so that no additional agitation was necessary.

Due to the thickening of the slurry by the intermediately formed wegscheiderite, the process can only be operated at a maximal initial magma density of 18%-weight sodium bicarbonate.

The long residence time and the slow, continuous recrystallization were found to produce particularly large, well shaped anhydrate crystals, which yielded a bulk density of

1440kg/m<sup>3</sup>. It therefore appears possible, that this process produces a super dense soda of increased bulk density and better flow-ability than the previously described mixed solvent recrystallization processes.

### **10.3. Economical Evaluation**

All of the presented processes are technically feasible and produce soda of commercial quality or better. To determine the economically most attractive solution, the required investment capital and the annual operating costs of the different processes were calculated. As basis, an annual production capacity of 500,000 tons of soda per year was chosen as a representative size for a major soda plant [1].

#### **10.3.1. Required Capital Investment**

The required investment capital is calculated from the cost of the required pieces of equipment of the plant. The dimensions of the equipment are calculated for a 500,000 t/a soda plant. The basic equipment costs are taken from the DACE cost tables of 2004 [23]. The required capital investment  $C_i$ , i.e. the cost for the turn-key plant, was derived by Eq. 4 from the total basic equipment cost  $C_{eq}$  by multiplication with the Lang-factors  $l_1$  and  $l_2$ , according to Sinnott [24].  $l_1$  introduces the costs for equipment design & engineering, the contractor's fee, and contingency.  $l_2$  reflects the overall installation and instrumentation costs from the basic equipment to the turn-key plant, i.e. costs for equipment erection, piping, insulation, electrical installation, power supply, lighting installation, instrumentation & control, process buildings & structures, ancillary buildings, offices & workshops.

#### **Lang factors [24]**

<b><math>l_1</math></b>	<b>1.4</b>
<b><math>l_2</math> (for solid-fluid processing)</b>	<b>3.15</b>

$$C_i = l_1 \cdot l_2 \cdot C_{eq}$$

Eq. 10-4

The total basic equipment cost  $C_{eq}$  is the sum of the costs  $c_{eq}$  of the basic pieces of equipment.

$$C_{eq} = \sum c_{eq} \quad \text{Eq. 10-5}$$

For the presented processes, the basic pieces of equipment consist of:

- **Vessels**
- **Calciners & Dryers**
- **Vacuum Pumps & Compressors**
- **Belt Filters**
- **Pumps & Powder Feeders**
- **Heat Exchangers**

The methods of calculation of the dimensions of the equipment are summarized below. All equipment in contact with the salt slurry or the salt solution is constructed from stainless steel (AISI 316) and priced accordingly.

#### 10.3.1.1. Vessels

The vessels, i.e. the crystallizers, are dimensioned for the set production capacity of 500,000 t/a and the required residence time  $\tau$ .

$$V_{vessel} = \dot{V}_{slurry} \cdot \tau \quad \text{Eq. 10-6}$$

This required residence time depends on the process performed in the respective vessel.

The residence time in a specific process was determined based on:

1. optimal crystal growth
  - for monohydrate and trona growth in evaporative crystallization (MH, TEC) [1]
  - for monohydrate and anhydrate growth in MSDR and 3-step MSRR [15, 16]
  - for anhydrate growth in all MSRR processes [19, 20]
2. complete crystal dissolution
  - for the trona dissolution in 1-step MSRR [19, 20]
  - for the trona dissolution in 2-step MSRR [19, 20]

3. given reaction rate

- for the bicarbonate decomposition in all MSRR processes [19 - 21]

The rates of growth, dissolution and reaction in these processes depend on a range of process conditions, like the concentration or supersaturation of species in solution, temperature, mixed solvent composition, intensity of carbon dioxide stripping and mixing intensity/agitation power. The chosen residence times (given in the process descriptions) have been calculated and experimentally verified to guarantee 99.5%-weight conversion to super dense soda for the crystallization, dissolution and reaction rates at the chosen process conditions. The chosen operating conditions have been obtained from experimental optimization [15, 16, 19 - 21]. These conditions allow stable operation of the respective process and yield a product of high mean particle size and bulk density.

The volume flows of slurry in the process are determined from the experimentally determined, maximum magma density  $M$  [kg solid/ kg slurry], the required flow of the respective solid for the desired production capacity (500,000 t/a), and a operation time  $t_a$  of 8760 hrs per year (24 hrs/day, 365 days/a):

$$\dot{V}_{slurry} = \frac{\dot{m}_{solid}}{M \cdot \rho_{slurry} \cdot t_a} \quad \text{Eq. 10-7}$$

All Mixed Solvent Recrystallization processes have in common, that they only require a minimal amount of evaporation to remove the released crystal water of the recrystallization of trona to maintain the water content of the mixed solvent constant. Therefore, the crystallization vessels do not require the large vapor heads of the common evaporative crystallizers. In the MSRR processes on the other hand carbon dioxide stripping is required, with the volume fraction of strip gas (air) amounting to 5 to 8 %-vol of the crystallizer content. This requires a bubbling/degassing volume in the top section of the crystallizer of ca. 15 to 25% of the slurry hold-up volume to minimize mixed solvent entrainment in the strip gas.

Still, the mixed solvent re-crystallizers are smaller in dimensions and therefore less expensive for the same slurry content than evaporative crystallizers, for which the vapor head is calculated as 30% of the slurry hold-up volume.

In the given cost of the vessels, the cost for stirrer and stirrer motor are included, where such equipment is required for the operation of the crystallizer, i.e. not for the reactive recrystallization vessels, which are mixed by gas-lift with the strip gas (air).

#### *10.3.1.2. Calciners and Dryers*

The calciners are dimensioned to process the respective solid feed, transfer sufficient energy in the solid for the calcination reaction and remove the formed water and/or carbon dioxide by ventilation. The dryers are dimensioned to evaporate adhering moisture up to 3%-weight of the dry solid feed, which is removed by ventilation and condensed in a build in heat exchanger.

Calciners and dryers are designed as rotary-drum type equipment with included electromotors for the rotation, and build-in ventilation systems as well as vapor condensers.

#### *10.3.1.3. Vacuum Pumps and Compressors*

The dimensions of the vacuum pumps in the evaporative crystallization processes (MH, TEC) and the compressors for the strip gas in the MSRR processes are based on the gas flow rate ( $\text{Nm}^3/\text{sec}$ ) and the power to bring the gas stream to the required pressure.

The gas flow rate is derived for the evaporative crystallization processes from the fraction of the dissolved gas in the treated brine. The steam flow from the evaporative crystallizers is condensed in barometric condensers, so that only the non-condensable gas fraction of the steam has to be evacuated by vacuum pump to maintain the vacuum in the crystallizer. It was estimated, that this gas fraction would amount to max. 1%-weight of the processed brine, i.e. up 1 to 3%-weight of the occurring water vapor.

The power requirement of the vacuum pumps is calculated for the isothermal compression of the gas stream from the low-pressure level  $p_1$  to atmospheric pressure  $p_2$ , according to Strauß [25]:

$$P_{VP} = \frac{1}{\xi_{VP}} \cdot \int_{p_1}^{p_2} \dot{V}(p) dp = \frac{1}{\xi_{VP}} \cdot \dot{V}(p_1) \cdot p_1 \cdot \ln\left(\frac{p_2}{p_1}\right) \quad \text{Eq. 10-8}$$

The efficiency  $\xi_{VP}$  of the vacuum pumps is estimated as 0.35.

The required strip gas flow rate in the MSRR processes is estimated based on the occurring carbon dioxide formation rates. The strip gas flow is set to about 6 to 7 times the volume flow of the formed carbon dioxide in the crystallizers. This results in a strip gas hold-up of 5 to 8%-vol of the slurry volume (superficial velocity of 0.2 to 0.3 m/sec). The power requirement of the strip gas compressors is calculated for adiabatic compression with a compressor efficiency  $\xi_C$  of 0.8:

$$P_C = \frac{1}{\xi_C} \cdot \int_{p_1}^{p_2} \dot{V}(p) dp = \frac{\dot{V}(p_1)}{\xi_C} \cdot p_1 \cdot \frac{\kappa}{\kappa-1} \cdot \left[ \left(\frac{p_2}{p_1}\right)^{\frac{\kappa-1}{\kappa}} - 1 \right] \quad \text{Eq. 10-9}$$

The prices for compressors and vacuum pumps for the estimated gas flow rates and power requirements are taken from the DACE cost tables [23].

#### 10.3.1.4. Belt Filters

The cost of the belt filters is estimated from the required filter surface area [23]. The belt filters are designed as horizontal belt filters operated at intermittent vacuum. The required area is calculated from the product slurry mass and volume flow from the preceding crystallization, the solid fraction of the slurry, the specific resistance of the filter cake (based on cake porosity, specific cake surface area and solution viscosity), the applied vacuum (pressure difference) and the amount of required washing liquid (saturated brine).

$$v_{filtrate} = \frac{\Delta p_{vacuum}}{\eta_{filtrate} \cdot R_{cake}} \quad [\text{m}^3/\text{m}^2/\text{sec}] \quad \text{Eq. 10-10}$$

$$A_{filter} = \frac{V_{filtrate}}{v_{filtrate}} \quad [\text{m}^2] \quad \text{Eq. 10-11}$$

The costs for vacuum pumps, solution pumps, electromotors and internal piping, which are integral, functional parts of the belt filters, are included in the given costs.

#### *10.3.1.5. Pumps and Powder Feeders*

The pumps and powder feeders are dimensioned according to the estimated flow rates from the material balance of the process for slurry, liquid and powder. Suitable equipment is chosen for these flow rate capacities and the required pumping heights from the DACE tables [23], which also list the power of the required electromotor. This motor power was used to estimate the power consumption of the pumps and powder feeders for the annual costs.

#### *10.3.1.6. Heat Exchangers*

The costs of the heat exchangers are taken from the DACE tables [23] based on the required heat transfer area. This area is calculated for each heat exchanger from the required heat flux  $Q$ , the driving temperature difference  $\Delta T$  (in many cases the logarithmic temperature difference) and the heat transfer coefficient  $k$ , which is estimated from empirical functions given by Perry [26]:

$$A = \frac{Q}{k \cdot \Delta T} \quad [\text{m}^2] \quad \text{Eq. 10-12}$$

The given heat exchanger costs are for the heat exchangers of the crystallizers, which are not necessarily integral parts of the crystallization vessels. They are designed as shell and tube heat exchangers, due to the ease of cleaning of this type of heat exchangers. The costs of heat exchangers, which are integral, functional parts of a piece of equipment, such as in the rotary calciners and drum dryers, are not included here, but in the costs of those units.

The heat exchangers are designed with a safety margin, i.e. equipment with a heat transfer area about 20% larger than the estimate of Eq. 12 is chosen.



### 10.3.2. Required Annual Costs (Operation Costs)

The required annual costs summarize the total required expenditure per year to operate a given process after construction, testing and transfer of the turn-key plant to the operator. Two values for the annual cost are given: The *total annual cost* and the *annual cost after the depreciation period*. The *total annual cost* includes the annual payments of capital costs (*annuity*, see below), while the *annual costs after the depreciation period* summarize the operation costs of the plant after the capital investment (estimated in the previous section) has been “paid back” from the profits of the operation.

In the given estimation of the annual costs the following cost factors were taken into account:

- **Capital Costs**
- **Taxes, Insurance and Royalties**
- **Maintenance**
- **Labor Cost**
- **Cost of Heating Utilities**
- **Cost of Cooling Utilities**
- **Cost of Electricity**
- **Cost of Other Utilities** (Solvent Replacement)

The content of each of these cost factors is explained below along with the method of estimation.

#### 10.3.2.1. Capital Costs

The capital invested in a chemical plant has to be earned back by the income generated from the plant’s operation. In common accounting practice, the plant is *depreciated* over a set period of time, the *depreciation period*. During this period, the capital investment  $C_i$  (a.k.a. *principal*) has to be paid back with *interest*. The interest represents either the interest rate of a loan of foreign capital, e.g. from a bank, or the required return-on-investment for the operator’s own (or the operator’s investor’s) capital.

The amount paid annually for capital interest will decrease, as the invested capital is recovered with the annual rates. I.e. the sum, for which interest is paid, decreases with the

annual rate payments. To simplify accounting, the payable amount over the depreciation period, i.e. the capital investment plus the incurred interest, is paid in a series of equal payments, the so-called *annuity* ( $a$ ), see Peters & Timmerhaus [30]:

$$a = C_i \cdot \frac{i \cdot (1+i)^n}{(1+i)^n - 1} \quad \text{Eq. 10-13}$$

For a chemical production plant of a bulk chemical commodity like soda, for which a stable market exists, it is reasonable to choose a depreciation period ( $n$ ) of 10 years. This means, that for the first ten years, 10% of the initial capital investment has to be paid as depreciation. For an investment of this seize, an annual capital interest rate ( $i$ ) of 6% is reasonable at the time, this estimation is made. This yields an annuity ( $a$ ) of 13.587% of the capital investment ( $C_i$ ) as annual capital cost.

After the depreciation period the capital costs are assumed to be zero.

#### *10.3.2.2. Taxes, Insurance and Royalties*

This cost factor covers the annual payments for governmental taxes, annual fees for the insurance of the plant and royalties for licenses of patents used in the process. Sinnott [24] assigns each of these items a global cost factor of 1% of the total capital investment of the plant. This rule is also employed here to assign these costs a value of 3% of the total capital investment  $C_i$  per year.

#### *10.3.2.3. Maintenance*

Maintenance covers the cost of the necessary inspections, overhauls, repairs and replacements in the plant. This includes work hours as well as costs of replacement parts of equipment. In accordance with Sinnott [24], the annual maintenance cost is estimated as 5% of the total capital investment  $C_i$  per year.

#### *10.3.2.4. Labor Cost*

Based on the plant size of the MH, MDSR and MSRR processes, a work shift plan is drawn up for the supervision and operation of the plant. It is estimated, that 4 operators

per shift are required with 5 shifts operating the plant 24hrs per day, 7days per week for a total of 20 operators. The basic labor cost of these operators is calculated from a salary of 45,000 €/a plus 13,500€/a for taxes, insurance and administration. To this basic labor cost, 20% is added for supervision staff (process engineers and plant manager), 20% for laboratory facilities and 50% for the plant overhead, i.e. company facilities, administration, security, etc., see Sinnott [24]. This yields a total annual labor cost of about 2,223,000 €/a.

The preceding TEC process is estimated to require 3 operators per shift with 5 shifts operating the plant 24hrs/day, 7days/week. This yields a total annual labor cost of about 1,667,000 €/a.

#### 10.3.2.5. Costs of Heating and Cooling Utilities

The required heat and cooling is calculated from the heat capacities, and the dissolution/crystallization, reaction, and vaporization/condensation enthalpies of the system. The required heating and cooling is supplied either by heat integration, 20°C cooling water, low-pressure steam (4 bar) of 150°C condensation temperature and high-pressure steam (30 bar) of 235°C condensation temperature. The high-pressure steam is actually only applied in the trona and sodium bicarbonate calcinations steps where temperatures above 140°C are required. The utility costs are summarized in Table 1.

**Table 10-1:** Costs of heating and cooling utilities from the DACE tables [23]

Utility	Cost	
cooling water	0.075	€/m <sup>3</sup>
low pressure steam (4 bar, 150°C)	15,-	€/t
high pressure steam (30 bar, 235°C)	19,-	€/t
electrical power (average)	0.085	€/kWh

#### 10.3.2.6. Cost of Electricity

The required annual electrical power is calculated from the power requirements of all the electromotors in the plant, which drive the pumps, vacuum pumps, and compressors,

rotate the drum dryers and calciners, and operate the moving parts of the belt filters. These power requirements are either calculated from the required performance (including an efficiency factor) as in the case of the vacuum pumps, compressors and rotational motors, or taken from the required capacity of the electromotor of the respective piece of equipments as given in the DACE tables [23]. The average price of electricity is taken from the DACE listings [23] as 0.085€/hWh

#### *10.3.2.7. Cost of Other Utilities*

The two other major utilities used in the process are water and the antisolvent ethylene glycol. The water added to the crystallization and recrystallization processes is assumed to be of drinking water quality. Ethylene glycol of technical quality is sufficient for the mixed solvent processes. To compensate losses of solvent – antisolvent as well as water – it is assumed, that the complete solvent content of the crystallization vessels has to be replaced in the course of each year. This should provide a conservative estimation of the solvent loss, as this replacement is an important cost factor in the mixed solvent processes. The cost of drinking water is taken as 1.1 €/m<sup>3</sup> [23] and the cost of ethylene glycol as 0.869 €/kg [27, 28].

### **10.3.3. Economical Comparison of the Process Alternatives**

#### *10.3.3.1. Trona Processes*

Based on the case of the solution mining operation for a production of 500,000 metric tons of soda annually, 5 alternative processes are evaluated here. These alternatives are the monohydration (MH), the 1-step MSRR, the 2-Step MSRR, the 3-Step MSRR and the MSDR process, with the required capital investment and annual costs given in Table 2, 3 and 4, respectively. For all alternatives, trona is first recovered from the brine by evaporative crystallization (TEC, see Figure 2). As this part of the process is identical for all evaluated process alternatives, its cost is not included in the cost of the process alternatives, but given separately in Table 4.

**Table 10-2:** Cost Comparison of Trona Processes: Monohydration and 2-step MSRR process

<b><u>Equipment Costs</u></b>	<b><u>Monohydration (MH)</u></b>		<b><u>2-step MSRR</u></b>	
Vessels	3,986,904€	1,211m <sup>3</sup>	6,195,921€	2,292m <sup>3</sup>
Calciners & Dryers	1,742,376€	256m <sup>3</sup>	393,455€	76m <sup>3</sup>
Vacuum Pumps & Compressors	348,000€	155kW	1,344,000€	922kW
Belt Filters	389,442€	17m <sup>2</sup>	433,098€	15m <sup>2</sup>
Pumps & Powder Feeders	346,619€	292kW	318,951€	228kW
Heat Exchangers	2,430,000€	5,496m <sup>2</sup>	357,000€	356m <sup>2</sup>
<b>Total</b>	<b>9,243,341€</b>		<b>9,042,425€</b>	
<b>Lang Factors</b>				
<i>Design &amp; Engineering</i>	1.4		1.4	
<i>Installation &amp; Instrumentation</i>	3.15		3.15	
<b>Capital Investment</b>	<b>40,763,134€</b>		<b>39,877,094€</b>	
<b><u>Annual Costs</u></b>				
Taxes, Royalties & Insurance	1,171,371€	3.00%	1,139,014€	3.00%
Maintenance	1,952,285€	5.00%	1,898,357€	5.00%
Capital Cost	5,305,256€	13.59%	5,158,708€	13.59%
Labor Cost	2,223,000€	20pers.	2,223,000€	20pers.
Heating	15,678,697€	535,954MWh	3,561,532€	105,700MWh
Cooling	920,584€	323,068MWh	25,036€	3,728MWh
Electricity	529,686€	6232MWh	1,086,185€	12,780MWh
Utility (Solvent replacement)	4,971€		1,424,138€	
<b>Total</b>	<b>27,785,848€/a</b>		<b>16,515,969€/a</b>	
<b>After Depreciation Period</b>	<b>22,480,593€/a</b>		<b>11,357,261€/a</b>	

**Table 10-3:** Cost Comparison of Trona Processes: 1-Step MSRR and 3-step MSRR process

<b><u>Equipment Costs</u></b>	<b><u>1 Step MSRR</u></b>		<b><u>3 Step MSRR</u></b>	
Vessels	4,655,921€	1,684m <sup>3</sup>	3,111,004€	986m <sup>3</sup>
Calciners & Dryers	393,455€	76m <sup>3</sup>	393,455€	76m <sup>3</sup>
Vacuum Pumps & Compressors	896,000€	627kW	368,000€	39kW
Belt Filters	388,098€	14m <sup>2</sup>	388,098€	14m <sup>2</sup>
Pumps & Powder Feeders	284,695€	308kW	227,895€	308kW
Heat Exchangers	264,000€	241m <sup>2</sup>	1,742,000€	3,819m <sup>2</sup>
<b>Total</b>	<b>6,882,169€</b>		<b>6,230,452€</b>	
<b>Lang Factors</b>				
<i>Design &amp; Engineering</i>	1.4		1.4	
<i>Installation &amp; Instrumentation</i>	3.15		3.15	
<b>Capital Investment</b>	<b>30,350,365€</b>		<b>27,476,293€</b>	
<b><u>Annual Costs</u></b>				
Taxes, Royalties & Insurance	859,166€	3.00%	772,943€	3.00%
Maintenance	1,431,943€	5.00%	1,288,239€	5.00%
Capital Cost	3,891,247€	13.59%	3,500,738€	13.59%
Labor Cost	2,223,000€	20pers.	2,223,000€	20pers.
Heating	1,774,292€	55,003MWh	11,097,113€	398,674MWh
Cooling	12,754€	1,893MWh	1,004,932€	318,898MWh
Electricity	740,996€	8,718MWh	744,681€	8,761MWh
Utility (Solvent replacement)	885,481€		626,480€	
<b>Total</b>	<b>11,820,107€/a</b>		<b>21,258,126€/a</b>	
<b>After Depreciation Period</b>	<b>7,928,860€/a</b>		<b>17,757,388€/a</b>	

**Table 10-4:** Cost Comparison of Trona Processes: MSDR and Trona Evaporative Crystallization

<b><u>Equipment Costs</u></b>	<b><u>MSDR</u></b>		<b><u>Trona Evaporative Crystallization</u></b>	
Vessels	2,448,400€	786m <sup>3</sup>	2,859,750€	805m <sup>3</sup>
Calciners & Dryers	1,465,910€	251m <sup>3</sup>	0€	0m <sup>3</sup>
Vacuum Pumps & Compressors	0€	0kW	348,000€	193kW
Belt Filters	388,098€	14m <sup>2</sup>	376,647€	18m <sup>2</sup>
Pumps & Powder Feeders	200,580€	176kW	296,370€	198kW
Heat Exchangers	848,000€	983m <sup>2</sup>	2,793,000€	7,027m <sup>2</sup>
<b>Total</b>	<b>5,350,988€</b>		<b>6,673,767€</b>	
<b>Lang Factors</b>				
<i>Design &amp; Engineering</i>	1.4		1.4	
<i>Installation &amp; Instrumentation</i>	3.15		3.15	
<b>Capital Investment</b>	<b>23,597,857€</b>		<b>29,431,312 €</b>	
<b><u>Annual Costs</u></b>				
Taxes, Royalties & Insurance	656,590€	3.00%	833,109€	3.00%
Maintenance	1,094,317€	5.00%	1,388,515€	5.00%
Capital Cost	2,973,763€	13.59%	3,773,234€	13.59%
Labor Cost	2,223,000€	20pers.	1,667,250€	15pers.
Heating	8,589,443€	308,584MWh	9,834,419€	353,311MWh
Cooling	280,702€	92,563MWh	1,086,303€	336,352MWh
Electricity	180,725€	2,126MWh	487,223€	5.732MWh
Utility (Solvent replacement)	496,651€		6,039€	
<b>Total</b>	<b>16,495,192€/a</b>		<b>19,076,091€/a</b>	
<b>After Depreciation Period</b>	<b>13,521,428€/a</b>		<b>15,302,858€/a</b>	

The totally required capital investment as well as the total annual cost of the complete soda plant can thus be obtained by adding the cost of the TEC to the cost of the respective process alternative. The cost of the actual solution mining, i.e. the drilling of bore holes down to the soda strata, the cultivation of the brine caverns, and the recovery of the brine from the caverns, is not considered in this estimation. Also not included are the investment and the operating cost of necessary storage, packaging and shipping facilities.

Comparing the required capital investment of all process alternatives, it can be seen, that the commonly employed monohydration process requires the largest investment with about 40.76 M€, although the 2-step MSRR requires close to this amount with about 39.87 M€. The required capital investment for all other processes is estimated significantly lower with about 30.35 M€ for 1-step MSRR, about 27.48 M€ for 3-Step MSRR and about 23.60 M€ for MSDR.

The monohydration requires more equipment than the mixed solvent processes, i.e. two additional sets of calciners and one set of soda dissolution units. Also the heat exchangers in monohydration are larger, as more heat, i.e. for the evaporative crystallization, needs to be transferred in the process. The higher cost of the 2-step MSRR compared to the other mixed solvent processes stems from the cost of the larger vessels, as this process requires longer crystallizer residence time.

The MSDR process requires the lowest capital investment, because as it has a comparatively low residence time, requiring smaller crystallizers, and it requires no compressor for carbon dioxide stripping.

The annual costs of the monohydration process are also noticeably higher with about 27.75 M€ than the mixed solvent processes with about 21.26 M€ for 3-Step MSRR, about 16.52 M€ for 2-Step MSRR, about 11.82 M€ for 1-Step MSRR and about 16.50 M€ for MSDR. As can be seen from the listings of the annual costs in the Tables, the high operating costs of the monohydration stem from the cost for heating utilities, i.e. the cost of water evaporation. Even with multistage vacuum evaporation, comparatively large amounts of steam are required to procure the required heat of evaporation. The largest utility cost for the mixed solvent processes are solvent replacement, i.e. the cost of the



ethylene glycol, electricity, i.e. mainly for the strip gas compressors, and heating, to warm the circulated mixed solvent solution to the required process temperature. For the mixed solvent processes, those with the least temperature changes of the mixed solvent solution, especially the 1-step MSRR, have the lowest annual costs, as the heating of the large amounts of mixed solvent solution still has great impact on the operation costs. The 3-step MSRR with its large temperature changes consumes the largest amount of heating energy, and even with the previously mentioned additional heat integration (with savings of about 1,293 k€/a in heating and 334 k€/a in cooling costs), remains the least economically advantageous of the mixed solvent processes.

The most economically advantageous processes are the 1-Step MSRR and the MSDR process. While the MSDR process requires about 6.75 M€ less capital investment, the annual costs of the 1-step MSRR process are about 4.68 M€/a lower. The higher investment in comparison to the MSDR process would thus be earned back by the 1-step MSRR process in less than 1.5 years, after which the 1-step MSRR process would yield about 4.68 M€/a more profit. After depreciation, the annual cost savings of the 1-step MSRR process compared to the MSDR process would even be about 5.59 M€/a.

Compared to the monohydration process, the 1-step MSRR process yields a saving of about 10.41 M€ in investment capital and about 15.97 M€/a in annual costs – 14.55 M€/a after depreciation. Based on the savings in annual cost, replacing an existing (depreciated) monohydration process by a 1-step monohydration process would have a pay-back time  $t_b$  (the operation time needed to earn the invested capital from the savings/profit of the new process) of less than 3 years:

$$t_{b,1\text{-stepMSRR}} = \frac{C_{i,1\text{-stepMSRR}}}{a_{c,MH(\text{depreciated})} - a_{c,1\text{-stepMSRR}}} = \frac{30.35M\text{€}}{22.48M\text{€/a} - 11.82M\text{€/a}} = 2.85a$$

Even more cost efficient is the revamping of the existing monohydration plant to the 1-step MSRR process: The evaporative crystallizers of the monohydration process can be refitted for mixed solvent recrystallization, by reducing heat exchanger surface or installing smaller heat exchangers, removing the calciners, the vacuum pumps and

barometric condensers, and installing air compressors for carbon dioxide stripping and drum dryers for product drying. New belt filters for the recovery of the mixed solvent and more intensive washing of the product have to replace the existing belt filters of the monohydration process. The existing slurry (feed and product) pumps as well as much of the existing piping and instrumentation can most probably be reused.

In this way, the existing monohydration plant can be modified into a 1-step MSRR plant of about 2/3 (67.4%) of the desired capacity.

The drawback of revamping is of course, that production is stopped during the revamping period, which will amount to at least ½ year. This period will incur the operator loss of profit from product sales, which has to be taken into account for the economic evaluation of the revamping scenario. This loss in profit makes direct revamping an economically rather unattractive option. Revamping becomes a viable option, e.g., if the operator intends to significantly expand the production capacity, e.g. by 2/3 of the existing capacity of 500,000 t/a.

First, a new 500,000 t/a 1-step MSRR plant needs to be erected to supply the current production, while the existing monohydration plant is being revamped. The investment cost of the newly erected 1-step MSRR plant would amount to the cost given in Table 3, i.e. about 30.35 M€.

The cost of revamping the existing monohydrate plant is estimated as the installation cost of the new compressors, dryers, belt filters and heat exchangers, which amounts to about 5.70 M€. During the revamping period, the new 1-step MSRR plant cannot be depreciated, as it only takes over the function of the existing monohydration plant. After the revamping period, the capacity of the modified plant (67.4%) is added to the total production capacity for a new capacity of ca. 830,000 t/a.

Under these circumstances, the pay-back time of the change to the 1-step monohydration process is reduced to about 1½ years:

$$t_b = \frac{C_{i,1\text{-stepMSRR}} + 0.5 \cdot a_{d,1\text{-stepMSRR}} + C_{revamp} - 0.674 \cdot C_{i,1\text{-stepMSRR}}}{0.674 \cdot a_{c,1\text{-stepMSRR}} + a_{c,MH(depreciated)} - 1.674 \cdot a_{c,1\text{-stepMSRR}}}$$

$$= \frac{(1 - 0.674) \cdot 30.35 \text{ Mio€} + 0.5 \cdot 3.89 \text{ Mio€} + 5.70 \text{ Mio€}}{22.48 \text{ Mio€} / a - 11.82 \text{ Mio€} / a} = 1.64a$$

### 10.3.3.2. Bicarbonate Processes

For the conversion of solid sodium bicarbonate to soda and subsequent densification, the viable process alternatives considered are the MSRR process, the MSDR process and the monohydration process. The MSRR process requires with about 66.06 M€ the largest capital investment, due to the long residence times required by the process. These long residence times require a cascade of large crystallizers, which are the major cost factor for the capital investment. The monohydration process requires about 40.83 M€ and the MSDR process about 24.79 M€.

The saving in the capital investment with the MSDR process compared to the monohydration process again stems from the omission of the evaporative crystallization, which requires more heat exchanger surface and the multistage vacuum evaporation equipment.

While the annual costs with about 23.08 M€/a of the MSRR process are noticeably lower than those of the monohydration process with 28.39 M€/a, the MSDR process has also the lowest estimated annual costs with 16.97 M€/a.

While the savings in annual costs due to lower energy requirements for the MSRR process compared to the monohydration process are too low relative to the high investment costs to grant a reasonable pay-back time, the savings of the MSDR process make this process a very economically attractive process alternative. It requires about 16.04 M€ less capital investment than the monohydration process and the annual costs are lower by about 11.42 M€/a – or 9.24 M€ after the depreciation period.

The pay-back time  $t_b$  for the replacement of an existing (depreciated) monohydration process plant by a bicarbonate-MDSR plant is estimated to be about 4 years:

$$t_b = \frac{C_{i,MDSR(bicarb)}}{a_{c,MH(depreciated)} - a_{c,MDSR(bicarb)}} = \frac{24.79M \text{ €}}{23.08M \text{ € / a} - 16.97M \text{ € / a}} = 4.06a$$

**Table 10-5:** Cost Comparison of Bicarbonate Processes: Monohydration, MSRR and MSDR

<b>Equipment</b>						
<b>Costs</b>	<b>Monohydration (MEC)</b>		<b>MSRR (Bicarb)</b>		<b>MSDR (Bicarb)</b>	
Vessels	3,986,904€	1,211m <sup>3</sup>	10,585,000€	3,807m <sup>3</sup>	2,448,400€	766m <sup>3</sup>
Calciners & Dryers	1,757,376€	398m <sup>3</sup>	393,455€	74m <sup>3</sup>	1,735,910€	158m <sup>3</sup>
Vacuum Pumps & Compressors	348,000€	155kW	2,240,000€	1,483kW	0€	0kW
Belt Filters	389,442€	17m <sup>2</sup>	388,098€	13m <sup>2</sup>	388,098€	13m <sup>2</sup>
Pumps & Powder Feeders	346,619€	292kW	393,284€	230kW	200,580€	176kW
Heat Exchangers	2,430,000€	5,488m <sup>2</sup>	979,000€	99m <sup>2</sup>	848,000€	960m <sup>2</sup>
<b>Total</b>	<b>9,258,341€</b>		<b>14,978,837€</b>		<b>5,620,988€</b>	
<b>Lang Factors</b>						
Design & Engineering	1.4		1.4		1.4	
Installation & Instrumentation	3.15		3.15		3.15	
<b>Capital Investment</b>	<b>40,829,284€</b>		<b>66,056,671€</b>		<b>24,788,557€</b>	
<b>Annual Costs</b>						
Taxes, Royalties & Insurance	1,173,355€	3.00%	1,930,355€	3.00%	692,311€	3.00%
Maintenance	1,955,592€	5.00%	3,217,258€	5.00%	1,153,852€	5.00%
Capital Cost	5,314,244€	13.59%	8,742,770€	13.59%	3,135,547€	13.59%
Labor Cost	2,223,000€	20pers.	2,223,000	20Pers.	2,223,000€	20pers.
Heating	16,270,160€	557,203MWh	3,067,411€	110,200MWh	8,819,916€	316,864MWh
Cooling	920,584€	323,068MWh	18,110€	2,687MWh	284,230€	97,247MWh
Electricity	528,526€	6,218MWh	1,361,968€	16,023MWh	180,891€	2,128MWh
Utility (Solvent replacement)	4,970€		2,293,906€		485,172€	
<b>Total</b>	<b>28,390,431€/a</b>		<b>22,856,523€/a</b>		<b>16,974,919€/a</b>	
<b>After Depreciation Period</b>	<b>23,076,187€/a</b>		<b>14,113,754€/a</b>		<b>13,839,372€/a</b>	

#### **10.4. Bottom Line of the Economical Evaluation**

With prices for soda produced from trona in the United States in the range of 105 to 130 US\$ per short ton [29], corresponding to 97.20 to 120.35 € per metric ton, the sales value of the produced soda of a 500,000 t/a plant is about 50 to 60 M€/a. The estimated annual cost of production – calculated in this work - is in the range of 37.5 (depreciated plants) to 46.4 (non-depreciated plants) M€ for trona evaporative crystallization and monohydration. The costs for mining, storage, packaging and shipping are not even included in these sums. I.e. this leaves a margin of about 10 to 15 M€/a for mining, storage, packaging, shipping – and profit! An increase in profit of 15 M€/a due to savings in annual costs by a Mixed Solvent Process would thus at least double the annual profit.

#### **10.5. Conclusions**

Mixed solvent recrystallization [14-16, 18-21] produces soda of improved quality with respect to higher bulk density and improved mechanical stability in comparison to the current production processes, and it is more cost efficient than the commonly employed *monohydration* process. The currently employed processes all require evaporative crystallization and calcinations to produce densified soda. These process steps are very energy intensive, so that the cost for heating and cooling utilities constitutes a major fraction (55 to 68%) of the operation costs of these processes.

Since the evaporative crystallization and even the calcinations can be avoided with the presented mixed solvent processes, this allows for significant savings in operation costs and also in capital investment, as the equipment for calcination and multistage evaporative crystallization can be omitted. It is shown, that by employing mixed solvent recrystallization the operational cost of the production of soda from trona can be reduced by about 15 M€ per year and for the production of soda from sodium bicarbonate, as in the Solvay process [2, 3], by about 10 M€/a in comparison to the monohydration process for a 500,000 t/a soda production.

This yields pay-back times for the replacement of existing monohydration plants of less than 3 years for trona operations and about 4 years for bicarbonate operations.

## 10.6. Literature References

- [1] Garret, D.E., "Natural Soda Ash – Occurrences, Processing and Use", Van Nostrand – Reinhold (Publ.), New York, 1992, p. 30-416
- [2] Thieme, C., "sodium hydrogen carbonate" in Ullmann's Encyclopedia of Chemical Technology, 6<sup>th</sup> ed., 2000, electronic release, Wiley-VCH
- [3] Rant, Z., "Die Erzeugung von Soda nach dem Solvay-Verfahren", Ferdinand Enke Verlag, Stuttgart, 1968, pp. 300
- [4] Vanderzee, C.E., "Thermodynamic relations and equilibria in ( $\text{Na}_2\text{CO}_3 + \text{NaHCO}_3 + \text{H}_2\text{O}$ ): standard Gibbs energies of formation and other properties of sodium hydrogen carbonate, sodium carbonate heptahydrate, sodium carbonate decahydrate, trona: ( $\text{Na}_2\text{CO}_3 \cdot \text{NaHCO}_3 \cdot 2\text{H}_2\text{O}$ ), and Wegscheider's salt: ( $\text{Na}_2\text{CO}_3 \cdot 3\text{NaHCO}_3$ )", J. Chem. Thermodynamics, 14, 1982, p. 219-238
- [5] Vanderzee, C.E., Wigg, D.A., "The standard enthalpies of formation of Wegscheider's salt:  $\text{Na}_2\text{CO}_3 \cdot 3\text{NaHCO}_3(\text{s})$  and of trona:  $\text{Na}_2\text{CO}_3 \cdot \text{NaHCO}_3 \cdot 2\text{H}_2\text{O}(\text{s})$  at 298.15K", J. Chem. Thermodynamics, 13, 1981, p. 573-583
- [6] Haynes, H.W., "Solution Mining of Trona", In Situ, 21(4), 1997, p. 357-394
- [7] Aitala, R., Aitala, M., "Process Selection Criteria for Refining Trona to Commercial Products", The First International Soda Ash Conference (ISAC), June 1997, available on: <http://www.isonex.com/isacpaper.html>
- [8] Nasün-Saygili, G., Okutan, H., "Application of the solution mining process to the Turkish trona deposit", Hydrometallurgy, 42, 1996, p. 103-113
- [9] Nasün-Saygili, G., Okutan, H., "Mechanism of the dissolution of Turkish trona", Hydrometallurgy, 43, 1996, p. 317-329
- [10] Robertson, H.R., "Production of Dense Soda Ash", United States Patent 2,267,136, Solvay Process Company, NY, 1940
- [11] Bourne, D.J., Lamb, F.E., "Method of Producing Soda Ash", United States Patent 3,656,892, Duval Co., 1972
- [12] Lynn, G., United States Patent 1,907,987, Pittsburg Plateglass Co., 1933
- [13] Julien, A.P., Keene, P.A., United States Patent, 2,133,455, The Solvay Process Co., 1938
- [14] Oosterhof, H., Witkamp, G.J., van Rosmalen, G.M., "Evaporative Crystallization of Anhydrous Sodium Carbonate at Atmospheric Conditions", AIChE J., 47(10), 2001, p. 2220-2225

- [15] Oosterhof, H., de Graauw, J., Witkamp, G.J., van Rosmalen, G.M., "Continuous Double Recrystallization of Light Soda Ash into Super Dense Soda Ash", *Crystal Growth & Design*, 2 (2), 2002, p. 151-157
- [16] Oosterhof, H., Witkamp, G.J., van Rosmalen, G.M., "Antisolvent Crystallization of Anhydrous Sodium Carbonate at Atmospheric Conditions", *AIChE J.*, 47(3), 2001, p. 602-608
- [17] Mannion, L.E., "Sodium Carbonate Deposits" in: Lefond, S. (Editor), "Industrial Minerals and Rocks", American Institute of Mining, Metallurgical and Petroleum Engineers, Port City Press, Maryland (Baltimore), 1983, p. 1187-1206
- [18] Gärtner, R.S., Witkamp, G.J., "Wet Calcining of Trona (Sodium Sesquicarbonate) and Bicarbonate in a Mixed Solvent", *J. Crystal Growth*, 237-239 (3), 2002, p. 2199-2205
- [19] Gärtner, R.S., Seckler, M.M., Witkamp, G.J., "Recrystallization of Trona (Sodium Sesquicarbonate) into Soda (Sodium Carbonate Anhydrate) in a Mixed Solvent, Part I: Fundamental Conversion Steps", submitted for publication in *AIChE Journal* (Chapter 4)
- [20] Gärtner, R.S., Seckler, M.M., Witkamp, G.J., "Recrystallization of Trona (Sodium Sesquicarbonate) into Soda (Sodium Carbonate Anhydrate) in a Mixed Solvent, Part II: Alternative Recrystallization Routes", in preparation for publication (Chapter 5)
- [21] Gärtner, R.S., Seckler, M.M., Witkamp, G.J., "Reactive Recrystallization of Sodium Bicarbonate", submitted for publication to *Ind. Eng. Chem. Res.* (Chapter 3)
- [22] Ball, M.C., Snelling, Ch.M., Strachan, A.N., Strachan, R.M., J. "Thermal Decomposition of Solid Sodium Bicarbonate", *Chem. Soc. Faraday Trans. 1*, 82, 1986, p. 3709-3715
- [23] Dutch Association of Cost Engineers, "NAP DACE prijzenboekje", 22<sup>nd</sup> edition, Elsevier bedrijfsinformatie, Doetinchem, 2002
- [24] Sinnott, R.K., "Coulson & Richardson's Chemical Engineering – Vol. 6 Chemical Engineering Design", revised 2<sup>nd</sup> edition, "Chapter 6: Costing and Project Evaluation", Butterworth-Heinemann, London, 1997
- [25] Strauß, K., "Strömungsmechanik – Eine Einführung für Verfahreningenieure", VCH, Weinheim, 1991
- [26] Perry, R.H., Green, D.W., "Perry's Chemical Engineer's Handbook", 7<sup>th</sup> edition, "Section 11: Heat Transfer Equipment", McGraw-Hill, New York, 1997
- [27] ChemSpy.com, "Bulk chemicals price indication", <http://www.chemspy.com/cgi-bin/database.cgi>
- [28] Camford Chemical Report, "Chemical prices", <http://ed.icheme.org/costchem.html>

- [29] US Geological Survey, “Soda Ash Statistics and Information”,  
[http://minerals.usgs.gov/minerals/pubs/commodity/soda\\_ash/index.html](http://minerals.usgs.gov/minerals/pubs/commodity/soda_ash/index.html)
- [30] Peters, M.S., Timmerhaus, K.D., “Plant Design and Economics for Chemical Engineers”,  
2<sup>nd</sup> ed., McGraw-Hill, New York, 1968, pp 157



## SUMMARY

The basic concept of antisolvent crystallization and mixed solvent crystallization are quite similar. The decisive difference is that in antisolvent crystallization (or in most cases rather: precipitation), the antisolvent is added during the process to induce crystallization by dramatically decreasing the solubility of the product compound.

The strategy of mixed solvent crystallization is to employ a miscible co-solvent to modify the crystallization behavior of a system. By the use of a 'tailor-made' mixed solvent, the morphology, the growth rate, the metastable zone width, the solubility and even the stability of a solid phase can be modified. Thereby, this method offers significant potential to fundamentally improve crystallization processes, especially since it also has the potential of significant savings in energy consumption and operation costs as energy intensive evaporative crystallization steps can be avoided.

The technical challenge for this method is its application to the crystallization of chemical bulk products. While in the production of high-added-value products like pharmaceuticals, the replacement / recycling of the solvent might be a minor cost factor, it is of vital importance for bulk products, where the price of a ton of co-solvent can be higher than the price of the same amount of product. This cost factor has to be countered by an increased added value of the product, significant savings in production costs and efficient recycling of the solvent.

Oosterhof et al. [1-4] have successfully applied mixed solvent (re)crystallization in the densification of soda, employing a mixed solvent composed of ethylene glycol and water. They succeeded in developing a process for the production of soda of higher purity, mechanical stability and bulk density, a.k.a. *super dense soda*, at lower production costs than the currently employed industrial process.

The process of Oosterhof et al. [1-4] is limited to increasing the value of common light soda ash by a downstream densification. *The aim of this work was to develop complete,*

*novel process routes based on the concept of mixed solvent recrystallization for the production of super dense soda from all of the principal sources of sodium carbonate, i.e. to provide concepts to replace the current, energy-consumptive production routes.*

To obtain fundamental understanding of these new processes, the conversion mechanisms were studied, and thermodynamic and kinetic models developed, to not only allow proper control of the processes, but also their predictive modeling for optimization and scale-up. Also the incorporation of common impurities during the mixed solvent crystallization steps was studied as well as different process steps for the in-line removal of these impurities from the mixed solvent to allow its efficient and continuous recycling.

The most common industrial sources of sodium carbonate are sodium bicarbonate ( $\text{NaHCO}_3(\text{s})$ ), produced by the Solvay process [5], and trona ( $\text{Na}_2\text{CO}_3 \cdot \text{NaHCO}_3 \cdot 2\text{H}_2\text{O}(\text{s})$ ), which occurs as a natural ore at locations on all continents [6]. Both sources contain bicarbonate, which has to be converted to carbonate, to obtain pure soda. It was found in this work, that bicarbonate could be converted by thermal decomposition in the mixed solvent simultaneously to the mixed solvent recrystallization.

The reaction mechanisms and kinetics of the thermal decomposition of pure solid and dissolved bicarbonate in mixed solvent solution were investigated (Chapter 3). It was found, that bicarbonate decomposes preferentially in the dissolved state according to a first order mechanism that matched the one found in literature for aqueous solution. The solvent mediated decomposition results also in the recrystallization of solid sodium bicarbonate. As the bicarbonate decomposition in solution is a reversible process, it results in an equilibrium between dissolved bicarbonate and carbonate. Above a temperature of ca.  $90^\circ\text{C}$ , this results in the formation of trona as the stable solid phase in contact with aqueous solution, while sodium carbonate anhydrate (soda) is formed in mixed solvent solution. Interestingly, the limiting temperature of  $90^\circ\text{C}$  for the stability of solid sodium bicarbonate in solution was found to be independent of solvent composition. Additionally, the decomposition rate in mixed solvent solution is slower than in aqueous solution, which allowed good control of the carbonate supersaturation, created by the decomposition reaction, and the growth of the soda crystals.

The study of the conversion of trona (Chapter 4) revealed, that its recrystallization was driven by two separate effects: The instability of the crystal water and the bicarbonate decomposition. Both effects increased with temperature. While at low driving forces the trona recrystallized solution mediated, higher driving forces resulted in a pseudo solid-state conversion. The product of the pseudo solid-state conversion consisted of pseudomorphs, i.e. agglomerates of fine soda crystallites in the shape of the original trona crystal. These pseudomorphs are undesirable products, as they retain solvent and impurities and yield a low bulk density. The kinetics of the conversion mechanisms were determined (Chapter 4) and 3 different mixed solvent process routes were developed (Chapter 5) to avoid pseudomorph formation while balancing short process times with controlled crystal growth and high product bulk densities.

The recrystallization of solid sodium bicarbonate and trona to soda in the mixed solvent was only possible due to the significantly increased stability of the anhydrous soda compared to the aqueous system. The stabilities and solubilities of all occurring solid phases were determined for a range of temperatures and mixed solvent compositions (Chapter 6). It was found, that not only the stability range of soda increased with increasing ethylene glycol content, but also the one of wegscheiderite ( $\text{Na}_2\text{CO}_3 \cdot 3\text{NaHCO}_3(\text{s})$ ), while the stability ranges of all hydrates including trona strongly decreased.

The study of the impurity incorporation during the mixed solvent recrystallization steps (Chapter 2) showed that chloride, fluoride and borate were excluded from the monohydrate and anhydrate crystals. Sulfate was incorporated to a high degree, which even resulted in morphological changes of the formed monohydrate and anhydrate. Interestingly, mixed solid phases of carbonate and sulfate, which were observed in the aqueous system, did not appear in the mixed solvent system.

Reactive extraction (Chapter 7), ion exchange (Chapter 8) and electrodialysis (Chapter 9) were evaluated as possible methods for the in-line extraction of impurities from the mixed solvent recycle.

The application of reactive extraction was not promising for the in-line removal: For all of the tested reactive extraction systems, ethylene glycol was taken up into the extractant and vice versa. Therefore only the results of another reactive extraction study are given, as reactive extraction is an attractive option for similar applications.

The application of ion exchange was more successful. Chloride and sulfate were extracted with a decent degree of selectivity from the trona-saturated mixed solvent. The extraction was apparently enhanced by a partitioning ('salting out') effect between the mixed solvent bulk and the pore solution of the ion exchangers.

Also by electrodialysis, chloride and sulfate were extracted from the carbonate saturated mixed solvent, but here it was found, that the selectivity was reduced compared to the aqueous system. The electrical resistance for electrodialysis in the mixed solvent was increased by a factor of 8, due to the increased resistance of the more apolar mixed solvent solution. Still, electrodialysis offers a viable option for the desalting of a mixed solvent, due to the good retention of the ethylene glycol.

An economical evaluation (Chapter 10) of different mixed solvent (reactive) recrystallization process alternatives was done. Comparison to processes currently employed in industry, revealed that the mixed solvent processes offer the possibility for significant savings in investment capital and operation costs – in the Solvay process [5] as well as in the processing of solution-mined trona [6]. Savings in operation costs of 10 to 15 M€ for a 500.000t/a soda plant were estimated, resulting in payback times of 3 to 4 years. These savings mainly resulted from savings of 55 to 70% in energy-consumption, namely heating utilities.

## **Literature References**

- [1] Oosterhof, H., Witkamp, G.J., van Rosmalen, G.M., “Evaporative Crystallization of Anhydrous Sodium Carbonate at Atmospheric Conditions”, *AIChE J.*, 47(10), 2001, p. 2220-2225
- [2] Oosterhof, H., de Graauw, J., Witkamp, G.J., van Rosmalen, G.M., “Continuous Double Recrystallization of Light Soda Ash into Super Dense Soda Ash”, *Crystal Growth & Design*, 2, (2), 2002, p. 151-157
- [3] Oosterhof, H., Witkamp, G.J., van Rosmalen, G.M., “Antisolvent Crystallization of Anhydrous Sodium Carbonate at Atmospheric Conditions”, *AIChE J.*, 47(3), 2001, p. 602-608
- [4] Oosterhof, H., de Graauw, J., Witkamp, G.J., van Rosmalen, G.M., “Process for the production of sodium carbonate anhydrate”, European and US Patent application, 1998
- [5] Thieme, C., “sodium bicarbonate” in “Ullmann’s Encyclopedia of Chemical Technology”, 6<sup>th</sup> ed., 2000, electronic release, Wiley-VCH
- [6] Garret, D.E., “Natural Soda Ash – Occurrences, Processing, And Use”, Van Nostrand Reinhold (publ.), New York, 1991, p. 267-383

## ACKNOWLEDGEMENTS

With the scientific and engineering part said and done, I am left with expressing my gratitude to the many people, who have advised, supported and kept me company during the 6 years of research, study and especially writing for my PhD project.

First of all, my thanks go to my wonderful wife, Dima, for her contribution to this work not only in the form of patience and support during long nights of data processing, modeling and writing, writing, writing, but of course also for her great work in the design of the cover of this book.

Second, I would like to thank my promotor, Prof. dr. Geert-Jan Witkamp, and my advisor, Dr. Marcelo Martins Seckler, for their good advice and tireless efforts to review and improve my work, and Prof. emerita dr. Gerda M. van Rosmalen and Prof. emeritus dr. Jan de Graauw for taking the time to share their invaluable experience.

Third, I want to express my gratitude to the Membrane Technology Group of the University of Twente, especially to Prof. Dr. Matthias Wessling for the opportunity to perform research in his department and to Dr. Friedrich G. Wilhelm und Dr. Alberto Figioli for their advice and support, which made Chapter 9 possible.

A special ‘thanks’ goes to Dr. Sean D. Fleming for the contribution of his molecular modeling simulations to the research on impurity incorporation presented in Chapter 2. (Too bad the results were trashed, when the hard disk of your computer bought the farm. Months of work down the drain and we ended up with zip. That’s tough noogies, mate!)

And of course: my gratitude to my colleagues - PhD students, Post Docs, academic and analytical staff as well as mechanical and electronic workshop alike - at the Laboratory for Process Equipment of Delft University, which will always be a place with a special charm to me. Special thanks to Dr. Christof Kersch for bringing me there, to Dr. Anke M. Berends for adopting me into ‘her’ project, to Dr. Harald Oosterhof for passing ‘his’ project on to me, to Mr. Paul Durville and Mr. Michel van den Brink for their support and contribution to experiments and analysis, to my great colleagues of the Eutectic-Freezing-Crystallization Project – Daniela, Chrismono, Raymond, Elif and Marcos – and to all the others, who have been and still are great colleagues and good company.

## CURRICULUM VITAE

### Robert Sebastian Gärtner

born July 17<sup>th</sup>, 1972 in Borgå, Finland

- June 1992:** Abitur (High School Degree) at the Konrad-Adenauer-Gymnasium in Langenfeld (Rhld.), Germany
- 1996 – 1998:** Junior Research Assistant at the Chair of Technical Chemistry A, Faculty of Chemical Engineering (Chemietechnik), University of Dortmund
- April 1998:** Diplom-Ingenieur Chemietechnik (M.Sc. Chemical Engineering) from the University of Dortmund, Dortmund, Germany
- July 1998:** Start of PhD research at the Laboratory for Process Equipment, Delft University of Technology
- July 2002:** Start of Post Doc research at the Laboratory for Process Equipment, Delft University of Technology
- March 2005:** PhD in chemical engineering from Delft University of Technology

### *Publications*

Gärtner, R.S., Witkamp, G.J., “Regeneration of Mixed Solvent by Ion Exchange Resin: Selective Removal of Chloride and Sulfate“, submitted for publication in Separation Science and Technology

Gärtner, R.S., Witkamp, G.J., “Mixed Solvent Reactive Recrystallization of Trona (Sodium Sesquicarbonate) into Soda (Sodium Carbonate Anhydrate)“, submitted for publication in AIChE Journal

Gärtner, R.S., Seckler, M.M., Witkamp, G.J., “Reactive Recrystallization of Sodium Bicarbonate“, submitted for publication in Industrial & Engineering Chemistry Research

Pillay, V., Gärtner, R.S., Himawan, C., Seckler, M.M., Lewis, A.E., Witkamp, G.J., “The System  $\text{MgSO}_4 + \text{H}_2\text{O}$  at Eutectic Conditions and Thermodynamic Solubility Products of  $\text{MgSO}_4 \cdot 12\text{H}_2\text{O}(\text{s})$  and  $\text{MgSO}_4 \cdot 7\text{H}_2\text{O}(\text{s})$ “, accepted for publication in Journal of Chemical and Engineering Data

R.S. Gärtner, F.E. Genceli, D.O. Trambitas, G.J. Witkamp, "Impurity Gradients in Solution-Grown Ice and  $\text{MgSO}_4 \cdot 12\text{H}_2\text{O}$  crystals measured by Cryo-Laser-Ablation and High Resolution Induced Coupled Plasma Mass Spectrograph", accepted for publication in Journal of Crystal Growth

F.E. Genceli, R.S. Gärtner, G.J. Witkamp, „Eutectic Freeze Crystallization in 2nd Generation Cooled Disk Column Crystallizer for the System  $\text{MgSO}_4\text{-H}_2\text{O}$ “, accepted for publication in Journal of Crystal Growth

Gärtner, R.S., Wilhelm, F.G., Witkamp, G.J., Wessling, M., "Regeneration of Mixed Solvent by Electrodialysis: Selective Removal of Chloride and Sulfate", accepted for publication in Journal of Membrane Science

Gärtner, R.S., Seckler, M.M., Witkamp, G.J., "Solid Phases and their Solubilities in the System  $\text{Na}_2\text{CO}_3 + \text{NaHCO}_3 + \text{Ethylene Glycol} + \text{Water}$  from (50 to 90) $^\circ\text{C}$ ", Journal of Chemical and Engineering Data (2004), 49(1), p. 116-125

Gärtner, R.S., Berends, A.M., Witkamp, G.J., "Testing Calix(4)arenes for the Selective Removal of Aluminum from a Pickling Bath Solution", Journal of Supramolecular Chemistry, Vol. 2 (2002), p. 159-162

Gärtner, R.S., Seckler, M.M., Witkamp, G.J., "Shifting the Phase Stabilities in the Sodium Carbonate-Bicarbonate System by a Mixed Solvent", Proceedings of the BIWIC 2002 / 9<sup>th</sup> International Workshop on Industrial Crystallization, Sept. 11<sup>th</sup> & 12<sup>th</sup>, 2002, Halle, Germany, Martin-Luther-University Halle-Wittenberg (Publ.), 2002, p. 27-34

Gärtner, R.S., Seckler, M.M., Witkamp, G.J., "Super Dense Soda from Trona (Sodium Sesquicarbonate) and Bicarbonate by Reactive Recrystallization in a Mixed Solvent", Proceedings of the 15<sup>th</sup> International Symposium on Industrial Crystallization, Sept. 15<sup>th</sup>-18<sup>th</sup>, Sorrento, Italy, Chemical Engineering Transactions, Vol. II, 2002, p. 945-950

Gärtner, R.S., Strube, J., Schulte, M., "Process Development of Product Recovery and Solvent Recycling Steps of Chromatographic Separation Processes", Chemical Engineering Journal, Vol. 85, 2002, p. 273-288

Gärtner, R.S., Witkamp, G.J., "Wet Calcining of Trona (Sodium Sesquicarbonate) and Bicarbonate in a Mixed Solvent", Journal of Crystal Growth, Vol. 237-239, part 3, 2002, p. 2199-2205

Gärtner, R.S., Witkamp, G.J., "Wet Calcining of Trona in a Mixed Solvent", Proceedings of the BIWIC 2001 / 8<sup>th</sup> International Workshop on Industrial Crystallization, Sept. 18<sup>th</sup>-20<sup>th</sup>, 2001, Delft, The Netherlands, Doc Vision Delft (Publ.), 2001, p. 190-195

Gärtner, R.S., Berends, A.M., Witkamp, G.J., "Extraction of Aluminum from a Pickling Bath Solution by Liquid-Liquid Extraction with Calixarenes", Proceedings of "Metal Separation Technologies Beyond 2000: Combining Novel Chemistry with Processing", United Engineering Foundation, Kahuku, Oahu, Hawaii, June 13-18, 1999, The Minerals, Metals and Materials Society (Publ.), 1999, p. 315-326